FRONTIERS IN SYSTEMS NEUROSCIENCE – EDITORS' PICK 2021

EDITED BY: Olivia Gosseries and Maria V. Sanchez-Vives
PUBLISHED IN: Frontiers in Systems Neuroscience

frontiers Research Topics

frontiers

ISSN 1664-8714
ISBN 978-2-88971-173-4
DOI 10.3389/978-2-88971-173-4

About Frontiers

Frontiers is more than just an open-access publisher of scholarly articles: it is a pioneering approach to the world of academia, radically improving the way scholarly research is managed. The grand vision of Frontiers is a world where all people have an equal opportunity to seek, share and generate knowledge. Frontiers provides immediate and permanent online open access to all its publications, but this alone is not enough to realize our grand goals.

Frontiers Journal Series

The Frontiers Journal Series is a multi-tier and interdisciplinary set of open-access, online journals, promising a paradigm shift from the current review, selection and dissemination processes in academic publishing. All Frontiers journals are driven by researchers for researchers; therefore, they constitute a service to the scholarly community. At the same time, the Frontiers Journal Series operates on a revolutionary invention, the tiered publishing system, initially addressing specific communities of scholars, and gradually climbing up to broader public understanding, thus serving the interests of the lay society, too.

Dedication to Quality

Each Frontiers article is a landmark of the highest quality, thanks to genuinely collaborative interactions between authors and review editors, who include some of the world's best academicians. Research must be certified by peers before entering a stream of knowledge that may eventually reach the public - and shape society; therefore, Frontiers only applies the most rigorous and unbiased reviews.
Frontiers revolutionizes research publishing by freely delivering the most outstanding research, evaluated with no bias from both the academic and social point of view. By applying the most advanced information technologies, Frontiers is catapulting scholarly publishing into a new generation.

What are Frontiers Research Topics?

Frontiers Research Topics are very popular trademarks of the Frontiers Journals Series: they are collections of at least ten articles, all centered on a particular subject. With their unique mix of varied contributions from Original Research to Review Articles, Frontiers Research Topics unify the most influential researchers, the latest key findings and historical advances in a hot research area! Find out more on how to host your own Frontiers Research Topic or contribute to one as an author by contacting the Frontiers Editorial Office: frontiersin.org/about/contact

FRONTIERS IN SYSTEMS NEUROSCIENCE – EDITORS' PICK 2021

Topic Editors:
Olivia Gosseries, University of Liège, Belgium
Maria V. Sanchez-Vives, Institut de Recerca Biomèdica August Pi i Sunyer (IDIBAPS), Spain

Citation: Gosseries, O., Sanchez-Vives, M. V., eds. (2021). Frontiers in Systems Neuroscience – Editors' Pick 2021. Lausanne: Frontiers Media SA. doi: 10.3389/978-2-88971-173-4

Table of Contents

frontiers in Systems Neuroscience

ORIGINAL RESEARCH
published: 15 January 2019
doi: 10.3389/fnsys.2018.00074

Abnormal Cortico-Cerebellar Functional Connectivity in Autism Spectrum Disorder

Taiane Coelho Ramos[1], *Joana Bisol Balardin*[2], *João Ricardo Sato*[3] *and André Fujita*[1]*

[1] *Department of Computer Science, Institute of Mathematics and Statistics, University of São Paulo, São Paulo, Brazil,* [2] *Brain Institute, Hospital Israelita Albert Einstein, São Paulo, Brazil,* [3] *Center of Mathematics, Computation, and Cognition, Universidade Federal do ABC, Santo André, Brazil*

The cerebral cortex and the cerebellum are spatially remote areas that are connected by complex circuits that link both primary and associative areas. Previous studies have revealed abnormalities in autism spectrum disorder (ASD); however, it is not clear whether cortico-cerebellar connectivity is differentially manifested in the disorder. To explore this issue, we investigated differences in intrinsic cortico-cerebellar functional connectivity between individuals with typical development (TD) and those with ASD. To this end, we used functional magnetic resonance imaging (fMRI) of 708 subjects under a resting state protocol provided by the ABIDE I Consortium. We found that people with ASD had diminished functional connectivity between the cerebellum and the following cortical regions: (i) right fusiform gyrus, (ii) right postcentral gyrus, (iii) right superior temporal gyrus, (iv) right middle temporal gyrus, and (v) left middle temporal gyrus. All of these regions are involved in many cognitive systems that contribute to commonly affected functions in ASD. For right fusiform gyrus, right superior temporal gyrus, and left middle temporal gyrus, we reproduced the results in an independent cohort composed of 585 subjects of the ABIDE II Consortium. Our results points toward a consistent atypical cortico-cerebellar connectivity in ASD.

Keywords: cortico-cerebellar connectivity, autism spectrum disorders, ASD, resting-state fMRI, cerebellum, functional connectivity, underconnectivity, ABIDE

OPEN ACCESS

Edited by:
Mikhail Lebedev,
Duke University, United States

Reviewed by:
Pere Berbel,
Universidad Miguel Hernández de Elche, Spain
Sergio E. Lew,
Universidad de Buenos Aires, Argentina
Hanna Bronisława Cygan,
Institute of Physiology and Pathology of Hearing (IFPS), Poland

***Correspondence:**
André Fujita
fujita@ime.usp.br

Received: *10 September 2018*
Accepted: *27 December 2018*
Published: *15 January 2019*

Citation:
Ramos TC, Balardin JB, Sato JR and Fujita A (2019) Abnormal Cortico-Cerebellar Functional Connectivity in Autism Spectrum Disorder. Front. Syst. Neurosci. 12:74. doi: 10.3389/fnsys.2018.00074

1. INTRODUCTION

Autism spectrum disorders (ASD) are mainly characterized by repetitive behavior and social impairment, including differentiated sensitivity to sound and touch and difficulty in recognizing non-verbal language and facial expressions (American Psychiatric Association, 2013). These symptoms may affect a child's cognitive development, which may prevent self-sufficiency in adulthood. One out of 68 children in the U.S. (Christensen, 2016) and 1% of the population worldwide (Elsabbagh et al., 2012) are estimated to have ASD. Despite this high incidence, the pathophysiology of ASD is still unclear. Therefore, additional studies are needed to better understand the underlying mechanisms and develop proper treatments for ASD.

Cerebellar abnormalities have been implicated in ASD (Fatemi et al., 2012), as suggested by studies correlating ASD to a reduced number and size of Purkinje cells (Fatemi et al., 2002; Bauman and Kemper, 2005) and cerebellar vermis hypoplasia (Courchesne et al., 1988; Hashimoto et al., 1995; Webb et al., 2009). Moreover, cerebellar lesions in premature children may result in symptoms similar to ASD (Limperopoulos et al., 2014).

Although the cerebellum was originally considered a motor structure, (Schmahmann, 2010; Noroozian, 2014; Baumann et al., 2015; Hoche et al., 2016) identified its role in cognitive, social, and emotional abilities, in special by observations of the cerebellar cognitive affective syndrome (Schmahmann, 2004). Its involvement in these functions may be explained by the vast white matter pathways connecting the cerebellum to functionally heterogeneous cortical regions (Glickstein, 1992; Ramnani, 2006). Functional cortical-cerebellar connectivity studies suggest a correlation between the cerebellar activity and several cortical regions, particularly correlation between the cerebellar frontal lobe and temporal, auditory, superior temporal, somatosensory, motor, and premotor regions and between the cerebellar posterior lobe and posterior parietal regions and the prefrontal cortex (O'Reilly et al., 2010; Buckner et al., 2011). In addition, meta-studies report cerebellar activity related to higher cognitive domains, including language, verbal working memory, and emotional processing (Stoodley and Schmahmann, 2009; Buckner, 2013; Keren-Happuch et al., 2014).

Currently, ASD is believed to be a disorder related more to differential brain connectivity than to the activity in a specific brain region (Müller et al., 2011; Maximo et al., 2014). Thus, it is natural to ask whether cortico-cerebellar connections are differentiated in ASD compared to typical development (TD). Attempts to answer this question are usually based on diffusion imaging studies, most of which show decreased Fractional Anisotropy (FA) suggesting a weaker structural connectivity in participants with ASD (Catani et al., 2008; Brito et al., 2009; Hanaie et al., 2013) (for a review, see Crippa et al., 2016). Task-driven fMRI studies reported decreased functional cortico-cerebellar connectivity during finger tapping task (Mostofsky et al., 2009) and verb generation task (Verly et al., 2014) in children with ASD.

A potential technique for studying neural connectivity is resting-state fMRI (rs-fMRI). rs-fMRI measures fluctuations in the blood oxygen level-dependent (BOLD) signal when a subject is not performing any specific task (Biswal et al., 1995). The brain areas and their respective correlations between the BOLD signals form the functional network (Fox and Raichle, 2007), which has been shown to be a good approximation of structural connections (Smith et al., 2009). However, few rs-fMRI studies focus specifically on cortico-cerebellar connectivity alterations in ASD. To the best of our knowledge, the study by Khan et al. (2015) is the only one that aimed at assessing functional cortico-cerebellar connectivity using rs-fMRI. The authors found a general cortico-cerebellar overconnectivity in children and adolescents with ASD, in special in sensori-motor networks, accompanied by underconnectivity in supramodal networks. They relate these results with previous findings of early overgrowth of the white matter, possibly leading to poorly assembled networks.

Considering the evidence, the current study aimed to identify brain regions with differential functional connectivity with the cerebellum in ASD, using rs-fMRI in a public large discovery sample (ABIDE I dataset) and to validate the findings in a validation sample (ABIDE II dataset). To the best of our knowledge, this is the first work to assess functional cortico-cerebellar connectivity that reproduced results on an independent dataset.

2. MATERIALS AND METHODS

To test our hypothesis of differential cortico-cerebellar functional connectivity between subjects with TD and those with ASD, we downloaded a large fMRI dataset from the ABIDE I Consortium and confirmed the results using an independent dataset (ABIDE II).

2.1. Functional MRI Data

We downloaded two large resting-state fMRI datasets, namely, ABIDE I and ABIDE II. ABIDE I is composed of 573 individuals with TD and 539 individuals with ASD (totaling 1 112 subjects). ABIDE II is composed of 593 individuals with TD and 521 individuals with ASD (totaling 1 114 subjects). After preprocessing (described in section 2.2.), the ABIDE I dataset was composed of 432 subjects with TD (348 males, mean age $\pm$ standard deviation of 18.21 $\pm$ 8.04) and 276 individuals with ASD (241 males, 18.42 $\pm$ 8.38). The ABIDE II dataset was composed of 316 subjects with TD (208 males, 12.80 $\pm$ 5.61) and 269 individuals with ASD (234 males, 13.93 $\pm$ 7.07). Both are available on the ABIDE Consortium website (http://fcon_1000.projects.nitrc.org/indi/abide/). According to the ABIDE repository, the acquisition methods and protocols were approved by the corresponding local Institutional Review Boards (i.e., the review boards and their regulations at the California Institute of Technology, Carnegie Mellon University, ETH Zürick, Georgetown University, Indiana University, Kennedy Krieger Institute, University of Leuven, Ludwig Maximilians University Munich, New York University, Oregon Health and Science University, Institute of Living at Hartford Hospital, University of Pittsburgh, Social Brain Lab, San Diego State University, Stanford University, Trinity Center for Health Sciences, University of California Davis, University of California Los Angeles, University of Michigan, University of Utah School of Medicine, Yale School of Medicine) and were performed in accordance with Health Insurance Portability and Accountability Act (HIPAA) guidelines and the 1,000 Functional Connectomes Project/International Data-sharing Initiative (http://fcon_1000.projects.nitrc.org/) protocols. Written informed consent was obtained from all the participants. All data distributed via the ABIDE website were fully anonymized in compliance with the HIPAA privacy rules, and no protected health information was included. The imaging protocols are considered to be equivalent across different institutes. Further details about this dataset can be obtained from the ABIDE consortium website.

2.2. Image Preprocessing

We preprocessed the imaging data using the Athena pipeline (www.nitrc.org/plugins/mwiki/index.php/neurobureau:AthenaPipeline). The pipeline focused on providing systematic processing of fMRI data, including the following main steps: exclusion of the first four scans; slice timing correction;

deoblique dataset; correction for head movements; masking the volumes to exclude non-brain regions; co- registration of the mean image to the respective anatomic image of the subject; spatial normalization to MNI space ($4 \times 4 \times 4$ mm resolution); extraction of BOLD (Ogawa et al., 1990) time series from white matter (WM) and cerebrospinal-fluid (CSF); removing the effects of WM, CSF, motion, and trend using multiple linear regression; temporal band-pass filter ($0.009 < f < 0.08$ Hz); and spatially smoothing the filtered data using a Gaussian filter (FWHM = 6 mm). All these steps were performed by using the following software: Analysis of Functional NeuroImages (AFNI) (http://afni.nimh.nih.gov/afni) and the fMRIB Software Library (FSL) (http://fsl.fMRIb.ox.ac.uk/fsl/fslwiki/). To define the 116 ROIs considered in this study, we used the Automated Anatomical Labeling (AAL) atlas (Tzourio-Mazoyer et al., 2002). We identified 25 ROIs comprising the ventricles by using the Montreal Neurological Institute (MNI) atlas, and we removed them. The head coil coverage available in the scanners may vary depending on the model, which may lead to a lack of reading of part of the cerebellum for some subjects. Thus, to avoid artifacts, we adopted a masking procedure to constrain the statistics only to ROIs with a mean voxels sampling of 80% across participants. An image was created from the overlay plot to represent the percentage of valid voxels in each cerebellar ROI (see **Figure S1**). We found that ROIs from I-VI lobes and the vermis region matched this criterion. Thus, we considered 79 ROIs (65 cortical and 14 cerebellar) for further analysis. Subjects' head movements during MRI scanning could lead to spurious correlations between ROIs; thus, we carried out the "scrubbing" procedure (Power et al., 2012) to remove frames affected by head movement. We removed frames that presented both framewise displacement (FD) greater than 0.5 mm and DVARS greater than 0.5% ΔBOLD (Power et al., 2012). Preceding and following frames that did not meet these criteria were not removed. Subjects that had more than 5% of the total number of scans removed by scrubbing were excluded from the analysis. Head motion across the dataset is measured by the FD, which presents a mean of 0.137 mm and standard deviation of 0.102 mm on the study dataset (ABIDE I) and a mean of 0.169 mm with standard deviation of 0.132 mm on the independent dataset (ABIDE II). A total of 93 subjects (53 TD and 40 ASD) in the study dataset (ABIDE I) and 45 subjects (24 TD and 21 ASD) in the independent dataset (ABIDE II) had scans removed by the scrubbing process.

We considered both autism and Asperger syndrome as parts of the ASD as suggested by the Diagnostic and Statistical Manual of Mental Disorders 5th edition (DSM-5) (American Psychiatric Association, 2013).

2.3. Cortico-Cerebellar Functional Connectivity Analysis

To summarize, reduce the number of variables, and enhance the statistical power, for each subject in the sample, we applied the principal component analysis (PCA) on the 14 cerebellar ROI time series. Then, for each subject, we selected the principal components (PCs) that explained at least 95% of the data variance. Thus, each subject had a different number of PCs used for the analyses (average of 9.25 PCs with standard deviation of 1.19).

Next, to identify the cortical regions that are functionally associated with the cerebellum, for each subject, we carried out a linear regression with the cortical ROI time series as response variables and the PCs of the cerebellum obtained by the PCA for the subject as predictor variables. The adjusted R^2 (coefficient of determination) was considered as a measure of functional connectivity between the cortical ROI and the cerebellum.

To test if the functional connectivity was different between the TD and ASD groups for each cortical ROI, we performed a linear regression using the measure of functional connectivity (the adjusted R^2 obtained for each subject in the previous step) as the response variable and the diagnostic group (TD or ASD) as the predictor variable. To reduce age, gender, and site effects, we included them as covariates in this linear model. All p-values were corrected for multiple tests by using the False Discovery Rate (FDR) (Benjamini and Hochberg, 1995) approach (we considered all 65 tests, one for each cortical ROI). The corrected p-value threshold considered to be statistically significant was set at 5%.

3. RESULTS

First, we carried out the procedures described in the sections 2.2. and 2.3. using the ABIDE I dataset. In summary, for each subject, we carried out a linear regression between the fMRI time series of each cortical ROI and the cerebellum. To represent the neural activity of the cerebellum, we used the cerebellar PCs representing 95% of the variance of the time series in this region. We estimated the R^2 value of this regression as a measure of connectivity between each cortical ROI and the cerebellum as a whole. Then, we carried out a second linear regression between the R^2 values obtained in the previous linear regression and the group (TD or ASD), by including age, gender, and site as covariates. We identified five cortical ROIs (**Figure 1**) that are differentially associated with the cerebellum between the typical development (TD) and autism spectrum disorder (ASD) groups, namely, the right fusiform gyrus [$\beta = -0.042$, t-value = -3.689, $p = 0.005$ —t-test (GLM)], the right postcentral gyrus [$\beta = -0.038$, t-value = -3.131, $p = 0.027$ — t-test (GLM)], the right superior temporal gyrus [$\beta = -0.034$, t-value = -3.082, $p = 0.027$ –t-test (GLM)], the right middle temporal gyrus [$\beta = -0.039$, t-value = -3.783, $p < 0.001$ —t-test (GLM)], and the left middle temporal gyrus [$\beta = -0.056$, t-value = -5.481, $p = 0.005$ —t-test (GLM)]. All p-values were corrected for FDR. **Figure 2** presents the barplots for the cortico-cerebellar functional connectivity measurements (adjusted R^2) for the TD and ASD groups for each of the five cortical ROIs. It is important to mention that for all of the identified cortical regions, the cortico-cerebellar functional connectivity in the ASD group was statistically lower than that in the TD group.

Then, to check the reproducibility of the findings, we tested these five differential cortico-cerebellar connectivity areas on an independent dataset composed of 585 subjects collected from 11 sites available in the ABIDE II consortium. The criteria for selecting the participants and the preprocessing procedure adopted for the independent dataset were the same

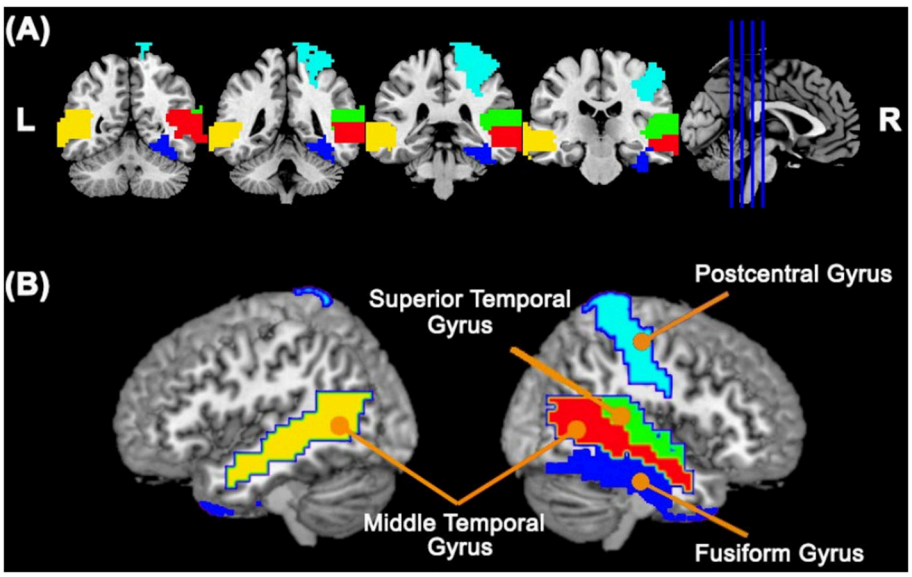

FIGURE 1 | Cortical ROIs with a differential association with the cerebellum between TD and ASD groups obtained by analyzing the ABIDE I dataset. Panels **(A,B)** represent coronal slices and two lateral views of the brain, respectively. The colors represent the cortical ROIs that differentially associated with the cerebellum between TD and ASD groups, namely, the right fusiform gyrus, right postcentral gyrus, right superior temporal gyrus, right middle temporal gyrus, and left middle temporal gyrus.

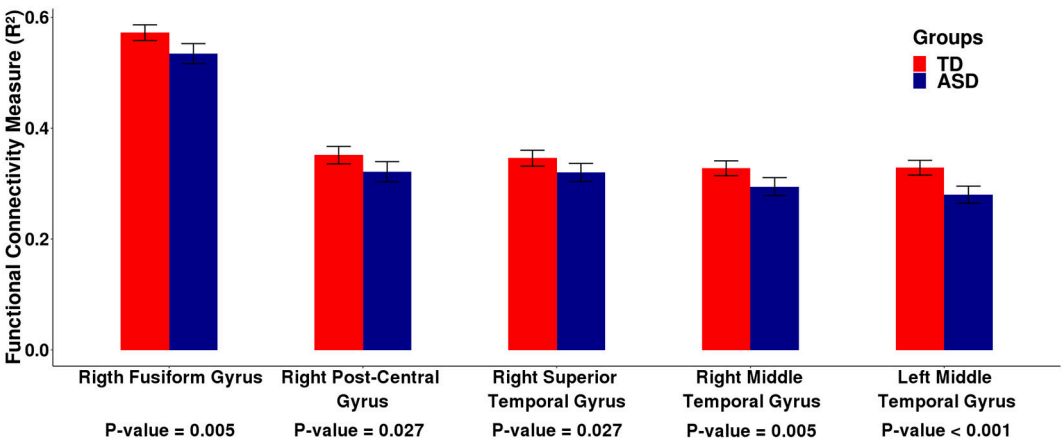

FIGURE 2 | Barplots of the functional connectivity measure (R^2) between the cortical ROI and the cerebellum obtained by analyzing the ABIDE I dataset. Each pair of bars represent the mean functional connectivity measurements between the cortical ROI and the cerebellum for the TD and ASD groups, respectively. The error bars represent 95% confidence interval. *P*-values were obtained by linear regression with the measure of functional connectivity (R^2) as the response variable and the diagnostic group (TD or ASD) as the predictor variable with age, gender, and site as covariates. All *p*-values were corrected for multiple tests by FDR. Note that the mean functional connectivity measurement (R^2) is significantly lower in the ASD group compared to the TD group, suggesting decreased functional cortico-cerebellar connectivity in the ASD group.

as described for the ABIDE I dataset in the section 2.2. In this validation analysis, three out of five cortical ROIs, namely, the right fusiform gyrus [$\beta = -0.028$, t-value = -2.193, $p = 0.047$ —t-test (GLM)], the right superior temporal gyrus [$\beta = -0.044$, t-value = -3.495, $p = 0.002$ —t-test (GLM)], and the left middle temporal gyrus [$\beta = -0.033$, t-value = -2.583, $p = 0.025$—t-test (GLM)], confirmed the reduced functional connectivity in the ASD group (p-values corrected for multiple tests by FDR). The barplots for the functional connectivity measures (adjusted R^2) of these three cortical regions are shown in **Figure 3**. It is important to mention that the cortico-cerebellar functional connectivity in the ASD group was statistically lower than that in the TD group, as observed in the previous dataset. For some brief results on difference in intracortical connectivity between groups, see **Figures S2**, **S3**.

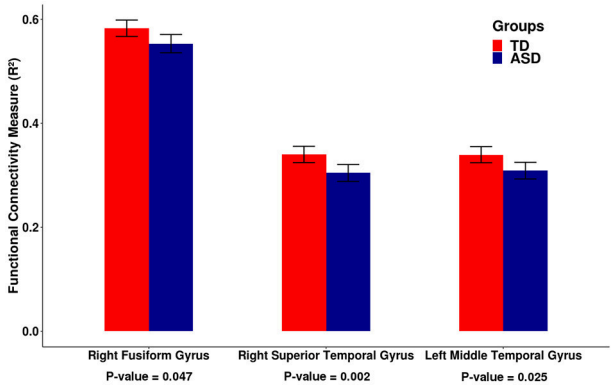

FIGURE 3 | Barplots of the functional connectivity measure (R^2) between the cortical ROI and the cerebellum for an independent dataset (ABIDE II). Each pair of bars represent the mean functional connectivity measurements between the cortical ROI and the cerebellum for the TD and ASD groups, respectively. The error bars represent 95% confidence interval. *P*-values were obtained by linear regression with the measure of functional connectivity (R^2) as the response variable and the diagnostic group (TD or ASD) as the predictor variable with age, gender, and site as covariates. All *p*-values were corrected for multiple tests by FDR. Note that the median functional connectivity measurement (R^2) is significantly lower in the ASD group compared to the TD group, suggesting decreased functional cortico-cerebellar connectivity in the ASD group. These data confirm the findings that were obtained by analyzing the ABIDE I dataset.

4. DISCUSSION

In this study, we investigated the differences in the intrinsic cortico-cerebellar functional connectivity between individuals with TD and those with ASD. We found that people with ASD had diminished functional connectivity between the cerebellum and several cortical regions, including the right postcentral, middle temporal, superior temporal, and fusiform gyri and the left middle temporal gyrus. For the right fusiform gyrus, the right superior temporal gyrus, and the left middle temporal gyrus, the validity of the results was confirmed in a large independent sample (ABIDE II).

Our results are in line with previous studies based on diffusion tensor imaging (DTI) suggesting alterations in structural connectivity in ASD. These studies show reduced values of fractional anisotropy (FA) in the white matter of individuals with ASD (Shukla et al., 2010; Libero et al., 2016) and abnormal development of such white matter pathways in young children on the spectrum (Ben Bashat et al., 2007; Wolff et al., 2012). In addition, there are studies showing specifically reduced FA in the temporal lobe (Barnea-Goraly et al., 2004; Lee et al., 2007), in agreement with our results of reduced functional connectivity in the right middle and superior temporal gyri and left middle temporal gyrus.

Abnormal functional connectivity in the cerebellum has been reported in ASD, albeit with mixed results. For example, cortico-cerebellar functional overconnectivity in the sensorimotor regions and underconnectivity in the supramodal regions were previously described in children and adolescents with ASD (Khan et al., 2015). In adolescents with ASD, reduced connectivity was also shown in the right crus I and several contralateral cerebral regions, including the superior frontal gyrus, middle frontal gyrus, thalamus, and anterior cingulate gyrus, as well as in the precentral gyrus (Verly et al., 2014). In our replication study, a prominent pattern of reduced connectivity in ASD was observed in the lateral temporal cortex. This variation among the results in the different studies may reflect differential alterations in connectivity related to patient characteristics (i.e., age, disease duration, and symptom severity) or image analysis methods, as previously discussed in the autism literature (Ecker et al., 2015). Although the nature and direction of functional connectivity differences in ASD remain inconclusive, our results add to the evidence indicating decreased cortico-cerebellar functional connectivity in patients.

The specific cortical regions that exhibited ASD-related altered functional connectivity with the cerebellum have also been linked to symptoms and traits of autism. For example, differences in frontocerebellar circuits have been associated with motor impairments and stereotyped repetitive behaviors (Floris et al., 2016), and the lateral temporal cortex and fusiform gyrus appear to mediate social processing deficits (for a review, see Just et al., 2012). Altogether, these findings suggest that differences in cortico-cerebellar functional connectivity in organized somatomotor and associative networks may contribute to the clinical manifestations in ASD, although further studies are needed to establish a direct association between our findings and autistic symptoms.

The neurobiological mechanisms underlying the diminished cortico-cerebellar functional connectivity in ASD observed in our study remain speculative. The communication of the cerebellum with the cerebral cortex has been associated with a closed-loop system in which the cerebellum returns projections to the cerebral cortex via the thalamus (for a review, see Ramnani, 2006). In this context, cortico-cerebellar connectivity differences could emerge from developmental alterations in both thalamo-cortical and/or extrinsic cortico-cortical projections. In fact, prior ASD studies using diffusion tensor MRI have detected differences in microstructural integrity of tracts connecting thalamus with motor and somatosensory cortices (Nair et al., 2013), and also of the corpus callosum (Alexander et al., 2007). It is important to note, however, that microstructural alterations have also been reported in cerebellar tracts (e.g., intracerebellar fibers and right superior cerebellar output peduncle) (Catani et al., 2008). Thus, the extent to which the observed functional differences relates to anatomy is unknown and requires investigation.

Moreover, the challenges in the reproducibility of neuroimaging findings (Griffanti et al., 2016) and the influence of small sample size in the reliability of results (Button et al., 2013) have been much discussed in the current scientific literature. A major strength of this study is the reproducibility of most of the results in a large sample of similar individuals from the ABIDE II dataset (Di Martino et al., 2017). On the other hand, there are limitations that need to be taken into consideration. The estimation of cerebellar zones coupled to cerebral regions was compromised by the fact that there was no full coverage of the cerebellum in most individuals,

particularly in the posterior region. Therefore, further studies are required to comprehensively examine ASD-related differences in cortico-cerebellar functional connectivity. Importantly, both the ABIDE I and ABIDE II datasets are multicentric, with heterogeneous acquisition parameters across sites. Thus, to minimize the site effect in our analysis, we included it as a covariate in group-level statistics as described in the section 2.3. It is also important to highlight that since the ROIs were divided according to anatomical regions, they could exhibit functional heterogeneity, possibly leading to ambiguous functional connectivity.

In conclusion, our results suggest that ASD displays atypical reduced intrinsic functional cortico-cerebellar connectivity in specific networks, which is consistent with the idea that ASD is a disorder characterized by abnormalities in neural connections (Hoppenbrouwers et al., 2014).

AUTHOR CONTRIBUTIONS

TR and AF conceived the analyses. TR conducted the analyses. TR, JB, JS, and AF analyzed the results and reviewed the manuscript. All authors read and approved the final version of the manuscript.

ACKNOWLEDGMENTS

TR was partially supported by the Coordenação de Aperfeiçoamento de Pessoal de Nível Superior - Brasil (CAPES) (051/2013) and CNPq (141492/2017-1). AF was partially supported by the São Paulo Research Foundation (2013/07375-0, 2015/01587-0, 2016/13422-9, 2018/17996-5), CNPq (304876/2016-0), CAPES (Finance Code 001), Alexander von Humboldt Foundation, and Medical Academy of Sciences–Newton Advanced Fund. The authors would like to thank the ABIDE Consortium for making the fMRI database publicly available.

SUPPLEMENTARY MATERIAL

The Supplementary Material for this article can be found online at: https://www.frontiersin.org/articles/10.3389/fnsys.2018.00074/full#supplementary-material

REFERENCES

Alexander, A. L., Lee, J. E., Lazar, M., Boudos, R., DuBray, M. B., Oakes, T. R., et al. (2007). Diffusion tensor imaging of the corpus callosum in autism. *Neuroimage* 34, 61–73. doi: 10.1016/j.neuroimage.2006.08.032

American Psychiatric Association (2013). *Diagnostic and Statistical Manual of Mental Disorders (DSM-5®)*. Arlington, VA: American Psychiatric Pub.

Barnea-Goraly, N., Kwon, H., Menon, V., Eliez, S., Lotspeich, L., and Reiss, A. L. (2004). White matter structure in autism: preliminary evidence from diffusion tensor imaging. *Biol. Psychiatry* 55, 323–326. doi: 10.1016/j.biopsych.2003.10.022

Bauman, M. L., and Kemper, T. L. (2005). Neuroanatomic observations of the brain in autism: a review and future directions. *Int. J. Dev. Neurosci.* 23, 183–187. doi: 10.1016/j.ijdevneu.2004.09.006

Baumann, O., Borra, R. J., Bower, J. M., Cullen, K. E., Habas, C., Ivry, R. B., et al. (2015). Consensus paper: the role of the cerebellum in perceptual processes. *Cerebellum* 14, 197–220. doi: 10.1007/s12311-014-0627-7

Ben Bashat, D., Kronfeld-Duenias, V., Zachor, D. A., Ekstein, P. M., Hendler, T., Tarrasch, R., et al. (2007). Accelerated maturation of white matter in young children with autism: a high b value DWI study. *Neuroimage* 37, 40–47. doi: 10.1016/j.neuroimage.2007.04.060

Benjamini, Y., and Hochberg, Y. (1995). Controlling the false discovery rate: a practical and powerful approach to multiple testing. *J. R. Stat. Soc. Ser. B Methodol.* 57, 289–300. doi: 10.1111/j.2517-6161.1995.tb02031.x

Biswal, B., Yetkin, F. Z., Haughton, V. M., and Hyde, J. S. (1995). Functional connectivity in the motor cortex of resting human brain using echo-planar MRI. *Magn. Reson. Med.* 34, 537–541. doi: 10.1002/mrm.1910340409

Brito, A. R., Vasconcelos, M. M., Domingues, R. C., Hygino da Cruz, L. C., Rodrigues Lde, d. S., Gasparetto, E. L., et al. (2009). Diffusion tensor imaging findings in school-aged autistic children. *J. Neuroimaging* 19, 337–343. doi: 10.1111/j.1552-6569.2009.00366.x

Buckner, R. L. (2013). The cerebellum and cognitive function: 25 years of insight from anatomy and neuroimaging. *Neuron* 80, 807–815. doi: 10.1016/j.neuron.2013.10.044

Buckner, R. L., Krienen, F. M., Castellanos, A., Diaz, J. C., and Yeo, B. T. T. (2011). The organization of the human cerebellum estimated by intrinsic functional connectivity. *J. Neurophysiol.* 106, 2322–2345. doi: 10.1152/jn.00339.2011

Button, K. S., Ioannidis, J. P., Mokrysz, C., Nosek, B. A., Flint, J., Robinson, E. S., et al. (2013). Power failure: why small sample size undermines the reliability of neuroscience. *Nat. Rev. Neurosci.* 14:365. doi: 10.1038/nrn3475

Catani, M., Jones, D. K., Daly, E., Embiricos, N., Deeley, Q., Pugliese, L., et al. (2008). Altered cerebellar feedback projections in Asperger syndrome. *Neuroimage* 41, 1184–1191. doi: 10.1016/j.neuroimage.2008.03.041

Christensen, D. L. (2016). Prevalence and characteristics of autism spectrum disorder among children aged 8 years — autism and developmental disabilities monitoring network, 11 sites, United States, 2012. *MMWR Surveill. Summar.* 65,1–23. doi: 10.15585/mmwr.ss6503a1

Courchesne, E., Yeung-Courchesne, R., Press, G. A., Hesselink, J., and Jernigan, T. (1988). Hypoplasia of cerebellar vermal lobules VI and VII in autism. *New Engl. J. Med.* 318, 1349–1354. doi: 10.1056/NEJM198805263182102

Crippa, A., Del Vecchio, G., Busti Ceccarelli, S., Nobile, M., Arrigoni, F., and Brambilla, P. (2016). Cortico-cerebellar connectivity in autism spectrum disorder: what do we know so far? *Front. Psychiatry* 7:20. doi: 10.3389/fpsyt.2016.00020

Di Martino, A., O'Connor, D., Chen, B., Alaerts, K., Anderson, J. S., Assaf, M., et al. (2017). Enhancing studies of the connectome in autism using the autism brain imaging data exchange II. *Sci. Data* 4:170010. doi: 10.1038/sdata.2017.10

Ecker, C., Bookheimer, S. Y., and Murphy, D. G. M. (2015). Neuroimaging in autism spectrum disorder: brain structure and function across the lifespan. *Lancet Neurol.* 14, 1121–1134. doi: 10.1016/S1474-4422(15)00050-2

Elsabbagh, M., Divan, G., Koh, Y.-J., Kim, Y. S., Kauchali, S., Marcín, C., et al. (2012). Global prevalence of autism and other pervasive developmental disorders. *Autism Res.* 5, 160–179. doi: 10.1002/aur.239

Fatemi, S. H., Aldinger, K. A., Ashwood, P., Bauman, M. L., Blaha, C. D., Blatt, G. J., et al. (2012). Consensus paper: pathological role of the cerebellum in autism. *Cerebellum* 11, 777–807. doi: 10.1007/s12311-012-0355-9

Fatemi, S. H., Halt, A. R., Realmuto, G., Earle, J., Kist, D. A., Thuras, P., et al. (2002). Purkinje cell size is reduced in cerebellum of patients with autism. *Cell. Mol. Neurobiol.* 22, 171–175. doi: 10.1023/A:1019861721160

Floris, D. L., Barber, A. D., Nebel, M. B., Martinelli, M., Lai, M.-C., Crocetti, D., et al. (2016). Atypical lateralization of motor circuit functional connectivity in children with autism is associated with motor deficits. *Mol. Autism* 7:35. doi: 10.1186/s13229-016-0096-6

Fox, M. D., and Raichle, M. E. (2007). Spontaneous fluctuations in brain activity observed with functional magnetic resonance imaging. *Nat. Rev. Neurosci.* 8, 700–711. doi: 10.1038/nrn2201

Glickstein, M. (1992). The cerebellum and motor learning. *Curr. Opin. Neurobiol.* 2, 802–806.

Griffanti, L., Rolinski, M., Szewczyk-Krolikowski, K., Menke, R. A., Filippini, N., Zamboni, G., et al. (2016). Challenges in the reproducibility of clinical studies with resting state fmri: an example in early parkinson's disease. *Neuroimage* 124, 704–713. doi: 10.1016/j.neuroimage.2015.09.021

Hanaie, R., Mohri, I., Kagitani-Shimono, K., Tachibana, M., Azuma, J., Matsuzaki, J., et al. (2013). Altered microstructural connectivity of the superior cerebellar peduncle is related to motor dysfunction in children with autistic spectrum disorders. *Cerebellum* 12, 645–656. doi: 10.1007/s12311-013-0475-x

Hashimoto, T., Tayama, M., Murakawa, K., Yoshimoto, T., Miyazaki, M., Harada, M., et al. (1995). Development of the brainstem and cerebellum in autistic patients. *J. Autism Dev. Dis.* 25, 1–18.

Hoche, F., Guell, X., Sherman, J. C., Vangel, M. G., and Schmahmann, J. D. (2016). Cerebellar contribution to social cognition. *Cerebellum* 15, 732–743. doi: 10.1007/s12311-015-0746-9

Hoppenbrouwers, M., Vandermosten, M., and Boets, B. (2014). Autism as a disconnection syndrome: a qualitative and quantitative review of diffusion tensor imaging studies. *Res. Autism Spect. Disord.* 8, 387–412. doi: 10.1016/j.rasd.2013.12.018

Just, M. A., Keller, T. A., Malave, V. L., Kana, R. K., and Varma, S. (2012). Autism as a neural systems disorder: a theory of frontal-posterior underconnectivity. *Neurosci. Biobehav. Rev.* 36, 1292–1313. doi: 10.1016/j.neubiorev.2012.02.007

Keren-Happuch H., Chen, S.-H. A., Ho, M.-H. R., and Desmond, J. E. (2014). A meta-analysis of cerebellar contributions to higher cognition from pet and fMRI studies. *Hum. Brain Mapp.* 35, 593–615. doi: 10.1002/hbm.22194

Khan, A. J., Nair, A., Keown, C. L., Datko, M. C., Lincoln, A. J., and Müller, R.-A. (2015). Cerebro-cerebellar resting-state functional connectivity in children and adolescents with autism spectrum disorder. *Biol. Psychiatry* 78, 625–634. doi: 10.1016/j.biopsych.2015.03.024

Lee, J. E., Bigler, E. D., Alexander, A. L., Lazar, M., DuBray, M. B., Chung, M. K., et al. (2007). Diffusion tensor imaging of white matter in the superior temporal gyrus and temporal stem in autism. *Neurosci. Lett.* 424, 127–132. doi: 10.1016/j.neulet.2007.07.042

Libero, L. E., Burge, W. K., Deshpande, H. D., Pestilli, F., and Kana, R. K. (2016). White matter diffusion of major fiber tracts implicated in autism spectrum disorder. *Brain Connect.* 6, 691–699. doi: 10.1089/brain.2016.0442

Limperopoulos, C., Chilingaryan, G., Sullivan, N., Guizard, N., Robertson, R. L., and du Plessis, A. J. (2014). Injury to the Premature cerebellum: outcome is related to remote cortical development. *Cereb. Cortex* 24, 728–736. doi: 10.1093/cercor/bhs354

Maximo, J. O., Cadena, E. J., and Kana, R. K. (2014). The implications of brain connectivity in the neuropsychology of autism. *Neuropsychol. Rev.* 24, 16–31. doi: 10.1007/s11065-014-9250-0

Mostofsky, S. H., Powell, S. K., Simmonds, D. J., Goldberg, M. C., Caffo, B., and Pekar, J. J. (2009). Decreased connectivity and cerebellar activity in autism during motor task performance. *Brain* 132(Pt 9), 2413–2425. doi: 10.1093/brain/awp088

Müller, R.-A., Shih, P., Keehn, B., Deyoe, J. R., Leyden, K. M., and Shukla, D. K. (2011). Underconnected, but how? A survey of functional connectivity MRI studies in autism spectrum disorders. *Cereb. Cortex* 21, 2233–2243. doi: 10.1093/cercor/bhq296

Nair, A., Treiber, J. M., Shukla, D. K., Shih, P., and Müller, R.-A. (2013). Impaired thalamocortical connectivity in autism spectrum disorder: a study of functional and anatomical connectivity. *Brain* 136, 1942–1955. doi: 10.1093/brain/awt079

Noroozian, M. (2014). The role of the cerebellum in cognition: beyond coordination in the central nervous system. *Neurol. Clin.* 32, 1081–1104. doi: 10.1016/j.ncl.2014.07.005

Ogawa, S., Lee, T. M., Kay, A. R., and Tank, D. W. (1990). Brain magnetic resonance imaging with contrast dependent on blood oxygenation. *Proc. Natl. Acad. Sci. U.S.A.* 87, 9868–9872.

O'Reilly, J. X., Beckmann, C. F., Tomassini, V., Ramnani, N., and Johansen-Berg, H. (2010). Distinct and overlapping functional zones in the cerebellum defined by resting state functional connectivity. *Cereb. Cortex* 20, 953–965. doi: 10.1093/cercor/bhp157

Power, J. D., Barnes, K. A., Snyder, A. Z., Schlaggar, B. L., and Petersen, S. E. (2012). Spurious but systematic correlations in functional connectivity MRI networks arise from subject motion. *Neuroimage* 59, 2142–2154. doi: 10.1016/j.neuroimage.2011.10.018

Ramnani, N. (2006). The primate cortico-cerebellar system: anatomy and function. *Nat. Rev. Neurosci.* 7, 511–522. doi: 10.1038/nrn1953

Schmahmann, J. D. (2004). Disorders of the cerebellum: ataxia, dysmetria of thought, and the cerebellar cognitive affective syndrome. *J. Neuropsychiatry Clin. Neurosci.* 16, 367–378. doi: 10.1176/jnp.16.3.367

Schmahmann, J. D. (2010). The role of the cerebellum in cognition and emotion: personal reflections since 1982 on the dysmetria of thought hypothesis, and its historical evolution from theory to therapy. *Neuropsychol. Rev.* 20, 236–260. doi: 10.1007/s11065-010-9142-x

Shukla, D. K., Keehn, B.,and Müller, R. A. (2010). Tract-specific analyses of diffusion tensor imaging show widespread white matter compromise in autism spectrum disorder. *J. Child Psychol. Psychiatry* 52, 286–295. doi: 10.1111/j.1469-7610.2010.02342.x

Smith, S. M., Fox, P. T., Miller, K. L., Glahn, D. C., Fox, P. M., Mackay, C. E., et al. (2009). Correspondence of the brain's functional architecture during activation and rest. *Proc. Natl. Acad. Sci. U.S.A.* 106, 13040–13045. doi: 10.1073/pnas.0905267106

Stoodley, C. J., and Schmahmann, J. D. (2009). Functional topography in the human cerebellum: a meta-analysis of neuroimaging studies. *Neuroimage* 44, 489–501. doi: 10.1016/j.neuroimage.2008.08.039

Tzourio-Mazoyer, N., Landeau, B., Papathanassiou, D., Crivello, F., Etard, O., Delcroix, N., et al. (2002). Automated anatomical labeling of activations in SPM using a macroscopic anatomical parcellation of the MNI MRI single-subject brain. *Neuroimage* 15, 273–289. doi: 10.1006/nimg.2001.0978

Verly, M., Verhoeven, J., Zink, I., Mantini, D., Peeters, R., Deprez, S., et al. (2014). Altered functional connectivity of the language network in ASD: role of classical language areas and cerebellum. *Neuroimage Clin.* 4, 374–382. doi: 10.1016/j.nicl.2014.01.008

Webb, S. J., Sparks, B.-F., Friedman, S. D., Shaw, D. W. W., Giedd, J., Dawson, G., et al. (2009). Cerebellar vermal volumes and behavioral correlates in children with autism spectrum disorder. *Psychiatry Res. Neuroimaging* 172, 61–67. doi: 10.1016/j.pscychresns.2008.06.001

Wolff, J. J., Gu, H., Gerig, G., Elison, J. T., Styner, M., Gouttard, S., et al. (2012). Differences in white matter fiber tract development present from 6 to 24 months in infants with autism. *Am. J. Psychiatry* 169, 589–600. doi: 10.1176/appi.ajp.2011.11091447

Conflict of Interest Statement: The authors declare that the research was conducted in the absence of any commercial or financial relationships that could be construed as a potential conflict of interest.

frontiers in Systems Neuroscience

METHODS
published: 07 May 2019
doi: 10.3389/fnsys.2019.00020

DeepBehavior: A Deep Learning Toolbox for Automated Analysis of Animal and Human Behavior Imaging Data

Ahmet Arac[1]*, *Pingping Zhao*[1], *Bruce H. Dobkin*[1], *S. Thomas Carmichael*[1] and *Peyman Golshani*[1,2,3]

[1] Department of Neurology and University of California, Los Angeles, Los Angeles, CA, United States, [2] Semel Institute for Neuroscience and Human Behavior, University of California, Los Angeles, Los Angeles, CA, United States, [3] West Los Angeles Veterans Affairs Medical Center, Los Angeles, Los Angeles, CA, United States

Detailed behavioral analysis is key to understanding the brain-behavior relationship. Here, we present deep learning-based methods for analysis of behavior imaging data in mice and humans. Specifically, we use three different convolutional neural network architectures and five different behavior tasks in mice and humans and provide detailed instructions for rapid implementation of these methods for the neuroscience community. We provide examples of three dimensional (3D) kinematic analysis in the food pellet reaching task in mice, three-chamber test in mice, social interaction test in freely moving mice with simultaneous miniscope calcium imaging, and 3D kinematic analysis of two upper extremity movements in humans (reaching and alternating pronation/supination). We demonstrate that the transfer learning approach accelerates the training of the network when using images from these types of behavior video recordings. We also provide code for post-processing of the data after initial analysis with deep learning. Our methods expand the repertoire of available tools using deep learning for behavior analysis by providing detailed instructions on implementation, applications in several behavior tests, and post-processing methods and annotated code for detailed behavior analysis. Moreover, our methods in human motor behavior can be used in the clinic to assess motor function during recovery after an injury such as stroke.

Keywords: behavior analysis, deep learning, motor behavior, social behavior, human kinematics

OPEN ACCESS

Edited by:
Jonathan B. Fritz, University of Maryland, College Park, United States

Reviewed by:
Raúl G. Paredes, National Autonomous University of Mexico, Mexico
Vijay Mohan K. Namboodiri, University of North Carolina at Chapel Hill, United States

***Correspondence:**
Ahmet Arac
aarac@mednet.ucla.edu

Received: *07 January 2019*
Accepted: *18 April 2019*
Published: *07 May 2019*

Citation:
Arac A, Zhao P, Dobkin BH, Carmichael ST and Golshani P (2019) DeepBehavior: A Deep Learning Toolbox for Automated Analysis of Animal and Human Behavior Imaging Data. Front. Syst. Neurosci. 13:20. doi: 10.3389/fnsys.2019.00020

INTRODUCTION

A major goal in neuroscience research is to understand the relationship between neural function and behavior (National Institute of Health BRAIN 2025: A Scientific Vision, 2014). In order to understand this relationship, a vast array of exciting technologies have been developed over the years to characterize the structure and record the activity of neuronal populations (Real et al., 2017), as well as to modulate neuronal activity at cellular resolution and millisecond timescale (Deisseroth, 2015). In contrast, the development of behavioral analysis has lagged, with indirect measurements and a reductionist approach (Krakauer et al., 2017). This is, in part, due to a lack of tools to do automated and detailed analysis of behavior.

Observation and description of natural animal behavior has been fundamental to ethology (Tinbergen, 1963). Although modern high-speed video can record the natural behavior of animals

in exquisite detail, analysis of these recordings can be extremely difficult. The blinded observation and description of the video-recordings can take much longer than the time needed to record them, and these observations are highly subjective. Thus, tools that automate the analysis of these videos are needed for faster and more objective description of the video recordings. Several methods have been developed for this purpose: For example, classical machine vision techniques combined with depth imaging can identify patterns of behavior (Wiltschko et al., 2015). However, this requires special depth cameras and is not generalizable to all types of images. Other studies have used machine vision techniques with unsupervised data analysis (Vogelstein et al., 2014; Robie et al., 2017). While unsupervised analysis is very promising to identify patterns inherent to the data, it is not easy to apply the classical machine vision techniques to different behavior/experimental settings. While the commercial systems can provide off-the-shelf solutions for some behavioral tests, they are not open-source, thus limiting any type of modification, and their application to other behavioral tests. Automated tools that can easily be implemented and generalized to many different behavior tests are needed.

Advances in the deep learning field present opportunities for the automated analysis of images (LeCun et al., 2015). More specifically, convolutional neural networks (CNN), a class of deep neural networks, are most commonly used for image analysis. They are made up of nodes ("neurons") with learnable/trainable weights and biases, and the architecture is comprised of width, height (similar to images) and depth (a third dimension of activation volume) (Lecun et al., 1998). There have been recent advances in the field with several different CNN architectures (Krizhevsky et al., 2012; He et al., 2015; Szegedy et al., 2015) resulting in faster and more accurate outcomes.

Recently, deep learning applications have been used in behavior imaging data analysis (Stern et al., 2015; Mathis et al., 2018; Pereira et al., 2018). The first one of these studies created their own network architecture (Stern et al., 2015) which can limit the implementation of the technique and its broad use. The other two approaches (Mathis et al., 2018; Pereira et al., 2018) showed successful implementation of the CNNs to behavior imaging data analysis, both of them focusing on body pose estimation in animals. One of these used transfer learning approach on only one network architecture (Mathis et al., 2018), whereas the other one trained the network from scratch and achieved similarly good results (Pereira et al., 2018). These two approaches focused on animal pose estimation. While this provides useful information for behaviors where the pose detection of individual body parts is important, it cannot perform direct object recognition (for example distinguishing an apple vs. an orange). Specifically, it cannot distinguish two mice in different positions (vertical vs. horizontal) or identify a mouse performing a specific behavior (such as grooming). Therefore, these networks would detect body positions but not recognize that position/behavior directly. In order to identify these specific behaviors or body positions, these algorithms would require inferences based on the pose coordinates of body parts. Moreover, both studies used only one neural network architecture, thus limiting the user from trying and comparing different network architectures. Additionally, they did not provide post-processing methods for 3D kinematic analysis.

Similarly, motor behavior analysis in humans has also lagged. Currently, the most commonly used clinical motor function assessment tests are based on subjective scoring of the outcome (whether a task is completed fully, partially or not at all). These types of clinical motor impairment scores (i.e., Fugl-Meyer, Action Research Arm Test) are based on ordinal scales, and are insensitive to detect the meaningful changes in the motor function. Moreover, this is important because this type of simple and inexact motor impairment scores or, even worse, disability scores (modified Rankin Score) are not adequate (Bernhardt et al., 2017), and may not accurately reflect true recovery (Kitago et al., 2013). It is important to distinguish between the compensatory movements and true recovery, which can best be done via kinematic analysis (Cirstea and Levin, 2000; Kitago et al., 2013; Krakauer and Carmichael, 2017). Kinematic analysis reveals the timing and typicality of movements, and allows compensatory actions to be distinguished from true recovery of function (Krakauer and Carmichael, 2017). Moreover, it also provides objective metrics that have the potential to capture the movement quality. However, performing kinematic analysis on human motor behaviors can be challenging. Various sensors, reflective markers, external devices, or robotics have been used to perform kinematic analyses (Krebs et al., 2014). The complexity and cost of these devices greatly limits their generalized use. Moreover, using external devices may also alter the natural behavior itself. Thus, marker-less, automated analysis methods are needed for clinical assessment of motor function.

Here, we present a deep learning toolbox and post-processing methods. We name this toolbox DeepBehavior. We expand the deep learning applications for animal behavior imaging analysis by using two different CNN architectures in three different rodent behaviors (food pellet reaching task and two social behaviors). We demonstrate three dimensional (3D), marker-less kinematic analysis of reaching movement in mice. We provide detailed analysis of social behavior when two mice are interacting with post-processing methods. We show evidence that transfer learning approach accelerates training of the network with these types of images. Furthermore, we also demonstrate how CNNs can be used in clinical settings to assess motor function to perform 3D kinematic analysis of motor function in humans.

MATERIALS AND METHODS

Animals

All animal procedures were approved by the University of California, Los Angeles, Department of Laboratory Animal Medicine Institutional Animal Care and Use Committee, and were in accordance with the AAALAC and NIH guidelines. The animals used in this study were either GAD2CrexAi9 or C57Bl6/J mice, and both male and female mice were included. The age range of mice was 10–16 weeks-old.

Human Subjects

A 35-year-old, healthy adult was recorded. A written informed consent was obtained prior to the recording in accordance

with the Declaration of Helsinki. The consent included the use of video recordings for research, education, publication and public presentation.

Skilled Food Pellet Reaching Test

We have developed an apparatus for head-fixed mice to perform a reaching task for a food pellet. This apparatus is 3D printed (Shapeways, New York, NY) and has an arm that controls a platform with scotch and yoke mechanism. The arm is controlled by a small servo motor (Sparkfun, Niwok, CO). This is connected to a plexiglass cylindrical food pellet dispenser that is controlled by a stepper motor (Sparkfun, Niwok, CO). This releases one food pellet at a time. The apparatus automatically detects the pellet removal with an infrared light sensor, and provides a new pellet in the same exact position. During this time, the animal's paw is video recorded at 124 frames per second by two, monochrome, USB3.0, CMOS cameras (ThorLabs, Newton, NJ) at 448x460 pixel image size. The videos were recorded by using StreamPix software (Norpix, Montreal, QC, Canada) and were saved as ".seq" files. Then, a custom-written Python script was used to generate ".png" images and ".avi" video files from the ".seq" files. The servo and stepper motors and the infrared sensors are all controlled by an Arduino circuit board with a custom designed PCB shield. The cameras were triggered by a function generator (Siglent Technologies, Solon, OH). The animals were trained in this setup for 2 weeks until they were reaching for the food pellets on their own repetitively.

Three-Chamber Test for Sociability

We have custom built a plexiglass box (60 × 45 × 45 cm) with three chambers divided by plexiglass walls with spaces (45 × 19 × 45 cm) on them to allow exploration. Each side chamber has an upside down wired cup with one of them empty and the other one with a stranger mouse inside. The experimental animal is gently placed in the middle chamber, and is allowed to explore for 10 min. During this time, the whole apparatus is recorded from the top by using a Logitech web camera at 30 frames per second. In some recordings, the mouse wears a miniaturized fluorescence microscope on the head for simultaneous calcium imaging recordings. We calculate the time exploring each cup and their percentages of total time.

Social Interaction in Home Cage Test

For this test, two mice (one with a miniaturized microscope) were placed in a custom made, 45 × 45 cm plexiglass chamber, and their interaction was recorded from top view by using a monochrome, USB3, BlackflyS camera (Flir, Richmond, BC, Canada) at 30 frames per second.

Human Motor Behavior Recording System

We have built a stereo camera system with two high speed (170 Hz) color CMOS cameras (Flir, Richmond, BC, Canada). The cameras were fixed (62 inches apart from each other) on a foldable optical aluminum rail (McMaster-Carr) so that their positions and angles were fixed relative to each other. The orientation of cameras was almost orthogonal to each other. The cameras were connected to each other with a general I/O cable to provide synchronization between the cameras, and to a laptop computer with 32GB RAM for data acquisition. SpinView software (Flir, Richmond, BC, Canada) was used to acquire the videos. The aluminum rail that the cameras were fixed on was then placed on a tripod. The videos were recorded at 1,280 × 1,024 pixels resolution and at 170 frames per second. For reaching test, the subject sat on a chair and while sitting straight up reached for a ball hanging from the ceiling. For supination/pronation task, the subject sat on a chair and alternately rotated both hands.

Converting Videos to Single Frame Images

The Streampix software saves the images in ".seq" format (reaching task). Using Python PIMS (Phyton image sequence) package, and a custom Python script, we convert these video files to folders of images in ".png" format. We then make ".avi" format video by using ffmpeg. To process the ".avi" videos (social behavior), we use ffmpeg.

Creating Training and Test Datasets

In order to train the neural networks, we used custom written Python scripts to obtain bounding box coordinates for the paw positions. This script creates ".json" files that include x1, x2, y1, and y2 coordinates of the bounding boxes for each image in a folder. A different set of images were also labeled using the same script but then used as a test dataset. These ".json" files and the folders of corresponding raw images are then used as the training and test datasets for the GoogLeNet network (Stewart et al., 2016). This network model was written in Python and Tensorflow (Google) framework. We determined the size of the training dataset as described in the Results section. Because there is only one bounding box to be labeled, the labeling process is rather fast (we were able to label 100 images in ∼20 min). For the two-mouse interaction assay, we use a different custom script to label the images because the format this network uses is different. It requires labeling the position, as well as the size, of the bounding box relative to the size of the image in both x and y directions. Another difference is that we can label up to 80 classes (in our case, it was 8: for each mouse body, nose, head, and tail).

Human Pose Detection

We used OpenPose neural network architecture to detect the human poses in the videos (Cao et al., 2017). This network uses a non-parametric representation, which is referred to as Part Affinity Fields (PAFs), to learn to associate body parts with individuals in the image. This network model is implemented in C++ and Caffe. We then use a 10 × 7 checkerboard with 115 × 115 mm square sizes to calibrate the cameras. The camera calibration and 3D pose calculations were all done in MATLAB (Mathworks, Natick, MA).

Training the Neural Networks

We trained the networks, assessed their performance and used them for new image analysis on a computer with a TITAN X Pascal and Quadro P6000 graphics processor units (NVIDIA). The operating system was Ubuntu 16.0 with LinuxMint 18. CUDA 8.0, CUDNN 5.0 and Python 2.7 were used. On this computer, with one GPU in use, training the first network

architecture (for food pellet reaching task) takes ∼8 h for 600,000 iterations. Processing new images on the trained network takes ∼ 50 ms per image again with one GPU. Similarly, training YOLO v3 takes ∼12–14 h for 180,000 iterations, and new images are processed on the trained network at 30 frames per second with one GPU. Processing new images on OpenPose occurs at 3–4 Hz with two GPUs.

Code to Obtain Kinematic Data

Both algorithms in mice and humans generates the positions in ".json" files. We process these files in custom written code in MATLAB (Mathworks, Natick, MA) to obtain each joint's position from each camera view. We then combine two camera views to obtain the 3D positions. We used 4 × 6 checkerboard with 4.5 × 4.5 mm square size for mouse paw videos camera calibration. After obtaining the 3D position of joints or paws, we calculate several parameters such as the velocities, trajectories, shoulder and elbow angles as well as the supination angles all with custom written MATLAB codes. All of our code is open-source and available on our GitHub page at www.github.com/aarac/DeepBehavior.

RESULTS

3D Marker-Less Paw Detection During Skilled Reaching Task

Food pellet reaching in rodents is a commonly used motor behavior task to study motor learning and motor recovery (Farr and Whishaw, 2002; Guo et al., 2015). However, even simple motor behaviors such as reaching, when examined in detail, can be very difficult to define and quantify. Traditionally, performance in this task has been measured either by the percentage of the attempts in which the mouse is able to grab and eat the pellet (success rate), or with subjective scoring of each step of movement by a blinded observer (Farr and Whishaw, 2002). We have modified this task to include an apparatus for head-fixed mice to allow for future simultaneous imaging and electrophysiological recordings of the brain (**Figure 1A**). In this setup, the mouse is head-fixed and performs a reaching task for a food pellet. During this time, the food pellet is delivered by an automated food pellet delivery system after detection of the pellet removal (**Supplementary Figure 1**). During performance of the task, the animal's paw movements are video-recorded with high-speed cameras from two angles (**Supplementary Figure 1**). The cameras are triggered by a function generator to enable inter-camera synchronization. In order to detect the paw position in these video frames, we used a CNN model with an architecture of GoogLeNet (Szegedy et al., 2015, 2016) followed by an LSTM (long short-term memory) layer in TensorFlow (Stewart et al., 2016). This network model detects several outputs based on a set threshold value for LSTM (**Supplementary Figures 2A–C**). We trained this network with manually labeled images as described below. We obtained the initial weights of the GoogLeNet after training it first with ImageNet dataset. In order to manually label the images, we used a custom Python script which enabled placement of a bounding box around the paw and registered the coordinates of that bounding box in a separate text document. The input for this algorithm is the raw video frames, and the output is the coordinates of a bounding box around the right paw (**Figures 1B,C**; **Video 1**). The algorithm also provides a confidence score for each detection that can be useful for post-processing. Of note, we trained only one network with images from both front view and side view cameras. This network can detect the right paw position in both types of images.

In order to obtain 3D positions of the paw movements, we first calibrated the cameras with 24 checkerboard images (**Supplementary Figures 3A,B**), using a camera calibration toolbox in MATLAB (Bouguet, 2015). This toolbox creates a 3D cartesian coordinate system (**Supplementary Figure 3C**), which then provides the 3D position of a point when 2D positions of that point is given from the two camera views. By using this, we combined the 2D positions of paws detected by the neural network, and obtained the 3D trajectories of paw movements (**Figure 1D**; **Video 2**). After obtaining 3D coordinates, the kinematic data such as the distance traveled, time spent during the movement, maximum and average velocities can be calculated from these data (**Figure 1E**).

Social Behavior Analysis in the Three-Chamber Social Interaction Test

Similar to the paw detection method, we show that the same network can be used to analyze the three-chamber social interaction test. In this test, there are three chambers that the mouse can freely explore. In one chamber there is an empty wired cup, in another chamber a wired cup with a stranger mouse inside, and the third chamber is empty (**Figure 1F**). The mouse can freely move and explore all three chambers. The traditional analysis measures the times spent exploring/interacting with the wired cups, as the normal mice spend more time with the cup that has the stranger mouse. In order to perform this type of analysis automatically, we detect and track the head of the mouse throughout its exploration of the chambers using the same network architecture and methods as described above. We also detect the position of the chambers and when the head of the mouse is close enough to the chambers, we count it as interaction (**Figure 1G**; **Video 3**). With this type of analysis, we can measure the interaction times with either cup automatically. Moreover, the analysis also provides the position of the animal at any given time (**Figure 1H**). This allows calculation of whether the mouse is moving from one chamber to another, the precise timing of interactions, interaction counts, and the mouse's velocity as it explores the chambers.

Transfer Learning Results in Faster and More Reliable Training

Large datasets are required for training CNNs to obtain accurate results that generalize well. However, to create custom applications, one needs to create manually labeled training datasets from custom images. This can be challenging as labeling tens to hundreds of thousands of images manually is time-consuming and cumbersome, and defeats the purpose of creating an automated tool that should be easily modifiable. In order to overcome this, the transfer learning approach has been

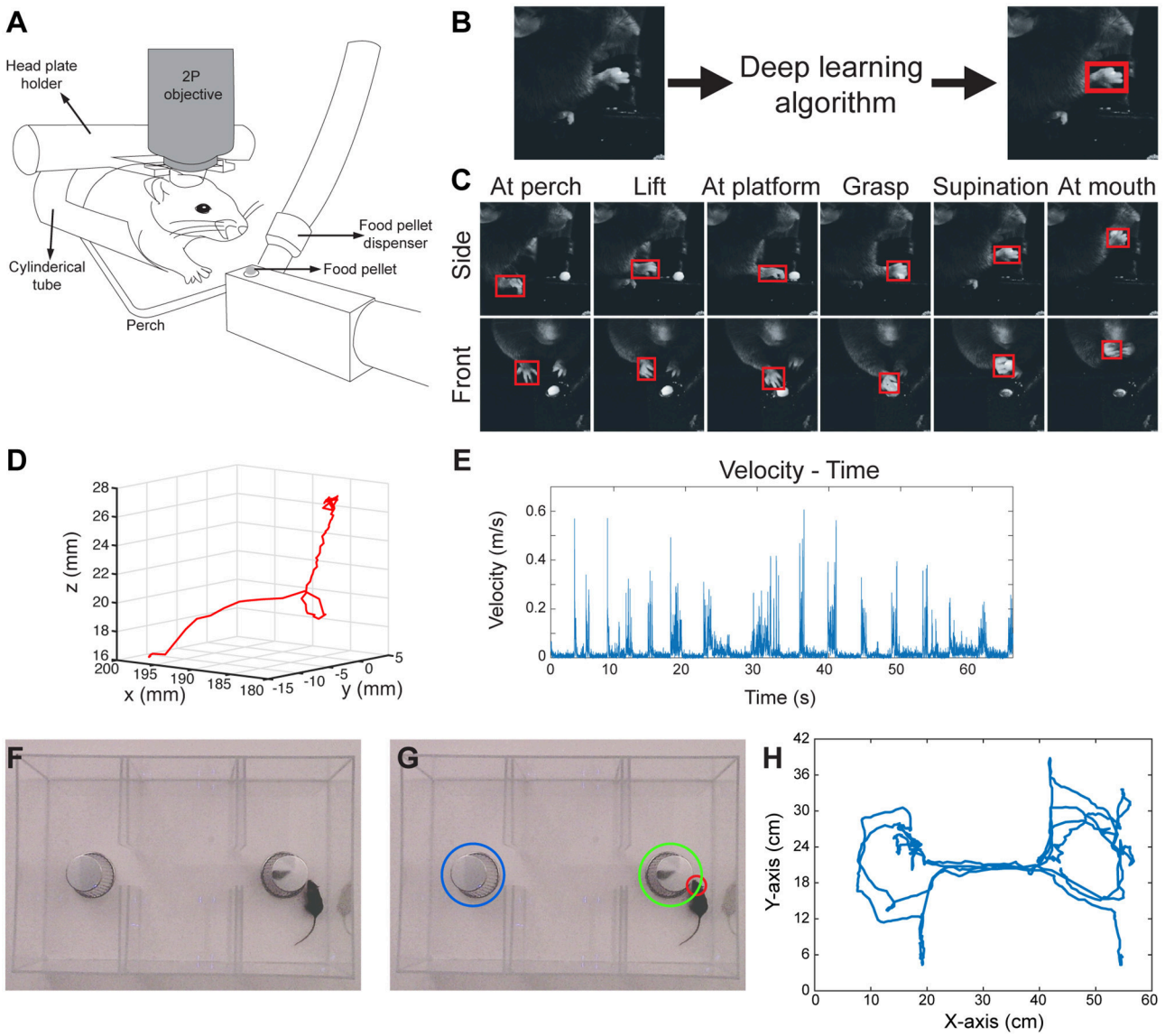

FIGURE 1 | 3D paw kinematics and three-chamber social behavior analysis in mice. **(A)** Schematic of skilled food pellet reaching task in head-fixed mice. This setup allows simultaneous two-photon (2P) calcium imaging or electrophysiological recordings. **(B)** An example of the data processing with feeding of raw video frames to the deep learning algorithm to obtain the coordinates of a bounding box around the paw. **(C)** Representative images showing detected paws from two camera views when the paw is in different positions. **(D)** 3D trajectory of a single reaching attempt obtained from 2D coordinates of paw positions in two camera views. **(E)** Kinematic parameters such as velocity-time graphs can be obtained from the 3D trajectories. **(F)** Raw video-frame of three-chamber test. **(G)** Representative analysis showing detection of the head of the mouse (red circle), and the cup with a stranger mouse in (green circle), and without a mouse (blue circle). **(H)** Trajectory of the mouse seen in Video-3.

proposed. In this approach, the network model is first trained with another larger dataset such as ImageNet (with 1.2 million images in one thousand classes) with random initialization of the weights, followed by re-training with a smaller dataset with custom images. This method improves performance significantly (Mahajan et al., 2018). However, behavioral video recordings contain images with less variability given that they are recorded under one condition (compared to the high variability of the larger datasets such as ImageNet). Thus, the network may overfit the model when trained with random initialization. This, however, may not matter to the experimenter as it will be used to analyze only the same type of images. In fact, one (Mathis et al., 2018) of the two deep learning methods for behavior analysis in the literature uses transfer learning whereas the other (Pereira et al., 2018) does not. Thus, it is not clear whether transfer learning is really necessary to obtain good results in these types of experiments. To test whether the transfer learning approach is better with images of behavioral videos, we trained two networks with the same architecture. One of them was trained with random initialization of weights using Xavier initialization, and the other

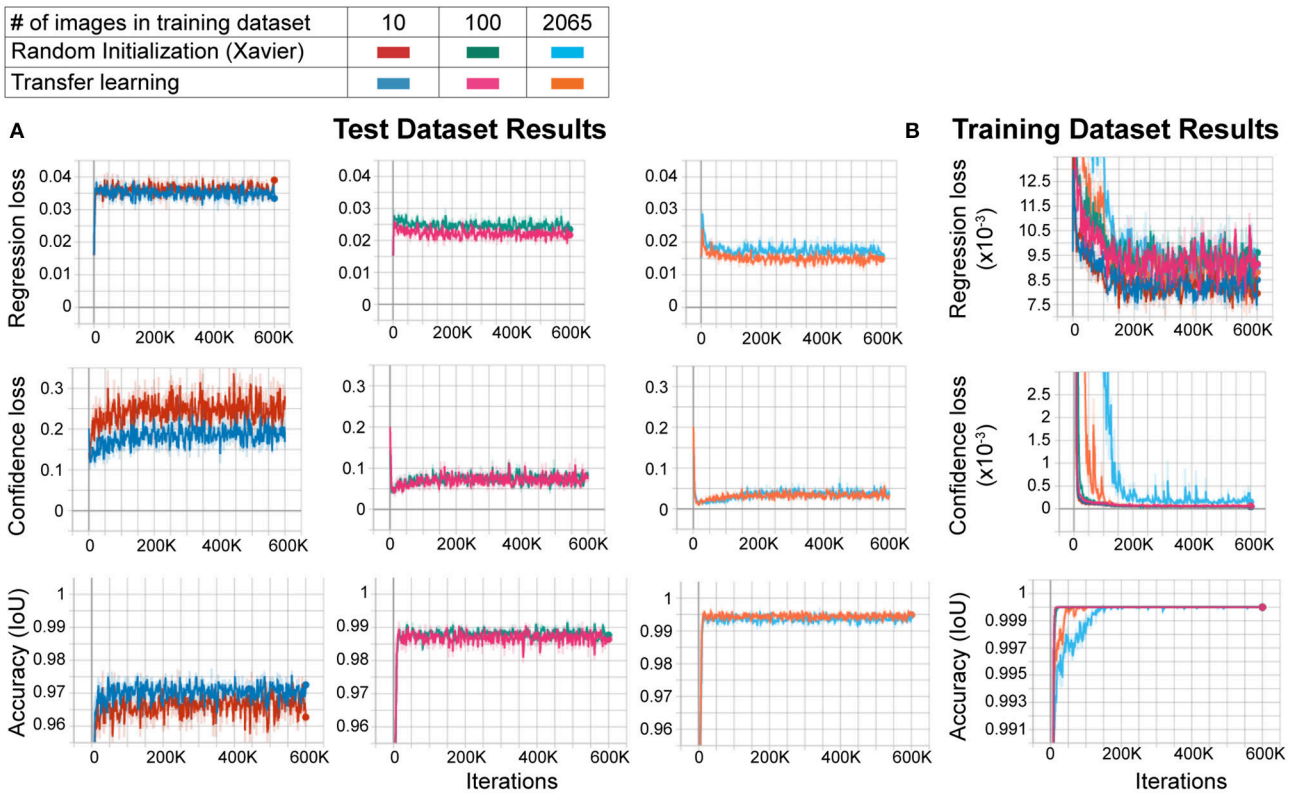

FIGURE 2 | Transfer learning results in faster and more reliable training. **(A)** Training results of the test dataset. As the training dataset size increases from 10 images to 2,065 images, the regression and confidence losses decrease, and the accuracy (IoU: intersection over union) increases. For each training dataset size, transfer learning results in more accurate training compared to random initialization (low regression and confidence losses, and high accuracy). **(B)** Training results of the training dataset. Note that the transfer learning training curves in the 2,065 training dataset size group converge faster and stay stable throughout the training, meaning more reliable training.

with the transfer learning approach. We used different sizes of training datasets (10, 100, and 2065 images) and the same test dataset (230 images) for each training. We found that the transfer learning approach resulted in greater accuracy (lower regression and confidence losses, and higher accuracy) with each training dataset size (**Figure 2A**). Moreover, as expected, increasing training dataset size improved the accuracy while decreasing confidence and regression loss (**Figure 2A**). As the training dataset size increased, this difference between transfer learning and random initialization decreased. However, transfer learning resulted in faster and more reliable training as evidenced by faster convergence and more stability on confidence loss and accuracy of the training dataset (**Figure 2B**). These results show that even with these types of behavior images with less variability, the transfer learning approach is better than training a naïve network (random initialization of weights).

Our overall workflow is shown in **Figure 3**. After acquisition of behavior videos, we split them into individual frames. Next, we choose images semi-randomly based on the different positions of the mice or paws depending on the content of the videos. We then label them manually using custom scripts, and train the network that is already pre-trained with ImageNet dataset. For the above network, we recommend starting with 200–300 manually labeled images. We train the network and then test the performance on a new video. This will show what kind of errors the network makes (such as misdetection, multiple detections, etc.). We then choose some of these images where the network had a difficulty in obtaining good results, manually label them, and add them into the training dataset and retrain the network. After a few iterations, the network becomes more generalizable within that image category.

Analysis of Social Interaction of Two Mice

Similar to the above example, the same approach can be expanded to the use of other network architectures. As an example, in social interaction assay, a stranger mouse is placed in a 45 × 45 cm chamber with another mouse which has a miniaturized microscope (Cai et al., 2016) (miniscope) attached to its head (**Figure 4A**). Their interaction is recorded from the top (bird's eye view). The interaction time between them is then recorded. This behavior assay can be powerful especially when combined with imaging of different brain regions during social behavior by using miniscopes (Cai et al., 2016). The mice can interact by sniffing nose-to-nose, nose-to-body, nose-to-tail. One difficulty in the literature has been the detection and tracking of these two mice throughout the recording. To analyze these

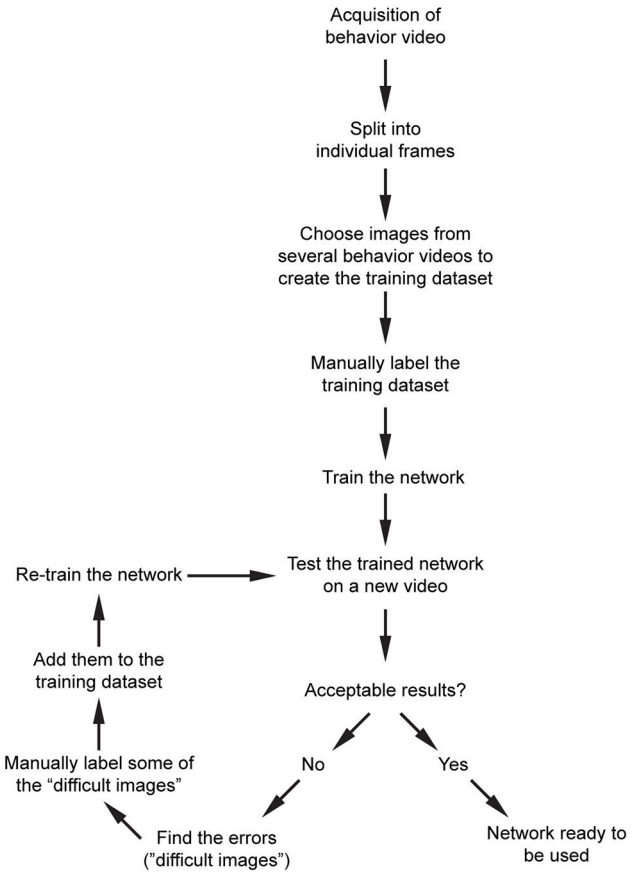

FIGURE 3 | Proposed workflow for processing of the raw behavior video and training the network. After pre-processing of the videos, and initial training of the network, an iterative training algorithm allows selection of images with high variability, resulting in more generalizable training for that dataset. After the images are processed, they can be used for post-processing.

videos, when the training dataset is created, we manually label images of the mouse without miniscope and with miniscope separately. We detect their nose, head, body, and tail (**Figure 4B**; **Video 4**). We use YOLO version-3 (Redmon and Farhadi, 2018) as the CNN architecture (**Supplementary Table**). This network is pre-trained with COCO dataset. After detecting the mice throughout the video, we do post-processing in MATLAB. We first separate each mouse and obtain their movement trajectories throughout the recording session (**Figure 4C**). We then measure the distance between their body centers, and the distance below a certain threshold is accepted as a close contact (**Figure 4D**). With this, we can obtain exactly when they are in close contact, the duration of contact, and their velocities throughout the recording session (**Figure 4E**). We then go into each "close contact" epoch and calculate the distances between each animal's nose and tail and the other animal's nose or tail. Interestingly, this gives unique interaction patterns. For example, in one close contact, mouse-A approaches mouse-B from behind (nose-to-tail interaction), but then mouse-B responds to this and turns around, and the interaction becomes nose-to-nose (**Figure 4F**; **Video 5**). In another example, the interaction is only a short nose-to-nose sniffing (**Figure 4G**; **Video 6**).

3D Human Pose Detection for Clinical Motor Function Assessment

Similar to rodent behavior analysis, the clinical motor function assessment in humans currently relies on subjective scoring of movements with ordinal scales. Performing detailed kinematic analysis in a clinical setting is challenging, and the best available techniques use robotics, exo-skeletons, sensors or externally attached markers. However, these external devices may affect the nature of the behavior. To overcome these problems, we have developed a two-camera stereo video recording system. With this system, we record the movement of the subjects at 170 frames per second, and importantly, the subjects do not need to put on any markers, or wear any sensors or special equipment. We then use a CNN (OpenPose) that was trained to detect the joint poses in humans (Wei et al., 2016; Cao et al., 2017; Simon et al., 2017) from two camera views (**Figure 5A**). After this, we calibrate the cameras and reconstruct the 3D models (including the individual finger joints) (**Figure 5B**; **Video 7**). As an example, we recorded a subject performing reaching movement toward a hanging ball, and then plotted the wrist movement trajectories for 10 reaches (**Figure 5C**), and calculated several kinematic parameters such as elbow and wrist velocities (**Figures 5D,E**). Moreover, after using dynamic time alignment kernels (Santarcangelo and Xiao, 2015) we can calculate the Euclidean distance between these kernels and cluster them (**Figure 5F**). This method identifies the similar reaches based on their trajectories in an unsupervised manner. Furthermore, from the 3D positions of joints, we can calculate the shoulder vs. body and elbow angles (**Figures 5G,H**).

In order to analyze forearm/hand movements, we recorded the subject during an alternating supination/pronation task (**Figure 6A**). We can reconstruct the 3D model of the hands with individual finger joints (**Figures 6B,C** and **Video 8**). With this task, we can calculate the supination angles (rotation angle along the forearm axis) from the 3D models (**Figure 6D**). We then use dynamic time warping to align these supination angle curves and calculate the Euclidean distance between them. By using hierarchical clustering on these calculated Euclidean distances, we can identify similar movement patterns (**Figure 6E**). This analysis robustly clustered the right and left hand movements as well as the different movement patterns for each hand in a healthy subject (**Figure 6E**).

DISCUSSION

Here, we present easy-to-use methodology on how to use CNNs for behavior imaging data analysis in mice and humans. Specifically, we use three different neural network architectures and five different behavior tasks. We present methods and share tips on how to train neural networks to achieve good accuracy, and provide methods for post-processing of the data. This approach can be applied to most, if not all, of the available CNN architectures.

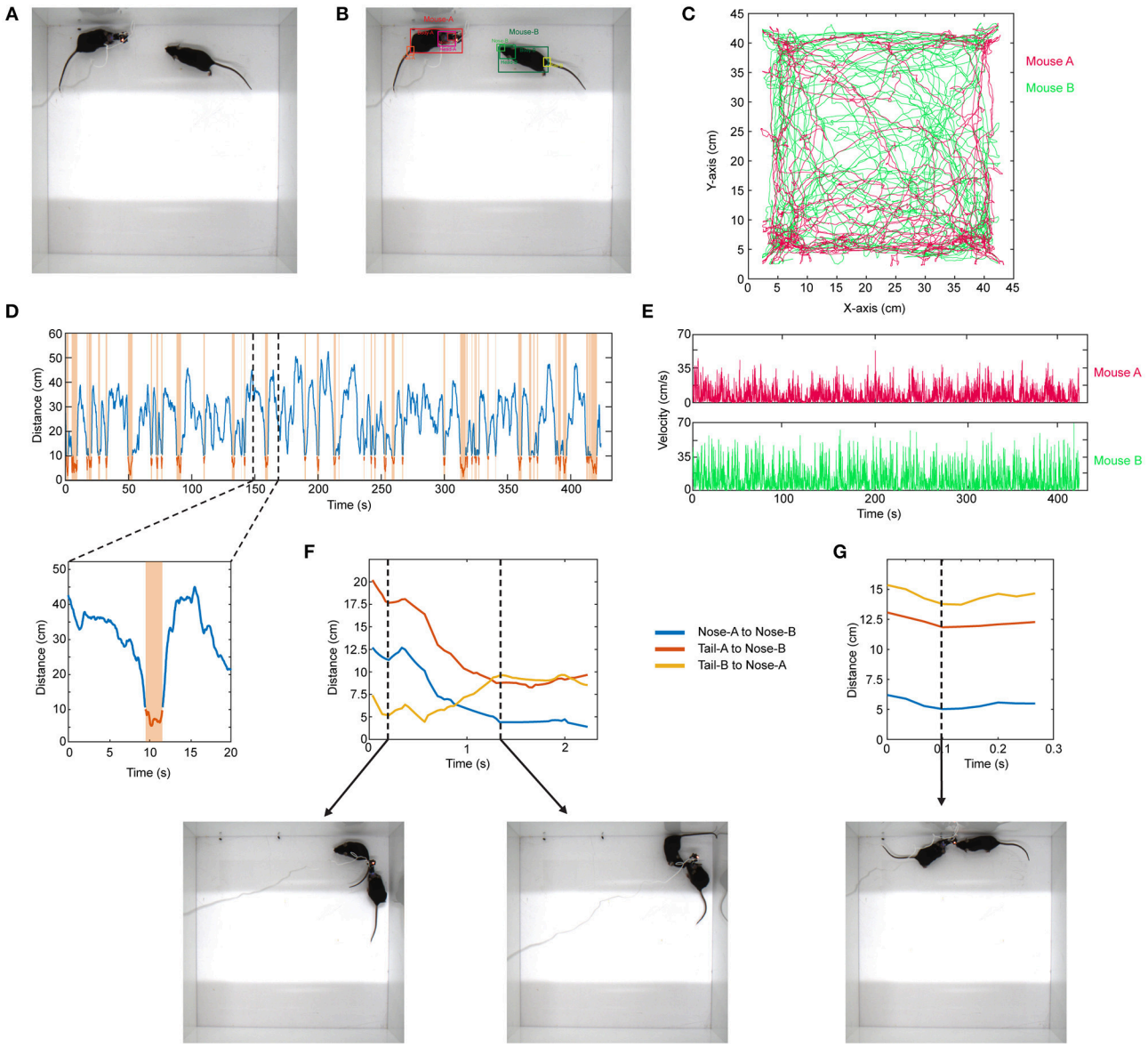

FIGURE 4 | Detection of two mice separately during social interaction and post-processing of data. **(A)** Representative raw video frame when two mice are interacting in a 45 × 45 cm chamber. Of note, one of the mice has a miniscope installed on the head to do calcium imaging of neuronal activity. **(B)** Detection of two mice separately (as mouse **A** and mouse **B**) by using YOLO v3 CNN. **(C)** Trajectories of body positions of these two mice in one session of interaction (~7 min). **(D)** The distance between two mice over time during the interaction session. The time periods when two mice are critically close to each other to allow any kind of interaction are marked and highlighted by orange color. A higher magnification of one of these close contacts is shown in the lower panel. **(E)** The velocity vs. time graphs can be obtained for each mouse throughout their interaction. **(F)** A representative distance time graph over one of the close contacts. The distances are between noses, or nose and tails of two mice. In panel **(F)**, the close contact starts as mouse B sniffing mouse A's rear (shorter distance between tail-B to nose-A) but then turns into a nose-to-nose interaction. **(G)** A representative distance time graph over one of the close contacts showing a short nose-to-nose interaction between two mice.

The transfer learning approach generally provides very good results requiring minimal number of images that need to be manually labeled for training dataset (Mahajan et al., 2018). Given the low variability of images in the videos obtained in the animal studies compared to larger datasets such as ImageNet, one argument is that overfitting may not cause significant problem given that the test images are all in the same category. However, we show that even with this type of similar image sets with low variability, the transfer learning approach makes the training faster and more reliable. Thus, the transfer learning approach should be considered for these types of analyses. The network models used in this study are chosen for their ease of use, and the same technical approach can be applied to other available network models, or any future network architecture. As the deep learning field grows and generates better and faster network architectures, those new models (or the existing ones) can be used with a similar approach.

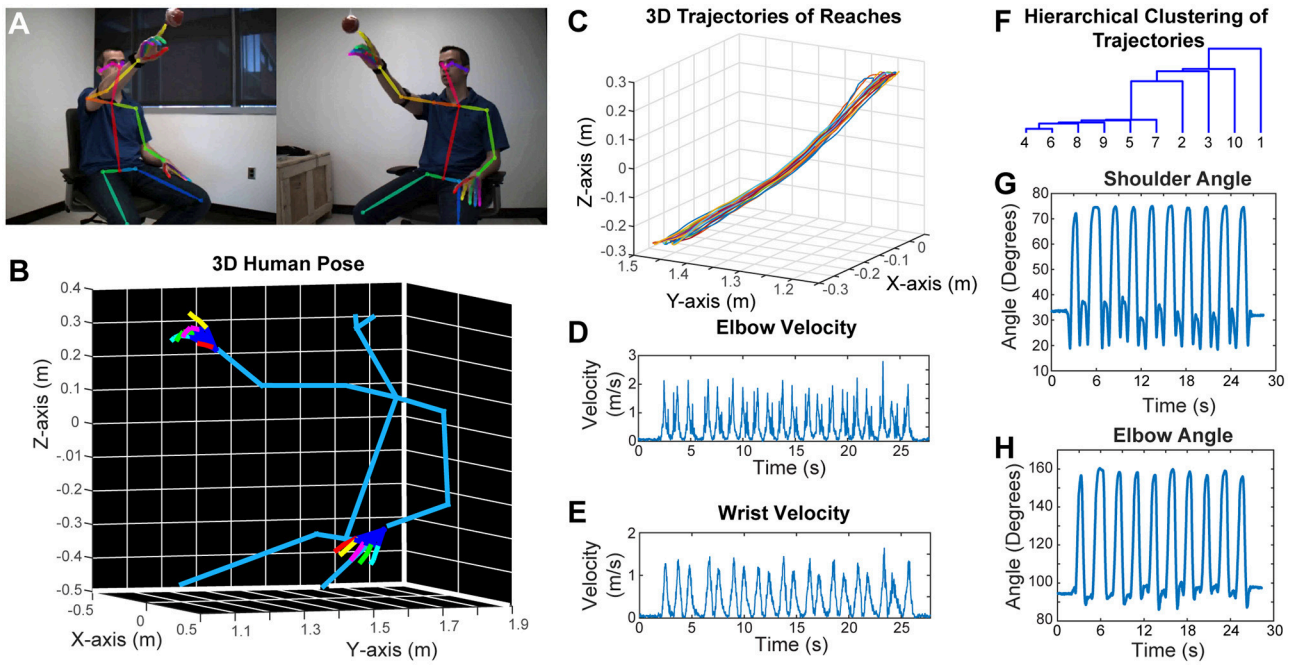

FIGURE 5 | Marker-less detection of human pose with 3D kinematics. **(A)** Representative images from the stereo camera system with two cameras that have different angles, with detection of joint poses on these 2D images. **(B)** 3D model reconstructed after calibration of the two camera views in panel **(A)**, showing accurate detection of joint positions down to individual finger joints. **(C)** 3D trajectories of air reaches of the subject in panel **(A)**, there are 10 reaches with superimposed reach trajectories. Velocity vs. time graphs for right elbow **(D)** and right wrist **(E)** during these 10 reaches. **(F)** Hierarchical clustering of these 10 reaches based on the dynamic time aligned kernels of the 3D trajectories. The numbers indicate the reach number. **(G)** Shoulder vs. body angles during these 10 reaches obtained from the 3D positions. H. Elbow (arm vs. forearm) angles during the 10 reaches. All the kinematic parameters **(D,E,G,H)** were obtained from the 3D model (as seen in panel **B**).

The traditional analysis for the food pellet reaching task in rodents evaluates whether the animal can successfully grab the food pellet over a number of reach attempts (success rate). A more sophisticated method (Farr and Whishaw, 2002) breaks down this movement into different stages, and gives subjective scores based on how close they are to a predefined normal movement. However, this type of scoring system is subjective and is dependent on an evaluator watching the videos in slow motion (almost frame by frame), thus requiring significant amount of time to analyze. To overcome this, a reflective marker that is glued on the paw can be tracked (Azim et al., 2014). However, this method fails when the marker is occluded. Alternatively, traditional computer vision classifier algorithms can be used for marker-less detection of paw (Guo et al., 2015). However, these algorithms need to be trained for each video.

Deep learning applications for behavioral analysis have recently been developed (Mathis et al., 2018; Pereira et al., 2018). One (Mathis et al., 2018) of these applications uses the transfer learning approach whereas the other one does not (Pereira et al., 2018). However, these require separate training for each camera view and lack the post-processing code for kinematic analysis. While these methods are very useful, we are expanding the behavior analysis tools available for the neuroscience community.

We extend the use of same methodology into different social behavior tasks. In the three-chamber test, the traditional analysis approach has been manual measurement of interaction times with the cups (Moy et al., 2004). By using the same network architecture that we used for paw detection, we first detect the head of the mouse, and track it as the mouse explores all three chambers. This type of analysis provides more relevant information than just the interaction times, it also lowers the time spent for analysis significantly.

In the other social behavior test of two mice interacting, the traditional analysis was based on just the interaction of two mice (Kim et al., 2015). However, this analysis is very limited. Using the same transfer learning approach, but this time a different network architecture, we can automatically track two mice, one of them wearing a miniaturized microscope. Because the algorithm recognizes these mice separately (one with the miniaturized microscope, the other without), we can distinguish them even after a very close contact. The analysis also provides whether the mice are moving, and if so, their velocities, the interaction type (nose-to-nose vs. nose-to-tail sniffing), the time that they start approaching to each other, etc. This type of detailed analysis is important in identifying the details of the social interaction.

Clinical motor impairment scores (i.e., Fugl-Meyer, Action Research Arm Test) are insensitive to detect the meaningful changes in the motor function. Moreover, they may not even reflect accurate motor behavior. When tested after constraint-induced movement therapy for stroke victims, although these measurement scales showed benefit, the kinematics of how patients performed these movements didn't change,

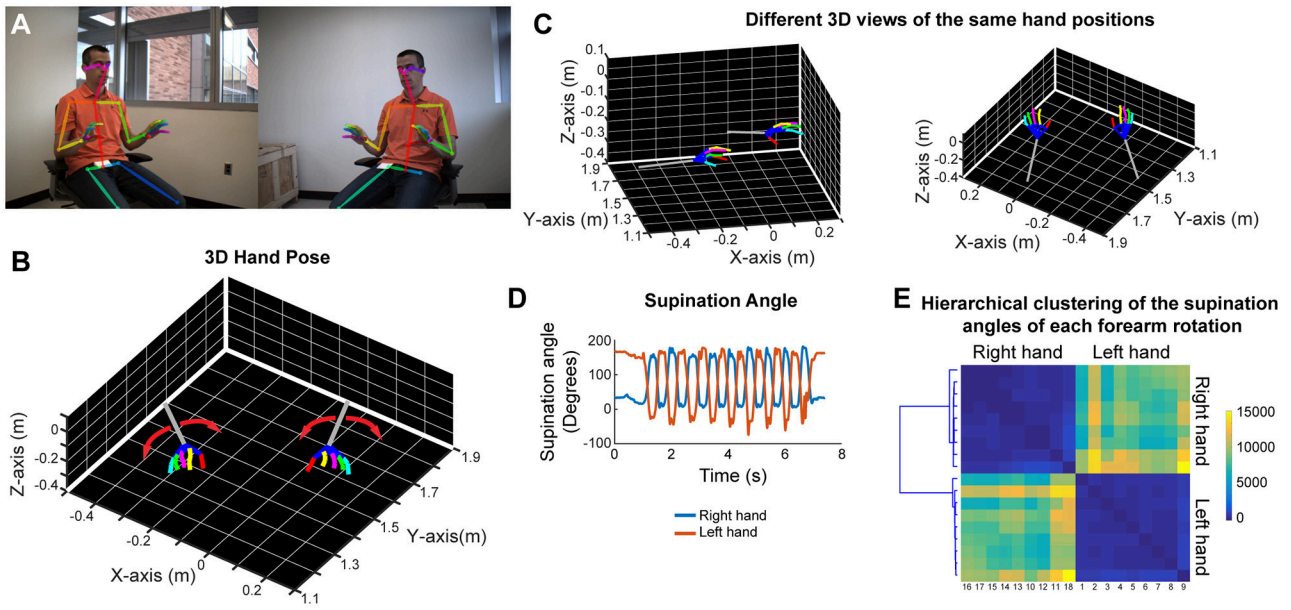

FIGURE 6 | Marker-less detection of fine hand/finger movements in 3D. **(A)** Representative images from the stereo camera system, focusing more on the hand movements, with detection of the joint poses in 2D images. **(B)** Representative 3D models of both hands and forearms while the subject is doing alternating supination/pronation movements. **(C)** 3D views from different angles of the same hand positions as in panels **(A,B)**. **(D)** Supination angles (rotation angles of the forearm) of both right and left hands during nine repetitive movements. **(E)** Hierarchical clustering based on the Euclidean distance between the supination angle curves of each rotation (supination and pronation) after these curves were aligned by dynamic time warping. Please note distinct clustering of right and left hand rotations as well as the heterogeneity among rotations within each hand.

suggesting compensatory mechanisms rather than true recovery (Kitago et al., 2013). Kinematic analysis has the potential to provide information on multi-joint coordination and motor control mechanisms (Alt Murphy and Häger, 2015). Here, we demonstrate that by using video recording in a standardized way, more meaningful data with 3D kinematic parameters can easily be collected in clinical settings. The setup of the hardware is also straightforward and very portable, making it feasible to obtain data at bedside. This type of kinematic analysis reduces subjectivity by capturing whole limb movements and replacing ordinal scales with continuous ones. Moreover, this setup can be expanded in simple but meaningful ways, such as adding simultaneous electromyographic recordings in a few key muscles of interest. However, before its clinical use, one needs to perform clinimetric studies such as reliability, validity, measurement error, responsiveness to abnormal motor function, etc., but these are beyond the focus of the current study. Several kinematic metrics such as task completion time, number of movement onsets, path length ratio, number of velocity peaks, joint angles and angular velocities have been proposed to provide objective evaluation of the movement quality (de los Reyes-Guzman et al., 2014). However, more longitudinal studies are required to enable a detailed understanding of recovery patterns after injury such as stroke.

Elucidating the behavior in detail is critical to understanding the brain-behavior relationship (Krakauer et al., 2017). The tools provided here have the potential to define the behavior in more detail, and when combined with other tools to study the brain, will likely help dissect out the brain-behavior relationship. Overall, we show proof of principle of the technique using several neural network architectures and different ways of analyzing several behavior tasks in mice and humans. In the future, with the advances in the deep learning field, faster and more sophisticated methods can likely be used with the same approach.

ETHICS STATEMENT

All animal procedures were approved by the University of California, Los Angeles, Department of Laboratory Animal Medicine Institutional Animal Care and Use Committee, and were in accordance with the AAALAC and NIH guidelines. A written informed consent was obtained from both of them prior to the recording in accordance with the Declaration of Helsinki. The consent included the use of video recordings for research, education, publication and public presentation. The protocol was approved by The UCLA Institutional Review Boards in The UCLA Office of the Human Research Protection Program (OHRPP).

AUTHOR CONTRIBUTIONS

AA and PG conceptualized and designed the study and wrote the manuscript with input from all authors. AA performed all the coding, implementation of the software, performed the video recordings, and analyzed the data. PZ assisted with performing

video recordings, and design of the study. BD and SC helped with the design and provided guidance.

FUNDING

This study was supported by NIH R25NS065723 (SC and AA), NIH K08NS109315 (AA), NVIDIA GPU grant (AA), Dr. Miriam and Sheldon G. Adelson Medical Research Foundation (BD), and the following grants (PG): NIH U01 NS094286, R01MH101198, R01NS090930, R01 MH105427, U54HD87101, R01NS099137, NSF 1700308.

ACKNOWLEDGMENTS

We would like to thank the Golshani lab members for frequent discussions and support. We also thank NVIDIA for generously donating Quadro-P6000 through the GPU grant.

SUPPLEMENTARY MATERIAL

The Supplementary Material for this article can be found online at: https://www.frontiersin.org/articles/10.3389/fnsys.2019.00020/full#supplementary-material

REFERENCES

Alt Murphy, M., and Häger, C. K. (2015). Kinematic analysis of the upper extremity after stroke - how far have we reached and what have we grasped? *Phys. Ther. Rev.* 20, 137–155. doi: 10.1179/1743288X15Y.0000000002

Azim, E., Jiang, J., Alstermark, B., and Jessell, T. M. (2014). Skilled reaching relies on a V2a propriospinal internal copy circuit. *Nature* 508, 357–363. doi: 10.1038/nature13021

Bernhardt, J., Hayward, K. S., Kwakkel, G., Ward, N. S., Wolf, S. L., Borschmann, K., et al. (2017). Agreed definitions and a shared vision for new standards in stroke recovery research: the stroke recovery and rehabilitation roundtable taskforce. *Neurorehabil. Neural. Repair*. 31, 793–799. doi: 10.1177/1545968317732668

Bouguet, J. Y. (2015). *Camera Calibration Toolbox for Matlab: California Institute of Technology*. Available online at: http://www.vision.caltech.edu/bouguetj/calib_doc/

Cai, D. J., Aharoni, D., Shuman, T., Shobe, J., Biane, J., Song, W., et al. (2016). A shared neural ensemble links distinct contextual memories encoded close in time. *Nature* 534, 115–118. doi: 10.1038/nature17955

Cao, Z., Simon, T, Wei, S. E., and Sheikh, Y. (2017). "Realtime multi-person 2D pose estimation using part affinity fields," in *arXiv* 1611.

Cirstea, M. C., and Levin, M. F. (2000). Compensatory strategies for reaching in stroke. *Brain 123 (Pt* 5), 940–953. doi: 10.1093/brain/123.5.940

de los Reyes-Guzman, A., Dimbwadyo-Terrer, I., Trincado-Alonso, F., Monasterio-Huelin, F., Torricelli, D., and Gil-Agudo, A. (2014). Quantitative assessment based on kinematic measures of functional impairments during upper extremity movements: a review. *Clin. Biomech.* 29, 719–727. doi: 10.1016/j.clinbiomech.2014.06.013

Deisseroth, K. (2015). Optogenetics: 10 years of microbial opsins in neuroscience. *Nat. Neurosci.* 18, 1213–1225. doi: 10.1038/nn.4091

Farr, T. D., and Whishaw, I. Q. (2002). Quantitative and qualitative impairments in skilled reaching in the mouse (Mus musculus) after a focal motor cortex stroke. *Stroke* 33, 1869–1875. doi: 10.1161/01.STR.0000020714.48349.4E

Guo, J. Z., Graves, A. R., Guo, W. W., Zheng, J., Lee, A., Rodriguez-Gonzalez, J., et al. (2015). Cortex commands the performance of skilled movement. *Elife* 4:e10774. doi: 10.7554/eLife.10774

He, K., Zhang, X., Ren, S., and Sun, J. (2015). "Deep residual learning for image recognition," in *2016 IEEE Conference on Computer Vision and Pattern Recognition (CVPR)*. doi: 10.1109/CVPR.2016.90

Kim, Y., Venkataraju, K. U., Pradhan, K., Mende, C., Taranda, J., Turaga, S. C., et al. (2015). Mapping social behavior-induced brain activation at cellular resolution in the mouse. *Cell Rep.* 10, 292–305. doi: 10.1016/j.celrep.2014.12.014

Kitago, T., Liang, J., Huang, V. S., Hayes, S., Simon, P., Tenteromano, L., et al. (2013). Improvement after constraint-induced movement therapy: recovery of normal motor control or task-specific compensation? *Neurorehabil. Neural Repair* 27, 99–109. doi: 10.1177/1545968312452631

Krakauer, J. W., and Carmichael, S. T. (2017). *Broken Movement: The Neurobiology of Motor Recovery After Stroke. Cambridge, MA: The MIT Press.*

Krakauer, J. W., Ghazanfar, A. A., Gomez-Marin, A., MacIver, M. A., and Poeppel, D. (2017). Neuroscience needs behavior: correcting a reductionist bias. *Neuron* 93, 480–490. doi: 10.1016/j.neuron.2016.12.041

Krebs, H. I., Krams, M., Agrafiotis, D. K., DiBernardo, A., Chavez, J. C., Littman, G. S., et al. (2014). Robotic measurement of arm movements after stroke establishes biomarkers of motor recovery. *Stroke* 45, 200–204. doi: 10.1161/STROKEAHA.113.002296

Krizhevsky, A., Sutskever, I., and Hinton, G. E. (2012). "ImageNet classification with deep convolutional neural networks," in *Paper Presented at the Proceedings of the 25th International Conference on Neural Information Processing Systems*, Vol 1. (Nevada, CA).

LeCun, Y., Bengio, Y., and Hinton, G. (2015). Deep learning. *Nature* 521, 436–444. doi: 10.1038/nature14539

Lecun, Y., Bottou, L., Bengio, Y., and Haffner, P. (1998). Gradient-based learning applied to document recognition. *Proc. IEEE* 86, 2278–2324. doi: 10.1109/5.726791

Mahajan, D. G., Ramanathan, V. R., He, K., Paluri, M., Li, Y., Bharambe, A., et al. (2018). "Exploring the Limits of Weakly Supervised Pretraining," in *arXiv* 1805(00932v1). doi: 10.1007/978-3-030-01216-8_12

Mathis, A., Mamidanna, P., Cury, K. M., Abe, T., Murthy, V. N., Mathis, M. W., et al. (2018). DeepLabCut: markerless pose estimation of user-defined body parts with deep learning. *Nat. Neurosci.* 21, 1281–1289. doi: 10.1038/s41593-018-0209-y

Moy, S. S., Nadler, J. J., Perez, A., Barbaro, R. P., Johns, J. M., Magnuson, T. R., et al. (2004). Sociability and preference for social novelty in five inbred strains: an approach to assess autistic-like behavior in mice. *Genes Brain Behav.* 3, 287–302. doi: 10.1111/j.1601-1848.2004.00076.x

National Institute of Health BRAIN 2025: A Scientific Vision (2014). Available online at: https://www.braininitiative.nih.gov/pdf/BRAIN2025_508C.pdf (accessed June 5, 2014)

Pereira, T. D., Aldarondo, D. E., Willmore, L., Kislin, M., Wang, S. S. H., Murthy, M., et al. (2018). "Fast animal pose estimation using deep neural networks," in *bioRxiv* 331181. doi: 10.1101/331181

Real, E., Asari, H., Gollisch, T., and Meister, M. (2017). Neural circuit inference from function to structure. *Curr. Biol.* 27, 189–198. doi: 10.1016/j.cub.2016.11.040

Redmon, J., and Farhadi, A. (2018). "YOLOv3: An incremental improvement," in *Computer Vision and Pattern Recognition.* eprint arXiv:1804.02767.

Robie, A. A., Hirokawa, J., Edwards, A. W., Umayam, L. A., Lee, A., Phillips, M. L., et al. (2017). Mapping the neural substrates of behavior. *Cell* 170, 393–406 e328. doi: 10.1016/j.cell.2017.06.032

Santarcangelo, J. Z., and Xiao, P. (2015). "Dynamic time-alignment k-means kernel clustering for time sequence clustering," in *2015 IEEE International Conference on Image Processing (ICIP)* (Toronto, ON).

Simon, T., Joo, H., Matthews, I., and Sheikh, Y. (2017). "Hand keypoint detection in single images using multiview bootstrapping," in *Hand Keypoint Detection in Single Images using Multiview Bootstrapping* (Atlanta, GA). doi: 10.1109/CVPR.2017.494

Stern, U., He, R., and Yang, C. H. (2015). Analyzing animal behavior via classifying each video frame using convolutional neural networks. *Sci. Rep.* 5:14351. doi: 10.1038/srep14351

Stewart, R., Andriluka, M., and Ng, A. Y. (2016). "End-to-end people detection in crowded scenes," in *Paper Presented at the 2016 IEEE Conference on Computer Vision and Pattern Recognition (CVPR)* (Stanford, CA).

Szegedy, C., Vanhoucke, V., Ioffe, S., Shlens, J., and Wojna, Z. (2016). "Rethinking the inception architecture for computer vision," in *Paper Presented at the 2016 IEEE Conference on Computer Vision and Pattern Recognition (CVPR)* (Mountain View, CA).

Szegedy, C., Wei, L., Yangqing, J., Sermanet, P., Reed, S., Anguelov, D., et al. (2015). "Going deeper with convolutions," in *Paper Presented at the 2015 IEEE Conference on Computer Vision and Pattern Recognition (CVPR)* (Mountain View, CA).

Tinbergen, N. (1963). On aims and methods of ethology. *Z. Tierpsychol.* 20, 410–433. doi: 10.1111/j.1439-0310.1963.tb01161.x

Vogelstein, J. T., Park, Y., Ohyama, T., Kerr, R. A., Truman, J. W., Priebe, C. E., et al. (2014). Discovery of brainwide neural-behavioral maps via multiscale unsupervised structure learning. *Science* 344, 386–392. doi: 10.1126/science.1250298

Wei, S. E., Ramakrishna, V., Kanade, T., and Sheikh, Y. (2016). "Convolutional Pose Machines. eprint arXiv:1602.00134," in *2016 IEEE Conferenceon Computer Vision and Pattern Recognition (CVPR)* (Atlanta, GA). doi: 10.1109/CVPR.2016.511

Wiltschko, A. B., Johnson, M. J., Iurilli, G., Peterson, R. E., Katon, J. M., Pashkovski, S. L., et al. (2015). Mapping sub-second structure in mouse behavior. *Neuron* 88, 1121–1135. doi: 10.1016/j.neuron.2015.11.031

Conflict of Interest Statement: The authors declare that the research was conducted in the absence of any commercial or financial relationships that could be construed as a potential conflict of interest.

frontiers in Systems Neuroscience

ORIGINAL RESEARCH
published: 02 August 2019
doi: 10.3389/fnsys.2019.00034

Neuroradiological Changes Following Single or Repetitive Mild TBI

*Praveen Kulkarni[1], Thomas R. Morrison[1], Xuezhu Cai[1], Sade Iriah[1], Neal Simon[2,3], Julia Sabrick[1], Lucas Neuroth[1] and Craig F. Ferris[1]**

[1] Center for Translational NeuroImaging, Northeastern University, Boston, MA, United States, [2] Azevan Pharmaceuticals, Bethlehem, PA, United States, [3] Department of Biological Sciences, College of Arts and Sciences, Lehigh University, Bethlehem, PA, United States

Objectives: To test the hypothesis that there are differences in neuroradiological measures between single and repeated mild traumatic brain injury using multimodal MRI.

Methods: A closed-head momentum exchange model was used to produce one or three mild head injuries in young adult male rats compared to non-injured, age and weight-matched controls. Six–seven weeks post-injury, rats were studied for deficits in cognitive and motor function. Seven–eight weeks post-injury changes in brain anatomy and function were evaluated through analysis of high resolution T2 weighted images, resting-state BOLD functional connectivity, and diffusion weighted imaging with quantitative anisotropy.

Results: Head injuries occurred without skull fracture or signs of intracranial bleeding or contusion. There were no significant differences in cognitive or motors behaviors between experimental groups. With a single mild hit, the affected areas were limited to the caudate/putamen and central amygdala. Rats hit three times showed altered diffusivity in white matter tracts, basal ganglia, central amygdala, brainstem, and cerebellum. Comparing three hits to one hit showed a similar pattern of change underscoring a dose effect of repeated head injury on the brainstem and cerebellum. Disruption of functional connectivity was pronounced with three mild hits. The midbrain dopamine system, hippocampus, and brainstem/cerebellum showed hypoconnectivity. Interestingly, rats exposed to one hit showed *enhanced* functional connectivity (or hyperconnectivity) across brain sites, particularly between the olfactory system and the cerebellum.

Interpretation: Neuroradiological evidence of altered brain structure and function, particularly in striatal and midbrain dopaminergic areas, persists long after mild repetitive head injury. These changes may serve as biomarkers of neurodegeneration and risk for dementia later in life.

Keywords: Parkinson's disease, dopamine, dementia, hyperconnectivity, microglia activation, cerebellum, suprachiasmatic nucleus (SCN), olfactory system diseases

OPEN ACCESS

Edited by:
James W. Grau,
Texas A&M University, United States

Reviewed by:
Ramesh Raghupathi,
Drexel University, United States
Sandy R. Shultz,
Monash University, Australia
Rebekah Mannix,
Boston Children's Hospital, Harvard Medical School, United States

***Correspondence:**
Craig F. Ferris
c.ferris@northeastern.edu;
c.ferris@neu.edu

Received: *15 December 2018*
Accepted: *10 July 2019*
Published: *02 August 2019*

Citation:
Kulkarni P, Morrison TR, Cai X, Iriah S, Simon N, Sabrick J, Neuroth L and Ferris CF (2019) Neuroradiological Changes Following Single or Repetitive Mild TBI. Front. Syst. Neurosci. 13:34. doi: 10.3389/fnsys.2019.00034

INTRODUCTION

Traumatic brain injuries (TBIs) are responsible for over 2.8 million emergency room visits and 50,000 deaths in the United States each year (Taylor et al., 2017). Mild TBI is characterized as a negligible loss of consciousness with minimal neuropathology (Ruff et al., 2009; Menon et al., 2010) and is estimated to account for 70–90% of all TBI cases (Gardner and Yaffe, 2015; Astafiev et al., 2016). Mild TBI following a single incident is difficult to detect, most cognitive and behavioral deficits usually resolve within weeks of the head injury, and few cases result in extended recovery time periods (Lovell et al., 2003; McCrea et al., 2003; Iverson, 2005; Losoi et al., 2016). However, a more pernicious, long-lasting condition may arise with repeated incidents of mild TBI (rmTBI) (Guskiewicz et al., 2003). Repeated mild TBI is associated with more severe and protracted cognitive, motor, and behavioral complications that may last for months and even years (De Beaumont et al., 2009, 2012; Omalu et al., 2010). Even after the remission of symptoms, there is accumulating evidence of persistent brain injuries (Nakamura et al., 2009; Mayer et al., 2011; Palacios et al., 2017; Rajesh et al., 2017; Vergara et al., 2017) that carry an increased risk of dementia, including Alzheimer's disease, chronic traumatic encephalopathy, and Parkinson's disease later in life (Plassman et al., 2000; McKee et al., 2009; Gavett et al., 2011; Konrad et al., 2011; Sivanandam and Thakur, 2012; Jafari et al., 2013; Faden and Loane, 2015; Gardner and Yaffe, 2015; Jenkins et al., 2018).

The objective of this study was to use a momentum exchange model of head injury in rat to characterize neuroradiological differences between single and repeated mild TBI. To this end, we used diffusion weighted imaging (DWI) with indices of anisotropy registered to a 3D MRI rat atlas and computational analysis to identify putative changes in gray matter microarchitecture across 173 brain areas in control and experimental rats hit one or three times. In addition, resting-state BOLD functional connectivity (rsFC) was employed to evaluate alterations in global functional neural circuitry. These MRI protocols were selected due to their clinical use in diagnosing and following the progression of rmTBI after remission of symptoms (Nakamura et al., 2009; Mayer et al., 2011; Palacios et al., 2017; Rajesh et al., 2017; Vergara et al., 2017) as well as their utility in identifying biomarkers of neurodegenerative disease (Wu et al., 2009; Hacker et al., 2012; Koch et al., 2012; Teipel et al., 2013; Zhang et al., 2015). We adapted the momentum exchange model developed by the National Football League to study player concussions and designed for preclinical studies by Viano et al. (2009) to scale to humans. The velocity of head movement and energy transfer was calculated and scaled to mimic a mild concussive injury in humans. This injury was defined by the absence of skull fractures, prolonged loss of consciousness, or signs of intracranial bleeding, which are seen in TBIs classified as moderate or severe (Hardman and Manoukian, 2002).

MATERIALS AND METHODS

Animals

Adult, male Sprague Dawley rats (300–400 g) were purchased from Charles River Laboratories (Wilmington, MA, United States). Animals were housed in Plexiglas cages (two per cage) and maintained in ambient temperature (22–24°C) on a 12:12 light:dark cycle (lights on at 07:00 a.m.). Food and water were provided *ad libitum*. All methods and procedures described were approved by the Northeastern University Institutional Animal Care and Use Committee (IACUC). The Northeastern facility is AAALAC accredited with OLAW Assurance and is registered with the USDA. All housing, care, and use followed the Guide for the Care and Use of Laboratory Animals (8th Addition) and the Animal Welfare Act.

Momentum Exchange Model

Working with engineers at Animals Imaging Research, LLC (Holden, MA, United States), we replicated the pneumatic pressure drive, 50 g compactor (see **Supplementary Figure 1**) described by Viano et al. (2009) and reliably produced the 7.4, 9.3, and 11.2 m/s impact velocities described for mild, medium, and severe rat head injury, respectively. This same model was further refined and used to test the behavioral effects of mild TBI controlling for the axis of injury, rotational force, and head acceleration in different directions(Mychasiuk et al., 2016). Our impact created linear acceleration with some rotation. The data reported here all came from the 7.4 m/s impact velocities as determined using high-speed video recordings. The impact piston was directed to the top of the skull, midline, in the approximate area of Bregma. All control and TBI rats were anesthetized with 2% isoflurane. Rats were awake and ambulatory within 5–7 min after anesthesia and concussion. This impact regimen produced no signs of contusion (see **Supplementary Figure 2**). Rats were observed twice daily, in the morning and early evening, for the first week after TBI and weekly thereafter. Body weights were taken two to three times/week for the first week and then weekly. Buprenorphine treatment was available for pain and distress, but it was deemed unnecessary based upon behavioral observations and response to handling. There were no unplanned mortalities over the course of the study.

The impact regimen was based on a rich body of data detailing the effects of acute and rmTBI in various rodent models (Shultz et al., 2012; Xiong et al., 2013; Aungst et al., 2014; Fidan et al., 2016). Studies were scheduled one (n = 13) or three (n = 9) concussive head impacts under 2% isoflurane anesthesia, with a 48-h interval between each impact. Control rats (n = 9) were exposed to isoflurane anesthesia three times with 48 h intervals to control for the effects of anesthesia. Rats were not tested for neurological deficits after head injury; instead, they were returned to their home cage after their final TBI and left undisturbed for 6 weeks. Between 6 and 7 weeks after head injury, all animals were tested for cognitive and motor behavior. Between 7 and 8 weeks post injury all animals were imaged. Rats were euthanized with a combination of

carbon dioxide asphyxiation until the cessation of respiration followed by thoracotomy.

Neuroimaging

Imaging sessions were conducted using a Bruker Biospec 7.0T/20-cm USR horizontal magnet (Bruker, Billerica, MA, United States) and a 20-G/cm magnetic field gradient insert (ID = 12 cm) capable of a 120-μs rise time. Radio frequency signals were sent and received with a quadrature volume coil built into the animal restrainer (Animal Imaging Research, Holden, MA, United States). The design of the restraining system included a padded head support obviating the need for ear bars helping to reduce animal discomfort while minimizing motion artifact. All rats were imaged under 1–2% isoflurane while keeping a respiratory rate of 40–50/min. At the beginning of each imaging session, a high-resolution anatomical data set was collected using the RARE pulse sequence with following parameters, 35 slice of 0.7 mm thickness; field of view (FOV) 3 cm; 256 × 256; repetition time (TR) 3900 ms; effective echo time (TE) 48 ms; NEX 3; 6 min 14 s acquisition time.

Diffusion Weighted Imaging – Quantitative Anisotropy

Diffusion weighted imaging was acquired with a spin-echo echo-planar-imaging (EPI) pulse sequence having the following parameters: TR/TE = 500/20 ms, eight EPI segments, and 10 non-collinear gradient directions with a single *B*-value shell at 1000 s/mm^2 and one image with a *B*-value of 0 s/mm^2 (referred to as B_0). Geometrical parameters were: 48 coronal slices, each 0.313 mm thick (brain volume) and with in-plane resolution of 0.313 × 0.313 mm^2 (matrix size 96 × 96; FOV 30 mm^2). The imaging protocol was repeated two times for signal averaging. Each DWI acquisition took 35 min and the entire MRI protocol lasted ca. 70 min. Image analysis included DWI analysis of the DW-3D-EPI images to produce the maps of fractional anisotropy (FA) using a 3D MRI Rat Brain Atlas©(Ekam Solutions LLC, Boston, MA, United States). DWI analysis was completed with MATLAB and MedINRIA (1.9.0[1]) software. Because sporadic excessive breathing during DWI acquisition can lead to significant image motion artifacts that are apparent only in the slices sampled when motion occurred, each image (for each slice and each gradient direction) was screened, prior to DWI analysis. If found, acquisition points with motion artifacts were eliminated from analyses.

For statistical comparisons between rats, each brain volume was registered to the 3D rat atlas allowing voxel- and region-based statistics. All image transformations and statistical analyses were carried out using the in-house MIVA software[2]. For each rat, the B_0 image was co-registered with the B_0 template (using a six-parameter rigid-body transformation). The co-registration parameters were then applied on the DWI indexed maps for the different indices of anisotropy. Normalization was performed on the maps since they provided the most detailed visualization of brain structures and allowed for more accurate normalization. The normalization parameters were then applied to all DWI indexed maps that were then smoothed with a 0.3-mm Gaussian kernel. To ensure that FA and RD values were not affected significantly by the pre-processing steps, the "nearest neighbor" option was used following registration and normalization.

Statistical differences in measures of DWI between experimental groups were determined using a nonparametric Mann–Whitney *U*-test (alpha set at 5%). The formula below was used to account for false discovery from multiple comparisons.

$$P(i) \leq \frac{i}{V}\frac{q}{c(V)},$$

where $P(i)$ is the *p*-value based on the *t*-test analysis. Each of 171 regions of interest (ROIs) (i) within the brain containing (V) ROIs was ranked in order of its probability value (**Table 1**). The false-positive filter value q was set to 0.2 and the predetermined $c(V)$ was set to unity (Benjamini and Hochberg, 1995). The corrected probability is noted on each table.

Resting-State Functional Connectivity

Scans were collected using a spin-echo triple-shot EPI sequence [imaging parameters: matrix size = 96 × 96 × 20 (H × W × D), TR/TE = 1000/15 ms, voxel size = 0.312 × 0.312 × 1.2 mm, slice thickness = 1.2 mm, with 200 repetitions, time of acquisition 10 min]. There are numerous studies detailing the benefits of multi-shot EPI in BOLD imaging (Menon et al., 1997; Hoogenraad et al., 2000; Poser and Norris, 2009; Swisher et al., 2012; Kang et al., 2015). We avoided using single shot EPI because of its sever geometrical distortion at high field strengths (≥7T) and loss of effective spatial resolution as the readout period increases (Farzaneh et al., 1990; Jesmanowicz et al., 1998; Hoogenraad et al., 2000). There is also the possibility of signal loss in single shot EPI due to accumulated magnetic susceptibility or field inhomogeneity (Kang et al., 2015).

Preprocessing in this study was accomplished by combining Analysis of Functional NeuroImages (AFNI_17.1.12[3]), FMRIB Software library (FSL, v5.0.9[4]), Deformable Registration via Attribute Matching and Mutual-Saliency Weighting (DRAMMS 1.4.1[5]), and MATLAB (Mathworks, Natick, MA, United States). Brain tissue masks for resting-state functional images were manually drawn using 3DSlicer[6] and applied for skull-stripping. Motion outliers (i.e., data corrupted by extensive motion) were detected in the dataset and the corresponding time points were recorded so that they could be regressed out in a later step. Functional data were assessed for the presence of motion spikes. Any large motion spikes were identified and removed from the time-course signals. This filtering step was followed by slice timing correction from interleaved slice acquisition order. Head motion correction (six motion parameters) was carried out using the first volume as a reference image. Normalization was completed by registering functional data to the 3D MRI Rat Brain Atlas©using affine registration through DRAMMS. The

[1]http://www-sop.inria.fr/asclepios/software/MedINRIA/index.php
[2]http://ccni.wpi.edu/
[3]http://afni.nimh.nih.gov/afni/
[4]http://fsl.fmrib.ox.ac.uk/fsl/
[5]https://www.cbica.upenn.edu/sbia/software/dramms/index.html
[6]https://www.slicer.org/

TABLE 1 | Measures of motor behavior.

Apparatus and parameter	Control	1-Hit	3-Hit	Statistics
Balance beam				
Total foot faults	2.0 ± 0.7	2.2 ± 0.6	2.8 ± 0.9	$F = 0.31$, $p = 0.74$[a]
Faults per segment:				
Wide	0.3 ± 0.1	0.5 ± 0.2	0.5 ± 0.2	–
Middle	0.2 ± 0.1	0.1 ± 0.1	0.3 ± 0.2	$p < 0.01$[b]
Thin	0.5 ± 0.2	0.6 ± 0.1	0.6 ± 0.1	$p < 0.02$[b]
Goal box latency (s)	12.7 ± 2.2	9.9 ± 1.2	14.7 ± 3.7	$F = 0.99$, $p = 0.38$[a]
Rota-rod				
Fall latency (s)	107.8 ± 9.7	83.2 ± 9.6	100.5 ± 19.8	$F = 1.05$, $p = 0.36$[a]

Data represent mean ± SEM. For balance beam testing, there were no significant differences between groups for goal box latency [$F(2,27) = 0.99$, $p > 0.1$] or total foot faults [$F(2,27) = 0.30$, $p > 0.1$]. Similarly there was no difference between groups for fall latency on the rota-rod task [$F(2,27) = 1.05$, $p > 0.1$]. Analysis of balance beam performance, in terms of the widths of the three specific beam segments (i.e., Wide, Middle, and Thin), resulted in a significant main effect of segment width [$F(2,52) = 11.7$, $p < 0.0001$] with all groups showing a higher number of foot faults on the thinnest and middle portion of the beam compared to the widest portion of the beam ($p < 0.05$ for both). [a]Non-significant; [b]significant.

MRI rat atlas containing 173 annotated brain regions was used for segmentation. Data are reported in 166 brain areas, as five regions in the brain atlas were excluded from analysis due to the large size of three brains. These brains fell slightly outside our imaging FOV and thus we did not get any signal from the extreme caudal tip of the cerebellum. Whole brains that contain all ROIs are needed for analyses so rather than excluding the animals, we removed the brain sites across all animals. After quality assurance, band-pass filtering (0.01–0.1 Hz) was preformed to reduce low-frequency drift effects and high-frequency physiological noise for each subject. The resulting images were further detrended and spatially smoothed (full width at half maximum = 0.8mm). Finally, regressors comprised of motion outliers, the six motion parameters, the mean white matter, and cerebrospinal fluid time series were fed into general linear models for nuisance regression to remove unwanted effects.

The region-to-region functional connectivity method was performed in this study to measure the correlations in spontaneous BOLD fluctuations. A network is comprised of nodes and edges; nodes being the brain ROI and edges being the connections between regions. Data are reported in 166 brain areas, as five regions in the 3D MRI Rat Brain Atlas were excluded from analysis due to the large size of three brains that fell slightly outside then FOV excluding signal from the most caudal tip of the cerebellum. Voxel time series data were averaged in each node based on the residual images using the nuisance regression procedure. Pearson's correlation coefficients across all pairs of nodes (14,535 pairs) were computed for each subject among all three groups to assess the interregional temporal correlations. The r-values (ranging from −1 to 1) were z-transformed using the Fisher's Z transform to improve normality. 166 × 166 symmetric connectivity matrices were constructed with each entry representing the strength of edge. Group-level analysis was performed to look at the functional connectivity in the experimental groups. The resulting Z-score matrices from one-group t-tests were clustered using the K-nearest neighbors clustering method to identify how nodes cluster together and form resting-state networks. A Z-score threshold of $|Z| = 2.3$ was applied to remove spurious or weak node connections for visualization purposes.

Behavioral Testing

The novel object recognition (NOR) task was used to assess episodic learning and memory (Bevins and Besheer, 2006; Antunes and Biala, 2012). The apparatus consisted of a black cube-shaped Plexiglass box (L: 60.9, W: 69.2, H: 70.5 cm) with no lid, indirectly illuminated with two 40 W incandescent bulbs. Animals were placed in the empty box (15 min) for acclimation on day 1. On day 2, for the familiar phase (5 min), animals were placed in the box with two identical objects arranged in diagonal corners, 5 cm from each wall. After a 90 min rest period in their home cage, animals were placed back in the box for the novel phase (3 min) with one of the familiar objects and a novel object.

The Barnes Maze was used to assess spatial learning and memory (Barnes, 1979; Fox et al., 1998; Harrison et al., 2009). The maze consists of a circular platform (121 cm in diameter, elevated 40 cm), with 18 escape holes along the perimeter at 30 cm intervals. A black, removable enclosed Plexiglas goal box was positioned under a single escape hole on the underside of the maze (L:40.0 × W:12.7 × H:7.6 cm) in the same position relative to the testing room across all trials. Between trials, the maze was rotated 45 degrees and the goal box shifted accordingly for cardinal consistency. Animals were placed inside the goal box for 1 min and then under an enclosed container at the center of the circular platform for 30 s, that was then lifted to start the trial. If animals did not find the goal box within the test period (4 min), they were gently nudged into the box and allowed to stay for 1 min, and then placed back in their home cages between trials (three trials/day for 4 days). For both the NOR and the Barnes maze, all trials were video recorded and analyzed using manual methods by experimenters blind to treatment condition and verified with automated scoring using ANY-maze® software (Stoelting, Wood Dale, IL, United States).

A tapered balance beam (Dragonfly Inc., Ridgeley, WV, United States) and rota-rod were used to measure motor behavior (Williams et al., 2005; Sackheim et al., 2017). The balance beam

(L: 150 cm, W: 5.5 cm tapering down to 1.5 cm, elevated 120 cm) was equally divided into three sections (L:47 cm each; "wide," "middle," "thin" sections) that were lined with touch-sensitive sensor ledges (width: 2 cm) that ran the length of the beam and were arranged on each side, 4 cm below the surface of the beam to count paw slips (or *foot faults*). At the start of the maze ("wide" section) was a wooden start platform, and at the end of the beam (immediately following the "thin" section) was a black enclosed Plexiglas goal box. After 2 days of training (three trials per day), animals were tested (three trials/day for 2 days). Prior to each trial, animals were placed inside the goal box for 1 min. Animals were then placed on a start platform and timed for traversing into the goal box, where they remained for 1 min, and were then placed back in their home cage until the next trial (30 min intertrial interval).

Following 2 days of training (three trials/day), animals were tested over 2 days (three trials/day) using the rota-rod by placing them on a rotating cylinder (diameter: 4 cm) that rotated at an increasing frequency starting at 1 rpm and increasing linearly at a 0.1 v/t2 acceleration rate for a total of 210 s ending at a max frequency of 50 rpm. Latency to fall off the rod was recorded for each animal and averaged across trials and days. For all behavioral measures, GraphPad Prism version 6.0 (GraphPad Software, La Jolla, CA, United States) was used for statistical analyses. One-sample *t*-tests assessed differences from chance levels (i.e., =50%) of exploration in the NOR task, for each experimental group individually. Comparisons among groups were conducted using one-way analysis of variance (ANOVA) or mixed ANOVAs followed by Fisher's protected least significant difference *post hoc* test.

RESULTS

Cognitive and Motor Behavior

Across days, there was a significant main effect of testing day on goal box latency in the Barnes maze test [$F(3,81) = 9.3$, $p < 0.0001$], with no significant difference between groups [$F(2,27) = 0.38$, $p > 0.1$, **Figure 1**]. All groups had significantly shorter latencies to enter the goal box on testing day 3 ($p < 0.0001$), and 4 ($p < 0.0001$) compared to day 1. In addition, all groups showed shorter latencies on the last day of testing compared to the second day of testing ($p < 0.01$). In the NOR, single-sample *t*-tests showed that control, one, and three hit animals [$t(11) = 6.84$, $p < 0.0001$; $t(9) = 3.86$, $p < 0.01$; and $t(7) = 4.9$, $p < 0.001$, respectively] all had a significantly greater preference for the novel object that was beyond chance (>50%) during the novel phase (**Figure 1**). The DWI and rsFC data showed no evidence of alterations in the hippocampal complex as shown in **Figures 2**, **3**. **Table 1** summarizes the results of locomotor testing and shows no differences between the groups.

Diffusion Weighted Imaging and Quantitative Anisotropy

Measures of anisotropy at 7–8 weeks post injury were registered to the 3D MRI Rat Atlas with 173 segmented brain areas to identify possible changes in gray matter microarchitecture (Kulkarni et al., 2015). The data for FA are shown in **Figure 2**. These probability heat maps show statistical differences between the one and three hit groups compared to controls. The right column of activation maps shows three hits compared to one hit. The effects on FA from a single hit were limited to the dorsal striatum and central amygdala. However, rats exposed to three hits showed significant FA changes in the olfactory system, basal ganglia, central amygdala, cerebellum, and deep cerebellar nuclei. Many of the same differences are noted when comparing three hits to one hit, evidence of a dose effect with repeated mild head injuries (see **Supplementary Tables 1–3**).

Resting-State Functional Connectivity

The delineated areas in the two correlation matrices in **Figure 3** show that a single hit favors an increase in rsFC, while repeated hits show reduced rsFC. For example, the posterior cerebellum of the one hit group shows a much larger cluster than both the three hit and control animals. Indeed, this area has grown to include the paramedian lobule, crus 1 and 2, cerebellar lobules 7, 8, 9, and 10 plus the deep cerebellar nuclei. The rsFC between brain regions for the three experimental groups are shown in the right-hand panels of **Figure 3** for the olfactory system/prefrontal cortex, suprachiasmatic n. (SCN) of the hypothalamus, and the midbrain dopaminergic system. The areas in red comprise the key nodes for each panel. For instance, the olfactory system is made up of the three layers of the olfactory bulb and the anterior olfactory nucleus. In control rats, these combined areas have significant functional connections to the marked areas of the adjacent prefrontal ctx (e.g., rostral piriform, ventral, medial and lateral orbital cortex, and the tenia tecta, highlighted in yellow). The 3D organization of these brain areas and the others is shown in the glass brains. Rats hit once showed increase functional connectivity 7 weeks post injury that includes the anterior cerebellum (three to five lobules) and deep cerebellar nuclei (lateral and interposed). In contrast, rats exposed to three hits have reduced connectivity that is limited only to the olfactory bulb. The SCN, the key node in the brain controlling circadian rhythms and sleep/wake cycles, has functional connections with adjacent areas of the hypothalamus in control rats that are reduced with one hit and eliminated with three hits.

The ventral tegmental area (VTA) as well as the substantia nigra compacta (SNc) and reticularis (SNr) make up the core nodes of the midbrain dopaminergic system. From these regions, control animals have diffuse connectivity to areas in the amygdala, hypothalamus, thalamus, medulla oblongata, and cerebellum. Following a single mild hit, the functional connectivity primarily coalesces around the thalamus. Animals exposed to repeated TBI showed reduced connectivity compared to the other groups, and had no connectivity between the SN and the VTA.

The sensitivity of the cerebellum and its efferent connections to the brain through the deep cerebellar nuclei was examined further by seeding the combined lateral, fastigial, and interposed nuclei, and mapping areas of connectivity in the one and three hit groups that were significantly different from control (**Figure 4**). In addition, the posterior cerebellum was also seeded using an aggregate of multiple areas (6–10 lobules, cupola, crus 1 and 2, paramedian, and paraflocculus). The purpose of this

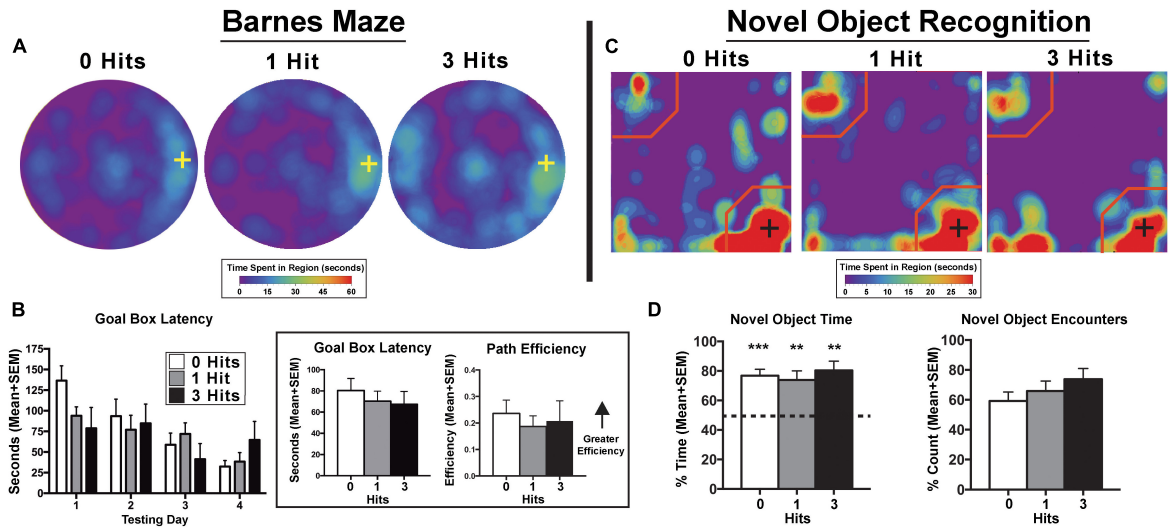

FIGURE 1 | Cognition testing. **(A)** Barnes maze heat maps for the last day of testing. Qualitatively, on the last day of testing, animals exposed to three hits spent more time on the maze searching for the goal box, however, this effect failed to reach quantitative significance. **(B)** Search patterns for the Barnes maze goal box resulted in no significant differences between groups across days for all maze parameters including goal box latency and path efficiency. There was a main effect of path efficiency on the Barnes maze with all experimental groups showing relatively steady increases across days [$F(3,81) = 3.29$, $p < 0.05$] (Inset). When averaged over days, there were no significant differences between groups for goal box latency [$F(2,27) = 0.20$, $p = 0.82$] or path efficiency [$F(2,27) = 0.22$, $p = 0.80$]. **(C)** Novel object recognition (NOR) – novel phase heat maps (averaged across days). Qualitative data show an equal pattern of exploration across groups with the greatest amount of time spent in close proximity to the novel object indicated by the presence of red on the lower right corner of the maps. **(D)** Quantitative data reflect qualitative patterns and show that all three treatment groups spent a greater than chance amount of time (i.e., >50%) with the novel object. Conversely, there were no differences between hit groups for the NOR index [$F(2,27) = 0.34$, $p > 0.1$], total time exploring the novel object [$F(2,27) = 0.57$, $p > 0.1$], or the percentage of novel object encounters during the novel phase [$F(2,27) = 1.16$, $p > 0.1$]. Crosses on heat maps indicate goal box location and novel object location on the Barnes maze and NOR, respectively. $^{**}p < 0.05$, $^{***}p < 0.01$ for single sample *t*-test.

seeding strategy was to identify putative afferent connections to the posterior cerebellum given its enhanced functional connectivity following a single concussion. For the one hit group, there was strong connectivity with the olfactory bulb, prelimbic ctx, tenia tecta, and endopiriform ctx (sections E and F). The amygdala (central, medial, and basal, section D), hippocampus (CA3 dorsal and ventral, CA1 dorsal, sections D and C), motor ctx (section D), and medulla oblongata (olivary n., vestibular n. principle sensory n. trigeminal, and parvicellular reticular n., sections A and B) all showed strong connectivity to the posterior cerebellum. These cerebellar connections were fewer and less significant with repeated concussions. The reorganization of functional connectivity in the cerebellum and brainstem shown in **Figures 3**, **4** compliment the FA data (**Figure 2**), which showed alterations in water diffusion and putative gray matter microarchitecture across many of the same brain areas. The Excel files with the raw Z scores for all brain areas for zero, one and three hit conditions are provided in **Supplementary Tables 4A–C**.

DISCUSSION

The study was designed to evaluate the long-term neuroradiological consequences of one versus three mild repetitive head injuries using the momentum exchange model. The model had the expected effect of delivering repetitive mild head injury without signs of contusion. This model enabled the question – are there any differences between a single mild hit and three mild hits to the head delivered over the course of several days? The imaging data from DWI and rsFC collected 7–8 weeks post injury were very different between a single and three mild hits and suggest a reorganization of gray matter microarchitecture and functional neural circuitry to repetitive head injury.

One vs. Three TBI

A single, mild TBI caused few changes in indices of anisotropy reflecting minor alterations in central water diffusion. With three concussions, there was evidence of white and gray matter injury, and loss of connectivity between various regions of the brain. This was consistent with several human and animal studies that showed that repetitive injury separated by short intervals poses a greater risk than single insults or multiple head injuries separated by longer intervals (Laurer et al., 2001; Yoshiyama et al., 2005; Meehan et al., 2012; Prins et al., 2013; Silverberg et al., 2013; Bolton and Saatman, 2014; Weil et al., 2014).

The availability and utilization of glucose necessary for brain function following repeated head injury appears to play a critical role in recovery (Selwyn et al., 2016). The change in brain metabolism following injury is triphasic, with an initial period of hyperglycolysis followed by depressed glucose metabolism and finally recovery (Yoshino et al., 1991; Ginsberg et al., 1997; Bergsneider et al., 2000, 2001; Selwyn et al., 2016). The reduction in glucose metabolism may reflect a "dormant" period helping

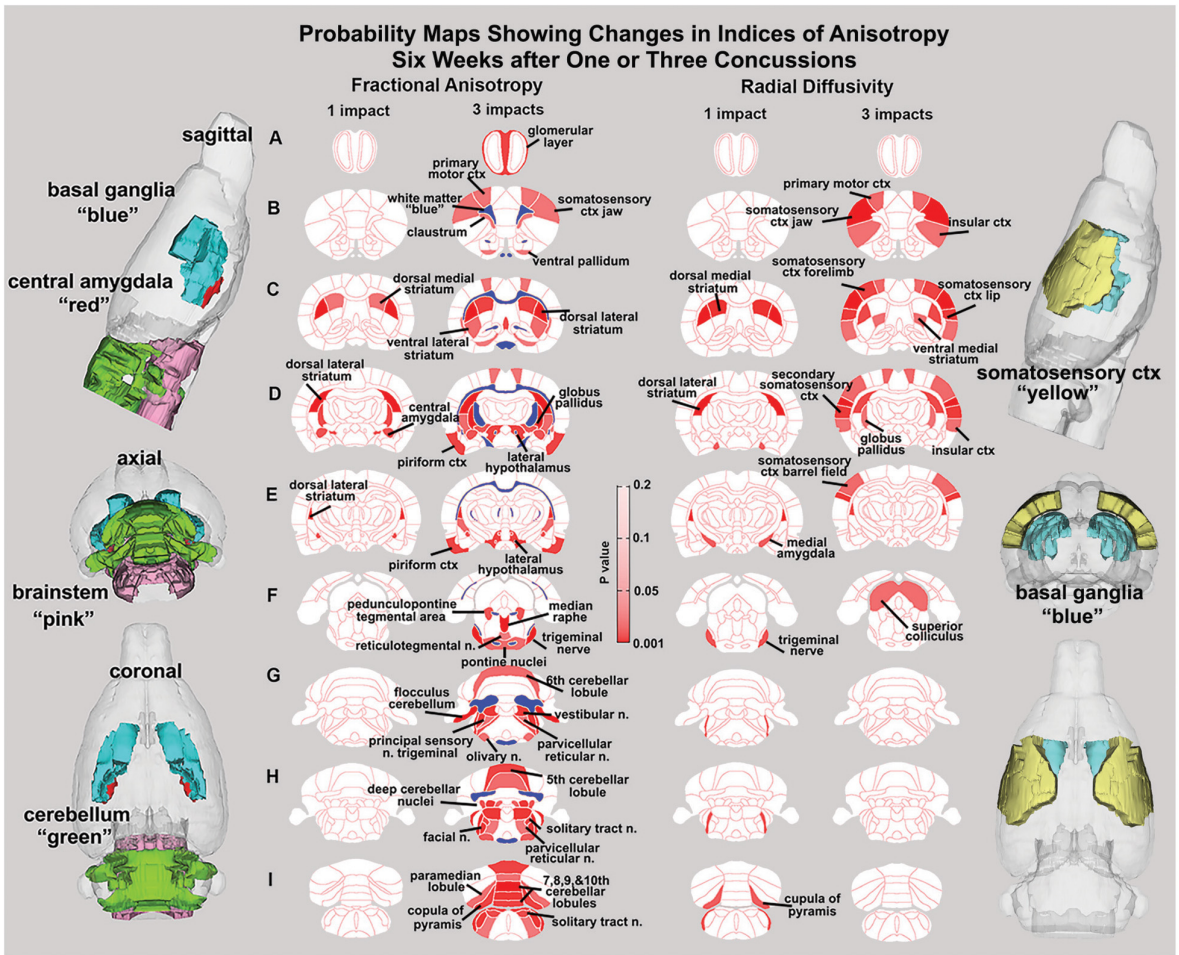

FIGURE 2 | Diffusion weighted imaging. Shown are 2D probability maps with quantitative anisotropy highlighting the brain areas (pink/red) that are significantly different in FA between one (n = 13) and three (n = 9). Most of these areas are associated with the basal ganglia, cerebellum, and brainstem. The 3D representations of these areas are presented in different orthogonal directions to the left. The forebrain areas shown in sections **B–D** are near the impact site and include the underlying ctx and striatum (caudate/putamen), while the hindbrain areas (sections **F–I**) include various components of the pons and medulla oblongata that are associated with arousal (raphe, parvicellular reticular, pedunculopontine tegmental, reticulotegmental areas), sensory integration (principle sensory n, facial n, vestibular n.), and autonomic regulation (solitary tract n.). The pontine and olivary nuclei have efferent connections to the cerebellum as do the many sensory nuclei in medulla. The posterior cerebellum comprising the vermis (5th–10th cerebellar lobules), flocculus, paramedian lobules, cupola of the pyramis, and deep cerebellar n. were all affected with three hits.

in recovery. In a recent study, Selwyn et al. (2016) looked at repeated head injury in rodents timed to coincided with this "dormant" phase of glucose metabolism and reported greater neurological damage and deficits in motor function compared to injury at other times. Concussions that occur closer together have greater cognitive and behavioral consequences, with deficits that can be present up to year later in preclinical models (Selwyn et al., 2016). In accord with this finding, a repeated imaging study showed that at multiple time points both during and after repeated head strikes, FA and mean diffusivity, as well as axial and radial diffusivity, continue to change across various regions of the brain (Qin et al., 2018).

Diffusion Weighted Imaging

There were few changes in indices of anisotropy at 7–8 weeks following a single hit. Those that occurred were localized to the central and medial amygdala, and the dorsal/ventral striatum (caudate/putamen). These areas are related to the control of emotion and dopaminergic regulation of motor function, respectively (Lanteaume et al., 2007; Fazio et al., 2011; Smith and Lane, 2015). Rats exposed to three hits showed significant changes in FA within the white matter tracts, olfactory system, basal ganglia, central amygdala, cerebellum, and deep cerebellar nuclei. Comparing three hits to one hit showed a similar pattern of change underscoring a dose effect of repeated head injury on the brainstem and cerebellum. The decrease in FA values in white matter tracts following head injury is well established in the clinical literature (Shenton et al., 2012) and again reported by Wright et al. (2017) in rmTBI using the momentum exchange model and most recently by Fidan et al. (2018) in a closed head cortical impact model. The resulting putative changes to gray matter microarchitecture show a distinct

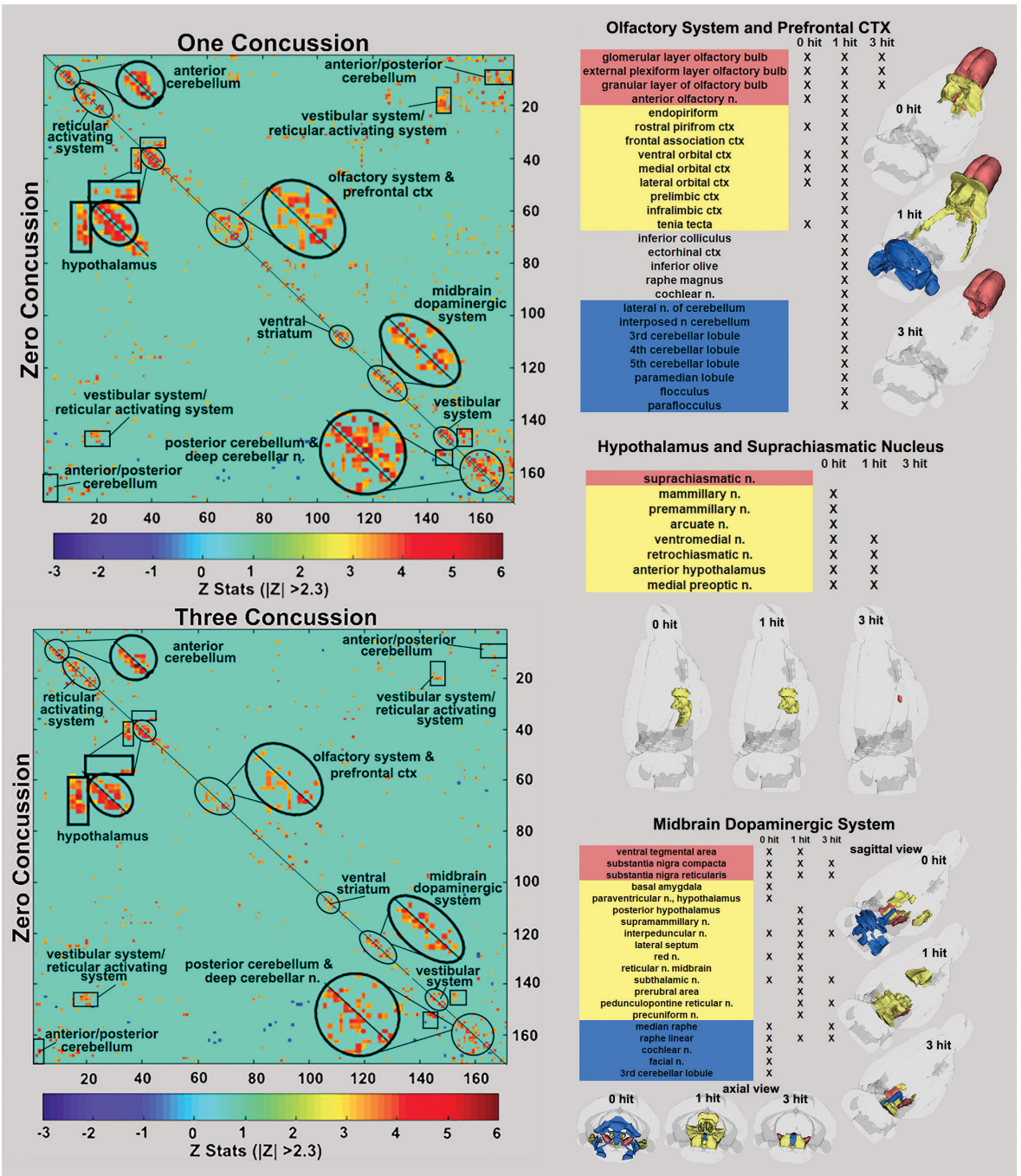

FIGURE 3 | Functional connectivity correlation matrices. Shown are correlation matrices of 166 rat brain areas for rsFC comparing controls to one concussion (top left) and three concussions (bottom left). Each dark red pixel for control rats represents 1 of 166 brain areas that is significantly correlated with other brain areas. The brain areas with significant correlations appear as clusters because they are contiguous in their neuroanatomy and function. The diagonal line separates the control and one concussed groups. The pixels for one concussion are a mirror image of those pixels (i.e., brain areas for controls). Interesting, rats with a single concussion (n = 13) showed greater rsFC within the anterior and posterior cerebellum and deep cerebellar n., olfactory system, and prefrontal ctx when compared to no hit controls (n = 9).

separation between forebrain and hindbrain (see 3D sagittal representation in **Figure 2**). These results align with numerous reports showing that the cerebellum is particularly vulnerable to mild TBI (Bolton and Saatman, 2014; Ordek et al., 2014; Nathan et al., 2015; Schroeter et al., 2015; Meabon et al., 2016; Manktelow et al., 2017). Furthermore, in a recent study, rsFC data from human mTBI patients identified altered connectivity to the cerebellum as an important biomarker (Vergara et al., 2017).

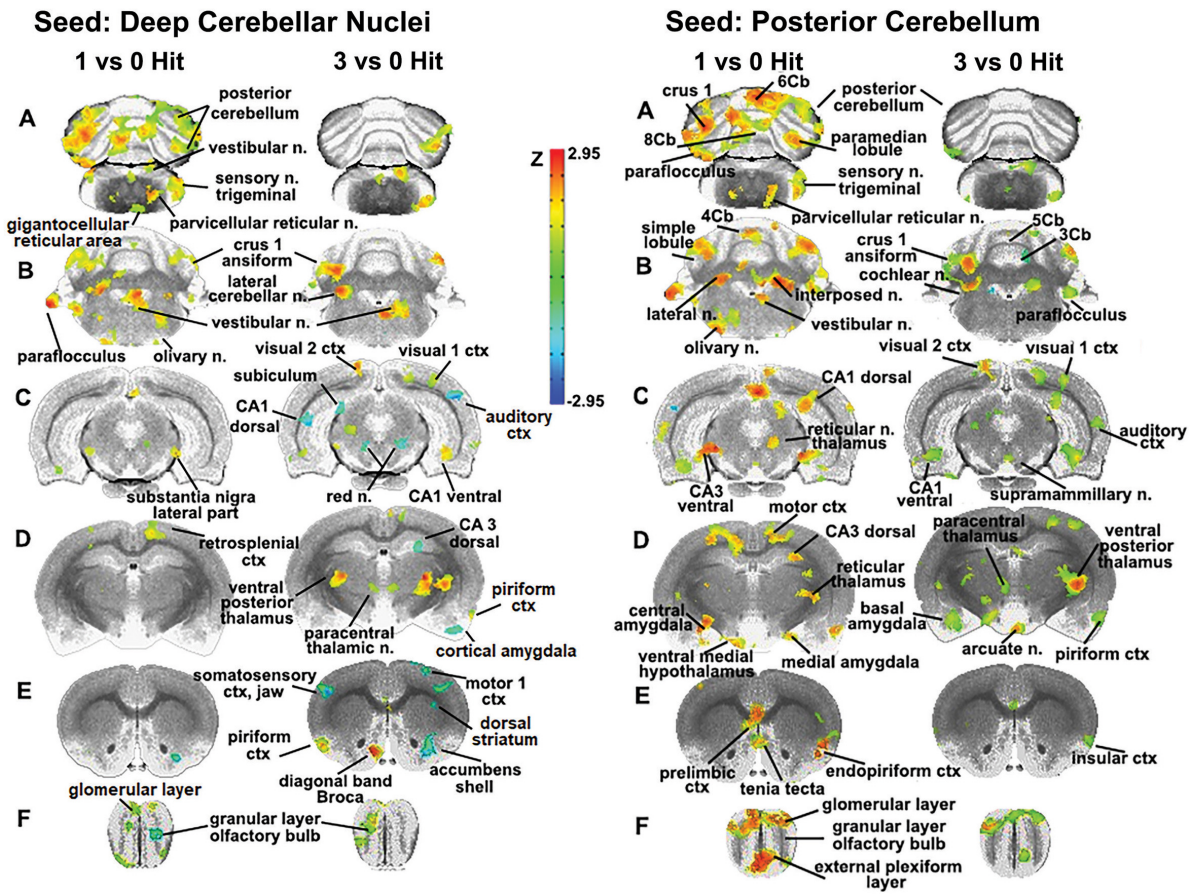

FIGURE 4 | Seeding the cerebellum. The deep cerebellar nuclei (lateral, fastigial, and interposed) and collective areas comprising the posterior cerebellum served as seeds point to focus on the connectivity of the brain to the cerebellum following one and three concussions (hits) as compared to 0 hit sham controls. Areas denoted in red/yellow are significantly greater than control while blue are significantly less than control. Sections **A** and **B** show increased connectivity between the deep cerebellar nuclei and the posterior cerebellum (lobules 5–9), crus 1 of the ansiform lobule, and parafloculus in one hit rats. Additionally, the primary sensory n. of the trigeminal nerve, vestibular n., parvicellular reticular n., and the olivary n. of the underlying medulla oblongata are all part of the enhanced functional connectivity that is present in one hit rats compared to control animals. These same cerebellar/brain stem connections were reduced in the three hit rats (controls < three hit < one hit, sections **A** and **B**). At the level of the pons (section **C**) there is clear bilateral connectivity to the lateral part of the SN in one hit rats and, to a lesser degree, a unilateral connection in the three hit rats. Three hit rats show a reduced connectivity (blue) in the red n., dorsal CA1, and dorsal subiculum of the hippocampus (three hit < control) but an increased connectivity in the ventral CA1, visual 1 and 2 cortices (control < three hit). At the level of the thalamus (section **D**) there is only one area that differs between one hit and control animals, the retrosplenial ctx. In contrast, the three hit rats show enhanced bilateral connectivity in the ventral posterior thalamus and paracentral thalamic n., and reduced connectivity in dorsal CA3 hippocampus and piriform ctx. At the level of the striatum (section **E**) there is reduced connectivity in one and three hit rats in the accumbens shell (one hit ≤ three hit < control). Three hit rats show a bilateral reduction in the primary somatosensory cortex representing the jaw, a unilateral reduction in connectivity to the motor ctx, and enhanced connectivity in the piriform ctx and diagonal band of Broca.

Related to this finding, data from retired military personnel show that decreased metabolic activity in the cerebellum is negatively correlated with the number of blast-related mild TBIs (Selwyn et al., 2016). Given the heterogeneity of TBIs, the consistency of alterations to cerebellar function due to head injury in both humans and across animal models suggests that the cerebellum is an important region for characterizing the progression of head injury.

Resting-State Functional Connectivity: Midbrain Dopamine System

This study included a global analysis of rsFC of 166 brain regions extending from the rostral-most portion of the olfactory bulb to the caudal brainstem and cerebellum. Animals hit once showed a combination of hyper- and hypoconnectivity across several networks, while rats concussed three times presented with only hypoconnectivity (**Figure 3**). The altered connectivity of the midbrain dopaminergic system demonstrates injury-dependent hypoconnectivity and reorganization of an extended neural network to a smaller cluster. The VTA and SN make up the core nodes of the midbrain dopaminergic system and have diffuse connectivity to areas in the amygdala, hypothalamus, thalamus, medulla oblongata, and cerebellum in control animals. Following a single concussion, functional connectivity primarily coalesces around the thalamus. This clustering, or "small-world" effect (Bassett and Bullmore, 2009; Nakamura et al., 2009; Roy et al., 2017), shortens the pathway

length or aggregate neural connections, reducing the metabolic cost of signal transduction. Repeated concussions show reduced connectivity in these areas compared to one concussion and control groups, as well as loss of connectivity between the SN and the VTA. Both the SN and the VTA contain a high density of dopamine (DA) neurons, and the loss of functional connections with afferent brain regions due to depletion of these DA neurons is associated with Parkinson's disease onset. The midbrain DA system and its projections to the striatum may be particularly sensitive to TBI. There are numerous preclinical studies reporting damage to the midbrain dopaminergic system and striatum months after moderate to severe TBI (Hicks et al., 1996; Bales et al., 2009; Hutson et al., 2011; Acosta et al., 2015, 2017; Impellizzeri et al., 2016; Liu et al., 2017). The damage is characterized by loss of DA neurons in the SN, increased accumulation of α-synuclein aggregates and putative Lewy bodies, and neuroinflammation marked by activated microglia. The data reported here show rmTBI-induced hypoconnectivity in the SN and VTA, along with altered DWI in the basal ganglia. These data corroborate an expanding literature that head injury is a risk factor for development of Parkinson's later in life (Jafari et al., 2013; Crane et al., 2016; Taylor et al., 2016; Gardner et al., 2018; Jenkins et al., 2018).

Resting-State Functional Connectivity: Olfactory System/Cerebellum

One of the more interesting observations from rsFC is the relationship between the olfactory system and the cerebellum. Non-concussed rats showed the olfactory bulb and anterior olfactory n. have close adjacent connections to the orbital and piriform cortices. Six–seven weeks post injury, rats concussed only once showed increased connectivity in the forebrain olfactory system and limbic ctx with hindbrain regions that include the anterior cerebellum (three to five lobules) and deep cerebellar nuclei (lateral and interposed). In contrast, rats exposed to three concussions had reduced connectivity limited only to the olfactory bulb and isolated from the anterior olfactory n.

BOLD imaging in response to odors that involve both systems show brain activation in the olfactory cortex, insula, thalamus, and cerebellum (Pellegrino et al., 2017). Indeed, the cerebellum is consistently activated in human imaging studies that use an odor stimulus (Mainland et al., 2005). While the pathway from the olfactory bulbs to cerebellum has not yet been defined, the circuitry appears to cross over the midline as lesions in the left cerebellum impair odor processing in the contralateral nostril (Mainland et al., 2005). Moreover, data based on changing odor intensity suggest that the intranasal trigeminal system may be responsible for odor-induced activation of the cerebellum (Iannilli et al., 2011; Pellegrino et al., 2017). Disrupted olfaction is commonly found long after initial head trauma in TBI patients (Schofield et al., 2014) and is a highly prevalent, early symptom of Parkinson's and Alzheimer's disease (Doty et al., 1988, 1992; Mesholam et al., 1998; Katzenschlager and Lees, 2004).

Resting-State Functional Connectivity: Cerebellum

The sensitivity of the cerebellum and its efferent connections to the brain through the cerebellar nuclei was examined by seeding the combined dentate, fastigial, and interposed nuclei as well as the posterior cerebellum, and then mapping their connectivity. The cerebellum has reciprocal interactions with much of the brain (Witter and De Zeeuw, 2015). Excitatory outputs from the cerebellar nuclei impact the motor and somatosensory cortices (Allen and Tsukahara, 1974), thalamus (Kalil, 1981; Aumann and Horne, 1996; Aumann et al., 1996), hypothalamus, amygdala, basal ganglia (Hoshi et al., 2005; Bostan et al., 2010; Chen et al., 2014), and hippocampus (Onuki et al., 2015). A single concussion increased connectivity between the cerebellar nuclei and the posterior cerebellum. The primary sensory n. of the trigeminal nerve, vestibular n., parvicellular reticular n., and olivary n. of the underlying medulla oblongata, all of which have reciprocal connections with the cerebellum (Teune et al., 2000; Witter and De Zeeuw, 2015), are part of the enhanced functional circuitry that we observed. The posterior cerebellum showed connectivity in the hindbrain that was similar to the cerebellar nuclei, with additional connections with the limbic ctx, amygdala, and hippocampus. The functional connectivity to these brain regions is consistent with the growing literature on cerebellar involvement in emotion and cognition and its reciprocal connections to these areas (Snider and Maiti, 1976; Heath et al., 1978; Haines et al., 1984; Sacchetti et al., 2002; Schutter and van Honk, 2006; Rogers et al., 2011; Calcagnoli et al., 2015).

The altered connectivity observed after seeding the cerebellar nuclei and posterior cerebellum following three concussions showed a loss of "small worldness," with reduced connectivity with the cerebellum as well as the underlying brainstem. The motor ctx, basal ganglia, hippocampus, and amygdala showed negative connectivity compared to controls. The sensitivity of these areas to rmTBI may be a risk factor for the cognitive, emotional, and/or motor dysfunction associated with neurodegenerative diseases. For example, similar to our three hit model, Alzheimer's patients show decreased functional connectivity between the hippocampus and the cerebellum (Allen et al., 2007), and elderly individuals with mild cognitive impairment show reduced connectivity of the hippocampus within a functional network that includes the cerebellum (Bai et al., 2009). In line with our three hit rsFC data, functional connectivity is reduced in Parkinson's patients between the amygdala and the contralateral cerebellum, and also between the amygdala and the putamen (Hu et al., 2015).

Limitations and Considerations

This model using momentum exchange for rmTBI and neuroradiology to assess changes in brain structure and function potentially mirrors the human experience and condition. We were unable to identify any changes in cognitive or motor function at 6–7 weeks post injury in one or three hit rats. While it is possible that cognitive and motor deficits would

have been revealed with different assays, our assessments showed no overt problems with general health and behavior. However, noninvasive imaging using DWI and rsFC protocols revealed significant alterations in putative gray and white matter architecture and functional connectivity 7–8 weeks post injury, a duration comparable to over 4 years in a human life (11.8 adult rat days = 1 human year) (Sengupta, 2013). In the context of translational neuroscience, this would be sustained injury in humans. The absence of any overt behavioral deficits after an extended period following injury is consistent with mild concussions in humans.

As previously reported, the momentum exchange model for rmTBI produces a constellation of neurological deficits that resolve within a week of head injury (Mychasiuk et al., 2016; Wright et al., 2017). Therefore, it is likely that rats had recovered from these earlier neurological deficits but it cannot be certain. While we tested for cognitive and motor behaviors it would have been of interest had we tested for changes in affective behavior given the reports that head injury in different rodent models of mild TBI increase anxiety (Petraglia et al., 2014; Rowe et al., 2016). Still another, and probably a more relevant behavioral measurement, would have been sleep/waking activity given the loss of functional coupling in the SCN (Castriotta et al., 2007).

These studies were done on adult male rats. Recently, there have been numerous reports addressing sex differences in rmTBI and the vulnerability of adolescence given the increased incidence of head injury in organized sports (Lovell et al., 2003; McCrea et al., 2004; Broshek et al., 2005; Colvin et al., 2009). Wright et al. (2017) clearly showed sex differences in behavior, imaging, and molecular markers in 30–38-day adolescent rats following rmTBI with momentum exchange. RmTBI using control cortical impact on immature 18-day male mice causes changes in white matter FA values and neurochemistry (Fidan et al., 2018). Would the neuroradiological data presented here be different between males and females and dependent upon age of injury?

Recently, there have been many preclinical studies using MRI to interrogate the brain following rmTBI (Wright et al., 2016; Fidan et al., 2018; Meconi et al., 2018; Wortman et al., 2018). DTI is routinely done but the focus is primarily on white matter and only then is predefined areas such as the corpus callosum. The DWI described here with quantitative anisotropy combining a 3D rat MRI atlas with 173 segmented and annotated areas with computational analysis provides an unbiased global interrogation of the brain for subtle changes in gray and white matter microarchitecture (Kulkarni et al., 2015). We are not aware of any preclinical rmTBI studies that use rsFC to follow the long-term consequences of mild head injury. This imaging method is becoming more important in the clinic to diagnose brain function in asymptomatic patients as noted below and focused attention in the clinic on the cerebellum as a biomarker of rmTBI. When our rsFC data are analyzed using the rat MRI atlas, global networks of functional coupling can be reconstructed. Indeed, without this capability the changes in cerebellum and positive correlation with the olfactory system would not have been noted.

It is generally held that the abatement of biopsychosocial deficits is accompanied by a parallel resolution of neuroradiological evidence of brain injury. Indeed, the preclinical images studies cited above show both recovery of behavior and DWI measures shortly after head injury. This was not the case in this study as DWI and rsFC measures in the 1- or 3-hit groups persisted for 7–8 weeks post injury. Similar to the present results, Rajesh et al. (2017) using rsFC reported that neural disruptions and structural insult in mTBI may persist up to 10 years following injury in subjects with normal cognitive function. Hypoconnectivity in the forebrain thought to be responsible for initial cognitive deficits persisted for years after injury and cognitive recovery, suggesting the brain may compensate for disrupted function through reorganization. A time lapse of 7–8 weeks in an adult rat's life is comparable to 4–5 years in humans (Sengupta, 2013), and thus the continued presence of injury after rmTBI suggests that the hyper- and hypoconnectivity observed in these studies may persist for an extended period.

The site of impact was limited to the rostral cranium at the level of bregma, directly affecting the underlying motor ctx. Although striking this specific site may have produced a unique mechanical force responsible for the observed global changes as described by Mychasiuk et al. (2016), we believe that the neurological effects of TBI are more generalized and agnostic to the site of impact. While concussions can occur on any part of the head, the general neuropathology is reasonably similar among cases. The cerebellum has been recognized as being particularly vulnerable to mTBI (Peskind et al., 2011; Nathan et al., 2015; Meabon et al., 2016; Vergara et al., 2017) and neuroradiological evidence of cerebellar dysfunction has been advanced as a diagnostic biomarker of TBI (Vergara et al., 2017). Our findings of changes in cerebellar connectivity in response to impact to the forebrain support this position. Previously, we addressed whether general markers of dysfunction reliably occur after TBI between subjects and found that concussive injuries to the forebrain or hindbrain of rats result in a similar pattern of neuropathology in the amygdala, hippocampus, and thalamus (Kulkarni et al., 2015).

One of the confounds in preclinical TBI research is the use of anesthesia during head impact as required by many IACUCs. Nonetheless, there are published methods for awake closed head injury and resulting studies with rmTBI in rats reporting behavioral and imaging data that are not dissimilar from that reported with anesthesia (Wright et al., 2016). Anesthesia was used in these studies for both head impact and imaging. The rsFC data were necessarily collected under low dose isoflurane anesthesia to minimize motion artifact and physiological stress (Guilfoyle et al., 2013). Although not optimal, numerous studies comparing anesthetized and conscious states show similar rsFC data (Jonckers et al., 2014; Gorges et al., 2017).

CONCLUSION

Recent clinical studies report mild TBI early in life is a significant risk factor for future dementia (Taylor et al., 2016;

Gardner et al., 2018; Jenkins et al., 2018; Richardson et al., 2018). The momentum exchange model developed by the National Football League to study player concussions was adapted for use in rats to produce mild concussions without neuroradiological evidence of brain contusions or changes in cognitive or motor behavior. Nonetheless, 7–8 weeks post injury there are significant changes in brain gray matter microarchitecture and function as determined by MRI. The midbrain dopaminergic system and striatum are particularly vulnerable to rmTBI. The sensitivity of the cerebellum to rmTBI corroborates findings in the clinic and may represent a key biomarker in the diagnosis of head injury. Building on the present findings can provide an opportunity to more fully characterize recovery from mild TBI, the efficacy of early intervention strategies to resolve structural and functional alterations, and the risk of dementia later in life associated with mild repetitive TBI.

ETHICS STATEMENT

All methods and procedures described were approved by the Northeastern University IACUC. The Northeastern facility is AAALAC accredited with OLAW Assurance and is registered with the USDA. All housing, care, and use followed the Guide for the Care and Use of Laboratory Animals (8th Addition) and the Animal Welfare Act.

AUTHOR CONTRIBUTIONS

CF, PK, NS, and LN: experimental design, resources, and manuscript preparation. PK, XC, SI, TM, and JS: data generation and analysis.

FUNDING

This work was funded by the Program Consortium BUILD Award (UL1MD009605/RL5MD009590/TL4MD009635) to CF. This work appeared as a preprint in BioRxiv.

ACKNOWLEDGMENTS

We want to thank Gloria Hoffman, Mary Lang, and Laporsha Kennedy from the Morgan State University for their preliminary work using immunohistochemistry to identify microglia activation following head injury.

SUPPLEMENTARY MATERIAL

The Supplementary Material for this article can be found online at: https://www.frontiersin.org/articles/10.3389/fnsys.2019.00034/full#supplementary-material

REFERENCES

Acosta, S. A., Tajiri, N., de la Pena, I., Bastawrous, M., Sanberg, P. R., Kaneko, Y., et al. (2015). Alpha-synuclein as a pathological link between chronic traumatic brain injury and Parkinson's disease. *J. Cell Physiol.* 230, 1024–1032. doi: 10.1002/jcp.24830

Acosta, S. A., Tajiri, N., Sanberg, P. R., Kaneko, Y., and Borlongan, C. V. (2017). Increased amyloid precursor protein and Tau expression manifests as key secondary cell death in chronic traumatic brain injury. *J. Cell Physiol.* 232, 665–677. doi: 10.1002/jcp.25629

Allen, G., Barnard, H., McColl, R., Hester, A. L., Fields, J. A., Weiner, M. F., et al. (2007). Reduced hippocampal functional connectivity in Alzheimer disease. *Arch. Neurol.* 64, 1482–1487.

Allen, G. I., and Tsukahara, N. (1974). Cerebrocerebellar communication systems. *Physiol. Rev.* 54, 957–1006. doi: 10.1152/physrev.1974.54.4.957

Antunes, M., and Biala, G. (2012). The novel object recognition memory: neurobiology, test procedure, and its modifications. *Cogn. Process.* 13, 93–110. doi: 10.1007/s10339-011-0430-z

Astafiev, S. V., Zinn, K. L., Shulman, G. L., and Corbetta, M. (2016). Exploring the physiological correlates of chronic mild traumatic brain injury symptoms. *Neuroimage Clin.* 11, 10–19. doi: 10.1016/j.nicl.2016.01.004

Aumann, T. D., and Horne, M. K. (1996). Ramification and termination of single axons in the cerebellothalamic pathway of the rat. *J. Comp. Neurol.* 376, 420–430.

Aumann, T. D., Rawson, J. A., Pichitpornchai, C., and Horne, M. K. (1996). Projections from the cerebellar interposed and dorsal column nuclei to the thalamus in the rat: a double anterograde labelling study. *J. Comp. Neurol.* 368, 608–619.

Aungst, S. L., Kabadi, S. V., Thompson, S. M., Stoica, B. A., and Faden, A. I. (2014). Repeated mild traumatic brain injury causes chronic neuroinflammation, changes in hippocampal synaptic plasticity, and associated cognitive deficits. *J. Cereb. Blood Flow Metab.* 34, 1223–1232. doi: 10.1038/jcbfm.2014.75

Bai, F., Zhang, Z., Watson, D. R., Yu, H., Shi, Y., Yuan, Y., et al. (2009). Abnormal functional connectivity of hippocampus during episodic memory retrieval processing network in amnestic mild cognitive impairment. *Biol. Psychiatry* 65, 951–958. doi: 10.1016/j.biopsych.2008.10.017

Bales, J. W., Wagner, A. K., Kline, A. E., and Dixon, C. E. (2009). Persistent cognitive dysfunction after traumatic brain injury: a dopamine hypothesis. *Neurosci. Biobehav. Rev.* 33, 981–1003. doi: 10.1016/j.neubiorev.2009.03.011

Barnes, C. A. (1979). Memory deficits associated with senescence: a neurophysiological and behavioral study in the rat. *J. Comp. Physiol. Psychol.* 93, 74–104. doi: 10.1037/h0077579

Bassett, D. S., and Bullmore, E. T. (2009). Human brain networks in health and disease. *Curr. Opin. Neurol.* 22, 340–347. doi: 10.1097/WCO.0b013e32832d93dd

Benjamini, Y., and Hochberg, Y. (1995). Controlling the false discovery rate: a practical and powerful approach to multiple testing. *J. R. Stat. Soc. Ser. B* 57, 289–300. doi: 10.1111/j.2517-6161.1995.tb02031.x

Bergsneider, M., Hovda, D. A., Lee, S. M., Kelly, D. F., McArthur, D. L., Vespa, P. M., et al. (2000). Dissociation of cerebral glucose metabolism and level of consciousness during the period of metabolic depression following human traumatic brain injury. *J. Neurotrauma* 17, 389–401. doi: 10.1089/neu.2000.17.389

Bergsneider, M., Hovda, D. A., McArthur, D. L., Etchepare, M., Huang, S. C., Sehati, N., et al. (2001). Metabolic recovery following human traumatic brain injury based on FDG-PET: time course and relationship to neurological disability. *J. Head Trauma Rehabil.* 16, 135–148. doi: 10.1097/00001199-200104000-00004

Bevins, R. A., and Besheer, J. (2006). Object recognition in rats and mice: a one-trial non-matching-to-sample learning task to study 'recognition memory'. *Nat. Protoc.* 1, 1306–1311. doi: 10.1038/nprot.2006.205

Bolton, A. N., and Saatman, K. E. (2014). Regional neurodegeneration and gliosis are amplified by mild traumatic brain injury repeated at 24-hour intervals. *J. Neuropathol. Exp. Neurol.* 73, 933–947. doi: 10.1097/NEN.0000000000000115

Bostan, A. C., Dum, R. P., and Strick, P. L. (2010). The basal ganglia communicate with the cerebellum. *Proc. Natl. Acad. Sci. U.S.A.* 107, 8452–8456. doi: 10.1073/pnas.1000496107

Broshek, D. K., Kaushik, T., Freeman, J. R., Erlanger, D., Webbe, F., and Barth, J. T. (2005). Sex differences in outcome following sports-related concussion. *J. Neurosurg.* 102, 856–863. doi: 10.3171/jns.2005.102.5.0856

Calcagnoli, F., Kreutzmann, J. C., de Boer, S. F., Althaus, M., and Koolhaas, J. M. (2015). Acute and repeated intranasal oxytocin administration exerts anti-aggressive and pro-affiliative effects in male rats. *Psychoneuroendocrinology* 51, 112–121. doi: 10.1016/j.psyneuen.2014.09.019

Castriotta, R. J., Wilde, M. C., Lai, J. M., Atanasov, S., Masel, B. E., and Kuna, S. T. (2007). Prevalence and consequences of sleep disorders in traumatic brain injury. *J. Clin. Sleep Med.* 3, 349–356.

Chen, C. H., Fremont, R., Arteaga-Bracho, E. E., and Khodakhah, K. (2014). Short latency cerebellar modulation of the basal ganglia. *Nat. Neurosci.* 17, 1767–1775. doi: 10.1038/nn.3868

Colvin, A. C., Mullen, J., Lovell, M. R., West, R. V., Collins, M. W., and Groh, M. (2009). The role of concussion history and gender in recovery from soccer-related concussion. *Am. J. Sports Med.* 37, 1699–1704. doi: 10.1177/0363546509332497

Crane, P. K., Gibbons, L. E., Dams-O'Connor, K., Trittschuh, E., Leverenz, J. B., Keene, C. D., et al. (2016). Association of traumatic brain injury with late-life neurodegenerative conditions and neuropathologic findings. *JAMA Neurol.* 73, 1062–1069. doi: 10.1001/jamaneurol.2016.1948

De Beaumont, L., Henry, L. C., and Gosselin, N. (2012). Long-term functional alterations in sports concussion. *Neurosurg. Focus* 33:E8. doi: 10.3171/2012.9.FOCUS12278

De Beaumont, L., Theoret, H., Mongeon, D., Messier, J., Leclerc, S., Tremblay, S., et al. (2009). Brain function decline in healthy retired athletes who sustained their last sports concussion in early adulthood. *Brain* 132(Pt 3), 695–708. doi: 10.1093/brain/awn347

Doty, R. L., Deems, D. A., and Stellar, S. (1988). Olfactory dysfunction in parkinsonism: a general deficit unrelated to neurologic signs, disease stage, or disease duration. *Neurology* 38, 1237–1244.

Doty, R. L., Stern, M. B., Pfeiffer, C., Gollomp, S. M., and Hurtig, H. I. (1992). Bilateral olfactory dysfunction in early stage treated and untreated idiopathic Parkinson's disease. *J. Neurol. Neurosurg. Psychiatry* 55, 138–142. doi: 10.1136/jnnp.55.2.138

Faden, A. I., and Loane, D. J. (2015). Chronic neurodegeneration after traumatic brain injury: alzheimer disease, chronic traumatic encephalopathy, or persistent neuroinflammation? *Neurotherapeutics* 12, 143–150. doi: 10.1007/s13311-014-0319-5

Farzaneh, F., Riederer, S. J., and Pelc, N. J. (1990). Analysis of T2 limitations and off-resonance effects on spatial resolution and artifacts in echo-planar imaging. *Magn. Reson. Med.* 14, 123–139. doi: 10.1002/mrm.1910140112

Fazio, L., Blasi, G., Taurisano, P., Papazacharias, A., Romano, R., Gelao, B., et al. (2011). D2 receptor genotype and striatal dopamine signaling predict motor cortical activity and behavior in humans. *Neuroimage* 54, 2915–2921. doi: 10.1016/j.neuroimage.2010.11.034

Fidan, E., Foley, L. M., New, L. A., Alexander, H., Kochanek, P. M., Hitchens, T. K., et al. (2018). Metabolic and structural imaging at 7 tesla after repetitive mild traumatic brain injury in immature rats. *ASN Neuro* 10:1759091418770543. doi: 10.1177/1759091418770543

Fidan, E., Lewis, J., Kline, A. E., Garman, R. H., Alexander, H., Cheng, J. P., et al. (2016). Repetitive mild traumatic brain injury in the developing brain: effects on long-term functional outcome and neuropathology. *J. Neurotrauma* 33, 641–651. doi: 10.1089/neu.2015.3958

Fox, G. B., Fan, L., LeVasseur, R. A., and Faden, A. I. (1998). Effect of traumatic brain injury on mouse spatial and nonspatial learning in the Barnes circular maze. *J. Neurotrauma* 15, 1037–1046. doi: 10.1089/neu.1998.15.1037

Gardner, R. C., Byers, A. L., Barnes, D. E., Li, Y., Boscardin, J., Yaffe, K., et al. (2018). and risk of Parkinson disease: a chronic effects of neurotrauma consortium study. *Neurology* 90, e1771–e1779. doi: 10.1212/WNL.0000000000005522

Gardner, R. C., and Yaffe, K. (2015). Epidemiology of mild traumatic brain injury and neurodegenerative disease. *Mol. Cell Neurosci.* 66(Pt B), 75–80. doi: 10.1016/j.mcn.2015.03.001

Gavett, B. E., Stern, R. A., and McKee, A. C. (2011). Chronic traumatic encephalopathy: a potential late effect of sport-related concussive and subconcussive head trauma. *Clin. Sports Med.* 30, 179–188. doi: 10.1016/j.csm.2010.09.007

Ginsberg, M. D., Zhao, W., Alonso, O. F., Loor-Estades, J. Y., Dietrich, W. D., and Busto, R. (1997). Uncoupling of local cerebral glucose metabolism and blood flow after acute fluid-percussion injury in rats. *Am. J. Physiol.* 272(6 Pt 2), H2859–H2868.

Gorges, M., Roselli, F., Muller, H. P., Ludolph, A. C., Rasche, V., and Kassubek, J. (2017). Functional connectivity mapping in the animal model: principles and applications of resting-state fMRI. *Front. Neurol.* 8:200. doi: 10.3389/fneur.2017.00200

Guilfoyle, D. N., Gerum, S. V., Sanchez, J. L., Balla, A., Sershen, H., Javitt, D. C., et al. (2013). Functional connectivity fMRI in mouse brain at 7T using isoflurane. *J. Neurosci. Methods* 214, 144–148. doi: 10.1016/j.jneumeth.2013.01.019

Guskiewicz, K. M., McCrea, M., Marshall, S. W., Cantu, R. C., Randolph, C., Barr, W., et al. (2003). Cumulative effects associated with recurrent concussion in collegiate football players: the NCAA concussion study. *JAMA* 290, 2549–2555.

Hacker, C. D., Perlmutter, J. S., Criswell, S. R., Ances, B. M., and Snyder, A. Z. (2012). Resting state functional connectivity of the striatum in Parkinson's disease. *Brain* 135(Pt 12), 3699–3711. doi: 10.1093/brain/aws281

Haines, D. E., Dietrichs, E., and Sowa, T. E. (1984). Hypothalamo-cerebellar and cerebello-hypothalamic pathways: a review and hypothesis concerning cerebellar circuits which may influence autonomic centers affective behavior. *Brain Behav. Evol.* 24, 198–220. doi: 10.1159/000121317

Hardman, J. M., and Manoukian, A. (2002). Pathology of head trauma. *Neuroimaging Clin. N. Am.* 12, 175–187.

Harrison, F. E., Hosseini, A. H., and McDonald, M. P. (2009). Endogenous anxiety and stress responses in water maze and Barnes maze spatial memory tasks. *Behav. Brain Res.* 198, 247–251. doi: 10.1016/j.bbr.2008.10.015

Heath, R. G., Dempesy, C. W., Fontana, C. J., and Myers, W. A. (1978). Cerebellar stimulation: effects on septal region, hippocampus, and amygdala of cats and rats. *Biol. Psychiatry* 13, 501–529.

Hicks, R., Soares, H., Smith, D., and McIntosh, T. (1996). Temporal and spatial characterization of neuronal injury following lateral fluid-percussion brain injury in the rat. *Acta Neuropathol.* 91, 236–246. doi: 10.1007/s004010050421

Hoogenraad, F. G., Pouwels, P. J., Hofman, M. B., Rombouts, S. A., Lavini, C., Leach, M. O., et al. (2000). High-resolution segmented EPI in a motor task fMRI study. *Magn. Reson. Imaging* 18, 405–409. doi: 10.1016/s0730-725x(00)00127-2

Hoshi, E., Tremblay, L., Feger, J., Carras, P. L., and Strick, P. L. (2005). The cerebellum communicates with the basal ganglia. *Nat. Neurosci.* 8, 1491–1493. doi: 10.1038/nn1544

Hu, X., Song, X., Yuan, Y., Li, E., Liu, J., Liu, W., et al. (2015). Abnormal functional connectivity of the amygdala is associated with depression in Parkinson's disease. *Mov. Disord.* 30, 238–244. doi: 10.1002/mds.26087

Hutson, C. B., Lazo, C. R., Mortazavi, F., Giza, C. C., Hovda, D., and Chesselet, M. F. (2011). Traumatic brain injury in adult rats causes progressive nigrostriatal dopaminergic cell loss and enhanced vulnerability to the pesticide paraquat. *J. Neurotrauma* 28, 1783–1801. doi: 10.1089/neu.2010.1723

Iannilli, E., Bitter, T., Gudziol, H., Burmeister, H. P., Mentzel, H. J., Chopra, A. P., et al. (2011). Differences in anosmic and normosmic group in bimodal odorant perception: a functional- MRI study. *Rhinology* 49, 458–463. doi: 10.4193/Rhino11.110

Impellizzeri, D., Campolo, M., Bruschetta, G., Crupi, R., Cordaro, M., Paterniti, I., et al. (2016). Traumatic brain injury leads to development of Parkinson's disease related pathology in mice. *Front. Neurosci.* 10:458. doi: 10.3389/fnins.2016.00458

Iverson, G. L. (2005). Outcome from mild traumatic brain injury. *Curr. Opin. Psychiatry* 18, 301–317.

Jafari, S., Etminan, M., Aminzadeh, F., and Samii, A. (2013). Head injury and risk of Parkinson disease: a systematic review and meta-analysis. *Mov. Disord.* 28, 1222–1229. doi: 10.1002/mds.25458

Jenkins, P. O., De Simoni, S., Bourke, N. J., Fleminger, J., Scott, G., Towey, D. J., et al. (2018). Dopaminergic abnormalities following traumatic brain injury. *Brain* 141, 797–810. doi: 10.1093/brain/awx357

Jesmanowicz, A., Bandettini, P. A., and Hyde, J. S. (1998). Single-shot half k-space high-resolution gradient-recalled EPI for fMRI at 3 Tesla. *Magn. Reson. Med.* 40, 754–762. doi: 10.1002/mrm.1910400517

Jonckers, E., Delgado y Palacios, R., Shah, D., Guglielmetti, C., Verhoye, M., and Van der Linden, A. (2014). Different anesthesia regimes modulate the functional connectivity outcome in mice. *Magn. Reson. Med.* 72, 1103–1112. doi: 10.1002/mrm.24990

Kalil, K. (1981). Projections of the cerebellar and dorsal column nuclei upon the thalamus of the rhesus monkey. *J. Comp. Neurol.* 195, 25–50. doi: 10.1002/cne.901950105

Kang, D., Sung, Y. W., and Kang, C. K. (2015). Fast imaging technique for fMRI: consecutive multishot echo planar imaging accelerated with GRAPPA technique. *Biomed. Res. Int.* 2015:394213. doi: 10.1155/2015/394213

Katzenschlager, R., and Lees, A. J. (2004). Olfaction and Parkinson's syndromes: its role in differential diagnosis. *Curr. Opin. Neurol.* 17, 417–423. doi: 10.1097/01.wco.0000137531.76491.c2

Koch, W., Teipel, S., Mueller, S., Benninghoff, J., Wagner, M., Bokde, A. L., et al. (2012). Diagnostic power of default mode network resting state fMRI in the detection of Alzheimer's disease. *Neurobiol. Aging* 33, 466–478. doi: 10.1016/j.neurobiolaging.2010.04.013

Konrad, C., Geburek, A. J., Rist, F., Blumenroth, H., Fischer, B., Husstedt, I., et al. (2011). Long-term cognitive and emotional consequences of mild traumatic brain injury. *Psychol. Med.* 41, 1197–1211. doi: 10.1017/S0033291710001728

Kulkarni, P., Kenkel, W., Finklestein, S. P., Barchet, T. M., Ren, J., Davenport, M., et al. (2015). Use of anisotropy, 3D segmented atlas, and computational analysis to identify gray matter subcortical lesions common to concussive injury from different sites on the cortex. *PLoS One* 10:e0125748. doi: 10.1371/journal.pone.0125748

Lanteaume, L., Khalfa, S., Regis, J., Marquis, P., Chauvel, P., and Bartolomei, F. (2007). Emotion induction after direct intracerebral stimulations of human amygdala. *Cereb. Cortex* 17, 1307–1313. doi: 10.1093/cercor/bhl041

Laurer, H. L., Bareyre, F. M., Lee, V. M., Trojanowski, J. Q., Longhi, L., Hoover, R., et al. (2001). Mild head injury increasing the brain's vulnerability to a second concussive impact. *J. Neurosurg.* 95, 859–870. doi: 10.3171/jns.2001.95.5.0859

Liu, M., Bachstetter, A. D., Cass, W. A., Lifshitz, J., and Bing, G. (2017). Pioglitazone attenuates neuroinflammation and promotes dopaminergic neuronal survival in the nigrostriatal system of rats after diffuse brain injury. *J. Neurotrauma* 34, 414–422. doi: 10.1089/neu.2015.4361

Losoi, H., Silverberg, N. D., Waljas, M., Turunen, S., Rosti-Otajarvi, E., Helminen, M., et al. (2016). Recovery from mild traumatic brain injury in previously healthy adults. *J. Neurotrauma* 33, 766–776. doi: 10.1089/neu.2015.4070

Lovell, M. R., Collins, M. W., Iverson, G. L., Field, M., Maroon, J. C., Cantu, R., et al. (2003). Recovery from mild concussion in high school athletes. *J. Neurosurg* 98, 296–301. doi: 10.3171/jns.2003.98.2.0296

Mainland, J. D., Johnson, B. N., Khan, R., Ivry, R. B., and Sobel, N. (2005). Olfactory impairments in patients with unilateral cerebellar lesions are selective to inputs from the contralesional nostril. *J. Neurosci.* 25, 6362–6371. doi: 10.1523/jneurosci.0920-05.2005

Manktelow, A. E., Menon, D. K., Sahakian, B. J., and Stamatakis, E. A. (2017). Working memory after traumatic brain injury: the neural basis of improved performance with methylphenidate. *Front. Behav. Neurosci.* 11:58. doi: 10.3389/fnbeh.2017.00058

Mayer, A. R., Mannell, M. V., Ling, J., Gasparovic, C., and Yeo, R. A. (2011). Functional connectivity in mild traumatic brain injury. *Hum. Brain Mapp.* 32, 1825–1835. doi: 10.1002/hbm.21151

McCrea, M., Guskiewicz, K. M., Marshall, S. W., Barr, W., Randolph, C., Cantu, R. C., et al. (2003). Acute effects and recovery time following concussion in collegiate football players: the NCAA concussion study. *JAMA* 290, 2556–2563.

McCrea, M., Hammeke, T., Olsen, G., Leo, P., and Guskiewicz, K. (2004). Unreported concussion in high school football players: implications for prevention. *Clin. J. Sport Med.* 14, 13–17. doi: 10.1097/00042752-200401000-00003

McKee, A. C., Cantu, R. C., Nowinski, C. J., Hedley-Whyte, E. T., Gavett, B. E., Budson, A. E., et al. (2009). Chronic traumatic encephalopathy in athletes: progressive tauopathy after repetitive head injury. *J. Neuropathol. Exp. Neurol.* 68, 709–735. doi: 10.1097/NEN.0b013e3181a9d503

Meabon, J. S., Huber, B. R., Cross, D. J., Richards, T. L., Minoshima, S., Pagulayan, K. F., et al. (2016). Repetitive blast exposure in mice and combat veterans causes persistent cerebellar dysfunction. *Sci. Transl. Med.* 8:321ra326. doi: 10.1126/scitranslmed.aaa9585

Meconi, A., Wortman, R. C., Wright, D. K., Neale, K. J., Clarkson, M., Shultz, S. R., et al. (2018). Repeated mild traumatic brain injury can cause acute neurologic impairment without overt structural damage in juvenile rats. *PLoS One* 13:e0197187. doi: 10.1371/journal.pone.0197187

Meehan, W. P. III, Zhang, J., Mannix, R., and Whalen, M. J. (2012). Increasing recovery time between injuries improves cognitive outcome after repetitive mild concussive brain injuries in mice. *Neurosurgery* 71, 885–891.

Menon, D. K., Schwab, K., Wright, D. W., Maas, A. I., and Demographics and Clinical Assessment Working Group of the International and Interagency Initiative toward Common Data Elements for Research on Traumatic Brain Injury and Psychological Health (2010). Position statement: definition of traumatic brain injury. *Arch. Phys. Med. Rehabil.* 91, 1637–1640. doi: 10.3766/jaaa.15123

Menon, R. S., Thomas, C. G., and Gati, J. S. (1997). Investigation of BOLD contrast in fMRI using multi-shot EPI. *NMR Biomed.* 10, 179–182.

Mesholam, R. I., Moberg, P. J., Mahr, R. N., and Doty, R. L. (1998). Olfaction in neurodegenerative disease: a meta-analysis of olfactory functioning in Alzheimer's and Parkinson's diseases. *Arch. Neurol.* 55, 84–90.

Mychasiuk, R., Hehar, H., Candy, S., Ma, I., and Esser, M. J. (2016). The direction of the acceleration and rotational forces associated with mild traumatic brain injury in rodents effect behavioural and molecular outcomes. *J. Neurosci. Methods* 257, 168–178. doi: 10.1016/j.jneumeth.2015.10.002

Nakamura, T., Hillary, F. G., and Biswal, B. B. (2009). Resting network plasticity following brain injury. *PLoS One* 4:e8220. doi: 10.1371/journal.pone.0008220

Nathan, D. E., Oakes, T. R., Yeh, P. H., French, L. M., Harper, J. F., Liu, W., et al. (2015). Exploring variations in functional connectivity of the resting state default mode network in mild traumatic brain injury. *Brain Connect.* 5, 102–114. doi: 10.1089/brain.2014.0273

Omalu, B. I., Hamilton, R. L., Kamboh, M. I., DeKosky, S. T., and Bailes, J. (2010). Chronic traumatic encephalopathy (CTE) in a national football league player: case report and emerging medicolegal practice questions. *J. Forensic Nurs.* 6, 40–46. doi: 10.1111/j.1939-3938.2009.01064.x

Onuki, Y., Van Someren, E. J., De Zeeuw, C. I., and Van der Werf, Y. D. (2015). Hippocampal-cerebellar interaction during spatio-temporal prediction. *Cereb. Cortex* 25, 313–321. doi: 10.1093/cercor/bht221

Ordek, G., Proddutur, A., Santhakumar, V., Pfister, B. J., and Sahin, M. (2014). Electrophysiological monitoring of injury progression in the rat cerebellar cortex. *Front. Syst. Neurosci.* 8:197. doi: 10.3389/fnsys.2014.00197

Palacios, E. M., Yuh, E. L., Chang, Y. S., Yue, J. K., Schnyer, D. M., Okonkwo, D. O., et al. (2017). Resting-state functional connectivity alterations associated with six-month outcomes in mild traumatic brain injury. *J. Neurotrauma* 34, 1546–1557. doi: 10.1089/neu.2016.4752

Pellegrino, R., Drechsler, E., Hummel, C., Warr, J., and Hummel, T. (2017). Bimodal odor processing with a trigeminal component at sub- and suprathreshold levels. *Neuroscience* 363, 43–49. doi: 10.1016/j.neuroscience.2017.07.030

Peskind, E. R., Petrie, E. C., Cross, D. J., Pagulayan, K., McCraw, K., Hoff, D., et al. (2011). Cerebrocerebellar hypometabolism associated with repetitive blast exposure mild traumatic brain injury in 12 Iraq war Veterans with persistent post-concussive symptoms. *Neuroimage* 54(Suppl. 1), S76–S82. doi: 10.1016/j.neuroimage.2010.04.008

Petraglia, A. L., Plog, B. A., Dayawansa, S., Chen, M., Dashnaw, M. L., Czerniecka, K., et al. (2014). The spectrum of neurobehavioral sequelae after repetitive mild traumatic brain injury: a novel mouse model of chronic traumatic encephalopathy. *J. Neurotrauma* 31, 1211–1224. doi: 10.1089/neu.2013.3255

Plassman, B. L., Havlik, R. J., Steffens, D. C., Helms, M. J., Newman, T. N., Drosdick, D., et al. (2000). Documented head injury in early adulthood and risk of Alzheimer's disease and other dementias. *Neurology* 55, 1158–1166. doi: 10.1212/wnl.55.8.1158

Poser, B. A., and Norris, D. G. (2009). Investigating the benefits of multi-echo EPI for fMRI at 7 T. *Neuroimage* 45, 1162–1172. doi: 10.1016/j.neuroimage.2009.01.007

Prins, M. L., Alexander, D., Giza, C. C., and Hovda, D. A. (2013). Repeated mild traumatic brain injury: mechanisms of cerebral vulnerability. *J. Neurotrauma* 30, 30–38. doi: 10.1089/neu.2012.2399

Qin, Y., Li, G. L., Xu, X. H., Sun, Z. Y., Gu, J. W., and Gao, F. B. (2018). Brain structure alterations and cognitive impairment following repetitive mild head impact: an in vivo MRI and behavioral study in rat. *Behav. Brain Res.* 340, 41–48. doi: 10.1016/j.bbr.2016.08.008

Rajesh, A., Cooke, G. E., Monti, J. M., Jahn, A., Daugherty, A. M., and Kramer, A. (2017). Differences in brain architecture in remote mild traumatic brain injury. *J. Neurotrauma* 34, 3280–3287. doi: 10.1089/neu.2017.5047

Richardson, J. S., Guzauskas, G. F., Fann, J. R., Temkin, N. R., Bush, N. E., Bell, K. R., et al. (2018). Economic evaluation of telephone-based concussion management for combat-related mild traumatic brain injury. *J. Telemed. Telecare* 24, 282–289. doi: 10.1177/1357633X17696586

Rogers, T. D., Dickson, P. E., Heck, D. H., Goldowitz, D., Mittleman, G., and Blaha, C. D. (2011). Connecting the dots of the cerebro-cerebellar role in cognitive function: neuronal pathways for cerebellar modulation of dopamine release in the prefrontal cortex. *Synapse* 65, 1204–1212. doi: 10.1002/syn.20960

Rowe, R. K., Ziebell, J. M., Harrison, J. L., Law, L. M., Adelson, P. D., and Lifshitz, J. (2016). Aging with traumatic brain injury: effects of age at injury on behavioral outcome following diffuse brain injury in rats. *Dev. Neurosci.* 38, 195–205. doi: 10.1159/000446773

Roy, A., Bernier, R. A., Wang, J., Benson, M., French, J. J. Jr., Good, D. C., et al. (2017). The evolution of cost-efficiency in neural networks during recovery from traumatic brain injury. *PLoS One* 12:e0170541. doi: 10.1371/journal.pone.0170541

Ruff, R. M., Iverson, G. L., Barth, J. T., Bush, S. S., Broshek, D. K., Policy, N. A. N., et al. (2009). Recommendations for diagnosing a mild traumatic brain injury: a national academy of neuropsychology education paper. *Arch. Clin. Neuropsychol.* 24, 3–10. doi: 10.1093/arclin/acp006

Sacchetti, B., Baldi, E., Lorenzini, C. A., and Bucherelli, C. (2002). Cerebellar role in fear-conditioning consolidation. *Proc. Natl. Acad. Sci.U.S.A.* 99, 8406–8411. doi: 10.1073/pnas.112660399

Sackheim, A. M., Stockwell, D., Villalba, N., Haines, L., Scott, C. L., Russell, S., et al. (2017). Traumatic brain injury impairs sensorimotor function in mice. *J. Surg. Res.* 213, 100–109. doi: 10.1016/j.jss.2017.02.016

Schofield, P. W., Moore, T. M., and Gardner, A. (2014). Traumatic brain injury and olfaction: a systematic review. *Front. Neurol.* 5:5. doi: 10.3389/fneur.2014.00005

Schroeter, M. L., Mueller, K., Arelin, K., Sacher, J., Holiga, S., Kratzsch, J., et al. (2015). Serum neuron-specific enolase is related to cerebellar connectivity: a resting-state functional magnetic resonance imaging pilot study. *J. Neurotrauma* 32, 1380–1384. doi: 10.1089/neu.2013.3163

Schutter, D. J., and van Honk, J. (2006). An electrophysiological link between the cerebellum, cognition and emotion: frontal theta EEG activity to single-pulse cerebellar TMS. *Neuroimage* 33, 1227–1231. doi: 10.1016/j.neuroimage.2006.06.055

Selwyn, R. G., Cooney, S. J., Khayrullina, G., Hockenbury, N., Wilson, C. M., Jaiswal, S., et al. (2016). Outcome after repetitive mild traumatic brain injury is temporally related to glucose uptake profile at time of second injury. *J. Neurotrauma* 33, 1479–1491. doi: 10.1089/neu.2015.4129

Sengupta, P. (2013). The laboratory rat: relating its age with Human's. *Int. J. Prev. Med.* 4, 624–630.

Shenton, M. E., Hamoda, H. M., Schneiderman, J. S., Bouix, S., Pasternak, O., Rathi, Y., et al. (2012). Review of magnetic resonance imaging and diffusion tensor imaging findings in mild traumatic brain injury. *Brain Imaging Behav.* 6, 137–192. doi: 10.1007/s11682-012-9156-5

Shultz, S. R., Bao, F., Omana, V., Chiu, C., Brown, A., and Cain, D. P. (2012). Repeated mild lateral fluid percussion brain injury in the rat causes cumulative long-term behavioral impairments, neuroinflammation, and cortical loss in an animal model of repeated concussion. *J. Neurotrauma* 29, 281–294. doi: 10.1089/neu.2011.2123

Silverberg, N. D., Lange, R. T., Millis, S. R., Rose, A., Hopp, G., Leach, S., et al. (2013). Post-concussion symptom reporting after multiple mild traumatic brain injuries. *J. Neurotrauma* 30, 1398–1404. doi: 10.1089/neu.2012.2827

Sivanandam, T. M., and Thakur, M. K. (2012). Traumatic brain injury: a risk factor for Alzheimer's disease. *Neurosci. Biobehav. Rev.* 36, 1376–1381.

Smith, R., and Lane, R. D. (2015). The neural basis of one's own conscious and unconscious emotional states. *Neurosci. Biobehav. Rev.* 57, 1–29. doi: 10.1016/j.neubiorev.2015.08.003

Snider, R. S., and Maiti, A. (1976). Cerebellar contributions to the Papez circuit. *J. Neurosci. Res.* 2, 133–146. doi: 10.1002/jnr.490020204

Swisher, J. D., Sexton, J. A., Gatenby, J. C., Gore, J. C., and Tong, F. (2012). Multishot versus single-shot pulse sequences in very high field fMRI: a comparison using retinotopic mapping. *PLoS One* 7:e34626. doi: 10.1371/journal.pone.0034626

Taylor, C. A., Bell, J. M., Breiding, M. J., and Xu, L. (2017). Traumatic brain injury-related emergency department visits, hospitalizations, and deaths - United States, 2007 and 2013. *MMWR Surveill. Summ.* 66, 1–16. doi: 10.15585/mmwr.ss6609a1

Taylor, K. M., Saint-Hilaire, M. H., Sudarsky, L., Simon, D. K., Hersh, B., Sparrow, D., et al. (2016). Head injury at early ages is associated with risk of Parkinson's disease. *Parkinsonism Relat. Disord.* 23, 57–61. doi: 10.1016/j.parkreldis.2015.12.005

Teipel, S. J., Grothe, M., Lista, S., Toschi, N., Garaci, F. G., and Hampel, H. (2013). Relevance of magnetic resonance imaging for early detection and diagnosis of Alzheimer disease. *Med. Clin. N. Am.* 97, 399–424. doi: 10.1016/j.mcna.2012.12.013

Teune, T. M., van der Burg, J., van der Moer, J., Voogd, J., and Ruigrok, T. J. (2000). Topography of cerebellar nuclear projections to the brain stem in the rat. *Prog. Brain Res.* 124, 141–172. doi: 10.1016/s0079-6123(00)24014-4

Vergara, V. M., Mayer, A. R., Damaraju, E., Kiehl, K. A., and Calhoun, V. (2017). Detection of mild traumatic brain injury by machine learning classification using resting state functional network connectivity and fractional anisotropy. *J. Neurotrauma* 34, 1045–1053. doi: 10.1089/neu.2016.4526

Viano, D. C., Hamberger, A., Bolouri, H., and Saljo, A. (2009). Concussion in professional football: animal model of brain injury–part 15. *Neurosurgery* 64, 1162–1173; discussion1173. doi: 10.1227/01.NEU.0000345863.99099.C7

Weil, Z. M., Gaier, K. R., and Karelina, K. (2014). Injury timing alters metabolic, inflammatory and functional outcomes following repeated mild traumatic brain injury. *Neurobiol. Dis.* 70, 108–116. doi: 10.1016/j.nbd.2014.06.016

Williams, A. J., Hartings, J. A., Lu, X. C., Rolli, M. L., Dave, J. R., and Tortella, F. C. (2005). Characterization of a new rat model of penetrating ballistic brain injury. *J. Neurotrauma* 22, 313–331. doi: 10.1089/neu.2005.22.313

Witter, L., and De Zeeuw, C. I. (2015). Regional functionality of the cerebellum. *Curr. Opin. Neurobiol.* 33, 150–155. doi: 10.1016/j.conb.2015.03.017

Wortman, R. C., Meconi, A., Neale, K. J., Brady, R. D., McDonald, S. J., Christie, B. R., et al. (2018). Diffusion MRI abnormalities in adolescent rats given repeated mild traumatic brain injury. *Ann. Clin. Transl. Neurol.* 5, 1588–1598. doi: 10.1002/acn3.667

Wright, D. K., O'Brien, T. J., Shultz, S. R., and Mychasiuk, R. (2017). Sex matters: repetitive mild traumatic brain injury in adolescent rats. *Ann. Clin. Transl. Neurol.* 4, 640–654. doi: 10.1002/acn3.441

Wright, D. K., Trezise, J., Kamnaksh, A., Bekdash, R., Johnston, L. A., Ordidge, R., et al. (2016). Behavioral, blood, and magnetic resonance imaging biomarkers of experimental mild traumatic brain injury. *Sci. Rep.* 6:28713. doi: 10.1038/srep28713

Wu, T., Wang, L., Chen, Y., Zhao, C., Li, K., and Chan, P. (2009). Changes of functional connectivity of the motor network in the resting state in Parkinson's disease. *Neurosci. Lett.* 460, 6–10. doi: 10.1016/j.neulet.2009.05.046

Xiong, Y., Mahmood, A., and Chopp, M. (2013). Animal models of traumatic brain injury. *Nat. Rev. Neurosci.* 14, 128–142. doi: 10.1038/nrn3407

Yoshino, A., Hovda, D. A., Kawamata, T., Katayama, Y., and Becker, D. P. (1991). Dynamic changes in local cerebral glucose utilization following cerebral conclusion in rats: evidence of a hyper- and subsequent hypometabolic state. *Brain Res.* 561, 106–119. doi: 10.1016/0006-8993(91)90755-k

Yoshiyama, Y., Uryu, K., Higuchi, M., Longhi, L., Hoover, R., Fujimoto, S., et al. (2005). Enhanced neurofibrillary tangle formation, cerebral atrophy, and cognitive deficits induced by repetitive mild brain injury in a transgenic tauopathy mouse model. *J. Neurotrauma* 22, 1134–1141. doi: 10.1089/neu.2005.22.1134

Zhang, Y., Wu, I. W., Buckley, S., Coffey, C. S., Foster, E., Mendick, S., et al. (2015). Diffusion tensor imaging of the nigrostriatal fibers in Parkinson's disease. *Mov. Disord.* 30, 1229–1236. doi: 10.1002/mds.26251

Conflict of Interest Statement: CF has a financial interest in Animal Imaging Research, the company that makes the RF electronics and holders for animal imaging. NS is a consultant for Azevan Pharmaceuticals, Inc., serves as an officer, and holds equity in the company.

The remaining authors declare that the research was conducted in the absence of any commercial or financial relationships that could be construed as a potential conflict of interest.

frontiers in Systems Neuroscience

REVIEW
published: 21 August 2019
doi: 10.3389/fnsys.2019.00040

Whisker-Mediated Touch System in Rodents: From Neuron to Behavior

Mehdi Adibi[1,2,3]*

[1] School of Psychology, University of New South Wales, Sydney, NSW, Australia, [2] Tactile Perception and Learning Lab, International School for Advanced Studies (SISSA), Trieste, Italy, [3] Padua Neuroscience Center, University of Padua, Padua, Italy

A key question in systems neuroscience is to identify how sensory stimuli are represented in neuronal activity, and how the activity of sensory neurons in turn is "read out" by downstream neurons and give rise to behavior. The choice of a proper model system to address these questions, is therefore a crucial step. Over the past decade, the increasingly powerful array of experimental approaches that has become available in non-primate models (e.g., optogenetics and two-photon imaging) has spurred a renewed interest for the use of rodent models in systems neuroscience research. Here, I introduce the rodent whisker-mediated touch system as a structurally well-established and well-organized model system which, despite its simplicity, gives rise to complex behaviors. This system serves as a behaviorally efficient model system; known as nocturnal animals, along with their olfaction, rodents rely on their whisker-mediated touch system to collect information about their surrounding environment. Moreover, this system represents a well-studied circuitry with a somatotopic organization. At every stage of processing, one can identify anatomical and functional topographic maps of whiskers; "barrelettes" in the brainstem nuclei, "barreloids" in the sensory thalamus, and "barrels" in the cortex. This article provides a brief review on the basic anatomy and function of the whisker system in rodents.

Keywords: rodents, whisker system, vibrissae, vibrissal system, somatosensory, barrel field, thalamic barreloids

OPEN ACCESS

Edited by:
Ilan Lampl,
Weizmann Institute of Science, Israel

Reviewed by:
Vassiliy Tsytsarev,
University of Maryland, College Park, United States
Sylvain Crochet,
École Polytechnique Fédérale de Lausanne, Switzerland
Mickey London,
Hebrew University of Jerusalem, Israel

***Correspondence:**
Mehdi Adibi
m.adibi@unsw.edu.au

Received: *22 August 2018*
Accepted: *02 August 2019*
Published: *21 August 2019*

Citation:
Adibi M (2019) Whisker-Mediated Touch System in Rodents: From Neuron to Behavior. Front. Syst. Neurosci. 13:40. doi: 10.3389/fnsys.2019.00040

1. INTRODUCTION

A fundamental goal of systems neuroscience is to identify how sensory stimuli are represented in neuronal activity, and how the activity of sensory neurons is "read out" by downstream neuronal structures to generate behavior. Researchers dissect this goal into the following questions:

1. What elemental features of sensory stimuli are encoded in the neuronal activity of sensory neurons?
2. How is each elemental feature represented in the activity of sensory neurons?
3. How do the downstream neuronal areas decode the activity of sensory neurons?
4. How does spatial and temporal context affect the efficiency with which single neurons and neuronal ensembles encode sensory stimuli?
5. How does the activity of neurons give rise to perception and ultimately behavior?

Over the past decade, the increasingly powerful array of experimental approaches such as optogenetics and two-photon imaging which has become available in non-primate models, particularly in rodents, has spurred a renewed interest for the use of rodents in neuroscience research. The aim of this article is to introduce the rodent whisker-mediated touch system as a model system suitable for investigating the fundamental questions in systems neuroscience.

This model serves as an anatomically well-established and behaviorally efficient system; as nocturnal animals, rodents rely on their whisker-mediated touch system to collect information about their surrounding environment. Moreover, this system represents a well-studied circuitry with an elegant structural organization. At every stage of processing, one can identify anatomical and functional topographic maps of whiskers. These clusters are referred to as "barrelettes" in the brainstem nuclei, "barreloids" in the thalamus, and "barrels" in the cortex. Mapping studies have revealed that whisker-related areas occupy a relatively large proportion of neural tissue at trigeminal medullar level (28%) (Nord, 1967), at the level of thalamic sensory nuclei (27%) (Emmers, 1965), and at the cortical level (20%) (Welker, 1971).

In the following sections, I first provide a brief introduction to the basic anatomy and then the function of the whisker system in rodents.

2. THE WHISKER-MEDIATED TOUCH SYSTEM

2.1. Vibrissae and Follicles

Rat vibrissae, or whiskers, form a grid-wise layout on either side of the snout. The main distinction of the vibrissae from ordinary hairs is their large follicles which contain dense nerve terminals and sensory receptors. As mechanical transducers, the vibrissae mediate the transfer of the touch signal into these receptors. The vibrissae are categorized into two classes: (i) the micro-vibrissae, which are short and thin hairs around the nose tip, and (ii) macro-vibrissae, which are the long stiff mystacial hairs caudal to micro-vibrissae on the whisker pad (Brecht et al., 1997). Macro-vibrissae consist of four follicles in rows A and B, seven to nine follicles in row C, D and E, and four straddlers ($\alpha, \beta, \gamma, \delta$) straddling between rows caudal to the mystacial pad (see **Figure 1**).

These two classes of vibrissae are believed to be functionally distinct (Vincent, 1912; Brecht et al., 1997); the macro-vibrissae transmit spatial information such as localization in space, as they sweep the environment by intrinsic muscles. However micro-vibrissae are considered to be involved in acquisition of detailed tactile information for object and texture recognition. Nevertheless, there is evidence from behavioral studies demonstrating that rodents are able to perform texture and vibration discrimination tasks using their macro-vibrissae (Carvell and Simons, 1990; Krupa et al., 2001; von Heimendahl et al., 2007; Adibi and Arabzadeh, 2011; Morita et al., 2011; Adibi et al., 2012).

The nerve terminals and mechanoreceptors around the vibrissa shaft are of various types, morphologies and distributions (Melaragno and Montagna, 1953) including Merkel cell-neurite complexes, lanceolate receptors, Ruffini corpuscles—sometimes referred to as reticular endings—and free nerve endings (Renehan and Munger, 1986; Rice et al., 1986; Ebara et al., 2002). Different receptors show different tuning properties and sensitivity to a variety of tactile stimulus parameters such as amplitude, frequency, duration, velocity, acceleration and direction of whisker deflections/motion (Fitzgerald, 1940; Kerr and Lysak, 1964; Zucker and Welker, 1969; Hahn, 1971; Pubols et al., 1973; Dykes, 1975; Gibson and Welker, 1983a,b; Lichtenstein et al., 1990). These receptors also exhibit different profiles of adaptation. Merkel cells are the most prominent mechanoreceptors. These receptors adapt slowly to sustained whisker deflections, whereas lanceolate receptors and simple corpuscles are rapidly-adapting (Iggo and Muir, 1969; Zucker and Welker, 1969; Munger et al., 1971; Gottschaldt et al., 1973; Pubols et al., 1973; Dykes, 1975).

Each follicle is innervated by 150–200 myelinated and 100 unmyelinated distal axons of trigeminal ganglion neurons (Lee and Woolsey, 1975; Waite and Cragg, 1982; Renehan and Munger, 1986; Rice et al., 1986, 1997; Henderson and Jacquin, 1995). These axons arborize around the hair shaft, sensing movements in different directions.

2.2. Whisking

Whisking is the rhythmic cyclic vibrissae sweeping action, consisting of repetitive forward (protraction) and backward (retraction) movements at an average frequency of about 8 Hz (Welker, 1964; Wineski, 1983; Carvell et al., 1991). Whisking is often synchronous to respiratory, head, and nose movements, suggesting coordination of activity among many muscle groups (Welker, 1964; Cao et al., 2012). Berg and Kleinfeld (2003) observed two different patterns of whisking; the first pattern, referred to as the exploratory whisking, consists of wide-angle sweeps with a frequency range of 1 to 5 Hz in bouts of 1 to 10 s. The whisking frequency within a bout remains remarkably constant, while it changes between bouts (Vincent, 1912; Welker, 1964; Wineski, 1983; Carvell and Simons, 1990; Carvell et al., 1991). The second pattern of whisking consists of small-amplitude high-frequency (ranging from 15 to 25 Hz) sweeps for a period of 0.5 to 1 s while whiskers are thrust forward in a dense pattern (Carvell and Simons, 1990, 1995; Berg and Kleinfeld, 2003). This pattern resembles the dense focalized arrangement of photoreceptors in the retina fovea, and is therefore referred to as "foveal whisking". Movement of the follicle is controlled by the facial motor nerve. Macro-vibrissae are moved by two sets of striated musculatures (Dörfl, 1982; Wineski, 1983, 1985); the intrinsic and extrinsic muscles. Intrinsic muscles lack a bony attachment and have their origin and insertions in the skin (Dörfl, 1982). They are associated with individual whiskers and generate the forward whisker motion (protraction) by pulling the base of the follicle backwards (Carvell et al., 1991). Extrinsic muscles are located superficially in the mystacial pad with no direct connection with follicles. They move all whiskers together (Wineski, 1983, 1985; Dörfl, 1985; Carvell et al., 1991). On the basis of anatomical observations, Dörfl (1982, 1985) and Wineski (1985) concluded that mystacial pad muscles move the whiskers forward (protraction), whereas backward motion (retraction) is mainly a result of the elastic properties of the facial tissue, and is therefore passive. A more recent finding, however, demonstrated that retraction is under the active muscular control as well (Berg and Kleinfeld, 2003).

Whisking is controlled by a neuronal oscillator located in the vibrissa-related region of intermediate reticular formation

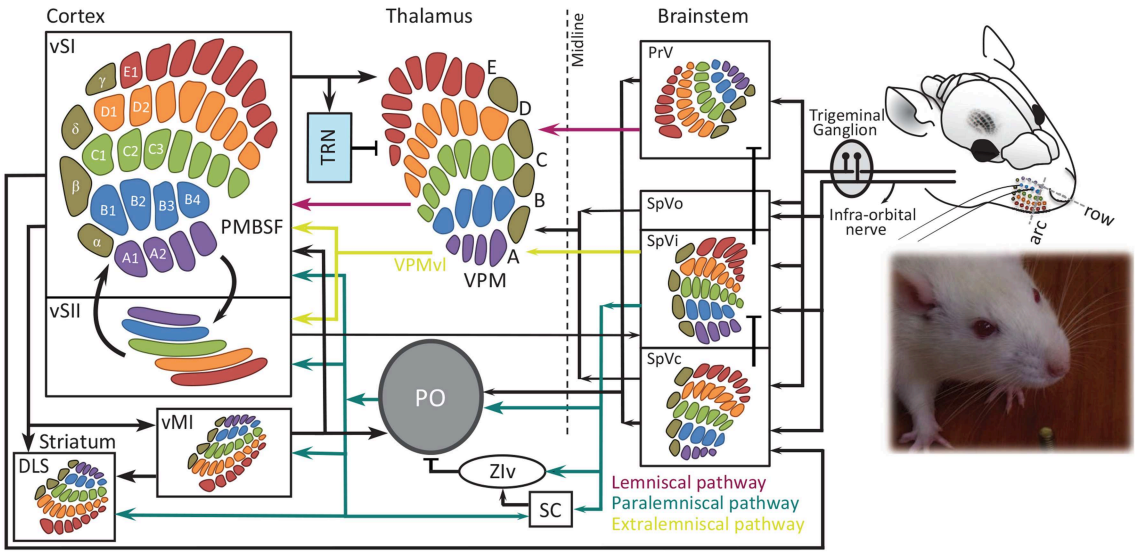

FIGURE 1 | Schematic representation of whisker-barrel system. Each whisker is identified by a unique letter-number combination corresponding to its row (A to E from dorsal to ventral) and arc (identified by numbers 1, 2 and etcetera from caudal to rostral), with α, β, γ, and δ straddlers between rows. Colors indicate rows. Barrel, barreloid and barrelets are redrawn from Durham and Woolsey (1984). PMBSF, posterior-medial barrel sub-field; PO, posterior thalamic nucleus; PrV, principal trigeminal nucleus; SC, superior colliculus; SpVi, spinal trigeminal nuclei pars interpolaris; SpVo, pars oralis; SpVc, pars caudalis; TRN, thalamic reticular nucleus; VPM, ventro-posterior medial nucleus; vMI, vibrissal primary motor cortex; vSI, vibrissal primary somatosensory cortex; vSII, secondary somatosensory cortex with the somatotopic map from Benison et al. (2007); DLS, dorsolateral striatum; Zlv, ventral zona inserta. The evidence for somatotopic map in vM1 is provided in Ferezou et al. (2007) and Sreenivasan et al. (2016).

of the medulla (vIRt) (Moore et al., 2013, 2014; Deschênes et al., 2016). This region includes facial premotor neurons and neurons that their spiking activity is either in phase or in anti-phase with whisking protraction. Selective lesions in vIRt abolish whisking on the side of the lesion, and activation of the vIRt by iontophoretic injection of kainic acid (KA) induces long episodes of whisking under light ketamine anesthesia (Moore et al., 2014). Glycinergic/GABAergic neurons in vIRt rhythmically inhibit vibrissa facial motoneurons innervating the intrinsic muscles (Deschênes et al., 2016), suggesting that rhythmic whisking is driven by inhibition. During whisking, the intrinsic muscles protracting individual whiskers follow the whisking oscillation, while extrinsic muscles that move the mystacial pad follow the breathing rhythm. Both rhythms are phase-locked during sniffing (rapid rhythmic breathing) (Deschênes et al., 2012; Kleinfeld et al., 2014). This is compatible with the unidirectional connections from the pre-Bötzinger complex—the inspiratory oscillator for respiration located in medulla adjacent to IRt (Feldman and Kam, 2015)—to vIRt, revealing the contribution of pre-Bötzinger complex to the mystacial pad control by driving the extrinsic muscles together with the potential contribution of putative parafacial neurons that receive their input from pre-Bötzinger complex (Deschênes et al., 2016). There are no bilateral vIRt to vIRt connections. Thus, the bilateral synchronization of whisking is mediated by the medullary commissural fibers connecting the left and right pre-Bötzinger complexes (Deschênes et al., 2016).

Whiskers on the right and left sides can move asymmetrically and asynchronously (Knutsen et al., 2006; Towal and Hartmann, 2008). Additionally, rostral and caudal whiskers on a single side of the snout can sometimes move independently. Recently, using a three-dimensional model of the vibrissal array, Huet and Hartmann (2014) quantified the search space during whisking and protraction. According to their calculations, the parabolic intrinsic curvature of the whiskers increases the volume of the search space by over 40% compared to that of the straight whiskers, while the elevation—whisker's angle relative to the horizontal plane—and torsion—torsional rotation of a whisker about its own axis—had modest effect on the search space. Elevation and torsion, however, affect the trajectory of the whisker tips. Dynamics of whisker movement reveal a rodent's expectations about the environment (Mitchinson et al., 2007; Grant et al., 2009). During locomotion, direction and speed of running are coupled with average whisker position (Towal and Hartmann, 2006, 2008; Mitchinson et al., 2011; Sofroniew et al., 2014). The fine-scale kinematics of the whisking motion in freely moving rodents, however, is difficult to characterize. Machine learning techniques such as deep learning (Hong et al., 2015), visually enhanced whiskers for tracking using florescent dyes (Rigosa et al., 2017) and precise controlled locomotion in virtual reality for head-fixed animal (Sofroniew et al., 2014) are promising future approaches for high precision characterization of whisker motion kinematics during locomotion.

2.3. Trigeminal Ganglion

Trigeminal ganglion (also called semilunar ganglion) consists of the cell bodies of pseudo-unipolar neurons with their proximal axons innervating the ipsilateral brainstem trigeminal complex

(BTC) (Vincent, 1913; Ma and Woolsey, 1984) and their distal axons innervating the vibrissae follicles. Each ganglion cell innervates only one whisker follicle (Fitzgerald, 1940; Zucker and Welker, 1969; Dykes, 1975; Gibson and Welker, 1983a; Rice et al., 1986; Lichtenstein et al., 1990). The trigeminal ganglion is somatotopically organized with caudal arcs represented dorsally, and dorsal rows represented medially (Zucker and Welker, 1969; Lichtenstein et al., 1990). Early studies indicate that a great majority of the ganglion cells are slowly adapting (Fitzgerald, 1940; Kerr and Lysak, 1964; Zucker and Welker, 1969; Lichtenstein et al., 1990, but see Pubols et al., 1973; Gibson and Welker, 1983b). The rapidly adapting ganglion cells have generally higher velocity thresholds (Zucker and Welker, 1969; Lichtenstein et al., 1990). Different trigeminal ganglion units show various tuning properties, with evidence suggesting sensitivity to the following parameters: amplitude, frequency, duration, velocity, acceleration and direction of whisker deflections/motion (Fitzgerald, 1940; Kerr and Lysak, 1964; Zucker and Welker, 1969; Hahn, 1971; Pubols et al., 1973; Dykes, 1975; Gibson and Welker, 1983a,b; Lichtenstein et al., 1990). These neurons are highly sensitive to whisker deflection with over 50% of units responding to $<1^\circ$ of whisker deflection (Gibson and Welker, 1983a). The spontaneous activity of these units is considered to be zero (Zucker and Welker, 1969; Gibson and Welker, 1983a; Lichtenstein et al., 1990), and any discharge is potentially attributed to the high sensitivity of the units to tiny movements such as pneumatic vibrations, mechanical hysteresis of hair shaft, or tissue damage caused by microelectrode penetration (Gibson and Welker, 1983a).

2.4. Brainstem Trigeminal Complex (BTC)

Traditionally, the whisker-recipient trigeminal complex in the brainstem is subdivided into the principal sensory nucleus (PrV) and the spinal nucleus (SpV). The latter is further subdivided rostro-caudally into 3 sub-nuclei: oralis (SpVo), interpolaris (SpVi) and caudalis (SpVc) (Arvidsson, 1982; Ma and Woolsey, 1984). Trigeminal nuclei neurons receive inputs from trigeminal ganglion cells and form discrete aggregated neuronal clusters—called barrelettes—in each nucleus except for SpVo (Erzurumlu and Killackey, 1980; Durham and Woolsey, 1984; Bates and Killackey, 1985; Chiaia et al., 1991; Ma, 1991; Jacquin et al., 1993). Brainstem barrelettes preserve the somatotopic organization of whiskers on the mystacial pad (Belford and Killackey, 1979; Hayashi, 1980; Arvidsson, 1982). Each barrelette is about 55 μm in diameter and 1.2 mm long along the rostro-caudal direction and contains 160–200 neurons (Timofeeva et al., 2003). The PrV and SpVi sub-nuclei provide the majority of the projections to the thalamus. Similar to first-order neurons in trigeminal ganglion, the more sensitive BTC units (with low velocity thresholds) were slowly adapting, whereas the less sensitive units (high velocity thresholds) were rapidly adapting.

A majority of PrV barrelette neurons have barrelette-bounded dendritic trees (Jacquin et al., 1993; Veinante and Deschênes, 1999). These neurons mainly project into single barreloids—neuronal aggregates representing individual whiskers—of the ventro-posterior medial nucleus (VPM) in the contralateral thalamus (Jacquin et al., 1988; Veinante and Deschênes, 1999). Other groups of neurons in PrV with large multipolar somata and expansive dendritic branches spread over multiple barrelettes (Jacquin et al., 1988; Jacquin and Rhoadesi, 1990; Veinante and Deschênes, 1999), and also respond to multiple whiskers. This population mainly projects into the posterior thalamic nucleus (POm) in thalamus, tectum, superior colliculus, zona incerta, the medial part of the medial geniculate nucleus (MGm), inferior olive and medial dorsal part of VPM (VPMdm) (Huerta et al., 1983; Bruce et al., 1987; Bennett-Clarke et al., 1992; Van Ham and Yeo, 1992; Williams et al., 1994; Veinante and Deschênes, 1999). The electrophysiological studies identified two broad classes of neurons in PrV; tonic neurons which represent a single whisker, and phasic units which are driven by single or multiple whiskers (Shipley, 1974; Veinante and Deschênes, 1999; Minnery and Simons, 2003; Minnery et al., 2003).

Neurons in SpVi spread their dendritic arbors into a broader area across multiple barrelettes, and thus respond to multiple whiskers (Woolston et al., 1982; Jacquin et al., 1986). These neurons project to different brain areas, such as ventrobasal complex (mainly ventro-lateral VPM, VPMvl), the zona incerta, superior colliculus, medial geniculate nucleus, cerebellum and spinal cord (Erzurumlu and Killackey, 1980; Huerta et al., 1983; Silverman and Kruger, 1985; Jacquin et al., 1989; Van Ham and Yeo, 1992; Williams et al., 1994). SpVc also projects to VPMvl similar to the thin axons of SpVi. SpVo sends a few axons only to POm (Veinante et al., 2000).

2.5. Thalamus

VPM, POm and the intralaminar thalamic nuclei form the major thalamic targets of second-order neurons of brainstem trigeminal complex (Williams et al., 1994; Diamond, 1995; Veinante and Deschênes, 1999). The vibrissae representation area in VPM is somatotopically organized into discrete finger-like structures, called barreloids (van der Loos, 1976). Barreloids are oblong cylinder-like structures, with a length of 500–900 μm and contain 250 to 300 neurons each (van der Loos, 1976; Saporta and Kruger, 1977; Land et al., 1995; Timofeeva et al., 2003; Oberlaender et al., 2012). The size of the barreloids is positively correlated with the length of whiskers (Haidarliu and Ahissar, 2001). Cells within a barreloid have receptive fields composed of one principal and several surrounding whiskers (Friedberg et al., 1999). POm is more homogeneous than VPM, with no barreloid-like structures. However, there is evidence that POm is organized topographically (Diamond et al., 1992; Alloway et al., 2003). Compared to VPM cells, the receptive field of POm neurons is larger (6–8 whiskers) (Diamond et al., 1992). Moreover, POm neurons show a weaker response to single whisker deflections than VPM neurons do, and unlike VPM neurons, POm neurons exhibit less preference to a particular principal whisker (Diamond et al., 1992). Instead, POm neurons are strongly driven by simultaneous disturbance of multiple whiskers.

Thalamic barreloids receive three main inputs:

1. an ascending excitatory input from the principal trigeminal nucleus (PrV),

2. an excitatory corticothalamic input from the barrel field in the primary somatosensory cortex (SI),
3. an inhibitory input from the thalamic reticular nucleus.

In all of these pathways, terminal fields of axons are mainly confined to the barreloid representing the corresponding principal whisker of their receptive field (Williams et al., 1994; Veinante and Deschênes, 1999; Desilets-Roy et al., 2002; Varga et al., 2002). The distal dendritic arbors of a proportion of VPM cells, however, spread in the surrounding barreloids, leading to a cross-whisker interaction (Varga et al., 2002). In contrast to the sensory-thalamic nuclei for other modalities, there are few, if any, dendrodendritic synapses and no local axon collaterals and inhibitory interneurons in rat VPM (Barbaresi et al., 1986; Harris, 1986).

Afferents of VPMdm neurons of thalamic barreloids arborize in the corresponding neuronal aggregates—barrels—in layer IV of primary somatosensory cortex and form a one-to-one connection between the VPM barreloids and cortical barrels (Herkenham, 1980; Jensen and Killackey, 1987; Chmielowska et al., 1989; Lu and Lin, 1993). Multi-barrel projections of VPM neurons have never been observed. However, some axonal innervations into septal regions surrounding the barrels were found. Thalamic reticular nucleus and the upper part of layer VI of barrel field in SI are innervated by collaterals of the ascending projections from VPM (Jones, 1975; Herkenham, 1980; Jensen and Killackey, 1987; Chmielowska et al., 1989; Lu and Lin, 1993). The VPMvl neurons do not directly project to the barrels. They receive presynaptic inputs from the caudal division of SpVi and branch their axons in the secondary somatosensory cortex (SII) as well as septal and dysgranular zone in SI (Pierret et al., 2000) and form the extralemniscal pathway (Yu et al., 2006). An additional ascending pathway parallel to lemniscal pathway originates from multi-whisker PrV neurons passing through the head of the thalamic barreloids (Urbain and Deschênes, 2007). The neurons in the head of barreloids have multi-whisker receptive fields, innervate layer 4 septa and receive corticothalamic feedback from layer 6 of vibrissal MI (Urbain and Deschênes, 2007; Furuta et al., 2009). Hence it suggests this pathway is involved in relaying information related to the phase of whisking.

POm projects to almost all sensory-motor areas of the neocortex, including the primary somatosensory, secondary somatosensory (SII), perirhinal, insular and motor cortices, and to a lesser extent to thalamic reticular nucleus (Deschênes et al., 1998). The laminar distribution of the terminal fields of POm projection to cortex are mainly to layers Va and I (Deschênes et al., 1998). Similarly, POm axon terminals in SI are distributed from upper layer V to layer I of the dysgranular zone and interbarrel septa, as well as in layers V and I of the barrels (Herkenham, 1986; Koralek et al., 1988; Lu and Lin, 1993; Deschênes et al., 1998).

The thalamic reticular nucleus (TRN) with ventrobasal thalamic nuclei forms an inhibitory feedback loop which is believed to play role in thalamic spindling (Steriade et al., 1985; Fuentealba and Steriade, 2005), sleep-related thalamocortical oscillations (Steriade et al., 1993; Pinault, 2004; Fernández et al., 2018b), arousal (Steriade et al., 1986, 1993; Lewis et al., 2015), and selective attention (Skinner and Yingling, 1977; Crick, 1984). Optogenetic activation of TRN switches the thalamocortical firing pattern from tonic to bursting and enhances cortical spindles and delta waves (Halassa et al., 2011; Lewis et al., 2015). Neurons in the reticular nucleus receive vibrissae-related input from cortical Layer VI neurons in SI (Bourassa et al., 1995), collaterals from thalamocortical neurons in VPM and POm (Harris, 1987), as well as inputs from neighboring neurons in reticular nucleus (Landisman et al., 2002). In turn, they send their GABAergic inhibitory projections back to ventrobasal nucleus and POm (Scheibel and Scheibel, 1966; Pinault et al., 1995; Lam and Sherman, 2007). These inhibitory back-projections can account for the inter-barreloid inhibition in VPM (Desilets-Roy et al., 2002; Lavallée and Deschênes, 2004). While the topographic organization of the reticular neurons that project to VPM is somatotopic, no somatotopic map was found in the reticular neurons projecting to POm (Pinault et al., 1995).

In addition to thalamic reticular nucleus, a group of thalamic nuclei—termed extra-reticular inhibitory system—innervate POm with prominent GABAergic inhibitory projections (Bokor et al., 2005; Lavallée et al., 2005). The extra-reticular inhibitory system includes the anterior pretectal nucleus (APT) (Bokor et al., 2005), zona incerta (Barthó et al., 2002; Trageser and Keller, 2004; Lavallée et al., 2005) and pars reticulate division of substantia nigra (Buzsaki, 2009). Zona incerta (ZI) and APT are reciprocally connected, both project to PO and brainstem motor centers and receive layer V cortical inputs (Terenzi et al., 1995; May et al., 1997). ZI receives direct whisker input from both PrV and SpVi (Kolmac et al., 1998; Simpson et al., 2008) in addition to input from SI (Mitrofanis and Mikuletic, 1999; Barthó et al., 2007). Neurons in the dorsal and ventral divisions of ZI exhibit multi-whisker receptive fields (Nicolelis et al., 1992) with partial somatotopy in dorsal division and a complete somatotopic organization in ventral division (Nicolelis et al., 1992; Shaw and Mitrofanis, 2002). The ventral division of the zona incerta (ZIv) receives the main input from SpVi (Kolmac et al., 1998) and serves as a relay by feed-forward GABAergic inhibition of thalamocortical neurons in higher order thalamic nuclei including the paralemniscal pathway and POm for whisker-related motor activity (Trageser and Keller, 2004; Lavallée et al., 2005). The activation of vibrissal motor cortex suppresses vibrissal responses in ZIv (Urbain and Deschênes, 2007), providing a dis-inhibition mechanism for sensory gating in higher order thalamic nuclei during whisker-related motor activity and active touch. For a thorough review refer to Mitrofanis (2005).

2.6. Barrel Field Cortex

The cortical vibrissae representation in rodents is formally referred to as the posterior-medial barrel sub-field (PMBSF) and occupies about 20% of the somatosensory cortex (Zucker and Welker, 1969; Welker, 1971). The cortex is organized in 6 layers (**Figure 2**). In rodents, Layer IV of the vibrissae region of primary somatosensory cortex—referred to as the granular zone—contains anatomically distinguishable clusters of neurons called "barrels" (Woolsey and van der Loos, 1970).

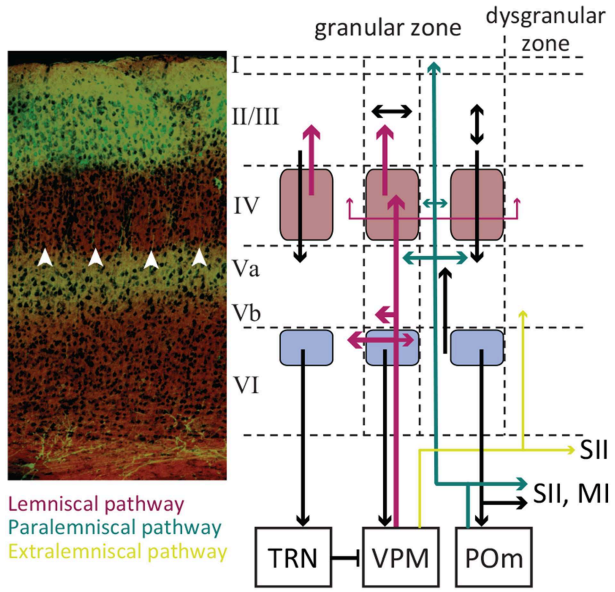

FIGURE 2 | The laminar organization of SI. A coronal section of the somatosensory cortex with cresyl violet Nissl Staining (left panel). The white arrowheads indicate barrels in layer IV. Excitatory neurons in layer II/III are GFP labeled with their terminals in Layer Va. The laminar pathway containing glutamatergic excitatory projections from VPM to layer IV and sparsely to layers Vb and VI (labeled red). The paralaminar pathway containing the projections from POm to layer Va and I (labeled cyan). The pink boxes represent the barrels, and the light purple boxes represent infrabarrels. Adopted from Petersen (2007) and modified. Immunohistology and confocal microscopy image by Ehsan Kheradpezouh and Mehdi Adibi.

Each elliptically shaped barrel is approximately 0.3–0.5 mm in maximal diameter (Hodge et al., 1997) and contains an average of 2500 neurons (Woolsey and van der Loos, 1970; Lee and Woolsey, 1975; Jones and Diamond, 1995). Barrels are somatotopically arranged in an identical order as the whiskers on the snout, with the most dorsal posterior whiskers being represented by the most lateral posterior barrels (Woolsey and van der Loos, 1970). Neurons within each barrel produce their strongest and fastest response to the stimulation of the anatomically-associated whisker, also known as the "principal" whisker (Welker, 1971). There is a precise one-to-one connection between thalamic barreloids and cortical barrels, with no evidence of a multi-barrel innervation by thalamocortical axons (Bernardo and Woolsey, 1987; Chmielowska et al., 1989; Agmon et al., 1995; Land et al., 1995). In rats, there are sparse-celled regions between barrels called septa (Woolsey and van der Loos, 1970; Welker and Woolsey, 1974). Inter-barrel septa together with regions surrounding the barrel field form the dysgranular zone.

There are two main types of neurons in layer IV barrels: spiny stellate and star-pyramidal excitatory neurons, and GABAergic interneurons. Both excitatory and inhibitory neurons receive direct inputs from VPM. Neurons in layer IV heavily project into supragranular layer II/III within the same cortical column (along the barrel). Septal neurons project above septum to layer II/III and to some extent coarsely to surrounding barrels, secondary somatosensory cortex (SII) and primary motor cortex (Feldmeyer et al., 1999; Kim and Ebner, 1999; Petersen and Diamond, 2000; Chakrabarti and Alloway, 2006). Some layer IV barrel axons innervate into the adjacent barrels as well (Kim and Ebner, 1999; Petersen and Diamond, 2000; Brecht and Sakmann, 2002). The targets of layer II/III neurons include the adjacent barrel layer II/III, layer V, primary and secondary motor cortices, secondary somatosensory cortex, dysgranular zone, perirhinal temporal association cortex, dorsolateral striatum and the contralateral SI (Koralek et al., 1990; Hayama and Ogawa, 1997; Kim and Ebner, 1999; Yamashita et al., 2018). The laminar organization of neurons along a barrel form functional barrel columns across cortical layers which mainly represent the barrel's principal whisker.

Thalamic afferents innervate layer Vb and VI neurons concurrently to layer IV neurons (Constantinople and Bruno, 2013). Their synapses with layer V pyramidal neurons reliably elicit action potentials (Constantinople and Bruno, 2013). Axons of the layer V pyramidal neurons ramify extensively within this layer with ascending collaterals targeting the supragranular layers and descending collaterals projecting to infragranular layer VI (Thomson and Bannister, 2003; Lübke and Feldmeyer, 2010; Feldmeyer, 2012; Ramaswamy and Markram, 2015). Layer Va is predominantly populated by slender-tufted pyramidal neurons characterized by their slender apical dendrites, while layer Vb is predominantly populated by thick-tufted pyramidal neurons characterized by pyramidal-like somas and thick apical dendrites and the untufted pyramidal cells (Ramaswamy and Markram, 2015). The pyramidal neurons in layer Va (both slender and thick-tufted) may function as integrators of lemniscal and paralemiscal thalamic pathways through monosynaptic connections with layer IV spiny stellate neurons (Feldmeyer et al., 2005). The layer Vb thick-tufted pyramidal neurons mainly project to anterior midbrain and thalamic nuclei, including the posterior thalamus, ZI and APT. These projections maintain the somatotopic organization beyond the cortex (Sumser et al., 2017). For a detailed recent review of the neuroanatomy and physiology of the layer V refer to Ramaswamy and Markram (2015).

Layer VI is the main source of corticothalamic feedback projections (Bourassa et al., 1995; Feldmeyer, 2012). Corticothalamic neurons, in addition to projections to sensory thalamic nuclei, ramify both excitatory and inhibitory neurons in layer IV as well as pyramidal neurons in layer Va (Feldmeyer, 2012; Harris and Mrsic-Flogel, 2013; Kim et al., 2014). Paired whole-cell recording (Lefort et al., 2009) and laser scanning photo-release of caged glutamate (Hooks et al., 2011) revealed layer VI inter-laminar input and output are weak. However, repetitive optogenetic excitation of layer VI corticothalamic neurons evokes action potentials in layer Va pyramidal neurons as well as fast-spiking interneurons in both layer IV and Va by activating facilitating synapses (Kim et al., 2014), while the overall effect on layer IV excitatory neurons is weak excitation or disynaptic inhibition (Kim et al., 2014). Layer VIa corticothalamic neurons form aggregated barrel-like structures (called infrabarrels) organized somatotopically align with the layer VI barrels (Crandall et al., 2017). Corticocortical

neurons, on the other hand, predominantly populate between infrabarrels. By optogenetic stimulation of VPM and POm thalamic nuclei, Crandall et al. (2017) found VIa corticocortical neurons receive strong synaptic input from both VPM and POm, whereas corticothalamic neurons exhibit weaker responses to VPM input and little response to POm. The receptive field properties of neurons in the barrel field are different across layers. The receptive fields in general have an excitatory center and excitatory surround structure; cortical neurons respond vigorously to the corresponding principal whisker as well as to the adjacent/surrounding whiskers with a weaker and delayed response (Simons, 1978; Armstrong-James and Fox, 1987). However, septal neurons similar to their presynaptic POm neurons, respond to multiple whiskers without preference to a certain whisker as principal (Armstrong-James and Fox, 1987; Brecht and Sakmann, 2002). Consistent with their pattern of connectivity, layer II/III neurons, show a broader receptive field with a lower response magnitude (Ito, 1985; Armstrong-James and Fox, 1987; Armstrong-James et al., 1992). Synaptic integration in layer V neurons is more complex, as these neurons receive input from layers II/III (Reyes and Sakmann, 1999), IV (Feldmeyer et al., 2005; Schubert et al., 2006), from other pyramidal neurons in the infragranular layers (Markram et al., 1997; Schubert et al., 2001), as well as substantial direct thalamic input (Bureau et al., 2006). This leads to broad receptive fields and sometimes whisker non-specific response profiles (Sachdev et al., 2001). For a more detailed review on SI laminar organization refer to Ahissar and Staiger (2010). Also, for a review on the functional organization of barrel cortex refer to Petersen (2007).

Across all cortical laminae, increasing the velocity/acceleration of stimuli applied to the principal whisker increased the amplitude of excitatory post synaptic potentials (EPSPs) and decreased their latency to peak (Wilent and Contreras, 2004). The changes in the EPSP were accompanied by a transient increase in the spiking activity of cortical neurons (Simons, 1978; Ito, 1985; Pinto et al., 2000; Arabzadeh et al., 2003; Wilent and Contreras, 2004; Adibi and Arabzadeh, 2011), typically followed by a rapid decline (within 10–20 ms of the response onset) to a lower level of tonic spiking rate. The synaptic response of supragranular (layer II/III) and infragranular (layer V and VI) neurons was on average delayed with respect to that of the granular (layer IV) neurons (Brecht and Sakmann, 2002; Brecht et al., 2003; Manns et al., 2004; Wilent and Contreras, 2004, but see Constantinople and Bruno, 2013). The peak of the spiking response of Layer IV neurons was followed by infragranular neurons' response peak and then by the response peak of layer II/III neurons (Wilent and Contreras, 2004). Layer IV neurons exhibit a short integration window of a few milliseconds compared to other layers. These findings suggest that layer IV neurons function as coincidence detectors, whereas supra- and infragranular circuits function as input integrators (Wilent and Contreras, 2004; Brecht, 2007). Layer V neurons are proposed to integrate lemniscal and paralemniscal inputs in addition to inputs from most or all cortical layers (Brecht, 2007). Layer IV, III and II, on the contrary, might operate as functionally segregated circuits contributing to separate lemniscal and paralemniscal processing streams (Brecht, 2007).

The sequence of cortical activation across layers is consistent with interlaminar interacortical local field potential recordings and current source analysis which exhibit early current sinks in layer IV followed by activation of layers II/III and V (Di et al., 1990; Agmon and Connors, 1991; Kenan-Vaknin and Teyler, 1994). Multi-electrode array electrophysiology from SI neurons revealed whisker deflection stimulation quenches trial-by-trial variability (Adibi et al., 2013b); the Fano factor, defined as the ratio of the variance of neuronal responses to their average, decreased as the stimulus intensity (and hence the population activity) increased (**Figures 3A,B**). This decrease is consistent with previous findings in areas V4 (Cohen and Newsome, 2009) and MT (Uka and DeAngelis, 2003; Osborne et al., 2004), premotor cortex (Churchland et al., 2006), and superior temporal sulcus (Oram, 2011) of monkeys (for a detailed review see Churchland et al., 2010). Stimulation quenches the correlation in trial-to-trial variability between neurons (noise correlation) (**Figures 3C,D**). Noise correlation is usually characterized in terms of the correlation coefficient of the spike counts for pairs of neurons. Using principal component analysis of neuronal responses, Adibi et al. (2013b) extended this measure to neuronal populations of larger than 2 neurons (see **Figure 3E**). The functional connectivity map constructed based on the strength of pairwise correlations of ongoing spontaneous activity of urethane-anesthetized rats recorded using 10 × 10 array of electrodes predicted the anatomical arrangement of electrodes on the sensory cortex (Sabri et al., 2016). Neurons with stronger correlations to the population during episodes of spontaneous activity, carried higher information about the sensory stimuli in their evoked response (**Figure 3F**). It is, however, not clear whether this higher level of correlations is due to common input from thalamus or originates from the cortical circuitry. Moreover, the correlation profile of electrode pairs during spontaneous activity predicted both signal and noise correlations (Adibi et al., 2014) during sensory stimulation (**Figures 3G,H**).

It has been demonstrated that barrel cortex neurons in anesthetized rats robustly encode the velocity of whisker motion (Simons, 1978; Pinto et al., 2000; Arabzadeh et al., 2003, 2004; Estebanez et al., 2012). The whisker motion features that these neurons encode form a common low-dimensional feature subspace of whisker motion, comprising linear combination of whisker velocity and position, and to a lesser extent whisker acceleration (Maravall et al., 2007; Estebanez et al., 2012). Estebanez et al. (2012) recently demonstrated that the feature encoding properties of cortical neurons differ depending on the level of spatial correlation in multi-whisker sensory stimuli. In addition to velocity, cortical neurons in the whisker-related area of SI exhibit directional selectivity (Simons, 1978; Simons and Carvell, 1989; Bruno and Simons, 2002; Wilent and Contreras, 2005; Puccini et al., 2006; Kremer et al., 2011).

The feedback projections from infragranular layers to the vibrissae-related thalamic sensory nuclei consist of three main routes:

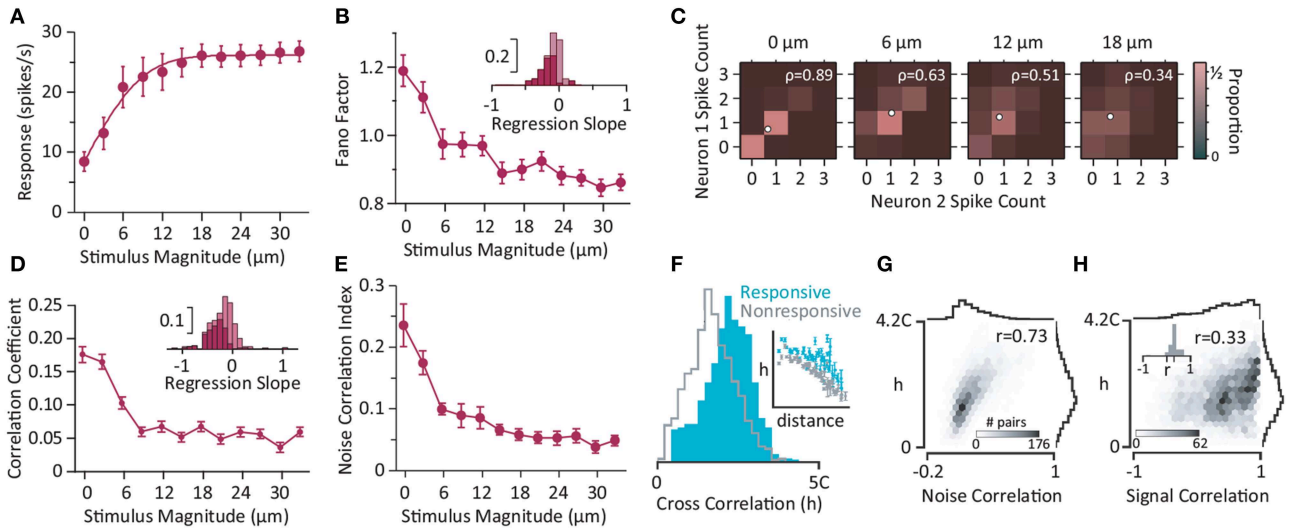

FIGURE 3 | Neural activity in somatosensory cortex. **(A)** The population activity increases with the magnitude of whisker deflection stimulation (single-cycle sine-wave at 80 Hz). Error bars represent the standard error of means across populations with more than five simultaneously recorded units ($n = 8$). **(B)** Trial-to-trial variations in neuronal response (in terms of Fano factor) as a function of stimulus intensity for single neurons ($n = 64$). The inset depicts the histogram of the linear regression slope of the Fano factor with respect to the z-scored neuronal activity for individual neurons. The dark bars correspond to recordings with a significant linear regression ($p<0.05$). **(C)** Color indicates the proportion of joint spike counts for a pair of simultaneously recorded neurons. White circles indicate mean spike counts for each stimulus. The Pearson's correlation coefficient of the spike counts is indicated by ρ for each panel. **(D)** The mean Pearson's correlation coefficient across all possible pairs of neurons ($n = 245$) as a function of stimulus intensity. Error bars indicate standard error of means. The inset depicts the histogram of regression slopes of noise correlation against average firing rate for pairs of neurons. Dark bars indicate the cases with significant linear regression ($p<0.05$). **(E)** The noise correlation index (Adibi et al., 2013b) as a function of stimulus magnitude averaged across populations containing at least five simultaneously recorded neurons (data from **A**). Error bars are standard error of mean across populations ($n = 8$). Most of the neurons exhibit a negative slope indicating Fano factor **(B)** and noise correlations decrease with firing rate. **(F)** The strength of correlation, denoted by h: the peak of the cross correlation of a pair of electrodes relative to the chance level (denoted by C). Electrodes were divided into two groups of "Responsive" and "Nonresponsive" based on the median of the mutual information between neuronal responses and whisker stimulation. The distribution of h values for Responsive pairs (where both electrodes were from the Responsive group; cyan) and Nonresponsive pairs (where both electrodes in a pair were from the Nonresponsive group; gray). The inset depicts the average and standard error of means of strength of correlation, h, across electrode pairs as a function of their distance for each category. **(G)** The histogram shows the joint distribution of h values and noise correlations. r represents the correlation coefficient. **(H)** Same as **(G)**, but for signal correlation. Inset depicts the histogram of r value calculated for groups of electrode pairs with identical distance. The distribution of r values is positive with a mean of 0.3 indicating that the positive correlation between h and signal correlation is independent of the distance between electrodes and is present across all distances. **(A–E)** are based on Adibi et al. (2013b), and **(F–H)** are from Sabri et al. (2016).

1. Neurons in the upper part of layer VI of a barrel exclusively project to the corresponding barreloid in VPM (Bourassa et al., 1995; Land et al., 1995) forming a reciprocal barreloid-barrel connection.
2. Neurons in the lower part of layer VI project to POm and also a major proportion of these axons make collaterals in VPM to form rostro-caudal rod-like bands representing an arc of vibrissae (Hoogland et al., 1987; Bourassa et al., 1995).
3. The corticothalamic projections of layer V cells exclusively terminate in POm (Bourassa et al., 1995).

The axons originated from layer VI along the inter-barrel septa exclusively target POm (Bourassa et al., 1995). The Layer VI corticothalamic axons, but not those of layer V give off collaterals in the reticular nucleus while traversing it (Bourassa et al., 1995; Deschênes et al., 1998).

The primary somatosensory cortex projects to the secondary somatosensory cortex, the primary motor cortex (MI), thalamus sensory nuclei, superior caliculus and dorsolateral neostriatum (White and DeAmicis, 1977; Carvell and Simons, 1986, 1987; Welker et al., 1988; Deschênes et al., 1998; Alloway et al., 2006; Chakrabarti and Alloway, 2006; Hattox and Nelson, 2007; Larsen et al., 2007). Also, the barrel cortices on two hemispheres are linked by a callosal connection (White and Czeiger, 1991). In turn, primary somatosensory cortex receives inputs from the secondary somatosensory cortex and motor cortex (Carvell and Simons, 1987; Kim and Ebner, 1999). Unlike in primates (Hsiao et al., 1993; Jiang et al., 1997; Iwamura, 1998; Mima et al., 1998; Karhu and Tesche, 1999; Salinas et al., 2000; Romo et al., 2002), little is known about the functional properties of the secondary somatosensory cortex in rodents, and this knowledge is limited to anesthetized preparations (Carvell and Simons, 1986; Kwegyir-Afful and Keller, 2004).

2.7. Parallel Ascending Subcortical Routes for Whisking and Touch Signals to Cortex

The whisker information from trigeminal complex is channeled to cortex through three parallel pathways (Pierret et al., 2000; Yu et al., 2006, also see **Figures 1**, **2**):

1. The lemniscal pathway is the major pathway through which the touch signal is channeled to cortex. This pathway includes

ipsilateral PrV barrelettes to contralateral VPMdm barreloids to cortical barrel columns layer IV and sparsely to Layer VI in SI. The lemniscal pathway conveys a combination of touch and whisking signals and is speculated to represent the "what" pathway (analogous to the ventral stream in the visual system).
2. The paralemniscal pathway channels the sensory information from rostral part of alaminar spinal trigeminal nucleus (nucleus interpolaris or SpVi) into the thalamic posterior medial nucleus (POm), and then to the following cortical areas: layer I and Va of SI, the septal regions, SII, MI and superior colliculus. The paralemniscal pathway primarily conveys whisking signals, which can be employed to form sensory-motor coordination and positional reference signals during exploration/whisking (Ahissar et al., 2000; Kleinfeld et al., 2006). Hence the paralemniscal pathway is speculated to represent the "where" system in somatosensation in rodents (analogous to the dorsal stream in the visual system).
3. The extralemniscal pathway conveys touch information from SpVc and caudal division of SpVi to VPMvl thalamus and then to SII and the septal regions of SI cortex.

The lemniscal and paralemniscal pathways interact; the lemniscal pathway has been shown to suppress the paralemniscal pathway through cortically-activated rapid GABAergic inhibitory projections of zona incerta to POm (Lin et al., 1990; Nicolelis et al., 1992; Power et al., 1999).

3. PHYSIOLOGY AND FUNCTION

3.1. Modes of Whisker-Mediated Sensation

As in vision where controlled eye movements—saccades—enhance the efficacy of the visual system to browse the environment and extract relevant visual information, rodents sweep their mystacial vibrissae to scan the environment and collect behaviorally-relevant information. A body of literature referred to this purposively information-seeking manipulation of sensory apparatus as "active sensing" (Gibson, 1962; Aloimonos et al., 1988; Aloimonos, 1990; Szwed et al., 2003, 2006; Mitchinson et al., 2007; Grant et al., 2009; Sullivan et al., 2012). In the realm of engineering, however, "active sensing" against "passive sensing" means emitting energy (e.g., in electromagnetic form as in radar or in mechanical form as in sonar) and sensing the reflections of the emitted signal to obtain information about the medium/environment. To avoid this ambiguity, here, I follow the terminology as in Diamond and Arabzadeh (2013) which categorize the whisker-mediated perception in rodents into two modes: "generative" and "receptive."

Whisking is the self-generated exploratory whisker motion through which rodents sense their surrounding environment in the "generative mode." This generative mode of whisking is used in the perception of surface textures, identification of objects and shapes, estimation of distances and localization of objects. As a whisker comes in contact with an object or palpates the object, its instantaneous motion changes following every contact and release from the surface with high acceleration and high velocity—stick-slip events. The sequence of these stick-slip events along with the self-generated component of the whisker motion uniquely reconstructs the kinetics of surface and determines the texture of a surface, or the shape or location of an object. A body of research has focused on quantification of behavioral capacities and characterization of whisker motion and its consecutive neuronal activity in the generative mode. These include a variety of behavioral tasks or simulated conditions such as texture discrimination (Carvell and Simons, 1990; Guić-Robles et al., 1992; Prigg et al., 2002; Arabzadeh et al., 2005; von Heimendahl et al., 2007; Diamond et al., 2008; Itskov et al., 2011; Morita et al., 2011; Zuo et al., 2011), identification of shape and size of objects (Brecht et al., 1997; Harvey et al., 2001; Polley et al., 2005), distance, gap and aperture width detection (Hutson and Masterton, 1986; Guic-Robles et al., 1989; Harris et al., 1999; Jenkinson and Glickstein, 2000), object localization (Knutsen et al., 2006; Mehta et al., 2007; Ahissar and Knutsen, 2008; Knutsen and Ahissar, 2009; O'Connor et al., 2010) and natural exploratory whisking (Fee et al., 1997; Kleinfeld et al., 2002, 2006; O'Connor et al., 2002; Berg and Kleinfeld, 2003; Szwed et al., 2003; Ganguly and Kleinfeld, 2004; Knutsen et al., 2005). For other paradigms, such as width discrimination described in (Krupa et al., 2001) whisking may not be essential. However, I categorized such behavioral tasks in the generative mode as they require controlled head positioning and movements.

As in vision where fixating the gaze on a focal target provides more accurate visual information, in receptive mode, rats can immobilize their vibrissae to achieve efficient vibro-tactile signal collection from a mobile object. In vision, saccades during a fine visual task such as counting degrade the performance. Similarly, there is behavioral evidence that self-generated whisker motion reduces the rodent's performance when detecting vibrations (Ollerenshaw et al., 2012). This aspect of whisker-mediated sensation is less investigated in the literature (Hutson and Masterton, 1986) and research has been mainly limited to head-fixed rodents performing a go/no-go licking task (Stüttgen and Schwarz, 2008, 2010; Gerdjikov et al., 2010; Schwarz et al., 2010).

Recent studies revealed that the response dynamics of cortical neurons changes with the mode of sensation and the behavioral state (Fanselow and Nicolelis, 1999; Castro-Alamancos, 2004; Crochet and Petersen, 2006; Ferezou et al., 2006, 2007). The response of cortical neurons to whisker stimuli was suppressed in the generative mode compared to the receptive mode or quiescent state (Castro-Alamancos, 2004; Crochet and Petersen, 2006; Ferezou et al., 2006, 2007; Crochet et al., 2011). Likewise, neurons in rat auditory cortex show sensory-evoked response suppression during active behavioral states (Otazu et al., 2009). Additionally, fluctuations in local field and membrane potentials of layer II/III cortical neurons exhibit prominent slow synchrony during receptive mode (Crochet and Petersen, 2006; Poulet and Petersen, 2008; Gentet et al., 2010, 2012). In the generative mode during free whisking, however, membrane potential fluctuations were suppressed and desynchronized across nearby neurons. This cortical state of desynchrony was accompanied by an increase in the spiking activity of thalamocortical neurons (Poulet et al., 2012). Cutting the sensory peripheral afferents innervating whisker follicles did not affect the generative mode response suppression and desynchrony, indicating that its origin is not

peripheral (Poulet et al., 2012). Pharmacological inactivation of thalamocortical neurons, however, halted the generative-mode desynchronization. Consistently, optogenetic stimulation of thalamocortical neurons induced similar desynchronized cortical state (Poulet et al., 2012). For further details refer to the review article by Petersen and Crochet (2013).

3.2. Behavioral Approaches to Systems Neuroscience: Linking Circuitry and Function

How does neuronal activity give rise to sensation and ultimately perception? To what extent does the neuronal readout match the perception of whisker vibration? In order to draw a causal link between neuronal activity and sensorimotor, perceptual, and cognitive functions, it is crucial to develop appropriate behavioral methods and combine them with requisite methods of observation and perturbation of neuronal activity. The behavioral approaches in rodent model system are either based on native forms of natural behavior such as whisking, hence require minimum training—for instance, free navigation or exploration, whisking and aperture or gap crossing (Harris et al., 1999; Jenkinson and Glickstein, 2000; Crochet and Petersen, 2006; Celikel and Sakmann, 2007; Sofroniew et al., 2014; Kandler et al., 2018)—or paradigms embedded in an artificial task and require extensive training of the animal to interact with the environment and express specific behaviors in response to events and stimuli—in this context, neutral tactile stimuli such as textures, vibrations or object contacts. The body of literature mainly divides into two forms of behavioral tasks: (i) go/no-go or lick/no-lick, and (ii) two- or multiple-alternative-choice tasks.

Go/no-go (or lick/no-lick) tasks are often used in the head-fixed preparation predominantly in mice and sometimes in rats (Topchiy et al., 2009; Schwarz et al., 2010; Guo et al., 2014a; Fernández et al., 2018a; Helmchen et al., 2018). It provides the mechanical stability and a fixed head position ideal for precise whisker stimulation, whisker motion tracking, eye/pupil and gesture tracking, as well as electrophysiology (for instance, intracellular recording) and imaging from cortex (two-photon calcium imaging or voltage-sensitive dye imaging). To prevent learning about timing of the reward as a confounding cue, and to minimize impulsive or anticipatory responses based on the periodicity of the sensory events and reward, go/no-go tasks usually do not have a discrete trial structure, or the initiation of a trial is at random time instances with variable delays. The proportion of the trials followed by no-go should be precisely balanced in order to minimize excessive reinforcement of spontaneous incorrect go choices (false alarms) and to avoid formation of a bias toward go or no-go choices. Other limitations of the go/no-go tasks in head-fixed preparation include no re-enforcement (reward) for correct no-go choices, suppressed vestibular signals which may play a crucial role for coordination of whisking behavior and body movements, and relying on licking behavior with highly reflexive components (Keehn and Arnold, 1960; Schaeffer and Premack, 1961; Hulse and Suter, 1968) as a representation of a cognitive goal-directed behavior. Using conditioned level-press responses, Mehta et al. (2007) found that rats with only a single whisker combine touch and whisker movement to distinguish the location of objects at different angular positions along the sweep of whisker. The other limitation of go/no-go head-fixed tasks is the lack of control over motivational factors (e.g., satiation) affecting the likelihood of go choices. The motivation can be controlled by employing a self-initiation mechanism for trials. Go/no-go paradigm is commonly used to quantify the behavioral performances for detection of a stimulus or the detection of change (Stüttgen and Schwarz, 2008; Ollerenshaw et al., 2012; Bari et al., 2013) and discrimination of two sets of stimuli, one associated with go (and hence reward), and one associated with no-go (Mehta et al., 2007; Gerdjikov et al., 2010; O'Connor et al., 2010; Chen et al., 2013). Lee et al. (2016) applied a visuo-tactile detection go/no-go task in freely moving rats with the minimum level of temporal uncertainty; upon the initiation of a trial by nose-poke into a port, the sensory cue (whisker deflection or visual flicker) appeared after a delay of either 300 or 800 ms each of which with equal likelihood. After stimulus onset, the rat had a 500 ms window of opportunity to elicit the go choice and collect the reward. For a hypothetically "logical" rat, the optimal strategy is to detect the sensory stimulus only at the time instance associated to the short delay (300 ms). Upon no detection at 300 ms, the hypothetical rat makes an anticipatory non-sensory go choice at 800 ms, as the hazard rate for stimulus presentation (and hence reward delivery) at 800 ms equals 1 (i.e., absolute certainty). This non-sensory anticipatory strategy explains the faster response time to 800-ms stimulation compared to 300-ms stimulation observed in (Lee et al., 2016). Additionally, this strategy predicts a higher proportion of misses for short delay stimulation and higher hit rate for the long delay stimulation (see also Lee et al., 2019). Extracellular array recording from vSI neurons during this task revealed enhanced cortical activity to whisker stimulation with higher expectancy (likelihood compared to visual stimulus) (Lee et al., 2016, 2019). This supports a plausible multiplicative gain modulation of evoked responses or alternatively an additive modulation of baseline activity. This response enhancement may be induced by expectation or attentional factors, motor preparation or sensory events related to motor output (as the task lacks a delay after stimulus presentation to withhold the go choice and to separate stimulus presentation from choice), decision processes and motor output. This is a common drawback in go/no-go, and in particular, lick/no-lick paradigms. In contrast to go/no-go tasks in which it is difficult to distinguish a lack of motivation or lapses of attention from false rejections or correct rejections, two-alternative-choice tasks provide a clear distinction of correct, incorrect, and missed trials.

Two- or multiple-alternative-choice tasks can be divided into two main categories: sensory discrimination/comparison and categorization tasks (**Figure 4**). In sensory discrimination tasks, every trial includes presentation of two stimuli. Discrimination/comparison tasks take two forms depending on the association of the two choices with the stimuli. In the "comparative" discrimination (**Figure 4A**), the task is to compare an attribute of the two stimuli against each other [e.g., roughness of textures (Carvell and Simons, 1990), frequency (Adibi et al., 2012; Mayrhofer et al., 2012), magnitude (Adibi and Arabzadeh,

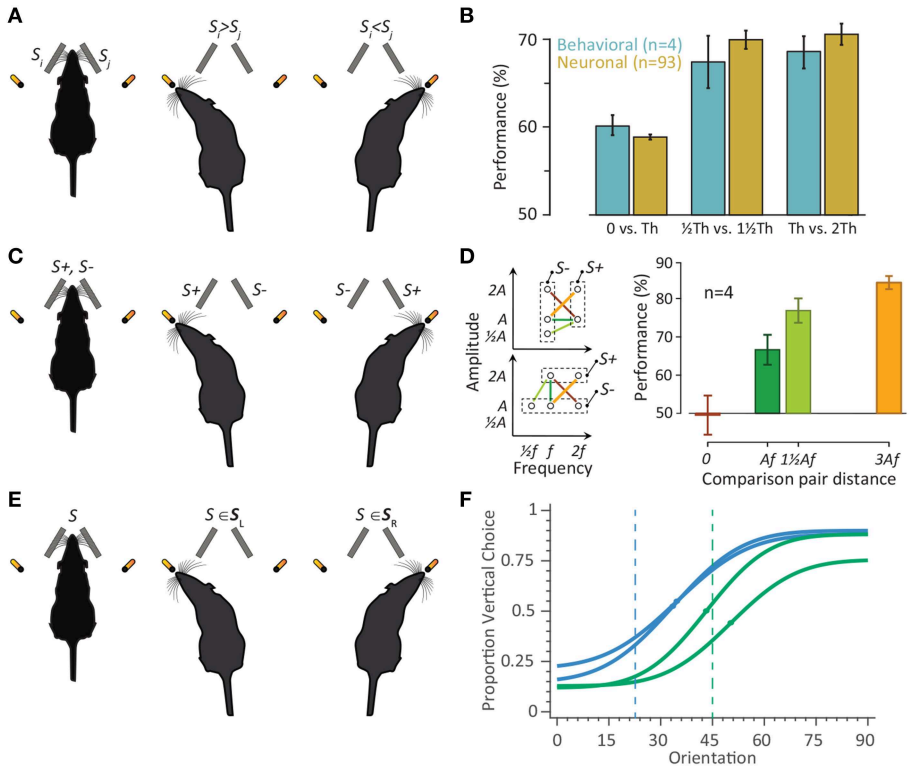

FIGURE 4 | The two-alternative-choice behavioral tasks in rodents. **(A)** Schematic representation of the comparative discrimination paradigm. On every trial, two vibrations S_i and S_j were presented. **(B)** Four rats were trained in the detection/discrimination task to identify the vibration with the higher amplitude. The neuronal performance is the average performance (based on the area under ROC) across single-units ($n = 35$) and multiunit clusters ($n = 58$) from Adibi and Arabzadeh (2011). For each neuron, the stimulus intensity whose detection performance was closest to 60% was chosen as detection threshold (*Th*). The stimuli corresponding to $\frac{1}{2}-$, $1\frac{1}{2}-$, and 2-fold *Th* were then selected for estimating the discrimination performances. The same threshold of 60% defined as detection threshold for rats. The rats performed the comparison task between $0 - Th$, $\frac{1}{2} - 1\frac{1}{2}$ and $Th - 2Th$. Error bars indicate standard error of means across rats or neurons. **(C)** Schematic representation of the categorical discrimination paradigm. Stimuli were defined as either S+ or S−. In each trial, one of the two vibrations was S+ and the other was S−. Having identified the S+ vibration, the rodent expressed its choice by turning toward the corresponding drinking spout. **(D)** (Left) Stimulus space. Each circle represents the frequency–amplitude combination of one stimulus. Two groups of rats were trained in the task. For one group (top-left), two frequencies ($f = 80$ Hz and $2f = 160$ Hz) and three amplitudes ($\frac{1}{2}A = 8$ μm, $A = 16\mu$m, and $2A = 32$ μm) were used to generate five vibrations, and for second group (bottom-left) three frequencies ($\frac{1}{2}f = 40$ Hz, $f = 80$ Hz and $2f = 160$ Hz) and two amplitudes ($A = 16$ μm and $2A = 32$ μm) were used to generate five vibrations. Stimuli that were presented together and had to be discriminated (paired stimuli) are connected by lines. The right panel shows the proportion of correct trials (performance) for the corresponding four stimulus-pairs averaged across rats. Error bars are s.e.m. across rats. Re-plotted from (Adibi et al., 2012). **(E)** The schematic representation of the categorization paradigm. The stimuli are divided into two categories of S_L and S_R, corresponding to left and right choices, respectively. A stimulus S was presented on every trial. The rat identifies the category which stimulus S belongs to. **(F)** Rats were trained to categorize the orientation of a 9.8 cm-diameter disc with alternating ridges and grooves by licking at one of the two reward spouts. Psychometric functions correspond to two rats trained to categorize orientations 0–45° as horizontal, and 45–90° as vertical (green), and another two rats trained to categorize orientations 0–22.5° as horizontal, and 22.5–90° as vertical (blue). The curves correspond to a Gaussian cumulative function fitted to data. The dots on each curve represent the perceptual decision boundary of each rat. The blue and green vertical dashed lines represent the categorization boundaries of 22.5° and 45°, respectively.

2011; Adibi et al., 2012; Fassihi et al., 2014, 2017), or duration (Fassihi et al., 2017) of two vibrations]. Each outcome of the comparison is associated with one of the two reward ports. The two stimuli may present simultaneously at two distinct positions (e.g., two whiskers, or two sides of snout Carvell and Simons, 1990; Adibi and Arabzadeh, 2011; Adibi et al., 2012) or at one position but at distinct time instances (Fassihi et al., 2014, 2017). In the "categorical" discrimination (**Figure 4C**), the stimuli are divided into two categories of rewarded/target (S+) vs. unrewarded/distractor (S−). Each trial comprises presentation of one stimulus from each of the two categories. The task is to select the choice associated to the position of the target/rewarded stimulus (Morita et al., 2011; Adibi et al., 2012; Mayrhofer et al., 2012; Musall et al., 2014).

In the categorization tasks, the stimuli are divided into two categories, each of which associated with one of the two choices (**Figure 4E**). On every trial, one stimulus is presented, and the task is to identify the category to which the stimulus belongs. Categorization tasks can be considered as a discrimination/comparison task against a reference or boundary dividing the physical feature space of the stimulus into two categories. Alternatively, it can be considered as a mapping of

individual stimuli with one of the two choices. Rodents can perform whisker-mediated tactile categorization tasks on sensory attributes such as textures (von Heimendahl et al., 2007; Zuo et al., 2011; Grion et al., 2016; Zuo and Diamond, 2019b), whisker deflection amplitude pattern (McGuire et al., 2016), aperture width (Krupa et al., 2001), location (Guo et al., 2014b; Li et al., 2015; Helmchen et al., 2018) and orientation (our recent data in **Figure 4F**, also see Nikbakht et al., 2018) of objects.

Discrimination and detection behavioral studies quantify the psychometric response function (the likelihood of the choices as a function of stimulus attribute) which along with the acquisition of neuronal activity allows linking the behavioral function to the neuronal activity. Comparison of the neuronal and psychophysical performances started in the late 1960s in the classic electrophysiological experiments in cat retina (Barlow and Levick, 1969; Barlow et al., 1971) and in the somatosensory cortex (Talbot et al., 1968; Mountcastle et al., 1972). Thereafter, more studies have combined psychophysical and neurophysiological experiments in order to relate neuronal responses to perception (Romo et al., 1998, 2000; Hernández et al., 2000; Salinas et al., 2000; Ress and Heeger, 2003; Luna et al., 2005; de Lafuente and Romo, 2006; Stüttgen and Schwarz, 2008) and decision making (Newsome et al., 1989; Shadlen et al., 1996; Romo et al., 2004; Hanks et al., 2006; Kiani et al., 2008). Instead of the traditional comparison of behavioral and neuronal thresholds or sensitivities, Adibi and Arabzadeh (2011) compared the non-linearity of the behavioral and neuronal response profiles to the amplitude of vibration. In a series of vibration detection and amplitude discrimination tasks, Adibi and Arabzadeh (2011) first quantified the detection threshold of both cortical neurons and rats (denoted by *Th*, **Figure 4B**). For near-threshold stimuli with identical amplitude difference, both the neuronal and behavioral discrimination performances surpassed the detection performances (**Figure 4B**). This is consistent with the accelerating nonlinearity of neurometric and psychometric functions at low stimulus intensities. The results revealed the nonlinearity in the neuronal response function predicts behavioral detection and discrimination performances. This study presents the first observation of the "pedestal effect"—frequently reported in human psychophysics—in animal literature. Using the same behavioral detection task, McDonald et al. (2014) showed rats' behavior indicated a dynamic stimulus sampling whereby stimulus sampling was continued until the stimulus was correctly identified or the rat experienced a false alarm. This is consistent with the recent evidence from texture identification task (Zuo and Diamond, 2019a,b) suggesting similar to primates, rats' choices are governed by bounded integration of primacy-weighted touch-by-touch evidence.

Previous electrophysiology studies identified the physical features of whisker motion that are encoded in the activity of cortical neurons to be the product of elemental features of whisker motion, its frequency (f) and amplitude (A) (Simons, 1978; Ito, 1985; Pinto et al., 2000; Arabzadeh et al., 2003, 2004). Consistently, behavioral studies revealed rats are unable to discriminate these elemental features independently of their product (Adibi et al., 2012); two groups of rats were trained to discriminate either based on the frequency or based on the amplitude of the vibrations delivered to both whisker pads. The stimulus pairs with identical Af product (marked in red, **Figure 4D**) were not discriminable, while the other stimulus pair with the same feature difference in the physical space (marked with orange, **Figure 4D**) were highly discriminable. In both groups, rats' performance in discriminating two stimuli is accounted for by the difference in Af but not by differences in either elemental feature (A and f) alone. This is consistent with the electrophysiological findings that neurons reduced the dimensionality of the stimulus from two features (A, f) to a single feature: the product Af (Arabzadeh et al., 2003, 2004). Af defines a real physical property: the speed of whisker motion averaged over cycles.

The bridge linking neuronal activity to perception is the readout mechanism of sensory neurons. The interlaced synaptic architecture of neural networks provides strong evidence for decoding by downstream neuronal structures based on "populations" of neurons rather than individual single neurons. Such a synaptic organization together with physiological properties of dendritic processes by which neurons receive information simulates an integration model in which the activity of neurons in the relevant population is summed with different weights. This provides a simple framework to investigate how a biologically plausible ideal observer of neuronal responses, a linear "decoder," extracts information about the stimuli. Linear decoders are simple in their structure and compatible with the architecture of the brain. With optimizing the weights, it provides an upper limit to the amount of information extractable from neuronal responses. There are two limiting factors affecting the reliability of the neuronal code for sensory stimuli: the response variability of individual neurons to a given stimulus, and co-variability (noise correlation) across the neurons. In our previous studies, we characterized the neuronal response statistics in terms of neuronal variability (Fano factor) and co-variability (noise correlation) and parsed out the effect of each of these components on the coding as well as decoding efficiency of cortical populations (Adibi et al., 2013a,b, 2014). Adibi et al. (2014) further quantified the effect of noise correlations on the optimal linear decoder and characterize the cost of ignoring noise correlations during decoding.

3.3. Motion Detection and Spatial Invariancy in Whisker-Mediated Touch System

A majority of neurons across different layers of the rat barrel cortex exhibit multi-whisker receptive fields (Simons, 1978; Armstrong-James and Fox, 1987; Moore and Nelson, 1998; Ghazanfar and Nicolelis, 1999; Brecht and Sakmann, 2002; Brecht et al., 2003). The spatial extent of the receptive field of a cortical neuron depends on the intra-cortical connections between barrel columns (Armstrong-James et al., 1991). Anatomical studies revealed that intra-cortical inter-barrel connections are stronger between barrels within a row (Bernardo et al., 1990a,b; Hoeflinger et al., 1995), with directionally-biased fiber projections into the anterior barrel (Hoogland et al., 1987; Bernardo et al., 1990a). Additionally, intra-cortical projections

from septal columns extend two to three barrels along the rows (Kim and Ebner, 1999). Consistently, the activity pattern of VPM and cortical neurons to single-whisker deflections is elongated along rows (Simons, 1978; Armstrong-James and Fox, 1987; Armstrong-James et al., 1992; Lee et al., 1994; Kleinfeld and Delaney, 1996). Electrophysiological studies also revealed that the multi-whisker interaction along rows and arcs is not symmetric. Suppressive two-whisker interactions have been reported to be more prominent during within-row stimulation than during within arc stimulation (Ego-Stengel et al., 2005), while within-arc multi-whisker stimulation yields more supra-linear response integration (Ghazanfar and Nicolelis, 1997; Ego-Stengel et al., 2005). However, multi-whisker interactions are highly dependent upon the temporal order and timing of the stimulation (Shimegi et al., 1999, 2000). Estebanez et al. (2012) demonstrated that the feature encoding properties of cortical neurons changes with the level of spatial correlation in multi-whisker sensory stimuli. In addition to its anatomical and functional importance, the rostro-caudal axis is behaviorally relevant. Through exploratory behavior, rats whisk (move their vibrissae) rostro-caudally, leading to a functional asymmetry between rows and arcs; as the whiskers palpate an object, whiskers within a row contact the object successively relative to their rostro-caudal position in the row, whereas whiskers within an arc usually contact the object nearly simultaneously. Thus, a potential function of within-arc facilitatory interactions might be to boost up the contact signal which is more likely to arise from whiskers within an arc. Alternatively, the spatiotemporal multi-whisker interactions could be an indication of cross-whisker motion detection (e.g., head relative to environment and vice versa) at the level of neurons in the rat primary somatosensory cortex or secondary somatosensory cortex (Jacob et al., 2008). Simple biologically-plausible models such as the Reichardt model (Hassenstein and Reichardt, 1956; Reichardt, 1961)—a correlation detector based on temporal delays—or energy models (Adelson and Bergen, 1985) provide plausible frameworks underlying movement detection in barrel cortex. Such motion detectors are more likely to be identified in SII or in the infra-granular layers of SI where neurons have broad multi-whisker receptive fields. In addition to information about the velocity of moving objects or the ego motion, such motion detectors can provide information about the location of objects with respect to head during whisking or head movements. A recent study (Curtis and Kleinfeld, 2009) showed that barrel neurons provide a representation of the position of contacted objects in a coordinate frame that is normalized to the trajectory of the motor output (i.e., phase of whisking). Contact was encoded independently of the angular whisker position and was shown to be invariant with respect to the amplitude and frequency of whisking. The representation of contact in a coordinate system that is dynamically normalized by the motor output provides the basis for encoding the spatiotemporal properties of an externally induced movement.

Le Cam et al. (2011) demonstrated that functional principal whisker—the whisker eliciting the strongest response with the shortest latency—differed based on the direction of whisker deflection along the rostro-caudal axis. The stimulus-induced changes in the spatial structure of the receptive field of the neurons was not limited to the principal whisker, and included stimulus-dependent changes in the size, response latency and receptive field center of mass. Although the neuronal mechanisms underlying these dynamic changes are not clear, they suggest invariancy of whisker position through whisking along the rostro-caudal axis; as the rat whisks, the position of the whiskers changes along the rostro-caudal axis with respect to the head leading to potential ambiguity about the position of an object in contact with the whisker. Such a dynamic shift in the receptive fields might help to adjust the position of contact with respect to the head instead of the whisker. This position invariant information can potentially give rise to whisker-mediated coordination, and contribute to spatiotopic representations in grid cells (Hafting et al., 2005) in the entorhinal cortex, head-direction cells in classic Papez circuit (Taube, 1998) and place cells (O'Keefe, 1976; O'keefe and Conway, 1978; O'Keefe and Nadel, 1978) in parahippocampal and hippocampal cortices.

3.4. Directional Selectivity in Whisker-Mediated Touch System

There are several lines of evidence that cortical neurons in the whisker area of SI exhibit directional selectivity (Simons, 1978; Simons and Carvell, 1989; Bruno and Simons, 2002; Wilent and Contreras, 2005; Puccini et al., 2006; Kremer et al., 2011; Kwon et al., 2018). Direction preference is also observed in the response of thalamic and trigeminal neurons (Shosaku, 1985; Lichtenstein et al., 1990; Hartings et al., 2000; Minnery et al., 2003; Timofeeva et al., 2003; Furuta et al., 2006; Bellavance et al., 2010). Although the directional selectivity in the periphery and brainstem originates in the uneven arborization of nerve terminals around the follicle (Lichtenstein et al., 1990), direction-dependent differences in the temporal profile of synaptic excitation and inhibition in barrels (Wilent and Contreras, 2005) and non-linear dendritic processes (Lavzin et al., 2012) also may contribute to the directional tuning in barrel cortex neurons. The directional selectivity decreases along the ascending whisker-to-barrel pathway. The functional and behavioral correlate of directional selectivity in the whisker-to-barrel system is not understood and it is not clear whether rats perceive the direction of vibro-tactile stimulus. However, several lines of research provide evidence against an angular selectivity readout such that leads to a sensation of direction. First, neurons with multi-whisker receptive fields in cortex and thalamus do not necessarily exhibit the same angular preference to different whiskers in their receptive field (Hemelt et al., 2010, but see Kida et al., 2005). Second, in the visual system, orientation selectivity arises from specific convergence of directionally non-tuned thalamic inputs in layer IV of striate cortex and gives rise to selectivity to more complex features along the cortical visual hierarchy. On the contrary, in the whisker-mediated touch system, directional selectivity exists in the peripheral sensory afferents innervating vibrissae follicles and gets weaker along the ascending whisker-to-barrel pathway. Thirdly, in contrast to visual system where the arrangement of neurons across the cortical surface forms a

precise "pinwheel"-like orientation preference topographic map (Hubel and Wiesel, 1974; Blasdel and Salama, 1986; Grinvald et al., 1986; Bonhoeffer and Grinvald, 1991; Ohki et al., 2005, 2006), the evidence on a topographic directional tuning map in barrel field of SI is weak and controversial in the literature. While directional preference mapping was observed in VPM (Timofeeva et al., 2003), neurons in layer IV barrels exhibit weak direction preference map (Bruno et al., 2003; Andermann and Moore, 2006). Weak correlation between the angular tuning and position of neurons with respect to the center of barrel column was observed in layer II/III of adult rats through tetrode recording (Andermann and Moore, 2006) as well as two-photon calcium imaging (Kremer et al., 2011). However, such an angular preference spatial mapping is absent in supra-granular layers in juvenile rats (Kerr et al., 2007). In layer II/III, two-photon imaging revealed orientation-specific responses were organized in a locally heterogeneous and spatially distributed manner (Kwon et al., 2018). Additionally, neurons with similar orientation preference exhibited higher correlation in their trial-to-trial response variability.

Although it has been shown that rats are capable of discriminating between different orientations of an object using all of their whiskers (Polley et al., 2005), direction selectivity of single cortical units may or may not contribute to this discrimination. Difference in the kinematics of the contact of multiple whiskers along with the ego head motions could provide the information about the orientation of an object. Thus, the extent to which rats can extract the direction of a vibro-tactile stimulus using only one whisker is not yet known. Recent findings revealed that mice learned to detect optical micro-stimulation of a sparse group of supra-granular neurons in SI (Huber et al., 2007), as well as the difference between temporal patterns of electrical micro-stimulation (Yang and Zador, 2012). As vibrations with different orientation elicit responses in distinct populations of cortical neurons, the rat might be able to use that population information to decode orientation. A key test is to see if rats generalize the learned behavior when stimulus is presented to another whisker.

3.5. Linking Cortical Function and Behavioral Context

A given sensory stimulus may convey different meanings depending on the time and context of its occurrence, requiring the organism to take different courses of action. Sensory processing also changes with behavioral context: for example, high amplitude oscillations (known as mu rhythm) are observed in sensorimotor areas when subjects are immobile with focused attention (Kuhlman, 1978; Rougeul et al., 1979; Bouyer et al., 1981). Similar oscillations were observed in membrane potentials recorded from layer II/III neurons of mice SI in receptive mode (Crochet and Petersen, 2006). In generative mode during free whisking, however, the synchronous fluctuations were suppressed and decorrelated (Crochet and Petersen, 2006; Poulet and Petersen, 2008; Gentet et al., 2010, 2012). Beyond the spontaneous oscillations, sensory stimuli delivered to whiskers of awake rats and mice evoked a smaller response amplitude in the generative mode compared to receptive mode (Castro-Alamancos, 2004; Ferezou et al., 2006, 2007). Similar response suppression during active behavior was observed in rat auditory cortex (Otazu et al., 2009), while a response enhancement was observed in visual cortex (Niell and Stryker, 2010; Keller et al., 2012). Functional interaction between sensory and motor areas at different behavioral modes (Matyas et al., 2010; Niell and Stryker, 2010; Keller et al., 2012) and thalamocortical synaptic depression (Castro-Alamancos and Oldford, 2002; Otazu et al., 2009; Poulet et al., 2012) could account for changes in the sensory-driven response dynamics during active behavior. Grion et al. (2016) reported increased hippocampal theta band oscillations during texture discrimination task compared to a memory task in rats. This was accompanied by an enhanced phase-lock synchronization between whisking rhythm, SI neuronal spiking activity and hippocampal theta oscillation. Future paired recordings from primary somatosensory cortex and primary motor cortex or sensorimotor thalamic areas in awake rodents are required to understand the functional role and interaction of these areas in sensory processing and sensation.

Cortical neurons process information on a background of ongoing activity with distinct spatiotemporal dynamics forming various cortical states. During wakefulness, cortical state changes constantly in relation to behavioral context, attentional level or general motor activity. A common observation in awake rodents is the rapid change in spontaneous cortical activity from high-amplitude, low-frequency fluctuations referred to as synchronized state (e.g., when animals are quiet), to faster and smaller fluctuations, referred to as desynchronized state (e.g., when animals are active). Fazlali et al. (2016) recently showed this re-organization of the activity of cortical networks strongly affects sensory processing. In the desynchronized state, cortical neurons showed lower stimulus detection threshold, higher response fidelity, and shorter response latency with a prominent enhanced late response. Interestingly, changes in the activity of a small population of locus coeruleus (LC) neurons preceded and predicted the changes in the cortical state: the cross-correlation of the LC firing profile with the cortical state was maximal at an average lag of -1.2 s.

3.6. Link to Perception

It is not clear how and where in neocortex the perception of the tactile information emerges. However, a prime candidate for perceptual judgments and navigation based on tactile information is the prefrontal cortex (PFC). Somatosensory cortex projects into the dorsal part of medial prefrontal cortex (mPFC) (Conde et al., 1995)—homolog of primate dorsolateral prefrontal cortex. There are several lines of evidence indicating that in rats, mPFC and in particular its dorsal bank is involved in memory and delayed tasks (Larsen and Divac, 1978; Thomas and Brito, 1980; Eichenbaum et al., 1983; Wolf et al., 1987; Brabander et al., 1991; Granon et al., 1994; Verma and Moghaddam, 1996, but see de Bruin et al., 1994; Sánchez-Santed et al., 1997; Ragozzino et al., 1998). Prefrontal cortex also projects to hippocampus both directly and indirectly through lateral entorhinal cortex. The entorhinal cortex gates sensory information to hippocampus and its lesioning impairs spatial representation (Brun et al., 2008).

Moreover, population dynamics of place-selective grid cells in the medial entorhinal cortex predict adaptive hippocampal remapping (Fyhn et al., 2007). Somatosensory cortex projects to the lateral entorhinal cortex through indirect projections via perirhinal cortex and also via weaker direct projections. This potentially forms an additional pathway of vibrissal information to hippocampus.

4. CONCLUDING REMARKS

Recent years have witnessed a revitalization of interest in rodent models not only in systems neuroscience, but also in the whole body of neuroscience research. This revitalization is partly due to availability of an increasingly powerful array of experimental approaches from optogenetics and two-photon imaging to whole-cell and intracellular electrophysiology and labeling that are challenging to apply to their full potential in primates. Availability of a broad range of genetically modified mouse lines offer scientists the tools to precisely target neuronal circuits and specific cell-types to study their function. The flat surface of the cortex in rodents without sulci and gyri along with its relatively small size is an asset for application of the state-of-the-art battery of techniques in observation and perturbation of neuronal activity. While the rodent somatosensory cortex is probably the most studied system in the literature, providing an immense amount of data from genome expression to cell types and neuronal circuitry, yet there is a huge gap in our understanding and knowledge about how this system functions. Filling this gap requires a comprehensive and coordinated drive from multiple disciplines including but not limited to cellular, systems, computational, behavioral and cognitive neuroscience.

The somatosensory system is an expert system in rodents. This system comprises one of the major channels through which rodents as nocturnal animals collect information about their surrounding environment, making this system an ideal model system to understand the neuronal computations and their underlying cellular and neuronal mechanisms in information processing and decision making. Recent studies reveal complex cognitive functions in rodent somatosensation previously reported in humans and primates such as evidence accumulation for optimal decision making and forming abstract concepts of noisy stimulation patterns (Fassihi et al., 2014; Zuo and Diamond, 2019b). Yet, further behavioral studies are required to unveil the cognitive abilities in rodents. The role of different connections and areas in this system (see **Figure 1**) such as vSII, vMI, TRN, ZI, and SC in different contextual and behavioral conditions is yet to be understood. Within cortical areas, the effect of different laminae and a variety of cell types (Narayanan et al., 2017) within this architecture on different aspects of sensory processing and behavior is not clear, and requires further investigation in future studies.

AUTHOR CONTRIBUTIONS

MA drafted and wrote the manuscript.

FUNDING

MA is supported by an CJ Martin Early Career Fellowship (GNT1110421) from the Australian National Health and Medical Research Council (NMHRC).

ACKNOWLEDGMENTS

The author would like to thank the members of the Tactile Perception and Learning Lab, SISSA, Italy and the Neural Coding Lab, JCSMR, ANU, Australia, particularly Mathew Diamond and Ehsan Arabzadeh for their comments. The author would like to express gratitude to all people who supported this work at the University of New South Wales and the University of Padova. The author also would like to thank Nelly Redolfi for the inspiration and support to complete this work.

REFERENCES

Adelson, E. H., and Bergen, J. R. (1985). Spatiotemporal energy models for the perception of motion. *J. Opt. Soc. Am. A* 2, 284–299.

Adibi, M., and Arabzadeh, E. (2011). A comparison of neuronal and behavioral detection and discrimination performances in rat whisker system. *J. Neurophysiol.* 105:356. doi: 10.1152/jn.00794.2010

Adibi, M., Clifford, C. W., and Arabzadeh, E. (2013a). Informational basis of sensory adaptation: entropy and single-spike efficiency in rat barrel cortex. *J. Neurosci.* 33, 14921–14926. doi: 10.1523/JNEUROSCI.1313-13.2013

Adibi, M., Diamond, M. E., and Arabzadeh, E. (2012). Behavioral study of whisker-mediated vibration sensation in rats. *Proc. Natl. Acad. Sci. U.S.A.* 109, 971–976. doi: 10.1073/pnas.1116726109

Adibi, M., McDonald, J. S., Clifford, C. W., and Arabzadeh, E. (2013b). Adaptation improves neural coding efficiency despite increasing correlations in variability. *J. Neurosci.* 33, 2108–2120. doi: 10.1523/JNEUROSCI.3449-12.2013

Adibi, M., McDonald, J. S., Clifford, C. W., and Arabzadeh, E. (2014). Population decoding in rat barrel cortex: optimizing the linear readout of correlated population responses. *PLoS Comput. Biol.* 10:e1003415. doi: 10.1371/journal.pcbi.1003415

Agmon, A., and Connors, B. W. (1991). Thalamocortical responses of mouse somatosensory (barrel) cortex *in vitro*. *Neuroscience* 41, 365–379. doi: 10.1016/0306-4522(91)90333-J

Agmon, A., Yang, L. T., Jones, E. G., and O'Dowd, D. K. (1995). Topological precision in the thalamic projection to neonatal mouse barrel cortex. *J. Neurosci.* 15, 549–561. doi: 10.1523/JNEUROSCI.15-01-00549.1995

Ahissar, E., and Knutsen, P. (2008). Object localization with whiskers. *Biol. Cybern.* 98, 449–458. doi: 10.1007/s00422-008-0214-4

Ahissar, E., Sosnik, R., and Haidarliu, S. (2000). Transformation from temporal to rate coding in a somatosensory thalamocortical pathway. *Nature* 406, 302–306. doi: 10.1038/35018568

Ahissar, E., and Staiger, J. (2010). S1 laminar specialization. *Scholarpedia* 5:7457. doi: 10.4249/scholarpedia.7457

Alloway, K. D., Hoffer, Z. S., and Hoover, J. E. (2003). Quantitative comparisons of corticothalamic topography within the ventrobasal complex and the posterior nucleus of the rodent thalamus. *Brain Res.* 968, 54–68. doi: 10.1016/S0006-8993(02)04265-8

Alloway, K. D., Lou, L., Nwabueze-Ogbo, F., and Chakrabarti, S. (2006). Topography of cortical projections to the dorsolateral neostriatum in rats: multiple overlapping sensorimotor pathways. *J. Compar. Neurol.* 499, 33–48. doi: 10.1002/cne.21039

Aloimonos, J. (1990). "Purposive and qualitative active vision," in *10th International Conference on Pattern Recognition*, Vol. 1, (Atlantic City, NJ), 346–360. doi: 10.1109/ICPR.1990.118128

Aloimonos, J., Weiss, I., and Bandyopadhyay, A. (1988). Active vision. *Int. J. Comput. Vis.* 1, 333–356. doi: 10.1007/BF00133571

Andermann, M. L., and Moore, C. I. (2006). A somatotopic map of vibrissa motion direction within a barrel column. *Nat. Neurosci.* 9, 543–551. doi: 10.1038/nn1671

Arabzadeh, E., Panzeri, S., and Diamond, M. E. (2004). Whisker vibration information carried by rat barrel cortex neurons. *J. Neurosci.* 24, 6011–6020. doi: 10.1523/JNEUROSCI.1389-04.2004

Arabzadeh, E., Petersen, R. S., and Diamond, M. E. (2003). Encoding of whisker vibration by rat barrel cortex neurons: implications for texture discrimination. *J. Neurosci.* 23, 9146–9154. doi: 10.1523/JNEUROSCI.23-27-09146.2003

Arabzadeh, E., Zorzin, E., and Diamond, M. E. (2005). Neuronal encoding of texture in the whisker sensory pathway. *PLoS Biol.* 3:e17. doi: 10.1371/journal.pbio.0030017

Armstrong-James, M., Callahan, C. A., and Friedman, M. A. (1991). Thalamo-cortical processing of vibrissal information in the rat. I. Intracortical origins of surround but not centre-receptive fields of layer IV neurones in the rat S1 barrel field cortex. *J. Compar. Neurol.* 303, 193–210. doi: 10.1002/cne.903030203

Armstrong-James, M., and Fox, K. (1987). Spatiotemporal convergence and divergence in the rat S1 "barrel" cortex. *J. Compar. Neurol.* 263, 265–281. doi: 10.1002/cne.902630209

Armstrong-James, M., Fox, K., and Das-Gupta, A. (1992). Flow of excitation within rat barrel cortex on striking a single vibrissa. *J. Neurophysiol.* 68, 1345–1358. doi: 10.1152/jn.1992.68.4.1345

Arvidsson, J. (1982). Somatotopic organization of vibrissae afferents in the trigeminal sensorynuclei of the rat studied by transganglionic transport of HRP. *J. Compar. Neurol.* 211, 84–92. doi: 10.1002/cne.902110108

Barbaresi, P., Spreafico, R., Frassoni, C., and Rustioni, A. (1986). GABAergic neurons are present in the dorsal column nuclei but not in the ventroposterior complex of rats. *Brain Res.* 382:305. doi: 10.1016/0006-8993(86)91340-5

Bari, B. A., Ollerenshaw, D. R., Millard, D. C., Wang, Q., and Stanley, G. B. (2013). Behavioral and electrophysiological effects of cortical microstimulation parameters. *PLoS ONE* 8:e82170. doi: 10.1371/journal.pone.0082170

Barlow, H. B., and Levick, W. R. (1969). Three factors limiting the reliable detection of light by retinal ganglion cells of the cat. *J. Physiol.* 200:1. doi: 10.1113/jphysiol.1969.sp008679

Barlow, H. B., Levick, W. R., and Yoon, M. (1971). Responses to single quanta of light in retinal ganglion cells of the cat. *Vis. Res.* 11(Suppl. 3), 87–101. doi: 10.1016/0042-6989(71)90033-2

Barthó, P., Freund, T., and Acsády, L. (2002). Selective GABAergic innervation of thalamic nuclei from zona incerta. *Eur. J. Neurosci.* 16, 999–1014. doi: 10.1046/j.1460-9568.2002.02157.x

Barthó, P., Slézia, A., Varga, V., Bokor, H., Pinault, D., Buzsáki, G., et al. (2007). Cortical control of zona incerta. *J. Neurosci.* 27, 1670–1681. doi: 10.1523/JNEUROSCI.3768-06.2007

Bates, C. A., and Killackey, H. P. (1985). The organization of the neonatal rat's brainstem trigeminal complex and its role in the formation of central trigeminal patterns. *J. Compar. Neurol.* 240, 265–287. doi: 10.1002/cne.902400305

Belford, G. R., and Killackey, H. P. (1979). Vibrissae representation in subcortical trigeminal centers of the neonatal rat. *J. Compar. Neurol.* 183, 305–321. doi: 10.1002/cne.901830207

Bellavance, M.-A., Demers, M., and Deschênes, M. (2010). Feedforward inhibition determines the angular tuning of vibrissal responses in the principal trigeminal nucleus. *J. Neurosci.* 30, 1057–1063. doi: 10.1523/JNEUROSCI.4805-09.2010

Benison, A. M., Rector, D. M., and Barth, D. S. (2007). Hemispheric mapping of secondary somatosensory cortex in the rat. *J. Neurophysiol.* 97, 200–207. doi: 10.1152/jn.00673.2006

Bennett-Clarke, C. A., Chiaia, N. L., Jacquin, M. F., and Rhoades, R. W. (1992). Parvalbumin and calbindin immunocytochemistry reveal functionally distinct cell groups and vibrissa-related patterns in the trigeminal brainstem complex of the adult rat. *J. Compar. Neurol.* 320, 323–338. doi: 10.1002/cne.903200305

Berg, R. W., and Kleinfeld, D. (2003). Rhythmic whisking by rat: Retraction as well as protraction of the vibrissae is under active muscular control. *J. Neurophysiol.* 89, 104–117. doi: 10.1152/jn.00600.2002

Bernardo, K. L., McCasland, J. S., and Woolsey, T. A. (1990a). Local axonal trajectories in mouse barrel cortex. *Exp. Brain Res.* 82, 247–253. doi: 10.1007/BF00231244

Bernardo, K. L., McCasland, J. S., Woolsey, T. A., and Strominger, R. N. (1990b). Local intra- and interlaminar connections in mouse barrel cortex. *J. Compar. Neurol.* 291, 231–255. doi: 10.1002/cne.902910207

Bernardo, K. L., and Woolsey, T. A. (1987). Axonal trajectories between mouse somatosensory thalamus and cortex. *J. Compar. Neurol.* 258, 542–564. doi: 10.1002/cne.902580406

Blasdel, G. G., and Salama, G. (1986). Voltage-sensitive dyes reveal a modular organization in monkey striate cortex. *Nature* 321, 579–585. doi: 10.1038/321579a0

Bokor, H., Frère, S. G., Eyre, M. D., Slézia, A., Ulbert, I., Lüthi, A., et al. (2005). Selective gabaergic control of higher-order thalamic relays. *Neuron* 45, 929–940. doi: 10.1016/j.neuron.2005.01.048

Bonhoeffer, T., and Grinvald, A. (1991). Iso-orientation domains in cat visual cortex are arranged in pinwheel-like patterns. *Nature* 353, 429–431. doi: 10.1038/353429a0

Bourassa, J., Pinault, D., and Deschênes, M. (1995). Corticothalamic projections from the cortical barrel field to the somatosensory thalamus in rats: a single-fibre study using biocytin as an anterograde tracer. *Eur. J. Neurosci.* 7, 19–30. doi: 10.1111/j.1460-9568.1995.tb01016.x

Bouyer, J. J., Montaron, M. F., and Rougeul, A. (1981). Fast fronto-parietal rhythms during combined focused attentive behaviour and immobility in cat: cortical and thalamic localizations. *Electroencephalogr. Clin. Neurophysiol.* 51, 244–252. doi: 10.1016/0013-4694(81)90138-3

Brecht, M. (2007). Barrel cortex and whisker-mediated behaviors. *Curr. Opin. Neurobiol.* 17, 408–416. doi: 10.1016/j.conb.2007.07.008

Brecht, M., Preilowski, B., and Merzenich, M. M. (1997). Functional architecture of the mystacial vibrissae. *Behav. Brain Res.* 84, 81–97. doi: 10.1016/S0166-4328(97)83328-1

Brecht, M., Roth, A., and Sakmann, B. (2003). Dynamic receptive fields of reconstructed pyramidal cells in layers 3 and 2 of rat somatosensory barrel cortex. *J. Physiol.* 553, 243–265. doi: 10.1113/jphysiol.2003.044222

Brecht, M., and Sakmann, B. (2002). Dynamic representation of whisker deflection by synaptic potentials in spiny stellate and pyramidal cells in the barrels and septa of layer 4 rat somatosensory cortex. *J. Physiol.* 543, 49–70. doi: 10.1113/jphysiol.2002.018465

Bruce, L. L., McHaffie, J. G., and Stein, B. E. (1987). The organization of trigeminotectal and trigeminothalamic neurons in rodents: a double-labeling study with fluorescent dyes. *J. Compar. Neurol.* 262, 315–330. doi: 10.1002/cne.902620302

Brun, V. H., Leutgeb, S. Q., Wu, H., Schwarcz, R., Witter, M. P., Moser, E. I., et al. (2008). Impaired spatial representation in CA1 after lesion of direct input from entorhinal cortex. *Neuron* 57, 290–302. doi: 10.1016/j.neuron.2007.11.034

Bruno, R. M., Khatri, V., Land, P. W., and Simons, D. J. (2003). Thalamocortical angular tuning domains within individual barrels of rat somatosensory cortex. *J. Neurosci.* 23, 9565–9574. doi: 10.1523/JNEUROSCI.23-29-09565.2003

Bruno, R. M., and Simons, D. J. (2002). Feedforward mechanisms of excitatory and inhibitory cortical receptive fields. *J. Neurosci.* 22, 10966–10975. doi: 10.1523/JNEUROSCI.22-24-10966.2002

Bureau, I., von Saint Paul, F., and Svoboda, K. (2006). Interdigitated paralemniscal and lemniscal pathways in the mouse barrel cortex. *PLoS Biol.* 4:e382. doi: 10.1371/journal.pbio.0040382

Buzsaki, G. (2009). *Rhythms of the Brain*. Oxford: Oxford University Press.

Cao, Y., Roy, S., Sachdev, R. N., and Heck, D. H. (2012). Dynamic correlation between whisking and breathing rhythms in mice. *J. Neurosci.* 32, 1653–1659. doi: 10.1523/JNEUROSCI.4395-11.2012

Carvell, G. E., and Simons, D. J. (1986). Somatotopic organization of the second somatosensory area (SII) in the cerebral cortex of the mouse. *Somatosens. Mot. Res.* 3, 213–237. doi: 10.3109/07367228609144585

Carvell, G. E., and Simons, D. J. (1987). Thalamic and corticocortical connections of the second somatic sensory area of the mouse. *J. Compar. Neurol.* 265, 409–427. doi: 10.1002/cne.902650309

Carvell, G. E., and Simons, D. J. (1990). Biometric analyses of vibrissal tactile discrimination in the rat. *J. Neurosci.* 10, 2638–2648. doi: 10.1523/JNEUROSCI.10-08-02638.1990

Carvell, G. E., and Simons, D. J. (1995). Task- and subject-related differences in sensorimotor behavior during active touch. *Somatosens. Mot. Res.* 12, 1–9. doi: 10.3109/08990229509063138

Carvell, G. E., Simons, D. J., Lichtenstein, S. H., and Bryant, P. (1991). Electromyographic activity of mystacial pad musculature during whisking behavior in the rat. *Somatosens. Mot. Res.* 8, 159–164. doi: 10.3109/08990229109144740

Castro-Alamancos, M. A. (2004). Absence of rapid sensory adaptation in neocortex during information processing states. *Neuron* 41, 455–464. doi: 10.1016/S0896-6273(03)00853-5

Castro-Alamancos, M. A., and Oldford, E. (2002). Cortical sensory suppression during arousal is due to the activity-dependent depression of thalamocortical synapses. *J. Physiol.* 541, 319–331. doi: 10.1113/jphysiol.2002.016857

Celikel, T., and Sakmann, B. (2007). Sensory integration across space and in time for decision making in the somatosensory system of rodents. *Proc. Natl. Acad. Sci. U.S.A.* 104, 1395–1400. doi: 10.1073/pnas.0610267104

Chakrabarti, S., and Alloway, K. (2006). Differential origin of projections from si barrel cortex to the whisker representations in SII and MI. *J. Compar. Neurol.* 498:624. doi: 10.1002/cne.21052

Chen, J. L., Carta, S., Soldado-Magraner, J., Schneider, B. L., and Helmchen, F. (2013). Behaviour-dependent recruitment of long-range projection neurons in somatosensory cortex. *Nature* 499:336. doi: 10.1038/nature12236

Chiaia, N. L., Bennett-Clarke, C. A., and Rhoades, R. W. (1991). Effects of cortical and thalamic lesions upon primary afferent terminations, distributions of projection neurons, and the cytochrome oxidase pattern in the trigeminal brainstem complex. *J. Compar. Neurol.* 303, 600–616. doi: 10.1002/cne.903030407

Chmielowska, J., Carvell, G. E., and Simons, D. J. (1989). Spatial organization of thalamocortical and corticothalamic projection systems in the rat smi barrel cortex. *J. Compar. Neurol.* 285, 325–338. doi: 10.1002/cne.902850304

Churchland, M. M., Byron, M. M., Cunningham, J. P., Sugrue, L. P., Cohen, M. R., Corrado, G. S., et al. (2010). Stimulus onset quenches neural variability: a widespread cortical phenomenon. *Nat. Neurosci.* 13, 369–378. doi: 10.1038/nn.2501

Churchland, M. M., Byron, M. M., Ryu, S. I., Santhanam, G., and Shenoy, K. V. (2006). Neural variability in premotor cortex provides a signature of motor preparation. *J. Neurosci.* 26, 3697–3712. doi: 10.1523/JNEUROSCI.3762-05.2006

Cohen, M. R., and Newsome, W. T. (2009). Estimates of the contribution of single neurons to perception depend on timescale and noise correlation. *J. Neurosci.* 29:6635. doi: 10.1523/JNEUROSCI.5179-08.2009

Conde, F., Mairelepoivre, E., Audinat, E., and Crepel, F. (1995). Afferent connections of the medial frontal-cortex of the rat. 2. Cortical and subcortical afferents. *J. Compar. Neurol.* 352, 567–593. doi: 10.1002/cne.903520407

Constantinople, C. M., and Bruno, R. M. (2013). Deep cortical layers are activated directly by thalamus. *Science* 340, 1591–1594. doi: 10.1126/science.1236425

Crandall, S. R., Patrick, S. L., Cruikshank, S. J., and Connors, B. W. (2017). Infrabarrels are layer 6 circuit modules in the barrel cortex that link long-range inputs and outputs. *Cell Rep.* 21, 3065–3078. doi: 10.1016/j.celrep.2017.11.049

Crick, F. (1984). Function of the thalamic reticular complex: the searchlight hypothesis. *Proc. Natl. Acad. Sci. U.S.A.* 81, 4586–4590. doi: 10.1073/pnas.81.14.4586

Crochet, S., and Petersen, C. C. (2006). Correlating whisker behavior with membrane potential in barrel cortex of awake mice. *Nat. Neurosci.* 9, 608–610. doi: 10.1038/nn1690

Crochet, S., Poulet, J. F., Kremer, Y., and Petersen, C. C. (2011). Synaptic mechanisms underlying sparse coding of active touch. *Neuron* 69, 1160–1175. doi: 10.1016/j.neuron.2011.02.022

Curtis, J. C., and Kleinfeld, D. (2009). Phase-to-rate transformations encode touch in cortical neurons of a scanning sensorimotor system. *Nat. Neurosci.* 12, 492–501. doi: 10.1038/nn.2283

de Brabander, J. M., de Bruin, J. P., and van Eden, C. G. (1991). Comparison of the effects of neonatal and adult medial prefrontal cortex lesions on food hoarding and spatial delayed alternation. *Behav. Brain Res.* 42, 67–75. doi: 10.1016/S0166-4328(05)80041-5

de Bruin, J., Sánchez-Santed, F., Heinsbroek, R., Donker, A., and Postmes, P. (1994). A behavioural analysis of rats with damage to the medial prefrontal cortex using the morris water maze: Evidence for behavioural flexibility, but not for impaired spatial navigation. *Brain Res.* 652, 323–333. doi: 10.1016/0006-8993(94)90243-7

de Lafuente, V., and Romo, R. (2006). Neural correlate of subjective sensory experience gradually builds up across cortical areas. *Proc. Natl. Acad. Sci. U.S.A.* 103:14266. doi: 10.1073/pnas.0605826103

Deschênes, M., Moore, J., and Kleinfeld, D. (2012). Sniffing and whisking in rodents. *Curr. Opin. Neurobiol.* 22, 243–250. doi: 10.1016/j.conb.2011.11.013

Deschênes, M., Takatoh, J., Kurnikova, A., Moore, J. D., Demers, M., Elbaz, M., et al. (2016). Inhibition, not excitation, drives rhythmic whisking. *Neuron* 90, 374–387. doi: 10.1016/j.neuron.2016.03.007

Deschênes, M., Veinante, P., and Zhang, Z.-W. (1998). The organization of corticothalamic projections: reciprocity versus parity. *Brain Res. Rev.* 28, 286–308. doi: 10.1016/S0165-0173(98)00017-4

Desilets-Roy, B., Varga, C., Lavallée, P., and Deschênes, M. (2002). Substrate for cross-talk inhibition between thalamic barreloids. *J. Neurosci.* 22, RC218–RC218. doi: 10.1523/JNEUROSCI.22-09-j0002.2002

Di, S., Baumgartner, C., and Barth, D. S. (1990). Laminar analysis of extracellular field potentials in rat vibrissa/barrel cortex. *J. Neurophysiol.* 63, 832–840. doi: 10.1152/jn.1990.63.4.832

Diamond, M. E. (1995). "Somatosensory thalamus of the rat," in *Cerebral Cortex: The Barrel Cortex of Rodents*, Vol. 11, eds E. G. Jones and I. T. Diamond (New York, NY: Plenum Press), 189–219.

Diamond, M. E., and Arabzadeh, E. (2013). Whisker sensory system: from receptor to decision. *Prog. Neurobiol.* 103, 28–40. doi: 10.1016/j.pneurobio.2012.05.013

Diamond, M. E., Armstrong-James, M., and Ebner, F. F. (1992). Somatic sensory responses in the rostral sector of the posterior group (POM) and in the ventral posterior medial nucleus (VPM) of the rat thalamus. *J. Compar. Neurol.* 318, 462–476. doi: 10.1002/cne.903180410

Diamond, M. E., Von Heimendahl, M., and Arabzadeh, E. (2008). Whisker-mediated texture discrimination. *PLoS Biol.* 6:e220. doi: 10.1371/journal.pbio.0060220

Dörfl, J. (1982). The musculature of the mystacial vibrissae of the white mouse. *J. Anat.* 135(Pt 1):147.

Dörfl, J. (1985). The innervation of the mystacial region of the white mouse: a topographical study. *J. Anat.* 142, 173–184.

Durham, D., and Woolsey, T. A. (1984). Effects of neonatal whisker lesions on mouse central trigeminal pathways. *J. Compar. Neurol.* 223, 424–447. doi: 10.1002/cne.902230308

Dykes, R. (1975). Afferent fibers from mystacial vibrissae of cats and seals. *J. Neurophysiol.* 38, 650–662. doi: 10.1152/jn.1975.38.3.650

Ebara, S., Kumamoto, K., Matsuura, T., Mazurkiewicz, J. E., and Rice, F. L. (2002). Similarities and differences in the innervation of mystacial vibrissal follicle-sinus complexes in the rat and cat: a confocal microscopic study. *J. Compar. Neurol.* 449, 103–119. doi: 10.1002/cne.10277

Ego-Stengel, V., Mello E Souza, T., Jacob, V., and Shulz, D. E. (2005). Spatiotemporal characteristics of neuronal sensory integration in the barrel cortex of the rat. *J. Neurophysiol.* 93, 1450–1467. doi: 10.1152/jn.00912.2004

Eichenbaum, H., Clegg, R. A., and Feeley, A. (1983). Reexamination of functional subdivisions of the rodent prefrontal cortex. *Exp. Neurol.* 79, 434–451. doi: 10.1016/0014-4886(83)90224-8

Emmers, R. (1965). Organization of the first and the second somesthetic regions (SI and SII) in the rat thalamus. *J. Compar. Neurol.* 124, 215–227. doi: 10.1002/cne.901240207

Erzurumlu, R. S., and Killackey, H. P. (1980). Diencephalic projections of the subnucleus interpolaris of the brainstem trigeminal complex in the rat. *Neuroscience* 5:1891. doi: 10.1016/0306-4522(80)90037-8

Estebanez, L., El Boustani, S., Destexhe, A., and Shulz, D. E. (2012). Correlated input reveals coexisting coding schemes in a sensory cortex. *Nat. Neurosci.* 15, 1691–1699. doi: 10.1038/nn.3258

Fanselow, E. E., and Nicolelis, M. A. (1999). Behavioral modulation of tactile responses in the rat somatosensory system. *J. Neurosci.* 19, 7603–7616. doi: 10.1523/JNEUROSCI.19-17-07603.1999

Fassihi, A., Akrami, A., Esmaeili, V., and Diamond, M. E. (2014). Tactile perception and working memory in rats and humans. *Proc. Natl. Acad. Sci. U.S.A.* 111, 2331–2336. doi: 10.1073/pnas.1315171111

Fassihi, A., Akrami, A., Pulecchi, F., Schönfelder, V., and Diamond, M. E. (2017). Transformation of perception from sensory to motor cortex. *Curr. Biol.* 27, 1585–1596. doi: 10.1016/j.cub.2017.05.011

Fazlali, Z., Ranjbar-Slamloo, Y., Adibi, M., and Arabzadeh, E. (2016). Correlation between cortical state and locus coeruleus activity: implications for sensory coding in rat barrel cortex. *Front. Neural Circuits* 10:14. doi: 10.3389/fncir.2016.00014

Fee, M. S., Mitra, P. P., and Kleinfeld, D. (1997). Central versus peripheral determinants of patterned spike activity in rat vibrissa cortex during whisking. *J. Neurophysiol.* 78, 1144–1149. doi: 10.1152/jn.1997.78.2.1144

Feldman, J. L., and Kam, K. (2015). Facing the challenge of mammalian neural microcircuits: taking a few breaths may help. *J. Physiol.* 593, 3–23. doi: 10.1113/jphysiol.2014.277632

Feldmeyer, D. (2012). Excitatory neuronal connectivity in the barrel cortex. *Front. Neuroanat.* 6:24. doi: 10.3389/fnana.2012.00024

Feldmeyer, D., Egger, V., Lübke, J., and Sakmann, B. (1999). Reliable synaptic connections between pairs of excitatory layer 4 neurones within a single 'barrel' of developing rat somatosensory cortex. *J. Physiol.* 521, 169–190. doi: 10.1111/j.1469-7793.1999.00169.x

Feldmeyer, D., Roth, A., and Sakmann, B. (2005). Monosynaptic connections between pairs of spiny stellate cells in layer 4 and pyramidal cells in layer 5a indicate that lemniscal and paralemniscal afferent pathways converge in the infragranular somatosensory cortex. *J. Neurosci.* 25, 3423–3431. doi: 10.1523/JNEUROSCI.5227-04.2005

Ferezou, I., Bolea, S., and Petersen, C. C. (2006). Visualizing the cortical representation of whisker touch: voltage-sensitive dye imaging in freely moving mice. *Neuron* 50, 617–629. doi: 10.1016/j.neuron.2006.03.043

Ferezou, I., Haiss, F., Gentet, L. J., Aronoff, R., Weber, B., and Petersen, C. C. (2007). Spatiotemporal dynamics of cortical sensorimotor integration in behaving mice. *Neuron* 56, 907–923. doi: 10.1016/j.neuron.2007.10.007

Fernández, L. M., Vantomme, G., Osorio-Forero, A., Cardis, R., Béard, E., and Lüthi, A. (2018b). Thalamic reticular control of local sleep in mouse sensory cortex. *eLife* 7:e39111. doi: 10.7554/eLife.39111

Fitzgerald, O. (1940). Discharges from the sensory organs of the cat's vibrissae and the modification in their activity by ions. *J. Physiol.* 98, 163–178. doi: 10.1113/jphysiol.1940.sp003841

Friedberg, M. H., Lee, S. M., and Ebner, F. F. (1999). Modulation of receptive field properties of thalamic somatosensory neurons by the depth of anesthesia. *J. Neurophysiol.* 81, 2243–2252. doi: 10.1152/jn.1999.81.5.2243

Fuentealba, P., and Steriade, M. (2005). The reticular nucleus revisited: intrinsic and network properties of a thalamic pacemaker. *Prog. Neurobiol.* 75, 125–141. doi: 10.1016/j.pneurobio.2005.01.002

Furuta, T., Kaneko, T., and Deschenes, M. (2009). Septal neurons in barrel cortex derive their receptive field input from the lemniscal pathway. *J. Neurosci.* 29, 4089–4095. doi: 10.1523/JNEUROSCI.5393-08.2009

Furuta, T., Nakamura, K., and Deschênes, M. (2006). Angular tuning bias of vibrissa-responsive cells in the paralemniscal pathway. *J. Neurosci.* 26, 10548–10557. doi: 10.1523/JNEUROSCI.1746-06.2006

Fyhn, M., Hafting, T., Treves, A., Moser, M. B., and Moser, E. I. (2007). Hippocampal remapping and grid realignment in entorhinal cortex. *Nature* 446, 190–194. doi: 10.1038/nature05601

Ganguly, K., and Kleinfeld, D. (2004). Goal-directed whisking increases phase-locking between vibrissa movement and electrical activity in primary sensory cortex in rat. *Proc. Natl. Acad. Sci. U.S.A.* 101, 12348–12353. doi: 10.1073/pnas.0308470101

Gentet, L. J., Avermann, M., Matyas, F., Staiger, J. F., and Petersen, C. C. H. (2010). Membrane potential dynamics of GABAergic neurons in the barrel cortex of behaving mice. *Neuron* 65, 422–435. doi: 10.1016/j.neuron.2010.01.006

Gentet, L. J., Kremer, Y., Taniguchi, H., Huang, Z. J., Staiger, J. F., and Petersen, C. C. H. (2012). Unique functional properties of somatostatin-expressing GABAergic neurons in mouse barrel cortex. *Nat. Neurosci.* 15, 607–612. doi: 10.1038/nn.3051

Gerdjikov, T. V., Bergner, C. G., Stüttgen, M. C., Waiblinger, C., and Schwarz, C. (2010). Discrimination of vibrotactile stimuli in the rat whisker system: behavior and neurometrics. *Neuron* 65, 530–540. doi: 10.1016/j.neuron.2010.02.007

Ghazanfar, A. A., and Nicolelis, M. A. (1997). Nonlinear processing of tactile information in the thalamocortical loop. *J. Neurophysiol.* 78, 506–510. doi: 10.1152/jn.1997.78.1.506

Ghazanfar, A. A., and Nicolelis, M. A. (1999). Spatiotemporal properties of layer V neurons of the rat primary somatosensory cortex. *Cereb. Cortex* 9, 348–361. doi: 10.1093/cercor/9.4.348

Gibson, J. (1962). Observations on active touch. *Psychol. Rev.* 69:477. doi: 10.1037/h0046962

Gibson, J. M., and Welker, W. I. (1983a). Quantitative studies of stimulus coding in first-order vibrissa afferents of rats. 1. receptive field properties and threshold distributions. *Somatosens. Mot. Res.* 1, 51–67. doi: 10.3109/07367228309144540

Gibson, J. M., and Welker, W. I. (1983b). Quantitative studies of stimulus coding in first-order vibrissa afferents of rats. 2. Adaptation and coding of stimulus parameters. *Somatosens. Mot. Res.* 1, 95–117. doi: 10.3109/07367228309144543

Gottschaldt, K. M., Iggo, A., and Young, D. W. (1973). Functional characteristics of mechanoreceptors in sinus hair follicles of the cat. *J. Physiol.* 235, 287–315. doi: 10.1113/jphysiol.1973.sp010388

Granon, S., Vidal, C., Thinus-Blanc, C., Changeux, J. P., and Poucet, B. (1994). Working memory, response selection, and effortful processing in rats with medial prefrontal lesions. *Behav. Neurosci.* 108:883. doi: 10.1037/0735-7044.108.5.883

Grant, R. A., Mitchinson, B., Fox, C. W., and Prescott, T. J. (2009). Active touch sensing in the rat: anticipatory and regulatory control of whisker movements during surface exploration. *J. Neurophysiol.* 101:862. doi: 10.1152/jn.90783.2008

Grinvald, A., Lieke, E., Frostig, R. D., Gilbert, C. D., and Wiesel, T. N. (1986). Functional architecture of cortex revealed by optical imaging of intrinsic signals. *Nature* 324, 361–364. doi: 10.1038/324361a0

Grion, N., Akrami, A., Zuo, Y., Stella, F., and Diamond, M. E. (2016). Coherence between rat sensorimotor system and hippocampus is enhanced during tactile discrimination. *PLoS Biol.* 14:e1002384. doi: 10.1371/journal.pbio.1002384

Guić-Robles, E., Jenkins, W. M., and Bravo, H. (1992). Vibrissal roughness discrimination is barrel cortex-dependent. *Behav. Brain Res.* 48, 145–152. doi: 10.1016/S0166-4328(05)80150-0

Guic-Robles, E., Valdivieso, C., and Guajardo, G. (1989). Rats can learn a roughness discrimination using only their vibrissal system. *Behav. Brain Res.* 31, 285–289. doi: 10.1016/0166-4328(89)90011-9

Guo, Z. V., Hires, S. A., Li, N., O'Connor, D. H., Komiyama, T., Ophir, E., et al. (2014a). Procedures for behavioral experiments in head-fixed mice. *PLoS ONE* 9:e88678. doi: 10.1371/journal.pone.0088678

Guo, Z. V., Li, N., Huber, D., Ophir, E., Gutnisky, D., Ting, J. T., et al. (2014b). Flow of cortical activity underlying a tactile decision in mice. *Neuron* 81, 179–194. doi: 10.1016/j.neuron.2013.10.020

Hafting, T., Fyhn, M., Molden, S., Moser, M. B., and Moser, E. I. (2005). Microstructure of a spatial map in the entorhinal cortex. *Nature* 436, 801–806. doi: 10.1038/nature03721

Hahn, J. (1971). Stimulus–response relationships in first-order sensory fibres from cat vibrissae. *J. Physiol.* 213, 215–226. doi: 10.1113/jphysiol.1971.sp009377

Haidarliu, S., and Ahissar, E. (2001). Size gradients of barreloids in the rat thalamus. *J. Compar. Neurol.* 429, 372–387.

Halassa, M. M., Siegle, J. H., Ritt, J. T., Ting, J. T., Feng, G., and Moore, C. I. (2011). Selective optical drive of thalamic reticular nucleus generates thalamic bursts and cortical spindles. *Nat. Neurosci.* 14, 1118–1120. doi: 10.1038/nn.2880

Hanks, T. D., Ditterich, J., and Shadlen, M. N. (2006). Microstimulation of macaque area LIP affects decision-making in a motion discrimination task. *Nat. Neurosci.* 9, 682–689. doi: 10.1038/nn1683

Harris, J. A., Petersen, R. S., and Diamond, M. E. (1999). Distribution of tactile learning and its neural basis. *Proc. Natl. Acad. Sci. U.S.A.* 96, 7587–7591. doi: 10.1073/pnas.96.13.7587

Harris, K. D., and Mrsic-Flogel, T. D. (2013). Cortical connectivity and sensory coding. *Nature* 503, 51–58. doi: 10.1038/nature12654

Harris, R. M. (1986). Morphology of physiologically identified thalamocortical relay neurons in the rat ventrobasal thalamus. *J. Compar. Neurol.* 251, 491–505. doi: 10.1002/cne.902510405

Harris, R. M. (1987). Axon collaterals in the thalamic reticular nucleus from thalamocortical neurons of the rat ventrobasal thalamus. *J. Compar. Neurol.* 258, 397–406. doi: 10.1002/cne.902580308

Hartings, J. A., Temereanca, S., and Simons, D. J. (2000). High responsiveness and direction sensitivity of neurons in the rat thalamic reticular nucleus to vibrissa deflections. *J. Neurophysiol.* 83, 2791–2801. doi: 10.1152/jn.2000.83.5.2791

Harvey, M. A., Bermejo, R., and Zeigler, H. P. (2001). Discriminative whisking in the head-fixed rat: optoelectronic monitoring during tactile detection and discrimination tasks. *Somatosens. Mot. Res.* 18, 211–222. doi: 10.1080/01421590120072204

Hassenstein, B., and Reichardt, W. (1956). Systemtheoretische analyse der zeit-, reihenfolgen-und vorzeichenauswertung bei der bewegungsperzeption des rüsselkäfers chlorophanus. *Z. Naturforsch.* 11, 513–524. doi: 10.1515/znb-1956-9-1004

Hattox, A. M., and Nelson, S. B. (2007). Layer V neurons in mouse cortex projecting to different targets have distinct physiological properties. *J. Neurophysiol.* 98, 3330–3340. doi: 10.1152/jn.00397.2007

Hayama, T., and Ogawa, H. (1997). Regional differences of callosal connections in the granular zones of the primary somatosensory cortex in rats. *Brain Res. Bull.* 43, 341–347. doi: 10.1016/S0361-9230(97)00018-X

Hayashi, H. (1980). Distributions of vibrissae afferent fiber collaterals in the trigeminal nuclei as revealed by intra-axonal injection of horseradish peroxidase. *Brain Res.* 183:442. doi: 10.1016/0006-8993(80)90478-3

Helmchen, F., Gilad, A., and Chen, J. L. (2018). Neocortical dynamics during whisker-based sensory discrimination in head-restrained mice. *Neuroscience* 368, 57–69. doi: 10.1016/j.neuroscience.2017.09.003

Hemelt, M. E., Kwegyir-Afful, E. E., Bruno, R. M., Simons, D. J., and Keller, A. (2010). Consistency of angular tuning in the rat vibrissa system. *J. Neurophysiol.* 104, 3105–3112. doi: 10.1152/jn.00697.2009

Henderson, T., and Jacquin, M. (1995). What makes subcortical barrels. *Cereb. Cortex* 11, 123–187. doi: 10.1007/978-1-4757-9616-2_3

Herkenham, M. (1980). Laminar organization of thalamic projections to the rat neocortex. *Science* 207:532. doi: 10.1126/science.7352263

Herkenham, M. (1986). New perspectives on the organization and evolution of nonspecific thalamocortical projections. *Cereb. Cortex* 5, 403–445. doi: 10.1007/978-1-4613-2149-1_11

Hernández, A., Zainos, A., and Romo, R. (2000). Neuronal correlates of sensory discrimination in the somatosensory cortex. *Proc. Natl. Acad. Sci. U.S.A.* 97:6191. doi: 10.1073/pnas.120018597

Hodge, C. Jr., Stevens, R. T., Newman, H., Merola, J., and Chu, C. (1997). Identification of functioning cortex using cortical optical imaging. *Neurosurgery* 41:1137. doi: 10.1097/00006123-199711000-00023

Hoeflinger, B. F., Bennett-Clarke, C. A., Chiaia, N. L., Killackey, H. P., and Rhoades, R. W. (1995). Patterning of local intracortical projections within the vibrissae representation of rat primary somatosensory cortex. *J. Compar. Neurol.* 354, 551–563. doi: 10.1002/cne.903540406

Hong, W., Kennedy, A., Burgos-Artizzu, X. P., Zelikowsky, M., Navonne, S. G., Perona, P., et al. (2015). Automated measurement of mouse social behaviors using depth sensing, video tracking, and machine learning. *Proc. Natl. Acad. Sci. U.S.A.* 112, E5351–E5360. doi: 10.1073/pnas.1515982112

Hoogland, P. V., Welker, E., and Van der Loos, H. (1987). Organization of the projections from barrel cortex to thalamus in mice studied with phaseolus vulgaris-leucoagglutinin and HRP. *Exp. Brain Res.* 68, 73–87. doi: 10.1007/BF00255235

Hooks, B. M., Hires, S. A., Zhang, Y.-X., Huber, D., Petreanu, L., Svoboda, K., et al. (2011). Laminar analysis of excitatory local circuits in vibrissal motor and sensory cortical areas. *PLoS Biol.* 9:e1000572. doi: 10.1371/journal.pbio.1000572

Hsiao, S. S., O'shaughnessy, D. M., and Johnson, K. O. (1993). Effects of selective attention on spatial form processing in monkey primary and secondary somatosensory cortex. *J. Neurophysiol.* 70, 444–447. doi: 10.1152/jn.1993.70.1.444

Hubel, D. H., and Wiesel, T. N. (1974). Sequence regularity and geometry of orientation columns in the monkey striate cortex. *J. Compar. Neurol.* 158, 267–293. doi: 10.1002/cne.901580304

Huber, D., Petreanu, L., Ghitani, N., Ranade, S., Hromádka, T., Mainen, Z., et al. (2007). Sparse optical microstimulation in barrel cortex drives learned behaviour in freely moving mice. *Nature* 451, 61–64. doi: 10.1038/nature06445

Huerta, M. F., Frankfurter, A., and Harting, J. K. (1983). Studies of the principal sensory and spinal trigeminal nuclei of the rat: projections to the superior colliculus, inferior olive, and cerebellum. *J. Compar. Neurol.* 220, 147–167. doi: 10.1002/cne.902200204

Huet, L. A., and Hartmann, M. J. (2014). The search space of the rat during whisking behavior. *J. Exp. Biol.* 17, 3365–3376. doi: 10.1242/jeb.105338

Hulse, S. H., and Suter, S. (1968). One-drop licking in rats. *J. Compar. Physiol. Psychol.* 66:536. doi: 10.1037/h0026339

Hutson, K. A., and Masterton, R. B. (1986). The sensory contribution of a single vibrissa's cortical barrel. *J. Neurophysiol.* 56, 1196–1223. doi: 10.1152/jn.1986.56.4.1196

Iggo, A., and Muir, A. (1969). The structure and function of a slowly adapting touch corpuscle in hairy skin. *J. Physiol.* 200:763. doi: 10.1113/jphysiol.1969.sp008721

Ito, M. (1985). Processing of vibrissa sensory information within the rat neocortex. *J. Neurophysiol.* 54, 479–490. doi: 10.1152/jn.1985.54.3.479

Itskov, P. M., Vinnik, E., and Diamond, M. E. (2011). Hippocampal representation of touch-guided behavior in rats: Persistent and independent traces of stimulus and reward location. *PLoS ONE* 6:e16462. doi: 10.1371/journal.pone.0016462

Iwamura, Y. (1998). Hierarchical somatosensory processing. *Curr. Opin. Neurobiol.* 8, 522–528. doi: 10.1016/S0959-4388(98)80041-X

Jacob, V., Le Cam, J., Ego-Stengel, V., and Shulz, D. E. (2008). Emergent properties of tactile scenes selectively activate barrel cortex neurons. *Neuron* 60, 1112–1125. doi: 10.1016/j.neuron.2008.10.017

Jacquin, M., Golden, J., and Panneton, W. (1988). Structure and function of barrel 'precursor' cells in trigeminal nucleus principalis. *Dev. Brain Res.* 43, 309–314. doi: 10.1016/0165-3806(88)90109-5

Jacquin, M. F., Barcia, M., and Rhoades, R. W. (1989). Structure-function relationships in rat brainstem subnucleus interpolaris: IV. Projection neurons. *J. Compar. Neurol.* 282, 45–62. doi: 10.1002/cne.902820105

Jacquin, M. F., Mooney, R. T., and Rhoades, R. W. (1986). Morphology, response properties, and collateral projections of trigeminothalamic neurons in brainstem subnucleus interpolaris of rat. *Exp. Brain Res.* 61, 457–468. doi: 10.1007/BF00237571

Jacquin, M. F., Renehan, W. E., Rhoades, R. W., and Panneton, W. M. (1993). Morphology and topography of identified primary afferents in trigeminal subnuclei principalis and oralis. *J. Neurophysiol.* 70, 1911–1936. doi: 10.1152/jn.1993.70.5.1911

Jacquin, M. F., and Rhoadesi, R. W. (1990). Cell structure and response properties in the trigeminal subnucleus oralis. *Somatosens. Mot. Res.* 7, 265–288. doi: 10.3109/08990229009144709

Jenkinson, E. W., and Glickstein, M. (2000). Whiskers, barrels, and cortical efferent pathways in gap crossing by rats. *J. Neurophysiol.* 84, 1781–1789. doi: 10.1152/jn.2000.84.4.1781

Jensen, K. F., and Killackey, H. P. (1987). Terminal arbors of axons projecting to the somatosensory cortex of the adult rat. I. The normal morphology of specific thalamocortical afferents. *J. Neurosci.* 7, 3529–3543. doi: 10.1523/JNEUROSCI.07-11-03529.1987

Jiang, W., Tremblay, F., and Chapman, C. (1997). Neuronal encoding of texture changes in the primary and the secondary somatosensory cortical areas of monkeys during passive texture discrimination. *J. Neurophysiol.* 77, 1656–1662. doi: 10.1152/jn.1997.77.3.1656

Jones, E., and Diamond, I. (1995). *The Barrel Cortex of Rodents*. New York, NY: Plenum Press.

Jones, E. G. (1975). Some aspects of the organization of the thalamic reticular complex. *J. Compar. Neurol.* 162, 285–308. doi: 10.1002/cne.901620302

Kandler, S., Mao, D., McNaughton, B. L., and Bonin, V. (2018). Encoding of tactile context in the mouse visual cortex. *bioRxiv* 199364. doi: 10.1101/199364

Karhu, J., and Tesche, C. (1999). Simultaneous early processing of sensory input in human primary (SI) and secondary (SII) somatosensory cortices. *J. Neurophysiol.* 81, 2017–2025. doi: 10.1152/jn.1999.81.5.2017

Keehn, J. D., and Arnold, E. M. (1960). Licking rates of albino rats. *Science* 132, 739–741. doi: 10.1126/science.132.3429.739

Keller, G. B., Bonhoeffer, T., and Hü bener, M. (2012). Sensorimotor mismatch signals in primary visual cortex of the behaving mouse. *Neuron* 74, 809–815. doi: 10.1016/j.neuron.2012.03.040

Kenan-Vaknin, G., and Teyler, T. J. (1994). Laminar pattern of synaptic activity in rat primary visual cortex: comparison of *in vivo* and *in vitro* studies employing the current source density analysis. *Brain Res.* 635, 37–48. doi: 10.1016/0006-8993(94)91421-4

Kerr, F. W., and Lysak, W. R. (1964). Somatotopic organization of trigeminal-ganglion neurones. *Arch. Neurol.* 11:593. doi: 10.1001/archneur.1964.00460240025003

Kerr, J. N., de Kock, C. P., Greenberg, D. S., Bruno, R. M., Sakmann, B., and Helmchen, F. (2007). Spatial organization of neuronal population

responses in layer 2/3 of rat barrel cortex. *J. Neurosci.* 27, 13316–13328. doi: 10.1523/JNEUROSCI.2210-07.2007

Kiani, R., Hanks, T. D., and Shadlen, M. N. (2008). Bounded integration in parietal cortex underlies decisions even when viewing duration is dictated by the environment. *J. Neurosci.* 28:3017. doi: 10.1523/JNEUROSCI.4761-07.2008

Kida, H., Shimegi, S., and Sato, H. (2005). Similarity of direction tuning among responses to stimulation of different whiskers in neurons of rat barrel cortex. *J. Neurophysiol.* 94, 2004–2018. doi: 10.1152/jn.00113.2004

Kim, J., Matney, C. J., Blankenship, A., Hestrin, S., and Brown, S. P. (2014). Layer 6 corticothalamic neurons activate a cortical output layer, layer 5a. *J. Neurosci.* 34, 9656–9664. doi: 10.1523/JNEUROSCI.1325-14.2014

Kim, U., and Ebner, F. (1999). Barrels and septa: separate circuits in rat barrel field cortex. *J. Compar. Neurol.* 408, 489–505.

Kleinfeld, D., Ahissar, E., and Diamond, M. E. (2006). Active sensation: insights from the rodent vibrissa sensorimotor system. *Curr. Opin. Neurobiol.* 16, 435–444. doi: 10.1016/j.conb.2006.06.009

Kleinfeld, D., and Delaney, K. R. (1996). Distributed representation of vibrissa movement in the upper layers of somatosensory cortex revealed with voltage-sensitive dyes. *J. Compar. Neurol.* 375, 89–108.

Kleinfeld, D., Deschênes, M., Wang, F., and Moore, J. D. (2014). More than a rhythm of life: breathing as a binder of orofacial sensation. *Nat. Neurosci.* 17:647. doi: 10.1038/nn.3693

Kleinfeld, D., Sachdev, R. N., Merchant, L. M., Jarvis, M. R., and Ebner, F. F. (2002). Adaptive filtering of vibrissa input in motor cortex of rat. *Neuron* 34, 1021–1034. doi: 10.1016/S0896-6273(02)00732-8

Knutsen, P. M., and Ahissar, E. (2009). Orthogonal coding of object location. *Trends Neurosci.* 32, 101–109. doi: 10.1016/j.tins.2008.10.002

Knutsen, P. M., Derdikman, D., and Ahissar, E. (2005). Tracking whisker and head movements in unrestrained behaving rodents. *J. Neurophysiol.* 93, 2294–2301. doi: 10.1152/jn.00718.2004

Knutsen, P. M., Pietr, M., and Ahissar, E. (2006). Haptic object localization in the vibrissal system: behavior and performance. *J. Neurosci.* 26, 8451–8464. doi: 10.1523/JNEUROSCI.1516-06.2006

Kolmac, C. I., Power, B. D., and Mitrofanis, J. (1998). Patterns of connections between zona incerta and brainstem in rats. *J. Compar. Neurol.* 396, 544–555.

Koralek, K. A., Jensen, K. F., and Killackey, H. P. (1988). Evidence for two complementary patterns of thalamic input to the rat somatosensory cortex. *Brain Res.* 463, 346–351. doi: 10.1016/0006-8993(88)90408-8

Koralek, K. A., Olavarria, J., and Kellackey, H. P. (1990). Areal and laminar organization of corticocortical projections in the rat somatosensory cortex. *J. Compar. Neurol.* 299, 133–150. doi: 10.1002/cne.902990202

Kremer, Y., Léger, J.-F., Goodman, D., Brette, R., and Bourdieu, L. (2011). Late emergence of the vibrissa direction selectivity map in the rat barrel cortex. *J. Neurosci.* 31, 10689–10700. doi: 10.1523/JNEUROSCI.6541-10.2011

Krupa, D. J., Matell, M. S., Brisben, A. J., Oliveira, L. M., and Nicolelis, M. A. (2001). Behavioral properties of the trigeminal somatosensory system in rats performing whisker-dependent tactile discriminations. *J. Neurosci.* 21, 5752–5763. doi: 10.1523/JNEUROSCI.21-15-05752.2001

Kuhlman, W. N. (1978). Functional topography of the human mu rhythm. *Electroencephalogr. Clin. Neurophysiol.* 44, 83–93. doi: 10.1016/0013-4694(78)90107-4

Kwegyir-Afful, E. E. and Keller, A. (2004). Response properties of whisker-related neurons in rat second somatosensory cortex. *J. Neurophysiol.* 92, 2083–2092. doi: 10.1152/jn.00262.2004

Kwon, S. E., Tsytsarev, V., Erzurumlu, R. S., and O'Connor, D. H. (2018). Organization of orientation-specific whisker deflection responses in layer 2/3 of mouse somatosensory cortex. *Neuroscience* 368, 46–56. doi: 10.1016/j.neuroscience.2017.07.067

Lam, Y. W., and Sherman, S. S. (2007). Different topography of the reticulothalmic inputs to first-and higher-order somatosensory thalamic relays revealed using photostimulation. *J. Neurophysiol.* 98, 2903–2909. doi: 10.1152/jn.00782.2007

Land, P. W., Buffer, S. A. Jr., and Yaskosky, J. D. (1995). Barreloids in adult rat thalamus: three-dimensional architecture and relationship to somatosensory cortical barrels. *J. Compar. Neurol.* 355, 573–588. doi: 10.1002/cne.903550407

Landisman, C. E., Long, M. M., Beierlein, M., Deans, M. R., Paul, D. L., and Connors, B. W. (2002). Electrical synapses in the thalamic reticular nucleus. *J. Neurosci.* 22, 1002–1009. doi: 10.1523/JNEUROSCI.22-03-01002.2002

Larsen, D. I., Wickersham, I. R., and Callaway, E. M. (2007). Retrograde tracing with recombinant rabies virus reveals correlations between projection targets and dendritic architecture in layer 5 of mouse barrel cortex. *Front. Neural Circuits* 1:5. doi: 10.3389/neuro.04.005.2007

Larsen, J., and Divac, I. (1978). Selective ablations within the prefrontal cortex of the rat and performance of delayed alternation. *Physiol. Psychol.* 6, 15–17. doi: 10.3758/BF03326684

Lavallée, P. and Deschênes, M. (2004). Dendroarchitecture and lateral inhibition in thalamic barreloids. *J. Neurosci.* 24, 6098–6105. doi: 10.1523/JNEUROSCI.0973-04.2004

Lavallée, P., Urbain, N., Dufresne, C., Bokor, H., Acsady, L., and Deschênes, M. (2005). Feedforward inhibitory control of sensory information in higher-order thalamic nuclei. *J. Neurosci.* 25:7489. doi: 10.1523/JNEUROSCI.2301-05.2005

Lavzin, M., Rapoport, S., Polsky, A., Garion, L., and Schiller, J. (2012). Nonlinear dendritic processing determines angular tuning of barrel cortex neurons *in vivo*. *Nature* 490, 397–401. doi: 10.1038/nature11451

Le Cam, J., Estebanez, L., Jacob, V., and Shulz, D. E. (2011). Spatial structure of multiwhisker receptive fields in the barrel cortex is stimulus dependent. *J. Neurophysiol.* 106, 986–998. doi: 10.1152/jn.00044.2011

Lee, C. C., Diamond, M. E., and Arabzadeh, E. (2016). Sensory prioritization in rats: behavioral performance and neuronal correlates. *J. Neurosci.* 36, 3243–3253. doi: 10.1523/JNEUROSCI.3636-15.2016

Lee, C. C. Y., Clifford, C. W. G., and Arabzadeh, E. (2019). Temporal cueing enhances neuronal and behavioral discrimination performance in rat whisker system. *J. Neurophysiol.* 121, 1048–1058. doi: 10.1152/jn.00604.2018

Lee, K. J., and Woolsey, T. A. (1975). A proportional relationship between peripheral innervation density and cortical neuron number in the somatosensory system of the mouse. *Brain Res.* 99, 349–353. doi: 10.1016/0006-8993(75)90035-9

Lee, S. M., Friedberg, M. H., and Ebner, F. F. (1994). The role of GABA-mediated inhibition in the rat ventral posterior medial thalamus. i. Assessment of receptive field changes following thalamic reticular nucleus lesions. *J. Neurophysiol.* 71, 1702–1715. doi: 10.1152/jn.1994.71.5.1702

Lefort, S., Tomm, C., Sarria, J.-C., and Petersen, C. C. (2009). The excitatory neuronal network of the c2 barrel column in mouse primary somatosensory cortex. *Neuron* 61, 301–316. doi: 10.1016/j.neuron.2008.12.020

Lewis, L. D., Voigts, J., Flores, F. J., Schmitt, L. I., Wilson, M. A., Halassa, M. M., et al. (2015). Thalamic reticular nucleus induces fast and local modulation of arousal state. *eLife* 4:e08760. doi: 10.7554/eLife.08760

Li, N., Chen, T.-W., Guo, Z. V., Gerfen, C. R., and Svoboda, K. (2015). A motor cortex circuit for motor planning and movement. *Nature* 519:51. doi: 10.1038/nature14178

Lichtenstein, S., Carvell, G. E., and Simons, D. G. (1990). Responses of rat trigeminal ganglion neurons to movements of vibrissae in different directions. *Somatosens. Mot. Res.* 7, 47–65. doi: 10.3109/08990229009144697

Lin, C., Nicolelis, M., Schneider, J., and Chapin, J. (1990). A major direct GABAergic pathway from zona incerta to neocortex. *Science* 248:1553. doi: 10.1126/science.2360049

Lu, S.-M., and Lin, R. C. (1993). Thalamic afferents of the rat barrel cortex: a light-and electron-microscopic study using phaseolus vulgaris leucoagglutinin as an anterograde tracer. *Somatosens. Mot. Res.* 10, 1–16. doi: 10.3109/08990229309028819

Lübke J. H., and Feldmeyer D. (eds.). (2010). The axon of excitatory neurons in the neocortex: projection patterns and target specificity," in *New Aspects of Axonal Structure and Function* (Boston, MA: Springer). doi: 10.1007/978-1-4419-1676-1_9

Luna, R., Hernández, A., Brody, C. D., and Romo, R. (2005). Neural codes for perceptual discrimination in primary somatosensory cortex. *Nat. Neurosci.* 8, 1210–1219. doi: 10.1038/nn1513

Ma, P. M. (1991). The barrelettes—architectonic vibrissal representations in the brainstem trigeminal complex of the mouse. normal structural organization. *J. Compar. Neurol.* 309, 161–199. doi: 10.1002/cne.903090202

Ma, P. M., and Woolsey, T. A. (1984). Cytoarchitectonic correlates of the vibrissae in the medullary trigeminal complex of the mouse. *Brain Res.* 306:374. doi: 10.1016/0006-8993(84)90390-1

Manns, I. D., Sakmann, B., and Brecht, M. (2004). Sub- and suprathreshold receptive field properties of pyramidal neurons in layers 5a and

5b of rat somatosensory barrel cortex. *J. Physiol.* 556, 601–622. doi: 10.1113/jphysiol.2003.053132

Maravall, M., Petersen, R. S., Fairhall, A. L., Arabzadeh, E., and Diamond, M. E. (2007). Shifts in coding properties and maintenance of information transmission during adaptation in barrel cortex. *PLoS Biol.* 5:e19. doi: 10.1371/journal.pbio.0050019

Markram, H., Lübke, J., Frotscher, M., Roth, A., and Sakmann, B. (1997). Physiology and anatomy of synaptic connections between thick tufted pyramidal neurones in the developing rat neocortex. *J. Physiol.* 500, 409–440. doi: 10.1113/jphysiol.1997.sp022031

Matyas, F., Sreenivasan, V., Marbach, F., Wacongne, C., Barsy, B., Mateo, C., et al. (2010). Motor control by sensory cortex. *Science* 330, 1240–1243. doi: 10.1126/science.1195797

May, P. J., Sun, W., and Hall, W. C. (1997). Reciprocal connections between the zona incerta and the pretectum and superior colliculus of the cat. *Neuroscience* 77, 1091–1114. doi: 10.1016/S0306-4522(96)00535-0

Mayrhofer, J. M., Skreb, V., von der Behrens, W., Musall, S., Weber, B., and Haiss, F. (2012). Novel two-alternative forced choice paradigm for bilateral vibrotactile whisker frequency discrimination in head-fixed mice and rats. *J. Neurophysiol.* 109, 273–284. doi: 10.1152/jn.00488.2012

McDonald, J. S., Adibi, M., Clifford, C. W., and Arabzadeh, E. (2014). Sampling time and performance in rat whisker sensory system. *PLoS ONE* 9:e116357. doi: 10.1371/journal.pone.0116357

McGuire, L. M., Telian, G., Laboy-Juárez, K. J., Miyashita, T., Lee, D. J., Smith, K. A., et al. (2016). Short time-scale sensory coding in s1 during discrimination of whisker vibrotactile sequences. *PLoS Biol.* 14:e1002549. doi: 10.1371/journal.pbio.1002549

Mehta, S. B., Whitmer, D., Figueroa, R., Williams, B. A., and Kleinfeld, D. (2007). Active spatial perception in the vibrissa scanning sensorimotor system. *PLoS Biol.* 5:e15. doi: 10.1371/journal.pbio.0050015

Melaragno, H. P., and Montagna, W. (1953). The tactile hair follicles in the mouse. *Anat. Record* 115, 129–149. doi: 10.1002/ar.1091150202

Miguelez Fernández, A. M. M., Burman, A., Martínez Cáceres, A. I., Mininni, C. J., Zanutto, B. S., and Lew, S. E. (2018a). A spherical treadmill system to train head-fixed adult rats. *J. Neurosci. Methods* 297, 22–30. doi: 10.1016/j.jneumeth.2017.12.018

Mima, T., Nagamine, T., Nakamura, K., and Shibasaki, H. (1998). Attention modulates both primary and second somatosensory cortical activities in humans: a magnetoencephalographic study. *J. Neurophysiol.* 80, 2215–2221. doi: 10.1152/jn.1998.80.4.2215

Minnery, B. S., Bruno, R. M., and Simons, D. J. (2003). Response transformation and receptive-field synthesis in the lemniscal trigeminothalamic circuit. *J. Neurophysiol.* 90, 1556–1570. doi: 10.1152/jn.00111.2003

Minnery, B. S., and Simons, D. J. (2003). Response properties of whisker-associated trigeminothalamic neurons in rat nucleus principalis. *J. Neurophysiol.* 89, 40–56. doi: 10.1152/jn.00272.2002

Mitchinson, B., Grant, R. A., Arkley, K., Rankov, V., Perkon, I., and Prescott, T. J. (2011). Active vibrissal sensing in rodents and marsupials. *Philos. Trans. R. Soc. B Biol. Sci.* 366, 3037–3048. doi: 10.1098/rstb.2011.0156

Mitchinson, B., Martin, C. J., Grant, R. A., and Prescott, T. J. (2007). Feedback control in active sensing: rat exploratory whisking is modulated by environmental contact. *Proc. R. Soc. B Biol. Sci.* 274, 1035–1041. doi: 10.1098/rspb.2006.0347

Mitrofanis, J. (2005). Some certainty for the "zone of uncertainty"? Exploring the function of the zona incerta. *Neuroscience* 130, 1–15. doi: 10.1016/j.neuroscience.2004.08.017

Mitrofanis, J., and Mikuletic, L. (1999). Organisation of the cortical projection to the zona incerta of the thalamus. *J. Compar. Neurol.* 412, 173–185.

Moore, C. I., and Nelson, S. B. (1998). Spatio-temporal subthreshold receptive fields in the vibrissa representation of rat primary somatosensory cortex. *J. Neurophysiol.* 80, 2882–2892. doi: 10.1152/jn.1998.80.6.2882

Moore, J. D., Deschênes, M., Furuta, T., Huber, D., Smear, M. C., Demers, M., et al. (2013). Hierarchy of orofacial rhythms revealed through whisking and breathing. *Nature* 497:205. doi: 10.1038/nature12076

Moore, J. D., Deschênes, M., Kurnikova, A., and Kleinfeld, D. (2014). Activation and measurement of free whisking in the lightly anesthetized rodent. *Nat. Protoc.* 9:1792. doi: 10.1038/nprot.2014.119

Morita, T., Kang, H., Wolfe, J., Jadhav, S. P., and Feldman, D. E. (2011). Psychometric curve and behavioral strategies for whisker-based texture discrimination in rats. *PLoS ONE* 6:e20437. doi: 10.1371/journal.pone.0020437

Mountcastle, V., LaMotte, R. B., and Carli, G. H. (1972). Detection thresholds for stimuli in humans and monkeys: comparison with threshold events in mechanoreceptive afferent nerve fibers innervating the monkey hand. *J. Neurophysiol.* 35, 122–136. doi: 10.1152/jn.1972.35.1.122

Munger, B. L., Pubols, L. M., and Pubols, B. H. (1971). The merkel rete papilla—a slowly adapting sensory receptor in mammalian glabrous skin. *Brain Res.* 29, 47–61. doi: 10.1016/0006-8993(71)90416-1

Musall, S., Von Der Behrens, W., Mayrhofer, J. M., Weber, B., Helmchen, F., and Haiss, F. (2014). Tactile frequency discrimination is enhanced by circumventing neocortical adaptation. *Nat. Neurosci.* 17:1567. doi: 10.1038/nn.3821

Narayanan, R. T., Udvary, D., and Oberlaender, M. (2017). Cell type-specific structural organization of the six layers in rat barrel cortex. *Front. Neuroanat.* 11:91. doi: 10.3389/fnana.2017.00091

Newsome, W. T., Britten, K. H., and Movshon, J. A. (1989). Neuronal correlates of a perceptual decision. *Nature* 341, 52–54. doi: 10.1038/341052a0

Nicolelis, M., Chapin, J., and Lin, R. (1992). Somatotopic maps within the zona incerta relay parallel GABAergic somatosensory pathways to the neocortex, superior colliculus, and brainstem. *Brain Res.* 577, 134–141. doi: 10.1016/0006-8993(92)90546-L

Niell, C. M., and Stryker, M. P. (2010). Modulation of visual responses by behavioral state in mouse visual cortex. *Neuron* 65, 472–479. doi: 10.1016/j.neuron.2010.01.033

Nikbakht, N., Tafreshiha, A., Zoccolan, D., and Diamond, M. E. (2018). Supralinear and supramodal integration of visual and tactile signals in rats: psychophysics and neuronal mechanisms. *Neuron* 97, 626–639. doi: 10.1016/j.neuron.2018.01.003

Nord, S. (1967). Somatotopic organization in the spinal trigeminal nucleus, the dorsal column nuclei and related structures in the rat. *J. Compar. Neurol.* 130, 343–356. doi: 10.1002/cne.901300406

Oberlaender, M., de Kock, C., Bruno, R., Ramirez, A., Meyer, H. S., Dercksen, V. J., et al. (2012). Cell type specific three-dimensional structure of thalamocortical circuits in a column of rat vibrissal cortex. *Cereb. Cortex* 22, 2375–2391. doi: 10.1093/cercor/bhr317

O'Connor, D. H., Clack, N. G., Huber, D., Komiyama, T., Myers, E. W., and Svoboda, K. (2010). Vibrissa-based object localization in head-fixed mice. *J. Neurosci.* 30:1947. doi: 10.1523/JNEUROSCI.3762-09.2010

O'Connor, S. M., Berg, R. W., and Kleinfeld, D. (2002). Coherent electrical activity between vibrissa sensory areas of cerebellum and neocortex is enhanced during free whisking. *J. Neurophysiol.* 87, 2137–2148. doi: 10.1152/jn.00229.2001

Ohki, K., Chung, S., Ch'ng, Y. H., Kara, P., and Reid, R. C. (2005). Functional imaging with cellular resolution reveals precise micro-architecture in visual cortex. *Nature* 433, 597–603. doi: 10.1038/nature03274

Ohki, K., Chung, S., Kara, P., Hübener, M., Bonhoeffer, T., and Reid, R. C. (2006). Highly ordered arrangement of single neurons in orientation pinwheels. *Nature* 442, 925–928. doi: 10.1038/nature05019

O'Keefe, J. (1976). Place units in the hippocampus of the freely moving rat. *Exp. Neurol.* 51, 78–109. doi: 10.1016/0014-4886(76)90055-8

O'keefe, J., and Conway, D. H. (1978). Hippocampal place units in the freely moving rat: why they fire where they fire. *Exp. Brain Res.* 31, 573–590. doi: 10.1007/BF00239813

O'keefe, J., and Nadel, L. (1978). *The Hippocampus as a Cognitive Map*. Oxford: Oxford University Press.

Ollerenshaw, D. R., Bari, B. A., Millard, D. C., Orr, L. E., Wang, Q., and Stanley, G. B. (2012). Detection of tactile inputs in the rat vibrissa pathway. *J. Neurophysiol.* 108, 479–490. doi: 10.1152/jn.00004.2012

Oram, M. (2011). Visual stimulation decorrelates neuronal activity. *J. Neurophysiol.* 105, 942–957. doi: 10.1152/jn.00711.2009

Osborne, L. C., Bialek, W., and Lisberger, S. G. (2004). Time course of information about motion direction in visual area MT of macaque monkeys. *J. Neurosci.* 24, 3210–3222. doi: 10.1523/JNEUROSCI.5305-03.2004

Otazu, G. H., Tai, L. H., Yang, Y., and Zador, A. M. (2009). Engaging in an auditory task suppresses responses in auditory cortex. *Nat. Neurosci.* 12, 646–654. doi: 10.1038/nn.2306

Petersen, C. C. (2007). The functional organization of the barrel cortex. *Neuron* 56, 339–355. doi: 10.1016/j.neuron.2007.09.017

Petersen, C. C., and Crochet, S. (2013). Synaptic computation and sensory processing in neocortical layer 2/3. *Neuron* 78, 28–48. doi: 10.1016/j.neuron.2013.03.020

Petersen, R. S., and Diamond, M. E. (2000). Spatial-temporal distribution of whisker-evoked activity in rat somatosensory cortex and the coding of stimulus location. *J. Neurosci.* 20, 6135–6143. doi: 10.1523/JNEUROSCI.20-16-06135.2000

Pierret, T., Lavallée, P., and Deschênes, M. (2000). Parallel streams for the relay of vibrissal information through thalamic barreloids. *J. Neurosci.* 20, 7455–7462. doi: 10.1523/JNEUROSCI.20-19-07455.2000

Pinault, D. (2004). The thalamic reticular nucleus: structure, function and concept. *Brain Res. Rev.* 46, 1–31. doi: 10.1016/j.brainresrev.2004.04.008

Pinault, D., Bourassa, J., and Deschênes, M. (1995). The axonal arborization of single thalamic reticular neurons in the somatosensory thalamus of the rat. *Eur. J. Neurosci.* 7, 31–40. doi: 10.1111/j.1460-9568.1995.tb01017.x

Pinto, D. J., Brumberg, J. C., and Simons, D. J. (2000). Circuit dynamics and coding strategies in rodent somatosensory cortex. *J. Neurophysiol.* 83:1158. doi: 10.1152/jn.2000.83.3.1158

Polley, D. B., Rickert, J. L., and Frostig, R. D. (2005). Whisker-based discrimination of object orientation determined with a rapid training paradigm. *Neurobiol. Learn. Mem.* 83, 134–142. doi: 10.1016/j.nlm.2004.10.005

Poulet, J. F., Fernandez, L. M., Crochet, S., and Petersen, C. C. (2012). Thalamic control of cortical states. *Nat. Neurosci.* 15, 370–372. doi: 10.1038/nn.3035

Poulet, J. F., and Petersen, C. C. (2008). Internal brain state regulates membrane potential synchrony in barrel cortex of behaving mice. *Nature* 454, 881–885. doi: 10.1038/nature07150

Power, B. D., Kolmac, C. I., and Mitrofanis, J. (1999). Evidence for a large projection from the zona incerta to the dorsal thalamus. *J. Compar. Neurol.* 404, 554–565.

Prigg, T., Goldreich, D., Carvell, G. E., and Simons, D. J. (2002). Texture discrimination and unit recordings in the rat whisker/barrel system. *Physiol. Behav.* 77, 671–675. doi: 10.1016/S0031-9384(02)00917-4

Pubols, B. H., Donovick, P. J., and Pubols, L. M. (1973). Opossum trigeminal afferents associated with vibrissa and rhinarial mechanoreceptors. *Brain Behav. Evol.* 7, 360–381. doi: 10.1159/000124423

Puccini, G. D., Compte, A., and Maravall, M. (2006). Stimulus dependence of barrel cortex directional selectivity. *PLoS ONE* 1:e137. doi: 10.1371/journal.pone.0000137

Ragozzino, M. E., Adams, S., and Kesner, R. P. (1998). Differential involvement of the dorsal anterior cingulate and prelimbic-infralimbic areas of the rodent prefrontal cortex in spatial working memory. *Behav. Neurosci.* 112:293. doi: 10.1037//0735-7044.112.2.293

Ramaswamy, S., and Markram, H. (2015). Anatomy and physiology of the thick-tufted layer 5 pyramidal neuron. *Front. Cell. Neurosci.* 9:233. doi: 10.3389/fncel.2015.00233

Reichardt, W. (1961). "Autocorrelation, a principle for the evaluation of sensory information by the central nervous system," in *Sensory Communication*, Chapter 17, ed W. Rosenblith (Cambridge: MIT Press), 303–317.

Renehan, W. E., and Munger, B. L. (1986). Degeneration and regeneration of peripheral nerve in the rat trigeminal system. I. Identification and characterization of the multiple afferent innervation of the mystacial vibrissae. *J. Compar. Neurol.* 246, 129–145. doi: 10.1002/cne.902460109

Ress, D., and Heeger, D. (2003). Neuronal correlates of perception in early visual cortex. *Nat. Neurosci.* 6:414. doi: 10.1038/nn1024

Reyes, A., and Sakmann, B. (1999). Developmental switch in the short-term modification of unitary epsps evoked in layer 2/3 and layer 5 pyramidal neurons of rat neocortex. *J. Neurosci.* 19, 3827–3835. doi: 10.1523/JNEUROSCI.19-10-03827.1999

Rice, F. L., Fundin, B. T., Arvidsson, J., Aldskogius, H., and Johansson, O. (1997). Comprehensive immunofluorescence and lectin binding analysis of vibrissal follicle sinus complex innervation in the mystacial pad of the rat. *J. Compar. Neurol.* 385, 149–184.

Rice, F. L., Mance, A., and Munger, B. L. (1986). A comparative light microscopic analysis of the sensory innervation of the mystacial pad. i. innervation of vibrissal follicle-sinus complexes. *J. Compar. Neurol.* 252, 154–174. doi: 10.1002/cne.902520203

Rigosa, J., Lucantonio, A., Noselli, G., Fassihi, A., Zorzin, E., Manzino, F., et al. (2017). Dye-enhanced visualization of rat whiskers for behavioral studies. *Elife* 6:e25290. doi: 10.7554/eLife.25290

Romo, R., Hernández, A., and Zainos, A. (2004). Neuronal correlates of a perceptual decision in ventral premotor cortex. *Neuron* 41, 165–173. doi: 10.1016/S0896-6273(03)00817-1

Romo, R., Hernández, A., Zainos, A., Brody, C. D., and Lemus, L. (2000). Sensing without touching psychophysical performance based on cortical microstimulation. *Neuron* 26, 273–278. doi: 10.1016/S0896-6273(00)81156-3

Romo, R., Hernández, A., Zainos, A., Lemus, L., and Brody, C. D. (2002). Neuronal correlates of decision-making in secondary somatosensory cortex. *Nat. Neurosci.* 5, 1217–1225. doi: 10.1038/nn950

Romo, R., Hernández, A., Zainos, A., and Salinas, E. (1998). Somatosensory discrimination based on cortical microstimulation. *Nature* 392, 387–390. doi: 10.1038/32891

Rougeul, A., Bouyer, J. J., Dedet, L., and Debray, O. (1979). Fast somato-parietal rhythms during combined focal attention and immobility in baboon and squirrel monkey. *Electroencephalogr. Clin. Neurophysiol.* 46, 310–319. doi: 10.1016/0013-4694(79)90205-0

Sabri, M. M., Adibi, M., and Arabzadeh, E. (2016). Dynamics of population activity in rat sensory cortex: network correlations predict anatomical arrangement and information content. *Front. Neural Circuits* 10:49. doi: 10.3389/fncir.2016.00049

Sachdev, R., Jenkinson, E., Zeigler, H., and Ebner, F. (2001). "Sensorimotor plasticity in the rodent vibrissa system," in *The Mutable Brain: Dynamic and Plastic Features of the Developing and Mature Brain*, Chapter 4, ed J. Kaas (Amsterdam: Harwood Academic Publishers), 140–188.

Salinas, E., Hernandez, A., Zainos, A., and Romo, R. (2000). Periodicity and firing rate as candidate neural codes for the frequency of vibrotactile stimuli. *J. Neurosci.* 20, 5503–5515. doi: 10.1523/JNEUROSCI.20-14-05503.2000

Sánchez-Santed, F., de Bruin, J. P., Heinsbroek, R. P., and Verwer, R. W. (1997). Spatial delayed alternation of rats in a t-maze: effects of neurotoxic lesions of the medial prefrontal cortex and of T-maze rotations. *Behav. Brain Res.* 84, 73–79. doi: 10.1016/S0166-4328(97)83327-X

Saporta, S., and Kruger, L. (1977). The organization of thalamocortical relay neurons in the rat ventrobasal complex studied by the retrograde transport of horseradish peroxidase. *J. Compar. Neurol.* 174, 187–208. doi: 10.1002/cne.901740202

Schaeffer, R. W., and Premack, D. (1961). Licking rates in infant albino rats. *Science* 134, 1980–1981. doi: 10.1126/science.134.3494.1980

Scheibel, M. E., and Scheibel, A. B. (1966). The organization of the nucleus reticularis thalami: a golgi study. *Brain Res.* 1, 43–62. doi: 10.1016/0006-8993(66)90104-1

Schubert, D., Kötter, R., Luhmann, H., and Staiger, J. (2006). Morphology, electrophysiology and functional input connectivity of pyramidal neurons characterizes a genuine layer Va in the primary somatosensory cortex. *Cereb. Cortex* 16, 223–236. doi: 10.1093/cercor/bhi100

Schubert, D., Staiger, J. F., Cho, N., Kötter, R., Zilles, K., and Luhmann, H. J. (2001). Layer-specific intracolumnar and transcolumnar functional connectivity of layer V pyramidal cells in rat barrel cortex. *J. Neurosci.* 21:3580. doi: 10.1523/JNEUROSCI.21-10-03580.2001

Schwarz, C., Hentschke, H., Butovas, S., Haiss, F., Stüttgen, M. C., Gerdjikov, T. V., et al. (2010). The head-fixed behaving rat - procedures and pitfalls. *Somatosens. Mot. Res.* 27, 131–148. doi: 10.3109/08990220.2010.513111

Shadlen, M. N., Britten, K. H., Newsome, W. T., and Movshon, J. A. (1996). A computational analysis of the relationship between neuronal and behavioral responses to visual motion. *J. Neurosci.* 16:1486. doi: 10.1523/JNEUROSCI.16-04-01486.1996

Shaw, V., and Mitrofanis, J. (2002). Anatomical evidence for somatotopic maps in the zona incerta of rats. *Anat. Embryol.* 206, 119–130. doi: 10.1007/s00429-002-0280-7

Shimegi, S., Akasaki, T., Ichikawa, T., and Sato, H. (2000). Physiological and anatomical organization of multiwhisker response interactions in the barrel cortex of rats. *J. Neurosci.* 20, 6241–6248. doi: 10.1523/JNEUROSCI.20-16-06241.2000

Shimegi, S., Ichikawa, T., Akasaki, T., and Sato, H. (1999). Temporal characteristics of response integration evoked by multiple whisker

stimulations in the barrel cortex of rats. *J. Neurosci.* 19, 10164–10175. doi: 10.1523/JNEUROSCI.19-22-10164.1999

Shipley, M. (1974). Response characteristics of single units in the rat's trigeminal nuclei to vibrissa displacements. *J. Neurophysiol.* 37, 73–90. doi: 10.1152/jn.1974.37.1.73

Shosaku, A. (1985). A comparison of receptive field properties of vibrissa neurons between the rat thalamic reticular and ventro-basal nuclei. *Brain Res.* 347, 36–40. doi: 10.1016/0006-8993(85)90886-8

Silverman, J. d., and Kruger, L. (1985). Projections of the rat trigeminal sensory nuclear complex demonstrated by multiple fluorescent dye retrograde transport. *Brain Res.* 361, 383–388. doi: 10.1016/0006-8993(85)91308-3

Simons, D. J. (1978). Response properties of vibrissa units in rat SI somatosensory neocortex. *J. Neurophysiol.* 41, 798–820. doi: 10.1152/jn.1978.41.3.798

Simons, D. J., and Carvell, G. E. (1989). Thalamocortical response transformation in the rat vibrissa/barrel system. *J. Neurophysiol.* 61:311. doi: 10.1152/jn.1989.61.2.311

Simpson, K., Wang, Y., and Lin, R. C. (2008). Patterns of convergence in rat zona incerta from the trigeminal nuclear complex: light and electron microscopic study. *J. Compar. Neurol.* 507, 1521–1541. doi: 10.1002/cne.21624

Skinner, J., and Yingling, C. (1977). Central gating mechanisms that regulate event-related potentials and behavior. *Prog. Clin. Neurophysiol.* 1, 30–69.

Sofroniew, N. J., Cohen, J. D., Lee, A. K., and Svoboda, K. (2014). Natural whisker-guided behavior by head-fixed mice in tactile virtual reality. *J. Neurosci.* 34, 9537–9550. doi: 10.1523/JNEUROSCI.0712-14.2014

Sreenivasan, V., Kyriakatos, A., Mateo, C., Jaeger, D., and Petersen, C. C. (2016). Parallel pathways from whisker and visual sensory cortices to distinct frontal regions of mouse neocortex. *Neurophotonics* 4:031203. doi: 10.1117/1.NPh.4.3.031203

Steriade, M., Deschênes, M., Domich, L., and Mulle, C. (1985). Abolition of spindle oscillations in thalamic neurons disconnected from nucleus reticularis thalami. *J. Neurophysiol.* 54, 1473–1497. doi: 10.1152/jn.1985.54.6.1473

Steriade, M., Domich, L., and Oakson, G. (1986). Reticularis thalami neurons revisited: activity changes during shifts in states of vigilance. *J. Neurosci.* 6, 68–81. doi: 10.1523/JNEUROSCI.06-01-00068.1986

Steriade, M., McCormick, D. A., and Sejnowski, T. J. (1993). Thalamocortical oscillations in the sleeping and aroused brain. *Science* 262, 679–685. doi: 10.1126/science.8235588

Stüttgen, M. C, and Schwarz, C. (2008). Psychophysical and neurometric detection performance under stimulus uncertainty. *Nat. Neurosci.* 11, 1091–1099. doi: 10.1038/nn.2162

Stüttgen, M. C., and Schwarz, C. (2010). Integration of vibrotactile signals for whisker-related perception in rats is governed by short time constants: comparison of neurometric and psychometric detection performance. *J. Neurosci.* 30, 2060–2069. doi: 10.1523/JNEUROSCI.3943-09.2010

Sullivan, J., Mitchinson, B., Pearson, M., Evans, M., Lepora, N., Fox, C., et al. (2012). Tactile discrimination using active whisker sensors. *Sens. J. IEEE* 12, 350–362. doi: 10.1109/JSEN.2011.2148114

Sumser, A., Mease, R. A., Sakmann, B., and Groh, A. (2017). Organization and somatotopy of corticothalamic projections from l5b in mouse barrel cortex. *Proc. Natl. Acad. Sci. U.S.A.* 114, 8853–8858. doi: 10.1073/pnas.1704302114

Szwed, M., Bagdasarian, K., and Ahissar, E. (2003). Encoding of vibrissal active touch. *Neuron* 40, 621–630. doi: 10.1016/S0896-6273(03)00671-8

Szwed, M., Bagdasarian, K., Blumenfeld, B., Barak, O., Derdikman, D., and Ahissar, E. (2006). Responses of trigeminal ganglion neurons to the radial distance of contact during active vibrissal touch. *J. Neurophysiol.* 95, 791–802. doi: 10.1152/jn.00571.2005

Talbot, W. H., Darian-Smith, I., Kornhuber, H. H., and Mountcastle, V. B. (1968). The sense of flutter-vibration: comparison of the human capacity with response patterns of mechanoreceptive afferents from the monkey hand. *J. Neurophysiol.* 31:301. doi: 10.1152/jn.1968.31.2.301

Taube, J. S. (1998). Head direction cells and the neurophysiological basis for a sense of direction. *Prog. Neurobiol.* 55, 225–256. doi: 10.1016/S0301-0082(98)00004-5

Terenzi, M. G., Zagon, A., and Roberts, M. H. (1995). Efferent connections from the anterior pretectal nucleus to the diencephalon and mesencephalon in the rat. *Brain Res.* 701, 183–191. doi: 10.1016/0006-8993(95)01001-8

Thomas, G. J., and Brito, G. N. (1980). Recovery of delayed alternation in rats after lesions in medial frontal cortex and septum. *J. Compar. Physiol. Psychol.* 94:808. doi: 10.1037/h0077834

Thomson, A. M., and Bannister, A. P. (2003). Interlaminar connections in the neocortex. *Cereb. Cortex* 13, 5–14. doi: 10.1093/cercor/13.1.5

Timofeeva, E., Mérette, C., Emond, C., Lavallée, P., and Deschênes, M. (2003). A map of angular tuning preference in thalamic barreloids. *J. Neurosci.* 23, 10717–10723. doi: 10.1523/JNEUROSCI.23-33-10717.2003

Topchiy, I. A., Wood, R. M., Peterson, B., Navas, J. A., Rojas, M. J., and Rector, D. M. (2009). Conditioned lick behavior and evoked responses using whisker twitches in head restrained rats. *Behav. Brain Res.* 197, 16–23. doi: 10.1016/j.bbr.2008.07.032

Towal, R. B., and Hartmann, M. J. (2006). Right–left asymmetries in the whisking behavior of rats anticipate head movements. *J. Neurosci.* 26, 8838–8846. doi: 10.1523/JNEUROSCI.0581-06.2006

Towal, R. B., and Hartmann, M. J. (2008). Variability in velocity profiles during free-air whisking behavior of unrestrained rats. *J. Neurophysiol.* 100, 740–752. doi: 10.1152/jn.01295.2007

Trageser, J. C., and Keller, A. (2004). Reducing the uncertainty: gating of peripheral inputs by zona incerta. *J. Neurosci.* 24, 8911–8915. doi: 10.1523/JNEUROSCI.3218-04.2004

Uka, T., and DeAngelis, G. (2003). Contribution of middle temporal area to coarse depth discrimination: comparison of neuronal and psychophysical sensitivity. *J. Neurosci.* 23, 3515–3530. doi: 10.1523/JNEUROSCI.23-08-03515.2003

Urbain, N., and Deschênes, M. (2007). Motor cortex gates vibrissal responses in a thalamocortical projection pathway. *Neuron* 56, 714–725. doi: 10.1016/j.neuron.2007.10.023

Urbain, N., and Deschênes, M. (2007). A new thalamic pathway of vibrissal information modulated by the motor cortex. *J. Neurosci.* 27, 12407–12412. doi: 10.1523/JNEUROSCI.2914-07.2007

van der Loos, H. (1976). Barreloids in mouse somatosensory thalamus. *Neurosci. Lett.* 2, 1–6. doi: 10.1016/0304-3940(76)90036-7

Van Ham, J. J., and Yeo, C. H. (1992). Somatosensory trigeminal projections to the inferior olive, cerebellum and other precerebellar nuclei in rabbits. *Eur. J. Neurosci.* 4, 302–317. doi: 10.1111/j.1460-9568.1992.tb00878.x

Varga, C., Sík, A., Lavallée, P., and Deschênes, M. (2002). Dendroarchitecture of relay cells in thalamic barreloids: a substrate for cross-whisker modulation. *J. Neurosci.* 22, 6186–6194. doi: 10.1523/JNEUROSCI.22-14-06186.2002

Veinante, P., and Deschênes, M. (1999). Single-and multi-whisker channels in the ascending projections from the principal trigeminal nucleus in the rat. *J. Neurosci.* 19:5085. doi: 10.1523/JNEUROSCI.19-12-05085.1999

Veinante, P., Jacquin, M. F., and Deschênes, M. (2000). Thalamic projections from the whisker-sensitive regions of the spinal trigeminal complex in the rat. *J. Compar. Neurol.* 420, 233–243.

Verma, A., and Moghaddam, B. (1996). NMDA receptor antagonists impair prefrontal cortex function as assessed via spatial delayed alternation performance in rats: modulation by dopamine. *J. Neurosci.* 16, 373–379. doi: 10.1523/JNEUROSCI.16-01-00373.1996

Vincent, S. B. (1912). *The Functions of the Vibrissae in the Behavior of the White Rat*. Chicago, IL: University of Chicago.

Vincent, S. B. (1913). The tactile hair of the white rat. *J. Compar. Neurol.* 23, 1–34. doi: 10.1002/cne.900230101

von Heimendahl, M., Itskov, P. M., Arabzadeh, E., and Diamond, M. E. (2007). Neuronal activity in rat barrel cortex underlying texture discrimination. *PLoS Biol.* 5:e305. doi: 10.1371/journal.pbio.0050305

Waite, P. M., and Cragg, B. G. (1982). The peripheral and central changes resulting from cutting or crushing the afferent nerve supply to the whiskers. *Proc. R. Soc. Lond. Ser. B Biol. Sci.* 214, 191–211. doi: 10.1098/rspb.1982.0004

Welker, C. (1971). Microelectrode delineation of fine grain somatotopic organization of (SMI) cerebral neocortex in albino rat. *Brain Res.* 26, 259–275. doi: 10.1016/S0006-8993(71)80004-5

Welker, C., and Woolsey, T. A. (1974). Structure of layer IV in the somatosensory neocortex of the rat: description and comparison with the mouse. *J. Compar. Neurol.* 158, 437–453. doi: 10.1002/cne.901580405

Welker, E., Hoogland, P. V., and Van der Loos, H. (1988). Organization of feedback and feedforward projections of the barrel cortex: a PHA-l study in the mouse. *Exp. Brain Res.* 73, 411–435. doi: 10.1007/BF00248234

Welker, W. (1964). Analysis of sniffing of the albino rat. *Behaviour* 22, 223–244. doi: 10.1163/156853964X00030

White, E. L., and Czeiger, D. (1991). Synapses made by axons of callosal projection neurons in mouse somatosensory cortex: emphasis on intrinsic

connections. *J. Compar. Neurol.* 303, 233–244. doi: 10.1002/cne.903030206

White, E. L., and DeAmicis, R. A. (1977). Afferent and efferent projections of the region in mouse sml cortex which contains the posteromedial barrel subfield. *J. Compar. Neurol.* 175, 455–481. doi: 10.1002/cne.901750405

Wilent, W. B., and Contreras, D. (2004). Synaptic responses to whisker deflections in rat barrel cortex as a function of cortical layer and stimulus intensity. *J. Neurosci.* 24, 3985–3998. doi: 10.1523/JNEUROSCI.5782-03.2004

Wilent, W. B., and Contreras, D. (2005). Dynamics of excitation and inhibition underlying stimulus selectivity in rat somatosensory cortex. *Nat. Neurosci.* 8, 1364–1370. doi: 10.1038/nn1545

Williams, M. N., Zahm, D. S., and Jacquin, M. F. (1994). Differential foci and synaptic organization of the principal and spinal trigeminal projections to the thalamus in the rat. *Eur. J. Neurosci.* 6, 429–453. doi: 10.1111/j.1460-9568.1994.tb00286.x

Wineski, L. (1983). Movements of the cranial vibrissae in the golden hamster (*Mesocricetus auratus*). *J. Zool.* 200, 261–280. doi: 10.1111/j.1469-7998.1983.tb05788.x

Wineski, L. (1985). Facial morphology and vibrissal movement in the golden hamster. *J. Morphol.* 183, 199–217. doi: 10.1002/jmor.1051830208

Wolf, C., Waksman, D., Finger, S., and Almli, C. R. (1987). Large and small medial frontal cortex lesions and spatial performance of the rat. *Brain Res. Bull.* 18, 1–5. doi: 10.1016/0361-9230(87)90025-6

Woolsey, T. A., and van der Loos, H. (1970). The structural organization of layer IV in the somatosensory region (SI) of mouse cerebral cortex. The description of a cortical field composed of discrete cytoarchitectonic units. *Brain Res.* 17, 205–242. doi: 10.1016/0006-8993(70)90079-X

Woolston, D. C., La Londe, J. R., and Gibson, J. M. (1982). Comparison of response properties of cerebellar- and thalamic-projecting interpolaris neurons. *J. Neurophysiol.* 48, 160–173. doi: 10.1152/jn.1982.48.1.160

Yamashita, T., Vavladeli, A., Pala, A., Galan, K., Crochet, S., Petersen, S., et al. (2018). Diverse long-range axonal projections of excitatory layer 2/3 neurons in mouse barrel cortex. *Front. Neuroanat.* 12:33. doi: 10.3389/fnana.2018.00033

Yang, Y., and Zador, A. M. (2012). Differences in sensitivity to neural timing among cortical areas. *J. Neurosci.* 32, 15142–15147. doi: 10.1523/JNEUROSCI.1411-12.2012

Yu, C., Derdikman, D., Haidarliu, S., and Ahissar, E. (2006). Parallel thalamic pathways for whisking and touch signals in the rat. *PLoS Biol.* 4:e124. doi: 10.1371/journal.pbio.0040124

Zucker, E., and Welker, W. (1969). Coding of somatic sensory input by vibrissae neurons in the rat's trigeminal ganglion. *Brain Res.* 12:138. doi: 10.1016/0006-8993(69)90061-4

Zuo, Y., and Diamond, M. E. (2019a). Rats generate vibrissal sensory evidence until boundary crossing triggers a decision. *Curr. Biol.* 29, 1415–1424. doi: 10.1016/j.cub.2019.03.016

Zuo, Y., and Diamond, M. E. (2019b). Texture identification by bounded integration of sensory cortical signals. *Curr. Biol.* 29, 1425–1435. doi: 10.1016/j.cub.2019.03.017

Zuo, Y., Perkon, I., and Diamond, M. (2011). Whisking and whisker kinematics during a texture classification task. *Philos. Trans. R. Soc. B Biol. Sci.* 366, 3058–3069. doi: 10.1098/rstb.2011.0161

Conflict of Interest Statement: The author declares that the research was conducted in the absence of any commercial or financial relationships that could be construed as a potential conflict of interest.

frontiers in Systems Neuroscience

REVIEW
published: 27 August 2019
doi: 10.3389/fnsys.2019.00037

Different Approaches to Modulation of Microglia Phenotypes After Spinal Cord Injury

Elvira Akhmetzyanova[1], Konstantin Kletenkov[1], Yana Mukhamedshina[1,2] and Albert Rizvanov[1]*

[1] OpenLab Gene and Cell Technologies, Institute of Fundamental Medicine and Biology, Kazan Federal University, Kazan, Russia, [2] Department of Histology, Cytology and Embryology, Kazan State Medical University, Kazan, Russia

Microglial cells, which are highly plastic, immediately respond to any change in the microenvironment by becoming activated and shifting the phenotype toward neurotoxicity or neuroprotection. The polarization of microglia/macrophages after spinal cord injury (SCI) seems to be a dynamic process and can change depending on the microenvironment, stage, course, and severity of the posttraumatic process. Effective methods to modulate microglia toward a neuroprotective phenotype in order to stimulate neuroregeneration are actively sought for. In this context, available approaches that can selectively impact the polarization of microglia/macrophages regulate synthesis of trophic factors and cytokines/chemokines in them, and their phagocytic function and effects on the course and outcome of SCI are discussed in this review.

Keywords: microglia, phenotypes, modulation, spinal cord injury, neuroregeneration

OPEN ACCESS

Edited by:
Preston E. Garraghty, Indiana University Bloomington, United States

Reviewed by:
John Gensel, University of Kentucky, United States
Michelle Hook, Texas A&M University, United States

****Correspondence:***
Yana Mukhamedshina
yana.k-z-n@mail.ru

Received: *20 April 2019*
Accepted: *29 July 2019*
Published: *27 August 2019*

Citation:
Akhmetzyanova E, Kletenkov K, Mukhamedshina Y and Rizvanov A (2019) Different Approaches to Modulation of Microglia Phenotypes After Spinal Cord Injury. Front. Syst. Neurosci. 13:37. doi: 10.3389/fnsys.2019.00037

INTRODUCTION

Spinal cord injury (SCI) is characterized by numerous pathologic reactions that involve every cell type of the central nervous system (CNS). The activation of microglial cells, which are the first to respond to nervous tissue damage, is one of the essential events of posttraumatic reactions (Gensel and Zhang, 2015). Activated microglia can synthesize not only trophic biomolecules such as neurotrophins, glutamate transporters, and antioxidants, but also effectors such as nitric oxide (NO) and pro-inflammatory cytokines that can be potentially neurotoxic (Persson et al., 2005; Lai and Todd, 2006; Hellwig et al., 2013). In addition to synthesis of many biomolecules, a phagocytic function of microglia is critically important also due to its essential for the removal of degenerating/lost neurons and neuroglial cells, and rearrangement or destruction of synaptic connections (Chen and Trapp, 2016; Jin and Yamashita, 2016; Wolf et al., 2017). Previous studies have shown that the activation of microglia is not a single phenomenon and that there are several different "states of activation" when microglia can have a selective neurotoxic or neuroprotective effect. Given the diversity of microglia functions, the M1/M2 paradigm is a simplified model that reflects two opposite effects on inflammatory responses. However, one should take into consideration that the microglia microenvironment *in vivo* is diverse and its phenotype may rarely shift directly to the other state.

MICROGLIA PHENOTYPES

To date, several states of microglia polarization have been described: they are classic activation (M1), alternative activation (M2a), alternative type II activation (M2b), and acquired deactivation (M2c). A number of investigators question whether microglia can acquire an M3 phenotype (Malyshev and Malyshev, 2015; Walker and Lue, 2015). A number of principal studies have identified which markers are specific for classically or alternatively activated microglia (Martinez et al., 2006; Martinez et al., 2013).

M1 microglia are capable of producing active oxygen species that promote a respiratory burst, as well as produce cytokines such as tumor necrosis factor-α (TNF-α), IL-1β, IL-6, and IL-12, thereby mediating inflammatory tissue damage (Liu et al., 2018). M1 microglia are involved in secondary damage after SCI, producing proinflammatory molecules and the formation of a glial scar, which, in turn, creates an environment at the site of injury that is adverse for neuroprotection. Therefore, this phenotype is commonly referred to as neurotoxic (Shechter and Schwartz, 2013; Fan et al., 2016). The phagocytic activity was shown to be inhibited in M1 polarization (Durafourt et al., 2012); at the same time, M1 microglia regulate synaptic pruning and labeling synapses for phagocytosis (Schafer et al., 2012).

Alternative activation is subdivided into two subcategories: M2a and M2b. M2à microglia are considered to respond to IL-4 and IL-13; to have an increased phagocytic activity; to produce an insulin-like growth factor-1, trophic polyamines, and anti-inflammatory cytokines such as IL-10; and to express G-CSF, GM-CSF, and CD209 (Martinez and Gordon, 2014; Franco and Fernandez-Suarez, 2015; Peferoen et al., 2015). The microglia of this type can eliminate cellular debris and stimulate tissue regeneration. M2b microglia are induced by ligation of immunoglobulin Fc-gamma-receptors that results in IL-12 expression, increased IL-10 secretion, and HLA-DR expression. This phenotype is also characterized by active phagocytosis and an increased expression of CD32 and CD64, which are detected in the cerebral microglia in Alzheimer's disease (Peress et al., 1993). M2c (acquired deactivation) polarization can be caused by the anti-inflammatory cytokine IL-10 or glucocorticoids, an increased expression of transforming growth factor (TGF), sphingosine kinase (SPHK1), and CD163, a membrane-bound receptor for haptoglobin/hemoglobin complexes (Wilcock, 2014). The polarization of microglia/macrophages toward the M2 phenotype occurs to resolve inflammation and degeneration as a whole; thus, this phenotype is characterized as neuroprotective. It is worth noting, however, that although the M2 phenotype of microglia/macrophages plays a positive role in neuroregeneration processes, it has an absolutely opposite role in the case of neoplastic processes in the CNS and has a pro-tumor action (Wu and Watabe, 2017).

A similar pattern of polarization is involved in peripheral macrophages that actively migrate after injury when the blood–brain barrier is damaged. It should be noted that most researchers do not distinguish between microglia and macrophages, subsuming them into the same cell population and using pan markers for their identification. This might be due to the lack of highly specific markers for resident microglia and macrophages migrating toward a site of injury (Franco and Fernandez-Suarez, 2015; Martin et al., 2017).

BEHAVIOR OF MICROGLIA/MACROPHAGES IN SPINAL CORD INJURY

It has been previously shown that microglia are activated within the first 24 h after SCI. In the acute period, polarization shifts primarily toward M1 microglia, which release proinflammatory cytokines and chemokines. This results in progression of inflammatory processes after primary mechanical injury (Lee et al., 2009; Nakajima et al., 2012). Shortly thereafter (2–3 days post-injury, dpi), blood monocytes that subsequently differentiate into macrophages phenotypically and morphologically indistinguishable from activated microglia migrate toward the site of injury (Donnelly and Popovich, 2008; Beck et al., 2010). The appearance of M2 microglia/macrophages and their secretion of anti-inflammatory cytokines and chemokines results in inhibiting excessive inflammatory reactions around the site of injury and stimulating regeneration of damaged spinal cord tissues (Gratchev et al., 2008; Varnum and Ikezu, 2012; Shechter and Schwartz, 2013; Weisser et al., 2013). M2 microglia/macrophages are shown to possess an increased phagocytic activity that promotes clearance of posttraumatic debris, leading to accelerated demyelination and resolution of the initial traumatic events (Redondo-Castro et al., 2013; Lampron et al., 2015; Orihuela et al., 2016; Akhmetzyanova et al., 2018).

The primary phase of microglia/macrophage activation peaks on 7 dpi; microglia are reactivated after 14 dpi and then peak on 60 dpi and remain for up to 180 dpi (Beck et al., 2008; Conta and Stelzner, 2008; Kigerl et al., 2009; Bellver-Landete et al., 2019). M1 and M2 microglia/macrophages co-exist at the injury site within the 1st week after SCI, with M1 cells prevailing. However, other researchers have demonstrated that there were no M2 cells and the population of M1 cells significantly decreased after 28 dpi (Kigerl et al., 2009; Francos-Quijorna et al., 2016). These results confirm data on the population of $ED1^+$ phagocytic macrophages/microglia, which peak by day 7 after SCI, significantly decreasing by 28 dpi and abruptly increasing again by 90 dpi (Beck et al., 2010). At the same time, Bellver-Landete et al. (2019) showed that activated, proliferating microglia play an important role in the healing process, having a positive effect on tissue sparing and functional recovery after SCI, and this effect persists for 5 weeks after SCI.

These phases of microglia/macrophage activation in SCI can be paralleled with changes observed in the population of macrophages when other tissues and organs are damaged. For example, at the end of the remodeling phase when the main healing processes are completed, macrophages are deactivated, and inflammation resolves. The behavior of microglia/macrophages whose number reduces significantly though variably by 2–4 weeks after SCI is possibly the same.

With effective healing, the level of macrophages in non-nervous tissues returns to normal within several weeks after injury in parallel with its healing. On the contrary, wounds that do not heal within 3 months result in a stable activation of macrophages that is a distinctive feature of chronicity (Sindrilaru et al., 2011). In turn, we observed a similar picture during the second phase of microglia/macrophage activation that seems to be triggered by ongoing neurodegeneration in response to which re-activation of these cells prevents a subsequent loss of function.

The polarization of microglia/macrophages after SCI seems to be a dynamic process and can be altered depending on the microenvironment, the stage of the posttraumatic process, and its severity (Kigerl et al., 2009; David and Kroner, 2011). This phenomenon has been demonstrated in several studies and has shown that the behavior of microglia/macrophages depended on the factors of activation, in particular, the type of cells that activated them and the specific activating molecule (Nakajima and Kohsaka, 2002; Nakajima and Kohsaka, 2004; Stout and Suttles, 2004; Shaked et al., 2005; Lai and Todd, 2006; Nakajima et al., 2006; Menzies et al., 2010). An effective method to modulate microglia toward a neuroprotective phenotype in order to stimulate neuroregeneration is actively sought for in addition to investigation into the factors of activation. For this purpose, new approaches are being developed and different biomolecules potentially possessing a selective effect on the polarization of microglia/macrophages regulate their synthesis of trophic factors, cytokines/chemokines, and a phagocytic function tested. The latter can be achieved by affecting the signaling pathways that control microglia activation and polarization, discussed in the following section.

MICROGLIAL SIGNALING PATHWAYS

It is now increasingly evident that there are various ways of activation for microglia that determine the generation of cells with divergent abilities (**Figure 1**). Toll-like receptors (TLRs) are a class of transmembrane receptors involved in the activation of cell-mediated immune response. Out of more than 10 TLRs, identified in both rodents and humans, microglia express at least 9 TLRs along with their adapter proteins (Laflamme et al., 2001; Bsibsi et al., 2002; Dalpke et al., 2002; Olson and Miller, 2004; Zhang et al., 2013). Previous studies have demonstrated TLR-dependent microglia activation in neurodegenerative disorders and different types of CNS injury (Heneka et al., 2005; Fernandez-Lizarbe et al., 2009; Song et al., 2011; Yao et al., 2013). A classical/canonical activation of the nuclear factor κB (NF-κB) signaling, which is essential for both acute and chronic inflammatory responses, is initiated by TLRs, as well as other cell surface receptors, including those for IL-1 and TNF (Shih et al., 2015; Noort et al., 2015). The activated NF-κB allows translocation to the nucleus that results in production of anti-inflammatory cytokines, release of reactive oxygen species (ROS), and microglia modulation toward the M1 phenotype (Pan et al., 2010; Taetzsch et al., 2015; Zhang et al., 2017). The activation of NF-κB transcription factors also plays a key role in neurogenesis, synaptic plasticity, and protection of neurons (O'Riordan et al., 2006; Ahn et al., 2008; Koo et al., 2010). Therefore, NF-κB should be selectively inhibited in microglia and possibly in astrocytes in order to neutralize its neurotoxic role and maintain the neuroprotective one (Brambilla et al., 2005; Crosio et al., 2011; Frakes et al., 2014).

In the presence of inflammation, microglia are activated by means of phosphorylation of p38 mitogen-activated protein kinase (p38/MAPK) and extracellular signal–regulated kinases (ERKs), thereby enhancing phagocytosis, chemotaxis, and the expression of proinflammatory cytokines (Wang et al., 2011; Fan et al., 2017). At the same time, the phosphorylation of p38/MAPK inhibited ULK1 kinase activity and reduced autophagy, allowing the full induction of the inflammatory process during microglia activation (He et al., 2018). The activation of glial cells and the p38/MAPK signaling pathway was demonstrated to be involved in the development of a chronic neuropathic pain that affects up to 80% of patients with SCI (Finnerup et al., 2001; Crown et al., 2008; Detloff et al., 2008). Therefore, p38/MAPK inhibitors are intensively used to reduce activation of the spinal microglia, to prevent/reverse the neuropathic pain symptoms and neuroinflammation in general (Rojewska et al., 2014; Cheng et al., 2015; Kim et al., 2016; Taves et al., 2016).

A phosphatidylinositol 3-kinase (PI3K)/protein kinase B (Akt)/mammalian target of rapamycin (mTOR) signaling pathway that is involved in neuropathic pain progression, as well as astrocyte and microglia activation, is known. Its inhibition reduces the ability of microglial cells to migrate and their number in the site of neurodegeneration (Guo et al., 2017). PI3K/Akt/mTOR is triggered through the CD74 receptor, whose activation is promoted by a macrophage migration inhibitory factor (MIF). The use of MIF suppresses the microglia M1 activation and mitigates the severity of secondary injury around the lesion site in the murine dorsal hemisection model of SCI (Emmetsberger and Tsirka, 2012). At the same time, there is quite contradictory evidence that this pathway affects the shift of the microglia/macrophage phenotype toward M1 or M2 stages (Wang G. et al., 2015; Wang et al., 2016). Therefore, the role of the PI3K/Akt/mTOR pathway in microglia activation and neuroregeneration as a whole following SCI is still controversial (Kanno et al., 2012; Chen et al., 2016). Some researchers relate this to the possibility of isoform-specific cross-talk between PI3K, Akt, and mTORC (Vergadi et al., 2017).

There are natural (phosphatase and tensin homolog deleted on chromosome 10, PTEN) and artificial (ZSTK474, NVP-BEZ235, LY294002, PI828, etc.) inhibitors of the PI3K/Akt/mTOR signaling pathway. PTEN is a lipid and protein phosphatase that has dual substrate specificity and serves as the main negative regulator of PI3K and the PI3K/Akt/mTOR signaling pathway by converting phosphatidylinositol (3,4,5)-trisphosphate (PIP3) into phosphatidylinositol (4,5)-biphosphate (P1P2). In a model of chronic peripheral nerve injury, the PTEN gene overexpression resulted from its delivery with an adenoviral vector (Ad5-PTEN) in the spinal cord. It significantly reduced activation of microglia and astrocytes and prevented a neuropathic pain (Huang et al., 2015). At the same time, such microglia modulation in neurotrauma therapy can negatively affect regeneration as the PTEN expression has been shown to be able to attenuate

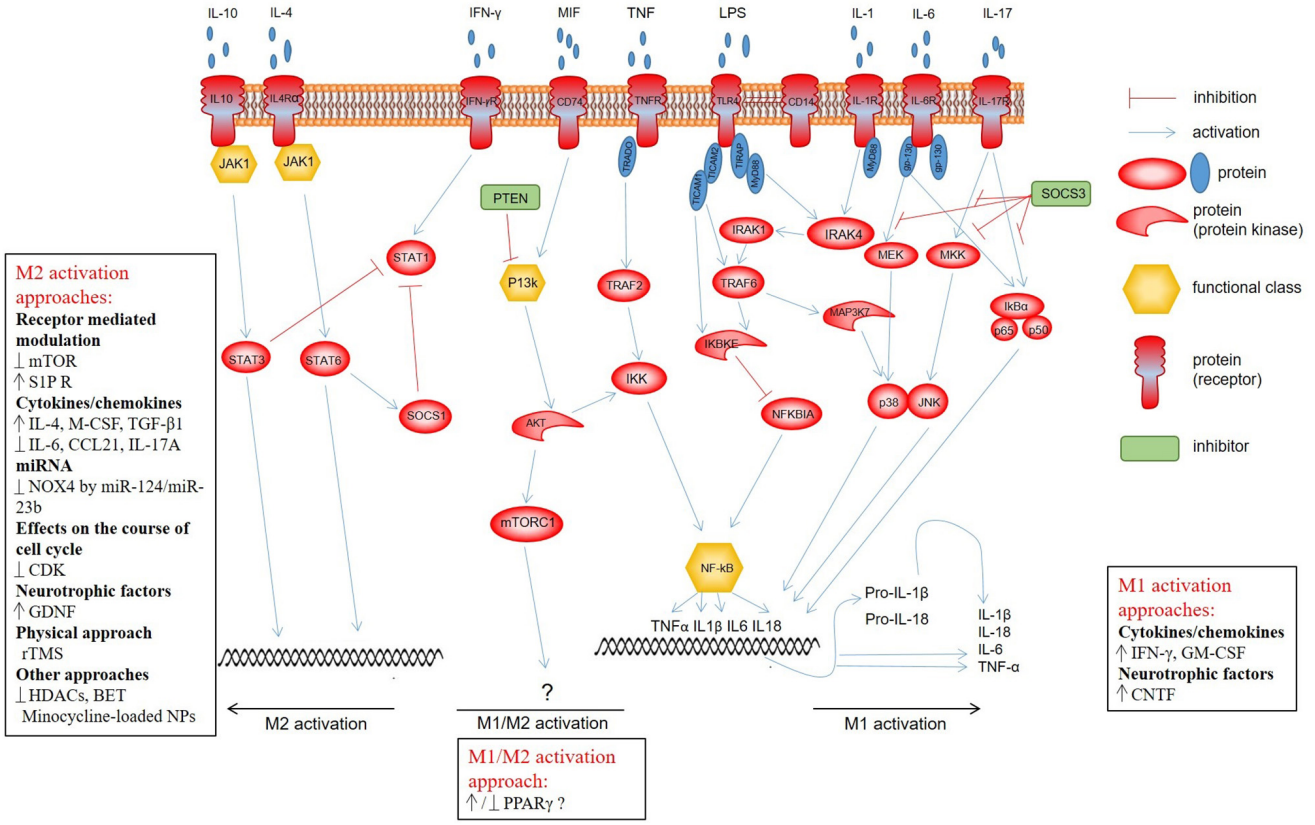

FIGURE 1 | Microglial signaling pathways determining development of cells with divergent abilities. Classical activation of the NF-κB signaling is initiated by TLRs, as well as other cell surface receptors, including specific IL-1 and TNF, and provides M1 polarization of microglia. PI3K/Akt/mTOR is triggered through the CD74 receptor, whose activation is promoted by MIF. There is quite contradictory evidence that this pathway affects the shift of the microglia/macrophage phenotype toward M1 or M2. Anti-inflammatory cytokines IL-10 and IL-4 induce STAT3 and STAT6 phosphorylation, respectively, via JAK1, which promotes polarization toward the M2 phenotype. The activation of STAT1, in turn, leads to polarization toward a neurotoxic M2 phenotype of microglia. Normally, there is a balance between the activation of STAT1 and STAT3/STAT6 that strictly regulates the microglia polarization and activity.

neuroprotection and lead to an impairment of axonal growth in particular (Zukor et al., 2013; Ohtake et al., 2014; Yin et al., 2018). Thus, the system regulation at the level of this enzyme is a quite dangerous process leading to disarrangement of oppositely directed processes.

A Janus tyrosine kinase (JAK)/signal transducer and activator of transcription (STAT) signaling pathway is one of the most important cascades triggered in response to many modulators of inflammation. Most studies focused on activation of the JAK/STAT3 signaling pathway in the case of neoplastic activity of microglia/macrophages (Zhang et al., 2009; Zhang et al., 2011; Oliva et al., 2012; Koscsó et al., 2013; Popiolek-Barczyk and Mika, 2016). As for microglia/macrophage modulation after SCI, anti-inflammatory cytokines IL-10 and IL-4 induce STAT3 and STAT6 phosphorylation, respectively, via JAK1, and promote polarization toward the M2 phenotype (Koscsó et al., 2013; Wang et al., 2014; Cianciulli et al., 2015; Popiolek-Barczyk and Mika, 2016). Activation of STAT1 and NF-κB transcription factors leads, in turn, to polarization toward a neurotoxic phenotype of microglia/macrophages. There is normally a balance between the activation of STAT1 and STAT3/STAT6 that strictly regulates the microglia/macrophage polarization and activity.

STAT3 is recognized as the main mediator of IL-6 and IL-17 functions (Camporeale and Poli, 2012). There are two main types of IL6 signalization: pro-inflammatory and anti-inflammatory. In microglia, the IL-6 pro-inflammatory signaling pathway is carried out through gp-130, which acts as an antagonist sequestering IL-6 (Hodes et al., 2016). Results obtained by Ma et al. (2010) indicate that SOCS3 can function as a negative regulator of NF-κB, p38 MAPK, and JNK signaling; moreover, an important role for SOCS3 in the regulation of IL-17 and IL-6/R-dependent induction of IL-6 was elucidated. Guerrero et al. (2012) demonstrated that classical microglia activation in mouse SCI could be inhibited by IL-6 blockade. Redondo-Castro et al. (2013) used glibenclamide, an inhibitor of ATP-sensitive potassium channels K_{ATP} to relieve a neuropathic pain in rats with SCI. The inhibition of IL-17, as a mediator of microglia activation, when injecting hyperforin enabled microglia polarization toward the M2 phenotype (Ma et al., 2018). Although studies to inhibit individual mediators of microglia activation demonstrate certain positive changes in

some neurodegenerative disorders, they cannot completely neutralize the neurotoxic potential of these cells that is related to their possible activation by means of a common regulator in a signaling cascade.

DIFFERENT APPROACHES TO MODULATION OF MICROGLIA/MACROPHAGES

Supplementary Table 1 contains published data available on the different approaches to modulation of microglia/macrophages *in vitro* and *in vivo*.

Receptor-Mediated Modulation

Peroxisome proliferator-activated receptor (PPARγ) is a key regulator of the microglia/macrophage M2 phenotype. It is a nuclear receptor capable of modulating inflammatory processes and controlling lipid and lipoprotein metabolism as well as glucose homeostasis (Chinetti et al., 2003; McTigue, 2008). PPARγ was shown to be immediately induced in monocyte differentiation into macrophages (Chinetti et al., 1998). In addition, activation of PPARγ signaling can suppress an inflammatory response by inhibiting NF-κB (Zolezzi et al., 2017). Therefore, PPARγ is described as the main anti-inflammatory regulator of macrophages (Ahmadian et al., 2013). Han et al. (2017) demonstrated that 6-Shogaol, a pungent constituent extracted from *Zingiber officinale* Roscoe can enhance PPARγ expression. Also, the addition of 6-Shogaol to an *in vitro* microglia culture could reduce the lipopolysaccharide-induced (LPS) expression of proinflammatory factors TNF-α, IL1β, IL6, and PGE2 as measured using ELISA. The use of a PPARγ agonist, rosiglitazone, was shown *in vitro* with PCR and flow cytometry to lead to monocyte modulation toward the M2 phenotype (Bouhlel et al., 2007). Additionally, in a murine brain injury model intravenously injected PPARγ activator, malibatol A, an anti-oxidant extracted from *Hopea hainanensis*, could shift the microglia phenotype toward M2 (Pan et al., 2015). Wen et al. (2018) compared the effects of intraperitoneal injections of the PPARγ agonist, rosiglitazone, and the PPARγ antagonist, GW9662, in a lateral fluid percussion injury model in mice. Using ELISA, real-time PCR and immunohistochemistry, they observed that 72 h after injury, expression levels of proinflammatory cytokines TNF-α, IL-1β, and IL-6 were significantly higher and that of anti-inflammatory IL-10 was lower in the group treated with GW9662. Further *in vitro* experiments in a primary culture of mouse microglia were conducted and results demonstrated that rosiglitazone increased the expression of M2 markers (CD206 and YM-1) and decreased that of M1 markers (TNF-α, IL-6, IL-1β, and IL-10). Interesting results were obtained by Park et al. (2007) using pioglitazone in a rat model of SCI. They showed that intraperitoneal injection of pioglitazone causes a decrease in the number of reactive macrophages, attenuates myelin loss, and improves functional recovery from SCI. The results of this study were confirmed by McTigue et al. (2007), where the rat electromagnetic SCI model again showed pioglitazone's ability to reduce the number of activated phagocytic microglia by 7 dpi.

Neuropeptides Y (NPY), Y1 receptor activators, suppress the innate immune response by reducing the release of interleukin-1β and NO, migration, and phagocytosis of activated microglial cells (Farzi et al., 2015). NPY were demonstrated to significantly restrain the microglia activation by inhibiting LPS-induced Fc-receptor-mediated phagocytosis (Ferreira et al., 2012). Macrophage antigen complex-1 receptor (MAC1R), a molecule mediating the macrophage activation in response to various stimuli, plays an important role in phagocytosis (Le Cabec et al., 2002). In fact, MAC1R is a key receptor for both toxins and classic acute-phase reactants such as fibrinogen, which activate microglia/macrophages manifesting in enhanced phagocytic activity and a release of ROS (Adams et al., 2007; Pei et al., 2007). The investigation of the role that NPY and MAC1R play in regulation of phagocytic activity of microglial cells is promising and requires further research.

Rapamycin, an inhibitor of the mTOR receptor in mammals, is involved in numerous cellular processes such as neuroprotection in neurodegenerative disorders (Ravikumar et al., 2004; Malagelada et al., 2010) and neuroregeneration after cerebral injury and SCI (Erlich et al., 2007; Kanno et al., 2012). Rapamycin inhibits the mTOR pathway by preventing the activation of p70S6K protein kinase (Schmelzle and Hall, 2000). Rapamycin neuroprotective properties are due to its ability to stimulate autophagy (Ravikumar et al., 2004; Malagelada et al., 2010). It is also involved in suppression of microglia activation and reduction of inflammation in the CNS by selective inhibition of the mTORC1 complex (Russo et al., 2009). *In vivo* studies using rat SCI model showed the ability of rapamycin to attenuate microglial activation and neuroinflammation processes by reducing the number of M1 cells and, as a result, TNF-α production (Chen et al., 2013; Song et al., 2015). However, Eldahan et al. (2018) caution against the use of rapamycin as a therapeutic intervention for SCI due to its toxic effects and exacerbation of cardiovascular dysfunction.

FTY720 is an agonist of the S1P receptor and a derivative of ISP-1 (myriocin), a metabolite of the Chinese fungus *Iscaria sinclairii*, as well as a sphingosine structural analog. This is a novel immunomodulator that promotes transplantability in numerous models by inhibiting lymphocytes. FTY720 plays the role of a switch in the polarization of microglia from M1 to M2 through the STAT3 protein activation that has been established in a white matter ischemic injury model (Qin et al., 2017). The results obtained also provide evidence that FTY720 has a protective effect against structural damage to the nodes of Ranvier and demyelination after hypoperfusion. It should be noted that, in some cases, FTY720 was effective in treating SCI but did not affect the activation of microglia/macrophages (Norimatsu et al., 2012; Wang J. et al., 2015).

Cytokines/Chemokines

Cytokines play an important role in posttraumatic processes; in particular, microglia cells can influence healing by controlling levels of some of them. Activating and blocking agents to

modulate inflammatory processes for most of these cytokines are under development. For example, IL-4 is considered the strongest polarizing cytokine for M2a microglia response. In the IL-4R-deficient mice SCI model, there was a decrease in the production of anti-inflammatory cytokines such as arginase, IL-1, and CCL2, which indicates the predominance of M1 microglia (Fenn et al., 2014). A single intraspinal injection of IL-4 48 h after SCI was shown to be sufficient to switch the microglia phenotype toward M2 and, what is more important, it was associated with improved functional recovery in mice with an SCI (Francos-Quijorna et al., 2016). Interestingly, in response to exposure, IL-4 can modulate the morphology of microglia *in vitro* from amoeboid (activated) to a more ramified (quiescent) one associated with a more activated phenotype; at the same time, IFN-γ and GM-CSF have the opposite effect (Rostam et al., 2017).

IL-6 is a key factor triggering inflammation after SCI; it also promotes microglia M1 activation (Bethea and Dietrich, 2002). An IL-6 blocking agent—monoclonal anti-mouse receptor antibody IL-6 (MR16-1)—administered into the site of SCI in mice promoted alternative M2 microglia activation and resulted in improved tissue integrity as well as an increased number of myelinated fibers (Guerrero et al., 2012). Moreover, inhibition of the EGFR/MAPK pathway that suppresses microglia activation and associated cytokine production decreases neuroinflammation-related secondary damage and thereby provides neuroprotection in rats after SCI (Qu et al., 2012). It is thought that EGFR can be a therapeutic target and inhibitors C225 and AG1478 have the potential to be used in the treatment of SCI (Qu et al., 2012). Chemokine CCL21 neutralization was also shown to reduce microglia M1 activation and to cause neuronal hyperexcitability of lateral posterior thalamic nuclei (Zhao et al., 2007).

IL-6 is a key cytokine accelerating the IL-17 production (Camporeale and Poli, 2012). IL-17 is a well-known proinflammatory cytokine associated with M1 activation of microglia (Kim and Moalem-Taylor, 2011; Zong et al., 2014). The inhibition of IL-17 as a mediator of microglia activation after hyperforin injection promoted microglia polarization toward the M2 phenotype in a murine acute cerebral mechanic trauma model (Ma et al., 2018). TGF-β1 is a polypeptide component of a transforming cytokine factor. It was shown in an *in vivo* murine stroke model that cerebro-ventricular injections of TGF-β1 promoted microglia M2 activation as well as improvement of functional recovery in mice (Taylor et al., 2017).

MicroRNA

Lately, special emphasis is being given to the role that miRNA plays in the pathogenesis of many diseases including diseases of the CNS. It has been shown that miRNA administration can be an effective therapeutic approach to the management of neurodegenerative processes. MiRNAs regulate the expression of a great number of genes by stimulating RNA interference pathway degradation or by preventing the translation of target genes. High miR-124 levels were reported in resident cerebral and spinal microglia, as well as their activation *in vitro* and *in vivo* to promote a decreased miR-124 expression (Ponomarev et al., 2011). miR-124 is considered to regulate the activity of microglia/macrophages by down-regulating the expression of CCAAT-enhancer-binding protein-α, a transcription factor regulating the differentiation of myeloid cells. Therefore, high miR-124 levels are thought to be required to maintain microglia in a quiescent state. Willemen et al. (2012) demonstrated that intrathecally injected miR-124 promoted the maintenance of microglia in this quiescent state and alleviated chronic posttraumatic processes in the spinal cord of rats with hyperalgesia. Im et al. (2012) reported similar results when injecting miR-23b intrathecally to mice in a neuropathic pain model. Based on their results, a return of miR-23b to normal levels decreased the expression of inflammatory proteins, reduced the number of $Iba1^+$ cells in the spinal cord tissue, and alleviated a neuropathic pain resulting from SCI.

Cell Cycle Modulation

It was found that exposure on a cell cycle course can also modulate cell phenotype. There were changes in cell cycle course following SCI and effects of systemic administration of delayed (24 h) flavopiridol, an inhibitor of major cyclin-dependent kinases, on functional recovery and histopathology in a rat SCI model (Wu et al., 2012). The treatment with flavopiridol attenuated the number of Iba-1^+-microglia in the intact tissue and, as a result, increased the myelinated area of the white matter. Moreover, flavopiridol attenuated the expression of Iba-1 and glactin-3, associated with microglia M1 activation and astrocyte reactivity by reducing the GFAP, NG2, and CHL1 expression.

Neurotrophic Factors

Although there are numerous approaches to modulate microglia in the CNS, the search for new approaches to effective polarization strictly toward a neuroprotective phenotype and introduction of results into clinical practice is still relevant. Neurotrophic factors are molecules that increase the potential of nervous system cells to proliferate, survive, migrate, and differentiate. For instance, a ciliary neurotrophic factor (CNTF) exerts a positive effect on reactive M1 microglia, promoting their survival and activation after intracerebral injection to mice *in vivo* (Kahn et al., 1995). However, Rocha et al. (2012) demonstrated that, on the contrary, a glial cell line-derived neurotrophic factor (GDNF) inhibited the activation of reactive M1 microglia *in vitro* (Rocha et al., 2012).

Selective modulation of microglia with recombinant adenoviruses carrying the GDNF gene *in vivo* seems promising. Zhuravleva et al. (2016) demonstrated that microglia transduction with an adenovirus encoding for GDNF (Ad5-GDNF) promoted a reduced phagocytic activity of these cells. We have conducted a study to evaluate effects of Ad5-GDNF transduction on the morphology and phenotype of microglial cells as well as effects of transplanting these cells on posttraumatic processes in the rat spinal cord. It was shown that microglia transduction with Ad5-GDNF down-regulated expression of CD45, but their transplantation into the site of a rat SCI did not

increase the area of intact tissue as compared to similar transplantation of Ad5-EGFP microglia with fair phagocytic activity (Akhmetzyanova et al., 2018).

Physical Methods

Repetitive transcranial magnetic stimulation of the motor cortex was shown to reduce microglia M1 activation after SCI and alleviated symptoms of neuropathic pain and allodynia (Kim et al., 2013). A method of physical exposure to alleviate SCI consequences is promising as it is non-invasive and has few side effects. However, this approach to treatment is just gaining ground and is not yet fully understood. Therefore a comprehensive assessment of modulation mechanisms triggered by a physical exposure is required.

Other Approaches

Lipopolysaccharide is an essential molecular component of the outer membrane of gram-negative bacteria and is recognized by an immune system as an invasion marker of bacterial pathogens. LPS is more often used to induce a potent immunological response and activate microglia/macrophages. It was found that pre-conditioning of microglia with LPS 48 h prior to transplantation enabled M2 polarization in mouse SCI (Hayakawa et al., 2014). The results obtained were evaluated by measuring the expression of mRNA markers of M1 (iNOS, CD86, and CD16) and M2 (arginase1 and CD206) microglia.

Histone deacetylases (HDACs) are proteins targeted to remove acetyl groups from lysine residues of target proteins. HDAC3 is most commonly found in the brain and is a regulator of inflammatory processes (Broide et al., 2007). HDAC3-deficient macrophages have a reduced ability to activate the expression of inflammatory genes in response to LPS stimulation (Chen et al., 2012). At the same time, it was found that HDAC3 is an epigenomic brake in macrophage alternative (M2) activation (Mullican et al., 2011). Malvaez et al. (2013) used protein mass spectrometry in the study *in vitro* to detect global molecular changes in resident microglia exposed to RGFP966, a selective HDAC3 inhibitor, by investigating a signaling pathway through which RGFP966 regulated an inflammation. They observed that RGFP966 could inhibit TLR and STAT3/5 signaling pathways of microglia M1 activation and that this resulted in an anti-inflammatory microglia response manifesting as a reduced expression of proinflammatory cytokines such as IL-6 and TNF-α (Xia et al., 2017). This is confirmed by another *in vitro* study, where it was shown in a primary culture that treatment with HDAC inhibitors promoted suppression of the innate immune activation of microglia (Kannan et al., 2013). A similar study demonstrated that HDAC3 arrest with the same selective inhibitor RGFP966 facilitated the shift toward an anti-inflammatory microglia response that resulted in gaining a neuroprotective phenotype by these cells and improved functional recovery in an SCI model *in vivo* (Kuboyama et al., 2017). Bromodomain and extraterminal (BET) proteins are readers of histone acetylation labels, thereby affecting the transcription of genes and thus playing an important role in regulation the expression of pro-inflammatory cytokine expression (Belkina et al., 2013). Sánchez-Ventura et al. (2019) investigated the influence of BET inhibitor JQ1 in polarizing microglia on bone-marrow-derived macrophage *in vitro* and *in vivo* in SCI mice and showed that JQ1 promotes polarization of microglia toward the M2 phenotype, reducing the expression of pro-inflammatory cytokines IL-6, IL-1β, and TNF-α and increasing the expression of anti-inflammatory cytokines Arg1 and CD206.

It was shown that an early administration of minocycline, a known anti-inflammatory agent, inhibiting poly (ADP-ribose) polymerase-1 (PARP-1), which both promotes cell death and inhibits microglia activation and an inflammation in general, can reduce a degree of neuronal hyperexcitability for up to 4 weeks after SCI (Alano et al., 2006; Tan, 2009). In addition, minocycline-loaded polymeric nanoparticles (NPs) injected into the site of an SCI can selectively target activated microglial cells and modulate their phenotypes toward the anti-inflammatory one by inhibiting PARP-1 and matrix metalloproteinases 2 and 9, which improves the course of secondary traumatic processes in a murine SCI model. The treatment with minocycline-loaded NPs resulted in a reduced activation and decreased proliferation of microglia around the site of injury. As a result, the decreased number of cells with a phagocytic phenotype switched toward quiescent microglia with a low CD68 staining level. The treatment with these particles appeared effective for 15 post-injury days and was related to a prolonged anti-inflammatory stimulus associated with microglia activation (Papa et al., 2013). Another study demonstrated that the administration of minocycline-loaded NPs in an acute period following trauma in a murine SCI model could effectively modulate resident microglial cells from M1 to M2 phenotype, which reduced a proinflammatory response, restored the nervous tissue integrity, and improved behavior test scores for up to 63 post-injury days (Papa et al., 2016).

CONCLUSION

Although there are many studies aimed at elucidating mechanisms of microglia/macrophage modulation, their phenotype, and role in various pathologies, currently, no effective methods to modulate microglia toward a neuroprotective phenotype in order to stimulate neuroregeneration are employed in clinical practice. In addition, there is an urgent need to develop a highly specific panel of markers for resident microglia and macrophages migrating to a site of pathology, as well as complete elucidation of every external (specifically activating molecules secreted by surrounding cells) and internal factor (signaling pathways) affecting the modulation of their phenotype.

AUTHOR CONTRIBUTIONS

EA was in charge of the collection of data on the approaches to modulation of microglia/macrophages and compilation of a table. KK was in charge of the collection of data on the

microglial signaling pathways. YM was in charge of the data collection about the microglia phenotypes and behavior of microglia/macrophages in the area of SCI and **Figure 1** drawing. AR was in charge of the article content compilation and manuscript writing.

FUNDING

This work was supported by a grant from the Russian Science Foundation, No. 18-75-00043 to YM.

ACKNOWLEDGMENTS

This work was performed in accordance with the Program of Competitive Growth of the Kazan Federal University.

SUPPLEMENTARY MATERIAL

The Supplementary Material for this article can be found online at: https://www.frontiersin.org/articles/10.3389/fnsys.2019.00037/full#supplementary-material

REFERENCES

Adams, R. A., Bauer, J., Flick, M. J., Sikorski, S. L., Nuriel, T., Lassmann, H., et al. (2007). The fibrin-derived γ377–395 peptide inhibits microglia activation and suppresses relapsing paralysis in central nervous system autoimmune disease. *J. Exp. Med.* 204, 571–582. doi: 10.1084/jem.20061931

Ahmadian, M., Suh, J. M., Hah, N., Liddle, C., Atkins, A. R., Downes, M., et al. (2013). PPARγ signaling and metabolism: the good, the bad and the future. *Nat. Med.* 19, 557–566. doi: 10.1038/nm.3159

Ahn, H. J., Hernandez, C. M., Levenson, J. M., Lubin, F. D., Liou, H. C., and Sweat, J. D. (2008). c-Rel, an NF-κB family transcription factor, is required for hippocampal long-term synaptic plasticity and memory formation. *Learn. Mem.* 15, 539–549. doi: 10.1101/lm.866408

Akhmetzyanova, E., Mukhamedshina, Y. O., Zhuravleva, M., Galieva, L., Kostennikov, A., Garanina, E., et al. (2018). Transplantation of microglia in the area of spinal cord injury in an acute period increases tissue sparing, but not functional recovery. *Front. Cell. Neurosci.* 12:507. doi: 10.3389/fncel.2018.00507

Alano, C. C., Kauppinen, T. M., Valls, A. V., and Swanson, R. A. (2006). Minocycline inhibits poly (ADP-ribose) polymerase-1 at nanomolar concentrations. *Proc. Natl. Acad. Sci.* 103, 9685–9690. doi: 10.1073/pnas.0600554103

Beck, A., Penner, R., and Fleig, A. (2008). Lipopolysaccharide-induced down-regulation of Ca2+ release-activated Ca2+ currents (ICRAC) but not Ca2+-activated TRPM4-like currents (ICAN) in cultured mouse microglial cells. *J. Physiol.* 586, 427–439. doi: 10.1113/jphysiol.2007.145151

Beck, K. D., Nguyen, H. X., Galvan, M. D., Salazar, D. L., Woodruff, T. M., and Anderson, A. (2010). Quantitative analysis of cellular inflammation after traumatic spinal cord injury: evidence for a multiphasic inflammatory response in the acute to chronic environment. *Brain* 133, 433–447. doi: 10.1093/brain/awp322

Belkina, A. C., Nikolajczyk, B. S., and Denis, G. V. (2013). BET protein function is required for inflammation: Brd2 genetic disruption and BET inhibitor JQ1 impair mouse macrophage inflammatory responses. *J. Immunol.* 190, 3670–3678. doi: 10.4049/jimmunol.1202838

Bellver-Landete, V., Bretheau, F., Mailhot, B., Vallières, N., Lessard, M., Janelle, M. E., et al. (2019). Microglia are an essential component of the neuroprotective scar that forms after spinal cord injury. *Nat. Commun.* 10, 518–536. doi: 10.1038/s41467-019-08446-0

Bethea, J. R., and Dietrich, D. W. (2002). Targeting the host inflammatory response in traumatic spinal cord injury. *Curr. Opin. Neurol.* 15, 355–360. doi: 10.1097/00019052-200206000-00021

Bouhlel, M. A., Derudas, B., Rigamonti, E., Dièvart, R., Brozek, J., Haulon, S., et al. (2007). PPARγ activation primes human monocytes into alternative M2 macrophages with anti-inflammatory properties. *Cell Metab.* 6, 137–143. doi: 10.1016/j.cmet.2007.06.010

Brambilla, R., Bracchi-Ricard, V., Hu, W. H., Frydel, B., Bramwell, A., Karmally, S., et al. (2005). Inhibition of astroglial nuclear factor κB reduces inflammation and improves functional recovery after spinal cord injury. *J. Exp. Med.* 202, 145–156. doi: 10.1084/jem.20041918

Broide, R. S., Redwine, J. M., Aftahi, N., Young, W., Bloom, F. E., and Winrow, C. J. (2007). Distribution of histone deacetylases 1–11 in the rat brain. *J. Mol. Neurosci.* 31, 47–58. doi: 10.1007/bf02686117

Bsibsi, M., Ravid, R., Gveric, D., and van Noort, J. M. (2002). Broad expression of toll-like receptors in the human central nervous system. *J. Neuropathol. Exp. Neurol.* 61, 1013–1021. doi: 10.1093/jnen/61.11.1013

Camporeale, A., and Poli, V. (2012). IL-6, IL-17 and STAT3: a holy trinity in auto-immunity? *Front Biosci.* 17:2306–2326.

Chen, C. H., Sung, C. S., Huang, S. Y., Feng, C. W., Hung, H. C., Yang, S. N., et al. (2016). The role of the PI3K/Akt/mTOR pathway in glial scar formation following spinal cord injury. *Exp. Neurol.* 278, 27–41. doi: 10.1016/j.expneurol.2016.01.023

Chen, H. C., Fong, T. H., Hsu, P. W., and Chiu, W. T. (2013). Multifaceted effects of rapamycin on functional recovery after spinal cord injury in rats through autophagy promotion, anti-inflammation, and neuroprotection. *J. Surg. Res.* 179, e203–e210. doi: 10.1016/j.jss.2012.02.023

Chen, X., Barozzi, I., Termanini, A., Prosperini, E., Recchiuti, A., Dalli, J., et al. (2012). Requirement for the histone deacetylase Hdac3 for the inflammatory gene expression program in macrophages. *Proc. Natl. Acad. Sci.U.S.A.* 109, 2865–2874. doi: 10.1073/pnas.1121131109

Chen, Z., and Trapp, B. D. (2016). Microglia and neuroprotection. *J. Neurochem.* 136, 10–17. doi: 10.1111/jnc.13062

Cheng, B., Lin, Y., Kuang, M., Fang, S., Gu, Q., Xu, J., et al. (2015). Synthesis and anti-neuroinflammatory activity of lactone benzoyl hydrazine and 2-nitro-1-phenyl-1H-indole derivatives as p38α MAPK inhibitors. *Chem. Biol. Drug Des.* 86, 1121–1130. doi: 10.1111/cbdd.12581

Chinetti, G., Fruchart, J. C., and Staels, B. (2003). Peroxisome proliferator-activated receptors: new targets for the pharmacological modulation of macrophage gene expression and function. *Curr. Opin. Lipidol.* 14, 459–468.

Chinetti, G., Griglio, S., Antonucci, M., Torra, I. P., Delerive, P., Majd, Z., et al. (1998). Activation of proliferator-activated receptors α and γ induces apoptosis of human monocyte-derived macrophages. *J. Biol. Chem.* 273, 25573–25580. doi: 10.1074/jbc.273.40.25573

Cianciulli, A., Dragone, T., Calvello, R., Porro, C., Trotta, T., Lofrumento, D. D., et al. (2015). IL-10 plays a pivotal role in anti-inflammatory effects of resveratrol in activated microglia cells. *Int. Immunopharmacol.* 24, 369–376. doi: 10.1016/j.intimp.2014.12.035

Conta, A. C., and Stelzner, D. J. (2008). Immunomodulatory effect of the purine nucleoside inosine following spinal cord contusion injury in rat. *Spinal Cord* 46, 39. doi: 10.1038/sj.sc.3102057

Crosio, C., Valle, C., Casciati, A., Iaccarino, C., and Carrì, M. T. (2011). Astroglial inhibition of NF-κB does not ameliorate disease onset and progression in a mouse model for amyotrophic lateral sclerosis (ALS). *PLoS One* 6:17187. doi: 10.1371/journal.pone.0017187

Crown, E. D., Gwak, Y. S., Ye, Z., Johnson, K. M., and Hulsebosch, C. E. (2008). Activation of p38 MAP kinase is involved in central neuropathic pain following spinal cord injury. *Exp. Neurol.* 213, 257–267. doi: 10.1016/j.expneurol.2008.05.025

Dalpke, A. H., Schäfer, M. K., Frey, M., Zimmermann, S., Tebbe, J., Weihe, E., et al. (2002). Immunostimulatory CpG-DNA activates murine microglia. *J. Immunol.* 168, 4854–4863. doi: 10.4049/jimmunol.168.10.4854

David, S., and Kroner, A. (2011). Repertoire of microglial and macrophage responses after spinal cord injury. *Nat. Rev. Neurosci.* 12, 388. doi: 10.1038/nrn3053

Detloff, M. R., Fisher, L. C., McGaughy, V., Longbrake, E. E., Popovich, P. G., and Basso, D. M. (2008). Remote activation of microglia and pro-inflammatory cytokines predict the onset and severity of below-level neuropathic pain after spinal cord injury in rats. *Exp. Neurol.* 212, 337–347. doi: 10.1016/j.expneurol.2008.04.009

Donnelly, D. J., and Popovich, P. G. (2008). Inflammation and its role in neuroprotection, axonal regeneration and functional recovery after spinal cord injury. *Exp. Neurol.* 209, 378–388. doi: 10.1016/j.expneurol.2007.06.009

Durafourt, B. A., Moore, C. S., Zammit, D. A., Johnson, T. A., Zaguia, F., Guiot, M. C., et al. (2012). Comparison of polarization properties of human adult microglia and blood-derived macrophages. *GLIA* 60, 717–727. doi: 10.1002/glia.22298

Eldahan, K. C., Cox, D. H., Gollihue, J. L., Patel, S. P., and Rabchevsky, A. G. (2018). Rapamycin exacerbates cardiovascular dysfunction after complete high-thoracic spinal cord injury. *J. Neurotrauma.* 35, 842–853. doi: 10.1089/neu.2017.5184

Emmetsberger, J., and Tsirka, S. E. (2012). Microglial inhibitory factor (MIF/TKP) mitigates secondary damage following spinal cord injury. *Neurobiol. Dis.* 47, 295–309. doi: 10.1016/j.nbd.2012.05.001

Erlich, S., Alexandrovich, A., Shohami, E., and Pinkas-Kramarski, R. (2007). Rapamycin is a neuroprotective treatment for traumatic brain injury. *Neurobiol. Dis.* 26, 86–93. doi: 10.1016/j.nbd.2006.12.003

Fan, H., Zhang, K., Shan, L., Kuang, F., Chen, K., Zhu, K., et al. (2016). Reactive astrocytes undergo M1 microglia/macrophages-induced necroptosis in spinal cord injury. *Mol. Neurodegener.* 11:14. doi: 10.1186/s13024-016-0081-8

Fan, Y., Xie, L., and Chung, C. Y. (2017). Signaling pathways controlling microglia chemotaxis. *Mol. Cells* 40, 163–168. doi: 10.14348/molcells.2017.0011

Farzi, A., Reichmann, F., and Holzer, P. (2015). The homeostatic role of neuropeptide Y in immune function and its impact on mood and behaviour. *Acta Physiol.* 213, 603–627. doi: 10.1111/apha.12445

Fenn, A. M., Hall, J. C., Gensel, J. C., Popovich, P. G., and Godbout, J. P. (2014). IL-4 signaling drives a unique arginase+/IL-1β+ microglia phenotype and recruits macrophages to the inflammatory CNS: consequences of age-related deficits in IL-4Rα after traumatic spinal cord injury. *J. Neurosci.* 34, 8904–8917. doi: 10.1523/jneurosci.1146-14.2014

Fernandez-Lizarbe, S., Pascual, M., and Guerri, C. (2009). Critical role of TLR4 response in the activation of microglia induced by ethanol. *J. Immunol.* 183, 4733–4744. doi: 10.4049/jimmunol.0803590

Ferreira, R., Santos, T., Cortes, L., Cochaud, S., Agasse, F., Silva, A. P., et al. (2012). Neuropeptide Y inhibits interleukin-1 beta-induced microglia motility. *J. Neurochem.* 120, 93–105. doi: 10.1111/j.1471-4159.2011.07541.x

Finnerup, N. B., Johannesen, I. L., Sindrup, S. H., Bach, F. W., and Jensen, T. S. (2001). Pain and dysesthesia in patients with spinal cord injury: a postal survey. *Spinal cord* 39, 256–262. doi: 10.1038/sj.sc.3101161

Frakes, A. E., Ferraiuolo, L., Haidet-Phillips, A. M., Schmelzer, L., Braun, L., Miranda, C. J., et al. (2014). Microglia induce motor neuron death via the classical NF-κB pathway in amyotrophic lateral sclerosis. *Neuron* 81, 1009–1023. doi: 10.1016/j.neuron.2014.01.013

Franco, R., and Fernandez-Suarez, D. (2015). Alternatively activated microglia and macrophages in the central nervous system. *Prog. Neurobiol.* 131, 65–86. doi: 10.1016/j.pneurobio.2015.05.003

Francos-Quijorna, I., Amo-Aparicio, J., Martinez-Muriana, A., and López-Vales, R. (2016). IL-4 drives microglia and macrophages toward a phenotype conducive for tissue repair and functional recovery after spinal cord injury. *GLIA* 64, 2079–2092. doi: 10.1002/glia.23041

Gensel, J. C., and Zhang, B. (2015). Macrophage activation and its role in repair and pathology after spinal cord injury. *Brain Res.* 1619, 1–11. doi: 10.1016/j.brainres.2014.12.045

Gratchev, A., Kzhyshkowska, J., Kannookadan, S., Ochsenreiter, M., Popova, A., Yu, X., et al. (2008). Activation of a TGF-β-specific multistep gene expression program in mature macrophages requires glucocorticoid-mediated surface expression of TGF-β receptor II. *J. Immunol.* 180, 6553–6555.

Guerrero, A. R., Uchida, K., Nakajima, H., Watanabe, S., Nakamura, M., Johnson, W. E., et al. (2012). Blockade of interleukin-6 signaling inhibits the classic pathway and promotes an alternative pathway of macrophage activation after spinal cord injury in mice. *J. Neuroinflammation.*9:40. doi: 10.1186/1742-2094-9-40

Guo, J. R., Wang, H., Jin, X. J., Jia, D. L., Zhou, X., and Tao, Q. (2017). Effect and mechanism of inhibition of PI3K/Akt/mTOR signal pathway on chronic neuropathic pain and spinal microglia in a rat model of chronic constriction injury. *Oncotarget* 8:52923. doi: 10.18632/oncotarget.17629

Han, J., Harris, R. A., and Zhang, X. M. (2017). An updated assessment of microglia depletion: current concepts and future directions. *Mol. Brain* 10:25. doi: 10.1186/s13041-017-0307-x

Hayakawa, K., Okazaki, R., Morioka, K., Nakamura, K., Tanaka, S., and Ogata, T. (2014). Lipopolysaccharide preconditioning facilitates M2 activation of resident microglia after spinal cord injury. *J. Neurosci. Res.* 92, 1647–1658. doi: 10.1002/jnr.23448

He, Y., She, H., Zhang, T., Xu, H., Cheng, L., Yepes, M., et al. (2018). p38 MAPK inhibits autophagy and promotes microglial inflammatory responses by phosphorylating ULK1. *J Cell Biol.* 217, 315–328. doi: 10.1083/jcb.201701049

Hellwig, S., Heinrich, A., and Biber, K. (2013). The brain's best friend: microglial neurotoxicity revisited. *Front. Cell. Neurosci.* 7:71. doi: 10.3389/fncel.2013.00071

Heneka, M. T., Sastre, M., Dumitrescu-Ozimek, L., Hanke, A., Dewachter, I., Kuiperi, C., et al. (2005). Acute treatment with the PPARγ agonist pioglitazone and ibuprofen reduces glial inflammation and Aβ1–42 levels in APPV717I transgenic mice. *Brain* 128, 1442–1453. doi: 10.1093/brain/awh452

Hodes, G. E., Ménard, C., and Russo, S. J. (2016). Integrating interleukin-6 into depression diagnosis and treatment. *Neurobiol. Stress* 4, 15–22. doi: 10.1016/j.ynstr.2016.03.003

Huang, Z., Luo, Q., Guo, Y., Chen, J., Xiong, G., Peng, Y., et al. (2015). Mycobacterium tuberculosis-induced polarization of human macrophage orchestrates the formation and development of tuberculous granulomas in vitro. *PLoS One* 10:e0129744. doi: 10.1371/journal.pone.0129744

Im, Y. B., Jee, M. K., Choi, J. I., Cho, H. T., Kwon, O. H., and Kang, S. K. (2012). Molecular targeting of NOX4 for neuropathic pain after traumatic injury of the spinal cord. *Cell Death Dis.* 3, E426. doi: 10.1038/cddis.2012.168

Jin, X., and Yamashita, T. (2016). Microglia in central nervous system repair after injury. *J. Biochem.* 159, 491–496. doi: 10.1093/jb/mvw009

Kahn, M. A., Ellison, J. A., Speight, G. J., and De Vellis, J. (1995). CNTF regulation of astrogliosis and the activation of microglia in the developing rat central nervous system. *Brain Res.* 685, 55–67. doi: 10.1016/0006-8993(95)00411-i

Kannan, V., Brouwer, N., Hanisch, U. K., Regen, T., Eggen, B. J., and Boddeke, H. W. (2013). Histone deacetylase inhibitors suppress immune activation in primary mouse microglia. *J. Neurosci. Res.* 91, 1133–1142. doi: 10.1002/jnr.23221

Kanno, H., Ozawa, H., Sekiguchi, A., Yamaya, S., Tateda, S., Yahata, K., et al. (2012). The role of mTOR signaling pathway in spinal cord injury. *Cell Cycle* 11, 3175–3179. doi: 10.4161/cc.21262

Kigerl, K. A., Gensel, J. C., Ankeny, D. P., Alexander, J. K., Donnelly, D. J., and Popovich, P. G. (2009). Identification of two distinct macrophage subsets with divergent effects causing either neurotoxicity or regeneration in the injured mouse spinal cord. *J. Neurosci.* 29, 13435–13444. doi: 10.1523/JNEUROSCI.3257-09.2009

Kim, B. W., More, S. V., Yun, Y. S., Ko, H. M., Kwak, J. H., Lee, H., et al. (2016). A novel synthetic compound MCAP suppresses LPS-induced murine microglial activation in vitro via inhibiting NF-kB and p38 MAPK pathways. *Acta Pharmacol. Sin.* 37, 334.–343

Kim, C. F., and Moalem-Taylor, G. (2011). Interleukin-17 contributes to neuroinflammation and neuropathic pain following peripheral nerve injury in mice. *J. Pain* 12, 370–383. doi: 10.1016/j.jpain.2010.08.003

Kim, J. Y., Choi, G. S., Cho, Y. W., Cho, H., Hwang, S. J., and Ahn, S. H. (2013). Attenuation of spinal cord injury-induced astroglial and microglial activation by repetitive transcranial magnetic stimulation in rats. *J. Korean Med. Sci.* 28, 295–299. doi: 10.3346/jkms.2013.28.2.295

Koo, J. W., Russo, S. J., Ferguson, D., Nestler, E. J., and Duman, R. S. (2010). Nuclear factor-κB is a critical mediator of stress-impaired neurogenesis and

depressive behavior. *Proc. Natl. Acad. Sci.U.S.A.* 107, 2669–2674. doi: 10.1073/pnas.0910658107

Koscsó, B., Csóka, B., Kókai, E., Németh, Z. H., Pacher, P., Virág, L., et al. (2013). Adenosine augments IL-10-induced STAT3 signaling in M2c macrophages. *J. Leukoc. Biol.* 94, 1309–1315. doi: 10.1189/jlb.0113043

Kuboyama, T., Wahane, S., Huang, Y., Zhou, X., Wong, J. K., Koemeter-Cox, A., et al. (2017). HDAC3 inhibition ameliorates spinal cord injury by immunomodulation. *Sci. Rep.* 7:8641. doi: 10.1038/s41598-017-08535-4

Laflamme, N., Soucy, G., and Rivest, S. (2001). Circulating cell wall components derived from gram-negative, not gram-positive, bacteria cause a profound induction of the gene-encoding Toll-like receptor 2 in the CNS. *J. Neurochem.* 79, 648–657. doi: 10.1046/j.1471-4159.2001.00603.x

Lai, A. Y., and Todd, K. G. (2006). Microglia in cerebral ischemia: molecular actions and interactions. *Can. J. Physiol. Pharmacol.* 84, 49–59. doi: 10.1139/Y05-143

Lampron, A., Larochelle, A., Laflamme, N., Préfontaine, P., Plante, M. M., Sánchez, M. G., et al. (2015). Inefficient clearance of myelin debris by microglia impairs remyelinating processes. *J. Exp. Med.* 212, 481–495. doi: 10.1084/jem.20141656

Le Cabec, V., Carréno, S., Moisand, A., Bordier, C., and Maridonneau-Parini, I. (2002). Complement receptor 3 (CD11b/CD18) mediates type I and type II phagocytosis during nonopsonic and opsonic phagocytosis, respectively. *J. Immunol.* 169, 2003–2009. doi: 10.4049/jimmunol.169.4.2003

Lee, K. D., Chow, W. N., Sato-Bigbee, C., Graf, M. R., Graham, R. S., Colello, R. J., et al. (2009). FTY720 reduces inflammation and promotes functional recovery after spinal cord injury. *J. Neurotrauma* 26, 2335–2344. doi: 10.1089/neu.2008.0840

Liu, X., Wen, S., Yan, F., Liu, K., Liu, L., Wang, L., et al. (2018). Salidroside provides neuroprotection by modulating microglial polarization after cerebral ischemia. *J. Neuroinflammation* 15:39. doi: 10.1186/s12974-018-1081-0

Ma, L., Pan, X., Zhou, F., Liu, K., and Wang, L. (2018). Hyperforin protects against acute cerebral ischemic injury through inhibition of interleukin-17A-mediated microglial activation. *Brain Res.* 1678, 254–261. doi: 10.1016/j.brainres.2017.08.023

Ma, X., Reynolds, S. L., Baker, B. J., Li, X., Benveniste, E. N., and Qin, H. (2010). IL-17 enhancement of the IL-6 signaling cascade in astrocytes. *J. Immunol.* 184, 4898–4906. doi: 10.4049/jimmunol.1000142

Malagelada, C., Jin, Z. H., Jackson-Lewis, V., Przedborski, S., and Greene, L. A. (2010). Rapamycin protects against neuron death in in vitro and in vivo models of Parkinson's disease. *J. Neurosci.* 30, 1166–1175. doi: 10.1523/JNEUROSCI.3944-09.2010

Malvaez, M., McQuown, S. C., Rogge, G. A., Astarabadi, M., Jacques, V., Carreiro, S., et al. (2013). HDAC3-selective inhibitor enhances extinction of cocaine-seeking behavior in a persistent manner. *Proc. Natl. Acad. Sci. U.S.A.* 110, 2647–2652. doi: 10.1073/pnas.1213364110

Malyshev, I., and Malyshev, Y. (2015). Current concept and update of the macrophage plasticity concept: intracellular mechanisms of reprogramming and M3 macrophage "switch" phenotype. *Biomed Res. Int.* 2015:341308. doi: 10.1155/2015/341308

Martin, E., El-Behi, M., Fontaine, B., and Delarasse, C. (2017). Analysis of microglia and monocyte-derived macrophages from the central nervous system by flow cytometry. *J. Vis. Exp.* 22:55781. doi: 10.3791/55781

Martinez, F. O., and Gordon, S. (2014). The M1 and M2 paradigm of macrophage activation: time for reassessment. *F1000prime Rep.* 6:13. doi: 10.12703/P6-13

Martinez, F. O., Gordon, S., Locati, M., and Mantovani, A. (2006). Transcriptional profiling of the human monocyte-to-macrophage differentiation and polarization: new molecules and patterns of gene expression. *J. Immunol.* 177, 7303–7311. doi: 10.4049/jimmunol.177.10.7303

Martinez, F. O., Helming, L., Milde, R., Varin, A., Melgert, B. N., Draijer, C., et al. (2013). Genetic programs expressed in resting and IL-4 alternatively activated mouse and human macrophages: similarities and differences. *Blood* 121, 57–69. doi: 10.1182/blood-2012-06-436212

McTigue, D. M. (2008). Potential therapeutic targets for PPAR after spinal cord injury. *PPAR Res.* 2008:517162. doi: 10.1155/2008/517162

McTigue, D. M., Tripathi, R., Wei, P., and Lash, A. T. (2007). The PPAR gamma agonist pioglitazone improves anatomical and locomotor recovery after rodent spinal cord injury. *Exp. Neurol.* 205, 396–406. doi: 10.1016/j.expneurol.2007.02.009

Menzies, F. M., Henriquez, F. L., Alexander, J., and Roberts, C. W. (2010). Sequential expression of macrophage anti-microbial/inflammatory and wound healing markers following innate, alternative and classical activation. *Clin. Exp. Immunol.* 160, 369–379. doi: 10.1111/j.1365-2249.2009.04086.x

Mullican, S. E., Gaddis, C. A., Alenghat, T., Nair, M. G., Giacomin, P. R., Everett, L. J., et al. (2011). Histone deacetylase 3 is an epigenomic brake in macrophage alternative activation. *Genes Dev.* 25, 2480–2488. doi: 10.1101/gad.175950.111

Nakajima, H., Uchida, K., Guerrero, A. R., Watanabe, S., Sugita, D., Takeura, N., et al. (2012). Transplantation of mesenchymal stem cells promotes an alternative pathway of macrophage activation and functional recovery after spinal cord injury. *J. Neurotrauma.* 29, 1614–1625. doi: 10.1089/neu.2011.2109

Nakajima, K., and Kohsaka, S. (2002). *Neuroprotective Roles of Microglia in the Central Nervous system, in Microglia in the Regenerating and Degenerating Central Nervous System*. Berlin: Springer, 188–208.

Nakajima, K., and Kohsaka, S. (2004). Microglia: neuroprotective and neurotrophic cells in the central nervous system. *Curr. Drug Targets Cardiovasc. Haematol. Disord.* 4, 65–84. doi: 10.2174/1568006043481284

Nakajima, K., Matsushita, Y., Tohyama, Y., Kohsaka, S., and Kurihara, T. (2006). Differential suppression of endotoxin-inducible inflammatory cytokines by nuclear factor kappa B (NFκB) inhibitor in rat microglia. *Neurosci. Lett.* 401, 199–202. doi: 10.1016/j.neulet.2006.03.014

Noort, A. R., Tak, P. P., and Tas, S. W. (2015). Non-canonical NF-κB signaling in rheumatoid arthritis: Dr Jekyll and Mr Hyde? *Arthritis Res. Ther.* 17:15. doi: 10.1186/s13075-015-0527-3

Norimatsu, Y., Ohmori, T., Kimura, A., Madoiwa, S., Mimuro, J., Seichi, A., et al. (2012). FTY720 improves functional recovery after spinal cord injury by primarily nonimmunomodulatory mechanisms. *Am. J. Pathol.* 180, 1625–1635. doi: 10.1016/j.ajpath.2011.12.012

Ohtake, Y., Park, D., Abdul-Muneer, P. M., Li, H., Xu, B., Sharma, K., et al. (2014). The effect of systemic PTEN antagonist peptides on axon growth and functional recovery after spinal cord injury. *Biomaterials* 35, 4610–4626. doi: 10.1016/j.biomaterials.2014.02.037

Oliva, A. A., Kang, Y., Sanchez-Molano, J., Furones, C., and Atkins, C. M. (2012). STAT3 signaling after traumatic brain injury. *J. Neurochem.* 120, 710–720. doi: 10.1111/j.1471-4159.2011.07610.x

Olson, J. K., and Miller, S. D. (2004). Microglia initiate central nervous system innate and adaptive immune responses through multiple TLRs. *J. Immunol.* 173, 3916–3924. doi: 10.4049/jimmunol.173.6.3916

Orihuela, R., McPherson, C. A., and Harry, G. J. (2016). Microglial M1/M2 polarization and metabolic states. *Br. J. Pharmacol.* 173, 649–665. doi: 10.1111/bph.13139

O'Riordan, K. J., Huang, I. C., Pizzi, M., Spano, P., Boroni, F., Egli, R., et al. (2006). Regulation of nuclear factor κB in the hippocampus by group I metabotropic glutamate receptors. *J. Neurosci.* 26, 4870–4879. doi: 10.1523/JNEUROSCI.4527-05.2006

Pan, J., Jin, J. L., Ge, H. M., Yin, K. L., Chen, X., Han, L. J., et al. (2015). Malibatol A regulates microglia M1/M2 polarization in experimental stroke in a PPARγ-dependent manner. *J. Neuroinflammation* 12:51. doi: 10.1186/s12974-015-0270-3

Pan, W., Yu, C., Hsuchou, H., and Kastin, A. J. (2010). The role of cerebral vascular NFκB in LPS-induced inflammation: differential regulation of efflux transporter and transporting cytokine receptors. *Cell. Physiol. Biochem.* 25, 623–630. doi: 10.1159/000315081

Papa, S., Caron, I., Erba, E., Panini, N., De Paola, M., Mariani, A., et al. (2016). Early modulation of pro-inflammatory microglia by minocycline loaded nanoparticles confers long lasting protection after spinal cord injury. *Biomaterials* 75, 13–24. doi: 10.1016/j.biomaterials.2015.10.015

Papa, S., Rossi, F., Ferrari, R., Mariani, A., De Paola, M., Caron, I., et al. (2013). Selective nanovector mediated treatment of activated proinflammatory microglia/macrophages in spinal cord injury. *ACS Nano* 7, 9881–9895. doi: 10.1021/nn4036014

Park, S. W., Yi, J. H., Miranpuri, G., Satriotomo, I., Bowen, K., Resnick, D. K., et al. (2007). Thiazolidinedione class of peroxisome proliferator-activated receptor γ agonists prevents neuronal damage, motor dysfunction, myelin loss, neuropathic pain, and inflammation after spinal cord injury in adult rats. *J. Pharmacol. Exp. Ther.* 320, 1002–1012. doi: 10.1124/jpet.106.113472

Peferoen, L. A., Vogel, D. Y., Ummenthum, K., Breur, M., Heijnen, P. D., Gerritsen, W. H., et al. (2015). Activation status of human microglia is dependent on lesion formation stage and remyelination in multiple sclerosis. *J. Neuropathol. Exp. Neurol.* 74, 48–63. doi: 10.1097/NEN.0000000000000149

Pei, Z., Pang, H., Qian, L. I., Yang, S., Wang, T., Zhang, W., et al. (2007). MAC1 mediates LPS-induced production of superoxide by microglia: the role of pattern recognition receptors in dopaminergic neurotoxicity. *GLIA* 55, 1362–1373. doi: 10.1002/glia.20545

Peress, N. S., Fleit, H. B., Perillo, E., Kuljis, R., and Pezzullo, C. (1993). Identification of FcγRI, II and III on normal human brain ramified microglia and on microglia in senile plaques in Alzheimer's disease. *J. Neuroimmunol.* 48, 71–79. doi: 10.1016/0165-5728(93)90060-c

Persson, M., Brantefjord, M., Hansson, E., and Rönnbäck, L. (2005). Lipopolysaccharide increases microglial GLT-1 expression and glutamate uptake capacity in vitro by a mechanism dependent on TNF-α. *Glia* 51, 111–120. doi: 10.1002/glia.20191

Ponomarev, E. D., Veremeyko, T., Barteneva, N., Krichevsky, A. M., and Weiner, H. L. (2011). MicroRNA-124 promotes microglia quiescence and suppresses EAE by deactivating macrophages via the C/EBP-α–PU. *Nat. Med.* 17, 64. doi: 10.1038/nm.2266

Popiolek-Barczyk, K., and Mika, J. (2016). Targeting the microglial signaling pathways: new insights in the modulation of neuropathic pain. *Curr. Med. Chem.* 23, 2908–2928. doi: 10.2174/0929867323666160607120124

Qin, C., Fan, W. H., Liu, Q., Shang, K., Murugan, M., Wu, L. J., et al. (2017). Fingolimod protects against ischemic white matter damage by modulating microglia toward M2 polarization via STAT3 pathway. *Stroke* 48, 3336–3346. doi: 10.1161/STROKEAHA.117.018505

Qu, W. S., Tian, D. S., Guo, Z. B., Fang, J., Zhang, Q., Yu, Z. Y., et al. (2012). Inhibition of EGFR/MAPK signaling reduces microglial inflammatory response and the associated secondary damage in rats after spinal cord injury. *J. Neuroinflammation* 9:178. doi: 10.1186/1742-2094-9-178

Ravikumar, B., Vacher, C., Berger, Z., Davies, J. E., Luo, S., Oroz, L. G., et al. (2004). Inhibition of mTOR induces autophagy and reduces toxicity of polyglutamine expansions in fly and mouse models of Huntington disease. *Nat. Genet.* 36, 585–595. doi: 10.1038/ng1362

Redondo-Castro, E., Hernández, J., Mahy, N., and Navarro, X. (2013). Phagocytic microglial phenotype induced by glibenclamide improves functional recovery but worsens hyperalgesia after spinal cord injury in adult rats. *Eur. J. Neurosci.* 38, 3786–3798. doi: 10.1111/ejn.12382

Rocha, S. M., Cristovão, A. C., Campos, F. L., Fonseca, C. P., and Baltazar, G. (2012). Astrocyte-derived GDNF is a potent inhibitor of microglial activation. *Neurobiol. Dis.* 47, 407–415. doi: 10.1016/j.nbd.2012.04.014

Rojewska, E., Popiolek-Barczyk, K., Jurga, A. M., Makuch, W., Przewlocka, B., and Mika, J. (2014). Involvement of pro-and antinociceptive factors in minocycline analgesia in rat neuropathic pain model. *J. Neuroimmunol.* 277, 57–66. doi: 10.1016/j.jneuroim.2014.09.020

Rostam, H. M., Reynolds, P. M., Alexander, M. R., Gadegaard, N., and Ghaemmaghami, A. M. (2017). Image based machine learning for identification of macrophage subsets. *Sci. Rep.* 7:3521. doi: 10.1038/s41598-017-03780-z

Russo, C. D., Lisi, L., Tringali, G., and Navarra, P. (2009). Involvement of mTOR kinase in cytokine-dependent microglial activation and cell proliferation. *Biochem. Pharmacol.* 78, 1242–1251. doi: 10.1016/j.bcp.2009.06.097

Sánchez-Ventura, J., Amo-Aparicio, J., Navarro, X., and Penas, C. (2019). BET protein inhibition regulates cytokine production and promotes neuroprotection after spinal cord injury. *J. Neuroinflammation* 16:124. doi: 10.1186/s12974-019-1511-7

Schafer, D. P., Lehrman, E. K., Kautzman, A. G., Koyama, R., Mardinly, A. R., Yamasaki, R., et al. (2012). Microglia sculpt postnatal neural circuits in an activity and complement-dependent manner. *Neuron* 74, 691–705. doi: 10.1016/j.neuron.2012.03.026

Schmelzle, T., and Hall, M. N. (2000). TOR, a central controller of cell growth. *Cell* 103, 253–262. doi: 10.1016/s0092-8674(00)00117-3

Shaked, I., Tchoresh, D., Gersner, R., Meiri, G., Mordechai, S., Xiao, X., et al. (2005). Protective autoimmunity: interferon-γ enables microglia to remove glutamate without evoking inflammatory mediators. *J. Neurochem.* 92, 997–1009. doi: 10.1111/j.1471-4159.2004.02954.x

Shechter, R., and Schwartz, M. (2013). Harnessing monocyte-derived macrophages to control central nervous system pathologies: no longer 'if' but 'how'. *J. Pathol.* 229, 332–346. doi: 10.1002/path.4106

Shih, R. H., Wang, C. Y., and Yang, C. M. (2015). NF-kappaB signaling pathways in neurological inflammation: a mini review. *Front. Mol. Neurosci.* 8:77. doi: 10.3389/fnmol.2015.00077

Sindrilaru, A., Peters, T., Wieschalka, S., Baican, C., Baican, A., Peter, H., et al. (2011). An unrestrained proinflammatory M1 macrophage population induced by iron impairs wound healing in humans and mice. *J. Clin. Invest.* 121, 985–997. doi: 10.1172/JCI44490

Song, M., Jin, J., Lim, J. E., Kou, J., Pattanayak, A., Rehman, J. A., et al. (2011). TLR4 mutation reduces microglial activation, increases Aβ deposits and exacerbates cognitive deficits in a mouse model of Alzheimer's disease. *J. Neuroinflammation* 8:92. doi: 10.1186/1742-2094-8-92

Song, Y., Xue, H., Liu, T. T., Liu, J. M., and Chen, D. (2015). Rapamycin plays a neuroprotective effect after spinal cord injury via anti-inflammatory effects. *J. Biochem. Mol. Toxicol.* 29, 29–34. doi: 10.1002/jbt.21603

Stout, R. D., and Suttles, J. (2004). Functional plasticity of macrophages: reversible adaptation to changing microenvironments. *J. Leukoc. Biol.* 76, 509–513. doi: 10.1189/jlb.0504272

Taetzsch, T., Levesque, S., McGraw, C., Brookins, S., Luqa, R., Bonini, M. G., et al. (2015). Redox regulation of NF-κB p50 and M1 polarization in microglia. *GLIA* 63, 423–440. doi: 10.1002/glia.22762

Tan, A. M. (2009). Early microglial inhibition preemptively mitigates chronic pain development after experimental spinal cord injury. *J. Rehab. Res. Dev.* 46, 123–133.

Taves, S., Berta, T., Liu, D. L., Gan, S., Chen, G., Kim, Y. H., et al. (2016). Spinal inhibition of p38 MAP kinase reduces inflammatory and neuropathic pain in male but not female mice: sex-dependent microglial signaling in the spinal cord. *Brain Behav. Immun.* 55, 70–81. doi: 10.1016/j.bbi.2015.10.006

Taylor, R. A., Chang, C. F., Goods, B. A., Hammond, M. D., Mac Grory, B., Ai, Y., et al. (2017). TGF-β1 modulates microglial phenotype and promotes recovery after intracerebral hemorrhage. *J. Clin. Invest.* 127, 280–292. doi: 10.1172/JCI88647

Varnum, M. M., and Ikezu, T. (2012). The classification of microglial activation phenotypes on neurodegeneration and regeneration in Alzheimer's disease brain. *Arch. Immunol. Ther. Exp.* 60, 251–266. doi: 10.1007/s00005-012-0181-2

Vergadi, E., Ieronymaki, E., Lyroni, K., Vaporidi, K., and Tsatsanis, C. (2017). Akt signaling pathway in macrophage activation and M1/M2 polarization. *J. Immunol.* 198, 1006–1014. doi: 10.4049/jimmunol.1601515

Walker, D. G., and Lue, L. F. (2015). Immune phenotypes of microglia in human neurodegenerative disease: challenges to detecting microglial polarization in human brains. *Alzheimers Res. Ther.* 7:56. doi: 10.1186/s13195-015-0139-9

Wang, G., Shi, Y., Jiang, X., Leak, R. K., Hu, X., Wu, Y., et al. (2015). HDAC inhibition prevents white matter injury by modulating microglia/macrophage polarization through the GSK3β/PTEN/Akt axis. *Proc. Natl. Acad. Sci.* 112, 2853–2858. doi: 10.1073/pnas.1501441112

Wang, J., Wang, J., Lu, P., Cai, Y., Wang, Y., Hong, L., et al. (2015). Local delivery of FTY720 in PCL membrane improves SCI functionbal recovery by reducing reactive astrogliosis. *Biomaterials* 62, 76–87. doi: 10.1016/j.biomaterials.2015.04.060

Wang, N., Liang, H., and Zen, K. (2014). Molecular mechanisms that influence the macrophage M1–M2 polarization balance. *Front. Immunol.* 5:614. doi: 10.3389/fimmu.2014.00614

Wang, P., He, Y., Li, D., Han, R., Liu, G., Kong, D., et al. (2016). Class I PI3K inhibitor ZSTK474 mediates a shift in microglial/macrophage phenotype and inhibits inflammatory response in mice with cerebral ischemia/reperfusion injury. *J. Neuroinflammation* 13:192. doi: 10.3389/fimmu.2014.00614

Wang, Y. P., Wu, Y., Li, L. Y., Zheng, J., Liu, R. G., Zhou, J. P., et al. (2011). Aspirin-triggered lipoxin A 4 attenuates LPS-induced pro-inflammatory responses by inhibiting activation of NF-κB and MAPKs in BV-2 microglial cells. *J. Neuroinflammation* 8:95. doi: 10.1186/s12974-016-0660-1

Weisser, S. B., McLarren, K. W., Kuroda, E., and Sly, L. M. (2013). Generation and characterization of murine alternatively activated macrophages. *Basic Cell Cult. Protoc.* 2013, 225–239. doi: 10.1007/978-1-62703-128-8_14

Wen, L., You, W., Wang, H., Meng, Y., Feng, J., and Yang, X. (2018). Polarization of microglia to the M2 phenotype in a peroxisome proliferator-activated receptor gamma–dependent manner attenuates axonal injury induced by traumatic brain injury in mice. *J. Neurotrauma* 35, 2330–2340. doi: 10.1089/neu.2017.5540

Wilcock, D. M. (2014). Neuroinflammatory phenotypes and their roles in Alzheimer's disease. *Neurodegener. Dis.* 13, 183–185. doi: 10.1007/s11307-017-1099-1

Willemen, H. L., Huo, X. J., Mao-Ying, Q. L., Zijlstra, J., Heijnen, C. J., and Kavelaars, A. (2012). MicroRNA-124 as a novel treatment for persistent hyperalgesia. *J. Neuroinflammation* 9:143. doi: 10.1186/1742-2094-9-143

Wolf, S. A., Boddeke, H. W. G. M., and Kettenmann, H. (2017). Microglia in physiology and disease. *Annu. Rev. Physiol.* 79, 619–643. doi: 10.1146/annurev-physiol-022516-034406

Wu, J., Stoica, B. A., Dinizo, M., Pajoohesh-Ganji, A., Piao, C., and Faden, A. I. (2012). Delayed cell cycle pathway modulation facilitates recovery after spinal cord injury. *Cell Cycle* 11, 1782–1795. doi: 10.4161/cc.20153

Wu, S. Y., and Watabe, K. (2017). The roles of microglia/macrophages in tumor progression of brain cancer and metastatic disease. *Front. Biosci.* 22:1805. doi: 10.2741/4573

Xia, M., Zhao, Q., Zhang, H., Chen, Y., Yuan, Z., Xu, Y., et al. (2017). Proteomic analysis of HDAC3 selective inhibitor in the regulation of inflammatory response of primary microglia. *Neural Plast* 2017:6237351. doi: 10.1155/2017/6237351

Yao, L., Kan, E. M., Lu, J., Hao, A., Dheen, S. T., Kaur, C., et al. (2013). Toll-like receptor 4 mediates microglial activation and production of inflammatory mediators in neonatal rat brain following hypoxia: role of TLR4 in hypoxic microglia. *J. Neuroinflammation* 10:23. doi: 10.1186/1742-2094-10-23

Yin, H., Shen, L., Xu, C., and Liu, J. (2018). Lentivirus-mediated overexpression of miR-29a promotes axonal regeneration and functional recovery in experimental spinal cord injury via PI3K/Akt/mTOR pathway. *Neurochem. Res.* 43, 2038–2046. doi: 10.1007/s11064-018-2625-5

Zhang, F., Zhong, R., Li, S., Fu, Z., Cheng, C., Cai, H., et al. (2017). Acute hypoxia induced an imbalanced M1/M2 activation of microglia through NF-κB signaling in Alzheimer's disease mice and wild-type littermates. *Front. Aging Neurosci.* 9:282. doi: 10.3389/fnagi.2017.00282

Zhang, L., Alizadeh, D., Van Handel, M., Kortylewski, M., Yu, H., and Badie, B. (2009). Stat3 inhibition activates tumor macrophages and abrogates glioma growth in mice. *GLIA* 57, 1458–1467. doi: 10.1002/glia.20863

Zhang, L., Liu, W., Alizadeh, D., Zhao, D., Farrukh, O., Lin, J., et al. (2011). S100B attenuates microglia activation in gliomas: possible role of STAT3 pathway. *GLIA* 59, 486–498. doi: 10.1002/glia.21118

Zhang, Y. K., Liu, J. T., Peng, Z. W., Fan, H., Yao, A. H., Cheng, P., et al. (2013). Different TLR4 expression and microglia/macrophage activation induced by hemorrhage in the rat spinal cord after compressive injury. *J. Neuroinflammation* 10:112. doi: 10.1186/1742-2094-10-112

Zhao, P., Waxman, S. G., and Hains, B. C. (2007). Modulation of thalamic nociceptive processing after spinal cord injury through remote activation of thalamic microglia by cysteine–cysteine chemokine ligand 21. *J. Neurosci.* 27, 8893–8902. doi: 10.1523/jneurosci.2209-07.2007

Zhuravleva, M., Rizvanov, A., and Mukhamedshina, Y. (2016). Effect of GDNF on morphology, proliferation, and phagocytic activity of rat neonatal cortex isolated microglia. *Bionanoscience* 6, 379–383. doi: 10.1007/s12668-016-0247-4

Zolezzi, J. M., Santos, M. J., Bastías-Candia, S., Pinto, C., Godoy, J. A., and Inestrosa, N. C. (2017). PPARs in the central nervous system: roles in neurodegeneration and neuroinflammation. *Biol. Rev.* 92, 2046–2069. doi: 10.1111/brv.12320

Zong, S., Zeng, G., Fang, Y., Peng, J., Tao, Y., Li, K., et al. (2014). The role of IL-17 promotes spinal cord neuroinflammation via activation of the transcription factor STAT3 after spinal cord injury in the rat. *Mediators Inflamm.* 2014:786947. doi: 10.1155/2014/786947

Zukor, K., Belin, S., Wang, C., Keelan, N., Wang, X., and He, Z. (2013). Short hairpin RNA against PTEN enhances regenerative growth of corticospinal tract axons after spinal cord injury. *J. Neurosci.* 33, 15350–15361. doi: 10.1523/JNEUROSCI.2510-13

Conflict of Interest Statement: The authors declare that the research was conducted in the absence of any commercial or financial relationships that could be construed as a potential conflict of interest.

frontiers in Systems Neuroscience

ORIGINAL RESEARCH
published: 10 January 2020
doi: 10.3389/fnsys.2019.00080

Neural Correlates of Vestibular Processing During a Spaceflight Analog With Elevated Carbon Dioxide (CO_2): A Pilot Study

*Kathleen E. Hupfeld[1], Jessica K. Lee[2], Nichole E. Gadd[3], Igor S. Kofman[3], Yiri E. De Dios[3], Jacob J. Bloomberg[4], Ajitkumar P. Mulavara[3] and Rachael D. Seidler[1,5]**

[1] Department of Applied Physiology and Kinesiology, University of Florida, Gainesville, FL, United States, [2] German Aerospace Center, Institute of Aerospace Medicine, Cologne, Germany, [3] KBR, Houston, TX, United States, [4] NASA Johnson Space Center, Houston, TX, United States, [5] Department of Neurology, University of Florida, Gainesville, FL, United States

Astronauts return to Earth from spaceflight missions with impaired mobility and balance; recovery can last weeks postflight. This is due in large part to the altered vestibular signaling and sensory reweighting that occurs in microgravity. The neural mechanisms of spaceflight-induced vestibular changes are not well understood. Head-down-tilt bed rest (HDBR) is a common spaceflight analog environment that allows for study of body unloading, fluid shifts, and other consequences of spaceflight. Subjects in this context still show vestibular changes despite being in Earth's gravitational environment, potentially due to sensory reweighting. Previously, we found evidence of sensory reweighting and reduced neural efficiency for vestibular processing in subjects who underwent a 70-day HDBR intervention. Here we extend this work by evaluating the impact of HDBR paired with elevated carbon dioxide (CO_2) to mimic International Space Station conditions on vestibular neural processing. Eleven participants (6 males, 34 ± 8 years) completed 30 days of HDBR combined with 0.5% atmospheric CO_2 (HDBR + CO_2). Participants underwent six functional magnetic resonance imaging (fMRI) sessions pre-, during, and post- HDBR + CO_2 while we measured brain activity in response to pneumatic skull taps (a validated method of vestibular stimulation). We also measured mobility and balance performance several times before and after the intervention. We found support for adaptive neural changes within the vestibular system during bed rest that subsequently recovered in several cortical and cerebellar regions. Further, there were multiple brain regions where greater pre- to post- *deactivation* was associated with *reduced* pre- to post- balance declines. That is, increased *deactivation* of certain brain regions associated with *better* balance post-HDBR + CO_2. We also found that, compared to HDBR alone (n = 13 males; 29 ± 3 years) HDBR + CO_2 is associated with greater increases in activation of multiple frontal, parietal, and temporal regions during vestibular stimulation. This suggests interactive or additive effects of bed rest and elevated CO_2. Finally, we found stronger correlations between pre- to post-HDBR + CO_2 brain changes and dependence on the visual system during balance for subjects who developed signs of Spaceflight-Associated Neuro-ocular Syndrome

OPEN ACCESS

Edited by:
Preston E. Garraghty, Indiana University Bloomington, United States

Reviewed by:
Rahul Goel, Stanford University, United States
Nora Petersen, European Space Agency (ESA), France

***Correspondence:**
Rachael D. Seidler
rachaelseidler@ufl.edu

Received: 18 September 2019
Accepted: 09 December 2019
Published: 10 January 2020

Citation:
Hupfeld KE, Lee JK, Gadd NE, Kofman IS, De Dios YE, Bloomberg JJ, Mulavara AP and Seidler RD (2020) Neural Correlates of Vestibular Processing During a Spaceflight Analog With Elevated Carbon Dioxide (CO_2): A Pilot Study. Front. Syst. Neurosci. 13:80. doi: 10.3389/fnsys.2019.00080

(SANS). Together, these findings have clear implications for understanding the neural mechanisms of bed rest and spaceflight-related changes in vestibular processing, as well as adaptation to altered sensory inputs.

Keywords: vestibular, fMRI, head-down-tilt bed rest (HDBR), carbon dioxide (CO_2), spaceflight

INTRODUCTION

Microgravity exposure poses unique challenges to human physiology: astronauts encounter body unloading, headward fluid shifts, altered vestibular and proprioceptive inputs, inflight and postflight spatial disorientation (Young et al., 1984), and confined quarters with carbon dioxide (CO_2) levels up to more than ten times higher than those on Earth (Law et al., 2014). Upon return to Earth, astronauts present with multi-systemic consequences, such as declining bone (Sibonga, 2013) and muscle mass (LeBlanc et al., 1995; Stein, 2013), cardiovascular changes (Hargens and Richardson, 2009), and mobility and balance difficulties (Mulavara et al., 2010; Cohen et al., 2012; Wood et al., 2015). Here we focus on the neural vestibular consequences of a spaceflight analog environment, as well as the neural mechanisms underlying declines in vestibularly mediated mobility and balance.

Animal studies have demonstrated peripheral vestibular changes with spaceflight; for instance, utricular afferents become hypersensitive to translational accelerations after return to Earth (Boyle et al., 2001). Although the specific mechanisms for these changes remain unknown, one possibility is that the brain reinterprets afferent sensory input during flight due to the lack of a gravitational reference vector for the otoliths. After return to Earth, this re-interpretation is in conflict with Earth's gravitational environment and results in postflight vestibular dysfunction (e.g., balance difficulties), followed by slow re-adaptation over the days and weeks following spaceflight (Young et al., 1984; Parker et al., 1985; Mulavara et al., 2010). Astronauts also present with decreased skin sensitivity on the soles of the feet following spaceflight (Lowrey et al., 2014), which has been attributed to in-flight sensory reweighting (i.e., the process of adjusting the magnitude of different sensory contributions to motor control) (Assländer and Peterka, 2014) in compensation for unreliable vestibular inputs in microgravity. A single-subject case study (Demertzi et al., 2016) and recent study of 11 cosmonauts (Pechenkova et al., 2019) examining resting-state and task-based functional magnetic resonance imaging (fMRI) connectivity found evidence for vestibular cortex reorganization and multisensory reweighting following long-duration spaceflight. This work provides preliminary evidence of flight-related central vestibular plasticity. Taken together, it is likely that spaceflight factors influence the neural correlates of vestibular processing; however, the precise mechanisms underlying such changes require further study.

Head-down-tilt bed rest (HDBR) is a common spaceflight analog intervention that permits ground-based study of how axial body unloading alters sensory inputs that subsequently impact neural vestibular processing and vestibular system plasticity. Subjects remain in bed with their head tilted down six degrees to mimic a subset of spaceflight consequences including headward fluid shifts, arterial pressure changes, axial body unloading, and reduced somatosensory input. Although gravitational vector input does not change during HDBR, there is evidence that, similar to spaceflight, axial body unloading contributes to sensory reweighting (Moore et al., 2010; Mulavara et al., 2018; Yuan et al., 2018b). Even though HDBR does not directly affect vestibular inputs, sensory reweighting is thought to affect neural vestibular processing during HDBR; more specifically, the vestibular nuclei receive inputs from the vestibular organs, in addition to proprioceptive signals from the limbs (Fredrickson et al., 1966; Rubin et al., 1979; Yates et al., 2000; Jian et al., 2002). If either vestibular or somatosensory inputs appear to be incorrect or abnormal, the central nervous system may use information from the other system to compensate and maintain performance (Bles et al., 1984; Dieringer, 1995; Horak and Hlavacka, 2001; Carriot et al., 2015). Thus, during HDBR, in the absence of normal somatosensory inputs to the foot, vestibular processing appears to be altered, with vestibular cues weighted more heavily (Mulavara et al., 2018). HDBR also results in reduced functional mobility and decreased postural stability, which are both behaviors that depend upon the vestibular system and multisensory integration (Reschke et al., 2009; Mulder et al., 2014; Koppelmans et al., 2015, 2017; Miller et al., 2018; Mulavara et al., 2018). Thus, taken together, HDBR provides an effective environment for studying neural vestibular adaptation and has applications for both space travel and for better understanding plasticity of the vestibular system and multisensory integration.

In recent years, several fMRI-compatible vestibular stimulation methods, including auditory tone bursts and pneumatic skull taps, have been used to map central vestibular processing networks (Schlindwein et al., 2008; Noohi et al., 2017). Two meta-analyses have revealed a diffuse vestibular processing network, including portions of insular cortex, premotor cortex, inferior parietal cortex, cingulate cortex, and the superior temporal gyri (Lopez et al., 2012a; Zu Eulenburg et al., 2012). However, the most commonly activated regions across several different vestibular stimulation methods were the parietal opercular area ("OP2") and retroinsular cortex; consequently, these regions are sometimes referred to as "vestibular cortex," and considered to be the core regions responsible for vestibular processing. In the present work, we stimulated the vestibular system during fMRI using pneumatic skull taps, which we have previously validated in young (Noohi et al., 2017) and older adults (Noohi et al., 2019), and successfully employed in our past HDBR work (Yuan et al., 2018b). Pneumatic skull taps elicit both activation in the vestibular cortex and deactivation in cross-modal sensory regions. Across both young and older adults, we have found

associations between greater *deactivation* of certain subcortical and cerebellar regions in response to vestibular stimulation and *better* static balance performance (Noohi et al., 2019). This suggests the importance of both brain activation and deactivation, potentially reflecting sensory reweighting, for successful vestibular functioning.

In our past HDBR work, using this skull tap technique, we identified longitudinal brain changes suggestive of upregulation of vestibular processing in response to reduced somatosensory input during 70 days of HDBR (Yuan et al., 2018b). We also found associations between increased frontal, parietal, and occipital brain activity and greater HDBR-related mobility and balance declines, suggestive of reduced neural efficiency post-HDBR (Yuan et al., 2018b). Further, we identified post-HDBR increases in resting state connectivity for a network including the vestibular cortex and the cerebellum (Cassady et al., 2016). These findings indicate that the neural correlates of vestibular processing are altered with HDBR and have functional implications for vestibularly mediated behaviors.

No previous work has investigated the neural correlates of vestibular processing during an intervention combining HDBR with elevated CO_2, which would better mimic the actual conditions on the International Space Station (ISS). Among other effects, exposure to heightened CO_2 increases blood flow to the brain (at least initially) due to cerebral vasodilation (Atkinson et al., 1990; Zhou et al., 2008) and mildly impairs visuomotor function (Manzey and Lorenz, 1998). Although *reduced* blood levels of CO_2 during voluntary hyperventilation have been associated with increased postural sway (Sakellari et al., 1997), it is unknown how *elevated* atmospheric CO_2 interacts with central or peripheral vestibular processing.

Here we used fMRI to test changes in the neural response to vestibular stimulation with 30 days of HDBR paired with elevated CO_2 (which we refer to as "HDBR + CO_2"). We hypothesized that similar brain changes would emerge compared to our past work (referred to as "HDBR"), including evidence for HDBR-related upregulation of vestibular networks and reduced neural efficiency. Further, we anticipated that the interaction of HDBR and elevated CO_2 would result in additive neural effects.

We addressed three primary aims in this small pilot sample (n = 11): (1) assess the time course of changes in the neural correlates of vestibular processing and recovery patterns with HDBR + CO_2; (2) examine the functional consequences of HDBR + CO_2 by associating brain changes with mobility and balance declines; and (3) characterize how HDBR + CO_2 differentially affects the neural correlates of vestibular processing compared to HDBR alone. We developed an additional, exploratory aim (4) after about half of the HDBR + CO_2 subjects developed signs of Spaceflight-Associated Neuro-ocular Syndrome (SANS) (Laurie et al., 2019), a condition which manifests with symptoms such as optic disk edema and is estimated to affect between approximately 16 and 50 percent of long-duration astronauts (i.e., those who have completed an ISS mission, which typically last for about 6 months) (Stenger et al., 2017). We characterized subgroup differences between those HDBR + CO_2 subjects who did and did not develop signs of SANS.

MATERIALS AND METHODS

HDBR + CO_2

Participants

Eleven healthy individuals (six males, five females; mean ± SD age = 34 ± 8 years) provided their written informed consent and participated in 30 days of HDBR + CO_2. This intervention was implemented within the larger study, VaPER (Visual impairment intracranial pressure and Psychological:envihab Research), in which separate investigators evaluated other physiological systems. All study procedures were approved by the local ethical commission of the regional medical association, Ärztekammer Nordrhein, as well as the University of Florida and NASA Institutional Review Boards.

Testing Timeline

Subjects were admitted to:envihab at the German Aerospace Center (Deutsches Zentrum für Luft- und Raumfahrt, DLR) in Cologne, Germany 14 days before the start of HDBR + CO_2. During this time, they completed two baseline data collection (*BDC*) sessions (**Figure 1**). Subjects then underwent 30 days of six-degree HDBR with approximately 0.5% (partial pressure = 3.8 mmHg) elevated atmospheric CO_2 (*HDT*), to match average ISS conditions (Law et al., 2014). Subjects kept a "strict" head-down-tilt position at all times, verified by 24/7 video monitoring. Subjects were instructed to always keep at least one shoulder in contact with the mattress. They were not permitted to use a pillow or to raise or stretch their legs aside from standardized physiotherapy sessions. Subjects remained at the facility for 14 days after HDBR + CO_2 and completed two recovery (*R*) data collection sessions during this time.

fMRI images were collected at six time points: two times pre-, two times during, and two times post-HDBR + CO_2 (**Figure 1**). Subjects completed mobility and balance testing on the same days as fMRI scans, except for the time points during HDBR + CO_2. Subjects completed one additional mobility and balance testing session on the first recovery day (R0). One individual began testing late and thus did not complete BDC 13; however, this individual did complete the second baseline session (BDC 7).

Head-Down-Tilt Bed Rest

Participants

Thirteen healthy individuals (all males; mean ± SD age = 29 ± 3 years) provided their written informed consent and participated in 70 days of HDBR. All study procedures were approved by the University of Michigan, University of Texas Medical Branch, and NASA Institutional Review Boards. These subjects represent a subset of the 18 total HDBR participants who received the same mode of vestibular stimulation caused by pneumatic skull taps as the HDBR + CO_2 cohort. There were no significant age differences between the HDBR + CO_2 and HDBR participants, and both cohorts

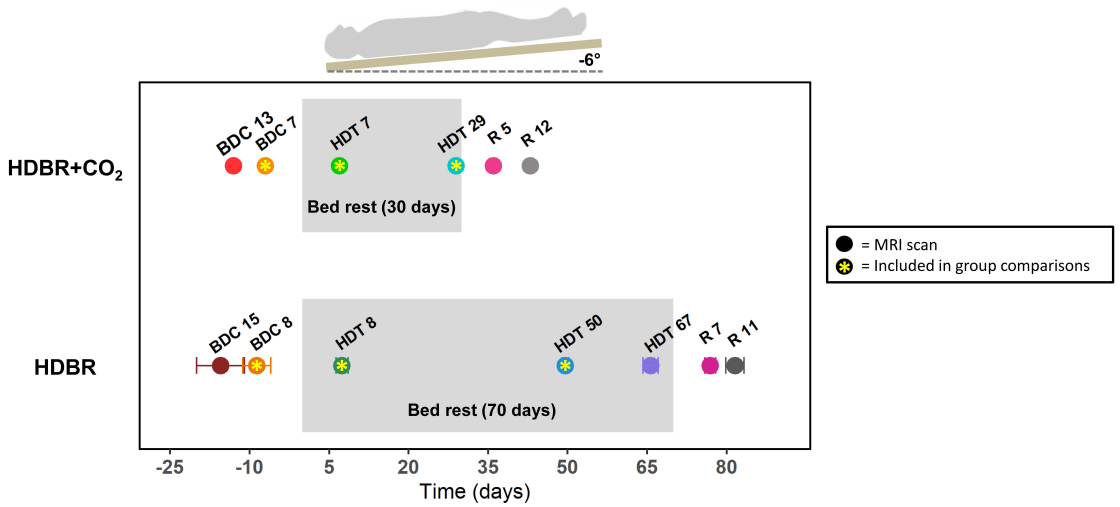

FIGURE 1 | Testing timeline. **Top:** testing timeline for the HDBR + CO_2 group, who completed 30 days of head-down-tilt bed rest (HDBR) with 0.5% elevated atmospheric CO_2. **Bottom:** testing timeline for the HDBR group, who completed 70 days of HDBR with normal atmospheric CO_2 levels. BDC, baseline data collection; HDT, head-down-tilt bed rest; R, recovery. Circles indicate the day for each MRI scan. Circles with asterisks represent the three time points used to create intercept and slope images for between-group comparisons. All HDBR + CO_2 subjects completed MRI scans on exactly the same days with respect to bed rest. There was some variability in testing days for the HDBR group; average day is plotted, with error bars indicating standard deviation. Mobility and balance data were collected at all time points for the HDBR + CO_2 group, with the exception of HDT 7 and HDT 29 (i.e., participants did not complete standing tasks *during* bed rest). One additional mobility and balance data collection took place on R0 for the HDBR + CO_2 group within ~3 h of first standing up. Mobility and balance scores at BDC 7 and R 0 were used for brain-behavior correlations with MRI data from BDC 7 and HDT 29.

passed a minimum physical fitness standard (i.e., an Air Force Class III equivalent physical examination) to participate (Lee et al., 2019a).

Testing Timeline

Participants were admitted to the NASA bed rest facility at the University of Texas Medical Branch, Galveston, TX, United States and completed two *BDC* sessions in the two weeks prior to starting HDBR (**Figure 1**). Participants underwent 70 days of HDBR with normal atmospheric CO_2 (*HDT*). They maintained a six-degree head-down-tilt at all times except for 30 min during each meal, when they were allowed to support their head with their hand. Subjects remained at the facility for 14 days after HDBR and completed two recovery (*R*) data collection sessions during this time. All participants were a part of larger bed rest studies; thus, the timelines for HDBR + CO_2 and HDBR were restricted by NASA and not identically matched between the two studies.

fMRI images were collected at seven time points: two times pre-, three times during, and two times post-HDBR (**Figure 1**). As we have previously reported neural vestibular changes with this intervention (Yuan et al., 2018b), here we use these fMRI data only for group comparisons with the HDBR + CO_2 group. We examine only the fMRI scans from BDC 8, HDT 8, and HDT 50, as these points fell closest in time to those collected pre- and during bed rest for the HDBR + CO_2 group and allowed us to compare slopes of change over time in the two groups. See Section "HDBR + CO_2 vs. HDBR Group Comparisons" for details on this analysis approach for making between-group comparisons that account for these differing testing timelines.

fMRI Data Collection

fMRI Acquisition

For the HDBR + CO_2 group, fMRI scans were collected on a 3 Tesla Siemens MRI scanner. A gradient echo T2*-weighted echo-planar imaging sequence was used to collect the fMRI scans: TR = 2.5 s, TE = 32 ms, flip angle = 90°, FOV = 192 × 192 mm, matrix = 64 × 64, slice thickness = 3.5 mm, voxel size = 3 × 3 × 3.5 mm^3, 37 slices, 96 volumes. A T1-weighted gradient-echo pulse sequence was also collected with parameters: TR = 1.9 s, TE = 2.4 ms, flip angle = 9°, FOV = 250 × 250 mm, matrix = 512 × 512, slice thickness = 1.0 mm, voxel size = 0.49 × 0.49 × 1.0 mm^3, 192 slices. Participants maintained the head-down-tilt position at all times using a foam wedge in the scanner. In addition, 0.5% CO_2 was continuously supplied during the HDBR + CO_2 intervention phase (through a mask and tank system when subjects were out of the environmentally controlled wing of the building).

For the HDBR group, fMRI scans were collected on a different 3 Tesla Siemens MRI scanner. A gradient echo T2*-weighted echo-planar imaging sequence was used to collect the fMRI scans: TR = 3.66 s, TE = 39 ms, flip angle = 90°, FOV = 240 × 240 mm, matrix = 94 × 94, slice thickness = 4 mm, slice gap = 1 mm, voxel size = 2.55 × 2.55 × 5.0 mm^3, 36 slices, 66 volumes. A T1-weighted gradient-echo pulse sequence was also collected with parameters: TR = 1.9 s, TE = 2.49 ms, flip angle = 9°, FOV = 270 × 270 mm, matrix = 288 × 288, slice thickness = 0.90 mm, voxel size = 0.94 × 0.94 × 0.90 mm^3, 192 slices. The HDBR participants did not maintain the head-down-tilt position in the scanner; they were supine instead.

Vestibular Stimulation

For both the HDBR + CO_2 and the HDBR cohorts, subjects received vestibular stimulation during fMRI. Subjects received skull taps via a pneumatic tactile pulse system [MR-compatible Pn Tactile Pulse System (PnTPS), Engineering Acoustics Inc.] placed over the lateral cheekbones (Noohi et al., 2017; Yuan et al., 2018b). The skull tapper used compressed air (50–55 psi) to power a small piston that delivered low-force taps (0.6 kg) to the cheekbone. We have recently shown that this approach is well tolerated by subjects, it activates vestibular cortical regions, it results in vestibular-evoked myogenic potentials in eye muscles, and it does not cause excessive head motion (Noohi et al., 2017).

Taps were delivered at 1 Hz, and each tapping block contained 24 taps. Both groups completed one fMRI run with five 24-s blocks of taps on the left cheekbone. Each block of taps was preceded and followed by 20-s rest periods. The HDBR group also completed a second run with taps to the right cheekbone; however, here we examine only the HDBR left tap run to enable direct comparison to the HDBR + CO_2 group. Of note, although the vestibular stimulation parameters and total sequence duration were identical between groups, as the HDBR + CO_2 fMRI sequence included a faster TR and more volumes (TR = 2.5 s; 96 volumes) than the HDBR sequence (TR = 3.66 s; 66 volumes), we acquired more data and thus had more statistical power for the HDBR + CO_2 group. This represents a potential limitation of the present work and is discussed further in Section "Limitations."

For both groups, the force of the taps was sufficiently low that they did not induce head motion that was greater than for other task runs. No subject moved more than 2.1 mm within any run, which is smaller than the size of one voxel.

fMRI Preprocessing and Subject-Level Analyses

Preprocessing

Image preprocessing was completed using Statistical Parametric Mapping 12 (SPM12, version 7219) (Ashburner et al., 2016) with MatLab R2016a, version 9.0. We used a standard SPM preprocessing pipeline for fMRI (Ashburner et al., 2016). All functional images were corrected for slice timing then realigned and resliced to correct for head motion. As an additional quality check, we used the Artifact Detection Tool (ART)[1] with motion threshold = 2.5 mm and global brain signal Z threshold = 9. There were no within-session movement outliers for either group. Only one individual in the HDBR + CO_2 group had a global intensity outlier present in 4 of 96 volumes for one session; we used the subject-level covariate outputted by ART to minimize effects of these volumes on group-level analyses.

After resetting the origins of each T1 image to the anterior commissure, the T1 images were coregistered to the mean functional image with separation of [2, 1 mm]. The T1 images were segmented using the SPM12 Dartel algorithm with a sampling distance of 1 mm. The forward deformation fields from the T1 segmentation were used to normalize the functional images and the T1 to MNI space. We used 7th degree B-spline normalization for optimal performance (Ashburner et al., 2016). The warped images were spatially smoothed with an 8 mm full−width at half−maximum three−dimensional Gaussian kernel.

Subject-Level Whole Brain Statistical Analyses

At the subject level, we calculated brain activity for each participant on a voxel-by-voxel basis for left cheekbone vestibular stimulation versus rest. We set the first level masking threshold to -infinity and masked out non-brain areas using the "mask_ICV.nii" SPM intracranial volume mask. This allowed for inclusion of all voxels in the first level general linear model (GLM), as opposed to the default SPM masking threshold of 0.80, which includes in the GLM only those voxels with a mean value $\geq$ 80% of the global signal. We included ART-derived head motion parameters as nuisance variables in the subject-level analyses.

Cerebellar Processing

To improve normalization of the cerebellum and avoid over-stretching (Diedrichsen, 2006; Diedrichsen et al., 2009), we applied specialized processing using portions of both the CEREbellum Segmentation (CERES) (Romero et al., 2017) pipeline and the Spatially Unbiased Infratentorial and cerebellar Template (SUIT) (Diedrichsen, 2006; Diedrichsen et al., 2009) pipeline. We used CERES to segment the cerebellum from each person's structural T1-weighted image. We then reset the origin of each individual's cerebellum segmentation in native space to fall within the space of the segment. This allowed us to coregister each subject's native space segmentation to the SUIT.nii template. We created binary gray matter, white matter, and full cerebellar masks from the CERES native space output and then used the suit_normalize_dartel function to obtain the Affine transformation matrix and flowfield needed to normalize these images into SUIT space.

We coregistered all of the slice timing-corrected, realigned/resliced (but *not* normalized) whole brain images to the T1-weighted whole brain image that was entered into the CERES pipeline and re-ran the subject-level statistical analyses described above on these *non*-normalized whole brain images. Then, using the Affine transformation and flowfield from normalizing the structural cerebellar segments to SUIT space, as well as each subject's native space full cerebellar mask, we applied suit_reslice_dartel to the whole brain functional images to reslice all of the images into SUIT space. Given the small size of cerebellar structures, we applied a 2 mm smoothing kernel to the final functional cerebellar images and masked all second-level statistical results with a binary version of the SUIT.nii template, to avoid any spillover off the cerebellum due to the spatial smoothing. We performed all second-level statistical analyses described below twice: once for the whole brain (excluding the cerebellum) and a second time for only the cerebellum.

[1] www.nitrc.org/projects/artifact_detect/

fMRI Group-Level Statistics

Neural Response to Vestibular Stimulation

To demonstrate that our pneumatic tapper method was eliciting the expected vestibular system response, we first tested the main effect of vestibular stimulation averaged across all sessions for the HDBR + CO_2 participants at peak-level $p < 0.0005$ (uncorrected), extent threshold = 10 voxels, controlling for age and sex differences.

Time Course of Neural Vestibular Response to HDBR + CO_2

Similar to our past work (Yuan et al., 2016, 2018a,b), we tested for regions of immediate and cumulative change during bed rest followed by both quick and gradual recovery of brain activation patterns during vestibular stimulation across all six time points. We used flexible factorial analysis (SPM's mixed model equivalent), controlling for age and sex, assuming independence between but not within subjects, and assuming equal variances between and within subjects (Gläscher and Gitelman, 2008; Kurth et al., 2010). We used several contrast vectors as weights for the statistical analyses to test the hypothesized relative level of activation during each session. Cumulative change (**Figure 2A**) was modeled as a progressive increase in activity across the course of HDBR + CO_2, with a peak at the end of HDBR + CO_2, and gradual restoration after the conclusion of HDBR + CO_2. Immediate change (**Figure 2B**) was assumed to onset shortly after the start of HDBR + CO_2, to maintain during HDBR + CO_2, and to end shortly after the conclusion of HDBR + CO_2. We hypothesized that recovery would be either quick (**Figure 2C**), occurring during bed rest (i.e., between HDT 7 and HDT 29), or that recovery would be more gradual, with altered brain activation patterns still evident at HDT 29 (**Figures 2A,B**). We tested for both increases and decreases in activation with each of these contrast shapes. To better detect within−subject changes with the complex longitudinal models used in this pilot study, the alpha level was set at $p < 0.001$ (uncorrected). We report clusters that are at least 10 voxels for the whole brain and $k = 5$ voxels for the cerebellum.

Correlations of Brain and Behavioral Changes With HDBR + CO_2

We computed brain activation differences during vestibular stimulation between the final pre- HDBR + CO_2 time point (BDC 7) and the final time point during HDBR + CO_2 (HDT 29). We also computed the change in mobility and balance scores from BDC 7 to the first post-HDBR + CO_2 time point, R0. To examine regions in which HDBR + CO_2 brain changes were associated with changes in mobility and balance performance, we used a one-sample *t*-test model controlling for age and sex and included the behavioral change score as a covariate of interest. For each model, we used the Statistical Non-Parametric Mapping (SnPM version 13)[2] (Nichols and Holmes, 2002) toolbox to run non-parametric permutation tests with 15,000 permutations, variance smoothing = 8 mm kernel for the whole brain analyses and 2 mm kernel for the cerebellar analyses, minimum cluster size = 10 voxels, and threshold = non-parametric $p < 0.0005$ (uncorrected). The SnPM toolbox is recommended for studies with small sample sizes that may not meet assumptions for parametric testing. The SnPM toolbox calculates pseudo *t*-statistic images and uses non-parametric permutation testing to assess for significance.

HDBR + CO_2 vs. HDBR Group Comparisons

To examine differences in neural response to vestibular stimulation between bed rest with and without elevated CO_2, we compared both baseline (i.e., intercept) differences between the HDBR + CO_2 and HDBR groups, as well as the slope of change in brain activation across bed rest. As each cohort followed a different testing timeline, we compared the three time points that fell the closest together in time between the groups (indicated by asterisks in **Figure 1**). As in our previous work (Yuan et al., 2016, 2018b), we calculated a regression intercept and slope for each person using the scans from these three time points. The last image collected before the start of HDBR + CO_2 or HDBR was treated as time = 0 days, assuming that pre-bed rest activation was stable. Calculating the regression intercept allowed us to examine baseline differences between groups, and calculating the regression slope allowed us to compare the rate of change in brain activation during vestibular stimulation between groups.

We used two sample *t*-tests to examine between-group differences in intercept and slope images. For all group comparisons, we used SnPM non-parametric permutation tests with 15,000 permutations, variance smoothing = 8 mm kernel for whole brain analyses and 2 mm kernel for cerebellar analyses, minimum cluster size = 10 voxels, and threshold = non-parametric $p < 0.0005$ (uncorrected). In each model, we accounted for age and sex differences. We excluded two individuals from the HDBR cohort from group analyses: one individual had severe artifacts in their HDT 50 scan, and another individual had abnormally high contrast values at the single-subject level, possibly also due to artifacts. Thus there were $n = 11$ subjects per group for group comparisons.

There were several differences between the HDBR + CO_2 and HDBR images. Images were collected on different scanners, HDBR images showed evidence of greater orbitofrontal dropout compared to HDBR + CO_2 images, and HDBR individuals presented with slightly smaller ventricles. To address this and remain conservative in our analyses, we do not report any between-group orbitofrontal results, and we report with caution one between-group result in close proximity to the ventricles. As these two groups represent highly unique cohorts who have undergone a rare, intensive bed rest intervention with nearly identical behavioral and neuroimaging protocols, we feel that it is still valuable to report on group differences between these two cohorts, although the results of these specific analyses should be interpreted with caution. As we previously reported on longitudinal neural vestibular changes and brain-behavior correlations for the HDBR group (Yuan et al., 2018b), the only HDBR results reported here are the group differences between HDBR + CO_2 and HDBR.

[2] http://warwick.ac.uk/snpm

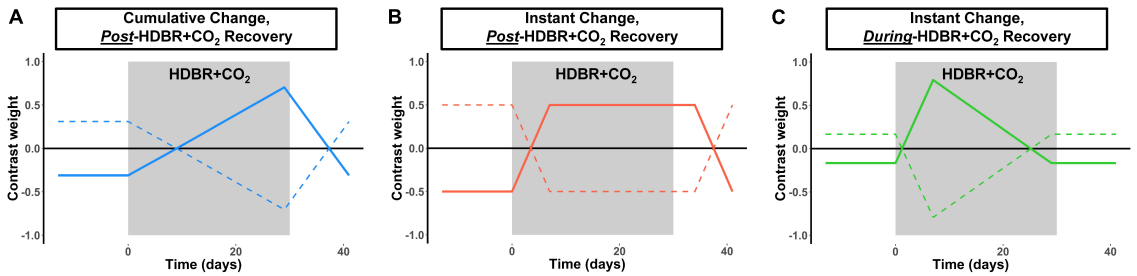

FIGURE 2 | Hypothesized changes in neural vestibular response to HDBR + CO_2. We hypothesized three different longitudinal patterns of brain change: **(A)** Cumulative change, in which brain changes would slowly increase over the course of HDBR + CO_2, followed by recovery after the conclusion of HDBR + CO_2. **(B)** Instant change, in which brain changes would immediately onset after the start of HDBR + CO_2, followed by recovery post-HDBR + CO_2. **(C)** Instant change, in which brain changes would immediately onset the start of HDBR + CO_2, but begin recovery *during* bed rest. We tested each of these hypotheses by using the contrast vectors shown here as weights in our longitudinal statistical model which assessed brain changes over all six time points for the HDBR + CO_2 group. Solid lines depict the positive version of each contrast; dotted lines depict the negative version of each contrast.

SANS Versus No-SANS Group Comparisons

We performed two exploratory analyses to examine group differences between those HDBR + CO_2 subjects who developed signs of SANS (SANS; $n = 5$; two males, three females) and those who did not (no-SANS; $n = 6$; four males, two females). First, we tested for differences between the intercept and slope images for each group. We conducted two-sample parametric t-tests with threshold $p < 0.0005$, $k = 10$. Non-parametric testing would not have been possible here, as less than 500 permutations exist for this combination of sample sizes.

Next, we tested for regions where the SANS versus no-SANS groups showed differences in the correlation between pre- to post-HDBR + CO_2 brain change and pre- to post- change in the ratio between the balance—eyes open and balance—eyes closed condition. This ratio score was calculated as: (balance—eyes open score/balance—eyes closed score) *100 and provides a metric of the degree to which an individual relies on vision for maintaining quiet upright stance. Each of these balance tasks is described in Section "Balance Testing." We selected to compare brain-behavior correlations only for this ratio score here because we previously identified significant differences between the two SANS subgroups on this measure, in which SANS individuals showed *greater increases* from pre- to post-HDBR + CO_2 in their reliance on vision during balance compared to no-SANS individuals (Lee et al., 2019a). One of the five SANS subjects was excluded from this analysis due to outlier values for the balance—eyes closed condition (described in Section "Balance Testing"). Thus there were $n = 4$ for the SANS group and $n = 6$ for the no-SANS group.

Mobility and Balance Testing: HDBR + CO_2 Cohort Only

Although the HDBR + CO_2 participants completed a battery of neurocognitive and sensorimotor assessments at each time point, here we focus on only mobility and balance testing, as these tasks were the most directly related to vestibular processing. We have previously published comprehensive behavioral profiles for both the HDBR + CO_2 (Lee et al., 2019a) and HDBR groups (Koppelmans et al., 2015), as well as vestibular brain-behavior correlations for the HDBR group (Yuan et al., 2018b).

Functional Mobility Test (FMT)

The Functional Mobility Test (FMT) is sensitive to the effects of spaceflight (Mulavara et al., 2010) and to the effects of bed rest (Reschke et al., 2009; Koppelmans et al., 2017). The FMT requires subjects to arise from a seated position and walk through a 6-m × 4-m two-part obstacle course consisting of foam hurdles, pylons, and bars. The first part of the course was completed on a hard floor, and the second part was completed on medium-density foam. Participants were instructed to walk through the course as quickly as possible without touching any of the obstacles. Participants repeated the FMT 10 times per session on five different testing days (**Figure 1**). Here we analyze only the total time needed to complete the course for the first trial of each session, as we have found this measure to be the most sensitive to intervention-related change. We excluded one subject from FMT analyses, as the subject showed substantial pre- to post- slowing (> ± 2.5 standard deviations from the group average pre- to post- change) and exerted considerable influence on group-level statistics. Thus there were $n = 10$ subjects for analyses involving FMT.

Balance Testing

Participants completed three balance tasks: (1) balance—eyes open; (2) balance—eyes closed; and (3) balance—eyes closed dynamic head tilt. Details of these tasks have been previously described (Mulder et al., 2014). Participants stood on a foam pad on top of a force platform (Leonardo Mechanograph, Novotec Medical GmbH, Pforzheim, Germany). Participants were instructed to maintain a comfortable stance, keep their arms folded across their chest and remain in a stable, upright posture for 30 s. Foot markers on the foam pad were used to ensure consistent foot placement across trials and between subjects. For the first two conditions, participants kept their head erect and eyes either open or closed. For the eyes closed dynamic head tilt condition, participants kept their eyes shut and made head pitch motions of ±20°, synchronized to a 0.33 Hz metronome tone. Participants repeated all conditions three times during each

testing session, and the order of conditions was semi-randomized to ensure that identical conditions did not repeat back-to-back. To minimize the effect of outlier trials, for each condition we examined the median score of the three trials. Scores are reported as equilibrium quotients (EQ), where 100% is a perfect score. EQ scores were calculated using instantaneous anterior-to-posterior peak-to-peak center-of-mass sway angle. For the eyes closed condition only, we excluded one subject, as the subject showed pre- to post-HDBR + CO_2 declines > ± 2 standard deviations from the group average and exerted considerable influence on group-level statistics. Thus there were $n = 10$ subjects for analyses involving balance-eyes closed scores, but there were $n = 11$ subjects for all other balance analyses.

Statistical Analyses of Behavioral Data

For completeness, we tested pre- to post- HDBR + CO_2 behavioral change, and we tested recovery for the mobility and balance tasks. In R 3.5.1 (R Core Team, 2013), using the last pre-bed rest time point (BDC 7) and the end of bed rest time point (HDT 29), we calculated a slope of pre- to post- performance change for each subject and conducted a one-sample *t*-test to determine if the group-average slope was different from 0. We also examined post-HDBR + CO_2 recovery trajectories for the three post-bed rest time points using a linear mixed model with restricted maximum likelihood (REML) estimation via the "lme" function. The model included a random intercept for subject (to allow for different starting points for each person) and the fixed effect of time. In each case, we were interested in whether the fixed effect of time was significant; we tested a quadratic fit for time for each measure as well, but the model including the linear effect of time performed better in all cases.

RESULTS

Neural Response to Vestibular Stimulation

Average BOLD signal during vestibular stimulation versus rest across all subjects and all time points is shown in **Figure 3** to illustrate the neural response to the skull tap method. In line with previous work (Lopez et al., 2012b; Zu Eulenburg et al., 2012; Noohi et al., 2017; Yuan et al., 2018b) vestibular stimulation resulted in activation of clusters in the right and left insula (**Table 1**). Also, as anticipated, we observed widespread deactivation of frontal, temporal, occipital, subcortical, and cerebellar regions. These results demonstrate that our skull tap method was able to engage the vestibular system and produce the expected neural response.

Time Course of Neural Vestibular Response to HDBR + CO_2

We identified multiple longitudinal changes in the neural response to vestibular stimulation across HDBR + CO_2, followed by recovery (**Figure 4** and **Table 2**). Several frontal, parietal, and temporal regions (**Figure 4A**) showed immediate *decreases in activation* with HDBR + CO_2, followed by recovery *during* the intervention and complete recovery by the final bed rest time point, HDT 29. For instance, right inferior temporal gyrus showed a conversion from *activation* to *deactivation* with the onset of HDBR + CO_2, followed by recovery of *activation* of this region by HDT 29.

Several other regions showed patterns of fast change, with changes sustaining throughout HDBR + CO_2 and not restoring until after the conclusion of bed rest. Right superior medial gyrus and right cerebellar lobule VI both showed *decreases in deactivation* and a conversion to *activation* with the start of bed rest, followed by recovery by 12 days post- bed rest. While neither of these clusters precisely overlaps with the regions that deactivated on average during vestibular stimulation (**Figure 3** and **Table 1**), other nearby parts of the superior medial gyrus and right cerebellar lobule VI did significantly deactivate in response to vestibular stimulation.

One brainstem cluster showed a fast *decrease in activation* with bed rest, with a conversion to *deactivation* of this region during HDBR + CO_2, followed by recovery. Of note, we did not find differences between the brain regions that emerged as significant for the "instant" versus "cumulative change post-HDBR + CO_2 recovery" contrasts, so we have reported only results for the instant change post-HDBR + CO_2 recovery contrasts.

Functional Behavioral Implications

Mobility and Balance Changes With HDBR + CO_2

Subjects showed pre- to post-HDBR + CO_2 declines in mobility, followed by a linear recovery pattern (**Figure 5** and **Table 3**); that is, participants were slower to complete the FMT obstacle course post-HDBR + CO_2, but sped back up by 12 days post-bed rest. The slope of decline in balance scores was only significant for the balance—eyes open condition; however, visually (**Figure 5**), there was a clear trend that HDBR + CO_2 negatively impacted balance across all three tasks. Similarly, only the balance—eyes closed dynamic head tilt condition showed a significant linear recovery pattern post-HDBR + CO_2, but again, visually, a recovery trend was evident post-bed rest for each of the balance tasks.

Brain—Behavior Correlations

We identified several dozen regions for which pre- to post-HDBR + CO_2 change in neural response to vestibular stimulation correlated with pre- to post- change in mobility and balance performance (**Figures 6A–D** and **Table 4**). In general, across all tasks and almost all clusters, we found that *greater deactivation* of various brain regions was associated with *reduced decline* or even improvement in behavioral measures. For instance, for the balance—eyes open condition, we found that *greater deactivation* of the right superior temporal gyrus (**Figure 6B**) associated with *less* balance decline and even balance improvement for a few individuals. That is, those with the greatest *decreases in activation* or *increases in deactivation* of this region had the *best* post-HDBR + CO_2 balance performance. Similarly, for the eyes closed and eyes closed dynamic head tilt balance conditions, we found that *greater* pre- to post- *deactivation* of right cerebellar lobule I-IV and supplementary motor area, respectively, was associated with *less balance decline* or even balance improvement (**Figures 6C,D**).

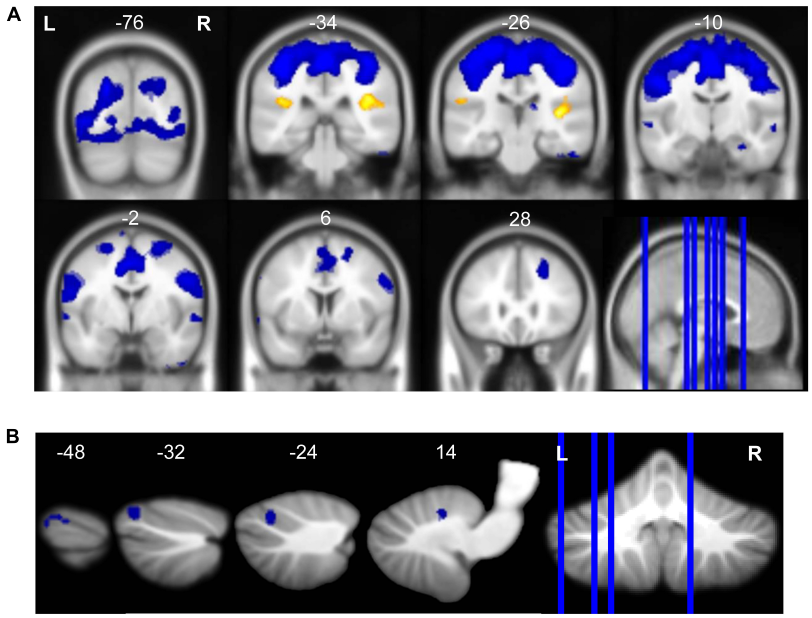

FIGURE 3 | Neural response to vestibular stimulation. Vestibular stimulation resulted in activation of insular cortex and widespread deactivation including **(A)** frontal, temporal, occipital, subcortical, and **(B)** cerebellar regions. Whole brain and cerebellar results are overlaid onto MNI **(A)** and SUIT **(B)** standard templates, respectively; $p < 0.0005$, $k = 10$; red = regions of activation; blue = regions of deactivation.

This relationship between *greater deactivation* and *reduced* behavioral decline held across the majority of brain regions that showed significant brain—behavior correlations, including sensorimotor cortex (i.e., supplementary motor area and postcentral gyrus), temporal cortex, occipital cortex, brainstem, and cerebellum (particularly, anterior cerebellum and crus I and II). In several cases, increased deactivation was found in regions that typically *deactivate* during vestibular stimulation (**Figure 3** and **Table 1**); for instance, this was the case for supplementary motor area, postcentral gyrus, and occipital gyrus (i.e., clusters marked with superscript "d" in **Table 4**).

There were only a few regions where *reduced* pre- to post-*deactivation* was more beneficial for post- HDBR + CO_2 mobility and balance performance. For instance, in the case of right cerebellar lobule VIIb (**Figure 6A**), *decreased deactivation* from pre- to post- was associated with *less* FMT slowing (i.e., less decline). Similarly, for the balance—eyes closed dynamic head tilt condition, *less deactivation* from pre- to post- in left cerebellar crus II was associated with *less* balance decline.

HDBR + CO_2 vs. HDBR Group Comparisons

Baseline (Intercept) Differences

Only three regions emerged where HDBR + CO_2 and HDBR had baseline differences in neural response to vestibular stimulation: left inferior temporal gyrus, right superior occipital gyrus, and brainstem (**Figure 7A** and **Table 5**). That is, both groups produced similar neural responses to vestibular stimulation pre-bed rest, and thus between-group slope differences can likely be attributed to intervention effects.

Slope Differences

There were five clusters across frontal, parietal, and temporal cortex where the HDBR + CO_2 group had a numerically *greater* slope of change in neural response to vestibular stimulation across the course of bed rest (**Figure 7B** and **Table 6**). Although no regions here overlapped with brain areas from the main effect analysis (**Figure 3** and **Table 1**), these clusters were located in close proximity to regions that are expected to show *deactivation* during vestibular stimulation. In general, the HDBR + CO_2 group showed *increases in activation* of these regions over the course of bed rest, as well as more within-group variability in neural response, compared to the HDBR group who generally showed *increases in deactivation* of these regions over the course of bed rest. For instance, in the left middle frontal gyrus (**Figure 7C**), the HDBR + CO_2 subjects showed a switch from *deactivation* of this region during vestibular stimulation at BDC 7 to *activation* of this region at HDT 29. The HDBR group showed the opposite pattern, changing from *activation* to *deactivation* of this region.

There was one cluster in the thalamus where the HDBR + CO_2 group showed a *reduced* slope of change compared to the HDBR group. Here the HDBR + CO_2 group exhibited *decreasing activation*, and ultimately *deactivation* of this region during vestibular stimulation at HDT 29, whereas the HDBR group exhibited a transition from *deactivation* of this region to *activation*.

SANS vs. No-SANS Group Differences

Five of the 11 HDBR + CO_2 participants developed signs of SANS, including optic disc edema. While this phenomenon is commonly reported following spaceflight (Lee et al., 2016), this

TABLE 1 | Regions of activation or deactivation in response to vestibular stimulation.

	Extent (k)	Peak T-value	Peak *p*-value	MNI coordinates (mm)		
				x	y	z
Activation						
Insular						
R Insula	374	5.269	1.092×10^{-6}	38	−24	8
L Rolandic Operculum	150	5.032	2.580×10^{-6}	−38	−36	20
Deactivation						
Frontal						
L Posterior-Medial Frontal Gyrus[a]	183,700	8.245	1.349×10^{-11}	−6	−16	60
R Middle Frontal Gyrus	487	4.775	6.469×10^{-6}	24	28	38
R Superior Medial Gyrus	12	3.791	1.821×10^{-4}	2	44	36
Temporal						
R Inferior Temporal Gyrus	111	4.375	6.067×10^{-6}	54	−30	−30
L Superior Temporal Gyrus	79	4.630	1.082×10^{-5}	−62	−6	−2
R Superior Temporal Gyrus	133	4.500	1.699×10^{-5}	60	−2	−4
R Parahippocampal Gyrus	37	4.224	4.372×10^{-5}	28	−14	−24
R Inferior Temporal Gyrus	30	4.068	7.380×10^{-5}	48	0	−48
R Olfactory Cortex	11	3.794	1.804×10^{-4}	4	10	−12
Occipital						
L Superior Occipital Gyrus[a]	5,868	6.151	4.065×10^{-8}	−22	−78	−32
Subcortical						
R Thalamus	25	4.163	5.373×10^{-5}	14	−24	16
R Caudate Nucleus	11	3.889	1.328×10^{-4}	8	14	8
Anterior Cerebellum						
R Cerebellar Lobule V	20	4.143	5.733×10^{-5}	14	−54	−21
Cerebellar Crus I						
L Cerebellar Crus I	49	4.165	5.335×10^{-5}	−24	−74	−29
L Cerebellar Crus I	10	4.033	8.289×10^{-5}	−48	−72	−31

Significance level set at $p < 0.0005$ and cluster size $k = 10$ for all analyses. Table shows all local maxima separated by more than 20 mm. Whole-brain results are listed first, followed by cerebellar results. Cortical regions were labeled using the AnatomyToolbox atlas via the SPM toolbox BSPMview. Cerebellar regions were labeled using the SUIT atlas. [a]*Portions of four deactivation clusters listed above passed Family Wise Error (FWE) < 0.05 correction:*

(1) L Posterior-Medial Frontal Gyrus: $k = 5{,}036$, FWE-corrected $p = 2.203 \times 10^{-6}$; MNI = −6, −16, 60
(2) L Superior Occipital Gyrus: $k = 60$, FWE-corrected $p = 0.003$; MNI = −22, −78, 32
(3) R Superior Frontal Gyrus: $k = 32$, FWE-corrected $p = 0.006$; MNI = 24, −10, 60
(4) L Inferior Occipital Gyrus: $k = 24$, FWE-corrected $p = 0.014$; MNI = −44, −78, 0

is the first bed rest study to induce such effects (Laurie et al., 2019), possibly due to the careful testing for SANS symptoms and the strict head-down-tilt conditions, or the addition of elevated CO_2. As SANS was not anticipated *a priori* but represents a substantial subgroup of the HDBR + CO_2 cohort, we conducted two exploratory analyses of this unique sample.

At $p < 0.0005$ and $k = 10$, there were no regions of intercept or slope difference between the SANS and no-SANS participants. We previously found that SANS individuals increased their reliance on visual information during balance from pre- to post-HDBR + CO_2 (Lee et al., 2019a); that is, SANS subjects had greater increases in their ratio of eyes open balance compared to eyes closed balance. Here we identified multiple frontal, parietal, temporal, and occipital regions where the SANS subjects showed stronger correlations with this balance ratio score compared to the no-SANS subjects (**Figure 8** and **Table 7**). For instance, SANS subjects showed a stronger correlation between *greater activation* of left middle frontal gyrus (**Figure 8**) and *increased* pre- to post-balance ratio score. Several of these clusters included regions typically activated during vestibular stimulation (indicated with a superscript "d" in **Table 7**). There were no regions of stronger correlation for the no-SANS subjects.

DISCUSSION

Key Findings

Here we identified changes in the neural correlates of vestibular processing with 30 days of HDBR + CO_2. We found multiple regions where brain activation during vestibular stimulation changed quickly after participants started HDBR + CO_2 and recovered either during or post-bed rest, providing support for adaptive plasticity of the vestibular system in response to altered sensory inputs. In multiple cases, *increased deactivation* of cortical and cerebellar areas was associated with *less* decline in balance from pre- to post-HDBR + CO_2, suggesting that

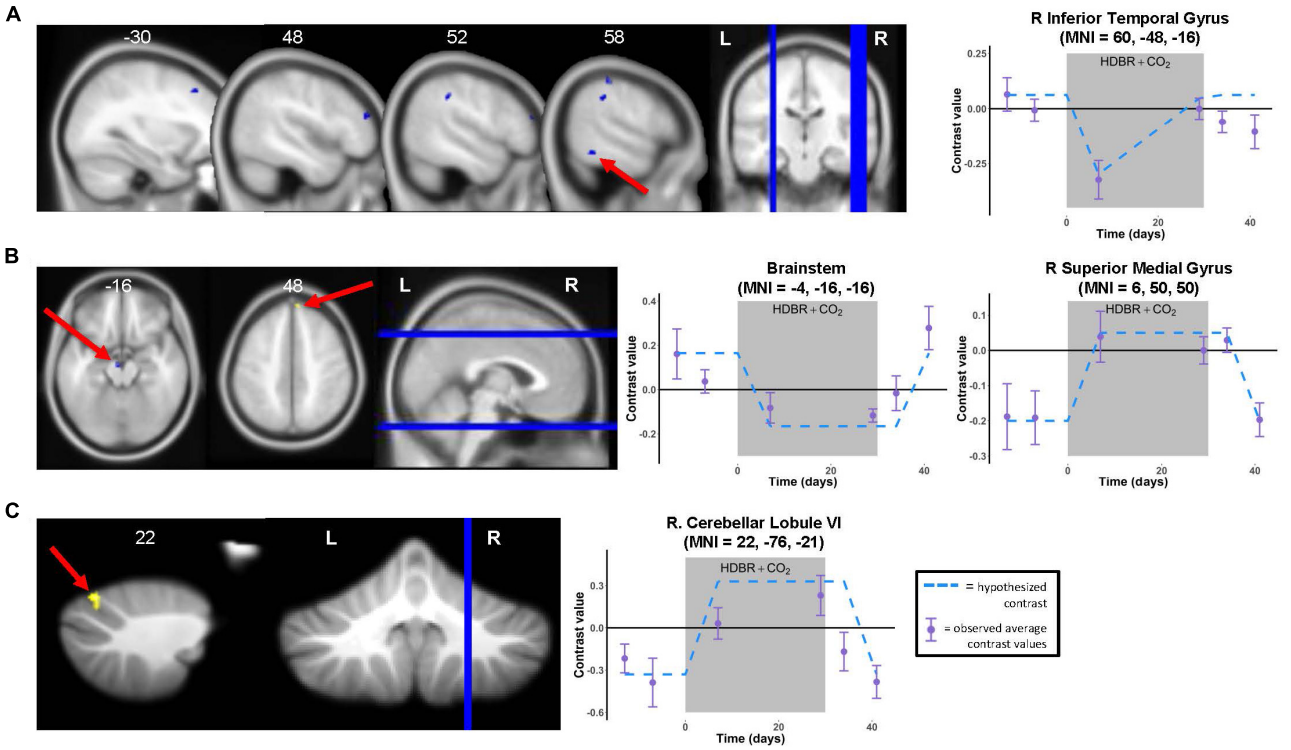

FIGURE 4 | Time course of neural vestibular response to HDBR + CO_2. Left panels: Regions showing whole brain **(A,B)** and cerebellar **(C)** longitudinal changes in activation during vestibular stimulation across the six time points. Whole brain and cerebellar results are overlaid onto MNI and SUIT standard templates, respectively; $p < 0.001$, $k = 10$ for whole brain analyses; $k = 5$ for cerebellar analyses. Three clusters survived $p < 0.0005$, $k = 10$ correction (see **Table 2**). Right panels: Example contrast values plotted for peak coordinate within the cluster with the largest T value in each case (cluster indicated by red arrow). Points represent group mean contrast values; error bars represent standard error. Dotted lines depict the hypothesized longitudinal contrasts for "instant decrease, during-HDBR + CO_2 recovery" **(A)**, "instant decrease, post-HDBR + CO_2 recovery" **(B)**, and "instant increase, post-HDBR + CO_2 recovery" **(B,C)**.

some of the adaptive neural changes during bed rest may benefit post-bed rest performance of vestibularly mediated behaviors. We found several differences for HDBR + CO_2 compared to HDBR subjects, suggesting interactive or additive effects of bed rest and CO_2. Finally, we noted differences in brain—behavior relationships for SANS versus no-SANS subjects, indicating the need for further study of bed rest-induced ocular symptoms.

Time Course of Neural Vestibular Response to HDBR + CO_2

Similar to our past work (Yuan et al., 2018b), we found multiple longitudinal changes in the neural response to vestibular stimulation, including in several areas in close proximity to regions typically involved in processing vestibular information, as well as in several regions that are not normally activated during vestibular stimulation. These responses could represent adaptive plasticity, in which the enhanced demands of neural processing of altered sensory inputs during HDBR + CO_2 are requiring greater neural resources. For instance, the finding of *decreased deactivation* in right superior medial gyrus and right cerebellar lobule VI (which are anatomically near to regions that, on average, deactivated in response to vestibular stimulation) suggests a compensatory response. That is, functional brain regions that typically deactivate in response to vestibular input are deactivating *less* during exposure to an altered sensory environment, potentially to allow for additional brain pathways to aid in processing the novel sensory information. Here, more specifically, it could be that down-weighting of somatosensory input during HDBR, paired with upweighting of vestibular input due to vestibular-somatosensory convergence at the vestibular nuclei (Mulavara et al., 2012), is resulting in a higher neural processing demand. The fast recovery of several of these regions *during* bed rest suggests an ability of the vestibular system to adjust rapidly to such altered sensory conditions.

In contrast to our past work (Yuan et al., 2018b), we did not identify any unique regions of slow, cumulative brain changes; instead, we found clusters that were statistically significant for both the immediate and cumulative models. This suggests that interactive effects of CO_2 with bed rest might accelerate neural vestibular changes. It could also be that CO_2-related increases in cerebral perfusion enhanced the BOLD signal (Corfield et al., 2001) for HDBR + CO_2 participants, making it easier to detect bed rest-related changes earlier during that intervention. Further, given that the HDBR + CO_2 intervention was about half the duration of the HDBR intervention, it could be that some of the slow, cumulative brain changes that we previously identified require longer than 30 days to develop.

TABLE 2 | Regions showing longitudinal increases and decreases in activation during vestibular stimulation across all six time points.

	Extent (k)	Peak *T*-value	Peak *p*-value	MNI coordinates (mm)		
				x	y	z
Instant Decrease, During-HDBR + CO_2 Recovery						
Frontal						
R Middle Frontal Gyrus[a]	21	−3.953	1.238×10^{-4}	48	46	20
L Middle Frontal Gyrus	15	−3.617	3.517×10^{-4}	−30	26	44
Parietal						
R Supramarginal Gyrus	12	−3.999	1.071×10^{-4}	58	−30	54
R Supramarginal Gyrus[a]	59	−3.835	1.798×10^{-4}	52	−36	38
Temporal						
R Inferior Temporal Gyrus[a,b]	46	−4.271	4.463×10^{-5}	60	−48	−16
Instant Increase, Post-HDBR + CO_2 Recovery						
Frontal						
R Superior Medial Gyrus[b]	15	3.781	2.123×10^{-4}	6	50	50
Anterior Cerebellum						
R Cerebellar Lobule VI[b]	9	4.093	7.938×10^{-5}	22	−76	−21
Instant Decrease, Post-HDBR + CO_2 Recovery						
Subcortical						
Brainstem[b]	15	−3.645	3.229×10^{-4}	−4	−16	−16

Clusters that emerged as significant were the same for the "instant, slow recovery" and "cumulative, slow recovery" increase and decrease contrasts. Thus here we report only the statistics for the instant increase and decrease contrasts. Significance level set at $p < 0.001$ and cluster size $k = 10$ for whole brain analyses and cluster size $k = 5$ for cerebellar analyses. Table includes all local maxima separated by more than 20 mm. Whole-brain results are listed first, followed by cerebellar results. Cortical regions were labeled using the AnatomyToolbox atlas via the SPM toolbox BSPMview. Cerebellar regions were labeled using the SUIT atlas. [a]*Portions of three "instant decrease, during HDBR + CO_2 recovery" clusters survived $p < 0.0005$ and $k = 10$ thresholding:*

(1) R Inferior Temporal Gyrus: $k = 24$
(2) R Middle Frontal Gyrus: $k = 12$
(3) R Supramarginal Gyrus: $k = 59$

[b]*Whole brain and cerebellar clusters with largest T value for each contrast; contrast values are plotted for the peak coordinate within each of these four clusters in* ***Figure 4****.*

Previously we found that HDBR resulted in upregulation of the vestibular system (Yuan et al., 2018b), which we attributed to either increased sensitivity of the vestibular system during HDBR or to reduced neural efficiency, in which greater activation of vestibular cortical regions would be needed to process vestibular information during HDBR. Here, we did not find clear evidence for reduced neural efficiency (Yuan et al., 2018b). That is, we did not identify any HDBR + CO_2-related *increases* in activation of vestibular cortical regions. This suggests that elevated CO_2 may augment vestibular processing, as this environment did not produce the same longitudinal reduction in neural efficiency as HDBR alone.

Functional Behavioral Implications

We identified predominantly regions for which *increased* pre- to post- *deactivation* during vestibular stimulation associated with *reduced* balance performance decline, or even performance improvement. This may represent adaptive plasticity during the HDBR + CO_2 intervention, in which some individuals show an enhancement of the expected cortical deactivation response, paired with a dampening of activity in other brain regions that could interfere with processing of vestibular information. This adaptive change could then later manifest as superior post-bed rest balance due to underlying increased specificity of activation of vestibular cortex and deactivation of other sensory regions during the balance tasks. More specifically, it could be that the reduced plantar somatosensory input during HDBR + CO_2 results in down-weighting of somatosensory input, but upweighting of vestibular input. While this reweighting is likely modulated at the level of the vestibular nuclei where the somatosensory and vestibular systems converge (Bles et al., 1984; Dieringer, 1995; Horak and Hlavacka, 2001; Carriot et al., 2015), this reorganization could plausibly manifest as increased deactivation of cortical sensorimotor processing regions, with those individuals who had the most successful reweighting processes presenting with enhanced preservation of balance abilities post- HDBR + CO_2. Given these possible mechanisms, it thus makes sense that we found the most numerous brain-behavior correlations for the eyes closed dynamic head tilt condition, as this condition most specifically tasks the vestibular system.

We similarly found evidence of brain-behavioral relationships in our past HDBR work for vestibular processing (Yuan et al., 2018b) and for neural control of foot movement (Yuan et al., 2018a). Further, we previously identified several regions for which *better* balance (i.e., reduced postural sway while standing on one leg) correlated with *greater deactivation* of the brainstem, cerebellar lobule VI, and crus I and II across healthy young and older adults at one time point (Noohi et al., 2019). This fits with the present work, as here we found several brainstem and

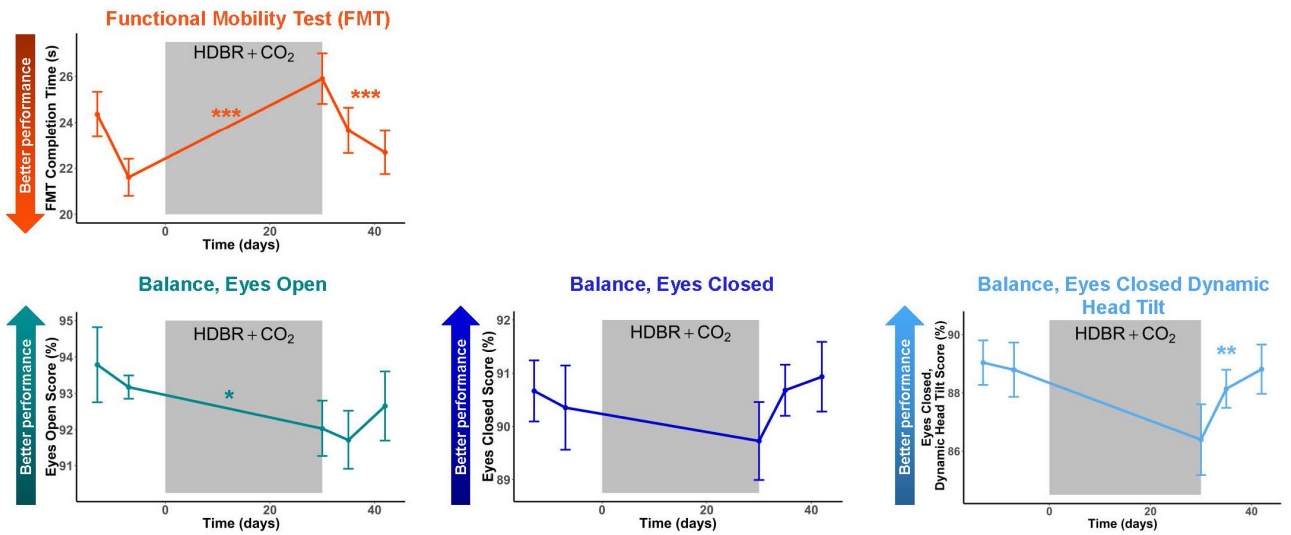

FIGURE 5 | Mobility and Balance Changes with HDBR + CO_2. Mobility and balance performance pre- and post-HDBR + CO_2. In general, participants showed performance declines followed by recovery post-HDBR + CO_2. The slope of behavioral decline was significant for FMT and a trend for the balance-eyes open condition. Participants showed a significant linear recovery trajectory for FMT and balance-eyes closed dynamic head tilt. Error bars represent standard error. *$p < 0.10$; **$p < 0.05$; ***$p < 0.001$.

TABLE 3 | Mobility and balance change with HDBR + CO_2 and recovery.

	Slope of Changes with HDBR + CO_2		Fixed Effect of Time During HDBR + CO_2 Recovery		
	***t*(DF)**	***p***	**Recovery Day β**	**t(DF)**	***p***
Functional Mobility Test (FMT)	5.45(9)	**<0.001*** **	−0.260	−5.35(19)	**<0.001*** **
Balance—eyes open	−1.91(10)	**0.085***	0.057	0.86(21)	0.398
Balance—eyes closed	−0.51(9)	0.622	0.087	1.38(19)	0.182
Balance—eyes closed dynamic head tilt	−1.74(10)	0.113	0.195	2.31(21)	**0.032****

*$p < 0.10$ (trend); **$p < 0.05$; ***$p < 0.001$.

cerebellar regions for which *greater* post-bed rest *deactivation* associated with *better* balance. Together, these findings provide further support for the notion that those with a more refined neural response to vestibular stimulation in the scanner (e.g., including *greater deactivation* of brainstem and cerebellum) likely also produce a more refined neural response during balance tasks outside of the scanner and therefore perform better.

Similarly, several mobile neuroimaging studies have identified that older adults exhibit poorer balance paired with *increased* brain activation during vestibular stimulation (Karim et al., 2013; Lin et al., 2017). For instance, using functional near-infrared spectroscopy (fNIRS), Lin et al. (2017) found greater activation in frontal and occipital regions during vestibular stimulation for older compared to middle-aged adults. This suggests compensatory processes in which older adults require greater neural resources to process the same vestibular information. This fits with the present findings, as those who had the largest post-bed rest balance declines also showed bed rest-related *increases in activation* or *reductions in deactivation* across various cortical regions, including frontal and occipital regions. It could be that, similar to older adults, these individuals were recruiting extra brain regions to aid in processing vestibular information in the scanner and then engaging similar compensatory over-recruitment mechanisms outside the scanner during the post-bed rest balance assessments, which ultimately resulted in poorer balance performance.

HDBR + CO_2 vs. HDBR Group Comparisons

CO_2-specific effects or interactive effects of bed rest and CO_2 may be contributing to the identified differences in slope of activation change for the HDBR + CO_2 group versus the HDBR group. CO_2 is a strong vasodilator and, among other effects, results in increased blood flow to the brain (Atkinson et al., 1990; Zhou et al., 2008), as well as increased intensity of the blood oxygen level-dependent (BOLD) signal measured by fMRI (Corfield et al., 2001). This increased cerebral perfusion could be contributing to the identified group differences here. Elevated CO_2 selectively favors frontal lobe perfusion (Bhogal et al., 2015); thus increased slope of change for frontal regions (e.g., middle frontal gyrus) among the HDBR + CO_2 group could be particularly related to perfusion effects on the BOLD signal. As brain deactivation is also an active process, the widespread

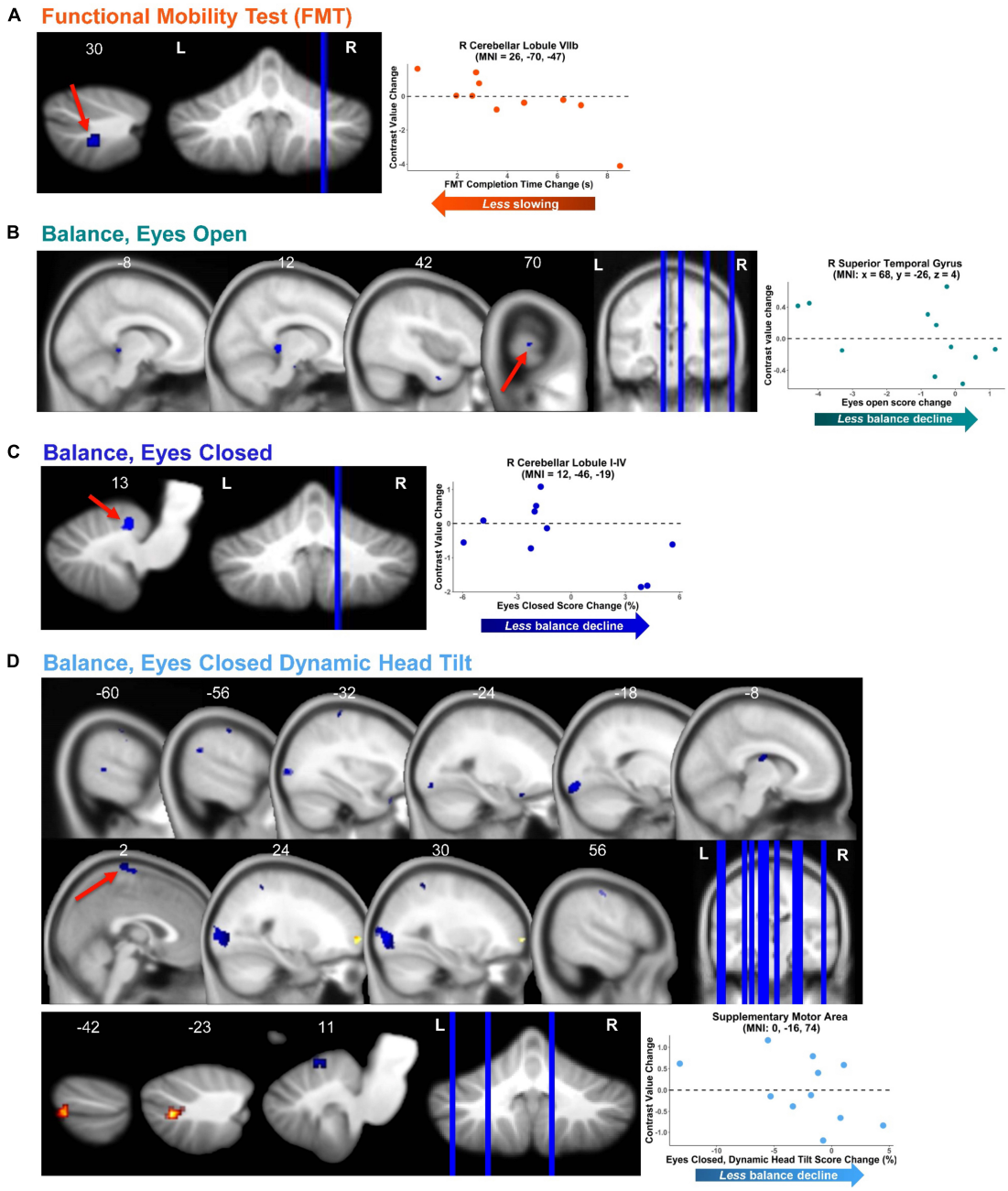

FIGURE 6 | Functional behavioral consequences. Brain—behavior correlations for functional mobility test (FMT; **A**) and three balance tasks **(B–D)**. Brain change was calculated as the difference in brain activation from pre-HDBR + CO_2 (time BDC 7) to the end of HDBR + CO_2 (time HDT 29). Behavior change was calculated as the difference in mobility and balance performance from pre-HDBR + CO_2 (time BDC 7) to post-HDBR + CO_2 (time R0). Whole brain and cerebellar results are overlaid onto MNI and SUIT standard templates, respectively; non-parametric $p < 0.0005$, $k = 10$. Warm colors indicate regions of positive correlation between brain change and behavior change. Cool colors indicate regions of negative correlation between brain change and behavior change. Right side correlation plots include contrast values extracted from peak coordinate inside an example cluster (indicated with red arrows), graphed against behavior change score.

increases in deactivation that we noted (which were generally associated with better behavioral performance) could also be influenced by CO_2-related perfusion effects.

It has been demonstrated that *decreased* CO_2 (through voluntary hyperventilation) negatively impacts postural sway, resulting in unsteadiness of balance (Sakellari et al., 1997). Although the mechanisms here are unknown, it has been suggested that hyperventilation disrupts vestibular system compensation, including interfering with central and peripheral somatosensory signals from the lower limbs (Sakellari et al., 1997). Here the differential effects between HDBR + CO_2 and HDBR subjects demonstrate that *increased* CO_2 may

TABLE 4 | Regions showing associations between pre- to post-HDBR + CO_2 differences in behavioral scores and pre- to post-HDBR + CO_2 change in brain activation during vestibular stimulation.

	Extent (*k*)	Peak *T*-value	Non-parametric Peak *p*-value	MNI coordinates (mm)		
				x	y	z
FMT[a], negative association						
Posterior Cerebellum						
R Cerebellar Lobule VIIb[c]	23	5.110	2.000×10^{-4}	26	−70	−47
Balance—eyes open, negative association						
Temporal						
R Superior Temporal Gyrus[c]	10	3.662	1.333×10^{-4}	68	−26	4
R Inferior Temporal Gyrus	12	3.205	4.000×10^{-4}	42	2	−36
Occipital						
R Lingual Gyrus	29	5.128	1.333×10^{-4}	12	−32	0
Subcortical						
Brainstem	10	3.812	2.667×10^{-4}	−8	−36	−4
Balance—eyes closed[b], negative association						
Anterior Cerebellum						
R Cerebellar Lobule I-IV[c]	12	6.895	2.000×10^{-4}	12	−46	−19
Balance—eyes closed, dynamic head tilt, positive association						
Frontal						
R Frontal Superior Orbital Cortex	55	4.196	2.000×10^{-4}	28	66	0
Cerebellar Crus						
L Cerebellar Crus II	10	4.821	2.667×10^{-4}	−22	−74	−41
L Cerebellar Crus I	15	4.103	6.667×10^{-5}	−40	−76	−41
Balance—eyes closed, dynamic head tilt, negative association						
Frontal						
R Precentral Gyrus	17	5.112	4.667×10^{-4}	56	−14	48
Supplementary Motor Area[c,d]	90	4.769	1.333×10^{-4}	0	−16	74
L Frontal Inferior Orbital Cortex	20	3.754	1.333×10^{-4}	−22	18	−22
L Precentral Gyrus[d]	14	3.524	4.667×10^{-4}	−30	−32	70
Parietal						
L Postcentral Gyrus	14	3.553	4.000×10^{-4}	−58	−20	50
Temporal						
R Fusiform Gyrus	549	6.929	1.333×10^{-4}	32	−86	2
L Superior Temporal Gyrus	45	5.165	2.000×10^{-4}	−54	−50	26
L Middle Temporal Gyrus	37	4.715	4.667×10^{-4}	−60	−40	4
Occipital						
L Lingual Gyrus	144	6.071	1.333×10^{-4}	−18	−92	−14
L Middle Occipital Gyrus[d]	51	5.560	2.667×10^{-4}	−34	−90	6
Subcortical						
L Thalamus	47	4.555	6.667×10^{-4}	−8	−14	20
Anterior Cerebellum						
Right Cerebellar Lobule V	12	6.018	2.000×10^{-4}	10	−62	−11

*Significance level set at non-parametric $p < 0.0005$ and cluster size $k = 10$ for all analyses. Table includes all local maxima separated by more than 20 mm. Whole-brain results are listed first, followed by cerebellar results. Cortical regions were labeled using the AnatomyToolbox atlas via the SPM toolbox BSPMview. Cerebellar regions were labeled using the SUIT atlas. [a]One outlier subject was excluded from FMT analyses so n = 10; see section "Materials and Methods." [b]One outlier subject excluded from balance—eyes closed analyses so n = 10; see section "Materials and Methods." [c]Indicates clusters for which values from peak coordinate within cluster are plotted against behavior change score in **Figure 6**. [d]Peak coordinate in cluster falls within region of brain deactivation in response to vestibular stimulation (**Figure 3** and **Table 1**).*

also disrupt normal vestibular processing and vestibular compensatory mechanisms.

SANS vs. No-SANS Group Differences

SANS subjects showed stronger correlations between pre- to post-HDBR + CO_2 change in balance ratio score and brain changes. This suggests a relationship between SANS status and visual contributions to balance. Higher ratio scores are associated with more reliance on external visual cues for balance. As those with the greatest *activation* of regions such as middle frontal gyrus also showed the greatest pre- to post- *increase* in visual dependence, this could indicate reduced neural efficiency—in which these individuals are recruiting extra brain regions to aid in processing of the same vestibular information. This indicates

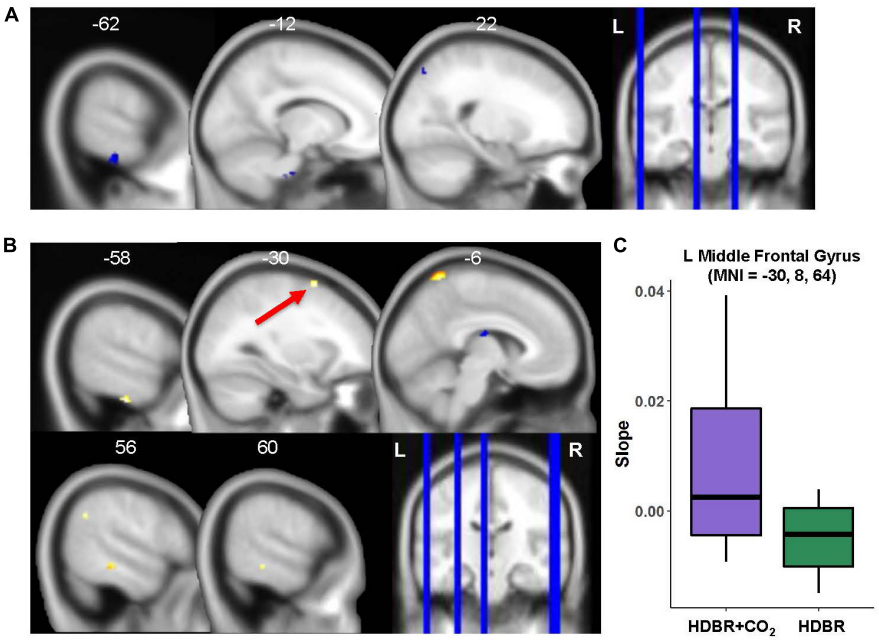

FIGURE 7 | HDBR + CO_2 vs. HDBR group comparisons. **(A)** Regions of intercept differences between HDBR + CO_2 and HDBR groups. **(B)** Regions of slope differences between HDBR + CO_2 and HDBR groups. Results overlaid onto MNI standard template; non-parametric $p < 0.0005$, $k = 10$. Cool colors indicate regions where the intercept or slope for the HDBR + CO_2 group was numerically less than the intercept or slope for the HDBR group. Warm colors indicate regions where the slope for the HDBR + CO_2 group was numerically greater than the slope for the HDBR group. **(C)** Example slope values extracted from L Middle Frontal Gyrus (i.e., the cluster with greatest *T* value for the HDBR + CO_2 > HDBR contrast). Here, the HDBR + CO_2 group showed *increased activation* of this region across bed rest, while the HDBR group showed *increased deactivation* of this region across bed rest.

TABLE 5 | Regions with intercept differences between HDBR + CO_2 and HDBR subjects.

	Extent (*k*)	Peak *T*-value	Non-parametric Peak *p*-value	MNI coordinates (mm)		
				x	*y*	*z*
HDBR + CO_2 < HDBR						
Temporal						
L Inferior Temporal Gyrus	56	4.692	6.667×10^{-5}	−62	−28	−28
Occipital						
R Superior Occipital Gyrus	10	3.798	2.668×10^{-4}	22	−76	52
Subcortical						
Brainstem	67	3.752	3.333×10^{-4}	−12	−22	−40

Significance level set at non-parametric p < 0.0005 and cluster size k = 10. Table includes all local maxima separated by more than 20 mm. Cortical regions were labeled using the AnatomyToolbox atlas via the SPM toolbox BSPMview. There were no significant intercept differences for the cerebellum.

reduced efficiency of the vestibular system that manifested behaviorally as greater reliance on the visual system during post-bed rest balance. These findings require validation in future studies to more clearly understand implications for the one third of astronauts who develop SANS (Lee et al., 2016).

Limitations

Limitations of the present work include the small pilot sample, lack of ambulatory control group, and differences in scanning timeline and parameters between the two groups. As the HDBR + CO_2 and HDBR groups were each part of separate, larger bed rest campaigns, the respective testing timelines were restricted by NASA and not matched between groups. Further, only males were included in the HDBR group, as these participants were control subjects for a different investigator's testosterone supplementation study. Although the vestibular stimulation parameters and sequence duration were identical between the HDBR + CO_2 and HDBR groups, these data were collected on two different Siemens scanners with two slightly different fMRI sequences. The HDBR + CO_2 fMRI sequence included a faster TR and more volumes (TR = 2.5 s; 96 volumes) than the HDBR sequence (TR = 3.66 s; 66 volumes). This amounts to greater statistical power for the HDBR + CO_2 group. While these differences represent a limitation of the between-group comparisons that we report here, multisite neuroimaging studies are increasing in popularity; such studies generally

TABLE 6 | Regions with differences in slope of activation change with bed rest between HDBR + CO_2 and HDBR subjects.

	Extent (*k*)	Peak *T*-value	Non-parametric Peak *p*-value	MNI coordinates (mm)		
				x	*y*	*z*
HDBR + CO_2 > HDBR						
Frontal						
L Middle Frontal Gyrus[a]	20	4.373	1.333×10^{-4}	−30	8	64
Parietal						
R Angular Gyrus	19	4.053	2.000×10^{-4}	56	−54	34
L Precuneus	88	3.899	6.667×10^{-5}	−6	−56	72
Temporal						
L Inferior Temporal Gyrus	27	4.313	6.667×10^{-5}	−58	−22	−32
R Inferior Temporal Gyrus	28	4.120	2.667×10^{-4}	60	−32	−12
HDBR + CO_2 < HDBR						
Subcortical						
L Thalamus	29	4.073	6.667×10^{-5}	−6	−14	20

Significance level set at non-parametric $p < 0.0005$ and cluster size $k = 10$. Table includes all local maxima separated by more than 20 mm. Cortical regions were labeled using the AnatomyToolbox atlas via the SPM toolbox BSPMview. There were no significant slope differences for the cerebellum. [a]Indicates cluster for which values from peak coordinate within cluster are plotted by group in ***Figure 7C****.*

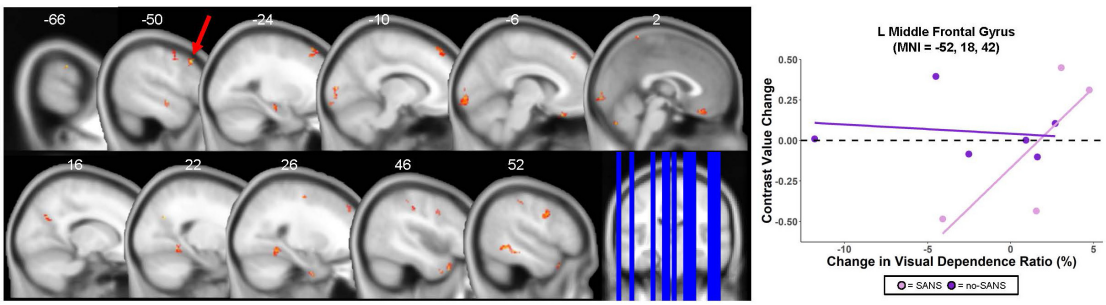

FIGURE 8 | SANS vs. No-SANS Group Differences. **Left:** regions in which HDBR + CO_2 participants who developed signs of Spaceflight-Associated Neuroocular Syndrome (SANS) showed a *stronger* correlation between pre- to post- change in brain activity during vestibular stimulation and pre- to post- change in balance ratio compared to those who did not develop signs of SANS (no-SANS). Balance ratio was calculated as: (balance—eyes open score/balance—eyes closed score) * 100. Results overlaid onto MNI standard template; non-parametric $p < 0.0005$, $k = 10$. One of the five SANS subjects was excluded from analysis here due to outlier values for their eyes closed balance score; thus $n = 4$ for the SANS group and $n = 6$ for the no-SANS group. **Right:** correlation between brain changes and visual dependence balance ratio change for an example cluster; SANS subjects are shown in pink, no-SANS subjects are shown in purple. Regression lines are shown for each group for reference only and do not represent the results of any statistical tests.

indicate that functional neuroimaging data is robust across sites (Costafreda et al., 2007; Biswal et al., 2010; Gountouna et al., 2010; Noble et al., 2017). Further, the analyses in the present work focus on differences in within-subject brain changes. That is, we have tested for between-group differences in within-person intercepts and slopes of change in brain activity. This makes the present results more robust to any introduced variance due to scanner or sequence differences.

Due to the limited pilot sample size, we use uncorrected *p*-values for the neuroimaging statistical tests to better detect within- and between-subject differences. Nonetheless, here we demonstrate for the first time the feasibility of characterizing vestibular brain changes during multiple weeks of bed rest combined with elevated CO_2. We present compelling preliminary findings based on these highly unique data, which should be validated in future work.

It should also be noted that it is difficult to fully generalize these bed rest findings to spaceflight. HDBR + CO_2 and HDBR mimic only some of the effects of spaceflight, such as body unloading, altered sensory input, and fluid shifts, but these analogs do not include all features of spaceflight that could impact vestibular processing. Finally, as is typical with the pneumatic skull tap method, the stimulus did not induce any vestibular perception, motion sensation, or movement in head position. Instead of using subjective perception of the vestibular stimulus, assessment of vestibular-evoked myogenic potentials in the eye muscles (oVEMPs) outside of the scanner was used to validate successful stimulation of vestibular organs.

Applications to Spaceflight and Future Directions

The present findings document changes in functional vestibular processing with spaceflight analog environments. These findings support that spaceflight factors do likely influence the neural correlates of vestibular processing; however, there is limited

TABLE 7 | Regions where SANS subjects showed *greater* correlations compared to no-SANS subjects between pre- to post HDBR + CO_2 change in visual dependence balance ratio and pre- to post-HDBR + CO_2 change in brain activation during vestibular stimulation.

	Extent (*k*)	Peak *T*-value	Peak *p*-value	MNI coordinates (mm)		
				x	*y*	*z*
SANS > no-SANS						
Frontal						
L Middle Frontal Gyrus[a]	120	62.762	1.930×10^{-7}	−52	18	42
L Superior Frontal Gyrus	121	47.969	5.650×10^{-7}	−16	42	52
R Paracentral Lobule	11	35.986	1.780×10^{-6}	2	−48	72
R Precentral Gyrus	56	26.726	5.826×10^{-6}	48	6	38
L Rectal Gyrus	56	25.731	6.775×10^{-6}	−2	30	-24
R Inferior Frontal Gyrus	11	23.941	9.027×10^{-6}	56	20	2
R Precentral Gyrus[b]	22	18.232	2.661×10^{-5}	28	−14	60
L Middle Orbital Gyrus	12	11.352	1.717×10^{-4}	−38	40	4
R Superior Frontal Gyrus	17	11.211	1.802×10^{-4}	28	42	44
L Precentral Gyrus	17	11.186	1.818×10^{-4}	−52	−4	52
Parietal						
R Postcentral Gyrus[b]	35	38.070	1.422×10^{-6}	38	−26	40
R Precuneus	34	33.849	2.272×10^{-6}	16	−66	30
L Superior Parietal Lobule	20	29.913	3.719×10^{-6}	−18	−62	46
R Postcentral Gyrus[b]	14	18.030	2.782×10^{-5}	48	−28	48
L Postcentral Gyrus	27	17.676	3.009×10^{-5}	−66	−20	34
R Postcentral Gyrus	12	14.543	6.500×10^{-5}	66	−8	24
Temporal						
L Hippocampus	24	64.347	1.747×10^{-7}	−28	−18	−18
R Medial Temporal Pole	32	27.635	5.099×10^{-6}	46	20	−34
R Fusiform Gyrus	10	24.758	7.898×10^{-6}	24	−4	−40
R Fusiform Gyrus	100	24.756	7.901×10^{-6}	22	−48	−8
R Inferior Temporal Gyrus	86	21.709	1.332×10^{-5}	52	−48	−6
R Inferior Temporal Gyrus	11	20.383	1.711×10^{-5}	60	−54	−20
L Middle Temporal Gyrus	17	19.939	1.867×10^{-5}	−50	−12	−10
L Fusiform Gyrus	11	19.920	1.874×10^{-5}	−36	−46	−22
L Fusiform Gyrus	14	18.070	2.757×10^{-5}	−38	−6	−38
R Medial Temporal Pole	13	16.837	3.647×10^{-5}	46	10	−38
Occipital						
R Middle Occipital Gyrus[b]	20	27.454	5.235×10^{-6}	30	−74	40
L Calcarine Gyrus	117	24.386	8.388×10^{-6}	−6	−96	−6
L Mid-Occipital Gyrus[b]	10	12.832	1.063×10^{-4}	−28	−84	14

*Significance level set at $p < 0.0005$ and cluster size $k = 10$. Table includes all local maxima separated by more than 20 mm. Cortical regions were labeled using the AnatomyToolbox atlas via the SPM toolbox BSPMview. There were no significant results for the cerebellum. [a]Indicates cluster for which values from peak coordinate within cluster are plotted against behavior change score in **Figure 8**. [b]Peak coordinate in cluster falls within region of brain deactivation in response to vestibular stimulation (**Figure 3** and **Table 1**).*

past work investigating vestibular processing in astronauts. Two previous studies suggest changes from pre- to post-spaceflight in resting-state (Demertzi et al., 2016) and task-based connectivity (Pechenkova et al., 2019) in brain networks that support vestibular function. Our past work has identified disrupted white matter structural connectivity in several tracts that underlie sensory integration and vestibular processes and associations of these brain changes with balance declines (Lee et al., 2019b). For instance, we found that astronauts with the *largest* spaceflight-associated balance disruptions also had the *greatest* white matter declines in the superior longitudinal fasciculus (Lee et al., 2019b), which connects the temporoparietal and prefrontal cortices and is thought to subserve vestibular functions (Spena et al., 2006). However, no studies to date have tested spaceflight-related changes in functional brain activity during processing of vestibular information. To address this critical literature gap, an ongoing prospective study by our group is measuring brain activity with the pneumatic skull tap paradigm at two time points before and four time points after astronauts complete ISS missions. Comparing these results with the present work will help to elucidate how additional microgravity factors not induced by bed rest (e.g., an altered gravitational vector) might affect the neural correlates of vestibular processing.

CONCLUSION

Here we demonstrate the feasibility of assessing longitudinal neural vestibular changes following 30 days of HDBR + CO_2. We identify support for specific effects of combined HDBR + CO_2 on vestibular processing, adaptive plasticity of the vestibular system during HDBR + CO_2 followed by fast and slow recovery, and relationships between adaptive plasticity and spared behavioral performance post-HDBR + CO_2. We note some differences between neural processing of vestibular information for HDBR + CO_2 versus HDBR subjects, as well as implications for dependence on visual cues during balance for SANs versus no-SANS subjects. Together, these findings contribute to understanding of how the vestibular system adapts to altered sensory inputs and to understanding of how spaceflight may influence the neural correlates of vestibular processing.

DATA AVAILABILITY STATEMENT

The raw data supporting the conclusions of this article will be made available by the authors, without undue reservation, to any qualified researcher.

ETHICS STATEMENT

The studies involving human participants were reviewed and approved by the local ethical commission of the regional medical association, Ärztekammer Nordrhein, as well as the University of Florida and NASA Institutional Review Boards. The patients/participants provided their written informed consent to participate in this study.

AUTHOR CONTRIBUTIONS

KH analyzed the vestibular fMRI data and mobility/balance behavioral data, created the figures and tables, and wrote the manuscript. JL collected and managed the data and participated in manuscript preparation. NG collected and analyzed the data. IK participated in project design and software development. YD collected and analyzed the data. JB, AM, and RS designed the project, secured funding, and led the interpretation and discussion of the results. All authors participated in revision of the manuscript.

FUNDING

This work was supported by grants to RS, AM, and JB from the National Aeronautics and Space Administration (NASA; 80NSSC17K0021), the National Space Biomedical Research Institute (NSBRI; NCC 9-58 and SA02802), and the National Institutes of Health and National Center for Advancing Translational Sciences (1UL1RR029876-01). Additionally, during completion of this work KH was supported by a National Science Foundation Graduate Research Fellowship under Grant Nos. DGE-1315138 and DGE-1842473, as well as training grant NIH T32-NS082128.

ACKNOWLEDGMENTS

The authors wish to gratefully acknowledge those at the: envihab facility in Cologne, Germany, including Dr. Edwin Mulder, the VaPER study staff, and the bed rest participants who volunteered their time, without whom this project would not have been possible.

REFERENCES

Ashburner, J., Barnes, G., Chen, C., Daunizeau, J., Flandin, G., Friston, K., et al. (2016). *SPM12 Manual*. Available at: http://web.mit.edu/spm_v12/manual.pdf (accessed September 2, 2019).

Assländer, L., and Peterka, R. J. (2014). Sensory reweighting dynamics in human postural control. *J. Neurophysiol.* 111, 1852–1864. doi: 10.1152/jn.00669.2013

Atkinson, J. L., Anderson, R. E., and Sundt, T. M. Jr. (1990). The effect of carbon dioxide on the diameter of brain capillaries. *Brain Res.* 517, 333–340. doi: 10.1016/0006-8993(90)91046-j

Bhogal, A. A., Philippens, M. E., Siero, J. C., Fisher, J. A., Petersen, E. T., Luijten, P. R., et al. (2015). Examining the regional and cerebral depth-dependent BOLD cerebrovascular reactivity response at 7 T. *Neuroimage* 114, 239–248. doi: 10.1016/j.neuroimage.2015.04.014

Biswal, B. B., Mennes, M., Zuo, X.-N., Gohel, S., Kelly, C., Smith, S. M., et al. (2010). Toward discovery science of human brain function. *Proc. Natl. Acad. Sci. U.S.A.* 107, 4734–4739. doi: 10.1073/pnas.0911855107

Bles, W., Jong, J. M. V., and Wit, G. D. (1984). Somatosensory compensation for loss of labyrinthine function. *Acta Otolaryngol.* 97, 213–221. doi: 10.3109/00016488409130982

Boyle, R., Mensinger, A. F., Yoshida, K., Usui, S., Intravaia, A., Tricas, T., et al. (2001). Neural readaptation to Earth's gravity following return from space. *J. Neurophysiol.* 86, 2118–2122. doi: 10.1152/jn.2001.86.4.2118

Carriot, J., Jamali, M., and Cullen, K. E. (2015). Rapid adaptation of multisensory integration in vestibular pathways. *Front. Syst. Neurosci.* 9:59. doi: 10.3389/fnsys.2015.00059

Cassady, K., Koppelmans, V., Reuter-Lorenz, P., De Dios, Y., Gadd, N., Wood, S., et al. (2016). Effects of a spaceflight analog environment on brain connectivity and behavior. *Neuroimage* 141, 18–30. doi: 10.1016/j.neuroimage.2016.07.029

Cohen, H. S., Kimball, K. T., Mulavara, A. P., Bloomberg, J. J., and Paloski, W. H. (2012). Posturography and locomotor tests of dynamic balance after long-duration spaceflight. *J. Vestib. Res.* 22, 191–196. doi: 10.3233/VES-2012-0456

Corfield, D., Murphy, K., Josephs, O., Adams, L., and Turner, R. (2001). Does hypercapnia-induced cerebral vasodilation modulate the hemodynamic response to neural activation? *Neuroimage* 13, 1207–1211. doi: 10.1006/nimg.2001.0760

Costafreda, S. G., Brammer, M. J., Vêncio, R. Z., Mourao, M. L., Portela, L. A., De Castro, C. C., et al. (2007). Multisite fMRI reproducibility of a motor task using identical MR systems. *J. Magn. Reson. Imaging* 26, 1122–1126. doi: 10.1002/jmri.21118

Demertzi, A., Van Ombergen, A., Tomilovskaya, E., Jeurissen, B., Pechenkova, E., Di Perri, C., et al. (2016). Cortical reorganization in an astronaut's brain after long-duration spaceflight. *Brain Struct. Funct.* 221, 2873–2876. doi: 10.1007/s00429-015-1054-3

Diedrichsen, J. (2006). A spatially unbiased atlas template of the human cerebellum. *Neuroimage* 33, 127–138. doi: 10.1016/j.neuroimage.2006.05.056

Diedrichsen, J., Balsters, J. H., Flavell, J., Cussans, E., and Ramnani, N. (2009). A probabilistic MR atlas of the human cerebellum. *Neuroimage* 46, 39–46. doi: 10.1016/j.neuroimage.2009.01.045

Dieringer, N. (1995). 'Vestibular compensation': neural plasticity and its relations to functional recovery after labyrinthine lesions in frogs and other vertebrates. *Prog. Neurobiol.* 46, 97–129. doi: 10.1016/0301-0082(94)00063-n

Fredrickson, J., Schwarz, D., and Kornhuber, H. (1966). Convergence and interaction of vestibular and deep somatic afferents upon neurons in the vestibular nuclei of the cat. *Acta Otolaryngol.* 61, 168–188. doi: 10.3109/00016486609127054

Gläscher, J., and Gitelman, D. (2008). *Contrast Weights in Flexible Factorial Design with Multiple Groups of Subjects* (London: SPM), 1–12.

Gountouna, V.-E., Job, D. E., Mcintosh, A. M., Moorhead, T. W. J., Lymer, G. K. L., Whalley, H. C., et al. (2010). Functional magnetic resonance imaging (fMRI) reproducibility and variance components across visits and scanning sites with a finger tapping task. *Neuroimage* 49, 552–560. doi: 10.1016/j.neuroimage.2009.07.026

Hargens, A. R., and Richardson, S. (2009). Cardiovascular adaptations, fluid shifts, and countermeasures related to space flight. *Respir. Physiol. Neurobiol.* 169, S30–S33. doi: 10.1016/j.resp.2009.07.005

Horak, F., and Hlavacka, F. (2001). Somatosensory loss increases vestibulospinal sensitivity. *J. Neurophysiol.* 86, 575–585. doi: 10.1152/jn.2001.86.2.575

Jian, B., Shintani, T., Emanuel, B., and Yates, B. (2002). Convergence of limb, visceral, and vertical semicircular canal or otolith inputs onto vestibular nucleus neurons. *Exp. Brain Res.* 144, 247–257. doi: 10.1007/s00221-002-1042-8

Karim, H., Fuhrman, S. I., Furman, J. M., and Huppert, T. J. (2013). Neuroimaging to detect cortical projection of vestibular response to caloric stimulation in young and older adults using functional near-infrared spectroscopy (fNIRS). *Neuroimage* 76, 1–10. doi: 10.1016/j.neuroimage.2013.02.061

Koppelmans, V., Bloomberg, J. J., De Dios, Y. E., Wood, S. J., Reuter-Lorenz, P. A., Kofman, I. S., et al. (2017). Brain plasticity and sensorimotor deterioration as a function of 70 days head down tilt bed rest. *PLoS One* 12:e0182236. doi: 10.1371/journal.pone.0182236

Koppelmans, V., Mulavara, A. P., Yuan, P., Cassady, K. E., Cooke, K. A., Wood, S. J., et al. (2015). Exercise as potential countermeasure for the effects of 70 days of bed rest on cognitive and sensorimotor performance. *Front. Syst. Neurosci.* 9:121. doi: 10.3389/fnsys.2015.00121

Kurth, F., Luders, E., and Gaser, C. (2010). *VBM8 Toolbox Manual*. Jena: University of Jena.

Laurie, S. S., Macias, B. R., Dunn, J. T., Young, M., Stern, C., Lee, S. M., et al. (2019). Optic disc edema after 30 days of strict head-down tilt bed rest. *Ophthalmology* 126, 467–468. doi: 10.1016/j.ophtha.2018.09.042

Law, J., Van Baalen, M., Foy, M., Mason, S. S., Mendez, C., Wear, M. L., et al. (2014). Relationship between carbon dioxide levels and reported headaches on the international space station. *J. Occup. Environ. Med.* 56, 477–483. doi: 10.1097/JOM.0000000000000158

LeBlanc, A., Rowe, R., Schneider, V., Evans, H., and Hedrick, T. (1995). Regional muscle loss after short duration spaceflight. *Aviat. Space Environ. Med.* 66, 1151–1154.

Lee, A. G., Tarver, W. J., Mader, T. H., Gibson, C. R., Hart, S. F., and Otto, C. A. (2016). Neuro-ophthalmology of space flight. *J. Neuroophthalmol.* 36, 85–91. doi: 10.1097/WNO.0000000000000334

Lee, J. K., De Dios, Y. E., Kofman, I. S., Mulavara, A. P., Bloomberg, J., and Seidler, R. D. (2019a). Head down tilt bed rest plus elevated CO2 as a spaceflight analog: effects on cognitive and sensorimotor performance. *Front. Hum. Neurosci.* 13:355. doi: 10.3389/fnhum.2019.00355

Lee, J. K., Koppelmans, V., Riascos, R. F., Hasan, K. M., Pasternak, O., Mulavara, A. P., et al. (2019b). Spaceflight-associated brain white matter microstructural changes and intracranial fluid redistribution. *JAMA Neurol.* 76, 412–419. doi: 10.1001/jamaneurol.2018.4882

Lin, C.-C., Barker, J. W., Sparto, P. J., Furman, J. M., and Huppert, T. J. (2017). Functional near-infrared spectroscopy (fNIRS) brain imaging of multi-sensory integration during computerized dynamic posturography in middle-aged and older adults. *Exp. Brain Res.* 235, 1247–1256. doi: 10.1007/s00221-017-4893-8

Lopez, C., Blanke, O., and Mast, F. (2012a). The human vestibular cortex revealed by coordinate-based activation likelihood estimation meta-analysis. *Neuroscience* 212, 159–179. doi: 10.1016/j.neuroscience.2012.03.028

Lopez, C., Schreyer, H.-M., Preuss, N., and Mast, F. W. (2012b). Vestibular stimulation modifies the body schema. *Neuropsychologia* 50, 1830–1837. doi: 10.1016/j.neuropsychologia.2012.04.008

Lowrey, C. R., Perry, S. D., Strzalkowski, N. D., Williams, D. R., Wood, S. J., and Bent, L. R. (2014). Selective skin sensitivity changes and sensory reweighting following short-duration space flight. *J. Appl. Physiol.* 116, 683–692. doi: 10.1152/japplphysiol.01200.2013

Manzey, D., and Lorenz, B. (1998). Effects of chronically elevated CO2 on mental performance during 26 days of confinement. *Aviat. Space Environ. Med.* 69, 506–514.

Miller, C. A., Kofman, I. S., Brady, R. R., May-Phillips, T. R., Batson, C. D., Lawrence, E. L., et al. (2018). Functional task and balance performance in bed rest subjects and astronauts. *Aerosp. Med. Hum. Perform.* 89, 805–815. doi: 10.3357/AMHP.5039.2018

Moore, S. T., Macdougall, H. G., and Paloski, W. H. (2010). Effects of head-down bed rest and artificial gravity on spatial orientation. *Exp. Brain Res.* 204, 617–622. doi: 10.1007/s00221-010-2317-0

Mulavara, A., Peters, B., Miller, C., Kofman, I., Reschke, M., Taylor, L., et al. (2018). Physiological and functional alterations after spaceflight and bed rest. *Med. Sci. Sports Exerc.* 50, 1961–1980. doi: 10.1249/MSS.0000000000001615

Mulavara, A., Ruttley, T., Cohen, H., Peters, B., Miller, C., Brady, R., et al. (2012). Vestibular-somatosensory convergence in head movement control during locomotion after long-duration space flight. *J. Vestib. Res.* 22, 153–166. doi: 10.3233/ves-2011-0435

Mulavara, A. P., Feiveson, A. H., Fiedler, J., Cohen, H., Peters, B. T., Miller, C., et al. (2010). Locomotor function after long-duration space flight: effects and motor learning during recovery. *Exp. Brain Res.* 202, 649–659. doi: 10.1007/s00221-010-2171-0

Mulder, E., Linnarsson, D., Paloski, W., Rittweger, J., Wuyts, F., Zange, J., et al. (2014). Effects of five days of bed rest with and without exercise countermeasure on postural stability and gait. *J. Musculoskelet. Neuronal Interact.* 14, 359–366.

Nichols, T. E., and Holmes, A. P. (2002). Nonparametric permutation tests for functional neuroimaging: a primer with examples. *Hum. Brain Mapp.* 15, 1–25. doi: 10.1002/hbm.1058

Noble, S., Scheinost, D., Finn, E. S., Shen, X., Papademetris, X., Mcewen, S. C., et al. (2017). Multisite reliability of MR-based functional connectivity. *Neuroimage* 146, 959–970. doi: 10.1016/j.neuroimage.2016.10.020

Noohi, F., Kinnaird, C., De Dios, Y., Kofman, I., Wood, S. J., Bloomberg, J. J., et al. (2019). Deactivation of somatosensory and visual cortices during vestibular stimulation is associated with older age and poorer balance. *PLoS One* 14:e0221954. doi: 10.1371/journal.pone.0221954

Noohi, F., Kinnaird, C., Dedios, Y., Kofman, I. S., Wood, S., Bloomberg, J., et al. (2017). Functional brain activation in response to a clinical vestibular test correlates with balance. *Front. Syst. Neurosci.* 11:11. doi: 10.3389/fnsys.2017.00011

Parker, D., Reschke, M., Arrott, A., Homick, J., and Lichtenberg, B. (1985). Otolith tilt-translation reinterpretation following prolonged weightlessness: implications for preflight training. *Aviat. Space Environ. Med.* 56, 601–606.

Pechenkova, E., Nosikova, I., Rumshiskaya, A., Litvinova, L., Rukavishnikov, I., Mershina, E., et al. (2019). Alterations of functional brain connectivity after long-duration spaceflight as revealed by fMRI. *Front. Physiol.* 10:761. doi: 10.3389/fphys.2019.00761

R Core Team (2013). *R: A Language and Environment for Statistical Computing*. Vienna: R Foundation for Statistical Computing.

Reschke, M. F., Bloomberg, J. J., Paloski, W. H., Mulavara, A. P., Feiveson, A. H., and Harm, D. L. (2009). Postural reflexes, balance control, and functional mobility with long-duration head-down bed rest. *Aviat. Space Environ. Med.* 80, A45–A54.

Romero, J. E., Coupé, P., Giraud, R., Ta, V.-T., Fonov, V., Park, M. T. M., et al. (2017). CERES: a new cerebellum lobule segmentation method. *Neuroimage* 147, 916–924. doi: 10.1016/j.neuroimage.2016.11.003

Rubin, A., Liedgren, S., Ödkvist, L., Larsby, B., and Aschan, G. (1979). Limb input to the cat vestibular nuclei. *Acta Otolaryngol.* 87, 113–122. doi: 10.3109/00016487909126395

Sakellari, V., Bronstein, A., Corna, S., Hammon, C., Jones, S., and Wolsley, C. (1997). The effects of hyperventilation on postural control mechanisms. *Brain J. Neurol.* 120, 1659–1673. doi: 10.1093/brain/120.9.1659

Schlindwein, P., Mueller, M., Bauermann, T., Brandt, T., Stoeter, P., and Dieterich, M. (2008). Cortical representation of saccular vestibular stimulation: VEMPs in fMRI. *Neuroimage* 39, 19–31. doi: 10.1016/j.neuroimage.2007.08.016

Sibonga, J. D. (2013). Spaceflight-induced bone loss: is there an osteoporosis risk? *Curr. Osteoporosis Rep.* 11, 92–98. doi: 10.1007/s11914-013-0136-5

Spena, G., Gatignol, P., Capelle, L., and Duffau, H. (2006). Superior longitudinal fasciculus subserves vestibular network in humans. *Neuroreport* 17, 1403–1406. doi: 10.1097/01.wnr.0000223385.49919.61

Stein, T. (2013). Weight, muscle and bone loss during space flight: another perspective. *Eur. J. Appl. Physiol.* 113, 2171–2181. doi: 10.1007/s00421-012-2548-9

Stenger, M. B., Tarver, W. J., Brunstetter, T., Gibson, C. R., Laurie, S. S., Lee, S., et al. (2017). *Evidence Report: Risk of Spaceflight Associated Neuro-Ocular Syndrome (SANS)*. Available at: https://humanresearchroadmap.nasa.gov/evidence/reports/SANS.pdf?rnd=0.434276635495143 (accessed February 15, 2018).

Wood, S. J., Paloski, W. H., and Clark, J. B. (2015). Assessing sensorimotor function following ISS with computerized dynamic posturography. *Aerosp. Med. Hum. Perform.* 86, A45–A53. doi: 10.3357/AMHP.EC07.2015

Yates, B., Jian, B., Cotter, L., and Cass, S. (2000). Responses of vestibular nucleus neurons to tilt following chronic bilateral removal of vestibular inputs. *Exp. Brain Res.* 130, 151–158. doi: 10.1007/s002219900238

Young, L. R., Oman, C. M., Watt, D., Money, K. E., and Lichtenberg, B. K. (1984). Spatial orientation in weightlessness and readaptation to earth's gravity. *Science* 225, 205–208. doi: 10.1126/science.6610215

Yuan, P., Koppelmans, V., Reuter-Lorenz, P., De Dios, Y., Gadd, N., Riascos, R., et al. (2018a). Change of cortical foot activation following 70 days of head-down bed rest. *J. Neurophysiol.* 119, 2145–2152. doi: 10.1152/jn.00693.2017

Yuan, P., Koppelmans, V., Reuter-Lorenz, P., De Dios, Y., Gadd, N., Wood, S., et al. (2018b). Vestibular brain changes within 70 days of head down bed rest. *Hum. Brain Mapp.* 39, 2753–2763. doi: 10.1002/hbm.24037

Yuan, P., Koppelmans, V., Reuter-Lorenz, P. A., De Dios, Y. E., Gadd, N. E., Wood, S. J., et al. (2016). Increased brain activation for dual tasking with 70-days head-down bed rest. *Front. Syst. Neurosci.* 10:71. doi: 10.3389/fnsys.2016.00071

Zhou, H., Saidel, G. M., and LaManna, J. C. (2008). Cerebral blood flow adaptation to chronic hypoxia. *Adv Exp Med Biol.* 614, 371–377. doi: 10.1007/978-0-387-74911-2_41

Zu Eulenburg, P., Caspers, S., Roski, C., and Eickhoff, S. B. (2012). Meta-analytical definition and functional connectivity of the human vestibular cortex. *Neuroimage* 60, 162–169. doi: 10.1016/j.neuroimage.2011.12.032

Conflict of Interest: The authors declare that the research was conducted in the absence of any commercial or financial relationships that could be construed as a potential conflict of interest.

The reviewer RG declared a past co-authorship with several of the authors AM and JB to the handling Editor.

frontiers in Systems Neuroscience

REVIEW
published: 24 January 2020
doi: 10.3389/fnsys.2019.00088

Plasticity in Limbic Regions at Early Time Points in Experimental Models of Tinnitus

Michelle R. Kapolowicz[1,2]* *and Lucien T. Thompson*[3]

[1]Center for Hearing Research, University of California, Irvine, Irvine, CA, United States, [2]Department of Otolaryngology-Head and Neck Surgery, School of Medicine, University of California, Irvine, Irvine, CA, United States, [3]Department of Neurobiology, School of Behavioral and Brain Sciences, The University of Texas at Dallas, Richardson, TX, United States

Tinnitus is one of the most prevalent auditory disorders worldwide, manifesting in both chronic and acute forms. The pathology of tinnitus has been mechanistically linked to induction of harmful neural plasticity stemming from traumatic noise exposure, exposure to ototoxic medications, input deprivation from age-related hearing loss, and in response to injuries or disorders damaging the conductive apparatus of the ears, the cochlear hair cells, the ganglionic cells of the VIIIth cranial nerve, or neurons of the classical auditory pathway which link the cochlear nuclei through the inferior colliculi and medial geniculate nuclei to auditory cortices. Research attempting to more specifically characterize the neural plasticity occurring in tinnitus have used a wide range of techniques, experimental paradigms, and sampled at different windows of time to reach different conclusions about why and which specific brain regions are crucial in the induction or ongoing maintenance of tinnitus-related plasticity. Despite differences in experimental methodologies, evidence reveals similar findings that strongly suggest that immediate and prolonged activation of non-classical auditory structures (i.e., amygdala, hippocampus, and cingulate cortex) may contribute to the initiation and development of tinnitus in addition to the ongoing maintenance of this devastating condition. The overarching focus of this review, therefore, is to highlight findings from the field supporting the hypothesis that abnormal early activation of non-classical sensory limbic regions are involved in tinnitus induction, with activation of these regions continuing to occur at different temporal stages. Since initial/early stages of tinnitus are difficult to control and to quantify in human clinical populations, a number of different animal paradigms have been developed and assessed in experimental investigations. Reviews of traumatic noise exposure and ototoxic doses of sodium salicylate, the most prevalently used animal models to induce experimental tinnitus, indicate early limbic

OPEN ACCESS

Edited by:
Josef P. Rauschecker, Georgetown University, United States

Reviewed by:
Marco Cambiaghi, University of Verona, Italy
Wilhelmina Mulders, University of Western Australia, Australia

***Correspondence:**
Michelle R. Kapolowicz
mkapolow@hs.uci.edu

Received: 24 September 2019
Accepted: 23 December 2019
Published: 24 January 2020

Citation:
Kapolowicz MR and Thompson LT (2020) Plasticity in Limbic Regions at Early Time Points in Experimental Models of Tinnitus. Front. Syst. Neurosci. 13:88. doi: 10.3389/fnsys.2019.00088

Abbreviations: ABR, acoustically evoked brainstem responses; AC, auditory cortex; ACC, anterior cingulate cortex; ALFF, amplitude of low-frequency fluctuations; Arc (arg3.1), activity-related cytoskeletal protein; BA, basal amygdala; BLA, basolateral amygdala; CA, cornu ammonis; CeA, central amygdala; CORT, corticosterone; dB SPL, decibels, sound pressure level; DCS, D-cycloserine; DCX, doublecortin; DG, dentate gyrus; Egr-1, early growth response 1; HPA, hypothalamic-pituitary-adrenal; IEG, immediate-early gene; IHC, inner hair cells; i.p., intraperitoneally; LA, lateral amygdala; LFP, local field potential; MeA, medial amygdala; MGN, medial geniculate nucleus; NBW, narrow band white noise; NR2B, NMDA receptor subunit 2B.

system plasticity (within hours, minutes, or days after initial insult), supports subsequent plasticity in other auditory regions, and contributes to the pathophysiology of tinnitus. Understanding this early plasticity presents additional opportunities for intervention to reduce or eliminate tinnitus from the human condition.

Keywords: tinnitus, amygdala, hippocampus, cingulate cortex, noise trauma, salicylate

INTRODUCTION

Tinnitus is described as a perception of sound(s), such as ringing, buzzing, or hissing, when no external sound is present. Tinnitus is the most widespread auditory disorder, steadily growing in incidence due to a rise in traumatic noise exposure (e.g., from combat, recreation, and work) and to an increase in the aging population (Rauschecker et al., 2010). Despite a growing amount of research effort focused on tinnitus, there still remains no consistent treatment or cure for this condition.

Systems-level approaches using neurophysiological and imaging techniques have shown numerous brain regions exhibit hyperactivity in tinnitus, in both classic lemniscal auditory regions (Arnold et al., 1996; Melcher et al., 2009) as well as in non-classic regions (Lockwood et al., 1998; Schlee et al., 2009) in human patients diagnosed with tinnitus. Despite the wide range of brain regions and networks seemingly altered in tinnitus, there is considerable disagreement in the literature as to where tinnitus initially manifests; i.e., there is no consensus as to the specific mechanisms or loci involved in the generation of tinnitus. While it is widely agreed that tinnitus is often triggered by cochlear damage resulting in maladaptive plasticity in the central auditory system (Mühlnickel et al., 1998), general scientific or clinical consensus regarding the consequences of this maladaptation has not emerged.

Overwhelming evidence shows that sensorineural hearing loss caused by either noise trauma (Dobie, 2008; Kujawa and Liberman, 2009) or exposure to ototoxic drugs, such as salicylate (Stypulkowski, 1990; Bisht and Bist, 2011; Yorgason et al., 2011), may result in a reduction in transmission of neural activity from the cochlea to the central auditory system. Consequently, activity in the central auditory system is enhanced at suprathreshold intensities. This compensatory increase in the central auditory system due to the loss of sensory input led to the dominant "central gain enhancement hypothesis" as a means to explain a potential mechanism for tinnitus induction (for a review, see Auerbach et al., 2014). Notably, Auerbach et al. (2014) also discuss central gain enhancement in non-lemniscal limbic regions, including the amygdala. Since debilitating tinnitus is often accompanied by negative emotions including anxiety, stress, depression, and sleep disturbances (Rizzardo et al., 1998), it is not surprising that evidence has accumulated showing that the amygdala, in addition to classic auditory structures, can be involved in tinnitus (e.g., Crippa et al., 2010). The amygdala has been widely accepted for its role in processing aversive auditory stimuli (e.g., Zald and Pardo, 2002), though alternative findings have been reported regarding auditory fear conditioning (Weinberger, 2011). The amygdala has reciprocal connections to the medial geniculate nucleus (MGN) and auditory cortex (A1; LeDoux and Farb, 1991). For example, it has been shown that when salicylate is applied locally to the amygdala, local field potential (LFP) responses in the A1 are greatly enhanced (Chen et al., 2012), consistent with the notion of central gain enhancement involving a limbic region of the brain.

Other hypotheses involving the aberrant filtering of auditory information by limbic regions have been put forth to explain the origin of tinnitus. Jastreboff and Jastreboff (2000) proposed that limbic hyperactivity observed in tinnitus patients plays a limited role, with this hyperactivity specifically causing the emotional reactions in tinnitus. However, Rauschecker et al. (2010) proposed that if limbic structures fail to block hyperactive signals generated in classic auditory structures, this "filter failure" leads to chronic forms of tinnitus. Both models assume that cortical regions are responsible for the origin of tinnitus. The latter model also asserts that certain limbic regions are responsible for the ability to cancel the tinnitus percept. Specifically, certain limbic regions may serve an inhibitory gating role for tinnitus perception by functioning as part of a feedback pathway from the amygdala to the auditory system. This inhibition may suppress tinnitus subcortically prior to reaching the A1 and consciousness. Rauschecker et al. (2010) focused on data from various human imaging studies, which give a clear picture of brain states well after the initial stages of tinnitus, but do not reflect potential plastic changes occurring at much earlier time points that can contribute to the initiation as well as the maintenance of tinnitus. Since humans do not present clinically until the disorder is readily apparent, assessment of early plasticity is best characterized in animal models of tinnitus (see **Figure 1** for diagram showing established connections linking known auditory structures with limbic structures).

Kraus and Canlon (2012) elaborated on the importance of limbic involvement, citing studies reporting evidence for reciprocal interactions between auditory areas and limbic regions contributing to the generation of tinnitus (e.g., Mühlau et al., 2006). Kraus and Canlon (2012) also discussed the potential role of limbic involvement in the stabilization or cancellation of tinnitus (as proposed by Rauschecker et al., 2010), noting that, since limbic and auditory systems are interconnected, tinnitus can affect emotional as well as cognitive processing, which can, in turn, affect auditory percepts. Kraus and Canlon (2012) focused their review on tinnitus linked to traumatic noise exposure. Although noise trauma is a common cause of tinnitus, it is important to determine whether other common causes of tinnitus, such as ototoxic medications, share similar mechanisms and time courses for development.

Evidence supporting the hypothesis that limbic regions play a strong role in the generation, induction, maintenance, and suppression of tinnitus has accrued, suggesting the limbic system

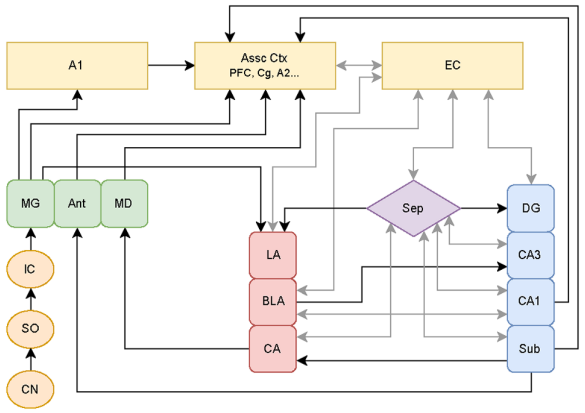

FIGURE 1 | Schematic of classical and non-classical auditory pathways. The medial geniculate nucleus of the thalamus (MG) can follow the classical auditory pathway to the primary auditory cortex (A1), or it can branch off to directly activate limbic pathways. These pathways may be stimulated simultaneously with parallel processing occurring between the amygdala-hippocampal circuits. Additional abbreviations: cochlear nucleus (CN), superior olive (SO), inferior colliculus (IC), anterior (Ant), medial dorsal (MD) thalamic nuclei, association cortices (Assoc Ctx), prefrontal cortex (PFC), cingulate (Cg), secondary auditory cortex (A2), entorhinal cortex (EC), septum (Sep), lateral (LA), basolateral (BLA), and central (CA) amygdaloid nuclei, and hippocampal subregions consisting of dentate gyrus (DG), cornu ammonis 3 (CA3), cornu ammonis 1 (CA1), subiculum (Sub). Circuitry compiled from established auditory-limbic connections as reported in Møller et al. (1992), Møller and Rollins (2002) and Kandratavicius et al. (2012) using draw.io online software (www.draw.io).

could be considered as a viable target for tinnitus treatment. Three key limbic regions are strongly implicated: the amygdaloid complex, the hippocampus, and the cingulate cortex. This review summarizes plasticity, excitation, and inhibition across early stages of tinnitus pathology resulting from either acute traumatic noise exposure or sodium salicylate treatment (the two most commonly used inductive paradigms in animals) in these key limbic regions. Hyperexcitability and other forms of plasticity within the amygdala, hippocampus, or cingulate cortex often occur immediately after initial exposure to either traumatic noise or to an ototoxic substance, and continues until well after behavioral evidence of tinnitus has been observed. Enhanced excitability within these limbic regions does not always co-occur with markers depicting decreases in inhibition (disinhibition). Remarkably, only a few studies to date have measured potential changes in inhibition in these key limbic regions in models of the development of tinnitus, so it is not currently possible to accurately characterize specific changes in inhibition in the early stages of tinnitus. The available evidence, however, supports the hypothesis that a maladaptive down-regulation of GABAergic neurotransmission occurs throughout the central auditory pathway in tinnitus (Wang et al., 2011; Richardson et al., 2012).

ANIMAL MODELS OF TINNITUS

Given the growing population of tinnitus sufferers worldwide, it has become essential to develop reliable animal models, both to understand its underlying mechanisms and in hope of developing treatments that can reverse tinnitus' maladaptive plasticity. Such models permit approaches beyond what is possible in human patients, with experiments capable of addressing individual neurons, reduced or enhanced networks, as well as characterizing the disorder at multiple time points. Animal models allow for use of invasive procedures with high spatial and temporal resolution. As noted, the two most common methods implemented to induce tinnitus in animal models are exposure to traumatic noise and treatment with high doses of sodium salicylate. These methods cause cochlear damage, which triggers a sequence of events leading to the development of tinnitus in both humans and in animal models. Both exposure to traumatic noise and treatment with high doses of sodium salicylate cause tinnitus in human populations, aiding translation from the laboratory to the clinic. For a detailed review of these two models, see von der Behrens (2014).

Traumatic noise exposure is one of the most common risk factors for tinnitus in human populations. Traumatic noise exposure has also been well established to induce tinnitus in animal models (e.g., Brozoski and Bauer, 2005; Turner et al., 2006; Engineer et al., 2011), though the parameters for induction are variable. Typically, a specific tone frequency is played at a high volume for 1–2 h either unilaterally or bilaterally while the animal is under anesthesia. Few studies, however, expose animals while they are freely behaving (which would be more analogous to human exposure conditions), hence the results from the noise trauma exposure are potentially confounded with the effects of anesthesia. For additional information on the role of anesthesia in tinnitus development, see von der Behrens (2014).

Since the probability of developing tinnitus after traumatic noise exposure is relatively inconsistent, researchers have also utilized paradigms consisting of treatment with ototoxic drugs, with sodium salicylate the most commonly used in animal models (Cazals, 2000). High doses of sodium salicylate, the active ingredient in aspirin, can cause temporary hearing loss and also consistently induces reversible tinnitus in both humans and animals (Jastreboff et al., 1988; Day et al., 1989; Jastreboff, 1990; Brien, 1993; Bauer et al., 1999; Chen et al., 2012). Salicylate inhibits cyclooxygenase and stimulates arachidonic acid production, which has been shown to facilitate NMDA receptor-mediated responses to glutamate released spontaneously by inner hair cells (IHC; Ruel et al., 2008). Treatment with salicylate is a useful paradigm to infer whether the neuronal enhancement seen after noise-induced hearing loss is also consistently seen in animals that are experiencing tinnitus, and its effects are rapid (Auerbach et al., 2014). For a thorough review of the salicylate model of tinnitus, see Stolzberg et al. (2012).

Animal models of tinnitus should ideally model human pathogenesis. It is widely suspected that traumatic noise exposure is the most common causative event for human tinnitus populations, which supports using an acoustic trauma paradigm to induce tinnitus in animals in preference over using an ototoxic substance. However, tinnitus induction *via* high doses of salicylate in animals yields a rapid (and higher percentage) onset of tinnitus. Given the widespread use of both methods

for tinnitus induction in animal models, this review will cover the neural correlates of both models within the amygdaloid complex, the hippocampus, and the cingulate cortex. Evidence will be summarized supporting the notion that outcomes from both methods of induction are consistently similar at early time points post-treatment. This review will also cover specific cases of animal models of noise trauma exposure which are not directly linked to tinnitus. Given that noise trauma is the most common cause of tinnitus and hearing loss, such animal models are important to be considered given that results from these noise trauma paradigms share similarities with reports from studies where behavioral evidence of tinnitus was also provided. Interestingly, while relatively homogenous outcomes are observed in these limbic structures (discussed below), traumatic noise exposure and salicylate affect classic auditory structures, including the cochlea and the central auditory system, in a much more heterogeneous manner. For more information on the divergence of observed mechanisms and patterns of maladaptive plasticity resulting from these two inductive paradigms in classical auditory pathway regions, see Eggermont (2016).

KEY LIMBIC REGIONS INVOLVED IN THE PATHOPHYSIOLOGY OF TINNITUS

Amygdaloid Complex

The amygdaloid complex (amygdala) is noted for processing emotionally salient information (Phelps and LeDoux, 2005). The amygdala is strongly involved in a range of behavioral functions and psychiatric disorders, and it has been implicated in tinnitus (e.g., De Ridder et al., 2006). The amygdala is divided into the lateral (LA), basal (BA), central (CeA) and medial (MeA) nuclei (LeDoux, 2007). The LA receives input from multiple sensory systems; the MeA receives information from the olfactory bulb; the CeA receives input from the viscerosensory cortex and sensory brainstem; the BA receives input from polymodal association cortex areas and from regions processing memory and cognition, i.e., it is linked functionally with the hippocampus (Kraus and Canlon, 2012). The LA is important in sound processing because it receives direct neuronal inputs from the MGN and from secondary auditory association areas (Sah et al., 2003; LeDoux, 2007). Additionally, auditory information reaching the LA through the MGN can signal this region to activate the hippocampus *via* output projections, which influence the sensitivity of neurons in the A1 (Chavez et al., 2009). Amygdalar responses to sound depend on how important the sound is in the individual's sensory environment (Klinge et al., 2010), and it is sensitive to stimuli with emotional valence (Anders et al., 2008). Activation of BA and LA neurons is critically involved in the maintenance of emotional salience (Sengupta et al., 2018) and in the processing of emotionally salient stimuli by hippocampal neurons (McIntyre et al., 2005; Farmer and Thompson, 2012; Lovitz and Thompson, 2015).

Hippocampus

The hippocampus is widely known for its involvement in learning and the formation of new memories. It is active in explicit or declarative memory (Dickerson and Eichenbaum, 2010), including episodic and semantic memory. The hippocampus is also involved with spatial memory (Thompson and Best, 1989, 1990; O'Keefe et al., 1998; Goble et al., 2009). Hippocampal synaptic integrity has also been shown to be impaired by hearing loss (Yu et al., 2011), and hippocampal neurogenesis is decreased by acoustic trauma (Liu et al., 2016). The hippocampus consists of several subregions: dentate gyrus (DG), cornu ammonis (CA) CA1, CA2, CA3, CA4 and adjacent subicular subregions. Major excitatory afferents enter the hippocampus from the entorhinal cortex (EC) *via* the perforant path, projecting to granule cells in the DG, which then project *via* the mossy fibers to CA3, with CA3 neurons projecting to CA1 *via* Schaffer collaterals, with major cortical efferents projecting from CA1 neurons; CA1 also projects to the subiculum, which has outputs to subcortical regions (Amaral et al., 2007). Once information leaves the hippocampus (*via* either CA1 or subicular projections), it can be passed directly to the lateral, basal and medial nuclei of the amygdala as well as to its intercalated cells (Kishi et al., 2006; Cenquizca and Swanson, 2007). The amygdala, *via* the lateral or basal nuclei, has direct projections to hippocampus as well *via* CA3, CA1 or the subiculum as well as indirect projections *via* the EC (Kraus and Canlon, 2012). Like the amygdala, the hippocampus also responds to sound by either direct or indirect input from various auditory association cortices (Mohedano-Moriano et al., 2007; Munoz-Lopez et al., 2010). There are also direct connections from CA1 to the auditory association cortex as well as to the primary A1 (Cenquizca and Swanson, 2007) which are involved in the formation of long-term auditory memories (Squire et al., 2001). The hippocampus is also indirectly connected to auditory regions *via* the front medial cortex, the insula and the amygdala (Kraus and Canlon, 2012).

Cingulate Cortex

The cingulate cortex is involved with emotional responsivity (Hadland et al., 2003; Vogt, 2005). It is also involved in learning (Aly-Mahmoud et al., 2017) and memory (Kozlovskiy et al., 2012). The cingulate has a major role in behavioral drive and regulation of affective behavior, e.g., it is involved in emotional processing and inhibitory control (Shackman et al., 2011; Holloway-Erickson et al., 2012; Xie et al., 2013). The cingulate gyrus is also critically involved in attentional processing and in sleep staging, with greatest activity observed in response to emotionally arousing stimuli in the waking state and during REM sleep periods crucial for memory consolidation (Oniani et al., 1989; Wang and Ikemoto, 2016). Wang and Ikemoto (2016), for example, found an increase in anterior cingulate cortex (ACC) neuronal firing which is influenced by hippocampal ripple activity during sleep and speculated that this aids in memory consolidation. Functional reciprocal connectivity between the ACC and the A1 has also been shown, particularly for auditory attention or by way of ACC-dependent modulation of spontaneous activity in the A1 (Benedict et al., 2002; Hunter et al., 2006; Mulert et al., 2007). The cingulate cortex also has extensive connections with the prefrontal cortex, amygdala, thalamus, and striatum, receives extensive inputs from pain

pathways, and contributes to the corticospinal tract (Vogt et al., 1979; Pandya et al., 1981; Finch et al., 1984; Vogt, 2005). The recognized role of the ACC in the pathophysiology of individuals suffering from chronic pain in the absence of nociceptive inputs (Fuchs et al., 2014; Sellmeijer et al., 2018) is consistent with the ACC also playing a significant role in tinnitus, driving the perceived ringing in the absence of auditory inputs (Chen et al., 2018). Enhanced activity in the cingulate cortex has also been observed in tinnitus distress (Vanneste et al., 2010; Vanneste and De Ridder, 2013).

CENTRAL CHANGES IN TRAUMATIC NOISE-EXPOSED ANIMALS

Amygdala

Supplementary Table S1 compares the species and methodologies used and briefly summarizes the results obtained examining aberrant plasticity in six experimental animal models of traumatic noise exposure in the amygdala at time points ranging from 45 min through 40 days post-exposure.

It was shown in Syrian golden hamsters that traumatic noise exposure with a 10 kHz tone at 125–127 dB SPL (decibels Sound Pressure Level) presented to the left ear for 4 h significantly increased expression of c-fos immunoreactivity in CeA, LA and basolateral amygdala (BLA; Zhang et al., 2003). No laterality of differences were observed other than in CeA, where concentrations were higher ipsilateral to the exposed ear 33–40 days post-exposure. Animals exposed to traumatic noise were also screened for behavioral evidence of tinnitus using a conditioned lick suppression/avoidance paradigm. Hearing loss was measured by examining thresholds of the acoustically evoked brainstem responses (ABR), which reflect differences in sound-induced auditory nerve activity and brainstem activity within the ventral cochlear nucleus (CN) and the ascending auditory nuclei. Zhang et al. (2003) also reported that expression of c-fos in a "stimulated," non-traumatic noise-exposed group (10 kHz tone, 80± dB SPL for 45 min) was increased in CeA, LA, and BLA immediately after this non-traumatic noise exposure, although the magnitude of this increase in this reduced exposure condition was not quantified nor compared across hemispheres. Neuronal expression of the immediate-early gene (IEG) product, c-fos, is one of a family of genes that are rapidly and transiently activated and translated in response to particular stimuli (Gall et al., 1998) and are widely used as a marker of neuronal activity. IEGs represent an early transcriptional and translational response mechanism activated in the first round of cellular responses to stimuli. C-fos plays a role in neuronal plasticity and is expressed when processing or associating novel sensory stimuli (Tischmeyer and Grimm, 1999). The immunocytochemical findings of Zhang et al. (2003) indicate that multiple amygdalar nuclei respond strongly to sound (traumatic and non-traumatic) at early (non-traumatic noise: c-fos upregulation observed immediately after sound exposure) and later time points (traumatic noise: c-fos upregulation observed at time points spanning over a month).

Wallhäusser-Franke et al. (2003) also investigated the effects of noise exposure on c-fos expression in the amygdala after freely behaving Mongolian gerbils were exposed to acute impulse noise exposure. A toy pistol was fired once close to each ear at a reported intensity level of 136–142 dB SPL. Gerbils were sacrificed at varying times post-impulse noise exposure (1, 3, 5 or 7 h). C-fos expressing cells were present bilaterally in MeA, LA and BLA, with the highest expression observed 1 h after noise exposure. C-fos immunoreactivity was only seen in CeA nuclei 7 h post-noise exposure, indicating a non-uniform increase in neuronal excitability in different amygdalar nuclei. Wallhäusser-Franke et al. (2003) also compared c-fos expression in other limbic brain regions, but reported the greatest IEG immunoreactivity was observed in the amygdala after acute impulse noise exposure.

C-fos immunoreactivity was, again, explored in relation to noise exposure by Mahlke and Wallhäusser-Franke (2004) in freely behaving Mongolian gerbils. Gerbils were acutely exposed to narrowband (1/3 octave) white noise (NBW) of 80 ± 5 dB SPL centered on either 1 or 8 kHz with a rise/fall time of 5 ms followed by an 800 ms pause for 10 min. Gerbils were perfused 3 h post-noise stimulation, and higher levels of c-fos expression were observed in LA, but rarely in CeA and minimally in MeA regardless of the noise condition. In addition to c-fos, arg 3.1 (activity-related cytoskeletal protein; also commonly referred to as "Arc"; henceforth, the term "Arc" will be maintained for consistency) immunoreactive neurons were also quantified. Arc is involved in long-term memory consolidation and synaptic plasticity (Plath et al., 2006). Arc mRNA and protein levels are mobilized by intense synaptic activity in glutamatergic neurons in an NMDA-receptor-dependent manner (Link et al., 1995; Steward and Worley, 2001). Arc binds to actin, is trafficked to dendrites, and accumulates at sites of synaptic activity where it is locally translated and induces homeostatic scaling of AMPA receptors and cellular structural modifications (Shepherd et al., 2006). Similar to their findings for c-fos, Mahlke and Wallhäusser-Franke (2004) found that NBW exposure increased Arc expression in LA 3 h post-exposure, with minimal expression observed at that time point in CeA or in MeA. Overall, they found that NBW did not elicit as much immunoreactivity as treatment with salicylate (results for salicylate treatment reported below). Moreover, they found that gerbils passively exposed to ambient background noise displayed comparable results in c-fos and Arc expression to gerbils exposed to NBW.

Singer et al. (2013) investigated BLA changes in Arc regulation in a rat model of tinnitus after varying intensities of sound exposure [80 dB SPL (a non-damaging condition) or more intense 100, 110 or 120 dB SPLs at 10 kHz]. Rats were bilaterally exposed to these sounds under anesthesia for 1–2 h, then sacrificed 6–30 days post-exposure. ABR waveform correlation factors were calculated, and the hearing thresholds of a subset of the animals were taken 6–14 days post-exposure. A further subset of animals was behaviorally trained and analyzed for tinnitus perception using an operant conditioned foraging task. A trend toward increased Arc mRNA expression was reported in the BLA of animals exposed to 110 dB SPL for 1–2 h. A separate group exposed to 120 dB SPL for 1–2 h exhibited behavioral

evidence of tinnitus; on day 14 after this initial noise exposure, these rats expressed reduced Arc mRNA and reduced Arc protein expression in BLA, similar to levels observed in controls. To better characterize this finding, the number of CtBP2/RIBEYE-positive particles in ribbon synapses of the IHC was also measured. Quantification of CtBP2/RIBEYE-positive particles allowed assessment of the degree of deafferentation/degeneration of cochlear hair cells, nerve terminals, and the connecting synapses (Khimich et al., 2005). These findings were related to the integrity of the ABR, and linked to Arc expression in BLA: Singer et al. (2013) observed that a failure to up-regulate Arc occurs after severe ribbon loss and is associated with reduced ABR waves and with behavioral evidence of tinnitus. Singer et al. (2013) also utilized the social stressor paradigm to elevate corticosterone (CORT) levels in rats exposed to 120 dB SPL for 1 h. The social stressor caused CORT levels to elevate within 48 h after the social stressor. Fourteen days after, when hearing capacity was analyzed, the mean ABR wave of the stressed animals showed more consistent maintenance of ABR waveforms compared to controls, indicating that CORT elevation may enable a more stable and persistent responsiveness to sound signals than otherwise would have been achieved. Noise trauma was given 2 days after stress priming Arc expression in groups with either moderate or high CORT levels at time of trauma. Those with significantly lower Arc expression in BLA were animals with higher CORT, while Arc up-regulation was observed with moderate CORT levels. This suggests that moderate stress may positively influence VIIIth nerve IHC ribbon numbers by recruiting Arc up-regulation proportional to the extent of damage at the IHC synapse following acoustic trauma, whereas very high or very low CORT levels at the time of trauma promote less protection from ribbon loss, leading to persistently reduced ABR wave sizes and a failure to up-regulate Arc expression.

Electrophysiological changes in BLA resulting from exposure to a 10 kHz tone at 105 dB SPL for 3 h have also been investigated using multichannel electrode arrays in rats with and without behavioral evidence of tinnitus at 2 and 6 week post-traumatic noise exposure by Zhang et al. (2016). Behavioral evidence of tinnitus was assessed at week 5–6 post-noise exposure using a gap-prepulse inhibition of the acoustic startle paradigm (also referred to as a gap detection acoustic startle reflex). This paradigm, originally suggested for studies involving animal models of tinnitus by Turner et al. (2006), provides a relatively fast screening for evidence of tinnitus in animals by assuming that if a background signal is perceptually similar to the animal's perception of tinnitus, then the animal will show poorer detection of a silent gap embedded in the background signal. Control animals experience the silent gap, and their reflexive startle responses on trials with this gap are lower in amplitude than on trials without the silent gap; in experimental animals the tinnitus "fills in the silence" on some or all gap trials, and their responses are similar to those of controls on non-gap trials. Zhang and colleagues also utilized a conditioned lick suppression paradigm (Pace et al., 2016) to assess behavioral evidence of tinnitus at 7 week post-noise exposure. Here, water-deprived rats were trained to lick a water spout when they heard narrowband sounds in order to receive water as a reward. If rats licked during silent trials, they received a mild foot shock to train them to only lick during narrowband noise trials. Post-noise exposure, rats were considered to have evidence of tinnitus if they increased licking behaviors during silent trials relative to baseline performance. Zhang et al. (2016) found significantly higher spontaneous BLA firing rates in rats with behavioral evidence of noise-induced tinnitus at 6 week post-noise exposure, but no alteration in firing observed at 2 week post-noise exposure when compared with rats that were exposed to the same noise that did not present with behavioral evidence of tinnitus. Essentially, 2 weeks after rats were exposed to traumatic noise, all had significant increases in spontaneous BLA firing rates, independent from behavioral evidence of tinnitus (assessment of behavioral evidence was only reported for weeks 5–7 post-noise exposure); however, spontaneous firing rates from rats without evidence of tinnitus (as reported for weeks 5–7) returned to basal levels 6 week post-noise exposure, whereas spontaneous BLA firing rates of rats presenting with evidence of tinnitus remained elevated. In the same study, Zhang et al. (2016) also reported significantly higher spontaneous neural synchrony in BLA of rats with behavioral evidence of tinnitus as compared to rats without evidence of tinnitus at both 2 and 6 week post-traumatic noise exposure, indicative of additional BLA plasticity in tinnitus.

Kapolowicz and Thompson (2016) also investigated changes in the amygdala after traumatic noise exposure. After bilaterally exposing freely behaving rats to 1 h of traumatic noise (16 kHz, 115 dB SPL), an upregulation of Arc protein expression was observed in the amygdaloid complex within 45–60 min post-noise exposure. To assure that changes were due to traumatic noise exposure rather than to the novelty of exposure to a sustained sound itself (novelty often up-regulates Arc expression in other brain regions), Kapolowicz and Thompson (2016) also tested the effect of non-traumatic noise exposure (16 kHz, 70 dB SPL) for the same duration and found no significant change in Arc protein expression for this condition relative to controls. In an attempt to understand if the observed upregulation of Arc resulting from traumatic noise exposure was linked to disinhibition, potential changes in GAD expression resulting from traumatic noise exposure were also quantified. GAD is the biosynthetic enzyme that catalyzes the decarboxylation of glutamate into the major inhibitory neurotransmitter, GABA, and it is expressed in two isoforms: GAD 65 and GAD 67 (Erlander et al., 1991). Kapolowicz and Thompson (2016) reported no significant changes in GAD 65 + GAD 67 after exposure to acute high-intensity noise. In order to see if the observed upregulation of Arc protein expression was linked to a stress response, Kapolowicz and Thompson (2016) also tested circulating serum CORT levels in rats exposed to traumatic noise at the same time point as animals were sacrificed (45–60 min post-sound exposure), but found no change in CORT when compared to controls at this early time point post-noise exposure. In the same study, the authors were also interested in whether D-cycloserine (DCS), an NMDA NR1 receptor partial agonist, would be able to reduce or prevent traumatic noise-related plastic changes in Arc protein expression. They found that, when intraperitoneally (i.p.) injected 15 min prior to the

start of sound exposure, acute traumatic noise-exposed rats treated with DCS did not exhibit an increase in Arc expression. Although the rats in this study were sacrificed within 1 h post-noise exposure, future research could monitor rats for behavioral evidence of tinnitus across relevant time intervals to determine how effective DCS could be in preventing, delaying, or reducing the manifestation of tinnitus.

Hippocampus

Supplementary Table S2 compares the species and methodologies used and briefly summarizes the results obtained examining aberrant plasticity in six experimental animal models of traumatic noise exposure in the hippocampus at multiple time points from 30 min to 10 weeks post-exposure.

Goble et al. (2009) reported plasticity-related changes in hippocampal CA1 neurons in freely behaving rats after acute bilateral noise exposure of 4 kHz at 104 dB SPL for 30 min. They reported that previously stable CA1 place cell responses were immediately altered after noise trauma and never re-stabilized to their original firing properties while being monitored and recorded for 24 h post-noise exposure. This noise-induced plasticity in place-field location specificity is noteworthy since prior work has demonstrated extreme stability of location-specific firing in the absence of specific changes in the spatial environment, stability persisting for periods of at least months at a time (Thompson and Best, 1989, 1990). After noise exposure sufficient to induce tinnitus, Goble et al. (2009) observed rapid (i.e., within $<$1 h) changes in place-field position, in spatial location correlation values, in grand-mean firing rates, in in-field and out-of-field firing rates, and in peak-firing rates compared to controls. These effects persisted for $>$24 h post-noise exposure and resulted in long-term plasticity in the spatial firing correlates of hippocampal neurons. Results from this study showed that evidence for plasticity resulting from traumatic noise exposure occurs in the hippocampus very rapidly after traumatic noise exposure and leads to long-term changes in hippocampal functional correlates.

Kraus et al. (2010) investigated whether neurogenesis in the hippocampal dentate subgranular zone was affected by a unilateral exposure to an acute 12 kHz tone at 126 dB SPL for 2 h in a rat model of tinnitus. When the animals were sacrificed 10 weeks post-noise exposure, they found that doublecortin (DCX; used for immunolabeling neuronal precursor cells) was reduced. DCX is a microtubule-associated protein expressed in neuronal precursor cells, but not in glial cells nor in neural stem cells from which the precursor cells develop. Upon migration and maturation into functional neurons, DCX expression is downregulated (Brown et al., 2003); DCX is thus a viable marker of neurogenesis. Immunolabeling of Ki67 (to label proliferating cells) was also reduced from exposure to the same acoustic trauma. Ki67 is a mitosis marker for cell proliferation that is expressed during all active phases of the cell cycle but absent in differentiated neurons (Scholzen and Gerdes, 2000). Taken together, Kraus et al.'s (2010) results were indicative that noise trauma impairs neurogenesis in the dentate of the hippocampus. All animals exposed to traumatic noise also exhibited sensory hair cell loss in their exposed ear. These animals were also tested for behavioral evidence of tinnitus using the gap-prepulse inhibition of the acoustic startle paradigm (Turner et al., 2006), and only a subset of rats presented behavioral evidence of tinnitus. While noise trauma specifically impaired later hippocampal neurogenesis, it did not necessarily lead to behavioral evidence of tinnitus in the gap-startle paradigm used.

Given the previous cited results showing early plastic changes in hippocampus due to traumatic noise exposure as well as others implicating the hippocampus in maintenance of tinnitus (Rauschecker et al., 2010; Roberts et al., 2010, 2013), Zheng et al. (2011) wanted to better characterize how hippocampal function might be impacted by acoustic noise exposure. Specifically, they investigated whether rats that had been exposed unilaterally to a 16 kHz tone at 110 dB SPL for 1 h would exhibit spatial memory deficits. Spatial memory deficits are linked to hippocampal functional impairments (e.g., in humans, Nunn et al., 1999; Guderian et al., 2015; in animals, Morris et al., 1982; Aggleton et al., 1986; Pioli et al., 2014). Using both T-maze and Morris water maze tasks, they found that spatial memory in rats with tinnitus was not impaired 2 months after exposure to acoustic trauma. They also utilized a lick suppression paradigm to confirm behavioral evidence of tinnitus in their rats 2 weeks and again at 10 months post-noise exposure, suggesting that some forms of hippocampal plasticity in tinnitus may not be directly linked to spatial memory impairments.

Singer et al. (2013) also examined whether changes in the hippocampus would be observed 14 days after various levels of noise exposure. They found an increase in Arc mRNA expression in CA1 after exposure to 100 and 110 dB SPL with a 10 kHz tone for 1 or 1.5 h. After 120 dB SPL exposure, however, Arc expression was no different from controls. These results were independent of whether rats were exposed to the noise for 1.5 h or only 1 h. This finding was further characterized by measuring the number of CtBP2/RIBEYE-positive particles in ribbon synapses of the IHC in order to determine the degree of deafferentation. The results were related to the integrity of the ABR and Arc expression in CA1 as in BLA: rats exposed to a 10 kHz tone at 120 dB SPL with behavioral evidence of tinnitus had the most severe IHC ribbon loss and most severe loss of ABR wave correlations (an 80% decline from baseline). Singer et al. (2013) also found that adding a social stressor 2 days prior to traumatic noise exposure raised circulating CORT levels in rats, which was linked to a more consistent maintenance of ABR waveforms compared to non-stressed controls. This effect indicates that CORT elevation allows for more stable and persistent responses to sound, a higher number of IHC ribbons, and greater mobilization of Arc mRNA in limbic regions (BLA and CA1 of the hippocampus). It suggests that moderately elevated circulating levels of CORT may serve a protective mechanism in both the cochlea and limbic regions, whereas high or very low levels of circulating CORT prevents this synaptic protection. This protection hypothesis is one that clearly deserves further study.

Kapolowicz and Thompson (2016) further investigated early plasticity in dorsal hippocampal processing of traumatic noise. Freely behaving rats were bilaterally exposed to either a 16 kHz

tone at 115 dB SPL, a 16 kHz tone at 70 dB SPL, or to silence, with exposure for each condition lasting 1 h. Rats were sacrificed 45 min-1 h after cessation of these sound conditions, and Arc protein expression was quantified for dorsal hippocampus; this time interval was selected to capture peak expression of transient Arc protein (McIntyre et al., 2005; Czerniawski et al., 2011; Holloway-Erickson et al., 2012). They found that Arc was upregulated after traumatic noise exposure (115 dB) but not after non-traumatic (70 dB) noise exposure. The authors also investigated potential changes in inhibition, using the biomarker GAD, after traumatic noise exposure. They found no significant changes in GAD 65 + 67 protein expression in the dorsal hippocampus. Kapolowicz and Thompson (2016) also examined whether the partial NMDA-receptor agonist, DCS, could maintain Arc protein expression at basal levels in the dorsal hippocampus after exposure to acoustic trauma: DCS did not prevent changes in Arc mobilization. The 6 mg/kg (ip) dose of DCS administered by Kapolowicz and Thompson (2016) was previously shown to increase hippocampal intrinsic excitability and Arc protein expression in non-noise exposed rats (Donzis and Thompson, 2014) as well as facilitate hippocampally-dependent memory in other species (Thompson et al., 1992; Thompson and Disterhoft, 1997). Although DCS functions as a partial agonist, it was predicted that, when paired with traumatic noise exposure, DCS would instead function antagonistically due to NMDA binding sites being saturated with less potent DCS competing off serine, the full agonist for the NMDA receptor, as observed in amygdala post-traumatic noise exposure with the same dosage. Relative to controls, Kapolowicz and Thompson (2016) observed elevated levels of Arc expression in dorsal hippocampus after treatment with DCS paired with traumatic noise exposure, similar to when rats were exposed to traumatic noise alone (without DCS treatment). Given that DCS was able to prevent elevation of Arc in the amygdala of traumatic noise-exposed rats treated with DCS, unlike for the dorsal hippocampus, future research should compare these results of DCS treatment with manipulations using serine, the endogenous ligand for NR1 subunits of NMDA receptors. Such an investigation would further address whether NMDA-receptor mediated plasticity is required at this early stage in tinnitus-related plasticity in the amygdala and in hippocampus.

Previous *in vitro* recordings found that long-term potentiation is inhibited within the CA1 region of the hippocampus after *in vivo* long-term exposure to high-intensity noise (Cunha et al., 2015). To further characterize this result, work from the same lab found that post-burst hyperpolarizations are increased due to a decrease in the h (hyperpolarization-activated) current; they also observed an increase in firing of CA1 pyramidal neurons, but the mechanism for this increase in excitability remained unknown (Cunha et al., 2018). Recently, Cunha et al. (2019) continued to better characterize this finding that high-intensity sound effects long term potentiation in CA1 hippocampal neurons using the same paradigm as their previous work, with rats exposed to high-intensity broadband noise (110 dB, 2–15 kHz, with a peak at 7 kHz) twice daily for 10 days, for 1 min each session. This pattern of noise exposure was meant to emulate exposure to a loud occupational/recreational sound in an animal model, as occupational and recreational sounds are common causes of auditory-related issues reported from both younger (Lercher et al., 2003) and older (Helfer et al., 2011) populations. Using *in vitro* whole-cell patch-clamp recordings to study synaptic transmission, they found that inhibitory GABAergic transmission is increased within CA1 after high-intensity noise exposure over the course of several days. They found no changes in excitatory glutamatergic activation of AMPA/kainate or NMDA receptors. While GABAergic enhancement is consistent with the observed inhibition of long-term potentiation in this paradigm, Cunha et al. (2019) speculated that this increase in inhibition could be compensatory and protective against loud sound exposure.

Cingulate

Supplementary Table S3 compares the species and methodologies used in two animal models exposed to traumatic noise exposure and briefly summarizes the results obtained examining potential changes in the cingulate cortex at different time points from 1 to 7 h post-exposure. The cingulate cortex is a limbic structure that has been less well-characterized regarding its prospective involvement in potentially tinnitus-inducing maladaptive plasticity. In much of the cognitive neuroscience literature (e.g., Stevens et al., 2011), important distinctions are drawn between anterior and posterior cingulate cortex, however in animal models exposed to traumatic noise, such a distinction is not always stipulated, or the focus is adhered to strictly the ACC. Henceforth in the present review, distinctions will be overtly stated if the distinction was provided in the original research. Otherwise, the general term of "cingulate cortex" will be used.

Wallhäusser-Franke et al. (2003) investigated how c-fos expression could be altered in various classic and non-classic auditory structures, including the ACC. They found that c-fos immunoreactivity in cingulate cortex was elevated in gerbils 1 h after being bilaterally exposed to impulse noise (136–142 dB SPL) but was reduced to control levels within 7 h post-traumatic noise exposure. Rapid and transient c-fos induction is associated with exposure to novel sensory stimuli (Tischmeyer and Grimm, 1999). The C-fos expression has been used to identify activation in various auditory regions, with upregulation found in relation to the significance of the acoustic signal (e.g., Carretta et al., 1999). Aligning with previously reported results, Wallhäusser-Franke et al.'s (2003) results described here are indicative that c-fos is also responsive to auditory stimuli within the ACC shortly after exposure to a traumatic sound.

Mahlke and Wallhäusser-Franke (2004) investigated potential changes in Arc and in c-fos immunoreactivity within the ACC of gerbils 3 h after 10 min of exposure to approximately 80 dB SPL NBW centered at two different frequencies (8 kHz or 1 kHz). They detected an upregulation of Arc within the ACC for both frequencies of noise exposure, but no significant differences due to treatment condition. Although they did not statistically analyze the expression of c-fos across groups, they also observed increases in c-fos immunoreactivity for all treatment conditions,

with c-fos expression always outnumbering Arc expression, though the magnitude of this difference was not given.

CENTRAL CHANGES IN ANIMALS TREATED WITH SALICYLATE

Amygdala

Supplementary Table S4 lists the species and methodologies utilized in five animal models exposed to sodium salicylate and briefly reports on the results obtained from these studies regarding potential changes in the amygdala at time points from 1 to 5 h post-exposure.

In the thorough study by Wallhäusser-Franke et al. (2003), the effect of impulse noise exposure on c-fos immunoreactivity was directly compared to the effects of treatment with either a high (350 mg/kg) or a low (50 mg/kg) dose of sodium salicylate in gerbils 3 h post-injection. The overall expression of c-fos in various brain regions revealed that c-fos immunoreactivity was lower after impulse noise exposure than after a high dose injection of salicylate. Within different amygdaloid nuclei (CeA, LA, BLA, and MeA), an abundance of labeled cells were observed bilaterally after a high dose of salicylate injection, whereas treatment with a low dose did not alter labeling from controls. The highest densities of c-fos expression were observed in the CeA.

Mahlke and Wallhäusser-Franke (2004) compared both Arc and c-fos immunoreactive expression resulting from either NBW exposure or salicylate treatment (350 mg/kg) in gerbils. Salicylate treated gerbils were further subdivided into groups also exposed to either ambient background noise or silence. Within the amygdaloid complex, Arc and c-fos immunoreactive neurons were substantially increased 5 h after salicylate injections compared to NBW stimulation, especially in CeA (where Arc and c-fos immunoreactive neurons were found exclusively after tinnitus-inducing treatments): Salicylate treatment combined with exposure to ambient background noise and salicylate treatment paired with exposure to silence led to strong Arc expression in CeA (mostly the lateral subdivision) as well as in LA, but expression was negligible in MeA. In comparison, gerbils exposed to NBW exhibited Arc staining of neurons in LA, but negligible staining in both CeA and MeA nuclei. Saline treatment paired with ambient background noise and saline treatment paired with silence showed only negligible expression of Arc in LA and none in CeA and MeA nuclei. After salicylate (both with and without ambient background noise), the amygdaloid complex presented with many more c-fos expressing neurons in CeA and LA nuclei than was observed in gerbils exposed to NBW. In comparison, after NBW exposure (paired with either ambient background noise or silence), c-fos immunoreactive neurons were always present in LA (a comparable expression to that seen for Arc) but rarely in CeA. Overall, higher levels of c-fos expression were observed compared to Arc expression, but the c-fos expression in MeA was minimal in all treatment groups.

Chen et al. (2012) investigated the effects of treatment with salicylate (300 mg/kg) on LFP and frequency receptive fields of neurons in LA in rats immediate after, 1 h, and 2 h post-treatment. They found that salicylate increased the amplitude of the LFP, making it hyperactive to sounds greater than 60 dB SPL. They also found that the frequency receptive fields of multiunit clusters in LA were also dramatically altered by salicylate: Neuronal activity at frequencies below 10 kHz and above 20 kHz was depressed at low intensities, but greatly enhanced for stimuli between 10 and 20 kHz (frequencies near the observed pitch of salicylate-induced tinnitus in rats). These frequency-dependent changes caused the frequency receptive fields of many LA neurons to migrate towards responses to 10–20 kHz stimuli (i.e., tonotopic reorganization), thereby amplifying activity in this frequency band. They also observed that the infusion of salicylate (20 ml, 2.8 mM) directly into LA enhanced sound-evoked activity in AC, i.e., increased LFP amplitude and enhanced AC neuronal activity at these same mid-frequencies, associated with the pitch of salicylate-induced tinnitus in rats.

In a separate study, Chen et al. (2014) further investigated changes in the excitability of LA neurons in rats 2 h post-treatment with salicylate (200 or 250 mg/kg). To identify electrophysiological changes within LA, sound-evoked LFPs and multiunit discharges were recorded before and after salicylate treatment. A subset of rats was trained on a two-alternative forced-choice identification task to test for behavioral evidence of tinnitus resulting from the salicylate treatment. Rats treated with doses of 200 and 250 mg/kg of sodium salicylate showed suprathreshold neuronal hyperexcitability in LA. Salicylate treatment also shortened the temporal response in LA. This salicylate-induced hyperactivity in LA indicates plastic changes occurring within LA during induction and early stages of tinnitus. Physiologically, salicylate treatment significantly enhanced sound-evoked neural activity in LA. The authors noted that the enhancement of sound-evoked activity occurred predominantly at the mid-frequencies [consistent with their findings in Chen et al. (2012), and again reflecting shifts of receptive fields of LA neurons towards the mid-frequency range post-treatment]. The increased number of mid-frequency neurons led to a relatively higher number of total spontaneous discharges in the mid-frequency range, regardless of whether or not the mean discharge rate of each LA neuron increased. Chen et al. (2014) speculated that this tonotopical overactivity in the mid-frequency range in quiet can potentially lead to a tonal sensation within this same range (i.e., tinnitus). The authors also suggested that this plasticity in LA may also contribute to the negative effect that many patients associate with their tinnitus.

Chen et al. (2015) additionally hypothesized that enhanced functional connectivity between hippocampal and auditory brain regions provides a substrate for assigning a spatial location to a phantom sound (findings summarized below), while coordinated activity between specific auditory areas and the amygdala may draw attention to and add emotional salience to neural activity in the auditory pathway. Thus, functionally coordinated activity within hippocampal, amygdalar and cortical networks may be essential for bringing tinnitus into consciousness. Although it

is beyond the scope of this present review to describe results observed in classic auditory structures, Chen et al. (2015) treated rats with sodium salicylate (300 mg/kg) and tested responses 2 h post-injection to investigate their hypothesis (A separate group of rats was treated with the same dose of salicylate and later tested for behavioral evidence of tinnitus using a two-alternative forced-choice paradigm to assure that their drug treatment could effectively serve as an animal model of tinnitus). Chen et al. (2015) found that salicylate vigorously amplified sound-evoked neural responses in LA *via* changes in LFP amplitude-intensity functions. These electrophysiological changes were compared with resting-state fMRI patterns, which revealed hyperactivity in the auditory network (i.e., inferior colliculus (IC), medial geniculate, and A1) with connections to amygdala and other regions *via* amplitude of low-frequency fluctuations (ALFF). Functional connectivity revealed enhanced coupling within the auditory network and other regions including the amygdala, further strengthening their hypothesis.

Hippocampus

Supplementary Table S5 summarizes the species and methodologies utilized in five animal models exposed to sodium salicylate and briefly reports on the results obtained from these studies regarding potential changes in the hippocampus at multiple time points from 2 h to up to 39 days post-exposure.

Wallhäusser-Franke et al. (2003) investigated the effects of treatment with either a single high dose (350 mg/kg) or a single low dose (50 mg/kg) injection of sodium salicylate in Mongolian gerbils 3 h post-treatment. They found bilateral expression of c-fos in both dentate and subiculum of the hippocampus in gerbils injected with the high dose of salicylate (a dose shown above to cause behavioral evidence of tinnitus in several animal models). In all regions assessed by Wallhäusser-Franke et al. (2003), including hippocampal regions, it was found that the greatest immunoreactivity was observed after this high dose treatment with salicylate when compared to the lower dose treatment group or to the group exposed to loud impulse noise.

Gong et al. (2008) examined potential changes in extrinsic excitation and inhibition in cultured rat neurons from the CA1 hippocampus during the *in vitro* bath application of sodium salicylate. Extracellular recordings showed that sodium salicylate enhanced the amplitude of evoked population spikes in a dose-dependent manner. Salicylate at 1 mM caused a leftward shift of the evoked EPSP curve, indicating an excitatory potentiation. This effect was reversible after washout. Salicylate had no effect on basal field EPSPs, suggesting that synaptic input remained unchanged during drug treatment. These results indicate that salicylate enhances the likelihood that EPSPs would cross the threshold to generate action potentials, reflecting increased excitation of CA1 neurons. Gong et al. (2008) also investigated possible changes in inhibition, and found that salicylate reduced GABAergic inhibition, leading to increased CA1 neuronal excitation. Both evoked (eIPSCs) and spontaneous (mIPSCs) were suppressed by salicylate with no change in input resistance. Only the amplitude, but not the frequency, of mIPSCs was reduced. Similarly, salicylate directly suppressed GABAaR-mediated whole-cell currents in cultured CA1, consistent with the effects on the amplitudes of mIPSCs and eIPSCs. Gong et al. (2008) concluded that salicylate reduces GABAergic transmission *via* suppression of GABAaR-mediated responses. These acute effects on inhibition were fully reversible by washout.

Chen et al. (2014) investigated the effect of treatment with salicylate (either 200 or 250 mg/kg) on rats 2 h post-treatment. Rats treated with both these doses showed suprathreshold hyperexcitability in the hippocampus (and in the amygdala, as detailed earlier). Again, this salicylate-induced hyperactivity is a consistent form of plastic change in the hippocampus. This electrophysiological plasticity was significant in recordings of sound-evoked LFPs and of multiunit discharges 2 h after treatment. Tinnitus-inducing treatment with salicylate significantly and rapidly enhanced sound-evoked neural activity in hippocampus. The enhancement of sound-evoked activity occurred predominantly at the mid-frequencies (as in the LA, described above), likely reflecting shifts of neuronal responses towards mid-frequency ranges post-salicylate treatment. Chen et al. (2014) explained that the increased number of mid-frequency responsive neurons would lead to a relatively higher number of total spontaneous discharges in the mid-frequency range, even though the mean discharge rate of each individual neuron need not increase. As also observed in LA, this tonotopical plasticity (frequency shift and hyperactivity) within the hippocampus in the mid-frequency range in quiet environments could lead to tonal mid-frequency sensations presenting as tinnitus. Again, Chen et al. (2014) tested a subset of rats given salicylate treatment for behavioral evidence of tinnitus and found that the treatment inducing early hippocampal plasticity also produced behavioral signs of tinnitus in this animal model.

Wu et al. (2015) investigated the effects of acute and chronic treatment with sodium salicylate (300 mg/kg) on CA1 hippocampal mRNA and on protein expression of Arc, Early growth response 1 (Egr-1), and NMDA receptor subunit 2B (NR2B). To reiterate, Arc expression has been shown to be involved mechanistically in long-term memory consolidation and synaptic plasticity (Plath et al., 2006). Egr-1 has been shown to be essential for the persistence of late-phase long-term potentiation within the hippocampus as well as the consolidation of several forms of long-term memory (Davis et al., 2010; Penke et al., 2014; Duclot and Kabbaj, 2017). NR2B is associated with NMDA receptor activation *via* glutamate binding, which is critical for age-dependent thresholds of plasticity and memory formation (Tang et al., 1999). Wu et al. (2015) acutely treated one group of rats with a single dose (300 mg/kg) of salicylate, and these rats were sacrificed 2 h post-treatment. Chronically treated groups were given salicylate once daily for 10 consecutive days, and sacrificed either on day 11 or put into in one of two recovery groups which were sacrificed on either day 25 or day 39. Wu et al. (2015) found that expression of Arc mRNA and protein were up-regulated after either acute or chronic salicylate treatments. Specifically, they reported an upregulation of Arc mRNA and protein expression after acute treatment, which further increased significantly for rats chronically treated with salicylate for 10 days. They also observed an increase in the number of presynaptic vesicles, the thickness of postsynaptic densities, and

an increase in synaptic interface curvature (i.e., expansion of synaptic area) in the group sacrificed on day 11. They also observed an upregulation of Egr-1 and NR2B mRNA and protein levels solely for rats chronically treated with salicylate. By day 25, expression for all three biomarkers returned to basal levels (intermediate intervals between 11 and 25 days post-treatment were not assessed).

As previously detailed, Chen et al. (2015) were interested in testing for enhanced functional connectivity between hippocampus and auditory areas in the acute salicylate-treated rat model of tinnitus. Chen and colleagues speculated that enhanced functional connectivity between the hippocampus and auditory areas might provide a substrate for assigning a spatial location to a phantom sound. In their experiments, rats were treated with sodium salicylate (300 mg/kg), and a separate group of rats given this same treatment were tested for behavioral evidence of tinnitus using a two-alternative forced-choice paradigm. Rats were tested before (baseline) and 2 h post-injection with MRI BOLD data acquisition. Similar to their results reported above for the amygdala, Chen et al. (2015) showed enhanced coupling between the auditory network and hippocampus.

Cingulate

Supplementary Table S6 displays the species and methodologies utilized in three animal models exposed to sodium salicylate and summarizes the results obtained from these studies regarding potential changes in the cingulate at different time points from 2 to 5 h post-exposure.

The cingulate cortex, another key limbic region investigated by Wallhäusser-Franke et al. (2003), showed elevation of c-fos labeled neurons 3 h after a high dose injection of salicylate (350 mg/kg) in gerbils. The authors noted this upregulation of c-fos specifically in the ACC subregion. This region has been implicated in pain processing (Hudson, 2000) and is often co-activated with the amygdala in affectively stressful autonomic responses.

Plasticity in the ACC after high dosage of salicylate was also reported by Mahlke and Wallhäusser-Franke (2004). After a 350 mg/kg dosage of sodium salicylate, they observed an upregulation of both Arc and c-fos expressing neurons in gerbils 5 h post-injection. C-fos expressing neurons outnumbered Arc expressing neurons after this high dose treatment with salicylate (They also reported a similar finding in the ACC after traumatic noise exposure, see above). They proposed that since layers 2 and 3 of the cingulate cortex are directly innervated by primary A1 (Budinger and Scheich, 2009), and they found that Arc immunoreactivity paralleled their findings of increases in Arc expression in A1, then this might entail that A1 activation may exert direct influence on the cingulate cortex.

A third group (Chen et al., 2014) reported no changes in cingulate cortical neuron excitability or frequency response after treatment with either 200 or 250 mg/kg of sodium salicylate, despite behavioral evidence of tinnitus observed in a subset of treated rats trained on a two-alternative forced-choice identification task. These experiments assessed changes in sound-evoked LFPs and in multiunit discharges 2 h post-treatment. Although Chen et al. (2014) observed no evident changes in cingulate cortex in this paradigm, hyperactivity was observed in both LA and hippocampus at this early time point, as described above.

CONCLUDING REMARKS AND FUTURE DIRECTIONS

In a variety of different animal models of tinnitus reviewed here, hyperexcitability, including increases in IEG expression, increased firing activity, and increased sensitivity to inputs, is consistently observed in multiple limbic (i.e., non-classical auditory) regions. The amygdala, the hippocampus, and the cingulate cortex are rapidly responsive to acoustic trauma, beginning immediately after cessation of noise exposure, and continue to exhibit plasticity well beyond the period after noise exposure ends. These same regions are also rapidly responsive to treatment with sodium salicylate sufficient to induce behavioral signs of tinnitus. These results of both early and sustained plasticity within these limbic regions support the hypothesis that non-classical auditory (i.e., limbic) regions play a vital role in both the manifestation and the maintenance of this common auditory disorder. Moreover, aberrant enhanced connectivity between limbic and classical auditory structures may contribute not only to the sensory sensation perceived as tinnitus but also to the emotional response to the percept of tinnitus, extending prior sensory gating hypotheses (Rauschecker et al., 2010) that do not address the potential involvement of limbic regions in the initiation of tinnitus. Further evidence for the potential involvement of limbic regions during the initiation phase of tinnitus is also reviewed by Kraus and Canlon (2012).

What currently remains unclear is the role that reduced inhibition plays early in tinnitus in these limbic regions. Considerable evidence of changes in inhibitory neurotransmission resulting from traumatic noise exposure have been well-characterized in classic auditory structures, and is beyond the scope of this review (e.g., Browne et al., 2012; Zheng et al., 2014; Heeringa and van Dijk, 2016). Also well-characterized are changes in inhibition in classic auditory regions resulting from ototoxic treatments such as sodium salicylate (e.g., Wang et al., 2006, 2016; Liu et al., 2007; Wu et al., 2018). However, considerably less research has focused on early changes in inhibition in limbic regions in animal models of tinnitus. This makes it difficult to assess whether reduced inhibition or other mechanisms may drive maladaptive hyperexcitability in different limbic regions in tinnitus. It is thus difficult to assess speculation that inhibitory gating from limbic regions may suppress the tinnitus percept at later time points in the clinical progression of this auditory disorder. At present, three separate investigations on changes in inhibition within limbic regions report conflicting results: one report found no changes in GAD expression within amygdala or hippocampus soon after acute noise trauma (Kapolowicz and Thompson, 2016), whereas Gong et al. (2008) found a decrease in inhibitory transmission in hippocampus after treatment with salicylate. Conversely, a more recent study reported an increase in GABAergic inhibition within the

hippocampus after prolonged exposure to high-intensity sound (Cunha et al., 2019). These disparate results come from studies with widely different methodologies, making it difficult to infer a clear role for inhibitory changes within these limbic regions in tinnitus.

Even if a decrease in inhibition contributes to hyperexcitability in some tinnitus models, rectifying such a change may not prevent the chronic tinnitus percept. Specifically, Zheng et al. (2014) found that after exposure to traumatic noise (16 kHz pure tone at 115 dB for 1 h), early (5 mg/kg s.c., 30 min, and every 24 h for five consecutive days post-noise exposure) or late (3 mg/day for 45 week beginning 17.5 week post-noise exposure) treatment with L-baclofen, a GABA-B receptor agonist, failed to prevent development of behavioral evidence of tinnitus in rats. If limbic regions are crucially involved from induction through maintenance of tinnitus, then the better detailed characterization of regional limbic inhibition at multiple time points is critically needed to better assess sensory gating hypotheses related to tinnitus percept and affect.

Tae et al. (2018) used a surface-based vertex analysis of data collected from magnetic resonance imaging to reveal evidence of atrophy in the basal and lateral nuclei of the right amygdala in tinnitus patients compared to controls. The authors speculated that such atrophy was due to patients' attempting to self-modulate their tinnitus percept by a kind of sensory gating, as suggested by Jastreboff (1990). Tae et al. (2018) also reported a decrease in left hippocampal volume correlating with an increase in tinnitus handicap inventory scores, with smaller hippocampi associated with greater self-reported functional impairment from tinnitus. Given that none of their tinnitus sufferers reported evidence of psychological disorders, Tae and coworkers hypothesized that decreased amygdala and hippocampal volume was directly related to the pathophysiology of tinnitus or sensory gating rather than to emotional distress. These results are insightful, suggesting that individuals who already have reduced limbic regional volume compared to the normal population may be more prone to experience tinnitus, or that specific pathologies in these regions can cause tinnitus.

A recent study supports the latter hypothesis: in mice, moderate noise exposure (80 dB SPL for 2 h/day) meant to simulate environmental noise caused an increase in oxidative stress and tau phosphorylation in hippocampus after just 1 week of exposure, whereas A1 did not become susceptible to such changes until after 3 weeks of noise exposure (Cheng et al., 2016). These results indicate that the hippocampus is more vulnerable at an earlier time point to potentially damaging sounds than classical auditory structures such as the A1. Although Cheng and colleagues did not investigate how increased vulnerability to potentially traumatic sounds may relate to initiation of tinnitus, their results indicate early vulnerability in these limbic regions and warrant further study.

The role played by stress hormones such as cortisol in humans (or corticosterone/CORT in rats) is unclear in limbic neuronal plasticity at early or late time points after tinnitus-inducing acoustic or salicylate treatments. Wallhäusser-Franke et al. (2003) proposed that tinnitus may be an indirect consequence of a loss of auditory input associated with stress. Surprisingly, Kapolowicz and Thompson (2016) found no change in circulating CORT levels in rats 1 h after traumatic noise exposure compared to controls. Singer et al. (2013) in fact reported that heightened stress can result in protection from acoustic trauma. These sparse and disparate experimental results suggest that the role of stress in noise trauma-related plasticity may be complex, and require more thorough investigation. Given data linking altered GABAergic activity with hypothalamic-pituitary-adrenal (HPA) axis function (Bowers et al., 1998; Dent et al., 2007; Cullinan et al., 2008) and that the amygdala and hippocampus are principle brain regions regulating HPA activity following psychological or emotional distress (Herman and Cullinan, 1997; Herman et al., 2003), one focus of future animal models of tinnitus should be to investigate direct relationships between altered inhibitory neurotransmission and hormonal and noradrenergic stress responses, and their impacts on neuronal function in these limbic regions.

As this current review shows, plasticity in both the amygdaloid complex and in the hippocampus, and to a lesser degree in the cingulate cortex, has been characterized in both the initiation and maintenance of experimental models of tinnitus. Prominent descriptions of tinnitus, such as the sensory gating hypothesis, should be updated to reflect evidence that limbic region function is altered not only in tinnitus maintenance but also at much earlier stages. Additional study of cingulate cortex plasticity in tinnitus models is needed to identify additional specific contributions to the development of tinnitus symptomology. The experimental results reviewed here suggest that limbic and other non-classical auditory brain regions are promising targets for researchers seeking a more comprehensive mechanistic understanding of the auditory disorder of tinnitus and may yield useful translational targets for improving treatment.

AUTHOR CONTRIBUTIONS

The manuscript was written, edited and expanded by MK and LT. Both authors contributed intellectually and practically to the work.

FUNDING

This work was supported by grant funding to LT from the American Tinnitus Association.

ACKNOWLEDGMENTS

We would like to thank Phillip Tran for assistance with a graphical representation of auditory-limbic circuitry.

SUPPLEMENTARY MATERIAL

The Supplementary Material for this article can be found online at: https://www.frontiersin.org/articles/10.3389/fnsys.2019.00088/full#supplementary-material.

REFERENCES

Aggleton, J. P., Hunt, P. R., and Rawlins, J. N. P. (1986). The effects of hippocampal lesions upon spatial and non-spatial tests of working memory. *Behav. Brain Res.* 19, 133–146. doi: 10.1016/0166-4328(86)90011-2

Aly-Mahmoud, M., Carlier, P., Salam, S. A., Houari Selmani, M., Moftah, M. Z., Esclapez, M., et al. (2017). Role of anterior cingulate cortex in instrumental learning: blockade of dopamine D1 receptors suppresses overt but not covert learning. *Front. Behav. Neurosci.* 11:82. doi: 10.3389/fnbeh.2017.00082

Amaral, D. G., Scharfman, H. E., and Lavenex, P. (2007). The dentate gyrus: fundamental neuroanatomical organization (dentate gyrus for dummies). *Prog. Brain Res.* 163, 3–22. doi: 10.1016/s0079-6123(07)63001-5

Anders, S., Eippert, F., Weiskopf, N., and Veit, R. (2008). The human amygdala is sensitive to the valence of pictures and sounds irrespective of arousal: an fMRI study. *Soc. Cogn. Affect. Neurosci.* 3, 233–243. doi: 10.1093/scan/nsn017

Arnold, W., Bartenstein, P., Oestreicher, E., Römer, W., and Schwaiger, M. (1996). Focal metabolic activation in the predominant left auditory cortex in patients suffering from tinnitus: a PET study with [18F]deoxyglucose. *ORL J. Otorhinolaryngol. Relat. Spec.* 58, 195–199. doi: 10.1159/000276835

Auerbach, B. D., Rodrigues, P. V., and Salvi, R. J. (2014). Central gain control in tinnitus and hyperacusis. *Front. Neurol.* 5:206. doi: 10.3389/fneur.2014.00206

Bauer, C. A., Brozoski, T. J., Rojas, R., Boley, J., and Wyder, M. (1999). Behavioral model of chronic tinnitus in rats. *Otolaryngol. Head Neck Surg.* 121, 457–462. doi: 10.1016/s0194-5998(99)70237-8

Benedict, R. H. B., Shucard, D. W., Santa Maria, M. P., Shucard, J. L., Abara, J. P., Coad, M. L., et al. (2002). Covert auditory attention generates activation in the rostral/dorsal anterior cingulate cortex. *J. Cogn. Neurosci.* 14, 637–645. doi: 10.1162/08989290260045765

Bisht, M., and Bist, S. S. (2011). Ototoxicity: the hidden menace. *Indian J. Otolaryngol. Head Neck Surg.* 63, 255–259. doi: 10.1007/s12070-011-0151-8

Bowers, G., Cullinan, W. E., and Herman, J. P. (1998). Region-specific regulation of glutamic acid decarboxylase (GAD) mRNA expression in central stress circuits. *J. Neurosci.* 18, 5938–5947. doi: 10.1523/jneurosci.18-15-05938.1998

Brien, J. A. (1993). Ototoxicity associated with salicylates. *Drug Saf.* 9, 143–148. doi: 10.2165/00002018-199309020-00006

Brown, J. P., Couillard-Després, S., Cooper-Kuhn, C. M., Winkler, J., Aigner, L., and Kuhn, H. G. (2003). Transient expression of doublecortin during adult neurogenesis. *J. Comp. Neurol.* 467, 1–10. doi: 10.1002/cne.10874

Browne, C. J., Morley, J. W., and Parsons, C. H. (2012). Tracking the expression of excitatory and inhibitory neurotransmission-related proteins and neuroplasticity markers after noise induced hearing loss. *PLoS One* 7:e33272. doi: 10.1371/journal.pone.0033272

Brozoski, T. J., and Bauer, C. A. (2005). The effect of dorsal cochlear nucleus ablation on tinnitus in rats. *Hear. Res.* 206, 227–236. doi: 10.1016/j.heares.2004.12.013

Budinger, E., and Scheich, H. (2009). Anatomical connections suitable for the direct processing of neuronal information of different modalities *via* the rodent primary auditory cortex. *Hear. Res.* 258, 16–27. doi: 10.1016/j.heares.2009.04.021

Carretta, D., Hervé-Minvielle, A., Bajo, V. M., Villa, A. E. P., and Rouiller, E. M. (1999). c-Fos expression in the auditory pathways related to the significance of acoustic signals in rats performing a sensory-motor task. *Brain Res.* 841, 170–183. doi: 10.1016/s0006-8993(99)01840-5

Cazals, Y. (2000). Auditory sensori-neural alterations induced by salicylate. *Prog. Neurobiol.* 62, 583–631. doi: 10.1016/s0301-0082(00)00027-7

Cenquizca, L. A., and Swanson, L. W. (2007). Spatial organization of direct hippocampal field CA1 axonal projections to the rest of the cerebral cortex. *Brain Res. Rev.* 56, 1–26. doi: 10.1016/j.brainresrev.2007.05.002

Crippa, A., Lanting, C. P., van Dijk, P., and Roerdink, J. B. T. (2010). A diffusion tensor imaging study on the auditory system and tinnitus. *Open Neuroimag. J.* 4, 16–25. doi: 10.2174/1874440001004010016

Chavez, C. M., McGaugh, J. M., and Weinberger, N. M. (2009). The basolateral amygdala modulates specific sensory memory representations in the cerebral cortex. *Neurobiol. Learn. Mem.* 91, 382–392. doi: 10.1016/j.nlm.2008.10.010

Chen, Y. C., Li, X., Liu, L., Wang, J., Lu, C. Q., Yang, M., et al. (2015). Tinnitus and hyperacusis involve hyperactivity and enhanced connectivity in auditory-limbic-arousal-cerebellar network. *Elife* 4:e06576. doi: 10.7554/eLife.06576

Chen, Y. C., Liu, S., Lv, H., Bo, F., Feng, Y., Chen, H., et al. (2018). Abnormal resting-state functional connectivity of the anterior cingulate cortex in unilateral chronic tinnitus patients. *Front. Neurosci.* 12:9. doi: 10.3389/fnins.2018.00009

Chen, G.-D., Manohar, S., and Salvi, R. (2012). Amygdala hyperactivity and tonotopic shift after salicylate exposure. *Brain Res.* 1485, 63–76. doi: 10.1016/j.brainres.2012.03.016

Chen, G.-D., Radziwon, K. E., Kashanian, N., Manohar, S., and Salvi, R. (2014). Salicylate-induced auditory perceptual disorders and plastic changes in nonclassical auditory centers in rats. *Neural Plast.* 2014:658741. doi: 10.1155/2014/658741

Cheng, L., Wang, S. H., Huang, Y., and Liao, X. M. (2016). The hippocampus may be more susceptible to environmental noise than the auditory cortex. *Hear. Res.* 333, 93–97. doi: 10.1016/j.heares.2016.01.001

Cullinan, W. E., Ziegler, D. R., and Herman, J. P. (2008). Functional role of local GABAergic influences on the HPA axis. *Brain Struct. Funct.* 213, 63–72. doi: 10.1007/s00429-008-0192-2

Cunha, A. O. S., Ceballos, C. C., de Deus, J. L., and Leão, R. M. (2018). Long-term high-intensity sound stimulation inhibits h current (Ih) in CA1 pyramidal neurons. *Eur. J. Neurosci.* 47, 1401–1413. doi: 10.1111/ejn.13954

Cunha, A. O. S., de Deus, J. L., Ceballos, C. C., and Leão, R. M. (2019). Increased hippocampal GABAergic inhibition after long-term high-intensity sound exposure. *PLoS One* 14:e0210451. doi: 10.1371/journal.pone.0210451

Cunha, A. O. S., de Oliveira, J. A. C., Almeida, S. S., Garcia-Cairasco, N., and Leão, R. M. (2015). Inhibition of long-term potentiation in the schaffer-CA1 pathway by repetitive high-intensity sound stimulation. *Neuroscience* 310, 114–127. doi: 10.1016/j.neuroscience.2015.09.040

Czerniawski, J., Ree, F., Chia, C., Ramamoorthi, K., Kumata, Y., and Otto, T. A. (2011). The importance of having arc: expression of the immediate-early gene arc is required for hippocampus-dependent fear conditioning and blocked by NMDA receptor antagonism. *J. Neurosci.* 31, 11200–11207. doi: 10.1523/jneurosci.2211-11.2011

Davis, S., Renaudineau, S., Poirier, R., Poucet, B., Save, E., and Laroche, S. (2010). The formation and stability of recognition memory: what happens upon recall? *Front. Behav. Neurosci.* 4:177. doi: 10.3389/fnbeh.2010.00177

Day, R. O., Graham, G. G., Bieri, D., Brown, M., Cairns, D., Harris, G., et al. (1989). Concentration-response relationships for salicylate-induced ototoxicity in normal volunteers. *Br. J. Clin. Pharmacol.* 28, 695–702. doi: 10.1111/j.1365-2125.1989.tb03562.x

De Ridder, D., Fransen, H., Francois, O., Sunaert, S., Kovacs, S., and Van De Heyning, P. (2006). Amygdalohippocampal involvement in tinnitus and auditory memory. *Acta Otolaryngol.* 126, 50–53. doi: 10.1080/03655230600895580

Dent, G., Choi, D. C., Herman, J. P., and Levine, S. (2007). GABAergic circuits and the stress hyporesponsive period in the rat: ontogeny of glutamic acid decarboxylase (GAD) 67 mRNA expression in limbic-hypothalamic stress pathways. *Brain Res.* 1138, 1–9. doi: 10.1016/j.brainres.2006.04.082

Dickerson, B. C., and Eichenbaum, H. (2010). The episodic memory system: neurocircuitry and disorders. *Neuropsychopharmacology* 35, 86–104. doi: 10.1038/npp.2009.126

Dobie, R. A. (2008). The burdens of age-related and occupational noise-induced hearing loss in the United States. *Ear Hear.* 29, 565–577. doi: 10.1097/aud.0b013e31817349ec

Donzis, E. J., and Thompson, L. T. (2014). D-Cycloserine enhances both intrinsic excitability of CA1 hippocampal neurons and expression of activity-regulated cytoskeletal (Arc) protein. *Neurosci. Lett.* 571, 50–54. doi: 10.1016/j.neulet.2014.04.035

Duclot, F., and Kabbaj, M. (2017). The role of early growth response 1 (EGR1) in brain plasticity and neuropsychiatric disorders. *Front. Behav. Neurosci.* 11:35. doi: 10.3389/fnbeh.2017.00035

Eggermont, J. J. (2016). Can animal models contribute to understanding tinnitus heterogeneity in humans? *Front. Aging Neurosci.* 8:265. doi: 10.3389/fnagi.2016.00265

Engineer, N. D., Riley, J. R., Seale, J. D., Vrana, W. A., Shetake, J. A., Sudanagunta, S. P., et al. (2011). Reversing pathological neural activity using targeted plasticity. *Nature* 470, 101–104. doi: 10.1038/nature09656

Erlander, M. G., Tillakaratne, N. J. K., Feldblum, S., Patel, N., and Tobin, A. J. (1991). Two genes encode distinct glutamate decarboxylases. *Neuron* 7, 91–100. doi: 10.1016/0896-6273(91)90077-d

Farmer, G. E., and Thompson, L. T. (2012). Learning-dependent plasticity of hippocampal CA1 pyramidal neuron postburst afterhyperpolarizations and increased excitability after inhibitory avoidance learning depend upon basolateral amygdala inputs. *Hippocampus* 22, 1703–1719. doi: 10.1002/hipo.22005

Finch, D. M., Derian, E. L., and Babb, T. L. (1984). Afferent fibers to rat cingulate cortex. *Exp. Neurol.* 83, 468–485. doi: 10.1016/0014-4886(84)90116-x

Fuchs, P. N., Peng, Y. B., Boyette-Davis, J. A., and Uhelski, M. L. (2014). The anterior cingulate cortex and pain processing. *Front. Integr. Neurosci.* 8:35. doi: 10.3389/fnint.2014.00035

Gall, C. M., Hess, U. S., and Lynch, G. (1998). Mapping brain networks engaged by, and changed by, learning. *Neurobiol. Learn. Mem.* 70, 14–36. doi: 10.1006/nlme.1998.3835

Goble, T. J., Møller, A. R., and Thompson, L. T. (2009). Acute high-intensity sound exposure alters responses of place cells in hippocampus. *Hear. Res.* 253, 52–59. doi: 10.1016/j.heares.2009.03.002

Gong, N., Zhang, M., Zhang, X. B., Chen, L., Sun, G. C., and Xu, T. L. (2008). The aspirin metabolite salicylate enhances neuronal excitation in rat hippocampal CA1 area through reducing GABAergic inhibition. *Neuropharmacology* 54, 454–463. doi: 10.1016/j.neuropharm.2007.10.017

Guderian, S., Dzieciol, A. M., Gadian, D. G., Jentschke, S., Doeller, C. F., Burgess, N., et al. (2015). Hippocampal volume reduction in humans predicts impaired allocentric spatial memory in virtual-reality navigation. *J. Neurosci.* 35, 14123–14131. doi: 10.1523/jneurosci.0801-15.2015

Hadland, K. A., Rushworth, M. F. S., Gaffan, D., and Passingham, R. E. (2003). The effect of cingulate lesions on social behaviour and emotion. *Neuropsychologia* 41, 919–931. doi: 10.1016/s0028-3932(02)00325-1

Heeringa, A. N., and van Dijk, P. (2016). The immediate effects of acoustic trauma on excitation and inhibition in the inferior colliculus: a Wiener-kernel analysis. *Hear. Res.* 331, 47–56. doi: 10.1016/j.heares.2015.10.007

Helfer, T. M., Jordan, N. N., Lee, R. B., Pietrusiak, P., Cave, K., and Schairer, K. (2011). Noise-induced hearing injury and comorbidities among postdeployment U.S. Army soldiers: April 2003-June (2009). *Am. J. Audiol.* 20, 33–41. doi: 10.1044/1059-0889(2011/10-0033)

Herman, J. P., and Cullinan, W. E. (1997). Neurocircuitry of stress: central control of the hypothalamo-pituitary-adrenocortical axis. *Trends Neurosci.* 20, 78–84. doi: 10.1016/s0166-2236(96)10069-2

Herman, J. P., Figueiredo, H., Mueller, N. K., Ulrich-Lai, Y., Ostrander, M. M., Choi, D. C., et al. (2003). Central mechanisms of stress integration: hierarchical circuitry controlling hypothalamo-pituitary-adrenocortical responsiveness. *Front. Neuroendocrinol.* 24, 151–180. doi: 10.1016/j.yfrne.2003.07.001

Holloway-Erickson, C. M., McReynolds, J. R., and McIntyre, C. K. (2012). Memory-enhancing intra-basolateral amygdala infusions of clenbuterol increase Arc and CaMKIIα protein expression in the rostral anterior cingulate cortex. *Front. Behav. Neurosci.* 6:17. doi: 10.3389/fnbeh.2012.00017

Hunter, M. D., Eickhoff, S. B., Miller, T. W. R., Farrow, T. F. D., Wilkinson, I. D., and Woodruff, P. W. R. (2006). Neural activity in speech-sensitive auditory cortex during silence. *Proc. Natl. Acad. Sci. U S A* 103, 189–194. doi: 10.1073/pnas.0506268103

Hudson, A. J. (2000). Pain perception and response: central nervous system mechanisms. *Can. J. Neurol. Sci.* 27, 2–16. doi: 10.1017/s0317167100051908

Jastreboff, P. J. (1990). Phantom auditory perception (tinnitus): mechanisms of generation and perception. *Neurosci. Res.* 8, 221–254. doi: 10.1016/0168-0102(90)90031-9

Jastreboff, P. J., Brennan, J. F., Coleman, J. K., and Sasaki, C. T. (1988). Phantom auditory sensation in rats: an animal model for tinnitus. *Behav. Neurosci.* 102, 811–822. doi: 10.1037/0735-7044.102.6.811

Jastreboff, P., and Jastreboff, M. M. (2000). Tinnitus retraining therapy (TRT) as a method for treatment of tinnitus and hyperacusis patients. *J. Am. Acad. Audiol.* 11, 162–177.

Kandratavicius, L., Lopes-Aguiar, C., Bueno-Júnior, L. S., Romcy-Pereira, R. N., Hallak, J. E. C., and Leite, J. P. (2012). Psychiatric comorbidities in temporal lobe epilepsy: possible relationships between psychotic disorders and involvement of limbic circuits. *Braz. J. Psychiatry* 34, 454–466. doi: 10.1016/j.rbp.2012.04.007

Kapolowicz, M. R., and Thompson, L. T. (2016). Acute high-intensity noise induces rapid Arc protein expression but fails to rapidly change GAD expression in amygdala and hippocampus of rats: effects of treatment with D-cycloserine. *Hear. Res.* 342, 69–79. doi: 10.1016/j.heares.2016.09.010

Khimich, D., Nouvian, R., Pujol, R., tom Dieck, S., Egner, A., Gundelfinger, E. D., et al. (2005). Hair cell synaptic ribbons are essential for synchronous auditory signalling. *Nature* 434, 889–894. doi: 10.1038/nature03418

Kishi, T., Tsumori, T., Yokota, S., and Yasui, Y. (2006). Topographical projection from thehippocampal formation to the amygdala: a combined anterograde and retro-grade tracing study in the rat. *J. Comp. Neurol.* 496, 349–368. doi: 10.1002/cne.20919

Klinge, C., Röder, B., and Büchel, C. (2010). Increased amygdala activation to emotional auditory stimuli in the blind. *Brain* 133, 1729–1736. doi: 10.1093/brain/awq102

Kozlovskiy, S. A., Vartanov, A. V., Nikonova, E. Y., Pyasik, M. M., and Velichkovsky, B. M. (2012). The cingulate cortex and human memory processes. *Psychol. Russ.* 5, 231–243. doi: 10.11621/pir.2012.0014

Kraus, K. S., and Canlon, B. (2012). Neuronal connectivity and interactions between the auditory and limbic systems. *Hear. Res.* 288, 34–46. doi: 10.1016/j.heares.2012.02.009

Kraus, K. S., Mitra, S., Jimenez, Z., Hinduja, S., Ding, D., Jiang, H., et al. (2010). Noise trauma impairs neurogenesis in the rat hippocampus. *Neuroscience* 167, 1216–1226. doi: 10.1016/j.neuroscience.2010.02.071

Kujawa, S. G., and Liberman, M. C. (2009). Adding insult to injury: cochlear nerve degeneration after "temporary" noise-induced hearing loss. *J. Neurosci.* 29, 14077–14085. doi: 10.1523/JNEUROSCI.2845-09.2009

LeDoux, J. (2007). The amygdala. *Curr. Biol.* 17, R868–R874. doi: 10.1016/j.cub.2007.08.005

LeDoux, J. E., and Farb, C. R. (1991). Neurons of the acoustic thalamus that project to the amygdala contain glutamate. *Neurosci. Lett.* 134, 145–149. doi: 10.1016/0304-3940(91)90527-z

Lercher, P., Evans, G. W., and Meis, M. (2003). Ambient noise and cognitive processes among primary schoolchildren. *Environ. Behav.* 35, 725–735. doi: 10.1177/0013916503256260

Link, W., Konietzko, U., Kauselmann, G., Krugt, M., Schwanke, B., Frey, U., et al. (1995). Somatodendritic expression of an immediate early gene is regulated by synaptic activity. *Proc. Natl. Acad. Sci. U S A* 92, 5734–5738. doi: 10.1073/pnas.92.12.5734

Liu, L., Shen, P., He, T., Chang, Y., Shi, L., Tao, S., et al. (2016). Noise induced hearing loss impairs spatial learning/memory and hippocampal neurogenesis in mice. *Sci. Rep.* 6:20374. doi: 10.1038/srep20374

Liu, Y., Zhang, H., Li, X., Wang, Y., Lu, H., Qi, X., et al. (2007). Inhibition of voltage-gated channel currents in rat auditory cortex neurons by salicylate. *Neuropharmacology* 53, 870–880. doi: 10.1016/j.neuropharm.2007.08.015

Lockwood, A. H., Salvi, R. J., Coad, M. L., Towsley, M. A., Wack, D. S., and Murphy, B. W. (1998). The functional neuroanatomy of tinnitus: evidence for limbic system links and neural plasticity. *Neurology* 50, 114–120. doi: 10.1212/wnl.50.1.114

Lovitz, E. S., and Thompson, L. T. (2015). Memory-enhancing intra-basolateral amygdala clenbuterol infusion reduces post-burst afterhyperpolarizations in hippocampal CA1 pyramidal neurons following inhibitory avoidance learning. *Neurobiol. Learn. Mem.* 119, 34–41. doi: 10.1016/j.nlm.2014.12.004

Mahlke, C., and Wallhäusser-Franke, E. (2004). Evidence for tinnitus-related plasticity in the auditory and limbic system, demonstrated by arg3.1 and c-fos immunocytochemistry. *Hear. Res.* 195, 17–34. doi: 10.1016/j.heares.2004.03.005

McIntyre, C. K., Miyashita, T., Setlow, B., Marjon, K. D., Steward, O., Guzowski, J. F., et al. (2005). Memory-influencing intra-basolateral amygdala drug infusions modulate expression of Arc protein in the hippocampus. *Proc. Natl. Acad. Sci. U S A* 102, 10718–10723. doi: 10.1073/pnas.0504436102

Melcher, J. R., Levine, R. A., Bergevin, C., and Norris, B. (2009). The auditory midbrain of people with tinnitus: abnormal sound-evoked activity revisited. *Hear. Res.* 257, 63–74. doi: 10.1016/j.heares.2009.08.005

Mohedano-Moriano, A., Pro-Sistiaga, P., Arroyo-Jimenez, M. M., Artacho-Pérula, E., Insausti, A. M., Marcos, P., et al. (2007). Topographical and laminar distribution of cortical input to the monkey entorhinal cortex. *J. Anat.* 211, 250–260. doi: 10.1111/j.1469-7580.2007.00764.x

Møller, A. R., Møller, M. B., and Yokota, M. (1992). Some forms of tinnitus may involve the extralemniscal auditory pathway. *Laryngoscope* 102, 1165–1171. doi: 10.1288/00005537-199210000-00012

Møller, A. R., and Rollins, P. R. (2002). The non-classical auditory pathways are involved in hearing in children but not in adults. *Neurosci. Lett.* 319, 41–44. doi: 10.1016/s0304-3940(01)02516-2

Morris, R. G. M., Garrud, P., Rawlins, J. N. P., and O'Keefe, J. (1982). Place navigation impaired in rats with hippocampal lesions. *Nature* 297, 681–683. doi: 10.1038/297681a0

Mühlau, M., Rauschecker, J. P., Oestreicher, E., Gaser, C., Röttinger, M., Wohlschläger, A. M., et al. (2006). Structural brain changes in tinnitus. *Cereb. Cortex* 16, 1283–1288. doi: 10.1093/cercor/bhj070

Mühlnickel, W., Elbert, T., Taub, E., and Flor, H. (1998). Reorganization of auditory cortex in tinnitus. *Proc. Natl. Acad. Sci. U S A* 95, 10340–10343. doi: 10.1073/pnas.95.17.10340

Mulert, C., Leicht, G., Pogarell, O., Mergl, R., Karch, S., Juckel, G., et al. (2007). Auditory cortex and anterior cingulate cortex sources of the early evoked gamma-band response: relationship to task difficulty and mental effort. *Neuropsychologia* 45, 2294–2306. doi: 10.1016/j.neuropsychologia.2007.02.020

Munoz-Lopez, M. M., Mohedano-Moriano, A., and Insausti, R. (2010). Anatomical pathways for auditory memory in primates. *Front. Neuroanat.* 4:129. doi: 10.3389/fnana.2010.00129

Nunn, J. A., Graydon, F. J. X., Polkey, C. E., and Morris, R. G. (1999). Differential spatial memory impairment after right temporal lobectomy demonstrated using temporal titration. *Brain* 122, 47–59. doi: 10.1093/brain/122.1.47

O'Keefe, J., Burgess, N., Donnett, J. G., Jeffery, K. J., and Maguire, E. A. (1998). Place cells, navigational accuracy, and the human hippocampus. *Philos. Trans. R. Soc. B Biol. Sci.* 353, 1333–1340. doi: 10.1098/rstb.1998.0287

Oniani, T. N., Mandzhavidze, S. D., Gvetadze, L. B., and Varazashvili, P. N. (1989). Dynamics of neuronal activity in the cingulate gyrus during the sleep-wake cycle. *Neurophysiology* 21, 596–602. doi: 10.1007/bf01051960

Pace, E., Luo, H., Bobian, M., Panekkad, A., Zhang, X., Zhang, H., et al. (2016). A conditioned behavioral paradigm for assessing onset and lasting tinnitus in rats. *PLoS One* 11:e0166346. doi: 10.1371/journal.pone.0166346

Pandya, D. N., Van Hoesen, G. W., and Mesulam, M. M. (1981). Efferent connections of the cingulate gyrus in the rhesus monkey. *Exp. Brain Res.* 42, 319–330. doi: 10.1007/bf00237497

Penke, Z., Morice, E., Veyrac, A., Gros, A., Chagneau, C., LeBlanc, P., et al. (2014). Zif268/Egr1 gain of function facilitates hippocampal synaptic plasticity and long-term spatial recognition memory. *Philos. Trans. R. Soc. B Biol. Sci.* 369:20130159. doi: 10.1098/rstb.2013.0159

Phelps, E. A., and LeDoux, J. E. (2005). Contributions of the amygdala to emotion processing: from animal models to human behavior. *Neuron* 48, 175–187. doi: 10.1016/j.neuron.2005.09.025

Pioli, E. Y., Gaskill, B. N., Gilmour, G., Tricklebank, M. D., Dix, S. L., Bannerman, D., et al. (2014). An automated maze task for assessing hippocampus-sensitive memory in mice. *Behav. Brain Res.* 261, 249–257. doi: 10.1016/j.bbr.2013.12.009

Plath, N., Ohana, O., Dammermann, B., Errington, M. L., Schmitz, D., Gross, C., et al. (2006). Arc/Arg3.1 is essential for the consolidation of synaptic plasticity and memories. *Neuron* 52, 437–444. doi: 10.1016/j.neuron.2006.08.024

Rauschecker, J. P., Leaver, A. M., and Muhlau, M. (2010). Tuning out the noise: limbic-auditory interactions in tinnitus. *Neuron* 66, 819–826. doi: 10.1016/j.neuron.2010.04.032

Richardson, B. D., Brozoski, T. J., Ling, L. L., and Caspary, D. M. (2012). Targeting inhibitory neurotransmission in tinnitus. *Brain Res.* 1485, 77–87. doi: 10.1016/j.brainres.2012.02.014

Rizzardo, R., Savastano, M., Maron, M. B., Mangialaio, M., and Salvadori, L. (1998). Psychological distress in patients with tinnitus. *J. Otolaryngol.* 27, 21–25.

Roberts, L. E., Eggermont, J. J., Caspary, D. M., Shore, S. E., Melcher, J. R., and Kaltenbach, J. A. (2010). Ringing ears: the neuroscience of tinnitus. *J. Neurosci.* 30, 14972–14979. doi: 10.1523/JNEUROSCI.4028-10.2010

Roberts, L. E., Husain, F. T., and Eggermont, J. J. (2013). Role of attention in the generation and modulation of tinnitus. *Neurosci. Biobehav. Rev.* 37, 1754–1773. doi: 10.1016/j.neubiorev.2013.07.007

Ruel, J., Chabbert, C., Nouvian, R., Bendris, R., Eybalin, M., Leger, C. L., et al. (2008). Salicylate enables cochlear arachidonic-acid-sensitive NMDA receptor responses. *J. Neurosci.* 28, 7313–7323. doi: 10.1523/JNEUROSCI.5335-07.2008

Sah, P., Faber, E. S. L., Lopez De Armentia, M., and Power, J. (2003). The amygdaloid complex: anatomy and physiology. *Physiol. Rev.* 83, 803–834. doi: 10.1152/physrev.00002.2003

Schlee, W., Hartmann, T., Langguth, B., and Weisz, N. (2009). Abnormal resting-state cortical coupling in chronic tinnitus. *BMC Neurosci.* 10:11. doi: 10.1186/1471-2202-10-11

Scholzen, T., and Gerdes, J. (2000). The Ki-67 protein: from the known and the unknown. *J. Cell. Physiol.* 182, 311–322. doi: 10.1002/(sici)1097-4652(200003)182:3<311::aid-jcp1>3.0.co;2-9

Sellmeijer, J., Mathis, V., Hugel, S., Li, X.-H., Song, Q., Chen, Q.-Y., et al. (2018). Hyperactivity of anterior cingulate cortex areas 24a/24b drives chronic pain-induced anxiodepressive-like consequences. *J. Neurosci.* 38, 3102–3115. doi: 10.1523/JNEUROSCI.3195-17.2018

Sengupta, A., Yau, J. O. Y., Jean-Richard-Dit-Bressel, P., Liu, Y., Millan, E. Z., Power, J. M., et al. (2018). Basolateral amygdala neurons maintain aversive emotional salience. *J. Neurosci.* 38, 3001–3012. doi: 10.1523/JNEUROSCI.2460-17.2017

Shackman, A. J., Salomons, T. V., Slagter, H. A., Fox, A. S., Winter, J. J., and Davidson, R. J. (2011). The integration of negative affect, pain and cognitive control in the cingulate cortex. *Nat. Rev. Neurosci.* 12, 154–167. doi: 10.1038/nrn2994

Shepherd, J. D., Rumbaugh, G., Wu, J., Chowdhury, S., Kuhl, D., Huganir, R. L., et al. (2006). Arc/Arg3.1 mediates homeostatic synaptic scaling of AMPA receptors. *Neuron* 52, 475–484. doi: 10.1016/j.neuron.2006.08.034

Singer, W., Zuccotti, A., Jaumann, M., Lee, S. C., Panford-Walsh, R., Xiong, H., et al. (2013). Noise-induced inner hair cell ribbon loss disturbs central arc mobilization: a novel molecular paradigm for understanding tinnitus. *Mol. Neurobiol.* 47, 261–279. doi: 10.1007/s12035-012-8372-8

Squire, L. R., Clark, R. E., and Knowlton, B. J. (2001). Retrograde amnesia. *Hippocampus* 11, 50–55. doi: 10.1002/1098-1063(2001)11:1<50::AID-HIPO1019>3.0.CO;2-G

Stevens, F. L., Hurley, R. A., and Taber, K. H. (2011). Anterior cingulate cortex: unique role in cognition and emotion. *J. Neuropsychiatry Clin. Neurosci.* 23, 120–125. doi: 10.1176/appi.neuropsych.23.2.121

Steward, O., and Worley, P. F. (2001). Selective targeting of newly synthesized Arc mRNA to active synapses requires NMDA receptor activation. *Neuron* 30, 227–240. doi: 10.1016/s0896-6273(01)00275-6

Stolzberg, D., Salvi, R. J., and Allman, B. L. (2012). Salicylate toxicity model of tinnitus. *Front. Syst. Neurosci.* 6:28. doi: 10.3389/fnsys.2012.00028

Stypulkowski, P. H. (1990). Mechanisms of salicylate ototoxicity. *Hear. Res.* 46, 113–146. doi: 10.1016/0378-5955(90)90144-e

Tae, W. S., Yakunina, N., Lee, W. H., Ryu, Y. J., Ham, H. K., Pyun, S. B., et al. (2018). Changes in the regional shape and volume of subcortical nuclei in patients with tinnitus comorbid with mild hearing loss. *Neuroradiology* 60, 1203–1211. doi: 10.1007/s00234-018-2093-2

Tang, Y.-P., Shimizu, E., Dube, G. R., Rampon, C., Kerchner, G. A., Zhuo, M., et al. (1999). Genetic enhancement of learning and memory in mice. *Nature* 401, 63–69. doi: 10.1038/43432

Thompson, L. T., and Best, P. J. (1989). Place cells and silent cells in the hippocampus of freely-behaving rats. *J. Neurosci.* 9, 2382–2390. doi: 10.1523/JNEUROSCI.09-07-02382.1989

Thompson, L. T., and Best, P. J. (1990). Long-term stability of the place-field activity of single units recorded from the dorsal hippocampus of freely behaving rats. *Brain Res.* 509, 299–308. doi: 10.1016/0006-8993(90)90555-p

Thompson, L. T., and Disterhoft, J. F. (1997). Age- and dose-dependent facilitation of associative eyeblink conditioning by D-cycloserine in rabbits. *Behav. Neurosci.* 111, 1303–1312. doi: 10.1037/0735-7044.111.6.1303

Thompson, L. T., Moskal, J. R., and Disterhoft, J. F. (1992). Hippocampus-dependent learning facilitated by a monoclonal antibody or D-cycloserine. *Nature* 359, 638–641. doi: 10.1038/359638a0

Tischmeyer, W., and Grimm, R. (1999). Activation of immediate early genes and memory formation. *Cell. Mol. Life Sci.* 55, 564–574. doi: 10.1007/s000180050315

Turner, J. G., Brozoski, T. J., Bauer, C. A., Parrish, J. L., Myers, K., Hughes, L. F., et al. (2006). Gap detection deficits in rats with tinnitus: a potential novel screening tool. *Behav. Neurosci.* 120, 188–195. doi: 10.1037/0735-7044.120.1.188

Vanneste, S., and De Ridder, D. (2013). Brain areas controlling heart rate variability in tinnitus and tinnitus-related distress. *PLoS One* 8:e59728. doi: 10.1371/journal.pone.0059728

Vanneste, S., Plazier, M., der Loo, E. V., de Heyning, P. V., Congedo, M., and De Ridder, D. (2010). The neural correlates of tinnitus-related distress. *NeuroImage* 52, 470–480. doi: 10.1016/j.neuroimage.2010.04.029

Vogt, B. A. (2005). Pain and emotion interactions in subregions of the cingulate gyrus. *Nat. Rev. Neurosci.* 6, 533–544. doi: 10.1038/nrn1704

Vogt, B. A., Rosene, D. L., and Pandya, D. N. (1979). Thalamic and cortical afferents differentiate anterior from posterior cingulate cortex in the monkey. *Science* 204, 205–207. doi: 10.1126/science.107587

von der Behrens, W. (2014). Animal models of subjective tinnitus. *Neural Plast.* 2014:741452. doi: 10.1155/2014/741452

Wallhäusser-Franke, E., Mahlke, C., Oliva, R., Braun, S., Wenz, G., and Langner, G. (2003). Expression of c-fos in auditory and non-auditory brain regions of the gerbil after manipulations that induce tinnitus. *Exp. Brain Res.* 153, 649–654. doi: 10.1007/s00221-003-1614-2

Wang, H., Brozoski, T. J., and Caspary, D. M. (2011). Inhibitory neurotransmission in animal models of tinnitus: maladaptive plasticity. *Hear. Res.* 279, 111–117. doi: 10.1016/j.heares.2011.04.004

Wang, D. V., and Ikemoto, S. (2016). Coordinated interaction between hippocampal sharp-wave ripples and anterior cingulate unit activity. *J. Neurosci.* 36, 10663–10672. doi: 10.1523/JNEUROSCI.1042-16.2016

Wang, X. X., Jin, Y., Luo, B., Sun, J. W., Zhang, J., Wang, M., et al. (2016). Sodium salicylate potentiates the GABAB-GIRK pathway to suppress rebound depolarization in neurons of the rat's medial geniculate body. *Hear. Res.* 332, 104–112. doi: 10.1016/j.heares.2015.11.013

Wang, H. T., Luo, B., Zhou, K. Q., Xu, T. L., and Chen, L. (2006). Sodium salicylate reduces inhibitory postsynaptic currents in neurons of rat auditory cortex. *Hear. Res.* 215, 77–83. doi: 10.1016/j.heares.2006.03.004

Weinberger, N. M. (2011). The medial geniculate, not the amygdala, as the root of auditory fear conditioning. *Hear. Res.* 274, 61–74. doi: 10.1016/j.heares.2010.03.093

Wu, C., Wu, X., Yi, B., Cui, M., Wang, X., Wang, Q., et al. (2018). Changes in GABA and glutamate receptors on auditory cortical excitatory neurons in a rat model of salicylate-induced tinnitus. *Am. J. Transl. Res.* 10, 3941–3955.

Wu, H., Xu, F.-L., Yin, Y., Da, P., You, X.-D., Xu, H.-M., et al. (2015). Salicylate-induced changes in immediate-early genes in the hippocampal CA1 area. *Mol. Med. Rep.* 12, 1625–1630. doi: 10.3892/mmr.2015.3608

Xie, K., Kuang, H., and Tsien, J. Z. (2013). Mild blast events alter anxiety, memory, and neural activity patterns in the anterior cingulate cortex. *PLoS One* 8:e64907. doi: 10.1371/journal.pone.0064907

Yorgason, J. G., Luxford, W., and Kalinec, F. (2011). *In vitro* and *in vivo* models of drug ototoxicity: studying the mechanisms of a clinical problem. *Expert Opin. Drug Metab. Toxicol.* 7, 1521–1534. doi: 10.1517/17425255.2011.614231

Yu, Y. F., Zhai, F., Dai, C. F., and Hu, J. J. (2011). The relationship between age-related hearing loss and synaptic changes in the hippocampus of C57BL/6J mice. *Exp. Gerontol.* 46, 716–722. doi: 10.1016/j.exger.2011.04.007

Zald, D. H., and Pardo, J. V. (2002). The neural correlates of aversive auditory stimulation. *NeuroImage* 16, 746–753. doi: 10.1006/nimg.2002.1115

Zhang, J. S., Kaltenbach, J. A., Wang, J., and Kim, S. A. (2003). Fos-like immunoreactivity in auditory and nonauditory brain structures of hamsters previously exposed to intense sound. *Exp. Brain Res.* 153, 655–660. doi: 10.1007/s00221-003-1612-4

Zhang, J., Luo, H., Pace, E., Li, L., and Liu, B. (2016). Psychophysical and neural correlates of noised-induced tinnitus in animals: intra- and inter-auditory and non-auditory brain structure studies. *Hear. Res.* 334, 7–19. doi: 10.1016/j.heares.2015.08.006

Zheng, Y., Hamilton, E., Begum, S., Smith, P. F., and Darlington, C. L. (2011). The effects of acoustic trauma that can cause tinnitus on spatial performance in rats. *Neuroscience* 186, 48–56. doi: 10.1016/j.neuroscience.2011.04.052

Zheng, Y., McPherson, K., and Smith, P. F. (2014). Effects of early and late treatment with L-baclofen on the development and maintenance of tinnitus caused by acoustic trauma in rats. *Neuroscience* 258, 410–421. doi: 10.1016/j.neuroscience.2013.11.032

Conflict of Interest: The authors declare that the research was conducted in the absence of any commercial or financial relationships that could be construed as a potential conflict of interest.

frontiers in Systems Neuroscience

ORIGINAL RESEARCH
published: 31 January 2020
doi: 10.3389/fnsys.2020.00004

Reversing Hemianopia by Multisensory Training Under Anesthesia

Huai Jiang, Benjamin A. Rowland and Barry E. Stein*

Department of Neurobiology and Anatomy, Wake Forest School of Medicine, Medical Center Boulevard, Winston-Salem, NC, United States

Hemianopia is characterized by blindness in one half of the visual field and is a common consequence of stroke and unilateral injury to the visual cortex. There are few effective rehabilitative strategies that can relieve it. Using the cat as an animal model of hemianopia, we found that blindness induced by lesions targeting all contiguous areas of the visual cortex could be rapidly reversed by a non-invasive, multisensory (auditory-visual) exposure procedure even while animals were anesthetized. Surprisingly few trials were required to reinstate vision in the previously blind hemisphere. That rehabilitation was possible under anesthesia indicates that the visuomotor behaviors commonly believed to be essential are not required for this recovery, nor are factors such as attention, motivation, reward, or the various other cognitive features that are generally thought to facilitate neuro-rehabilitative therapies.

Keywords: multisensory, rehabilitation, vision, cross-modal, hemianopia

OPEN ACCESS

Edited by:
Christopher I. Petkov, Newcastle University, United Kingdom

Reviewed by:
Andrew J. King, University of Oxford, United Kingdom
Kerstin Erika Schmidt, Federal University of Rio Grande do Norte, Brazil

****Correspondence:***
Benjamin A. Rowland
browland@wakehealth.edu

Received: *27 September 2019*
Accepted: *13 January 2020*
Published: *31 January 2020*

Citation:
Jiang H, Rowland BA and Stein BE (2020) Reversing Hemianopia by Multisensory Training Under Anesthesia. Front. Syst. Neurosci. 14:4. doi: 10.3389/fnsys.2020.00004

INTRODUCTION

Extensive damage to the visual cortex on one side of the brain produces blindness in the opposite hemifield (hemianopia) despite the sparing of other visual centers far from the site of the physical insult (Sand et al., 2013; Goodwin, 2014). Of special note is the superior colliculus (SC), a midbrain structure that plays a major role in detecting, localizing, and orienting to visual targets. Its multisensory neurons allow it to use non-visual cues to facilitate this process (Stein and Meredith, 1993), and its location in the midbrain ensures that it is not directly damaged by a hemianopia-inducing cortical insult. Yet, as shown in the cat model of hemianopia, the loss of visual responses in the multisensory layers of the SC and the total absence of visual detection and orientation responses to contralateral visual stimuli following lesions of visual cortex reveal that it too is compromised, presumably *via* secondary excitotoxic injuries that may alter other input structures such as the basal ganglia (Jiang et al., 2009, 2015). Interestingly, the dysfunction of SC appeared to be limited to its visual role. Its other sensory representations and sensorimotor roles remained intact: SC-mediated auditory and tactile detection and orientation responses were readily elicited (see also Sprague and Meikle, 1965).

Previously it was shown that hemianopia could be reversed using a non-invasive multisensory training paradigm (Jiang et al., 2015). The procedure consisted of presenting cross-modal combinations of spatiotemporally congruent auditory-visual cues in the blind hemifield of alert animals engaged in a sensory localization task. Because the animals were not deafened by the cortical lesion, they readily responded to the auditory-visual stimulus complex. After only a few

weeks of daily multisensory training sessions, a striking change occurred: not only could the animals now detect and localize a visual stimulus throughout the previously blind hemifield, but they could also discriminate elementary visual patterns there. Visual responses that had been lost in the multisensory layers of the ipsilesional SC also returned, and cortico-SC circuits normally engaged in multisensory integration (i.e., projections from the anterior ectosylvian sulcus, AES) were found to be crucial for the recovery. The recovery could not be induced by training with visual or auditory cues alone. In an important series of studies in human patients, Làdavas and colleagues (Bolognini et al., 2005; Leo et al., 2008; Passamonti et al., 2009; Dundon et al., 2015a,b) used a similar training paradigm and also met with success in evoking contralesional visual responses.

It is commonly believed that the success of this rehabilitative paradigm is a retraining of the visuomotor targeting behavior itself (see, review in Dundon et al., 2015a). In this case, the key factor would be the orienting action (initially elicited by the auditory stimulus) in the presence of the visual stimulus. Also, if true, it is reasonable to hypothesize that the effectiveness of this paradigm would be facilitated by other factors such as motivation, attention, arousal, and reinforcement, as these are commonly believed to enhance most neuro-rehabilitative therapies. An alternative explanation, however, is that the paradigm operates *via* the brain's inherent mechanisms for multisensory plasticity, which operate independent of these factors and can be engaged under anesthesia (Yu et al., 2013). In this case, the requirement would only be repeated, reliable exposure to the visual-auditory stimulus complex in the blinded hemifield. The present study examined this possibility directly.

MATERIALS AND METHODS

Adult mongrel cats (four male, three female) were obtained from a USDA-licensed commercial animal breeding facility (Liberty Labs, Waverly, NY, USA). The experimental procedures used were in compliance with the National Institutes of Health "Guide for the Care and Use of Laboratory Animals" (8th edition, NRC 2011) and approved by the Institutional Animal Care and Use Committee at Wake Forest School of Medicine. Each animal was first screened to ensure that it was tractable and responded to visual and auditory stimuli in both hemifields. All efforts were made to minimize the number of animals used.

Visual Detection and Orientation Testing

Visual orientation capabilities were quantitatively evaluated in a semicircular perimetry arena using previously described methods (see Jiang et al., 2015, see also **Figure 1A**). Animals were maintained at 80%–85% of body weight and obtained most of their daily food intake during, or immediately after, each behavioral session. Each animal was first trained to fixate directly ahead at a food reward held in forceps by one experimenter and protruded through a hole in the front wall of the apparatus 58 cm ahead at the 0° fixation point. Trial initiation was always contingent upon the animal establishing fixation. Once released by the animal handler (a second experimenter), the animal was required to move directly ahead to obtain the food reward. It was then trained to respond to the test stimulus (a white ping-pong ball at the end of a stick) presented at any 15° interval from 105° left to 105° right. This required little training as animals responded to the stimulus almost reflexively. Stimuli were presented manually and introduced suddenly from behind a black curtain while the animal was fixating. Additionally, on some trials, the ball remained hidden behind the opaque curtain and was tapped on the side of the apparatus to produce an auditory stimulus. If the animal oriented to and approached any test stimulus it was rewarded there, but could also move directly ahead to obtain a similar reward at the fixation point. The animal handler did not know the location of the upcoming test stimulus. This was determined by the experimenter holding the food reward, who also ensured that the trial did not begin if the animal had broken fixation. The verbal command "Go" triggered the release of the animal. "Catch trials" in which no stimulus was presented were interleaved with test trials at different locations to encourage the animal to minimize breaks in fixation, scanning movements, and "false" responses. Generally, in a given session, each of the 15° locations was tested at least 4–5 times. With few exceptions, the total number of trials/location was at least 100. The training criterion was an average of 95% correct responses. All animals reached criterion readily, had normal visual fields, and their weekly weight records revealed stable weight profiles.

Visual Cortex Ablation

Surgical procedures were conducted using sterile techniques. Animals were sedated with an initial injection of buprenorphine (0.005–0.01 mg/kg, i.m.) /acepromazine (0.05–0.1 mg/kg, i.m.) to render them tractable. Then, each animal was anesthetized with sodium pentobarbital (22–30 mg/kg, i.v; Jiang et al., 2009, 2015). Antibiotics (cefazolin, 20–30 mg/kg, i.m.) were provided preoperatively and, after the loss of reflexes to external stimuli, the animal was intubated through the mouth for later ventilation and placed in a stereotaxic head-holder and on a heating pad. A cannula was placed in the saphenous vein, and body temperature, expiratory CO_2, blood pressure, and heart rate were monitored *via* a SurgiVet Advisor (Smith Medical, Dublin, OH, USA) and maintained within normal physiological limits. The hair over the surgical site was removed and the area was coated with betadine. The scalp was opened, a craniotomy was made, the dura was reflected and the gray matter was aspirated. The lesion (see **Figure 2**) was made in the left hemisphere of one animal and the right hemisphere of six animals (prior work by Jiang et al., 2015 shows no hemispheric differences) to include the posterior three-fourths of the lateral and suprasylvian gyri, a portion of the posterior ectosylvian gyrus, the medial aspect of the cortex posterior to the cruciate gyrus above the splenial sulcus so that the lesion targeted Brodmann areas: 17, 18, 19, 20a, 20b, 21a, 21b, 5, 7, and the DLS, VLS, PS, PMLS, PLLS, AMLS, ALLS, and SVA, but always spared the AES. This large lesion causes degeneration of the ipsilesional lateral geniculate nucleus (LGN; **Figure 2**).

The lesion cavity was filled with moist gel foam, the cranial bone was replaced, and the incision closed with sutures. A corticosteroid anti-inflammatory (dexamethasone; 1 mg/kg,

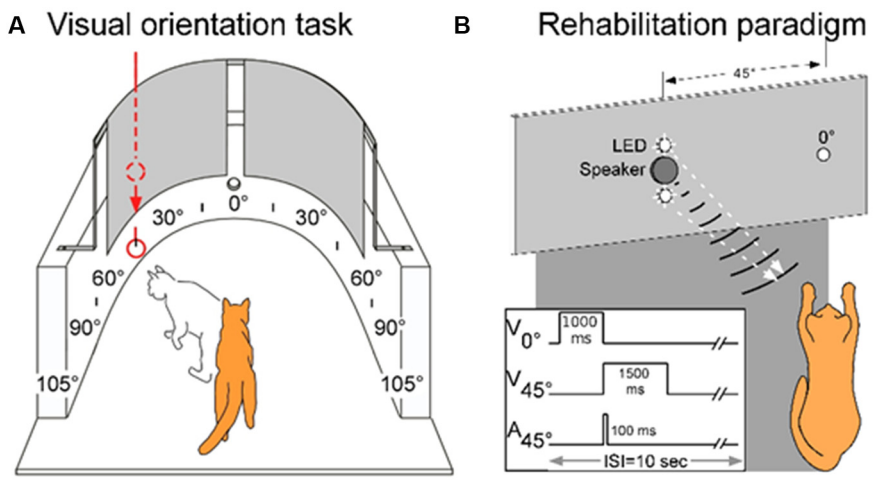

FIGURE 1 | The testing, training, and multisensory exposure paradigms. **(A)** Visual and auditory detection/localization capabilities were first assessed on both sides of space using a simple behavioral task. Cats were trained to fixate forward at 0° then orient to, and directly approach, a visual or auditory stimulus at any location in space. Visual stimuli were produced by lowering a ping pong ball below an obscuring curtain, and auditory stimuli were produced by tapping the ball against the apparatus wall while still obscured by the curtain. **(B)** Following surgery, a rehabilitation paradigm consisted of weekly sessions in which animals were exposed to cross-modal cues while anesthetized. As shown by the schematic at the lower left, the central LED (at 0°) of the display was briefly illuminated to signal the onset of the trial. It was followed by the combined LED-broadband noise burst at 45° in the contralesional hemifield. Traces illustrate the onset and duration of the stimuli. Panel **(A)** adapted from Jiang et al. (2015).

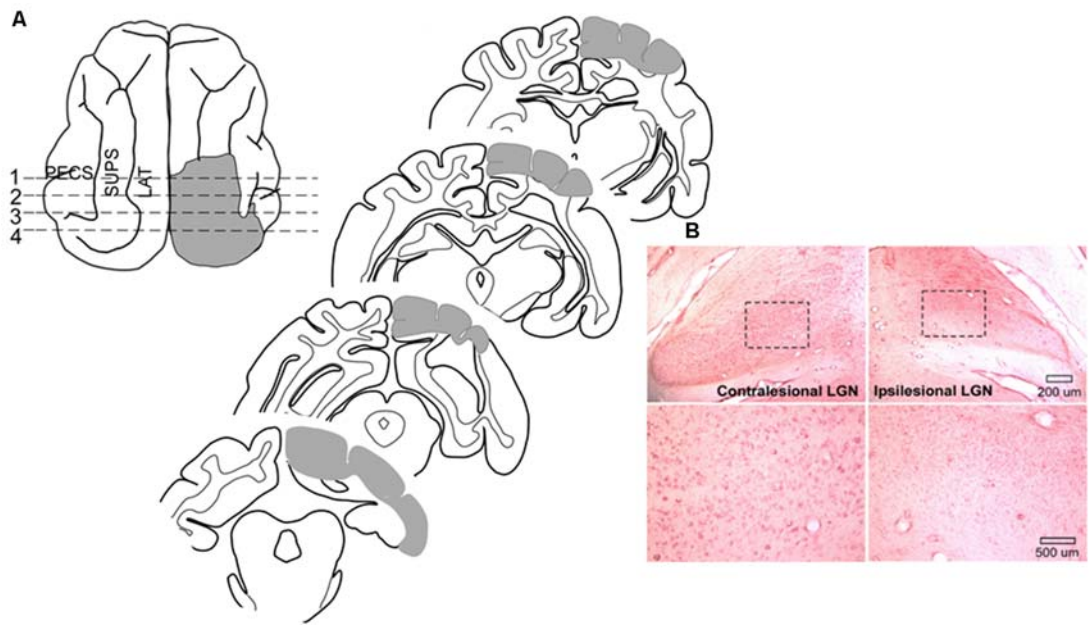

FIGURE 2 | Cortical areas ablated and degeneration of the Lateral Geniculate Nucleus (LGN). **(A)** Tracings of the brain regions ablated in one animal showing both the dorsal view and coronal sections. Ablated areas are indicated in gray. All animals received similar lesions. All lesions induced a profound contralesional hemianopia. **(B)** Microscopic images of the LGN in this animal. Zoomed images of the outlined area below reveal the near complete absence of large neurons in the LGN on the same side of the brain (ipsilesional).

i.m.) was given immediately after surgery to control edema, and analgesics (buprenorphine 0.005–0.01 mg/kg, i.m.) were routinely administered for a minimum of 24 h after surgery, and then provided daily as needed. The antibiotic cefazolin (20–30 mg/kg, i.m.) was given after surgery and continued as needed. Saline (50–200 ml, s.q. or i.v.) was provided to compensate for fluid loss. After the return of sternal recumbence and active locomotion, the animal was returned to its home cage.

Following surgery, each animal exhibited the characteristic tonic head deviation toward the lesion side and ipsiversive circling behavior that is associated with these lesions (Sprague, 1966; Sherman, 1977; Jiang et al., 2015). These symptoms resolved within 1 or 2 days. However, the absence of orientation to all manually presented visual stimuli and the total absence of blink-to-threat reflexes to contralesional visual stimuli persisted for the 3 month period used as the criterion for a "permanent" visual defect. The animal was then implanted with a head holding device to be used during rehabilitative training.

Animal Preparation for Multisensory Exposure and Electrophysiological Recording

Surgical procedures similar to those described above were used here. However, in this case, anesthesia was induced with ketamine hydrochloride (20–30 mg/kg, i.m.) and acepromazine maleate (0.05–0.1 mg/kg, i.m.), and maintained by artificial ventilation with isoflurane (0.5–4.0%). Expiratory CO_2 was maintained at 3.5%–4.5%, eyes were covered with a topical ophthalmic ointment and the craniotomy was made to provide access to the SC on both sides of the brain. A stainless-steel recording well/head-holder was fitted over the craniotomy and anchored to the skull with stainless-steel screws and dental acrylic (McHaffie and Stein, 1983). After a 10–14 day recovery period, multisensory rehabilitative exposures began.

During each of the exposure or recording sessions the animal was anesthetized in its home cage with ketamine hydrochloride (20–30 mg/kg, i.m.) and acepromazine maleate (0.05–0.1 mg/kg, i.m.). It was then transported to the experimental room. An endotracheal tube was inserted, and the animal was artificially respired. Its head was secured by attaching the head-holder to the stereotaxic frame without wounds or pressure points, and paralysis was induced with pancuronium bromide; (0.1 mg/kg, i.v.) to fix the eyes and pinnae. During the multisensory exposure period anesthesia, paralysis, and hydration were maintained *via* continuous intravenous infusion of ketamine hydrochloride (5–10 mg/kg/h) and pancuronium bromide (0.04–0.1 mg/kg/h) in 5% dextrose Ringer's solution (3–6 ml/h) through the saphenous vein. Blood pressure, heart rate, SpO_2 and respiratory CO_2 level were monitored continuously (Digital Vital Signs Monitor, SurgiVet V9200). End-tidal CO_2 was maintained at 3.5–4.5%. SpO_2 was maintained at >90%. Body temperature was kept at 37–38°C using a heating pad. The pupils were dilated with ophthalmic atropine sulfate (1%), and the eyes were fitted with contact lenses to focus them and prevent corneal drying.

The Multisensory Exposure Paradigm

Previous results have shown that extensive, repeated exposure to modality-specific visual or auditory stimuli in the blinded hemifield did not rehabilitate hemianopia, nor did exposure to visual-auditory pairs that were spatially or temporally incongruent (Jiang et al., 2015; Dakos et al., 2019a,b). Thus, all training trials contained spatiotemporally congruent visual-auditory stimulus pairs. The exposure sessions were conducted once/week and were preceded by a 2 h period of adaptation in a darkened room. In each exposure session, a pair of spatiotemporally congruent auditory-visual stimuli was repeatedly presented at 6-s intervals at 45° in the contralesional hemifield (**Figure 1B**). One animal was also tested with a series of auditory-visual exposures in the ipsilesional hemifield. The visual stimulus was presented for 1,500 ms against a dark background (∼0.75 cd/m^2). It was composed of a vertically-displaced pair of 10 mm white LEDs (the speaker for auditory stimulus delivery was located between the two LEDs), each covered by a diffusing filter made from a section of a white ping-pong ball (∼13.8 cd/m^2). The diameter of each light circle produced was approximately 5°. The center of the top circle was elevated approximately 2° above the animal's eyes and the bottom circle was approximately 7° below its eyes. The auditory stimulus was a broadband noise burst, 75 dB SPL against an ambient background of 48.4–52.7 dB SPL. It was presented for 100 ms. Animals received between 100 and 2,400 auditory-visual exposures per session. In one animal the number of stimulus presentations was varied in each session, in all others it was fixed at either: 100, 600, or 2,400 exposures/session.

Probing for Visual Recovery During the Multisensory Exposure Period

Rehabilitative success was assessed with "probe" trials in the perimetry arena (**Figure 1A**) on days in which there was no exposure session. These involved detecting the visual stimulus (the white ping-pong ball) at each of the target locations (see "Visual Detection and Orientation Testing" section above). Anesthetized exposure sessions were stopped at the first sign that contralesional visual orientation capabilities were restored. At that point, only behavioral assays were continued for a minimum of 2 months to verify the extent and persistence of the recovered function.

Electrophysiology Procedure

Animals were prepared for recording sessions (see above) after behavioral tests were completed. The purpose of these recordings was to determine whether visually-responsive neurons could be identified in the intermediate and deep layers of the SC of rehabilitated animals. Previous studies determined that this visual responsiveness is lost consequent to the lesions performed here and that it is restored concomitant with the return of the visually-guided behaviors tested here. Neuronal activity was recorded extracellularly with epoxylite-insulated tungsten microelectrodes (2–4 MΩ), then were bandpass-filtered, amplified, displayed on an oscilloscope, and subsequently processed to computer disc using a 1401+ hardware acquisition system (CED Systems, Cambridge, England). The single neuronal activity was sorted by running with CED Spike2 software. The visual receptive fields of isolated SC neurons were mapped on a Plexiglas hemisphere using a moving or stationary spot or bar of light from a hand-held ophthalmoscope. The presence of auditory responsiveness overlapping visual receptive fields was determined using broadband noise bursts (100 ms duration, 70 dB SPL) delivered from a movable speaker. For all quantitative tests, visual and auditory stimuli were presented repeatedly (n = 10–20 times/test, at 6–10 s intervals). Visual stimuli of various shapes and sizes were

presented through an electronically-controlled, galvanometer-driven mirror system. Auditory stimuli were controlled by a custom-built audio generator. The magnitudes of responses to visual and auditory stimuli presented alone and together in spatiotemporal concordance (i.e., simultaneously) were quantified as the mean number of stimulus-elicited impulses. Multisensory enhancement (ME) was quantified as the percent difference between the response elicited by a visual-auditory pair and the most robust response elicited by one of the component stimuli (Meredith and Stein, 1983).

Statistical Methods

All data are illustrated with the lesion depicted on the right side and the left side of space as contralesional. Data were analyzed for the central 180° of visual space in which pre-lesion visual performance was most reliable in all animals. Final stimulus detection and orientation accuracy were assessed with X^2 tests. Logistic regression was used to determine whether any significant differences in visual recovery were related to the different multisensory training conditions. This was accomplished by comparing regression models fit to data pooled across all animals (using nearest-neighbor interpolation to fill gaps) to models in which a single animal was extracted and fit separately from the pool. This allowed each animal's performance to be compared to the pooled data. The difference in deviances between the two models was evaluated against an X^2 distribution with 1 degree of freedom. The significance of physiological responses was evaluated with two-tailed *t*-tests.

Histological Evaluation of Cortical Lesions

At the termination of experimentation each animal was sedated with ketamine hydrochloride (20–30 mg/kg, i.m.) and acepromazine maleate (0.05–0.1 mg/kg i.m.) and, following the loss of reflexes, given a lethal dose of pentobarbital (100 mg/kg; i.p.). It was then perfused transcardially with 0.9% saline followed by 4% paraformaldehyde. The brain was removed, cut on a cryostat, and processed using routine histological procedures (neutral red staining; see **Figure 2**). The cortical lesion was reconstructed from photographs of the tissue block on the cryostat while serial coronal sections were taken. These were then referenced to standard anatomical maps (Scannell et al., 1996). Retrograde degeneration of the dorsal LGN was visualized microscopically.

RESULTS

Behavioral Results

The repeated presentation, to anesthetized animals, of congruent auditory-visual stimuli in the hemianopic field proved to be effective in rehabilitating hemianopia. Prior to the lesion, every animal achieved near-perfect performance in detecting visual stimuli at each tested location in the central 180° (**Figures 3**, **4**, "pre-lesion"). However, testing after a week of post-surgical recovery revealed that responses in contralesional space were entirely eliminated. Responses to visual stimuli in the ipsilesional (i.e., normal) hemifield remained intact, as did responses to auditory stimuli in both hemifields.

The hemianopia in each of these animals persisted throughout the post-surgical, pre-intervention period, which was a minimum of 3 months and in one case was extended to 15 months. After establishing that the defect was stable (**Figures 3**, **4**, "post-lesion"), multisensory exposure sessions began. In each case, the animal was anesthetized and paralyzed. After 3–7 weeks of these sessions, all animals began responding to visual stimuli in contralesional space. The delay between the start of the exposure sessions and the first signs of recovery was related to the density of exposures per session, but not systematically. There were no significant differences in the timing of recovery onset for animals given 600 exposures/session (range: 3–4 weeks) vs. 2,400 exposures/session (4 weeks; Wilcoxon test on days-until-recovery: $p = 0.63$), despite the four-fold increase in exposure density. However, reducing the density of exposures/session to 100 doubled the recovery period to 7 weeks. The timeline of six animals' exposure and recovery is described in **Table 1**. The table shows the total number of auditory-visual exposure trials, the number of exposure sessions, weeks of exposure, and the number of days between the start of the recovery, as well as when visual detection/localization performance had achieved pre-lesion levels. Data from the pilot animal (09NJO3) are not included despite its recovery, because cross-modal stimulus exposure was not systematic during this initial exploratory study (varying in frequency, timing, location, and identity).

Exposure sessions for each animal were terminated at the first appearance of contralesional visual responses. These initial responses always appeared at a location in central visual space (i.e., 15° or 30°, see **Figure 5**). The effective region expanded thereafter to more peripheral locations. However, within 1–2 weeks every animal reached ceiling performance at every contralesional location tested (**Figures 3**, **4**, "post-exposure"). This central-to-peripheral pattern was previously observed in animals rehabilitated while awake (Jiang et al., 2015), and occurred despite the fact that auditory-visual exposure stimuli were presented only at 45° in contralesional space. Apparently, the exposure location neither specifies the location at which responses will first be observed nor the extent of the restored visual field. The paradigm does not require exposure at every location to be successful. Furthermore, visual restoration did not vary systematically by exposure density and, except for the animal with 100 exposures/sessions, all animals recovered within approximately the same time period.

As a control, one animal was exposed to cross-modal stimuli (600 exposures/session for 9 weeks) at the homotopic location in the unaffected (ipsilesional) hemifield. These exposures failed to induce recovery. The animal was then switched to 600 exposures/session at 45° in the blind (contralesional) hemifield. It recovered at almost the same rate, and with the same pattern, as did its counterparts whose training began in the blind hemifield (**Figure 6**).

X^2 tests showed that each animal's visual detection and localization performance showed no significant deficit in the rehabilitated hemifield (from 15° to 90° of eccentricity, *p*-value range: 0.998–1, DF = 6). There was also no performance difference from that in ipsilesional space (*p*-value range: 0.993–1,

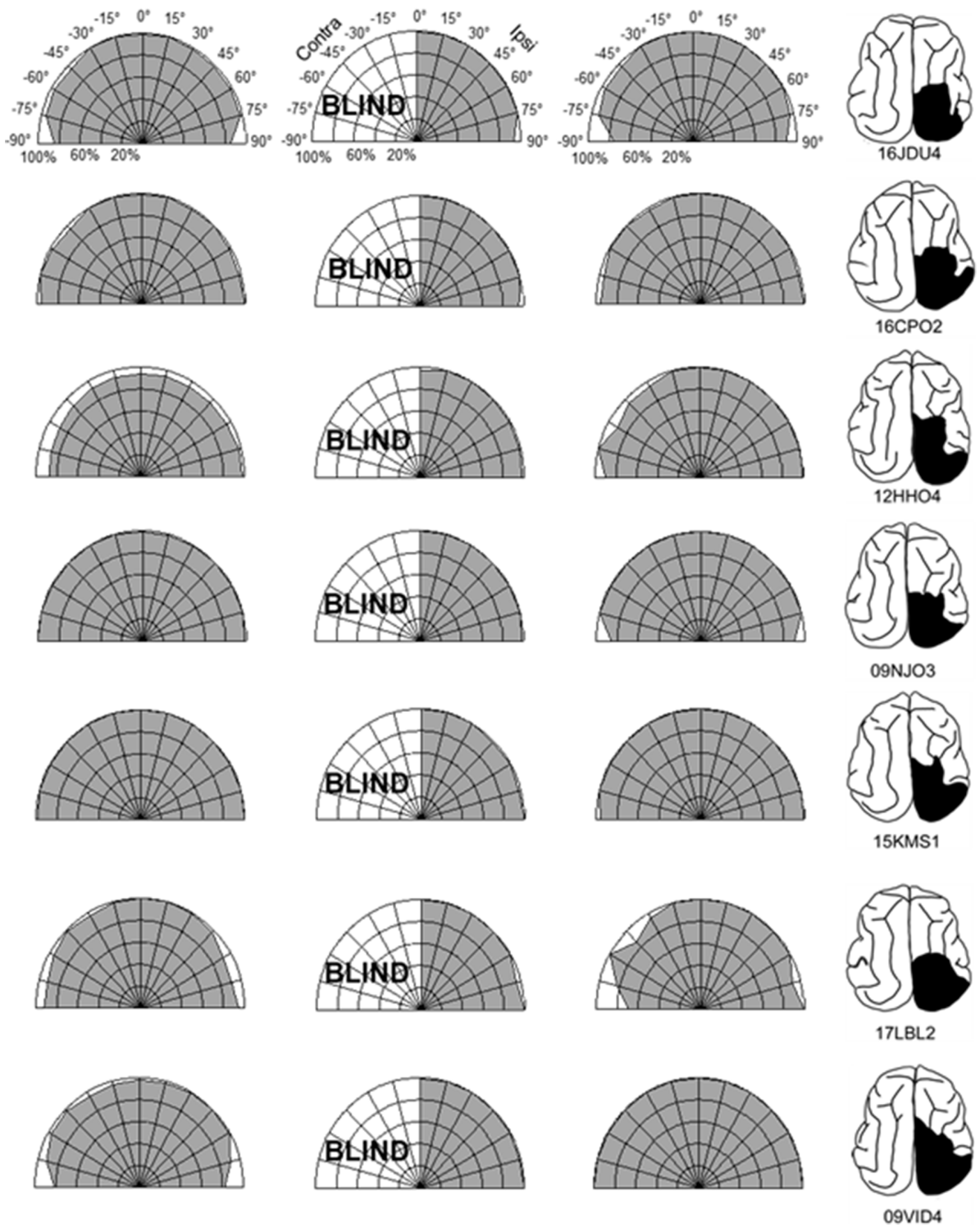

FIGURE 3 | Visual detection and orientation capabilities for each animal before the lesion (pre-lesion column), >3 months after the lesion (post-lesion), and after multisensory exposure (post-exposure). Polar charts depict the accuracy of responses to visual stimuli presented at eccentricities between 90° to the left and right of fixation (15° intervals). Concentric circles in the plot indicate accuracy increments of 20%. Performance of all animals at all locations was near-perfect prior to the lesion. After the lesion, responses to contralesional visual stimuli disappeared ("BLIND"), but returned to near-perfect following multisensory exposure. For illustration the contralesional hemifield is always drawn on the left.

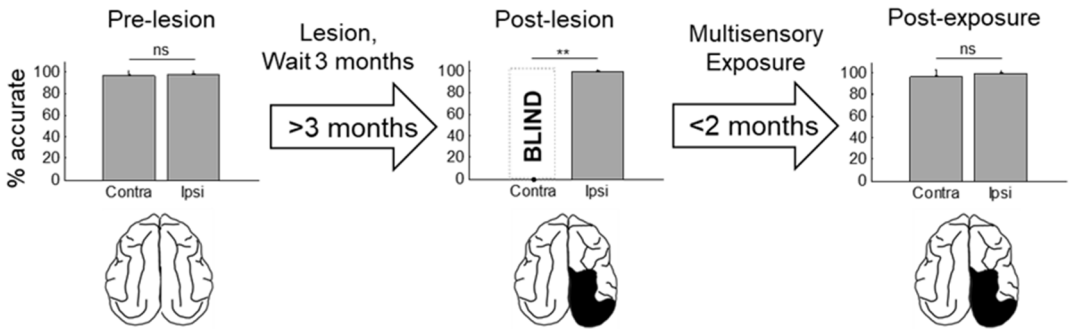

FIGURE 4 | Summary of the population results. Plotted is the percentage of accurate responses to visual stimuli averaged across animals and locations on the side of space ipsilateral (ipsi) and contralateral (contra) to the visual cortex lesion at three different time points: before the lesion (pre-lesion), >3 months after the lesion but before beginning the multisensory exposure series (post-lesion), and after the series was complete and behavior had stabilized (post-exposure, this required exposure sessions over several weeks). Error bars indicate the standard deviation across animals. Note that the results are highly consistent across animals. Dashed bar labeled "BLIND" indicates that, after the lesion and prior to rehabilitation, none of the animals detected visual stimuli at any tested location in contralesional space. Exemplar schematics of the lesion accompany each plot for illustration. ns, not significant, $^{**}p < 0.001$.

TABLE 1 | Exposure and recovery timelines for six animals (pilot animal excluded, see text).

Animal name	Exposures/Week	Exposures until the first contralesional response	Days from first contralesional response to full recovery
09VID4	600	2,400 (4 weeks)	6
12HHO4	600	3,000 (5 weeks)	7
15KMS1	2,400	12,000 (5 weeks)	10
16JDU4	100	800 (8 weeks)	5
16CPO2	600	2,400 (4 weeks)	7
17LBL2	600	3,000 (5 weeks)	8

The leftmost column indicates animal identity. The second column reports the number of weekly exposures. The third column shows the total number of auditory-visual exposures (and a number of weekly sessions), prior to the first response to a contralesional visual stimulus. The last column indicates the number of days between that first contralesional response and visual performance reaching pre-lesion levels. Each animal was tested with a 2–5 visual test/trials/location/day.

DF = 6), or from pre-lesion performance (p-value range: 0.990–1, DF = 6).

Electrophysiological Results

In the previous Jiang et al. (2015) study, it was noted that the superficial SC layers of hemianopic animals remained rich in visually-responsive neurons and that some visually-responsive neurons were also spared in the deeper, multisensory, layers of the SC. However, the spared deeper layer visual neurons had receptive fields that were restricted to central space (<15° from the midline). These neurons, which receive visual inputs directly from the retina and indirectly from extrastriate cortex in both hemispheres, play an important role in fixation (Baleydier, 1977; Baleydier et al., 1983; Ogasawara et al., 1984; Guitton and Munoz, 1991; Meredith and Ramoa, 1998) which was maintained in these animals. In contrast, the deep layer neurons that lost their visual responsiveness were those with more peripheral (e.g., >15° or more) receptive field centers, and which play a role in contralateral visuomotor responses (Stein and Clamann, 1981; Sparks, 1986; Jay and Sparks, 1987; Sparks and Hartwich-Young, 1989; Guitton and Munoz, 1991; Paré et al., 1994). This is consistent with the lost visual function observed here.

To determine whether visual responsiveness was also present in these deep layer neurons following rehabilitation under anesthesia, the same electrophysiological recording procedures used by Jiang et al. (2015) were conducted here in three animals.

Eighty-five neurons were recorded in the multisensory layers of the ipsilesional SC (n = 46 from an animal given 600 exposures/session, n = 29 from the animal given 100 exposures/session, and n = 10 from the animal given 2,400 exposures/session). Visually-responsive neurons were readily found in each of these animals (no inter-animal differences were observed, see exemplars in **Figure 7A**), and their pooled modality convergence patterns are shown in the left plot of **Figure 7B**. Many (74%, 58/78) of the visual receptive fields recorded in rehabilitated animals were very large and extended into central visual space. An overwhelming majority of these neurons were also overtly responsive to auditory inputs. The incidence of visually-responsive neurons also sensitive to the auditory modality (70%, 26/37) was roughly twice that expected given their incidence in the normal SC and in recordings from the contralesional SC of hemianopic animals (Meredith and Stein, 1986; Jiang et al., 2015). Given the high incidence (>30%) of "covert" multisensory neurons (one of the inputs is subthreshold, see Yu et al., 2013), this is likely to be an underestimate of neurons receiving an auditory input.

These data are consistent with the suggestion that the restoration of visual responsiveness depends on the cooperative interactions of convergent visual and auditory inputs onto the same neurons. Indeed, all but three (13/16) of the visually-responsive neurons in the recovered visual hemifield (receptive fields >15° of eccentricity) had their visual (and auditory) receptive fields encompassing the training site (45°; **Figure 7B**, right). The visual responses of these neurons were often modulated by auditory stimuli. In only a few cases was their

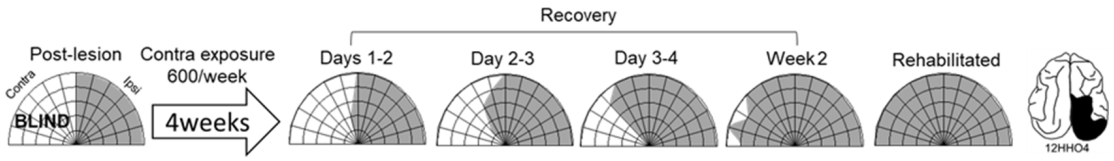

FIGURE 5 | Visual responsiveness recovered in a central-to-peripheral pattern. A hemianopic animal remained blind in contralesional space after 4 weeks of exposure sessions (600 auditory-visual exposures/session). Contralesional visual responses were first observed in the 5th week at 15°. The effective region expanded to 45° within several days (Day 0 was a day of exposure, and the results depicted were averaged over 2 days), and to at all contralesional locations tested within 2 weeks.

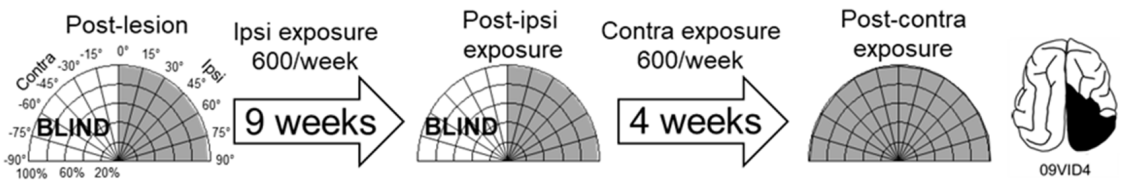

FIGURE 6 | Multisensory training in the unaffected (ipsilesional) hemifield failed to induce recovery from hemianopia. Nine weeks of ipsilesional multisensory exposure at 45° (600 exposures/session) failed to ameliorate the animal's hemianopia (conventions are the same as in **Figure 4**). At week 10 the cross-modal stimulus was moved to 45° in the blind (contralesional) hemifield. A series of exposures (600/session) at this location led to visual recovery within the same time frame as in animals that only had multisensory exposure in the blind hemifield.

ability to integrate cross-modal cues tested systematically, but this ability is a characteristic feature of multisensory neurons in the normal SC and was clearly evident in the exemplar presented in **Figure 7C**. Its visual-auditory response was significantly elevated above that elicited by either modality-specific component stimulus.

DISCUSSION

That visual responsiveness was restored in hemianopic animals by exposure to auditory-visual stimuli while they were anesthetized and paralyzed reveals that overt visuomotor behavior is not a requirement in this context, nor are any of the organismic variables that typically play important roles in learning and in rehabilitative therapies: e.g., alertness, explicit reward, engagement in the task, and many cognitive and motivational factors. Although this may seem surprising, it is consistent with work demonstrating similar visuomotor "recovery" after surgical intervention to remove sources of inhibitory influence from the intact hemisphere (Sprague and Meikle, 1965; Sprague, 1966; Sherman, 1977; Wallace et al., 1989, 1990; Lomber and Payne, 1996; Lomber et al., 2002).

The multisensory rehabilitation paradigm has also been shown to restore some visual responsiveness in human hemianopic populations (Bolognini et al., 2005; Dundon et al., 2015a; see also Purpura et al., 2017). However, some differences in the results have also been noted. Rehabilitated cats appear capable of extensive visual processing, including rudimentary pattern discrimination in the previously blind hemifield (Jiang et al., 2015). This strongly suggests that they are aware of those visual events. But rehabilitated human patients, despite being able to respond to visual stimuli in the previously blind hemifield, report a lack of awareness of those visual events. This may reflect a species difference, but may also reflect significant procedural differences. The absence of visual awareness in rehabilitated patients was concluded based on their reports when required to maintain fixation during visual stimulus presentation (i.e., they suppressed orientation responses). Given that visual responses to peripheral stimuli can also be suppressed in such a paradigm (including in the SC, e.g., see Rensink et al., 1997; Simons and Levin, 1997; Meredith and Ramoa, 1998), probably, the lack of visual awareness as a consequence of how the task constraints impacted the circuit. This possibility remains to be examined experimentally.

The anesthetized cross-modal exposure paradigm utilized here may not be a viable option for human patients; however, the current observations provide essential insights into the underlying process of recovery. Of particular interest is that the present findings, combined with the fact that exposure to auditory-alone or visual-alone stimuli are both ineffective in this rehabilitation (Jiang et al., 2015), strongly support the conclusion that recovery does not rely on merely drawing attention to the compromised hemifield. Rather, it appears to depend on mechanisms of multisensory plasticity that are engaged by cross-modal stimuli in the compromised hemifield. Violating the spatial or temporal requirements for SC multisensory integration in this paradigm also renders it ineffective in rehabilitation (see Dakos et al., 2019a,b). Repeated auditory-visual stimulation in the intact hemifield is ineffective in restoring vision, and had no salutary effect on subsequent multisensory exposure.

It is interesting to note how little experience with cross-modal stimuli was needed to induce recovery. In the paradigm,

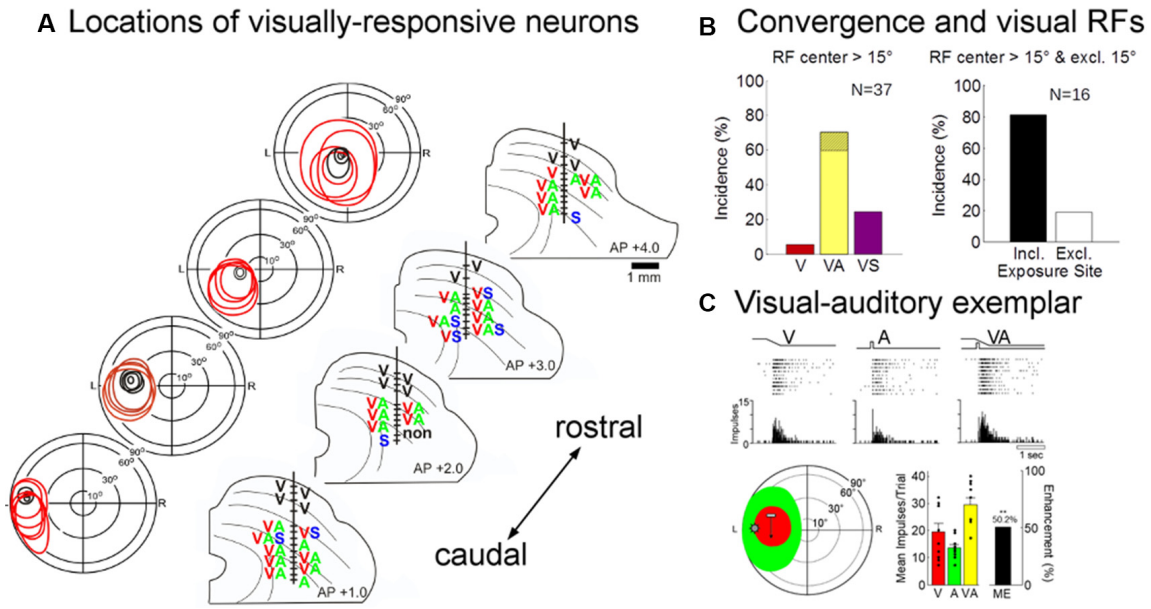

FIGURE 7 | Physiological recordings from the ipsilesional superior colliculus (SC) in an exemplar animal after rehabilitation. **(A)** Electrode penetrations were made in this animal at several different anterior-posterior positions in order to span the region in which visual responsiveness was lost (i.e., beyond the central 15°). The visual receptive fields, location, and modality convergence pattern for isolated neurons in these penetrations are indicated by letters (V, visual; A, auditory; S, somatosensory). Unisensory visual neurons are shown in black (note that all superficial layer visual neurons are unisensory). As in the normal SC, deeper layer visual receptive fields are far larger than their superficial counterparts, but maintain general spatial alignment with them. Note that almost all visually-responsive neurons in the region of interest were overtly multisensory. (**B**; Left) The population data show that a large proportion of the visually responsive neurons in the reactivated region were also overtly responsive to auditory stimuli (note that the hatched region on yellow bar shows that was also responsive to somatosensory stimuli, VAS). (Right) The receptive fields of these "recovered" neurons typically encompassed the 45° exposure site (incl) without encroaching on central space (15°). **(C)** The multisensory responses of one of these visual neurons are illustrated here in rasters and peristimulus time histograms at the top. The neuron's multisensory receptive fields are shown just below (red = V, green = A; icons show stimulus positions). Summary histograms (lower right) show the neuron's responses to the V and A stimuli individually and the multisensory enhancement (ME = 50.2%) evoked by their combination (**$p < 0.01$, 2-tailed *t*-test). Overlaid dot plots show response magnitude on each trial. Error bars indicate standard error of the mean.

stimulus exposures were provided every 6 s. Thus, animals rehabilitated by 600 exposures/session were given only 1 h of exposure per week, yet were recovered in approximately 4 weeks (4 h of exposure in total). Neither the speed of recovery nor its extent was significantly facilitated when the number of exposures was quadrupled from 600 to 2,400. When the number of exposures/session was reduced to 100, and exposure sessions only lasted for 10 min per week, recovery was initiated after 8 weeks (80 min of exposure in total). In both cases, the exposures represented a very small amount of the animals' total sensory experience during the rehabilitation period. These observations underscore the power that statistically regular sensory exposure has to reshape neural processing dynamics (see also Xu et al., 2017).

The rapidity with which visual responsiveness returned as a result of repeated exposure to cross-modal cues contrasts with the general intransigence of hemianopia under normal circumstances. Cross-modal events are a common feature of normal environments, and animals are likely to be exposed to thousands of such events in contralesional space every day. So, why is this "natural" multisensory exposure insufficient for rehabilitation while the laboratory exposure paradigm is so effective? One likely possibility is the difference in the density and regularity of the cross-modal events in these two circumstances. Cross-modal stimuli in the current rehabilitative paradigm were always congruent in space and time, and their individual physical features, spatiotemporal relationships, and iterative rates remained constant within and across exposure sessions. In a normal environment, a host of events gives rise to visual, auditory, and visual-auditory cues that can vary substantially in their physical features and in their cross-modal spatiotemporal relationships. Even repetition of the same event at different times in the non-laboratory environment is often accompanied by significant variation in the physical features and concordance of the cross-modal cues relative to the perceiver. Variation attributed to these and other sources can produce "contravening" experiences that may degrade the effectiveness of the stimuli in guiding underlying changes in the circuit.

The sensitivity of multisensory plasticity to regularity and congruency in cross-modal experience has been observed in other circumstances. Animals reared to adulthood in dark rooms, or with omnidirectional sound, have been deprived of the cross-modal experiences needed to develop the hallmark capability of normal SC neurons to integrate visual and auditory stimuli (Stein et al., 2014). Nevertheless, the later development of this capability in such animals can be rapidly initiated by repeatedly

exposing them to these spatiotemporally congruent cross-modal stimuli (Yu et al., 2010; Xu et al., 2012). This is far less effectively initiated by "natural" sensory experience in normal environments (Rowland et al., 2014; Xu et al., 2017).

It is important to note that repeated exposure to such congruent cross-modal stimuli also amplifies the responses of SC neurons to their modality-specific component responses (Yu et al., 2009, 2013). In each of these cases, multisensory exposure is effective in this regard even when animals are anesthetized as they were here (Yu et al., 2009, 2010; Xu et al., 2012). The dependence of recovery on multisensory exposure, the required integrity of the AES-SC projection for this training to be effective (Jiang et al., 2015), the paucity of other visually-responsive structures in lesioned animals, and prior work showing that permanent hemianopia is induced when both cortex and SC are damaged (Sherman, 1977; Wallace et al., 1990), all point to the critical role of the SC in this recovery process. However, the specific neurological changes that enable the return of visual responsiveness in the SC remain to be determined.

Yet, particularly interesting is that overt visually-guided behavior returned in a central-to-peripheral progression despite the single 45° exposure site and that once recovery was initiated in central space, no additional training was required for it to extend throughout the entire contralesional visual field (see also Lomber et al., 2002). There are several factors that may have been involved. Many of the rehabilitated visually-responsive neurons were found to have receptive fields that extended into central visual space. Given that the SC has a very high density of neurons representing central visual space and a rapidly decreasing proportion representing more peripheral locations, the critical number of active neurons needed to support visual behavior may have been first achieved at more central locations and then successively at more peripheral locations. In addition, the neurons representing the most central region of visual space that were retained after the cortical lesion may have exaggerated this effect by exerting a bias on localization decisions that steadily weakened as visual responses returned in neurons representing more peripheral locations. These possibilities also require further exploration.

It should be noted that removing all contiguous areas of the visual cortex likely produces significant and permanent functional consequences that were not explored here. Physiological changes in SC neurons have been noted with visual cortex lesions of varying extent and these include limiting the capabilities of SC neurons to respond selectively to direction or velocity of movement, and lowering the incidence of binocularity (e.g., see McIlwain and Fields, 1971; Rosenquist and Palmer, 1971; Ogasawara et al., 1984; Hardy and Stein, 1988). Perceptually, it is likely that the lesion compromises higher-order visual functions such as those related to the identity or meaning of visual events.

Also important to note is that a region of ipsilateral association cortex (the AES) distant from the lesion site appears to play a crucial role in supporting the restored SC visual activity. Removing AES after training-induced recovery reinstates the hemianopia and eliminates SC visual responses (Jiang et al., 2015). This is the case despite the fact that the lesion of visual cortex also deprives AES of major sources of visual input (Mucke et al., 1982; Norita et al., 1986; Olson and Graybiel, 1987; Scannell et al., 1996), which would have initially minimized its visual contribution to the SC. However, there is a likely active reconfiguration and functional alteration in the capabilities of the remaining visual circuits (Payne et al., 1996; Sorenson and Rodman, 1999; Bridge et al., 2008; Das et al., 2012), possibly enhancing their visual inputs to AES and, in turn, the effect of AES on the SC.

A prime candidate for supplying the critical visual inputs for this role is the superficial SC (see also, Casagrande et al., 1972). Its neurons can access AES *via* thalamocortical relays (Mucke et al., 1982; Olson and Graybiel, 1987; Abramson and Chalupa, 1988; Harting et al., 1991; Kelly et al., 2003), can provide it with a rich source of visual information, and, as noted above, these SC neurons retain their visual responsiveness after the hemianopia-inducing lesion. Indeed, they are often thought to play a role in the residual (albeit unconscious) visuomotor capabilities of human patients referred to as "blindsight" (Leh et al., 2006, 2010; Cowey, 2010; Tamietto et al., 2010; but see Schmid et al., 2010). They are also believed to be involved in one of many functional loops in the nervous system which, in this context, could allow one part of the SC (the purely visual superficial layers) to provide functionally relevant input to another part (its multisensory layers) *via* AES (McHaffie et al., 2005). But, to use that visual input, or any other input that survives the lesion, such as the sparse projections from retina (Wässle and Illing, 1980), pretectum (Edwards et al., 1979; Huerta and Harting, 1982), or directly from the overlying superficial SC (Casagrande et al., 1972; Behan and Appell, 1992; Schnupp et al., 1995; King et al., 1998; May, 2006), the circuit must be sensitive to the multisensory exposure paradigm. Once again this points to the multisensory SC neuron itself and/or its local circuit as a primary locus of the rehabilitative effect. This is consistent with the observation that the characteristic capability of ME was possible in the few neurons examined. This capability may have already been present before the hemianopia was resolved *via* the combination of subthreshold visual and suprathreshold auditory inputs. Whether this is actually the case, and whether the process could impact perception and overt behavior at this time is currently unknown (but see Ten Brink et al., 2015).

Whatever combination of circuit changes was induced by the current exposure paradigm to restore visual responsiveness in the previously blind hemifield, the organismic variables generally thought to be important in learning and in functional recovery from brain damage were not essential in this context. It is also an open question about whether or not they could facilitate this process. Using alert, interactive, and rewarded animals in a previous study, Jiang et al. (2015) found that a similar cross-modal rehabilitative paradigm was effective after 11–12 days. Although this is half or less the exposure duration required here with the anesthetized animal, suggesting a facilitation effect, that exposure paradigm involved sessions 5 days/week, whereas exposure sessions (albeit, with a higher density of trials) were provided to the anesthetized animal only once/week. When measured in terms of the number of hours of "training" that

led to rehabilitation, there was no obvious benefit of an alert behaving preparation. Although more controlled comparisons are clearly necessary before accepting what seems like a counterintuitive conclusion, the present findings do emphasize the sensitivity of the visual component of the multisensory circuit to the simple covariance of cross-modal cues. Repeated presentation of this stimulus complex led the circuit to regain many of its functional capabilities, thereby reversing hemianopia, and did so even when the host may have been unaware of the training experience.

DATA AVAILABILITY STATEMENT

The datasets generated for this study are available on request to the corresponding author.

ETHICS STATEMENT

The methods were in compliance with the National Institutes of Health "Guide for the Care and Use of Laboratory Animals" (8th edition, NRC 2011) and approved by the Institutional Animal Care and Use Committee at Wake Forest School of Medicine.

AUTHOR CONTRIBUTIONS

HJ participated in the research design, data collection, analysis, and manuscript writing. BR and BS participated in the research design, analysis, and manuscript writing.

FUNDING

This work was supported by National Institutes of Health (NIH) grant EY026916 and grants from the Johnston Foundation and the Tab Williams Family Foundation.

ACKNOWLEDGMENTS

We would like to thank Nancy London for technical assistance and for assistance in the preparation of this manuscript.

REFERENCES

Abramson, B. P., and Chalupa, L. M. (1988). Multiple pathways from the superior colliculus to the extrageniculate visual thalamus of the cat. *J. Comp. Neurol.* 271, 397–418. doi: 10.1002/cne.902710308

Baleydier, C. (1977). A bilateral cortical projection to the superior colliculus in the cat. *Neurosci. Lett.* 4, 9–14. doi: 10.1016/0304-3940(77)90116-1

Baleydier, C., Kahungu, M., and Mauguiere, F. (1983). A crossed corticotectal projection from the lateral suprasylvian area in the cat. *J. Comp. Neurol.* 214, 344–351. doi: 10.1002/cne.902140311

Behan, M., and Appell, P. P. (1992). Intrinsic circuitry in the cat superior colliculus: projections from the superficial layers. *J. Comp. Neurol.* 315, 230–243. doi: 10.1002/cne.903150209

Bolognini, N., Rasi, F., Coccia, M., and Làdavas, E. (2005). Visual search improvement in hemianopic patients after audio-visual stimulation. *Brain* 128, 2830–2842. doi: 10.1093/brain/awh656

Bridge, H., Thomas, O., Jbabdi, S., and Cowey, A. (2008). Changes in connectivity after visual cortical brain damage underlie altered visual function. *Brain* 131, 1433–1444. doi: 10.1093/brain/awn063

Casagrande, V. A., Harting, J. K., Hall, W. C., Diamond, I. T., and Martin, G. F. (1972). Superior colliculus of the tree shrew: a structural and functional subdivision into superficial and deep layers. *Science* 177, 444–447. doi: 10.1126/science.177.4047.444

Cowey, A. (2010). The blindsight saga. *Exp. Brain Res.* 200, 3–24. doi: 10.1007/s00221-009-1914-2

Dakos, A. S., Jiang, H., Stein, B. E., and Rowland, B. A. (2019a). Using the principles of multisensory integration to reverse hemianopia. *Cereb. Cortex* doi: 10.1093/cercor/bhz220 [Epub ahead of print].

Dakos, A. S., Walker, E. M., Jiang, H., Stein, B. E., and Rowland, B. A. (2019b). Interhemispheric visual competition after multisensory reversal of hemianopia. *Eur. J. Neurosci.* 50, 3702–3712. doi: 10.1111/ejn.14554

Das, A., Demagistris, M., and Huxlin, K. R. (2012). Different properties of visual relearning after damage to early versus higher-level visual cortical areas. *J. Neurosci.* 32, 5414–5425. doi: 10.1523/JNEUROSCI.0316-12.2012

Dundon, N. M., Bertini, C., Làdavas, E., Sabel, B. A., and Gall, C. (2015a). Visual rehabilitation: visual scanning, multisensory stimulation and vision restoration trainings. *Front. Behav. Neurosci.* 9:192. doi: 10.3389/fnbeh.2015.00192

Dundon, N. M., Làdavas, E., Maier, M. E., and Bertini, C. (2015b). Multisensory stimulation in hemianopic patients boosts orienting responses to the hemianopic field and reduces attentional resources to the intact field. *Restor. Neurol. Neurosci.* 33, 405–419. doi: 10.3233/rnn-140457

Edwards, S. B., Ginsburgh, C. L., Henkel, C. K., and Stein, B. E. (1979). Sources of subcortical projections to the superior colliculus in the cat. *J. Comp. Neurol.* 184, 309–329. doi: 10.1002/cne.901840207

Goodwin, D. (2014). Homonymous hemianopia: challenges and solutions. *Clin. Ophthalmol.* 8, 1919–1927. doi: 10.2147/opth.s59452

Guitton, D., and Munoz, D. P. (1991). Control of orienting gaze shifts by the tectoreticulospinal system in the head-free cat. I. Identification, localization, and effects of behavior on sensory responses. *J. Neurophysiol.* 66, 1605–1623. doi: 10.1152/jn.1991.66.5.1605

Hardy, S. C., and Stein, B. E. (1988). Small lateral suprasylvian cortex lesions produce visual neglect and decreased visual activity in the superior colliculus. *J. Comp. Neurol.* 273, 527–542. doi: 10.1002/cne.902730408

Harting, J. K., Huerta, M. F., Hashikawa, T., and van Lieshout, D. P. (1991). Projection of the mammalian superior colliculus upon the dorsal lateral geniculate nucleus: organization of tectogeniculate pathways in nineteen species. *J. Comp. Neurol.* 304, 275–306. doi: 10.1002/cne.903040210

Huerta, M. F., and Harting, J. K. (1982). The projection from the nucleus of the posterior commissure to the superior colliculus of the cat: patch-like endings within the intermediate and deep grey layers. *Brain Res.* 238, 426–432. doi: 10.1016/0006-8993(82)90118-4

Jay, M. F., and Sparks, D. L. (1987). Sensorimotor integration in the primate superior colliculus. I. Motor convergence. *J. Neurophysiol.* 57, 22–34. doi: 10.1152/jn.1987.57.1.22

Jiang, H., Stein, B. E., and McHaffie, J. G. (2009). Cortical lesion-induced visual hemineglect is prevented by NMDA antagonist pretreatment. *J. Neurosci.* 29, 6917–6925. doi: 10.1523/JNEUROSCI.3125-08.2009

Jiang, H., Stein, B. E., and McHaffie, J. G. (2015). Multisensory training reverses midbrain lesion-induced changes and ameliorates haemianopia. *Nat. Commun.* 6:7263. doi: 10.1038/ncomms8263

Kelly, L. R., Li, J., Carden, W. B., and Bickford, M. E. (2003). Ultrastructure and synaptic targets of tectothalamic terminals in the cat lateral posterior nucleus. *J. Comp. Neurol.* 464, 472–486. doi: 10.1002/cne.10800

King, A. J., Schnupp, J. W., and Thompson, I. D. (1998). Signals from the superficial layers of the superior colliculus enable the development of the auditory space map in the deeper layers. *J. Neurosci.* 18, 9394–9408. doi: 10.1523/JNEUROSCI.18-22-09394.1998

Leh, S. E., Johansen-Berg, H., and Ptito, A. (2006). Unconscious vision: new insights into the neuronal correlate of blindsight using diffusion tractography. *Brain* 129, 1822–1832. doi: 10.1093/brain/awl111

Leh, S. E., Ptito, A., Schönwiesner, M., Chakravarty, M. M., and Mullen, K. T. (2010). Blindsight mediated by an S-cone-independent collicular pathway: an fMRI study in hemispherectomized subjects. *J. Cogn. Neurosci.* 22, 670–682. doi: 10.1162/jocn.2009.21217

Leo, F., Bolognini, N., Passamonti, C., Stein, B. E., and Làdavas, E. (2008). Cross-modal localization in hemianopia: new insights on multisensory integration. *Brain* 131, 855–865. doi: 10.1093/brain/awn003

Lomber, S. G., and Payne, B. R. (1996). Removal of two halves restores the whole: reversal of visual hemineglect during bilateral cortical or collicular inactivation in the cat. *Vis. Neurosci.* 13, 1143–1156. doi: 10.1017/s0952523800007781

Lomber, S. G., Payne, B. R., Hilgetag, C. C., and Rushmore, J. (2002). Restoration of visual orienting into a cortically blind hemifield by reversible deactivation of posterior parietal cortex or the superior colliculus. *Commun. Biol.* 142, 463–474. doi: 10.1007/s00221-001-0957-9

May, P. J. (2006). The mammalian superior colliculus: laminar structure and connections. *Prog. Brain Res.* 151, 321–378. doi: 10.1016/s0079-6123(05)51011-2

McHaffie, J. G., Stanford, T. R., Stein, B. E., Coizet, V., and Redgrave, P. (2005). Subcortical loops through the basal ganglia. *Trends Neurosci.* 28, 401–407. doi: 10.1016/j.tins.2005.06.006

McHaffie, J. G., and Stein, B. E. (1983). A chronic headholder minimizing facial obstructions. *Brain Res. Bull.* 10, 859–860. doi: 10.1016/0361-9230(83)90220-4

McIlwain, J. T., and Fields, H. L. (1971). Interactions of cortical and retinal projections on single neurons of the cat's superior colliculus. *J. Neurophysiol.* 34, 763–772. doi: 10.1152/jn.1971.34.5.763

Meredith, M. A., and Ramoa, A. S. (1998). Intrinsic circuitry of the superior colliculus: pharmacophysiological identification of horizontally oriented inhibitory interneurons. *J. Neurophysiol.* 79, 1597–1602. doi: 10.1152/jn.1998.79.3.1597

Meredith, M. A., and Stein, B. E. (1983). Interactions among converging sensory inputs in the superior colliculus. *Science* 221, 389–391. doi: 10.1126/science.6867718

Meredith, M. A., and Stein, B. E. (1986). Visual, auditory, and somatosensory convergence on cells in superior colliculus results in multisensory integration. *J. Neurophysiol.* 56, 640–662. doi: 10.1152/jn.1986.56.3.640

Mucke, L., Norita, M., Benedek, G., and Creutzfeldt, O. (1982). Physiologic and anatomic investigation of a visual cortical area situated in the ventral bank of the anterior ectosylvian sulcus of the cat. *Exp. Brain Res.* 46, 1–11. doi: 10.1007/bf00238092

Norita, M., Mucke, L., Benedek, G., Albowitz, B., Katoh, Y., and Creutzfeldt, O. D. (1986). Connections of the anterior ectosylvian visual area (AEV). *Exp. Brain Res.* 62, 225–240. doi: 10.1007/bf00238842

Ogasawara, K., McHaffie, J. G., and Stein, B. E. (1984). Two visual corticotectal systems in cat. *J. Neurophysiol.* 52, 1226–1245. doi: 10.1152/jn.1984.52.6.1226

Olson, C. R., and Graybiel, A. M. (1987). Ectosylvian visual area of the cat: location, retinotopic organization, and connections. *J. Comp. Neurol.* 261, 277–294. doi: 10.1002/cne.902610209

Paré, M., Crommelinck, M., and Guitton, D. (1994). Gaze shifts evoked by stimulation of the superior colliculus in the head-free cat conform to the motor map but also depend on stimulus strength and fixation activity. *Exp. Brain Res.* 101, 123–139. doi: 10.1007/bf00243222

Passamonti, C., Bertini, C., and Làdavas, E. (2009). Audio-visual stimulation improves oculomotor patterns in patients with hemianopia. *Neuropsychologia* 47, 546–555. doi: 10.1016/j.neuropsychologia.2008.10.008

Payne, B. R., Lomber, S. G., Macneil, M. A., and Cornwell, P. (1996). Evidence for greater sight in blindsight following damage of primary visual cortex early in life. *Neuropsychologia* 34, 741–774. doi: 10.1016/0028-3932(95)00161-1

Purpura, G., Cioni, G., and Tinelli, F. (2017). Multisensory-based rehabilitation approach: translational insights from animal models to early intervention. *Front. Neurosci.* 11:430. doi: 10.3389/fnins.2017.00430

Rensink, R. A., O'Regan, J. K., and Clark, J. J. (1997). To see or not to see: the need for attention to perceive changes in scenes. *Psychol. Sci.* 8, 368–373. doi: 10.1111/j.1467-9280.1997.tb00427.x

Rosenquist, A. C., and Palmer, L. A. (1971). Visual receptive field properties of cells of the superior colliculus after cortical lesions in the cat. *Exp. Neurol.* 33, 629–652. doi: 10.1016/0014-4886(71)90133-6

Rowland, B. A., Jiang, W., and Stein, B. E. (2014). Brief cortical deactivation early in life has long-lasting effects on multisensory behavior. *J. Neurosci.* 34, 7198–7202. doi: 10.1523/JNEUROSCI.3782-13.2014

Sand, K. M., Midelfart, A., Thomassen, L., Melms, A., Wilhelm, H., and Hoff, J. M. (2013). Visual impairment in stroke patients—a review. *Acta Neurol. Scand. Suppl.* 127, 52–56. doi: 10.1111/ane.12050

Scannell, J. W., Sengpiel, F., Tovée, M. J., Benson, P. J., Blakemore, C., and Young, M. P. (1996). Visual motion processing in the anterior ectosylvian sulcus of the cat. *J. Neurophysiol.* 76, 895–907. doi: 10.1152/jn.1996.76.2.895

Schmid, M. C., Mrowka, S. W., Turchi, J., Saunders, R. C., Wilke, M., Peters, A. J., et al. (2010). Blindsight depends on the lateral geniculate nucleus. *Nature* 466, 373–377. doi: 10.1038/nature09179

Schnupp, J. W., King, A. J., Smith, A. L., and Thompson, I. D. (1995). NMDA-receptor antagonists disrupt the formation of the auditory space map in the mammalian superior colliculus. *J. Neurosci.* 15, 1516–1531. doi: 10.1523/JNEUROSCI.15-02-01516.1995

Sherman, S. M. (1977). The effect of superior colliculus lesions upon the visual fields of cats with cortical ablations. *J. Comp. Neurol.* 172, 211–229. doi: 10.1002/cne.901720203

Simons, D. J., and Levin, D. T. (1997). Change blindness. *Trends Cogn. Sci.* 1, 261–267. doi: 10.1016/S1364-6613(97)01080-2

Sorenson, K. M., and Rodman, H. R. (1999). A transient geniculo-extrastriate pathway in macaques? Implications for "blindsight". *Neuroreport* 10, 3295–3299. doi: 10.1097/00001756-199911080-00009

Sparks, D. L. (1986). Translation of sensory signals into commands for control of saccadic eye movements: role of primate superior colliculus. *Physiol. Rev.* 66, 118–171. doi: 10.1152/physrev.1986.66.1.118

Sparks, D. L., and Hartwich-Young, R. (1989). The deep layers of the superior colliculus. *Rev. Oculomot. Res.* 3, 213–255.

Sprague, J. M. (1966). Interaction of cortex and superior colliculus in mediation of visually guided behavior in the cat. *Science* 153, 1544–1547. doi: 10.1126/science.153.3743.1544

Sprague, J. M., and Meikle, T. H. Jr. (1965). The role of the superior colliculus in visually guided behavior. *Exp. Neurol.* 11, 115–146. doi: 10.1016/0014-4886(65)90026-9

Stein, B. E., and Clamann, H. P. (1981). Control of pinna movements and sensorimotor register in cat superior colliculus. *Brain Behav. Evol.* 19, 180–192. doi: 10.1159/000121641

Stein, B. E., and Meredith, M. A. (1993). *The Merging of the Senses.* Cambridge, MA: MIT Press.

Stein, B. E., Stanford, T. R., and Rowland, B. A. (2014). Development of multisensory integration from the perspective of the individual neuron. *Nat. Rev. Neurosci.* 15, 520–535. doi: 10.1038/nrn3742

Tamietto, M., Cauda, F., Corazzini, L. L., Savazzi, S., Marzi, C. A., Goebel, R., et al. (2010). Collicular vision guides nonconscious behavior. *J. Cogn. Neurosci.* 22, 888–902. doi: 10.1162/jocn.2009.21225

Ten Brink, A. F., Nijboer, T. C. W., Bergsma, D. P., Barton, J. J. S., and Van der Stigchel, S. (2015). Lack of multisensory integration in hemianopia: no influence of visual stimuli on aurally guided saccades to the blind hemifield. *PLoS One* 10:e0122054. doi: 10.1371/journal.pone.0122054

Wallace, S. F., Rosenquist, A. C., and Sprague, J. M. (1989). Recovery from cortical blindness mediated by destruction of nontectotectal fibers in the commissure of the superior colliculus in the cat. *J. Comp. Neurol.* 284, 429–450. doi: 10.1002/cne.902840309

Wallace, S. F., Rosenquist, A. C., and Sprague, J. M. (1990). Ibotenic acid lesions of the lateral substantia nigra restore visual orientation behavior in the hemianopic cat. *J. Comp. Neurol.* 296, 222–252. doi: 10.1002/cne.902960204

Wässle, H., and Illing, R.-B. (1980). The retinal projection to the superior colliculus in the cat: a quantitative study with HRP. *J. Comp. Neurol.* 190, 333–356. doi: 10.1002/cne.901900208

Xu, J., Yu, L., Rowland, B. A., Stanford, T. R., and Stein, B. E. (2012). Incorporating cross-modal statistics in the development and maintenance of multisensory integration. *J. Neurosci.* 32, 2287–2298. doi: 10.1523/JNEUROSCI.4304-11.2012

Xu, J., Yu, L., Rowland, B. A., and Stein, B. E. (2017). The normal environment delays the development of multisensory integration. *Sci. Rep.* 7:4772. doi: 10.1038/s41598-017-05118-1

Yu, L., Rowland, B. A., and Stein, B. E. (2010). Initiating the development of multisensory integration by manipulating sensory experience. *J. Neurosci.* 30, 4904–4913. doi: 10.1523/JNEUROSCI.5575-09.2010

Yu, L., Rowland, B. A., Xu, J., and Stein, B. E. (2013). Multisensory plasticity in adulthood: cross-modal experience enhances neuronal excitability and exposes silent inputs. *J. Neurophysiol.* 109, 464–474. doi: 10.1152/jn.00739.2012

Yu, L., Stein, B. E., and Rowland, B. A. (2009). Adult plasticity in multisensory neurons: short-term experience-dependent changes in the superior colliculus. *J. Neurosci.* 29, 15910–15922. doi: 10.1523/JNEUROSCI.4041-09.2009

Conflict of Interest: The authors declare that the research was conducted in the absence of any commercial or financial relationships that could be construed as a potential conflict of interest.

frontiers in Systems Neuroscience

ORIGINAL RESEARCH
published: 28 July 2020
doi: 10.3389/fnsys.2020.00048

Neural Working Memory Changes During a Spaceflight Analog With Elevated Carbon Dioxide: A Pilot Study

*Ana Paula Salazar[1], Kathleen E. Hupfeld[1], Jessica K. Lee[2], Nichole E. Beltran[3], Igor S. Kofman[3], Yiri E. De Dios[3], Edwin Mulder[2], Jacob J. Bloomberg[4], Ajitkumar P. Mulavara[3] and Rachael D. Seidler[1,5]**

[1] Department of Applied Physiology and Kinesiology, University of Florida, Gainesville, FL, United States, [2] Institute of Aerospace Medicine, German Aerospace Center, Cologne, Germany, [3] KBR, Houston, TX, United States, [4] NASA Johnson Space Center, Houston, TX, United States, [5] Department of Neurology, University of Florida, Gainesville, FL, United States

Spaceflight missions to the International Space Station (ISS) expose astronauts to microgravity, radiation, isolation, and elevated carbon dioxide (CO_2), among other factors. Head down tilt bed rest (HDBR) is an Earth-based analog for spaceflight used to study body unloading, fluid shifts, and other factors unrelated to gravitational changes. While in space, astronauts need to use mental rotation strategies to facilitate their adaptation to the ISS environment. Therefore, spatial working memory is essential for crewmember performance. Although the effects of HDBR on spatial working memory have recently been studied, the results are still inconclusive. Here, we expand upon past work and examine the effects of HDBR with elevated CO_2 (HDBR + CO_2) on brain activation patterns during spatial working memory performance. In addition, we compare brain activation between 30 days of HDBR + CO_2 and 70 days of HDBR to test the isolated effect of CO_2. Eleven subjects (6 males, 5 females; mean age = 34 ± 8 years) underwent six functional magnetic resonance imaging (fMRI) sessions pre-, during, and post-HDBR + CO_2. During the HDBR + CO_2 intervention, we observed decreasing activation in the right middle frontal gyrus and left regions of the cerebellum, followed by post-intervention recovery. We detected several correlations between brain and behavioral slopes of change with the HDBR + CO_2 intervention. For example, *greater* increases in activation in frontal, temporal and parietal regions were associated with *larger* spatial working memory improvements. Comparing the HDBR + CO_2 group to data from our previous 70-day HDBR study, we found *greater decreases* in activation in the right hippocampus and left inferior temporal gyrus for the HDBR + CO_2 group over the course of the intervention. Together, these findings increase our understanding of the neural mechanisms of HDBR, elevated levels of CO_2 and spaceflight-related changes in spatial working memory performance.

Keywords: cognition, spatial working memory, carbon dioxide, head down tilt bed rest, microgravity

OPEN ACCESS

Edited by:
Carlos Cepeda, University of California, Los Angeles, United States

Reviewed by:
Araceli Espinosa-Jeffrey, UCLA Department of Physiology, United States
Yaoying Ma, Binghamton University, United States

***Correspondence:**
Rachael D. Seidler
rachaelseidler@ufl.edu

Received: *17 April 2020*
Accepted: *29 June 2020*
Published: *28 July 2020*

Citation:
Salazar AP, Hupfeld KE, Lee JK, Beltran NE, Kofman IS, De Dios YE, Mulder E, Bloomberg JJ, Mulavara AP and Seidler RD (2020) Neural Working Memory Changes During a Spaceflight Analog With Elevated Carbon Dioxide: A Pilot Study. Front. Syst. Neurosci. 14:48. doi: 10.3389/fnsys.2020.00048

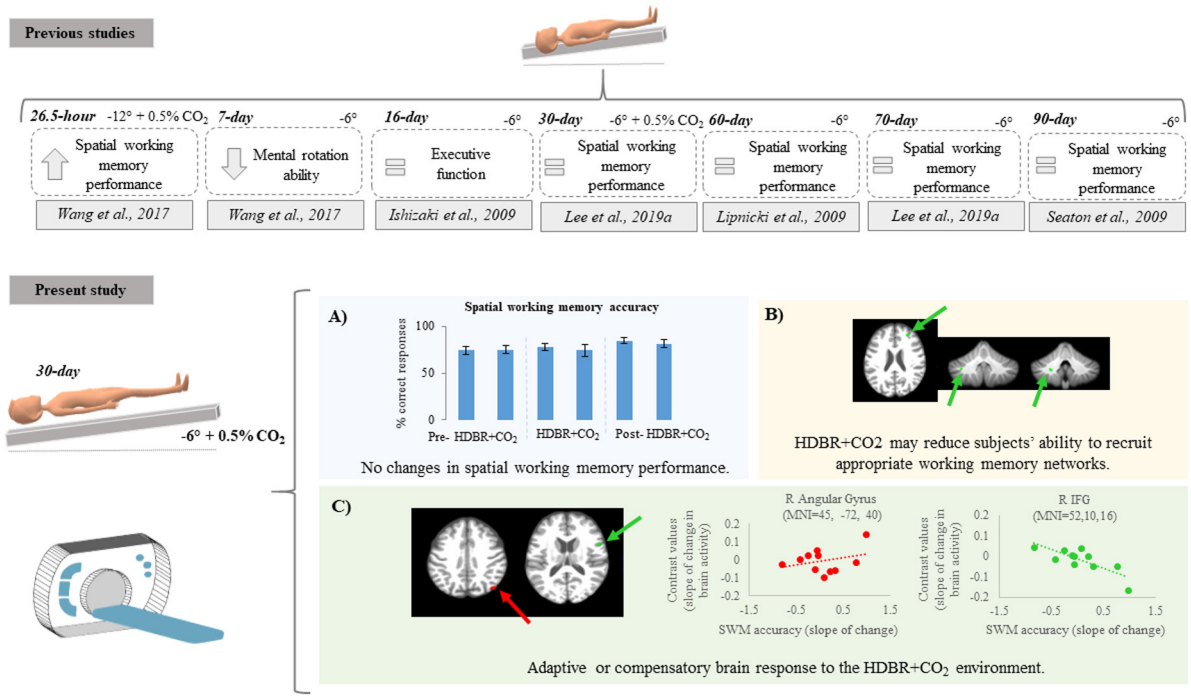

GRAPHICAL ABSTRACT | Top: previous findings regarding spatial working memory performance after bed rest protocols. Citations are presented in the Reference section. Bottom: Summary of findings from the present study showing **(A)** no differences in spatial working memory behavior performance; **(B)** decreasing activation in some brain regions suggesting that HDBR + CO_2 may reduce subjects' ability to recruit appropriate working memory networks; **(C)** positive and negative brain-behavior correlations suggesting adaptive or compensatory brain response to HDBR + CO_2.

INTRODUCTION

Spaceflight negatively affects human sensorimotor functioning and cognition (De la Torre, 2014). Cognitive performance in astronauts may be impaired by microgravity, radiation, noise, fatigue, and sleep deprivation, among other factors (De la Torre, 2014). Spatial orientation, mental rotation, and recognition are among the most common cognitive processes affected by spaceflight (De la Torre, 2014).

Mental rotation is a type of spatial working memory task in which a person imagines how an object would appear if it was rotated away from the presented orientation (Shepard and Metzler, 1971). Working memory is part of the short-term memory system, which involves a series of interactive processes that comprise the ability to temporarily maintain and manipulate information in the mind (Baddeley, 2017). Spatial working memory has an important role for executive function as well as sequence learning and sensorimotor adaptation (Seidler et al., 2012). Therefore, working memory is essential for successful crewmember performance. For instance, while in space, astronauts use mental rotation strategies to facilitate the recognition of objects and other astronauts' gestures.

Head down tilt bed rest (HDBR) is a well-established Earth-based analog of spaceflight used to investigate the physiological effects of microgravity on human performance (Moore et al., 2010). HDBR simulates the axial body unloading and fluid shifts toward the head that occur during spaceflight. Both spaceflight and HDBR impact sensorimotor function and are associated with modifications of brain structure and function in healthy individuals (Bock et al., 2010; Koppelmans et al., 2016; Roberts et al., 2017; Lee et al., 2019b). The effects of HDBR specifically on working memory remain unclear. Previous work assessed 20 males that underwent seven days of −6° HDBR. These individuals showed *reduced* mental rotation ability after three days of HDBR, but recovered after the end of HDBR, suggesting that short-duration HDBR temporarily impacts mental rotation abilities (Wang et al., 2017). Our group previously evaluated 17 males who underwent a 70-day HDBR intervention. We reported *improvements* in spatial working memory performance after 70 days of HDBR compared to baseline, suggestive of test practice effects (Cassady et al., 2016). Further, we found that working memory performance changes correlated with brain connectivity alterations (Cassady et al., 2016). This suggests that neuroplastic mechanisms may facilitate adaptation to the HDBR environment (Cassady et al., 2016).

In addition to microgravity, chronic exposure to elevated levels of carbon dioxide (CO_2) on the International Space Station (ISS) may also contribute to cognitive performance impairments (Manzey and Lorenz, 1998; Allen et al., 2019). Astronauts aboard the ISS often report hypercapnia-related symptoms such as headaches (Law et al., 2014), spatial disorientation, reduced attention and concentration, among other symptoms (Kanas and Manzey, 2008; De la Torre, 2014). Our group recently reported the effects of 30 days HDBR coupled with

elevated CO_2 on cognitive and sensorimotor performance (Lee et al., 2019a). Individuals in this cohort showed *improvements* in card rotation performance (i.e., a learning effect and no effect of the intervention) and *no changes* in cube rotation and working memory (Lee et al., 2019a). Although several recent studies have reported HDBR- and spaceflight-related changes in spatial working memory abilities (Leone et al., 1995; Lipnicki et al., 2009; Chen et al., 2013; Wang et al., 2017), there is still little understanding regarding how HDBR may affect the neural processing of spatial working memory. Further, no previous work has investigated neural spatial working memory changes with a combined HDBR and elevated CO_2, which better mimics the elevated CO_2 onboard the ISS (Law et al., 2014).

In the present pilot study, we examine the effects of 30 days of HDBR combined with elevated CO_2 levels (HDBR + CO_2) on the neural correlates of spatial working memory performance in eleven participants. We addressed two primary aims: (1) to investigate the time course of effects of a 30-day HDBR + CO_2 intervention on brain activation patterns during spatial working memory task performance; and (2) to determine whether any brain changes correlate with changes in spatial working memory performance. As a secondary aim, to investigate the additive effects of elevated CO_2 and long-duration HDBR, we compared the data here with those from our previous HDBR work (Yuan et al., 2016, 2018a; Koppelmans et al., 2017). This comparison was exploratory, given that the two HDBR interventions differed on several dimensions including the exposure duration.

MATERIALS AND METHODS

Participants and Testing Timeline

HDBR + CO_2

This longitudinal study conducted at:envihab in the German Aerospace Center, Cologne, Germany, included eleven participants (6 males, 5 females) with mean age of 34 ± 8 years at the beginning of the study. Participants were tested in six different time points: twice before the protocol started, twice during intervention and twice after the end of the bed rest (**Figure 1**). During the HDBR + CO_2 intervention, subjects maintained 6° head down tilt position while exposed to ambient 0.5% CO_2 (3.8 mmHg partial pressure of CO_2) (Law et al., 2014) at all times during 30 days. Oxygen and nitrogen levels were 20.9% and 78.6%, respectively. These small changes had no physiological effects neither affected the oxygen saturation. All participants received a controlled diet, had daily 8-h sleep opportunities (10:30 PM–6:30 AM) and were not allowed to use a pillow except when laying on their side.

Three days prior to bed rest and on the first day after bed rest blood draws were acquired to measure arterial partial pressure of carbon dioxide ($PaCO_2$). This was part of NASA's standard measures assessments.

All procedures were approved by the University of Florida and NASA Institutional Review Boards as well as by the local ethical commission of the regional medical association (Ärztekammer Nordrhein). All subjects provided written informed consent and received monetary compensation for their participation.

70-day HDBR

Sixteen individuals (all males; mean age = 29 ± 3 years) consented to participate in this study. All procedures were approved by the University of Michigan, University of Texas Medical Branch, and NASA Institutional Review Boards. All participants were admitted to the NASA bed rest facility at the University of Texas Medical Branch, Galveston, TX, United States and completed two baseline data collection sessions in the 2 weeks prior to starting HDBR. Subjects then underwent 70 days of HDBR intervention with normal atmospheric CO_2 (∼0.04%; 0.3 mmHg partial pressure of CO_2). During this campaign, participants remained lying down with a six-degree head down tilt at all times. They were allowed to use a pillow and to support their head with their hand during each meal (30 min). Subjects stayed at the facility for 14 days after HDBR and completed two recovery data collection sessions during this time (**Figure 1**).

Spatial Working Memory Behavioral Tasks

Spatial working memory behavioral tasks were acquired at all time points specified in **Figure 1**. Three different tasks were used to assess spatial working memory performance, as follows:

(1) *Spatial working memory task during functional magnetic resonance imaging (fMRI) (**Figure 2A**)*: This task was performed in the MRI scanner. Participants viewed a three-target set (three solid circles) for 500 ms. Following the presentation of this target set, participants saw a blank screen for 3000 ms (retention interval). During the retention interval, participants were instructed to mentally "connect the dots" and then mentally rotate the shape. After the retention interval, participants decided whether a subsequently presented probe set of open circles formed the same configuration as the target set they mentally rotated. Participants performed two runs of this task. Each run included 30 trials.

Participants also performed a control task in the MRI scanner (**Figure 2A**). The control task involved the presentation of three solid circles for 500 ms, followed by a 200 ms retention interval, then by the presentation of a single circle for 2500 ms. At this point, participants determined whether its spatial location matched that of a previously observed dot. Participants performed one run of this task consisting of 40 trials. This control task included all of the processes of the spatial working memory task, except for the working memory and mental rotation components. Thus, the subtraction of images from the control condition should reveal areas actively involved with spatial working memory maintenance and mental rotation while omitting those involved in visual processing and response button pressing (Reuter-Lorenz et al., 2000; Anguera et al., 2010).

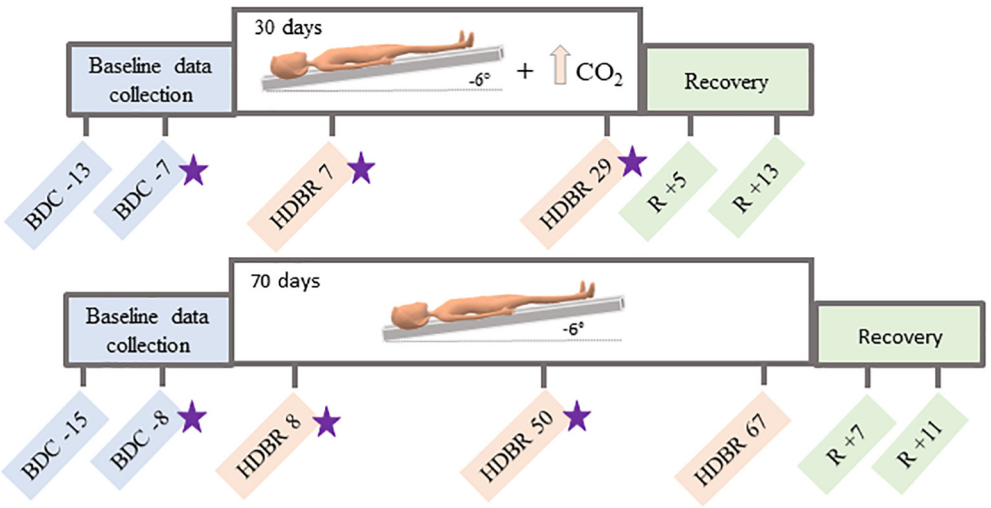

FIGURE 1 | Testing timelines. *Top:* testing timeline for the HDBR + CO_2 group, who completed 30 days of head down tilt bed rest (HDBR) with 0.5% atmospheric CO_2. *Bottom:* testing timeline for the HDBR group, who completed 70 days of HDBR with normal atmospheric CO_2 levels. BDC = baseline data collection; HDBR = head down tilt bed rest; R = recovery. Functional MRI and behavioral data were collected at all time points specified here. Stars indicate the three time points used to create the slope images for between-group comparisons.

For both tasks, we calculated the percentage of correct responses (spatial working memory and spatial working memory control accuracy).

(2) *Card rotation* (***Figure 2B***): Participants completed Thurstone's 2D card rotation test (Ekstrom et al., 1976). During each trial, they were presented with a 2D drawing of a card with an abstract shape. To the right of this card, there were eight drawings of the same card that were either only rotated or both rotated and mirrored. Participants determined which cards matched the initial drawing (S = same, i.e., only 2D rotated) and which cards were different (D = different, i.e., mirrored or flipped from the card at the beginning of the row). Time to complete the test (maximum time allowed is 3 min) and accuracy relative to completed trials were used as indicators of performance (Koppelmans et al., 2013; Cassady et al., 2016).

(3) *Cube rotation* (***Figure 2C***): Participants compared a collection of 3D cubes (Shepard and Metzler, 1988). During each trial, a 3D cube assemblage was presented on a computer screen for 3 s, followed by a blank screen for 2 s, and then two cube images. One of the two was a match to the target but was rotated three dimensionally; the other was a new cube assemblage. Participants indicated which cube image matched the target image by pressing a left or right button. Outcome measures for this task included reaction time and accuracy.

For both card and cube rotation assessments, the HDBR + CO_2 participants were in head down tilt while subjects from 70-day HDBR performed this task in the supine position (Koppelmans et al., 2013; Cassady et al., 2016).

fMRI Acquisition Parameters

HDBR + CO_2

Functional images were acquired on a 3 Tesla Siemens MRI scanner, using a gradient echo T2*-weighted echo-planar imaging sequence with the following parameters: TR = 2500 ms, TE = 32 ms, flip angle = 90°, FOV = 192 × 192 mm, matrix = 64 × 64, slice thickness = 3.5 mm, voxel size = 3 × 3 × 3.5 mm^3, 37 slices. A T1-weighted gradient-echo pulse sequence was also acquired: TR = 1.9 s, TE = 2.4 ms, flip angle = 9°, FOV = 250 × 250 mm, matrix = 512 × 512, slice thickness = 1.0 mm, voxel size = 0.49 × 0.49 × 1.0 mm^3, 192 slices. Participants maintained the head down tilt position in the scanner by lying on a wedge of foam; however, the head was supine in the head coil.

70-day HDBR

For the 70-day HDBR group, fMRI scans were acquired on a 3 Tesla Siemens MRI scanner using a gradient echo T2*-weighted echo-planar imaging sequence: Repetition time (TR) = 3.66 s, Echo time (TE) = 39 ms, flip angle = 90°, Field of view (FOV) = 240 × 240 mm, matrix = 94 × 94, slice thickness = 4 mm, slice gap = 1 mm, voxel size = 2.55 × 2.55 × 5.0 mm^3, 36 slices. A T1-weighted gradient-echo pulse sequence was also collected with parameters: TR = 1.9 s, TE = 2.49 ms, flip angle = 9°, FOV = 270 × 270 mm, matrix = 288 × 288, slice thickness = 0.90 mm, voxel size = 0.94 × 0.94 × 0.90 mm^3, 192 slices. Participants did not maintain the head down tilt position in the scanner.

fMRI Data Processing and Statistical Analyses

We used Statistical Parametric Mapping 12 (SPM12, version 7219) and MATLAB R2018a, version 9.0 for preprocessing and

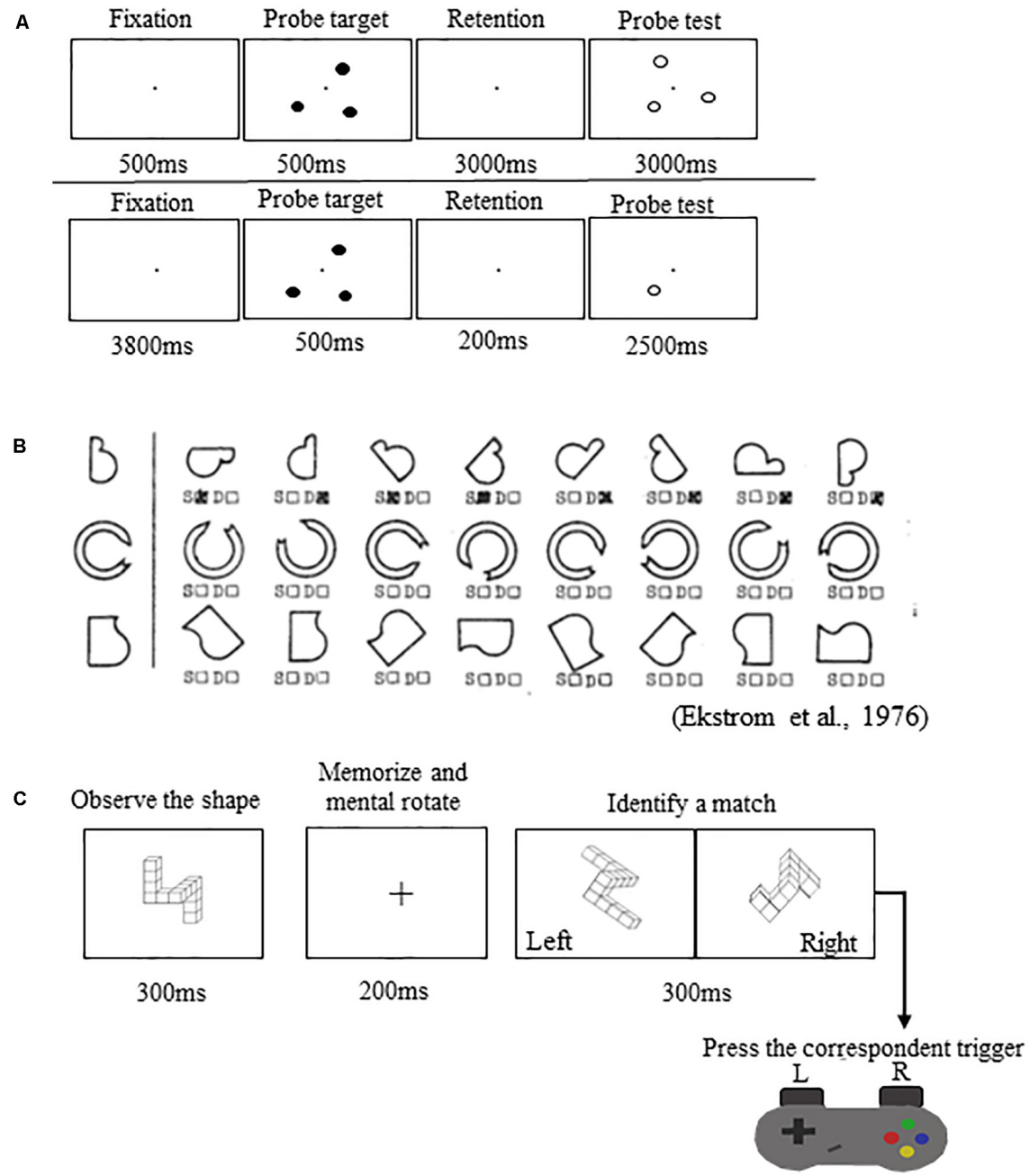

FIGURE 2 | Spatial working memory performance tasks. **(A)** *Top*: Spatial working memory task performed in the MRI scanner. *Bottom*: Spatial working memory control task performed in the MRI scanner. **(B)** Thurstone's 2D card rotation test. **(C)** Cube rotation task.

statistical analyses. We used a standard SPM preprocessing pipeline for fMRI. All functional images were slice timing and head motion corrected (realigned and resliced). Following these steps, the Artifact Detection Tool (ART)[1] was used as an additional quality check. We removed volumes with motion threshold equal or greater than 3 mm (i.e., approximately the size of one voxel for the HDBR + CO_2 group) and global brain signal Z threshold equal or greater than 9. Two individuals had movement outliers; for one of them the first 21 of 76 volumes were excluded, while the first 8 of 76 volumes were excluded for the other participant. We included head motion parameters outputted by ART as covariates in the subject-level analyses to minimize effects of these volumes on group-level analyses.

Next, whole brain fMRI images were normalized to MNI152 space using Advanced Normalization Tools (Avants et al., 2011), in a multi-step procedure. First, the

[1]www.nitrc.org/projects/artifact_detect/

T1 images were skull stripped using ImCalc (SPM12). Then, participant-specific templates were created using ANTs' *AntsMultivariateTemplateConstuction.sh* function. Next, these templates were normalized to MNI152 common space using ANTs' *AntsRegistration.sh* function. In order to normalize the images, we then created mean fMRI participant-specific templates (using ANTs' *AntsMultivariateTemplateConstuction.sh* function) and used these templates to coregister the functional images to the T1-specific templates. Coregistration was performed using *AntsRegistration.sh*. The resulting warp parameters were applied to the 4D EPI images using ANTs' *AntsApplyTransforms.sh* function. Finally, the normalized data were spatially smoothed with an 8 mm full-width half-maximum three-dimensional Gaussian kernel.

In addition to the whole brain normalization, we applied specialized processing using portions of both the CEREbellum Segmentation (CERES) (Romero et al., 2017) pipeline and the Spatially Unbiased Infratentorial Template (SUIT) (Diedrichsen, 2006; Diedrichsen et al., 2009) pipeline. The CERES pipeline was used to segment the cerebellum from each person's structural T1-weighted image. We then coregistered each subject's native space segmentation to the *SUIT.nii* template. Binary gray matter, white matter, and full cerebellar masks were created from the CERES native space output, and we then used the *suit_normalize_dartel* function to obtain the affine transformation matrix and normalize these images into SUIT space. Due to the small size of cerebellar structures, we applied a 2 mm full-width half-maximum three-dimensional Gaussian smoothing kernel to the normalized functional cerebellar images.

We calculated subject-level statistical analyses twice: once for the whole brain and a second time for the cerebellum. Brain activity was calculated for each participant on a voxel-by-voxel basis for the contrast spatial working memory > spatial working memory control. We set the first level masking threshold to -Infinity and masked out non-brain areas using the SPM intracranial volume mask.

fMRI Group-Level Statistical Analyses

Main Effect of Spatial Working Memory

To verify that our spatial working memory task elicited the expected brain activity, we calculated the main effect across all subjects and all sessions at peak-level of $p < 0.001$ (uncorrected), extent threshold = 10 voxels. In this model, we controlled for age and sex differences, i.e., these variables were included as covariates of no interest. For all analyses we used the contrast spatial working memory > control.

Time Course of Neural Spatial Working Memory Response to HDBR + CO_2

We first tested for brain regions that showed a pattern of cumulative change followed by post-HDBR + CO_2 recovery. These hypothesized cumulative change models are presented in **Figure 3**. For these longitudinal analyses, we used flexible factorial models controlling for age and sex assuming independence between subjects, and assuming equal variances between and within subjects (Gläscher and Gitelman, 2008). To better detect within-subject changes with the longitudinal model used in the present pilot study, the alpha level was set at $p < 0.0005$ (uncorrected), and the extent threshold was set at 10 voxels for the whole brain and 5 voxels for the cerebellum.

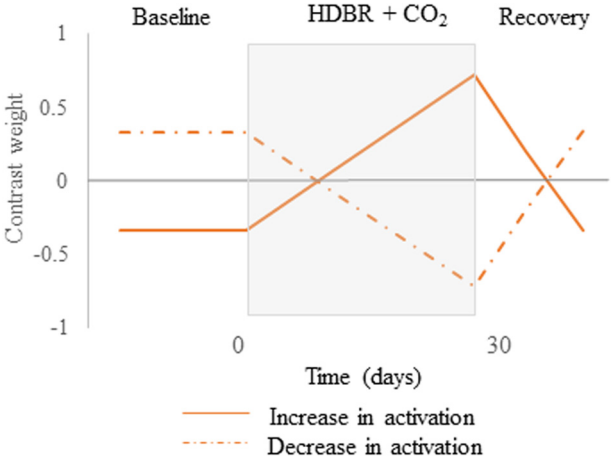

FIGURE 3 | Hypothesized contrast weights. Cumulative changes in neural spatial working memory response to HDBR + CO_2. Brain changes would slowly increase over the course of HDBR + CO_2, followed by recovery after the end of HDBR + CO_2. Solid lines represent the positive version while dotted lines describe the negative version of the contrast.

Brain-Behavioral Correlations

First, we computed the slope of changes in brain activation (Yuan et al., 2016, 2018b; Hupfeld et al., 2020) between the 2nd, 3rd, and 4th time points (**Figure 1**). These are the time points immediately before HDBR started and during HDBR, respectively. Additionally, we computed the slope of changes in behavioral performance on the spatial working memory, card rotation, and cube rotation tasks across the same time points. We then correlated the slope of brain changes with the slope of changes in spatial working memory performance. For these analyses, we used the Statistical Non-Parametric Mapping (SnPM version 13)[2] toolbox to run non-parametric permutation tests with 15,000 permutations, variance smoothing = 8 mm kernel for whole brain analyses and 2 mm kernel for cerebellar analyses, and controlling for age and sex. For these analyses, we used a non-parametric threshold of $p < 0.0005$ (uncorrected) and a minimum cluster size of 10 voxels for the whole brain and 5 voxels for the cerebellum.

HDBR + CO_2 vs. 70-day HDBR Group Comparisons

Given that each of the two bed rest studies followed a different testing timeline, to examine differences in neural response between HDBR with and without elevated CO_2, we compared only the slopes of change in brain activation between these two studies. We computed slopes of brain change for the 70-day HDBR group in an identical manner to those for the

[2]http://warwick.ac.uk/snpm

HDBR + CO_2 group. Additionally, for each group, we computed intercept images (i.e., baseline brain activation during spatial working memory). We then normalized the slope images using the formula: (slope image/intercept image); this allows us to compare between-group slope changes while accounting for baseline differences between the two groups.

We performed a two-sample *t*-test to test between-group differences in the normalized slope images. We used SnPM non-parametric permutation tests with 15,000 permutations, variance smoothing = 8 mm kernel for the whole brain analyses and 2 mm kernel for the cerebellar analyses, and controlling for age and sex. Statistical significance was determined by applying false discovery rate (FDR) $p < 0.05$ at the cluster-level (Nichols and Hayasaka, 2003).

Statistical Analyses

A paired sample one tailed *t*-test was performed to verify any increases pre- to post-HDBR + CO_2 in the $PaCO_2$ blood levels. Statistical significance was defined as $p < 0.05$.

We previously reported some statistical analyses of the spatial working memory behavioral data for the HDBR + CO_2 cohort (Lee et al., 2019a). Here, we further investigated the spatial working memory score using the following equation: Spatial working memory Score = Spatial working memory control accuracy – Spatial working memory accuracy. We did not have any outliers nor missing data. We conducted a linear mixed model regression analysis on the HDBR + CO_2 participants, entering time as a continuous variable to assess the effect of the intervention on spatial working memory score. We used R software version 3.6.0 for this analysis entering time as a continuous variable, and age and sex as covariates. We considered the first time point to be a practice session and thus excluded it from the analysis (Lee et al., 2019a).

RESULTS

We observed a small but significant increase in $PaCO_2$ from pre- (41.4 mmHg) to post- (43.4 mmHg) bed rest ($p < 0.05$).

Spatial Working Memory Behavioral Results

We did not observe an effect of HDBR + CO_2 on spatial working memory accuracy score ($\beta = 0.12$; $p = 0.39$). We previously reported the effects of HDBR + CO_2 on spatial working memory ($\beta = -0.03$; $p = 0.76$), spatial working memory control ($\beta = 0.10$; $p = 0.18$), card rotation (time: $\beta = -0.30$; $p < 0.01$; accuracy: $\beta = 0.11$; $p < 0.05$), and cube rotation (time: $\beta = -0.01$; $p = 0.18$ and accuracy: $\beta = -0.15$; $p = 0.15$) (Lee et al., 2019a). We only found effects of time on card rotation time and accuracy, in which subjects showed improvement in both measures across HDBR + CO_2 (Lee et al., 2019a).

Main Effect of Spatial Working Memory

The main effect of the spatial working memory task contrasted to the control task resulted in activation in the expected brain regions based on prior studies (Lamp et al., 2016). Specifically, we observed bilateral activation in several frontal, parietal, temporal and cerebellar regions (**Table 1** and **Figure 4**). We also found deactivation in parietal and occipital regions (**Table 1** and **Figure 4**).

Time Course of Neural Working Memory Response to HDBR + CO_2

Across HDBR + CO_2, we found *decreasing* activation in the right middle frontal gyrus and left dentate nucleus of the cerebellum, followed by recovery after the HDBR + CO_2 intervention

TABLE 1 | Brain regions showing activation or deactivation during spatial working memory.

	Extent (*k*)	Peak t-value	MNI coordinates (mm)		
			x	*y*	*z*
Activation					
Frontal					
R IFG (p. Opercularis)	3989	5.301	50	7	30
R IFG (p. Triangularis)	4049	4.884	44	30	20
L IFG (p. Opercularis)	4296	5.734	−52	8	32
L IFG (p. Triangularis)	1428	4.026	−44	30	20
L Posterior-medial frontal	1714	4.771	−6	16	51
Temporal					
R Fusiform gyrus	28771	8.009	34	−81	−8
R Middle occipital gyrus	28771	7.308	25	−92	10
Parietal					
R Superior parietal lobule	13689	6.279	27	−58	53
R Post-central gyrus	13689	5.031	54	−22	40
L Inferior parietal lobule	9058	5.087	−30	−56	59
L Post-central gyrus	9058	4.886	−43	−38	51
Occipital					
R Middle occipital gyrus	28771	7.308	25	−92	10
L Lingual gyrus	21522	8.799	−18	−92	−7
L Inferior occipital gyrus	21522	6.725	−43	−72	−9
Cerebellum					
L Cerebelum (Crus 1)	21522	3.333	−10	−77	−23
L Cerebelum (VIII)	167	3.890	−16	−68	−47
Deactivation					
Temporal					
R Middle temporal gyrus	2188	−5.441	58	−59	23
L Angular gyrus	1094	−4.144	−44	−76	39
L Middle temporal gyrus	1094	−3.486	−47	−56	16
Parietal					
R Precuneus	832	−3.705	3	−54	47
R Inferior parietal lobule	21	−3.577	56	−59	44
Occipital					
R Cuneus	326	−4.642	12	−96	20
L Superior occipital gyrus	93	−3.818	−23	−92	30
L Superior occipital gyrus	23	−3.553	−11	−104	15

Significance level set at non-parametric $p < 0.001$ and cluster size $k = 10$ for all analyses. Cortical regions labeled using the AnatomyToolbox atlas via the SPM toolbox BSPMview. Cerebellar regions labeled using the SUIT atlas. L = Left; R = Right.

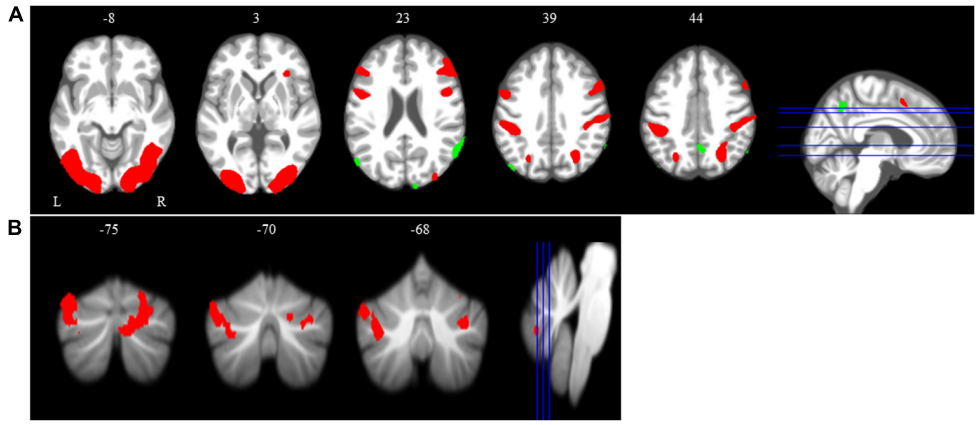

FIGURE 4 | Main effect of spatial working memory. The spatial working memory task resulted in widespread activation (red) and deactivation (green). Whole brain and cerebellar results are overlaid onto MNI **(A)** and SUIT **(B)** standard templates, respectively; $p < 0.001$, $k = 10$. Abbreviations: L = Left; R = Right.

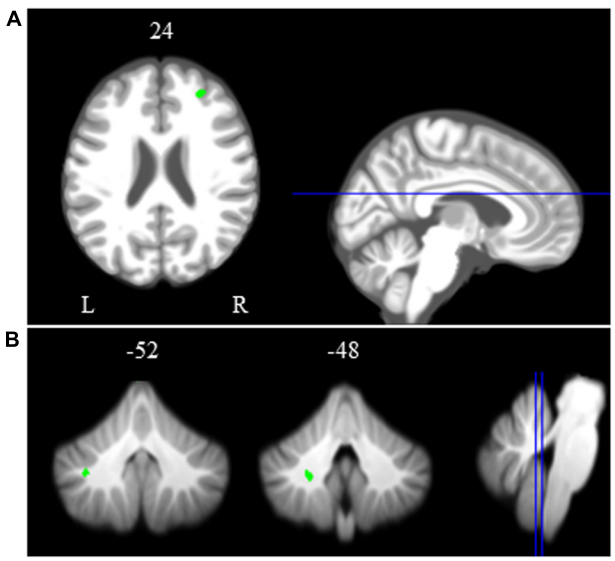

FIGURE 5 | Time course of neural spatial working memory response to HDBR + CO_2. Whole brain and cerebellar results showing decreases in activation (green) followed by recovery. Whole brain and cerebellar results are overlaid onto MNI **(A)** and SUIT **(B)** standard templates, respectively; $p < 0.0005$, $k = 10$ for whole brain analyses; $k = 5$ for cerebellar analyses. Abbreviations: L = Left; R = Right.

TABLE 2 | Brain regions showing cumulative changes during spatial working memory followed by recovery.

	Extent (*k*)	Peak *t*-value	MNI coordinates (mm)		
			x	*y*	*z*
Decreases in activation					
Frontal					
R Middle frontal gyrus	62	−3.969	28	44	24
Cerebellum					
L Dentate	8	−4.175	−22	−48	−41

Significance level set at non-parametric $p < 0.0005$ and cluster size $k = 10$ for the whole brain analyses and $k = 5$ for the cerebellum analyses. Cortical regions labeled using the AnatomyToolbox atlas via the SPM toolbox BSPMview. Cerebellar regions labeled using the SUIT atlas. L = Left; R = Right.

(**Figure 5** and **Table 2**). We did not observe any increases in brain activation followed by recovery in response to HDBR + CO_2.

Brain-Behavior Correlations

Spatial Working Memory Task

We identified several regions for which the slope of change in brain activity correlated with the slope of change in spatial working memory performance (**Figure 6A** and **Table 3**). For instance, for spatial working memory accuracy, we observed that *greater increases* in activation of the right angular gyrus were associated with *larger improvements* in spatial working memory performance. That is, subjects who performed this task with fewer errors presented with *greater increases* in activation of the right angular gyrus during the HDBR + CO_2 intervention. Further, a *greater decrease* in activation of the inferior frontal gyrus was correlated with *less decline* in spatial working memory accuracy. For the spatial working memory control task, we found that *greater increases* in activation of several brain regions, including parietal, temporal and occipital regions, correlated with *greater* accuracy increases. In addition, *greater decrease* in activation of the left lingual gyrus was correlated with *less decline* in the accuracy of the spatial working memory control task (**Figure 6B** and **Table 3**). Regarding the spatial working memory scores, we observed that *greater increases* in activation of the right superior temporal gyrus were correlated with *greater increases* in scores (**Figure 6C** and **Table 3**).

Card Rotation Task

We observed several brain regions for which the slope of change in brain activity correlated with the slope of change in card rotation accuracy (**Figure 7** and **Table 3**). We found that *greater increases* in activation of the left supramarginal gyrus correlated with *larger improvements* in card rotation accuracy, while *greater*

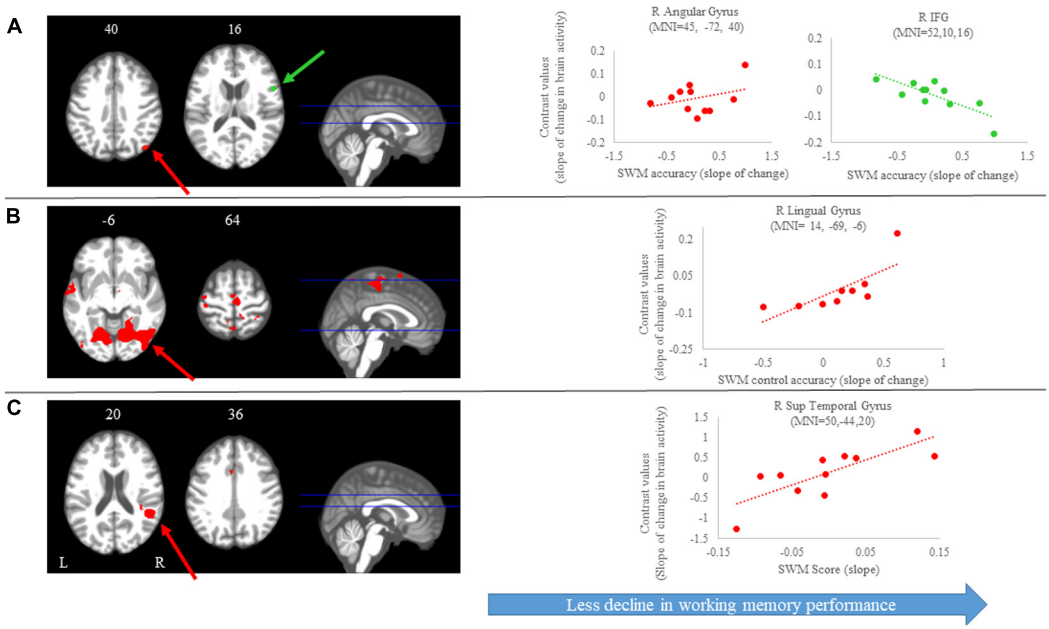

FIGURE 6 | Brain-behavior correlations (spatial working memory). Slope of changes in brain and behavior results showing positive (red) and negative (green) correlations. **(A)** Spatial working memory; **(B)** spatial working memory control; and **(C)** spatial working memory score. Whole brain results are overlaid onto the MNI standard template; $p < 0.0005$, $k = 10$. Right side correlation plots include contrast values extracted from the peak coordinate inside an example cluster (indicated with red or green arrows) graphed against the slope of changes in behavior results. Abbreviations: L = Left; R = Right; SWM = Spatial working memory.

decreases in activation of the left superior frontal gyrus, right angular gyrus, and left lingual gyrus correlated with *less decline* in this measure (**Figure 7** and **Table 3**). We did not observe brain and behavior correlation for the time to perform the card rotation task.

Cube Rotation Task

For the cube rotation task, we observed several regions in which the slope of change in brain activity correlated with the slope of change in cube rotation accuracy. We found that *greater increases* in activation of several brain regions, including frontal, parietal, temporal and subcortical regions, were correlated with *greater* accuracy increases. That is, participants who *increased activation* in these brain regions presented with *better* accuracy on this task. For the time to perform the cube rotation task, we found that those subjects who showed *increases activation* of the left postcentral gyrus, left fusiform gyrus, and right middle occipital gyrus required *less time* to perform the task (**Figure 8** and **Table 3**).

HDBR + CO_2 vs. 70-day HDBR Group Comparisons

Between-group normalized slope comparisons for HDBR + CO_2 and 70-day HDBR revealed differences in the right hippocampus and left inferior temporal gyrus (**Table 4**). That is, the HDBR + CO_2 group showed *greater decreases* in activation in both brain regions across the intervention in comparison to HDBR alone. These results were detected at the conservative, corrected statistical threshold of FDR < 0.05 (Nichols and Hayasaka, 2003).

DISCUSSION

This is the first study to investigate the effects of 30 days of HDBR combined with elevated CO_2 on brain activation during spatial working memory performance. While there were no group-level declines in spatial working memory performance, we observed *decreases* in brain activation in several cortical and cerebellar regions in response to the HDBR + CO_2 intervention, followed by recovery. In addition, we found that, in general, individuals who exhibited *greater increases* in brain activation also showed *less declines* in spatial working memory performance. The right superior temporal gyrus showed differential changes between the HDBR + CO_2 and 70-day HDBR groups, suggesting that elevated CO_2 levels may particularly affect the function of this brain region.

Spatial Working Memory Behavioral Results

Here, we found no differences in spatial working memory accuracy and score (which compares accuracy of the working memory condition to that of the control condition) or cube rotation time and accuracy across 30-days of HDBR + CO_2. Likewise, Ishizaki et al. (2009) evaluated the effects of a 16-day HDBR intervention on executive function in young healthy participants and found no intervention-related changes in performance. Seaton et al. (2009) also found no differences in

TABLE 3 | Brain regions showing associations between the slopes of change in brain and behavioral during spatial working memory.

	Extent (*k*)	Peak *t*-value	MNI coordinates (mm)		
			x	*y*	*z*
Spatial working memory task					
Positive correlation					
Parietal					
R Angular gyrus	36	4.3964	45	−72	40
Negative correlation					
Frontal					
R IFG (p. Opercularis)	12	5.2687	52	10	16
Spatial working memory control					
Positive correlation					
Frontal					
R Posterior-medial frontal	62	5.135	2	8	70
R Superior frontal gyrus	72	5.249	25	64	16
R IFG (p. Opercularis)	42	4.693	62	16	18
R Posterior-medial frontal	49	5.104	2	10	71
R Middle frontal gyrus	10	3.881	26	22	42
L Precentral gyrus	435	7.229	−40	−24	64
Insula					
L Insula lobe	74	4.626	−33	−29	22
Temporal					
R Superior temporal gyrus	182	6.253	48	−40	12
R Superior temporal gyrus	151	5.498	64	−12	12
R Superior temporal gyrus	89	6.537	53	−30	14
R Inferior temporal gyrus	248	6.552	46	−48	−16
R Medial temporal pole	256	8.568	34	14	−32
R Medial temporal pole	135	6.058	54	10	−20
R Medial temporal pole	17	5.584	60	6	−16
R Inferior temporal gyrus	77	3.341	43	−9	−34
R Temporal pole	32	3.049	48	5	−17
R Inferior temporal gyrus	10	3.508	58	−56	−20
L Middle temporal gyrus	40	5.870	44	−70	18
L Superior temporal gyrus	2192	12.836	−50	−16	10
L Superior temporal gyrus	2192	8.276	−50	−38	20
L Superior temporal gyrus	346	6.671	−56	0	−2
L Inferior temporal gyrus	96	3.870	−42	−42	−12
L Temporal pole	62	5.487	−32	10	−30
Parietal					
R Postcentral gyrus	796	5.512	26	−44	70
R Postcentral gyrus	151	7.760	60	−14	32
R Precuneus	91	4.977	2	−54	64
R Precuneus	45	3.772	4	−58	44
L Postcentral gyrus	2192	4.568	−58	−16	34
L Postcentral gyrus	435	10.650	−22	−34	78
Occipital					
R Lingual gyrus	8102	8.120	14	−69	−6
R Inferior occipital gyrus	3295	7.405	44	−68	−8
R Calcarine gyrus	966	4.887	24	−59	14
R Fusiform gyrus	41	5.093	40	−26	−30
R Fusiform gyrus	29	3.908	30	−6	−34
R Superior occipital gyrus	3295	7.760	18	−86	34
L Calcarine gyrus	155	7.554	−16	−100	0
L Fusiform gyrus	1482	5.699	−30	−76	−8
L Lingual gyrus	3295	8.011	14	−68	−6
L Superior occipital gyrus	40	6.671	−56	0	−2
L Inferior occipital gyrus	180	5.789	−43	−75	2
L Inferior occipital gyrus	70	5.356	−21	−101	−1
L Middle occipital gyrus	1482	7.826	−46	−70	4
Subcortical					
R Pallidum	38	3.691	24	−12	6
Negative correlation					
Occipital					
L Lingual gyrus	27	4.8595	−16	−102	−10
Spatial working memory Score					
Positive correlation					
Frontal					
R IFG (p. Opercularis)	15	3.8465	58	16	16
R Posterior-medial frontal	18	3.1255	−10	−14	58
L ACC	43	4.6595	−2	14	36
Temporal					
R Superior temporal gyrus	486	7.0509	50	−44	20
L Superior temporal gyrus	14	3.8465	−48	−8	2
Occipital					
R Fusiform gyrus	34	4.1826	28	−4	−38
Card rotation (accuracy)					
Positive correlation					
Parietal					
L Supramarginal gyrus	17	3.560	−62	−38	32
Negative correlation					
Frontal					
L Superior frontal gyrus	57	5.441	−20	−10	78
Parietal					
R Angular gyrus	42	4.006	42	−66	38
Occipital					
L Lingual gyrus	30	4.238	−32	−88	−10
Cube rotation (time)					
Positive correlation					
Parietal					
L Postcentral gyrus	47	3.2271	−18	−46	48
Occipital					
R Middle occipital gyrus	41	4.7345	32	−88	16
L Fusiform gyrus	29	4.2604	−24	−44	−10
Cube rotation (accuracy)					
Positive correlation					
Frontal					
R Precentral gyrus	96	4.600	48	−8	56
R Precentral gyrus	18	3.167	54	4	40
R Superior frontal gyrus	37	3.669	22	34	50
R Mid orbital gyrus	40	4.238	8	36	−6
Temporal					
R Middle temporal gyrus	68	4.307	64	−8	−12
R Middle temporal gyrus	24	3.516	52	−62	16
R ParaHippocampal gyrus	24	2.754	30	−4	−24

(Continued)

TABLE 3 | Continued

	Extent (*k*)	Peak *t*-value	MNI coordinates (mm)		
			x	*y*	*z*
R Fusiform gyrus	12	2.524	45	−36	−19
R Inferior temporal gyrus	16	4.576	54	−6	−34
L Middle temporal gyrus	71	4.378	−60	−10	−10
L Hippocampus	91	4.493	−20	−32	0
L Middle temporal gyrus	33	3.517	−50	−68	12
L Middle temporal gyrus	104	3.232	−64	−32	0
L Inferior temporal gyrus	17	3.232	−56	−16	−28
L Fusiform gyrus	15	2.821	−33	−36	−23
Parietal					
R Postcentral gyrus	15	3.028	62	−9	39
R Postcentral gyrus	15	2.366	63	−6	38
L Angular gyrus	30	3.588	−42	−74	42
Subcortical					
L Thalamus	29	2.783	−16	−23	14
L Pallidum	13	2.149	−22	−6	3

Significance level set at non-parametric $p < 0.0005$ and cluster size $k = 10$ for all analyses. Brain regions labeled using the AnatomyToolbox atlas via the SPM toolbox BSPMview. L = Left; R = Right; IFG = Inferior Frontal Gyrus; ACC = Anterior Cingulate Cortex.

cognition after 60 or 90 days of HDBR. In contrast, Wang et al. (2017) assessed male healthy subjects that underwent 7 days of HDBR and reported poorer mental rotation accuracy in comparison to baseline. Similarly, Lipnicki et al. (2009) studied the effects of 60-day HDBR and found declines in working memory performance. Another study also examined healthy young individuals regarding time-based prospective memory with an ongoing word recall task and identified impaired prospective memory during HDBR compared to baseline (Chen et al., 2013). Although the behavioral effects of HDBR on spatial working memory are mixed, it seems that long-duration HDBR largely does *not* affect working memory abilities, with only one study showing differences due to 7 days of HDBR.

Time Course of Spatial Working Memory Response to HDBR + CO_2

We identified decreasing activation in the right middle frontal gyrus and the cerebellar dentate nucleus, followed by recovery. These brain regions are involved in attention, mental rotation, and reorientation and are commonly activated during spatial working memory tasks (Thürling et al., 2012; Japee et al., 2015). Thus, these longitudinal changes suggest that HDBR + CO_2 may have reduced the subjects' ability to recruit appropriate working memory networks, or alternatively that it increased neural efficiency. We previously reported that the upward shift of the brain with both spaceflight (Koppelmans et al., 2016) and bed rest (Koppelmans et al., 2017) results in apparent reductions in gray matter volume of this region, which could potentially reflect gray matter compression. These structural brain changes may relate to the reduction in activation of this region during spatial working memory performance in the current study.

Brain-Behavior Correlations

We observed multiple brain-behavior correlations for the spatial working memory, 2D card rotation and 3D cube rotation tasks. Thus, although card rotation time and accuracy were the only behavioral metrics that changed with the intervention (Lee et al., 2019a), individual differences in performance changes in all tasks associated with individual differences in brain activity changes. We found that *greater increases* in activation in parietal, temporal, and occipital brain regions were correlated with *larger improvements* in spatial working memory accuracy. These associations may represent an adaptive or compensatory brain response to the HDBR + CO_2 environment. In the past, our group has demonstrated associations between changes in spatial working memory performance (assessed by cube and card rotation tasks) and changes in brain connectivity between sensorimotor seed regions and brain areas associated with spatial cognition after 70 days of HDBR (Cassady et al., 2016). Those participants who had the *greatest improvements* in spatial working memory performance showed the *greatest changes* in connectivity between the seed and target brain areas. Thus, in the present study, it could be that these brain-behavior associations represent an adaptive neural response and are related to HDBR more generally and not specifically to elevated levels of CO_2.

HDBR + CO_2 vs. 70-day HDBR Group Comparisons

As we did not observe group differences in spatial working memory behavioral performance between the HDBR + CO_2 and 70-day HDBR groups (Lee et al., 2019a), we expected to find few between-group differences in brain activation. We found that the HDBR + CO_2 group presented a steeper slope of change in brain activity in several brain regions. That is, participants who underwent 30 days of HDBR + CO_2 had *greater decreases* in activation in the right hippocampus and left inferior temporal gyrus than in HDBR alone. This was the only effect we observed that survived correction for multiple comparisons (FDR < 0.05). Previous functional neuroimaging studies have suggested that the inferior temporal gyrus is involved in several cognitive processes such as visual memory storage and cognitive learning (Miyashita, 1993). In the present study, *greater increases* in activation in the left inferior temporal gyrus was also correlated with *larger* improvements in cube rotation accuracy, which suggests compensatory network engagement to maintain performance during the intervention.

Similarly, the hippocampus plays an important role in long-term memory and working memory processing (Ni et al., 2017). Toepper et al. (2010) found activation in the right hippocampus when participants engaged in a spatial working memory task (Toepper et al., 2010). A more recent study with polar expeditioners who spent 14 months at the German Neumayer III station in Antarctica–a spaceflight analog model to study the effects of social isolation and environmental deprivation–observed reduced hippocampal volume in several regions following the expedition (Stahn et al., 2019). They also

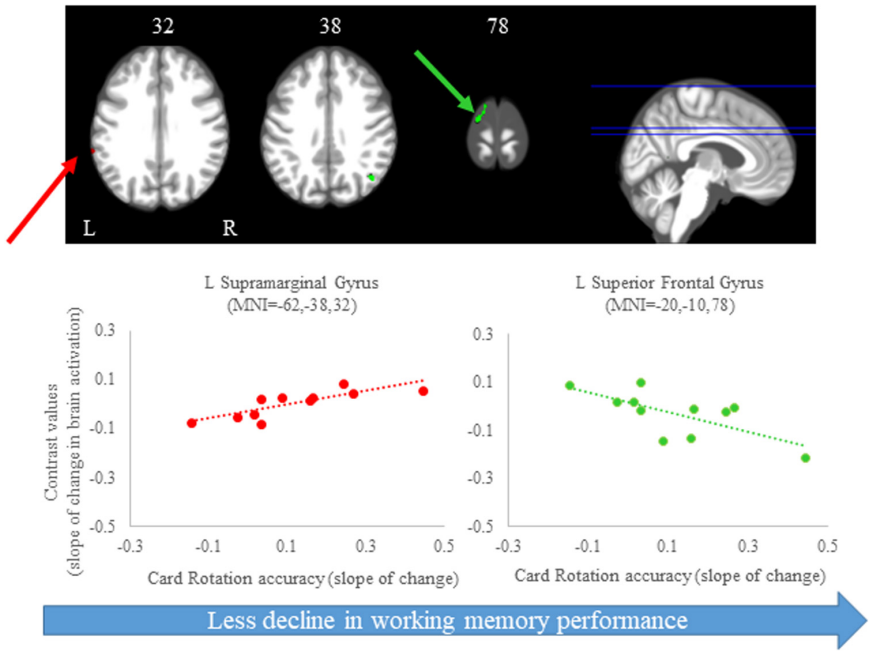

FIGURE 7 | Brain-behavior correlations (card rotation task). Slope of changes in brain and behavior results showing positive (red) and negative (green) correlations. *Top:* Whole brain results overlaid onto the MNI standard template; $p < 0.0005$, $k = 10$. *Bottom:* Correlation plots include contrast values extracted from the peak coordinate inside an example cluster (indicated with red or green arrows) graphed against the slope of changes in behavior results. Abbreviations: L = Left; R = Right.

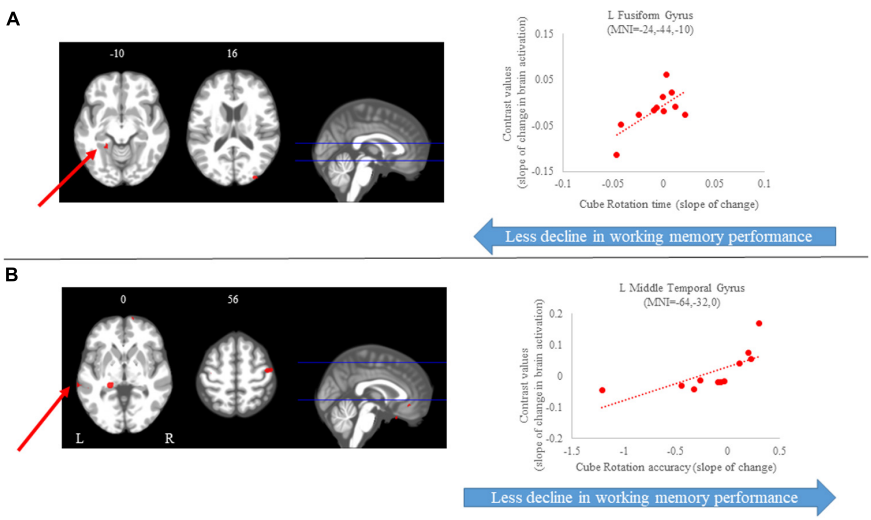

FIGURE 8 | Brain-behavior correlations (cube rotation task). Slope of changes in brain and behavior results showing positive (red) correlations. **(A)** Cube rotation time; and **(B)** cube rotation accuracy. Whole brain results are overlaid onto the MNI standard template; $p < 0.0005$, $k = 10$. Right side correlation plots include contrast values extracted from the peak coordinate inside an example cluster (indicated with red arrows) graphed against the slope of changes in behavior results. Abbreviations: L = Left; R = Right.

reported that reduced hippocampal volume was not associated with general cognitive performance, but it was correlated with performance on a spatial mental rotation task. Thus, it is possible that the hippocampal activation changes we observed here during the mental rotation working memory task occurred at least partly as a result of our subjects being isolated for 30 days.

Another recent study evaluated the effect of acute exposure to elevated levels of CO_2 (0.5%) during HDBR in comparison to HDBR alone on cognitive performance. They reported that subjects exposed to 26.5 h of 12° HDBR + CO_2 presented with greater accuracy and lower speed on the Visual Object Learning Task in comparison to HDBR alone (Basner et al., 2018).

TABLE 4 | Regions with differences in slope of change in brain activation during bed rest between HDBR + CO_2 and HDBR.

	Extent (*k*)	Peak *t*-value	MNI coordinates (mm)		
			x	*y*	*z*
HDBR + CO_2 < HDBR					
Temporal					
R Hippocampus	12	3.444	18	−40	14
L Inferior temporal gyrus	11	3.586	−66	−44	−14

Significance level set at FDR p < 0.05 and cluster size k = 10. Brain regions labeled using the AnatomyToolbox atlas via the SPM toolbox BSPMview. L = Left; R = Right.

Based on that finding, Scully et al., speculated that the medial temporal cortex and the hippocampus could be more sensitive to changes in CO_2 concentration, with concomitant improvement in memory performance (Scully et al., 2019). Our results are in agreement with their speculation since we observed that the elevated CO_2 levels combined with HDBR had a small effect on these same brain regions. However, we did not observe significant improvements in working memory performance; it could be that our task was not sensitive enough to detect subtle CO_2-induced changes in working memory performance. In combination, these studies support that medial temporal lobe and hippocampal changes with HDBR + CO_2 could be due to some combination of HDBR, CO_2, and/or isolation.

CO_2 has a vasodilation effect which results in increased brain blood flow (Atkinson et al., 1990; Zhou et al., 2008) and consequently increased intensity of the blood oxygen level-dependent (BOLD) signal measured by fMRI (Corfield et al., 2001). However, the effects of elevated CO_2 on brain perfusion are still inconclusive. In the present study, even though participants presented increases in their $PaCO_2$ levels from pre- to post-HDBR + CO_2 we did not see increases in brain activity in comparison to HDBR alone. Conversely, HDBR + CO2 presented greater decreases in activation in comparison to HDBR alone. On the other hand, a recent study from our group (again using the same subjects as in the present study) showed *greater increases* in activation of several regions during vestibular stimulation for the HDBR + CO_2 group in comparison to the 70-day HDBR group (Hupfeld et al., 2020). This result suggests interactive or additive effects of bed rest and elevated CO_2 for vestibular changes (Hupfeld et al., 2020), but not for spatial working memory changes. Therefore, again, elevated CO_2 effects seem to be task-specific rather than global effects of HDBR or CO_2.

Limitations

This study has several limitations. First, we had a small sample size and thus the results should be generalized with caution. Second, the testing timelines differed between the HDBR + CO_2 and 70-day HDBR groups; each group was part of a separate bed rest campaign. These data were collected on two different Siemens scanners with two slightly different fMRI sequences. The HDBR + CO_2 fMRI sequence included a faster TR than the 70-day HDBR sequence. However, we controlled for these differences as much as possible by using age and sex as covariates and by using slope comparisons to account for timeline differences (Yuan et al., 2016, 2018b; Hupfeld et al., 2020). Third, although the between-group comparison is FDR corrected (i.e., a more conservative statistical threshold), due to the limited pilot sample size, we used uncorrected *p*-values for the other neuroimaging statistical analyses to better detect within- and between-subject differences (Hupfeld et al., 2020). It is known that there is an upward shift of the brain and fluid redistribution during HDBR (Koppelmans et al., 2017), so it is not clear whether or how those changes interact with the functional brain changes seeing here. The fourth caveat of this study is that subjects on the HDBR + CO_2 group underwent stricter bed rest, so it is unclear whether the results found here are due to the effects of the elevated levels of CO_2 and/or the absence of a pillow in certain postures. Additionally, subjects in the HDBR campaign were scanned while supine, whereas those in the HDBR + CO_2 were maintained at −6°. Finally, it should also be mentioned that HDBR + CO_2 mimics only some of the effects of spaceflight, such as high levels of CO_2, body unloading and fluid shifts toward the head, so it is difficult to fully generalize these findings to spaceflight. Moreover, lung volumes are reduced in bed rest and microgravity but not with the same extent (West, 2000; Prisk, 2005), then elevated CO_2 levels may have larger effects on the ISS than on Earth.

CONCLUSION

We investigated the longitudinal neural effects of HDBR + CO_2 on spatial working memory. We observed decreases in activation in brain regions that are involved in attention, mental rotation and reorientation followed by recovery. This suggests that 30 days of HDBR combined with elevated CO_2 levels may reduce the ability to recruit these brain regions. These findings contribute to a better understanding of how the working memory system adapts to a spaceflight analog environment.

DATA AVAILABILITY STATEMENT

The raw data supporting the conclusions of this article will be made available by the authors, without undue reservation.

ETHICS STATEMENT

The studies involving human participants were reviewed and approved by the University of Florida Institutional Review Board. NASA Institutional Review Board. Local ethical commission of the regional medical association (Ärztekammer Nordrhein). The patients/participants provided their written informed consent to participate in this study.

AUTHOR CONTRIBUTIONS

AS analyzed the spatial working memory fMRI and behavioral data, created the figures and tables, and wrote the first draft

of the manuscript. KH assisted with fMRI preprocessing, fMRI statistical analyses, and preparation of the initial manuscript draft. JL and EM collected, analyzed, and managed the data. NB and YD collected and analyzed the data. IK participated in project design and software development. JB, AM, and RS designed the project, secured funding, and led the interpretation and discussion of the results. All authors participated in revision of the manuscript.

FUNDING

This work was supported by grants from the National Aeronautics and Space Administration (NASA; NNX11AR02G, and 80NSSC17K0021) and the National Space Biomedical Research Institute (NSBRI; SA02802) to RS, AM, and JB. Additionally, we thank support from a National Science Foundation Graduate Research Fellowship under Grant nos. DGE-1315138 and DGE-1842473, as well as training grant NIH T32-NS082128 to KH.

ACKNOWLEDGMENTS

The authors wish to acknowledge those at the: envihab facility in Cologne, Germany including the VaPER study staff, and the bed rest participants who volunteered their time, without whom this project would not have been possible.

REFERENCES

Allen, J. G., MacNaughton, P., Cedeno-Laurent, J. G., Cao, X., Flanigan, S., Vallarino, J., et al. (2019). Airplane pilot flight performance on 21 maneuvers in a flight simulator under varying carbon dioxide concentrations. *J. Expo. Sci. Environ. Epidemiol.* 29, 457–468. doi: 10.1038/s41370-018-0055-8

Anguera, J. A., Reuter-Lorenz, P. A., Willingham, D. T., and Seidler, R. D. (2010). Contributions of spatial working memory to visuomotor learning. *J. Cogn. Neurosci.* 22, 1917–1930. doi: 10.1162/jocn.2009.21351

Atkinson, J. L. D., Anderson, R. E., and Sundt, T. M. (1990). The effect of carbon dioxide on the diameter of brain capillaries. *Brain Res.* 517, 333–340. doi: 10.1016/0006-8993(90)91046-J

Avants, B. B., Tustison, N. J., Song, G., Cook, P. A., Klein, A., and Gee, J. C. (2011). A reproducible evaluation of ANTs similarity metric performance in brain image registration. *Neuroimage* 54, 2033–2044. doi: 10.1016/j.neuroimage.2010.09.025

Baddeley, A. D. (2017). "Working memory: theories, models, and controversies," in *Exploring Working Memory: Selected Works of Alan Baddeley* (London: Routledge Taylor & Francis Group). doi: 10.4324/9781315111261

Basner, M., Nasrini, J., Hermosillo, E., McGuire, S., Dinges, D. F., Moore, T. M., et al. (2018). Effects of -12° head-down tilt with and without elevated levels of CO2 on cognitive performance: the SPACECOT study. *J. Appl. Physiol.* 124, 750–760. doi: 10.1152/japplphysiol.00855.2017

Bock, O., Weigelt, C., and Bloomberg, J. J. (2010). Cognitive demand of human sensorimotor performance during an extended space mission: a dual-task study. *Aviat. Sp. Environ. Med.* 81, 819–824. doi: 10.3357/ASEM.2608.2010

Cassady, K., Koppelmans, V., Reuter-Lorenz, P., De Dios, Y., Gadd, N., Wood, S., et al. (2016). Effects of a spaceflight analog environment on brain connectivity and behavior. *Neuroimage* 141, 18–30. doi: 10.1016/j.neuroimage.2016.07.029

Chen, S., Zhou, R., Xiu, L., Chen, S., Chen, X., and Tan, C. (2013). Effects of 45-day -6° head-down bed rest on the time-based prospective memory. *Acta Astronaut.* 84, 81–87. doi: 10.1016/j.actaastro.2012.10.040

Corfield, D. R., Murphy, K., Josephs, O., Adams, L., and Turner, R. (2001). Does hypercapnia-induced cerebral vasodilation modulate the hemodynamic response to neural activation? *Neuroimage* 13(6 Pt 1), 1207–1211. doi: 10.1006/nimg.2001.0760

De la Torre, G. (2014). Cognitive neuroscience in space. *Life* 4, 281–294. doi: 10.3390/life4030281

Diedrichsen, J. (2006). A spatially unbiased atlas template of the human cerebellum. *Neuroimage* 33, 127–138. doi: 10.1016/j.neuroimage.2006.05.056

Diedrichsen, J., Balsters, J. H., Flavell, J., Cussans, E., and Ramnani, N. (2009). A probabilistic MR atlas of the human cerebellum. *Neuroimage* 46, 39–46. doi: 10.1016/j.neuroimage.2009.01.045

Ekstrom, R. B., French, J. W., and Harman, H. H. (1976). *Manual for Kit of Factor-Referenced Cognitive Tests*. Princeton, NJ: Education Testing Service.

Gläscher, J., and Gitelman, D. (2008). *Contrast Weights in Flexible Factorial Design with Multiple Groups of Subjects*. London: SPM, 1–12.

Hupfeld, K. E., Lee, J. K., Gadd, N. E., Kofman, I. S., De Dios, Y. E., Bloomberg, J. J., et al. (2020). Neural correlates of vestibular processing during a spaceflight analog with elevated carbon dioxide (co2): a pilot Study. *Front. Syst. Neurosci.* 13:80. doi: 10.3389/fnsys.2019.00080

Ishizaki, Y., Fukuoka, H., Tanaka, H., Ishizaki, T., Fujii, Y., Hattori-Uchida, Y., et al. (2009). Executive function on the 16-day of bed rest in young healthy men. *Acta Astronaut.* 64, 864–868. doi: 10.1016/j.actaastro.2008.10.006

Japee, S., Holiday, K., Satyshur, M. D., Mukai, I., and Ungerleider, L. G. (2015). A role of right middle frontal gyrus in reorienting of attention: a case study. *Front. Syst. Neurosci.* 9:23. doi: 10.3389/fnsys.2015.00023

Kanas, N., and Manzey, D. (2008). *Space Psychology and Psychiatry*. Dordrecht: Springer Netherlands. doi: 10.1007/978-1-4020-6770-9

Koppelmans, V., Bloomberg, J. J., De Dios, Y. E., Wood, S. J., Reuter-Lorenz, P. A., Kofman, I. S., et al. (2017). Brain plasticity and sensorimotor deterioration as a function of 70 days head down tilt bed rest. *PLoS One* 12:e0182236. doi: 10.1371/journal.pone.0182236

Koppelmans, V., Bloomberg, J. J., Mulavara, A. P., and Seidler, R. D. (2016). Brain structural plasticity with spaceflight. *npj Microgravity* 2:2. doi: 10.1038/s41526-016-0001-9

Koppelmans, V., Erdeniz, B., De Dios, Y. E., Wood, S. J., Reuter-Lorenz, P. A., Kofman, I., et al. (2013). Study protocol to examine the effects of spaceflight and a spaceflight analog on neurocognitive performance: extent, longevity, and neural bases. *BMC Neurol.* 13:205. doi: 10.1186/1471-2377-13-205

Lamp, G., Alexander, B., Laycock, R., Crewther, D. P., and Crewther, S. G. (2016). Mapping of the underlying neural mechanisms of maintenance and manipulation in visuo-spatial working memory using an n-back mental rotation task: a functional magnetic resonance imaging study. *Front. Behav. Neurosci.* 10:87. doi: 10.3389/fnbeh.2016.00087

Law, J., Van Baalen, M., Foy, M., Mason, S. S., Mendez, C., Wear, M. L., et al. (2014). Relationship between carbon dioxide levels and reported headaches on the international space station. *J. Occup. Environ. Med.* 56, 477–483. doi: 10.1097/JOM.0000000000000158

Lee, J. K., De Dios, Y., Kofman, I., Mulavara, A. P., Bloomberg, J. J., and Seidler, R. D. (2019a). Head down tilt bed rest plus elevated CO2 as a spaceflight analog: effects on cognitive and sensorimotor performance. *Front. Hum. Neurosci.* 13:355. doi: 10.3389/fnhum.2019.00355

Lee, J. K., Koppelmans, V., Riascos, R. F., Hasan, K. M., Pasternak, O., Mulavara, A. P., et al. (2019b). Spaceflight-associated brain white matter microstructural changes and intracranial fluid redistribution. *JAMA Neurol.* 76, 412–419. doi: 10.1001/jamaneurol.2018.4882

Leone, G., Lipshits, M., Gurfinkel, V., and Berthoz, A. (1995). Is there an effect of weightlessness on mental rotation of three-dimensional objects? *Cogn. Brain Res.* 2, 255–267. doi: 10.1016/0926-6410(95)90017-9

Lipnicki, D. M., Gunga, H. C., Belav?, D. L., and Felsenberg, D. (2009). Bed rest and cognition: effects on executive functioning and reaction time. *Aviat. Space Environ. Med.* 80, 1018–1024. doi: 10.3357/ASEM.2581.2009

Manzey, D., and Lorenz, B. (1998). Mental performance during short-term and long-term spaceflight. *Brain Res. Rev.* 28, 215–221. doi: 10.1016/S0165-0173(98)00041-1

Miyashita, Y. (1993). Inferior temporal cortex: where visual perception meets memory. *Annu. Rev. Neurosci.* 16, 245–263. doi: 10.1146/annurev.ne.16.030193.001333

Moore, S. T., MacDougall, H. G., and Paloski, W. H. (2010). Effects of head-down bed rest and artiWcial gravity on spatial orientation. *Exp. Brain Res.* 204, 617–622. doi: 10.1007/s00221-010-2317-0

Ni, B., Wu, R., Yu, T., Zhu, H., Li, Y., and Liu, Z. (2017). Role of the hippocampus in distinct memory traces: timing of match and mismatch enhancement revealed by intracranial recording. *Neurosci. Bull.* 33, 664–674. doi: 10.1007/s12264-017-0172-8

Nichols, T., and Hayasaka, S. (2003). Controlling the familywise error rate in functional neuroimaging: a comparative review. *Stat. Methods Med. Res.* 12, 419–446. doi: 10.1191/0962280203sm341ra

Prisk, G. K. (2005). The lung in space. *Clin. Chest Med.* 26, 415–438. doi: 10.1016/j.ccm.2005.05.008

Reuter-Lorenz, P. A., Jonides, J., Smith, E. E., Hartley, A., Miller, A., Marshuetz, C., et al. (2000). Age differences in the frontal lateralization of verbal and spatial working memory revealed by PET. *J. Cogn. Neurosci.* 12, 174–187. doi: 10.1162/089892900561814

Roberts, D. R., Albrecht, M. H., Collins, H. R., Asemani, D., Chatterjee, A. R., Spampinato, M. V., et al. (2017). Effects of spaceflight on astronaut brain structure as indicated on MRI. *N. Engl. J. Med.* 377, 1746–1753. doi: 10.1056/nejmoa1705129

Romero, J. E., Coupé, P., Giraud, R., Ta, V. T., Fonov, V., Park, M. T. M., et al. (2017). CERES: a new cerebellum lobule segmentation method. *Neuroimage* 147, 916–924. doi: 10.1016/j.neuroimage.2016.11.003

Scully, R. R., Basner, M., Nasrini, J., Lam, C. W., Hermosillo, E., Gur, R. C., et al. (2019). Effects of acute exposures to carbon dioxide on decision making and cognition in astronaut-like subjects. *npj Microgravity* 5:17. doi: 10.1038/s41526-019-0071-6

Seaton, K. A., Slack, K. J., Sipes, W. A., and Bowie, K. E. (2009). Cognitive functioning in long-duration head-down bed rest. *Aviat. Sp. Environ. Med.* 80(5 Suppl), A62–A65. doi: 10.3357/ASEM.BR09.2009

Seidler, R. D., Bo, J., and Anguera, J. A. (2012). Neurocognitive contributions to motor skill learning: the role of working memory. *J. Mot. Behav.* 44, 445–453. doi: 10.1080/00222895.2012.672348

Shepard, R. N., and Metzler, J. (1971). Mental rotation of three-dimensional objects. *Science* 171, 701–703. doi: 10.1126/science.171.3972.701

Shepard, S., and Metzler, D. (1988). Mental rotation: effects of dimensionality of objects and type of task. *J. Exp. Psychol. Hum. Percept. Perform.* 14, 3–11. doi: 10.1037/0096-1523.14.1.3

Stahn, A. C., Gunga, H. C., Kohlberg, E., Gallinat, J., Dinges, D. F., and Kühn, S. (2019). Brain changes in response to long Antarctic expeditions. *N. Engl. J. Med.* 381, 2273–2275. doi: 10.1056/NEJMc1904905

Thürling, M., Hautzel, H., Küper, M., Stefanescu, M. R., Maderwald, S., Ladd, M. E., et al. (2012). Involvement of the cerebellar cortex and nuclei in verbal and visuospatial working memory: a 7T fMRI study. *Neuroimage* 62, 1537–1550. doi: 10.1016/j.neuroimage.2012.05.037

Toepper, M., Markowitsch, H. J., Gebhardt, H., Beblo, T., Thomas, C., Gallhofer, B., et al. (2010). Hippocampal involvement in working memory encoding of changing locations: an fMRI study. *Brain Res.* 1354, 91–99. doi: 10.1016/j.brainres.2010.07.065

Wang, H., Duan, J., Liao, Y., Wang, C., Li, H., and Liu, X. (2017). Objects mental rotation under 7 days simulated weightlessness condition: an ERP study. *Front. Hum. Neurosci.* 11:553. doi: 10.3389/fnhum.2017.00553

West, J. B. (2000). Physiology of a microgravity environment historical perspectives: physiology in microgravity. *J. Appl. Physiol.* 89, 379–384. doi: 10.1152/jappl.2000.89.1.379

Yuan, P., Koppelmans, V., Reuter-Lorenz, P., De Dios, Y., Gadd, N., Riascos, R., et al. (2018a). Change of cortical foot activation following 70 days of head-down bed rest. *J. Neurophysiol.* 119, 2145–2152. doi: 10.1152/jn.00693.2017

Yuan, P., Koppelmans, V., Reuter-Lorenz, P., De Dios, Y., Gadd, N., Wood, S., et al. (2018b). Vestibular brain changes within 70 days of head down bed rest. *Hum. Brain Mapp.* 39, 2753–2763. doi: 10.1002/hbm.24037

Yuan, P., Koppelmans, V., Reuter-Lorenz, P. A., De Dios, Y. E., Gadd, N. E., Wood, S. J., et al. (2016). Increased brain activation for dual tasking with 70-days head-down bed rest. *Front. Syst. Neurosci.* 10:71. doi: 10.3389/fnsys.2016.00071

Zhou, H., Saidel, G. M., and Lamanna, J. C. (2008). Cerebral blood flow adaptation to chronic hypoxia. *Adv. Exp. Med. Biol.* 614, 371–377. doi: 10.1007/978-0-387-74911-2_41

Conflict of Interest: NB, IK, YD, and AM were employed by the company KBR.

The remaining authors declare that the research was conducted in the absence of any commercial or financial relationships that could be construed as a potential conflict of interest.

frontiers in Systems Neuroscience

REVIEW
published: 31 July 2020
doi: 10.3389/fnsys.2020.00045

Role of Ginkgolides in the Inflammatory Immune Response of Neurological Diseases: A Review of Current Literatures

*Chunrong Li, Kangding Liu, Shan Liu, Qiaolifan Aerqin and Xiujuan Wu**

Department of Neurology, Neuroscience Center, The First Hospital of Jilin University, Jilin University, Changchun, China

The inflammatory immune response (IIR) is a physiological or excessive systemic response, induced by inflammatory immune cells according to changes in the internal and external environments. An excessive IIR is the pathological basis for the generation and development of neurological diseases. Ginkgolides are one of the important medicinal ingredients in *Ginkgo biloba*. Many studies have verified that ginkgolides have anti-platelet-activating, anti-apoptotic, anti-oxidative, neurotrophic, and neuroimmunomodulatory effects. Inflammatory immunomodulation is mediated by inhibition of the mitogen-activated protein kinase (MAPK) and nuclear factor-kappa B (NF-κB) signaling pathways. They also inhibit the platelet-activating factor (PAF)-mediated signal transduction to attenuate the inflammatory response. Herein, we reviewed the studies on the roles of ginkgolides in inflammatory immunomodulation and suggested its potential role in novel treatments for neurological diseases.

Keywords: ginkgolides, inflammatory immune response, neurological diseases, multiple sclerosis, Guillain–Barré syndrome

OPEN ACCESS

Edited by:
James W. Grau,
Texas A&M University, United States

Reviewed by:
Marco Atzori,
Universidad Autónoma de San Luis Potosí, Mexico
Guisheng Zhou,
Nanjing University of Chinese Medicine, China

****Correspondence:***
Xiujuan Wu
wuxiujuan861003@126.com

Received: *08 February 2020*
Accepted: *17 June 2020*
Published: *31 July 2020*

Citation:
Li C, Liu K, Liu S, Aerqin Q and Wu X (2020) Role of Ginkgolides in The Inflammatory Immune Response of Neurological Diseases: A Review of Current Literatures. Front. Syst. Neurosci. 14:45. doi: 10.3389/fnsys.2020.00045

KEY POINTS

1. Ginkgolides have inflammatory immunomodulation effects, which are mediated by inhibition of the MAPK and TLR/MyD88/NF-κB signaling pathways.
2. TLR/MyD88/NF-κB signaling pathways are involved in the pathogenesis of some neurological diseases.
3. However, there are currently no comprehensive reviews about the regulatory effects of ginkgolides on the IIR.
4. Ginkgolides may represent a potential therapeutic target for neurological disorders in the future.

INTRODUCTION

The inflammatory immune response (IIR) is a physiological or excessive systemic response, induced by inflammatory immune cells based on the changes in the internal and external environments (Han et al., 2018). Inflammatory immune cells such as macrophages (MΦ), T lymphocytes, dendritic cells (DCs), some nonimmune cells, inflammatory immune cytokines, and related receptor signal transduction pathways are involved in the mechanisms underlying excessive IIR (Han et al., 2018). An excessive IIR is the pathological basis for the generation and development of neurological diseases, especially neurodegenerative and/or neuroimmune diseases, and ischemic cerebrovascular diseases (Ritzel et al., 2018; Voet et al., 2019). Regulating an excessive IIR has become a novel therapeutic target for neurological diseases. Ginkgolides are isolated and purified from the leaves of *Ginkgo biloba*. The ginkgo leaf extracts commonly contain flavonoids such as quercetin, kaempferol, myricetin, and terpene trilactone (Al-Adwani et al., 2019). The extracted terpene trilactone includes ginkgolide A (GA), B, C, M, J, and K and bilobalide (BB; Huang et al., 2014). As early as 1985, Braquet et al. discovered that ginkgolides, particularly GB, are platelet-activating factor (PAF) receptor (PAFR) antagonists, which contribute to the prevention of platelet aggregation and thrombosis (Braquent, 1985). The neuromodulatory effects of ginkgolides include promoting secretion of neurotrophic factors, anti-oxidant effects, increasing cerebral blood flow and circulation, modifying neurotransmission, and providing protection against apoptosis (Bastianetto et al., 2000; Zheng et al., 2000; Wang and Chen, 2005; Tchantchou et al., 2009; Ribonnet et al., 2011; Wei et al., 2017; **Table 1**). The regulatory effects of ginkgolides on IIR have recently been revealed. Ginkgolides can regulate IIR *via* PAF-mediated signal transduction, mitogen-activated protein kinase (MAPK), and toll-like receptor/myeloid differentiation primary response 88/nuclear factor-kappa B (TLR/MyD88/NF-κB) signaling pathways. Mediating an excessive IIR is a novel therapeutic target for neurological diseases, especially neurodegenerative diseases, ischemic cerebrovascular diseases, and/or neuroimmune diseases, but there are currently no comprehensive reviews on this topic. We herein summarize the articles about the effects of ginkgolides on the IIR, and we suggest a potential role for ginkgolides as a novel treatment for neurological disorders.

CHEMICAL AND PHARMACOLOGICAL CHARACTERISTICS OF GINKGOLIDES

Chemical Characteristics of Ginkgolides

Ginkgolides consist mainly of diterpenes and sesquiterpenes, which are the only natural substances with tertiary butyl functional groups [–C17 $(CH3)_3$]. As early as the 1930s, scholars had extracted and separated active components from *Ginkgo biloba* leaves (Strømgaard and Nakanishi, 2004). GA, GB, and BB in *G. biloba* were separately measured in the root, stem, and leaf by high-performance liquid chromatography in 1997 (Lu et al., 2017). The results demonstrated that quantities of GA, GB, and BB are high in the roots and leaves. Recently, GA, GB, GC, and BB have been further measured in the cortex and xylem of roots and branches (Lu et al., 2017). The diterpenoid lactones of ginkgolides have a unique 20-carbon skeleton structure, embedded with a tertiary butyl rarely found in natural compounds, and have a rigid skeleton formed by six five-membered rings, A–F. The diterpenoid lactones of *G. biloba* differ only in the number and position of hydroxyl groups, which can be converted into each other under certain conditions.

Platelet-Activating Factor-Mediated Signal Transduction in the Regulation of Inflammatory Immune Response of Ginkgolides

Pharmacological studies of ginkgolides are extensive (**Table 1**, **Figure 1**). Ginkgolides are natural PAFR antagonists that selectively and competitively antagonize PAF-induced platelet aggregation (Gui et al., 2007). It is well established that PAF signaling plays a pivotal role in the initiation and progression of inflammatory and thrombotic reactions, as well as in the cross talk between them (Stafforini et al., 2003). PAF is a lipid mediator of inflammation and has important functions in acute and chronic inflammation, emerging as an important factor in neural injury, such as ischemia/reperfusion (I/R) injury, stroke, inflammation, and multiple sclerosis (MS; Bellizzi et al., 2016; Wang et al., 2018). PAF works by binding to a unique G-protein-coupled, seven-transmembrane receptor, which contains an intronless protein coding region and activates multiple intracellular signaling pathways (Deng et al., 2019). The PAFR is considered to regulate all PAF actions through humoral, autocrine, and/or paracrine mechanisms. Kinases and phospholipases whose activation is induced by PAF include MAPK, protein kinase C (PKC), phosphatidylinositol 3-kinase (PI3K), protein tyrosine kinases, G-protein-coupled receptor kinase, and multiple intracellular signal transducers (Ishii and Shimizu, 2000). In addition, PAF regulates the expressions of interleukin (IL)-1, IL-6, IL-8, and pleiotropic cytokines (Hamel-Côté et al., 2019a,b). As an inflammatory factor, PAF plays an important role in many pathological conditions. It is remarkable that PAF is synthesized and released in both acute and chronic inflammatory animal models. PAF and PAF-like lipids bind to PAFR, which triggers a variety of intracellular signaling cascades and induces functional responses by PAFR-bearing cells, further initiating or amplifying inflammatory, thrombotic, or apoptotic events (Maerz et al., 2011). Thus, blocking PAFR signaling could possibly inhibit inflammation or ischemic injury. There is increasing evidence that GB protects against neural damage in a variety of circumstances and has beneficial effects on circulatory and inflammatory conditions due to pathophysiological effects of PAF (Golino et al., 1993). As an antagonist of the G-protein-coupled PAFR, GB is widely present on pivotal target cells of the inflammatory, immune, and hemostatic systems, and it competitively inhibits PAFR ligand binding (Gui et al., 2007; Maerz et al., 2011; **Figure 2**). Tran and colleagues investigated the roles of PAFR in the abnormal behaviors induced by phencyclidine (PCP) in mice, and they

TABLE 1 | Pharmacological characteristics of ginkgolides.

Pharmacological characteristics	Possible mechanisms	References
Anti-PAF	Competitively inhibits the binding of PAFR to ligands.	Gui et al. (2007) and Maerz et al. (2011)
Anti-apoptotic	Regulates anti-apoptotic protein Suppresses p-SAPK/JNK activation, reactive oxygen species, mitochondrial pro-apoptotic factors, PARP, and cytochrome *c* release.	Ahlemeyer et al. (1999) and Gu et al. (2012)
Anti-oxidative	Interferes with production of free oxygen radicals Protects the decrease in hippocampal Ca^{2+}/calmodulin-dependent protein kinase II activity.	Zalewska et al. (1996) and Pietri et al. (1997)
Neurotrophic effect	Up-regulates the expression of BDNF.	Wei et al. (2017)
Neuroimmunomodulatory effect	Inhibits TNF-α, IL-6, IL-1β and suppresses TLR4, NF-κB gene expressions.	Hu et al. (2011)

Note. PAF, platelet-activating factor; PAFR, platelet-activating factor receptor; PARP, poly (ADP-ribose) polymerase; p-SAPK, p-stress-activated protein kinase; JNK, c-Jun N-terminal kinase; BDNF, brain-derived neurotrophic factor; TNF-α, tumor necrosis factor α; IL, interleukin-6; TLR, toll-like receptor; NF-κB, nuclear factor-kappa B.

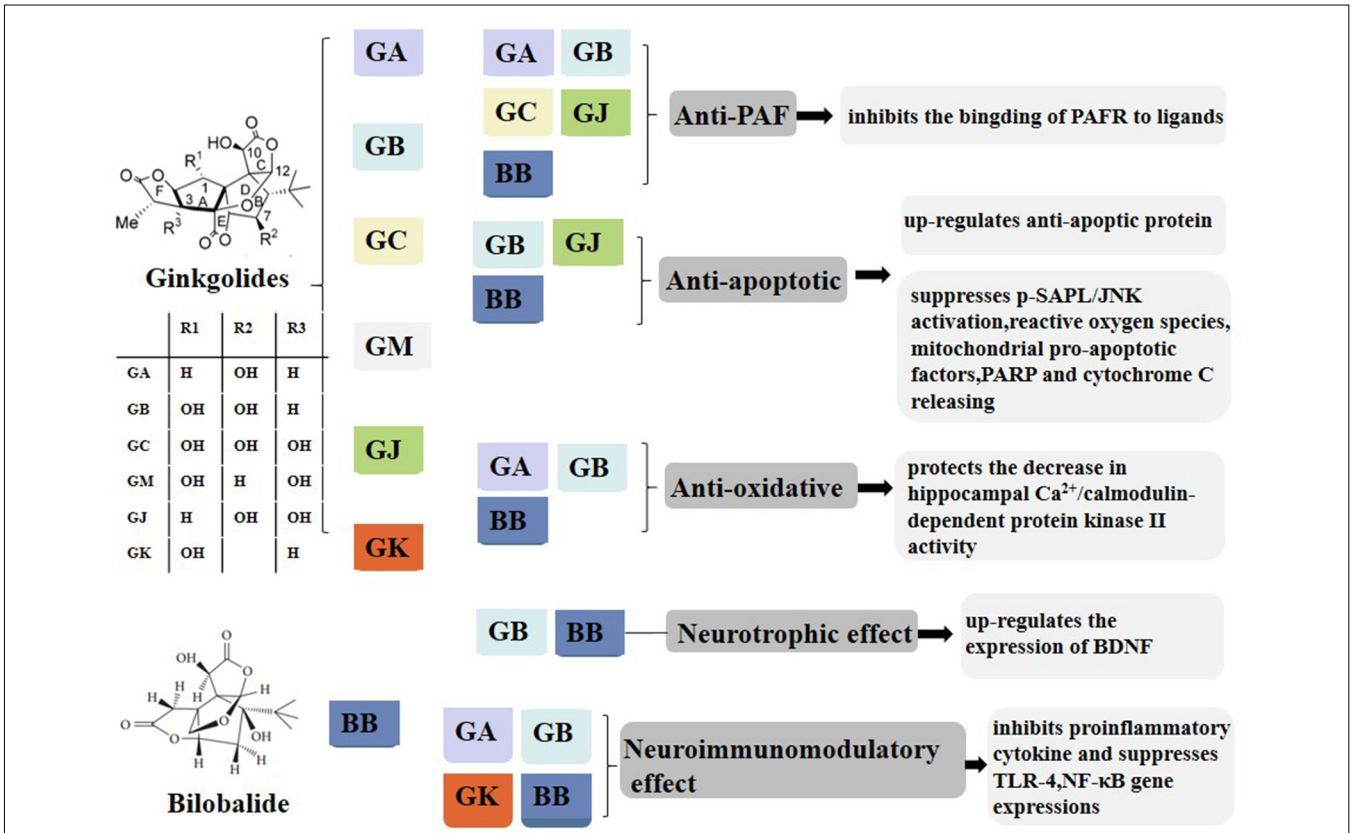

FIGURE 1 | Composition and pharmacological properties of ginkgolides. Ginkgolides are isolated and purified from the leaves of *Ginkgo biloba*. The ginkgo leaf extracts commonly contain flavonoids such as quercetin, kaempferol, myricetin, and terpene trilactone. The extracted terpene trilactone include ginkgolide A (GA), B, C, M, J, and K and bilobalide (BB). Ginkgolides have anti-PAF, anti-apoptotic, anti-oxidative, neurotrophic, and neuroimmunomodulatory effects. GA, ginkgolides A; BB, bilobalide; PAF, platelet-activating factor; PAFR, platelet-activating factor receptor; p-SAPK/JNK, phospho-stress-activated protein kinase/c-Jun N-terminal kinase; PARP, poly (ADP-ribose) polymerase; BDNF, brain-derived neurotrophic factor; TLR4, toll-like receptor-4; NF-κB, nuclear factor-kappa B.

found that treatment with PCP resulted in a virtual increase in nuclear translocation of NF-κB p65 and deoxyribonucleic acid (DNA) binding activity. These findings indicate that levels of the pro-inflammatory molecule NF-κB are increased through up-regulation of PAFR. They also found that GB significantly attenuates abnormal behaviors such as depression, sociability and cognitive impairment, and behavioral sensitization induced by PCP, in PAFR knockout mice. Moreover, GB attenuates PCP-induced increases in NF-κB p65 nuclear translocation and DNA binding activity (Tran et al., 2018). It was proposed for the first time that PAF/PAFR mediates dopaminergic degeneration *via* an NF-κB-dependent signaling process (Kim et al., 2013). Depletion of the PAFR gene, or GB, which itself is a PAFR antagonist, significantly attenuates the increase in NF-κB DNA binding activity (Kim et al., 2013). GB has also been shown to ameliorate colonic inflammation and decrease tumor number and load in mice, through the assessment of disease activity indexes, histological injury scores, leukocyte infiltration, and expression of pro-inflammatory cytokines such as tumor necrosis factor-α (TNF-α), IL-1β, and IL-6 (Sun et al., 2015). PAF

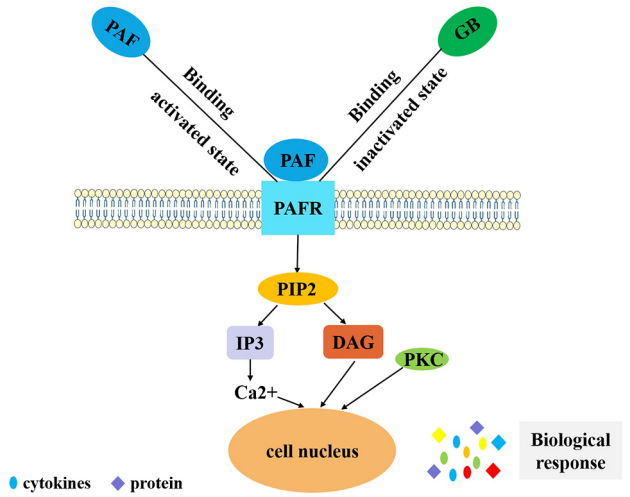

FIGURE 2 | PAF-mediated signal transduction of ginkgolides in the regulation of IIR. PAF binds to PAF receptor *in vivo*, and coupled with G protein, phospholipase C is activated and has an effect on phosphatidylinositol 4,5-bisphosphate. Phosphatidylinositol bisphosphate breakdown produces inositol triphosphate and diglyceride. Inositol triphosphate can induce intracellular calcium concentration increases and diglyceride can activate PKC. Finally, it exerts a biological effect by secreting cytokines and proteins. GB competitively inhibits PAF binding to PAFR in order to reduce the above series of reactions and play an anti-inflammatory role. PAF, platelet-activating factor; IIR, inflammatory immune response; PKC, protein kinase C; GB, ginkgolide B.PAF, platelet-activating factor; PAFR, platelet-activating factor receptor; GB, ginkgolide B; PIP2, phosphatidylinositol 4,5-bisphosphate; IP3, inositol 1,4,5-triphosphate; DAG, diacylglycerol; PKC, protein kinase C; IIR, inflammatory immune response.

regulates cytokines, which stimulates leukotriene synthesis and is associated with the pathogenesis of inflammatory processes (Maclennan et al., 2002). The PAFR is also involved in the microglial polarization modulatory effects of GB on increasing M2 signature gene expression, reducing M1 gene expression, increasing transforming growth factor-β (TGF-β) and IL-10 secretion, and decreasing IL-6 and TNF-α (Shu et al., 2016). Both GA and GB dose dependently inhibit the production of pro-inflammatory cytokines, such as TNF-α and IL-1, in lipopolysaccharide (LPS)-stimulated rat microglial cultures (Li et al., 2017).

Ginkgolides Regulate Mitogen-Activated Protein Kinase Signaling Pathways in the Inflammatory Immune Response

The effects of ginkgolides in inflammation and immunomodulation are gradually recognized. Administration of GB inhibits TNF-α, IL-6, and IL-1β production and suppresses TLR4 and NF-κB gene expression in an intracerebral hemorrhagic rat model (Hu et al., 2011). MAPK signaling is important for adjusting and controlling the structure and function of eukaryotic cells by transmitting signals from the cell membrane to the nucleus in response to a variety of extracellular stimuli, including neurotransmitters, hormones, inflammatory factors, viruses, growth factors, and inducer of oxidative stress (Elbirt et al., 1998; Sun and Nan, 2016). In MΦ and DC, p38 MAPK is activated by TLR and promotes the secretion of various pro-inflammatory and T cell polarization factors, such as TNF-α, interferon-γ (IFN-γ), IL-1β, IL-12, IL-6, and IL-23 (Aicher et al., 1999; Kikuchi et al., 2003). TLRs activate innate immunity through the early identification of pathogenic-associated molecular patterns in pathogens (Paul et al., 2018). These receptors also regulate adaptive immunity through up-regulating the expression of co-stimulatory molecules on the antigen presenting cell surface and the secretion of inflammatory cytokines, providing the second signal for T lymphocyte activation and inducing T lymphocyte differentiation. In T cells, p38 MAPK is activated by T cell receptor signaling, cytokines, and histamine (Berenson et al., 2006; Paul et al., 2018). c-Jun N-terminal kinase (JNK) and p38 are activated by a large number of immune receptors such as TLRs, TNFR, and IL-1R (Huang et al., 2009). JNK-mediated integration of T cell receptor and costimulation signals play a role in the stress-activated MAPK pathways in immune responses (Su et al., 2001). Coordinate immune response is one of the primary functions of stress-activated MAPK. It has been shown that pharmacological inhibition of p38 and JNK pathways is effective in treating or alleviating various inflammatory conditions (Kumar et al., 2003; Manning and Davis, 2003; Jeffrey et al., 2007).

In order to investigate whether *G. biloba* extract EGb761, which mainly contains flavonoids and terpene lactones, could reduce cerebral p-Tau levels and prevent Alzheimer's disease pathogenesis, human P301S tau mutant transgenic mice were fed with this compound for 5 months (Qin et al., 2018). It was found that the mouse cognitive function was improved, synaptophysin loss was attenuated, the cAMP response element binding protein phosphorylation in the mouse brain was recovered, and the p-Tau protein was decreased after treatment with EGb761 (Qin et al., 2018). Moreover, long-treatment with EGb761 also inhibited the activation of p38-MAPK and glycogen synthase kinase 3 in tau-transgenic mouse brains, the two key enzymes generating p-Tau. These all suggested that EGb761, especially the components of GA, BB, and flavonoids, enhanced autophagy, increased the degradation of phosphorylated tau in neurons, and reduced the generation of phosphorylated tau by inhibiting the activity of p38 MAPK and glycogen synthase kinase 3 (Qin et al., 2018). In addition, the neuroprotective effects of BB on cerebral ischemia and reperfusion injury are also associated with inhibition of pro-inflammatory mediator production and down-regulation of JNK1/2 and p38 MAPK activation (Jiang et al., 2014). Expression of MAPK/NF-κB signaling proteins, both *in vivo* and *in vitro*, has been evaluated by Hui and Fangyu (2017), who concluded that BB exerts gastroprotective effects *via* the activation of MAPK/NF-κB. In the study of Chen et al. (2017), high glucose-treated human umbilical vein endothelial cells (HUVECs) were subject to various concentrations of GB, and relative p38 MAPK phosphorylation was analyzed by western blot. The results demonstrated that GB can also inhibit p38 MAPK phosphorylation. Furthermore, they found that high glucose-induced expression of TLR4 was inhibited by p38 MAPK inhibitor SB203580. This indicates that p38 MAPK possibly participates in the positive feedback loop with TLR4 signaling and that GB restrains the course

(Chen et al., 2017; **Figure 3**). GB potently inhibited the expression of PF4 and CD40L in thrombin-activated platelets by inhibition of p38 MAPK phosphorylation. So GB might be a promising drug in atherosclerosis through inhibiting platelet function and reducing inflammation (Liu et al., 2014). In addition, GB also exerted anti-inflammatory and chondroprotective effects in LPS-induced chondrocytes by inhibiting LPS-induced MAPK pathway activation, suggesting that GB might be an underlying therapy for osteoarthritis (Hu et al., 2018). Collectively, ginkgolides play a role in the IIR by regulating MAPK signaling pathways, but the detailed mechanisms still need further investigations.

Toll-Like Receptor/Myeloid Differentiation Primary Response 88/Nuclear Factor-Kappa B Pathway in the Regulation of Inflammatory Immune Response

Myeloid differentiation primary response 88 (MyD88) is an adaptor protein of the toll/IL-1 receptor (TIR) signaling pathway. MyD88 has a TIR domain and can interact with other TIR domains in TIR family cells, mediating downstream signal transduction and playing a key role in TIR signaling pathway (Li and Qin, 2005). NF-κB is a protein that controls transcription of deoxyribonucleic acid, cytokine production, and cell survival and is also a major transcription factor involved with both the innate and adaptive immune response (Smith et al., 2006). Ginkgolides and BB not only inhibited IL-1β, IL-6, IL-8, IL-10, and TNF-α but also attenuated the levels of TLR2, TLR4, MyD88, Bak, and RIP3, which were induced by oxygen-glucose deprivation/reoxygenation (OGD/R) in BV2 microglial cells. Meanwhile, ginkgolides and BB also reduced p-TGF-β-activated kinase 1, p-IkBα, and p-IKKβ and suppressed the OGD/R-induced transfer of NF-κB p65 from the cytoplasm to the nucleus in BV2 microglial cells (Zhou Y. et al., 2016). These results showed that ginkgolides and BB protect BV2 microglial cells against OGD/R injury by inhibiting TLR2/4 signaling pathways (Zhou Y. et al., 2016). The therapeutic effects of GB on ischemic and hemorrhagic stroke are widely recognized. The modulatory effects on inflammatory-related gene expression, suppression of NF-κB and PI3K/Akt pathways, and TLR4/NF-κB are the main protective mechanisms of GB against stroke (Nabavi et al., 2015). Accumulating evidence demonstrated that GB can suppress gene expression of TLR4 and NF-κB; decrease concentrations of inflammatory cytokines such as TNF-α, IL-1β, and IL-6; and reduce the number of apoptotic neuronal cells in both intracerebral hemorrhage rat brain tissue and traumatic brain injury. These all suggested that GB may ameliorate inflammation by suppressing the expression of TLR4-NF-κB signaling pathway (Hu et al., 2011; Yu et al., 2012; Wan et al., 2017). GB also significantly attenuated activation of NF-κB and expression of TNF-α mRNA induced by LPS (Wu et al., 2016). In HUVECs, the expressions of inflammatory protein-intercellular adhesion molecule-1, the activation of IκB phosphorylation, and NF-κB induced by oxidized low-density lipoprotein are all inhibited by GB. The pharmacological effects of GB on the inflammatory response induced by ox-LDL in HUVECs may be associated with its inhibition of NF-κB activation and reduction of reactive oxygen species production (Li et al., 2009). Both GA and GB have ability to inhibit ischemia-induced NF-κB activation by IκBα degradation *via* suppression of the NF-κB-inducing kinase-IκB kinase pathway (Wang et al., 2008). GC also shows a beneficial effect against myocardial I/R injury *via* inhibition of inflammation, possibly *via* suppression of the CD-40-NF-κB signaling pathway and downstream inflammatory cytokine expression. These may offer an alternative treatment for myocardial I/R diseases (Zhang et al., 2018; **Figure 3**).

The neuroprotective effects of BB may be related to inhibiting the expression of NF-κB p65 protein and decreasing its nuclear translocation in the substantia nigra pars compacta of rats to prohibit the apoptosis of dopaminergic neurons (Li et al., 2008). GB can also protect cultured neurons from hypoxia- and glutamate-induced damage and inhibit neuronal apoptosis by down-regulating pro-apoptotic protein expression including Bcl-2-associated X protein and up-regulating anti-apoptotic protein expression (Ahlemeyer et al., 1999; Gu et al., 2012). The anti-apoptotic property of GB may also contribute to the suppression of p-SAPK/JNK activation and reactive oxygen species, inhibiting mitochondrial pro-apoptotic factors such as caspase-3, caspase-9, poly ADP-ribose polymerase, and cytochrome *c* (Gu et al., 2012). GB is also believed to interfere with the production of free radicals and protect against a decrease in hippocampal Ca^{2+}/calmodulin-dependent PKCII activity after cerebral ischemia (Zalewska et al., 1996; Pietri et al., 1997). Moreover, GA and GB decrease glutamate-induced damage of neuronal and hippocampal cells (Prehn and Krieglstein, 1993). Brain-derived neurotrophic factor (BDNF), a member of the neurotrophin family, is present in the mature brain and is implicated to decrease infarct volume and to improve neurological outcomes (Schäbitz et al., 2000, 2007). BDNF activates intracellular tyrosine receptor kinase B, MAPK, and the extracellular signal-regulated kinases to protect against ischemic stroke (Reichardt, 2006). Wei and colleagues found that GB can up-regulate the expression of BDNF in ischemic stroke by evaluating the therapeutic effects of GB in transient middle cerebral artery occlusion mice and OGD/R-treated N2a cells (Wei et al., 2017). Collectively, ginkgolides have anti-PAF, anti-apoptotic, anti-oxidative, neurotrophic, and neuroimmunomodulatory effects.

ROLES OF GINKGOLIDES IN THE INFLAMMATORY IMMUNE RESPONSE OF NEUROLOGICAL DISEASES

Inflammation and immune response, as an important mechanism, are directly involved in the occurrence of many diseases of the nervous system, such as Parkinson's disease (PD), ischemic stroke, MS, and Guillain–Barré syndrome (GBS). Ginkgolides might serve as a potential new treatment of these neurological diseases by regulating IIR (**Table 2**).

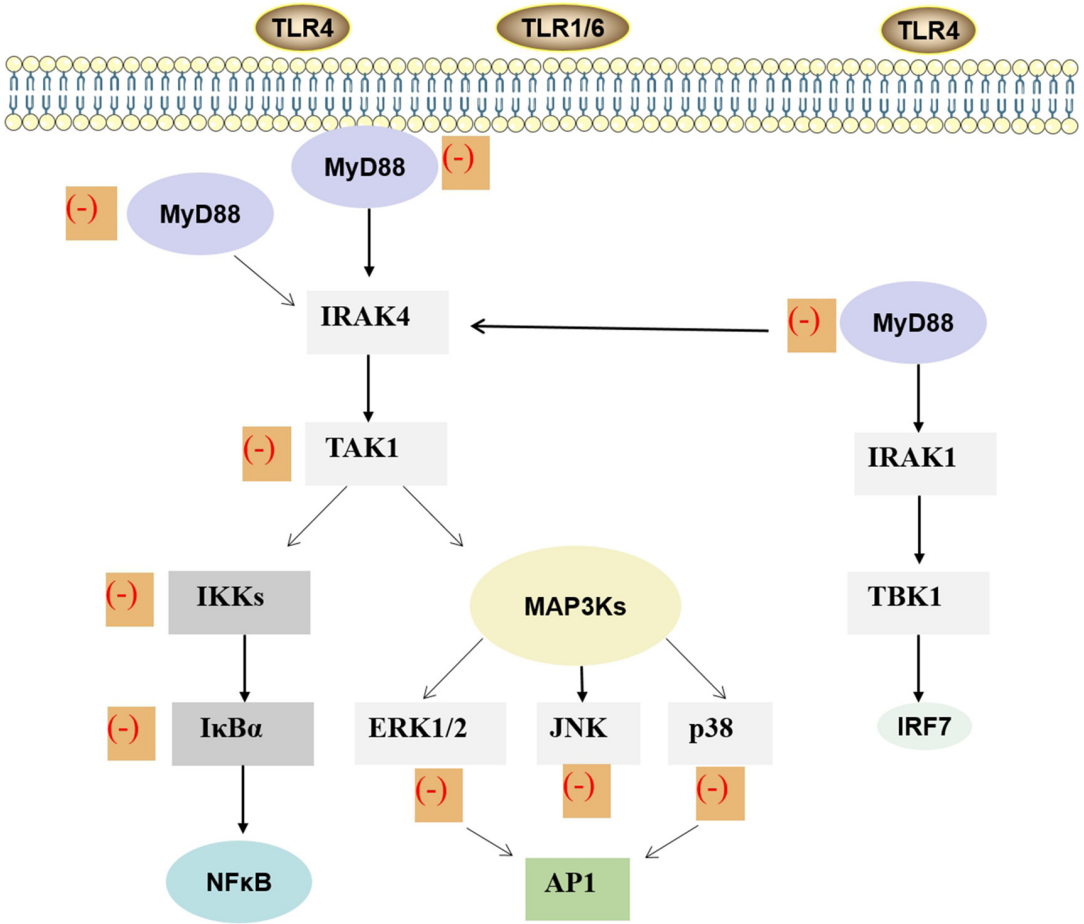

FIGURE 3 | MAPK and NF-κB signaling pathway of ginkgolides in the regulation of IIR. Lipopolysaccharide stimulates the dimerization of TLR4 and activates the conserved MAPK tertiary kinase cascade through MyD88, interleukin-1 receptor-associated kinase, which leads to the activation of transcription factors. Finally, it promotes the expression of inflammatory factors in target cells, thus participating in the inflammatory reaction process induced by lipopolysaccharide. As shown in the figure, ginkgolides have effects on MAPK and TLRs/MyD88/NF-κB signaling transduction pathway. It can down-regulate MyD88, transforming growth factor-β-activated kinase-1, IκB kinases, IκBα, extracellular signal-regulated protein kinase 1/2, extracellular signal-regulated JNK, and p38, ultimately reducing inflammation. MAPK, mitogen-activated protein kinase; NF-κB, nuclear factor-kappa B; IIR, inflammatory immune response; MyD88, myeloid differentiation primary response 88; TLR, toll-like receptor.TLR, toll-like receptor; MyD88, myeloid differentiation primary response 88; IRAK, interleukin-1 receptor-associated kinase; TAK1, transforming growth factor-β-activated kinase-1; IKK, IκB kinases; MAP3K, mitogen-activated protein kinase kinase kinase; ERK, extracellular signal-regulated protein-1; JNK, c-Jun amino-terminal kinase; NF-κB, nuclear factor-κB; AP1, activator protein-1; TBK1, TANK-binding kinase 1; IRF, interferon regulatory factor; IIR, inflammatory immune response.

Ginkgolides in Parkinson's Disease

PD is a common neurodegenerative disorder of the central nervous system (CNS), which is characterized by progressive loss of dopaminergic neurons of the substantia nigra pars compacta with a reduction of dopamine concentration in the striatum. The exact PD etiology remains unknown, but a variety of theories attempted to explain the causes of neuronal death and to identify possible triggers. It has been hypothesized that inflammation may underlay the neurodegenerative process, with the immune system playing a key role (Caggiu et al., 2019). A rat model of PD was produced with a unilateral infusion of 6-OHDA into the substantia nigra pars compacta. Different doses of BB were administered to the rat and locomotor activity and rotational behavior, and the expressions of NF-κB were tested after the 6-OHDA infusion. Finally, the study concluded that NF-κB activation contributes to the 6-OHDA-induced loss of dopaminergic neurons, and the inhibition of the NF-κB pathway is likely to be involved in the neuroprotective effect of BB (Li et al., 2008). The roles of ginkgolides in IIR are also supported by the study of Kim et al., wherein they found that GB can significantly attenuate the increase of the NF-κB DNA-binding activity induced by 1-methyl-4-phenyl-1,2,3,6-tetrahydropyridine (can induce PD rodent model through an NF-κB-dependent mechanism; Kim et al., 2013). Furthermore, PD model treatment with GB-nanocrystals (GB-NCs) can improve behavior, reduce dopamine deficiency, and elevate dopamine metabolite levels (Liu et al., 2020). Thus, BB and GB provide a therapeutic approach to rescue the PD by regulating IIR. Highly stabilized GB-NCs had small sizes, high rates of dissolution, and improved oral bioavailability and brain

TABLE 2 | Roles of ginkgolides in IIR in neurological diseases.

Diseases	Actions	Ingredients	References
Neurodegenerative diseases	Inhibition of the NF-κB.	BB	Li et al. (2008)
Ischemic stroke	Decreases infarct size, serum levels of pro-inflammatory factors, expressions of intercellular adhesion molecule-2 and E-selection.	GB	Gu et al. (2012)
	Down-regulates TLR4 and NF-κB.		
	Reduces microglial activation and promotes microglia/macrophage transferring from inflammatory M1 phenotype to M2 phenotype.		
	Suppresses ERK/MAPK pathway and inhibits Akt phosphorylation.		
	Reduces microglial activation and promotes microglia/macrophage transferring from inflammatory M1 phenotype to M2 phenotype.	GB	Gu et al. (2012)
	Suppresses ERK/MAPK pathway and inhibits Akt phosphorylation.	GB	Nabavi et al. (2015)
Neuroimmune diseases	Attenuates the inflammatory responses.	GB	Zhou J.-M. et al. (2016)
	Inhibits the expressions of TLR4 and MyD88.	GB	Chen et al. (2017)
	Regulates the TLR/MyD88/NF-κB.	Ginkgolides	Tran et al. (2018)

IIR, inflammatory immune response; NF-κB, nuclear factor-kappa B; BB, bilobalide; GB, ginkgolide B; TLR, toll-like receptor; ERK, extracellular regulated protein kinase; MAPK, mitogen-activated protein kinase; MyD88, myeloid differentiation factor 88.

uptake, which might make them effective drugs for anti-PD therapies in the future. But this field is nascent, and further explorations are needed.

Ginkgolides in Ischemic Stroke

Numerous studies have proven that neuroinflammation plays an important pathological role in ischemic stroke (Chen et al., 2020). Extracellular glutamate increased significantly after ischemia (Hsieh et al., 2017). And this extracellular glutamate can result in microglial activation and production of inflammatory mediators such as pro-inflammatory cytokines, adhesion molecules, and chemokines (Goldshmit et al., 2018). These inflammatory mediators can increase the severity of primary brain damages (Huang et al., 2018). TLR, NF-κB, and nitric oxide also play a crucial role in mediating signaling pathways in microglial activation and ischemic stroke-induced damage (Zheng et al., 2017; Zhao et al., 2019). A growing number of evidence has shown that administration with GB decreased infarct size, serum levels of pro-inflammatory factors (such as TNF-α, IL-6, and IL-1β), and expressions of intercellular adhesion molecule-2 and E-selectin; down-regulated TLR4 and NF-κB; and reduced microglial activation in transient middle cerebral artery occlusion-induced cerebral I/R injury in mice (Gu et al., 2012; Fan et al., 2020). Previous studies also proved that GB promoted microglia/macrophage transferring from inflammatory M1 phenotype to a protective, anti-inflammatory M2 phenotype *in vivo* or *in vitro* (Shu et al., 2016). Other mechanisms have been revealed that the anti-inflammatory activity of GB included suppression of ERK/MAPK pathway, inhibition of Akt phosphorylation, and down-regulation of p-TAK1, p-IkBα, and p-IKKβ (Nabavi et al., 2015; Fan et al., 2020). The effects of ginkgolides and BB in the cellular and signaling events of ischemic stroke, including inflammatory pathways and neuroprotection, have been validated in multiple preclinical studies. In the future, we might focus on the design and synthesis of ginkgolides and BB analogs with brain-targeting ability, which would cause effective and continuous therapy for CNS diseases.

Ginkgolides in Multiple Sclerosis

MS is a classic neuroinflammatory and immunological disease of the CNS, which is the second major neurological disease leading to the disability of young adults (Hassan-Smith and Douglas, 2011). In the pathogenesis of MS, antigens are ingested and recognized by antigen presenting cells (APCs) such as DCs, which leads to the activation of autoreactive T cells, leading to a series of pathological changes such as CNS inflammation, demyelination of myelin sheath, and destruction of axon (Mundt et al., 2019). DCs can initiate the autoreactive immune response in the pathogenesis of MS and promote and maintain immune tolerance on the other hand (Zhou Y. et al., 2016). PAF is a lipid mediator produced by cell activation, which participates in inflammatory reaction. In the process of inflammation and immune response, immunogen activates a series of signal transduction pathways in cells, which then triggers the expressions of cytokines and participates in inflammations and immune responses. NF-κB and MyD88 are critical intracellular signaling molecules. Recent studies suggested that NF-κB participates in the inflammatory immune responses induced by MΦ. Enhanced NF-κB activity can inhibit the transformation of M1 into M2, so as to strengthen and enlarge inflammation responses and aggravate tissue damages (Vogel et al., 2013). On the contrary, inhibiting the activity of NF-κB can increase the number and function of M2 cells and reduce inflammations and promote the recovery of diseases. MyD88 has a clear relationship with infectious diseases, tumors, and autoimmune diseases; and an MyD88-dependent pathway is considered as a vital target for intervention treatment of these diseases (Feng et al., 2016). TLR/MyD88 signaling pathway is closely related to the maturation of DCs and the secretion of inflammatory cytokines. TLR/MyD88 signaling pathway plays a key role in the pathogenesis of experimental allergic encephalomyelitis (EAE), a classical animal model of MS in human. The onset time of TLR9 knockout mice (TLR9−/−) is delayed compared with that of normal mice, and the clinical symptoms are mild (Prinz et al., 2006).

Ginkgolides regulate the TLR/MyD88/NF-κB signaling pathway and attenuate the inflammatory responses to inhibit

the productions of inflammatory factors mediated by OGD/R in microglial cells (Zhou Y. et al., 2016). GB plays a protective role in inhibiting the expressions of TLR4 and MyD88 induced by high glucose and then in alleviating the TLR4-mediated inflammatory responses in endothelial cells (Chen et al., 2017). As shown previously, ginkgolides have been proved to be a PAFR antagonist, significantly reducing the increase of nuclear translocation of NF-κB p65 induced by PCP (Tran et al., 2018). It has been reported that GB plays a role in PAFR antagonist and can effectively prevent synaptic damage in hippocampus of EAE mice without affecting microglial activation (Bellizzi et al., 2016). Recently, Yu et al. (2019) have observed the therapeutic potential of GK in experimental autoimmune neuritis (EAN) through possible cellular and molecular mechanisms, especially as a peripheral immunomodulatory, and provided that GK may be a promising naturally small molecule compound for treatment of MS in the future. Despite that ginkgolide treatment may represent a novel strategy for attenuating the inflammatory responses, the precise mechanism of ginkgolides in mediating IIR remains to be further explored.

Ginkgolides in Guillain–Barré Syndrome

GBS is an immune-mediated peripheral neuropathy, characterized by demyelination of peripheral nerve and nerve roots and infiltration of small vascular inflammatory cells. EAN is a useful animal model for conducting research on the pathogenesis and treatment of GBS (Liu et al., 2018). A variety of immune cell subsets and a complex network of cytokines are involved in the pathogenesis and progression of GBS/EAN, such as Th1, Th2, Th17, and regulatory T cells (Treg) cells (Zhang et al., 2013). The Th1 response is related to the acute phase response to the pathogen in GBS, whereas the Th2 response is associated with the recovery phase (Zhang et al., 2014). The IFN-γ, IL-6, and TNF-α levels in Th1 are increased in the acute phase of GBS, whereas those of TGF-β and IL-4 are increased during the recovery phase of GBS (Li et al., 2020). Moreover, the proportion of Th17 cells and the levels of IL-17A in the peripheral blood of GBS patients are increased in the acute phase of the disease, and those of IL-17A are related to the disability scale score of GBS (Kharwar et al., 2017). Tregs can abolish antigen-specific T cell proliferation and suppress the secretion of Th1 and Th2 cytokines (Zhang et al., 2013). Previous studies have suggested that Tregs play a critical role in immune responses in autoimmune diseases and that these cell numbers are reduced in patients with GBS and EAN animals, suggesting their crucial role in damage and repair in GBS (Harness and McCombe, 2008). In summary, $CD4^+$ T cells exert their effect by releasing effector cytokines, and the net effects of these Th cytokines determine the direction of immune responses and the consequence of GBS/EAN (Harness and McCombe, 2008; Nyati et al., 2011).

MΦ differentiate into two phenotypes after activation: classical activated M1, also known as pro-inflammatory type MΦ, and activated type M2, also known as anti-inflammatory type MΦ (Shapouri-Moghaddam et al., 2018). M1 are involved in the inflammatory damage of myelin sheath through the release of pro-inflammatory factors, such as IL-12, during the early course of GBS (Labonte et al., 2014). M2 are related to disease recovery by secreting anti-inflammatory cytokines in the later stage of GBS (Shen et al., 2018). $CD4^+$ T cells and MΦ could interact and promote with each other as the cytokines secreted by them are interconnected, intricate, and pleiotropic. These cytokines constitute a complex immune network in the pathogenesis of GBS/EAN. Previous studies have shown that TLRs play a pivotal role in the occurrence and development of GBS (Nyati and Prasad, 2014). Compared with healthy controls, mRNA levels of TLR2, TLR4, MyD88, and NF-κB were significantly increased in patients with GBS (Du et al., 2015). It was also found that significant up-regulation of TLR2 in sciatic nerves of EAN is correlated with disease severity (Zhang et al., 2009). Moreover, TLR signaling activates antigen presenting cells through MyD88-dependent or MyD88-independent pathways to initiate adaptive immunity (Nyati and Prasad, 2014). Thus, TLR, MyD88, and NF-κB are involved in the pathogenesis of GBS/EAN. Studies have also shown that expression of MyD88 in patients with GBS is increased (Du et al., 2015). We speculated that the roles of ginkgolides in GBS/EAN may be mediated by the regulation of MyD88/NF-κB, based on the fact that ginkgolides attenuate inflammatory responses by regulating the TLR/MyD88/NF-κB signaling pathway.

CONCLUSION

Ginkgolides are clinically used for neuroprotective treatment on reconvalescents of cerebral infarction. However, the cognition about its therapeutic mechanism is still lacking. Ginkgolides have several different biological effects including inhibiting platelet aggregation, preventing apoptosis and oxidation, providing nutrition to nerves, and regulating neuroimmunity. Nowadays, accumulating studies have reported that ginkgolides play an important role in regulating IIR *via* inhibiting the PAF-mediated signal transduction, MAPK, and NF-κB signaling pathways, which provide an insight into the novel clinical application of ginkgolides in some neurological disease therapy in the future.

AUTHOR CONTRIBUTIONS

CL carried out the literature review and drafted the manuscript. KL, SL, and QA helped to draft the manuscript. XW conceived, designed, and coordinated the study. All authors read and approved the final manuscript.

FUNDING

This study was supported by grants from The First Hospital, Jilin University, Changchun, the National Natural Science Foundation (No. 81771299).

REFERENCES

Ahlemeyer, B., Möwes, A., and Krieglstein, J. (1999). Inhibition of serum deprivation- and staurosporine-induced neuronal apoptosis by *Ginkgo biloba* extract and some of its constituents. *Eur. J. Pharmacol.* 367, 423–430. doi: 10.1016/s0014-2999(98)00903-0

Aicher, A., Shu, G. L., Magaletti, D., Mulvania, T., Pezzutto, A., Craxton, A., et al. (1999). Differential role for p38 mitogen-activated protein kinase in regulating CD40-induced gene expression in dendritic cells and B cells. *J. Immunol.* 163, 5786–5795.

Al-Adwani, D. G., Renno, W. M., and Orabi, K. Y. (2019). Neurotherapeutic effects of Ginkgo biloba extract and its terpene trilactone, ginkgolide B, on sciatic crush injury model: a new evidence. *PLoS One* 14:e0226626. doi: 10.1371/journal.pone.0226626

Bastianetto, S., Zheng, W. H., and Quirion, R. (2000). The *Ginkgo biloba* extract (EGb 761) protects and rescues hippocampal cells against nitric oxide-induced toxicity: involvement of its flavonoid constituents and protein kinase C. *J. Neurochem.* 74, 2268–2277. doi: 10.1046/j.1471-4159.2000.0742268.x

Bellizzi, M. J., Geathers, J. S., Allan, K. C., and Gelbard, H. A. (2016). Platelet-activating factor receptors mediate excitatory postsynaptic hippocampal injury in experimental autoimmune encephalomyelitis. *J. Neurosci.* 36, 1336–1346. doi: 10.1523/jneurosci.1171-15.2016

Berenson, L. S., Yang, J., Sleckman, B. P., Murphy, T. L., and Murphy, K. M. (2006). Selective requirement of p38alpha MAPK in cytokine-dependent, but not antigen receptor-dependent, Th1 responses. *J. Immunol.* 176, 4616–4621. doi: 10.4049/jimmunol.176.8.4616

Braquent, P. (1985). BN 52021 and related compounds: a new series of highly specific paf-acether receptor antagonists. *Prostaglandins* 30:687. doi: 10.1016/0090-6980(85)90031-0

Caggiu, E., Arru, G., Hosseini, S., Niegowska, M., Sechi, G., Zarbo, I. R., et al. (2019). Inflammation, infectious triggers, and Parkinson's disease. *Front. Neurol.* 10:122. doi: 10.3389/fneur.2019.00122

Chen, K., Sun, W., Jiang, Y., Chen, B., Zhao, Y., Sun, J., et al. (2017). Ginkgolide B suppresses TLR4-mediated inflammatory response by inhibiting the phosphorylation of JAK2/STAT3 and p38 MAPK in high glucose-treated HUVECs. *Oxid. Med. Cell. Longev.* 2017:9371602. doi: 10.1155/2017/9371602

Chen, S., Peng, J., Sherchan, P., Ma, Y., Xiang, S., Yan, F., et al. (2020). TREM2 activation attenuates neuroinflammation and neuronal apoptosis *via* PI3K/Akt pathway after intracerebral hemorrhage in mice. *J. Neuroinflammation* 17:168. doi: 10.1186/s12974-020-01853-x

Deng, M., Guo, H., Tam, J. W., Johnson, B. M., Brickey, W. J., New, J. S., et al. (2019). Platelet-activating factor (PAF) mediates NLRP3-NEK7 inflammasome induction independently of PAFR. *J. Exp. Med.* 216, 2838–2853. doi: 10.1084/jem.20190111

Du, Y., Zhang, G., Zhang, Z., Wang, Q., Ma, R., Zhang, L., et al. (2015). Toll-like receptor 2 and -4 are involved in the pathogenesis of the Guillain-Barré syndrome. *Mol. Med. Rep.* 12, 3207–3213. doi: 10.3892/mmr.2015.3730

Elbirt, K. K., Whitmarsh, A. J., Davis, R. J., and Bonkovsky, H. L. (1998). Mechanism of sodium arsenite-mediated induction of heme oxygenase-1 in hepatoma cells. Role of mitogen-activated protein kinases. *J. Biol. Chem.* 273, 8922–8931. doi: 10.1074/jbc.273.15.8922

Fan, Q., Zhou, J., Wang, Y., Xi, T., Ma, H., Wang, Z., et al. (2020). Chip-based serum proteomics approach to reveal the potential protein markers in the sub-acute stroke patients receiving the treatment of *Ginkgo Diterpene Lactone* Meglumine Injection. *J. Ethnopharmacol.* 260:112964. doi: 10.1016/j.jep.2020.112964

Feng, Z., Wang, Z., Yang, M., Zhou, L., and Bao, Y. (2016). Polysaccharopeptide exerts immunoregulatory effects *via* MyD88-dependent signaling pathway. *Int. J. Biol. Macromol.* 82, 201–207. doi: 10.1016/j.ijbiomac.2015.11.002

Goldshmit, Y., Jona, G., Schmukler, E., Solomon, S., Pinkas-Kramarski, R., and Ruban, A. (2018). Blood glutamate scavenger as a novel neuroprotective treatment in spinal cord injury. *J. Neurotrauma* 35, 2581–2590. doi: 10.1089/neu.2017.5524

Golino, P., Ambrosio, G., Ragni, M., Pascucci, I., Triggiani, M., Oriente, A., et al. (1993). Short-term and long-term role of platelet activating factor as a mediator of *in vivo* platelet aggregation. *Circulation* 88, 1205–1214. doi: 10.1161/01.cir.88.3.1205

Gu, J.-H., Ge, J.-B., Li, M., Wu, F., Zhang, W., and Qin, Z.-H. (2012). Inhibition of NF-κB activation is associated with anti-inflammatory and anti-apoptotic effects of Ginkgolide B in a mouse model of cerebral ischemia/reperfusion injury. *Eur. J. Pharm. Sci.* 47, 652–660. doi: 10.1111/j.1462-5822.2011.01720.x

Gui, C., Zhu, W., Chen, G., Luo, X., Liew, O. W., Puah, C. M., et al. (2007). Understanding the regulation mechanisms of PAF receptor by agonists and antagonists: molecular modeling and molecular dynamics simulation studies. *Proteins* 67, 41–52. doi: 10.1002/prot.21213

Hamel-Côté, G., Lapointe, F., Gendron, D., Rola-Pleszczynski, M., and Stankova, J. (2019a). Regulation of platelet-activating factor-induced interleukin-8 expression by protein tyrosine phosphatase 1B. *Cell Commun. Signal.* 17:21. doi: 10.1186/s12964-019-0334-6

Hamel-Côté, G., Lapointe, F., Véronneau, S., Mayhue, M., Rola-Pleszczynski, M., and Stankova, J. (2019b). Regulation of platelet-activating factor-mediated interleukin-6 promoter activation by the 48 kDa but not the 45 kDa isoform of protein tyrosine phosphatase non-receptor type 2. *Cell Biosci.* 9:51. doi: 10.1186/s13578-019-0316-9

Han, C., Li, Y., Wang, Y., Cui, D., Luo, T., Zhang, Y., et al. (2018). Development of inflammatory immune response-related drugs based on G protein-coupled receptor kinase 2. *Cell. Physiol. Biochem.* 51, 729–745. doi: 10.1159/000495329

Harness, J., and McCombe, P. A. (2008). Increased levels of activated T-cells and reduced levels of CD4/CD25+ cells in peripheral blood of Guillain-Barré syndrome patients compared to controls. *J. Clin. Neurosci.* 15, 1031–1035. doi: 10.1016/j.jocn.2007.09.016

Hassan-Smith, G., and Douglas, M. R. (2011). Management and prognosis of multiple sclerosis. *Br. J. Hosp. Med.* 72, M174–M176. doi: 10.12968/hmed.2011.72.sup11.m174

Hsieh, C.-H., Lin, Y.-J., Chen, W.-L., Huang, Y.-C., Chang, C.-W., Cheng, F.-C., et al. (2017). HIF-1α triggers long-lasting glutamate excitotoxicity *via* system x in cerebral ischaemia-reperfusion. *J. Pathol.* 241, 337–349. doi: 10.1002/path.4838

Hu, Y.-Y., Huang, M., Dong, X.-Q., Xu, Q.-P., Yu, W.-H., and Zhang, Z.-Y. (2011). Ginkgolide B reduces neuronal cell apoptosis in the hemorrhagic rat brain: possible involvement of Toll-like receptor 4/nuclear factor-kappa B pathway. *J. Ethnopharmacol.* 137, 1462–1468. doi: 10.1016/j.jep.2011.08.034

Hu, H., Li, Y., Xin, Z., and Zhanga, X. (2018). Ginkgolide B exerts anti-inflammatory and chondroprotective activity in LPS-induced chondrocytes. *Adv. Clin. Exp. Med.* 27, 913–920. doi: 10.17219/acem/70414

Huang, L., Ma, Q., Li, Y., Li, B., and Zhang, L. (2018). Inhibition of microRNA-210 suppresses pro-inflammatory response and reduces acute brain injury of ischemic stroke in mice. *Exp. Neurol.* 300, 41–50. doi: 10.1016/j.expneurol.2017.10.024

Huang, G., Shi, L. Z., and Chi, H. (2009). Regulation of JNK and p38 MAPK in the immune system: signal integration, propagation and termination. *Cytokine* 48, 161–169. doi: 10.1016/j.cyto.2009.08.002

Huang, P., Zhang, L., Chai, C., Qian, X.-C., Li, W., Li, J.-S., et al. (2014). Effects of food and gender on the pharmacokinetics of ginkgolides A, B, C and bilobalide in rats after oral dosing with ginkgo terpene lactones extract. *J. Pharm. Biomed. Anal.* 100, 138–144. doi: 10.1016/j.jpba.2014.07.030

Hui, S., and Fangyu, W. (2017). Protective effects of bilobalide against ethanol-induced gastric ulcer *in vivo/vitro*. *Biomed. Pharmacother.* 85, 592–600. doi: 10.1016/j.biopha.2016.11.068

Ishii, S., and Shimizu, T. (2000). Platelet-activating factor (PAF) receptor and genetically engineered PAF receptor mutant mice. *Prog. Lipid Res.* 39, 41–82. doi: 10.1016/s0163-7827(99)00016-8

Jeffrey, K. L., Camps, M., Rommel, C., and Mackay, C. R. (2007). Targeting dual-specificity phosphatases: manipulating MAP kinase signalling and immune responses. *Nat. Rev. Drug Discov.* 6, 391–403. doi: 10.1038/nrd2289

Jiang, M., Li, J., Peng, Q., Liu, Y., Liu, W., Luo, C., et al. (2014). Neuroprotective effects of bilobalide on cerebral ischemia and reperfusion injury are associated with inhibition of pro-inflammatory mediator production and down-regulation of JNK1/2 and p38 MAPK activation. *J. Neuroinflammation* 11:167. doi: 10.1186/s12974-014-0167-6

Kharwar, N. K., Prasad, K. N., Singh, K., Paliwal, V. K., and Modi, D. R. (2017). Polymorphisms of IL-17 and ICAM-1 and their expression in Guillain-Barré syndrome. *Int. J. Neurosci.* 127, 680–687. doi: 10.1080/00207454.2016.1231186

Kikuchi, K., Yanagawa, Y., Iwabuchi, K., and Onoé, K. (2003). Differential role of mitogen-activated protein kinases in CD40-mediated IL-12 production by immature and mature dendritic cells. *Immunol. Lett.* 89, 149–154. doi: 10.1016/s0165-2478(03)00134-2

Kim, B. K., Shin, E.-J., Kim, H.-C., Chung, Y. H., Dang, D.-K., Jung, B.-D., et al. (2013). Platelet-activating factor receptor knockout mice are protected from MPTP-induced dopaminergic degeneration. *Neurochem. Int.* 63, 121–132. doi: 10.1016/j.neuint.2013.05.010

Kumar, S., Boehm, J., and Lee, J. C. (2003). p38 MAP kinases: key signalling molecules as therapeutic targets for inflammatory diseases. *Nat. Rev. Drug Discov.* 2, 717–726. doi: 10.1038/nrd1177

Labonte, A. C., Tosello-Trampont, A.-C., and Hahn, Y. S. (2014). The role of macrophage polarization in infectious and inflammatory diseases. *Mol. Cells* 37, 275–285. doi: 10.14348/molcells.2014.2374

Li, R., Chen, B., Wu, W., Bao, L., Li, J., and Qi, R. (2009). Ginkgolide B suppresses intercellular adhesion molecule-1 expression *via* blocking nuclear factor-kappaB activation in human vascular endothelial cells stimulated by oxidized low-density lipoprotein. *J. Pharmacol. Sci.* 110, 362–369. doi: 10.1254/jphs.08275fp

Li, C., Luo, T., Cheng, Y., Liu, S., Qiao, L., Wu, X., et al. (2020). The effects of IVIg therapy on serum levels of neuropeptide Y and cytokines in Guillain-Barré syndrome. *Neurol. Sci.* 41, 295–303. doi: 10.1007/s10072-019-04063-3

Li, X., and Qin, J. (2005). Modulation of Toll-interleukin 1 receptor mediated signaling. *J. Mol. Med.* 83, 258–266. doi: 10.1007/s00109-004-0622-4

Li, Y., Wu, Y., Yao, X., Hao, F., Yu, C., Bao, Y., et al. (2017). Ginkgolide a ameliorates LPS-induced inflammatory responses *in vitro* and *in vivo*. *Int. J. Mol. Sci.* 18:794. doi: 10.3390/ijms18040794

Li, L.-Y., Zhao, X.-L., Fei, X.-F., Gu, Z.-L., Qin, Z.-H., and Liang, Z.-Q. (2008). Bilobalide inhibits 6-OHDA-induced activation of NF-κB and loss of dopaminergic neurons in rat substantia nigra. *Acta Pharmacol. Sinica* 29, 539–547. doi: 10.1111/j.1745-7254.2008.00787.x

Liu, X., Yan, Y., Bao, L., Chen, B., Zhao, Y., and Qi, R. (2014). Ginkgolide B inhibits platelet release by blocking Syk and p38 MAPK phosphorylation in thrombin-stimulated platelets. *Thromb. Res.* 134, 1066–1073. doi: 10.1016/j.thromres.2014.08.025

Liu, Y., Liu, W., Xiong, S., Luo, J., Li, Y., Zhao, Y., et al. (2020). Highly stabilized nanocrystals delivering Ginkgolide B in protecting against the Parkinson's disease. *Int. J. Pharm.* 577:119053. doi: 10.1016/j.ijpharm.2020.119053

Liu, R.-T., Zhang, M., Yang, C.-L., Zhang, P., Zhang, N., Du, T., et al. (2018). Enhanced glycolysis contributes to the pathogenesis of experimental autoimmune neuritis. *J. Neuroinflammation* 15:51. doi: 10.1186/s12974-018-1095-7

Lu, X., Yang, H., Liu, X., Shen, Q., Wang, N., Qi, L.-W., et al. (2017). Combining metabolic profiling and gene expression analysis to reveal the biosynthesis site and transport of ginkgolides in L. *Front. Plant Sci.* 8:872. doi: 10.3389/fpls.2017.00872

Maclennan, K. M., Darlington, C. L., and Smith, P. F. (2002). The CNS effects of Ginkgo biloba extracts and ginkgolide B. *Prog. Neurobiol.* 67, 235–257. doi: 10.1016/s0301-0082(02)00015-1

Maerz, S., Liu, C.-H., Guo, W., and Zhu, Y.-Z. (2011). Anti-ischaemic effects of bilobalide on neonatal rat cardiomyocytes and the involvement of the platelet-activating factor receptor. *Biosci. Rep.* 31, 439–447. doi: 10.1042/bsr20100128

Manning, A. M., and Davis, R. J. (2003). Targeting JNK for therapeutic benefit: from junk to gold?. *Nat. Rev. Drug Discov.* 2, 554–565. doi: 10.1038/nrd1132

Mundt, S., Greter, M., Flügel, A., and Becher, B. (2019). The CNS immune landscape from the viewpoint of a T cell. *Trends Neurosci.* 42, 667–679. doi: 10.1016/j.tins.2019.07.008

Nabavi, S. M., Habtemariam, S., Daglia, M., Braidy, N., Loizzo, M. R., Tundis, R., et al. (2015). Neuroprotective effects of ginkgolide B against ischemic stroke: a review of current literature. *Curr. Top. Med. Chem.* 15, 2222–2232. doi: 10.2174/1568026615666150610142647

Nyati, K. K., and Prasad, K. N. (2014). Role of cytokines and Toll-like receptors in the immunopathogenesis of Guillain-Barré syndrome. *Med. Inflamm.* 2014:758639. doi: 10.1155/2014/758639

Nyati, K. K., Prasad, K. N., Rizwan, A., Verma, A., and Paliwal, V. K. (2011). TH1 and TH2 response to Campylobacter jejuni antigen in Guillain-Barre syndrome. *Arch. Neurol.* 68, 445–452. doi: 10.1001/archneurol.2011.51

Paul, B., Rahaman, O., Roy, S., Pal, S., Satish, S., Mukherjee, A., et al. (2018). Activity-guided development of potent and selective toll-like receptor 9 antagonists. *Eur. J. Med. Chem.* 159, 187–205. doi: 10.1016/j.ejmech.2018.09.058

Pietri, S., Maurelli, E., Drieu, K., and Culcasi, M. (1997). Cardioprotective and anti-oxidant effects of the terpenoid constituents of *Ginkgo biloba* extract (EGb 761). *J. Mol. Cell. Cardiol.* 29, 733–742. doi: 10.1006/jmcc.1996.0316

Prehn, J. H., and Krieglstein, J. (1993). Platelet-activating factor antagonists reduce excitotoxic damage in cultured neurons from embryonic chick telencephalon and protect the rat hippocampus and neocortex from ischemic injury *in vivo*. *J. Neurosci. Res.* 34, 179–188. doi: 10.1002/jnr.490340205

Prinz, M., Garbe, F., Schmidt, H., Mildner, A., Gutcher, I., Wolter, K., et al. (2006). Innate immunity mediated by TLR9 modulates pathogenicity in an animal model of multiple sclerosis. *J. Clin. Invest.* 116, 456–464. doi: 10.1172/jci26078

Qin, Y., Zhang, Y., Tomic, I., Hao, W., Menger, M. D., Liu, C., et al. (2018). Ginkgo biloba extract EGb 761 and its specific components elicit protective protein clearance through the autophagy-lysosomal pathway in tau-transgenic mice and cultured neurons. *J. Alzheimers Dis.* 65, 243–263. doi: 10.3233/jad-180426

Reichardt, L. F. (2006). Neurotrophin-regulated signalling pathways. *Philos. Trans. R. Soc. Lond. B Biol. Sci.* 361, 1545–1564. doi: 10.1098/rstb.2006.1894

Ribonnet, L., Callebaut, A., Nobels, I., Scippo, M. L., Schneider, Y. J., De Saeger, S., et al. (2011). Modulation of CYP1A1 activity by a Ginkgo biloba extract in the human intestinal Caco-2 cells. *Toxicol. Lett.* 202, 193–202. doi: 10.1016/j.toxlet.2011.02.006

Ritzel, R. M., Lai, Y.-J., Crapser, J. D., Patel, A. R., Schrecengost, A., Grenier, J. M., et al. (2018). Aging alters the immunological response to ischemic stroke. *Acta Neuropathol.* 136, 89–110. doi: 10.1007/s00401-018-1859-2

Schäbitz, W. R., Sommer, C., Zoder, W., Kiessling, M., Schwaninger, M., and Schwab, S. (2000). Intravenous brain-derived neurotrophic factor reduces infarct size and counterregulates Bax and Bcl-2 expression after temporary focal cerebral ischemia. *Stroke* 31, 2212–2217. doi: 10.1161/01.str.31.9.2212

Schäbitz, W.-R., Steigleder, T., Cooper-Kuhn, C. M., Schwab, S., Sommer, C., Schneider, A., et al. (2007). Intravenous brain-derived neurotrophic factor enhances poststroke sensorimotor recovery and stimulates neurogenesis. *Stroke* 38, 2165–2172. doi: 10.1161/strokeaha.106.477331

Shapouri-Moghaddam, A., Mohammadian, S., Vazini, H., Taghadosi, M., Esmaeili, S.-A., Mardani, F., et al. (2018). Macrophage plasticity, polarization, and function in health and disease. *J. Cell. Physiol.* 233, 6425–6440. doi: 10.1002/jcp.26429

Shen, D., Chu, F., Lang, Y., Geng, Y., Zheng, X., Zhu, J., et al. (2018). Beneficial or harmful role of macrophages in guillain-barré syndrome and experimental autoimmune neuritis. *Med. Inflamm.* 2018:4286364. doi: 10.1155/2018/4286364

Shu, Z.-M., Shu, X.-D., Li, H.-Q., Sun, Y., Shan, H., Sun, X.-Y., et al. (2016). Ginkgolide B protects against ischemic stroke *via* modulating microglia polarization in mice. *CNS Neurosci. Ther.* 22, 729–739. doi: 10.1111/cns.12577

Smith, E. M., Gregg, M., Hashemi, F., Schott, L., and Hughes, T. K. (2006). Corticotropin Releasing Factor (CRF) activation of NF-kappaB-directed transcription in leukocytes. *Cell. Mol. Neurobiol.* 26, 1021–1036. doi: 10.1016/j.bbi.2006.04.075

Stafforini, D. M., McIntyre, T. M., Zimmerman, G. A., and Prescott, S. M. (2003). Platelet-activating factor, a pleiotrophic mediator of physiological and pathological processes. *Crit. Rev. Clin. Lab. Sci.* 40, 643–672. doi: 10.1080/714037693

Strømgaard, K., and Nakanishi, K. (2004). Chemistry and biology of terpene trilactones from Ginkgo biloba. *Angew. Chem.* 43, 1640–1658. doi: 10.1002/chin.200424256

Su, B., Cheng, J., Yang, J., and Guo, Z. (2001). MEKK2 is required for T-cell receptor signals in JNK activation and interleukin-2 gene expression. *J. Biol. Chem.* 276, 14784–14790. doi: 10.1074/jbc.m010134200

Sun, L., He, Z., Ke, J., Li, S., Wu, X., Lian, L., et al. (2015). PAF receptor antagonist Ginkgolide B inhibits tumourigenesis and angiogenesis in colitis-associated cancer. *Int. J. Clin. Exp. Pathol.* 8, 432–440.

Sun, J., and Nan, G. (2016). The mitogen-activated protein kinase (MAPK) signaling pathway as a discovery target in stroke. *J. Mol. Neurosci.* 59, 90–98. doi: 10.1002/anie.200300601

Tchantchou, F., Lacor, P. N., Cao, Z., Lao, L., Hou, Y., Cui, C., et al. (2009). Stimulation of neurogenesis and synaptogenesis by bilobalide and quercetin

via common final pathway in hippocampal neurons. *J. Alzheimers Dis.* 18, 787–798. doi: 10.3233/jad-2009-1189

Tran, T.-V., Park, S. J., Shin, E.-J., Tran, H.-Q., Jeong, J. H., Jang, C.-G., et al. (2018). Blockade of platelet-activating factor receptor attenuates abnormal behaviors induced by phencyclidine in mice through down-regulation of NF-κB. *Brain Res. Bull.* 137, 71–78. doi: 10.1016/j.brainresbull.2017.11.004

Voet, S., Srinivasan, S., Lamkanfi, M., and van Loo, G. (2019). Inflammasomes in neuroinflammatory and neurodegenerative diseases. *EMBO Mol. Med.* 11:e10248. doi: 10.15252/emmm.201810248

Vogel, D. Y. S., Vereyken, E. J. F., Glim, J. E., Heijnen, P. D. A. M., Moeton, M., van der Valk, P., et al. (2013). Macrophages in inflammatory multiple sclerosis lesions have an intermediate activation status. *J. Neuroinflammation* 10:35. doi: 10.1186/1742-2094-10-35

Wan, F., Zang, S., Yu, G., Xiao, H., Wang, J., and Tang, J. (2017). Ginkgolide B suppresses methamphetamine-induced microglial activation through TLR4-NF-κB signaling pathway in BV2 cells. *Neurochem. Res.* 42, 2881–2891. doi: 10.1007/s11064-017-2309-6

Wang, S.-J., and Chen, H.-H. (2005). Ginkgolide B, a constituent of Ginkgo biloba, facilitates glutamate exocytosis from rat hippocampal nerve terminals. *Eur. J. Pharmacol.* 514, 141–149. doi: 10.1016/j.ejphar.2005.03.027

Wang, E.-W., Han, Y.-Y., and Jia, X.-S. (2018). PAFR-deficiency alleviates myocardial ischemia/reperfusion injury in mice *via* suppressing inflammation, oxidative stress and apoptosis. *Biochem. Biophys. Res. Commun.* 495, 2475–2481. doi: 10.1016/j.bbrc.2017.12.132

Wang, X., Qin, Z.-H., Shi, H., Savitz, S. I., Qin, A.-P., Jiang, Y., et al. (2008). Protective effect of Ginkgolids (A+B) is associated with inhibition of NIK/IKK/IκB/NF-κB signaling pathway in a rat model of permanent focal cerebral ischemia. *Brain Res.* 1234, 8–15. doi: 10.1016/j.brainres.2008.07.102

Wei, H., Sun, T., Tian, Y., and Wang, K. (2017). Ginkgolide B modulates BDNF expression in acute ischemic stroke. *J. Korean Neurosurg. Soc.* 60, 391–396. doi: 10.3340/jkns.2016.1010.018

Wu, F., Shi, W., Zhou, G., Yao, H., Xu, C., Xiao, W., et al. (2016). Ginkgolide B functions as a determinant constituent of Ginkgolides in alleviating lipopolysaccharide-induced lung injury. *Biomed. Pharm.* 81, 71–78. doi: 10.1016/j.biopha.2016.03.048

Yu, W.-H., Dong, X.-Q., Hu, Y.-Y., Huang, M., and Zhang, Z.-Y. (2012). Ginkgolide B reduces neuronal cell apoptosis in the traumatic rat brain: possible involvement of toll-like receptor 4 and nuclear factor κB pathway. *Phytother. Res.* 26, 1838–1844. doi: 10.1002/ptr.4662

Yu, W.-B., Wang, Q., Chen, S., Cao, L., Tang, J., Ma, C.-G., et al. (2019). The therapeutic potential of ginkgolide K in experimental autoimmune encephalomyelitis *via* peripheral immunomodulation. *Int. Immunopharmacol.* 70, 284–294. doi: 10.1016/j.intimp.2019.02.035

Zalewska, T., Zabocka, B., and Domańska-Janik, K. (1996). Changes of Ca^{2+}/calmodulin-dependent protein kinase-II after transient ischemia in gerbil hippocampus. *Acta Neurobiol. Exp.* 56, 41–48. doi: 10.1016/0304-3940(96)12724-5

Zhang, R., Han, D., Li, Z., Shen, C., Zhang, Y., Li, J., et al. (2018). Ginkgolide C alleviates myocardial ischemia/reperfusion-induced inflammatory injury *via* inhibition of CD40-NF-κB pathway. *Front. Pharmacol.* 9:109. doi: 10.3389/fphar.2018.00109

Zhang, H.-L., Wu, L., Wu, X., and Zhu, J. (2014). Can IFN-γ be a therapeutic target in Guillain-Barré syndrome?. *Expert Opin. Ther. Targets* 18, 355–363. doi: 10.1517/14728222.2014.882899

Zhang, Z. Y., Zhang, Z., and Schluesener, H. J. (2009). Toll-like receptor-2, CD14 and heat-shock protein 70 in inflammatory lesions of rat experimental autoimmune neuritis. *Neuroscience* 159, 136–142. doi: 10.1016/j.neuroscience.2008.12.034

Zhang, H.-L., Zheng, X.-Y., and Zhu, J. (2013). Th1/Th2/Th17/Treg cytokines in Guillain-Barré syndrome and experimental autoimmune neuritis. *Cytokine Growth Factor Rev.* 24, 443–453. doi: 10.1016/j.cytogfr.2013.05.005

Zhao, J., Bi, W., Xiao, S., Lan, X., Cheng, X., Zhang, J., et al. (2019). Neuroinflammation induced by lipopolysaccharide causes cognitive impairment in mice. *Sci. Rep.* 9:5790. doi: 10.1186/s12974-015-0238-3

Zheng, Y., Bu, J., Yu, L., Chen, J., and Liu, H. (2017). Nobiletin improves propofol-induced neuroprotection *via* regulating Akt/mTOR and TLR 4/NF-κB signaling in ischemic brain injury in rats. *Biomed. Pharm.* 91, 494–503. doi: 10.1016/j.biopha.2017.04.048

Zheng, S. X., Zhou, L. J., Chen, Z. L., Yin, M. L., and Zhu, X. Z. (2000). Bilobalide promotes expression of glial cell line-derived neurotrophic factor and vascular endothelial growth factor in rat astrocytes. *Acta Pharmacol. Sinica* 21, 151–155.

Zhou, J.-M., Gu, S.-S., Mei, W. H., Zhou, J., Wang, Z. Z., and Xiao, W. (2016). Ginkgolides and bilobalide protect BV2 microglia cells against OGD/reoxygenation injury by inhibiting TLR2/4 signaling pathways. *Cell Stress Chaperones* 21, 1037–1053. doi: 10.1007/s12192-016-0728-y

Zhou, Y., Leng, X., Luo, S., Su, Z., Luo, X., Guo, H., et al. (2016). Tolerogenic dendritic cells generated with tofacitinib ameliorate experimental autoimmune encephalomyelitis through modulation of Th17/Treg balance. *J. Immunol. Res.* 2016:5021537. doi: 10.1155/2016/5021537

Conflict of Interest: The authors declare that the research was conducted in the absence of any commercial or financial relationships that could be construed as a potential conflict of interest.

Advantages of publishing in Frontiers

OPEN ACCESS
Articles are free to read for greatest visibility and readership

FAST PUBLICATION
Around 90 days from submission to decision

HIGH QUALITY PEER-REVIEW
Rigorous, collaborative, and constructive peer-review

TRANSPARENT PEER-REVIEW
Editors and reviewers acknowledged by name on published articles

Frontiers
Avenue du Tribunal-Fédéral 34
1005 Lausanne | Switzerland

Visit us: www.frontiersin.org
Contact us: frontiersin.org/about/contact

REPRODUCIBILITY OF RESEARCH
Support open data and methods to enhance research reproducibility

DIGITAL PUBLISHING
Articles designed for optimal readership across devices

FOLLOW US
@frontiersin

IMPACT METRICS
Advanced article metrics track visibility across digital media

EXTENSIVE PROMOTION
Marketing and promotion of impactful research

LOOP RESEARCH NETWORK
Our network increases your article's readership